1 2 9 0

UNIVERSIDADE Ð COIMBRA

Pedro Gil Girão dos Santos

HYBRID PERFORMANCE-BASED WOOD PANELS FOR A SMART CONSTRUCTION

Maio de 2020

Faculdade de Ciências e Tecnologia da Universidade de Coimbra

HYBRID PERFORMANCE-BASED WOOD PANELS FOR A SMART CONSTRUCTION

Pedro Gil Girão dos Santos

Tese no âmbito do Doutoramento em Engenharia Civil, Construções orientada pelos Professor Doutor Luís Manuel Cortesão Godinho, Professor Doutor João Pedro Ramôa Ribeiro Correia e Professor Doutor Alfredo Manuel Pereira Geraldes Dias e apresentada ao Departamento de Engenharia Civil da Faculdade de Ciências e Tecnologia da Universidade de Coimbra.

Maio de 2020

UNIVERSIDADE Ð
COIMBRA

FINANCIAMENTO

AGRADECIMENTOS

Quero começar por endereçar um agradecimento especial à *Fundação para a Ciência e a Tecnologia (FCT)*, como organismo financiador da bolsa de doutoramento ao abrigo do programa doutoral *EcoCoRe*, a qual garantiu não só a atribuição de um subsídio de bolsa, bem como o pagamento das propinas necessárias à frequência do curso de Doutoramento.

Quero endereçar um agradecimento especial ao comité científico do programa doutoral *EcoCoRe*, quer pela organização do programa doutoral em si, quer pelos eventos de '*Summer School*' promovidos, os quais permitiram não só dar a conhecer o trabalho desenvolvido pelos alunos, mas também a troca impressões, intercâmbio de ideias e disponibilização de conselhos, tão essenciais num percurso como é o desenvolvimento de uma tese de Doutoramento.

Um agradecimento especial à *Universidade de Coimbra (UC)* e, em particular, ao Departamento de Engenharia Civil, instituição que me acolheu durante todo o meu percurso académico, incluindo como estudante de Mestrado Integrado e como Bolseiro de Investigação, mas que também proporcionou todas as condições para o desenvolvimento do presente trabalho.

Um agradecimento especial ao *Centro de Inovação e Competências da Floresta (SerQ)*, pelas condições de excelência que proporcionou em termos de logística, equipamento e instalações oferecidas, sem as quais não teria sido possível o desenvolvimento de grande parte do trabalho aqui apresentado.

Um agradecimento especial ao *Institute for Sustainability and Innovation in Structural Engineering (ISISE)*, como unidade de investigação, que proporcionou instalações, equipamentos, software e funcionários, que foram essenciais ao desenvolvimento do trabalho.

Um agradecimento especial aos meus orientadores: Prof. Doutor Alfredo Dias, Prof. Doutor João Ramôa Correia e Prof. Doutor Luís Godinho. Sem eles, não teria sido possível ter chegado até aqui. A sua visão e domínio nas suas aéreas de investigação foi essencial para o bom desenrolar do plano de trabalhos que me propus desenvolver. Eles foram fundamentais ao longo de todo o percurso e foi a sua preciosa ajuda que me fez superar as dificuldades que foram surgindo, e que também me levou a investigar e a aprofundar certos aspetos do trabalho, cuja importância eu não me tinha inicialmente

momentos de convívio. Pelo salutar convívio, um agradecimento também aos outros colegas que conheci no SerQ: Bruno, Cláudia, Eduardo, João, Márcia, Patrícia, Raquel, Ricardo e Rita.

Às colegas do *Instituto de Investigação e Desenvolvimento Tecnológico para a Construção, Energia, Ambiente e Sustentabilidade (ITeCons)*, Eng. Andreia Cortês, Arq. Beatriz Marques e Eng. Beatriz Ferrer, pelo apoio dado, troca de impressões e simpatia.

Um agradecimento às empresas que me apoiaram, algumas delas inclusive de forma completamente gratuita, nomeadamente: à *Pedrosa & Irmãos, Lda* responsável pela produções de painéis, nomeadamente nas pessoas do Eng. Nelson Pedrosa e Doutor Telmo Morgado, à *Sika Portugal SA*, não somente pelo apoio técnico fornecido, nomeadamente nas pessoas dos Eng. Paulo Silva, Arq. Carla Gomes e Eng. Joel Oliveira, bem como pela cortesia demonstrada pela empresa na colaboração no fornecimento de material; à *Polirigido - Isolamentos Térmicos e Acústicos Lda*, especialmente na pessoa do Sr. Fernando Lira, pela disponibilidade demonstrada e pelos conselhos técnicos dados; à *Poliuretanos SA*, pela informação técnica disponibilizada; à *Amorim Isolamentos SA*, na pessoa do Sr. José Andrade, pela informação técnica disponibilizada; à *BASF Portugal*, especialmente na pessoa do Eng. Jaime Matos, pela informação técnica disponibilizada; à *Henkel & Cie. AG*, na pessoa do Eng. Dario Salzgeber, pela informação técnica disponibilizada.

RESUMO

A madeira lamelada-cruzada (cross-laminated timber, CLT), tendência moderna em termos de construção em madeira, demonstra elevado potencial para sistemas maciços de construção de madeira. O conceito dos painéis CLT (camadas ortogonais) reduz significativamente a anisotropia dos painéis, garante maior estabilidade física e permite ligações mais fáceis e eficientes entre os elementos e destes com outros componentes da construção, tornando esses painéis uma solução versátil para suportar cargas fora/ e no plano dos mesmos. Este sistema possui vantagens significativas em relação à construção das tradicionais estruturas leves de madeira, abrindo um campo completamente novo para o uso da madeira na construção. Por outro lado, como se trata de um sistema maciço de madeira, é necessário um volume significativo de matéria-prima para produzir os painéis, aspeto que é apontado como uma das principais barreiras para a implementação do CLT de uma forma mais abrangente, porventura devido aos custos associados.

Neste contexto, o objetivo da presente tese consistiu no desenvolvimento de uma solução de painel alternativa, ou pelo menos complementar, baseada em CLT, mas utilizando menos quantidade de madeira, combinando desempenho mecânico com melhor isolamento térmico e peso reduzido. A solução desenvolvida, denominada madeira isolada cruzada (cross-insulated timber, CIT), consiste em substituir a camada interna de um painel CLT de cinco camadas por uma à base de material de isolamento (espuma rígida de poliuretano), tendo, por isso, algumas semelhanças com o conceito de painel de madeira estrutural isolado (SIP).

Os principais aspetos focados nesta tese, tendo em vista o desenvolvimento do painel incluem: (i) a definição da estrutura do painel e dos possíveis materiais para a sua constituição; (ii) a caracterização dos materiais selecionados para o desenvolvimento do painel, incluindo as camadas adesivas; (iii) a caracterização mecânica dos painéis; (iv) a otimização funcional e económica dos painéis; (v) a avaliação do impacte ambiental dos painéis; (vi) a caracterização acústica dos painéis; e (vii) o desenvolvimento de sistemas de conexão para os painéis.

No primeiro aspeto, foi definida uma estrutura composta por um núcleo em espuma rígida de poliuretano entre dois pares de camadas cruzadas em madeira de Pinho bravo. Em alternativa, para as faces exteriores dos painéis, foi também considerada a Acácia Austrália.

No segundo aspeto, os resultados de caracterização dos materiais permitiram verificar o comportamento complexo da espuma de poliuretano, tendo-se observado um

comportamento não-linear e rotura dúctil em compressão e um comportamento linear e rotura frágil em tração. Da adesão entre materiais, concluiu-se que as adoção de pressões de aperto mais elevadas conduzem a uma melhor adesão dos mesmos e, dos ensaios de envelhecimento, concluiu-se que ao invés de uma redução da resistência, particularmente no poliuretano, houve um aumento da mesma devido à pós-reticulação do material.

No terceiro aspeto, foi possível verificar que o modo de rotura dominante nos ensaios de flexão foi o corte do núcleo. Os modelos analíticos identificados na revisão do estado-da-arte descreveram bem o comportamento inicial observado (linear) e, para descrever a fase não-linear observada, os modelos numéricos desenvolvidos demonstraram um bom nível de precisão.

No quarto aspeto, concluiu-se que a exigência de um desempenho térmico mínimo (envolvente exterior do edifício) torna a solução de painel desenvolvido na tese mais competitiva face aos painéis CLT.

No quinto aspeto, através de uma análise de ciclo-de-vida, concluiu-se que a produção de poliuretano e a assemblagem do painel constituem os processos de produção com maior impacte ambiental; dos cenários de fim-de-vida considerados, a opção de incineração com recuperação de energia revelou ser a que implica menores impactes. Da comparação com sistemas de CLT, concluiu-se que o painel desenvolvido implica, de uma forma geral, maiores impactes.

No sexto aspeto, verificou-se, o menor isolamento dos painéis de CIT face aos de CLT de igual espessura, devido à menor massa. Os modelos analíticos identificados no estado-da-arte para painéis sanduiche não se revelaram adequados para avaliação do isolamento a sons aéreos dos painéis, pelo que o modelo de Sharp para elementos isotrópicos e homogéneos com uma adaptação revelou uma melhor descrição dos mesmos; para descrição do isolamento a sons de percussão, a lei do invariante revelou-se eficaz.

No sétimo aspeto foram desenvolvidas várias ligações, sendo que uma delas foi testada experimentalmente, e cuja resistência se enquadrou dentro do previsto pelos modelos analíticos identificados no estado-da-arte.

Globalmente, o estudo realizado nesta tese mostrou que os painéis desenvolvidos têm potencial para complementar os atuais sistemas em CLT, nomeadamente no que diz respeito ao aos elementos da envolvente exterior.

Palavras-chave: madeira isolada cruzada; painéis sanduíche; produtos de madeira; caracterização do material; qualidade de colagem; teste estrutural; análise de ciclo de vida; desempenho acústico; ligações.

ABSTRACT

Cross-Laminated Timber (CLT), a modern trend in timber construction, shows high potential for massive timber construction systems. Compared to traditional systems, the CLT panels' layout (crosswise layers) significantly reduces the anisotropy of the panels, guarantees higher physical stability and allows for easier and more efficient connections between elements and other building components, making these panels a versatile solution to bear both out-of-plane and in-plane loads. This system has also significant advantages with respect to traditional wood light-frame construction, opening a completely new field for the use of timber in construction. On the other hand, as this is a massive wood system, a significant volume of wood raw material is required to produce the panels and this is pointed out as one of the main barriers for CLT implementation, perhaps due to the associated costs.

In this context, the objective of the present thesis consisted of the development of an alternative, or at least complementary, CLT based panel solution but using less amount of wood, combining mechanical performance with improved thermal insulation and reduced weight. Such solution, named cross insulated timber (CIT), consists of replacing the inner layer of a five-layer CLT panel by an alternative one made of insulation material (polyurethane rigid foam), and thus having some similarities with the structural insulated timber panel (SIP) concept.

The main aspects that are focused on this thesis for the panel development, include: (i) the definition of the panel layout and potential materials for its constitution; (ii) the characterization of the selected materials for the panel development, including the adhesive layers; (iii) the mechanical characterization of the panels; (iv) the functional and economic optimization of the panels; (v) the evaluation of the environmental impact of the panels; (vi) the acoustic characterization of the panels; (vii) the development of connection systems for the panels.

In the first aspect, a structure consisting of a polyurethane core between two pairs of Maritime pine crossed layers was defined. As an alternative to this, for the exterior faces of the panels, Acacia Australia was considered.

In the second aspect, the results of material characterization tests allowed to verify the complex behaviour of the polyurethane foam, which presents non-linear behaviour and ductile failure in compression, and linear behaviour and brittle failure in tension. From

the adhesion between materials, it was concluded that the adoption of higher bonding pressures leads to better adhesion of the same ones and, from the ageing tests, it was concluded that instead of a reduction in strength, particularly in polyurethane, there was a strength increase due to additional cross-linking due to post-curing.

In the third aspect, it was possible to verify that the dominant failure mode in the bending tests was core shearing. The analytical models identified in the state-of-the-art review described well the observed initial behaviour (linear) and, to describe the observed nonlinear phase, the numerical models developed demonstrated a good level of precision.

In the fourth aspect, it was concluded that the requirement of a minimum thermal performance (in the case of the exterior envelope of the building) makes the panel solution more competitive against CLT panels.

In the fifth aspect, through a life-cycle assessment, it was concluded that the production of polyurethane and the assembly of the panel constitute the production processes with the greatest environmental impact; among the considered end-of-life scenarios, the option of incineration with energy recovery proved to be the one with the least impacts. From the comparison with CLT systems, it was concluded that the developed panel presented, in general, greater impacts.

In the sixth aspect, less insulation of the CIT panels compared to the CLT panels of equal thickness was registered, due to the lower mass. The analytical models identified in the state-of-the-art for sandwich panels did not prove to be suitable for assessing the airborne sound insulation of the panels, so the Sharp model for isotropic and homogeneous elements with an adaptation provided more accurate predictions; for describing the insulation to impact sounds, the invariant law proved to be effective.

In the seventh aspect, several connections were developed, one of which was experimentally tested, and whose resistance fit within the predictions provided by the analytical models identified in the state-of-the-art.

Overall, the study conducted in this thesis showed that the developed panels have the potential to complement the current CLT systems, namely concerning the elements of the external envelope.

Keywords: cross-insulated timber; sandwich panels; wood products; material characterization; bonding quality; structural testing; life cycle assessment; acoustic performance; connections.

TABLE OF CONTENTS

LIST OF FIGURES

LIST OF TABLES

SIMBOLOGY

A_0	cross-section area of the layers compressed parallel to grain
C_{lf}	stiffness quota
D_{max}	maximum delamination
$D_{n,e}$	element-normalized level difference
D_{tot}	total delamination
E_c	elasticity modulus in compression
E_{dyn}	dynamic modulus of elasticity
E_t	elasticity modulus in tension
F_{crimp}	critical force that causes shear crimping
F_u	ultimate load
$L_{n,w}$	weighted normalised impact sound pressure level
L_n	normalized impact sound pressure level
L_w	sound level radiated per area
P_{cr}	Euler's buckling load
R_e	thermal resistance of the element
R_{se}	superficial external thermal resistance
R_{si}	superficial internal thermal resistance
R_w	airborne sound reduction index
T_g	glass transition temperature
$WF_{delamination}$	wood failure percentage after delamination test
$WF_{glue\ line}$	wood failure percentage for each split area
WF_{shear}	wood failure percentage after shear test
$WF_{tot,glue\ line}$	wood failure percentage for the sum of all split areas
X_d	design strength
b_{cut}	tip width of the cutter
b_t	tip width
c_0	speed of sound in air
d_c	core thickness
f_{11}	fundamental frequency
f_c	compressive strength
f_c	critical frequency
f_{dil}	dilatational resonant frequency
f_m	bending strength
f_t	tensile strength
f_v	shear strength

g_k	dead load, characteristic value
k_c	instability factor
k_{def}	deformation factor
k_m	factor related with the type of wood product
k_{mod}	modification factor
l_1	distance between the external deflection measurement points on bending test setup
$l_{glue\ line}$	perimeter of one glue line
l_j	finger length
$l_{max,delam}$	maximum delamination length
l_s	support length
l_t	tip gap
$l_{tot,delam}$	total delamination length
$l_{tot,glue\ line}$	sum of perimeters of all glue lines
$m_{0\%}$	dry mass of wood
q_k	imposed load, characteristic value
t_{ch}	time for start of charring
w_B	deflection due to the elastic extension of the faces
w_T	total deflection
w_u	deflection at the ultimate load for compression test
α_V	coefficient of volumetric shrinkage
γ_m	partial coefficient ($\gamma_m = \gamma_M$)
λ_{rel}	relative slenderness
ρ_{12}	wood density at relative humidity of 12%
σ_{wr}	wrinkling stress
$\bar{\tau}$	average transmission coefficient
ϵ_a	total axial shrinkage
ϵ_r	total radial shrinkage
ϵ_t	total tangential shrinkage
ϵ_v	total volumetric shrinkage
ΔH	horizontal shortening
ΔV	vertical extension
h	depth
δ	difference
δR	transmissibility
A	cross-sectional area; shear area; equivalent absorption area
C	convergence factor
D	sound level difference
E	modulus of elasticity

EI	bending stiffness
F	force; F-statistic (ANOVA)
G	shear modulus
$G\Omega_r$	effective shear stiffness
GA	shear stiffness
HR	moisture content
I	second moment of area
L	longitudinal; sound pressure level
M	bending moment
R	radial; airborne sound reduction
S	area
S	first moment of area
T	tangential; reverberation time
U	coefficient of thermal transmission
U	perimeter
V	shear force; volume
Z	acoustic impedance
a	distance between a support and the closest loading point on bending test setup; distance between the centres of gravity of layers 1 and n (SAV)
b	width
e	thickness; distance between centroids of the faces
ew	edgewise
f	frequency
fw	flatwise
k	distribution parameter; constant depending on the imperfections and quality of the face, core and bond
l	length; dimension
m	surface mass
p	pitch
p	sound pressure
$p-value$	probability that the F-statistic can take a value larger than a computed test statistic value (ANOVA)
t	thickness; time
w	deflection
z	distance between the centres of gravity of the layer and the full cross-section
γ	distortion; partial safety factors – EN 1990
ε	strain

ζ	fraction of critical damping
η	loss factor (chapter 8); conversion factor (chapter 6)
λ	Poisson' ratio
λ	thermal conductivity coefficient
μ	water vapour diffusion resistance factor
ρ	density
σ	normal stress
τ	shear stress; sound transmission coefficient
φ	creep coefficient
ψ	combination factors – EN 1990
ω	angular frequency

ABBREVIATIONS

1C	One-component
2C	Two-component
AB	Australian blackwood
ACB	Agglomerated Cork Board
AD	Acidification potential
ADP	Abiotic depletion potential
ANOVA	Analysis of variance
ASR	Adhesive spread rate
BEM	Boundary Element Method
BP	Bonding pressure
CIT	Cross Insulated Timber
CLT	Cross Laminated Timber
EP	Eutrophication potential
EPD	Environmental Product Declaration
EPI	Emulsion Polymer Isocyanate
EPS	Expanded Polystyrene
ER	Energy recover
ETA	European Technical Approval
FEM	Finite element model
GLT	Glued Laminated Timber
GWP100	Global warming potential for time horizon of 100 years
ICB	Expanded Insulation Corkboard
LCA	Life Cycle Assessment
LCI	Life Cycle Inventory
LCIA	Life Cycle Impact Assessment
LR	Longitudinal Radial
LT	Longitudinal Tangential
LVL	Laminated Veneer Lumber
MF	Melamine Formaldehyde
MP	Maritime pine
MUF	Melamine Urea Formaldehyde
ODP	Ozone layer depletion potential
OSB	Oriented Strand Board
PIR	Polyisocyanurate
POCP	Photochemical oxidation potential
PR	Phenolic Resin / Primer

PRF	Phenol Resorcinol Formaldehyde
PUR	Polyurethane
RW	Rock Wool
SAV	Shear analogy Method
SEA	Statistical Energy Analysis
SIP	Structural Insulated Panel
TBT	Timoshenko beam Theory
TL	Sound transmission loss
TR	Tangential Radial
UF	Urea Formaldehyde
WF	Wood failure percentage
WF	Wood Fibres
XPS	Extruded Polystyrene

1 INTRODUCTION

1.1 Context

Cross Laminated Timber (CLT) is a type of structural panel that consists of several layers of timber laminations, glued crosswise to produce a massive timber system (Crespell and Gagnon, 2010; FPInnovations, 2013) (Figure 1-1).
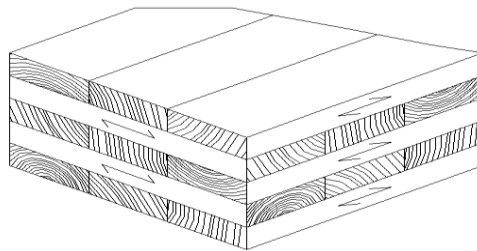
Figure 1-1 - Cross Laminated Timber: schematic layout.

The development of CLT started in the 1990s in Europe, motivated by the need of the sawmill industry to optimize the material cut from tree logs. The objective was to find higher value for the side boards (of excellent quality) that could be used as outer layers, while the inner boards (of lower quality) could be used as inner layers in the panels (Ansell, 2015). The CLT concept itself was not novel at the time, as it had been used in wood carpentry products, such as plywood. The novelty at the time was that such concept had never been used in panels of larger dimensions aimed for high demand structural purposes (Brandner et al, 2016).

The CLT layout concept, which significantly reduces the anisotropy of the panel, guarantees higher dimensional stability (e.g. reduced warping), allows easier and more efficient connections, making these panels a versatile solution for bearing either out-of-plane or in–plane loads. These characteristics allowed a new paradigm in the wood building construction, with CLT-made buildings becoming a competitive solution with respect to traditional masonry, steel and concrete structures (FPInnovations, 2013).

Some advantages and benefits of CLT are enumerated next (FPInnovations, 2013; Espinoza et al, 2016):

- High dimensional stability;

- Two-way action structural capabilities;
- Pre-fabrication, fast construction, little building site support requirements;
- Increased splitting resistance for some types of connections.

However, some disadvantages and issues exist (FPInnovations, 2013; Espinoza et al, 2016), namely:

- Less stiffness and strength in the main direction, when compared to traditional solutions (e.g. stress-laminated timber or glued-laminated timber), due to cross-layering;
- High wood volume required;
- Increased weight comparing to wood light-frame construction;
- Difficulties in rectifying the panels *in situ*;
- Need to use adhesives (less sustainability).

In some surveys conducted about CLT (Espinoza et al, 2016), the wood volume required is pointed out as one of the main barriers for CLT implementation. Indeed, recent research has been conducted to develop CLT optimized solutions, not only in terms of wood volume but also in terms of panel internal architecture, sustainability, thermal and acoustic insulation or increased load/span capacity.

One of the most obvious and efficient options when addressing the optimisation of CLT panels is the rational distribution of the raw material along the panels' height according to its quality. As in glued laminated timber (GLT), lower quality wood can be used in the inner layers with very insignificant loss of strength and stiffness.

As referred before, the original (or standard) CLT approach consists of alternate layers crossed at 90º (Figure 1-1). The fact that some of the inner layers are placed in a way that their wood fibres are normal to the span direction leads to a noticeable increase of shear deformation, which means that the CLT strength and stiffness is less than those of an equivalent panel with the wood fibre layers all aligned with the span direction. To minimize this disadvantage, some researchers, namely Chen (2011) and Buck et al (2016), tested an alternate angle for the inner layers (45º in relation to the span direction), leading to an increase of stiffness and strength along the span direction for panels loaded out-of-plane comparing to the standard solution.

Another approach involving lower stiffness and strength (compared to conventional CLT panels) but also lower wood volume employed and higher insulation consists of leaving voids in the panel structure filled with insulation material, for improved thermal

performance. Examples of such system are found in (Glasø and Nore, 2012) and the Panobloc systẽm (Franzoni et al, 2015; Panobloc, 2018).

Other solutions also include voids inside the panel structure, but aim at large span applications, such as box-type solutions: Chen (2011) and Montgomery (2014) proposed panels made of CLT flanges connected through metallic connectors to GLT internal webs; a five-layer CLT panel, where the central layer is substituted by a series of spaced beams, and which incorporates insulation in the voids is produced by Egoin (Egoin, 2015). Other options for large span applications include rib elements made with GLT webs and CLT flanges (KLH, 2015).

Regarding the connection system between layers, which ensures the composite action of the panel, besides the typical solution of glueing, other alternative systems can be found: metal nails (Chen, 2011 and Pang et al, 2017); wood dowels (Thoma, 2015); wood screws (Nur-Holz, 2015), or groove-tongue profiles (Smith, 2011).

These solutions are very interesting from a sustainability point of view (metal connectors can be separated from wood at the end-of-life of the panels and thus recycled, and CLT made with wood connectors is a 100% wood system); however, the mechanical performance of these systems is much more limited than glued CLT. For example, from bending tests conducted on glued CLT and nailed- CLT panels, (Chen, 2011) reports twice the resistance on the former system compared to the latter.

Beyond the above-referred solutions, another option, that is still open, is the replacement of one or more wood layers of a CLT panel by one or more layers made of a rigid insulation material. This is actually a concept similar to the one of the structural insulated panel (SIP), which consists of a sandwich panel type comprising an insulation layer between two external layers (also referred as faces or skins) made of a wood-based material (Kermani, 2006; SIPA, 2015) (Figure 1-2).
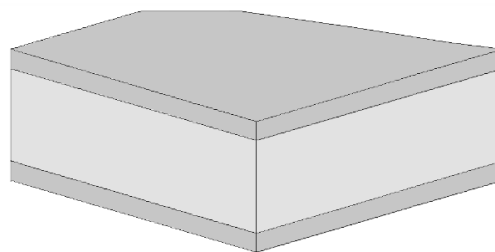
Figure 1-2 – Structural Insulated Panel: schematic layout

According to Panjehpour et al (2013), the SIP idea was firstly introduced in 1935 by the Forest Products Laboratory, in the USA, although according to Vinson (2005), the

sandwich concept itself is older. This system has a load bearing capacity that turns it into a cost effective alternative to traditional stud wall construction, reducing the need for structural framing (Kermani and Hairstans, 2006; Chen and Hao, 2015).

SIP presents advantages such as structural and insulation functions combined in a single manufactured system with relatively low self-weight. However, some issues are usually pointed out as disadvantages of SIP, namely the creep of the foam core and the poor fire resistance without protective coatings (Abbasi, 2014).

1.2 Motivation and objectives

Although some of the solutions previously presented include insulation material, they also present thermal bridging problems due to the inner rib elements. As referred in the previous paragraphs, a panel solution that combines the CLT and SIP concepts has not yet been developed, i.e. a panel with an inner layer fully composed of insulation material.

Such concept is idealized for a two pair of wood cross layers adhesively connected to an inner layer of insulation material, and is named Cross Insulated Timber (CIT) (Figure 1-3).
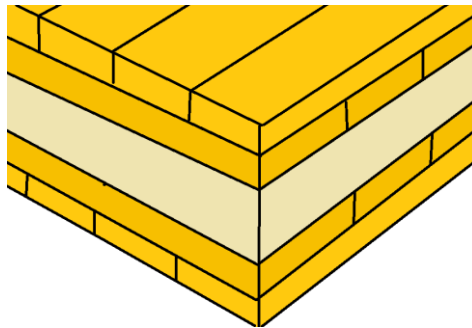
Figure 1-3 - Conceptual scheme of the developed panel, named Cross Insulated Timber.

The main purpose of this thesis is thus to develop and study a new kind of wood-based structural panel than can bear in-plane or out-plane loads, combining the advantages of CLT and SIP systems, namely:

- Adequate structural capacity with integrated thermal insulation;
- Optimized use of wood volume material;
- Low self-weight;
- Physical stability to hygrothermal variations;
- Possibility of versatility options for connections.

It should be noticed that SIPs are structurally more limited than CLT, due to the core material, which, typically, has increased thermal resistance, but at the same time has lower shear stiffness and strength. Due to such particularly, the panel to develop may not be an alternative, but a complement to CLT, especially for structural elements where thermal resistance is also required (i.e. external envelope).

Within the main goal of the thesis, the following objectives were set for the research:

i.   the definition of the panel layout and potential materials for its constitution;
ii.   the characterization of the selected materials for the panel development, including the adhesive layers;
iii. the mechanical characterization of the panels;
iv.   the functional and economic optimization of the panels;
v.   the evaluation of the environmental impact of the panels;
vi.   the acoustic characterization of the panels;
vii. the development of connection systems for the panels.

1.3 Methodology

To achieve the proposed objectives, the research methodologies pursued in this study are described next.

The first objective was developed through the following tasks:

- The definition of the panel layout;
- The identification of potential constituent materials for the panels.

In the first task, the analysis and comparison between different configurations of the panel layout was made, regarding their mechanical and physical performance, as well as their economic feasibility. The second task was developed through the identification and collection of information from the literature regarding possible materials for the development of the panels, focusing specifically on wood as the material for the faces of the panels. Regarding this aspect, one important target of this thesis was to promote the use of a natural renewable resource that is wood. It should be noticed that timber, in contrast to other building materials, has the particularity of being a "carbon storage", as a tree during its growth absorbs CO_2 from the atmosphere. The focus was also to use species found in Portuguese forest.

The second objective, the characterization of the selected materials for the panel development, including the adhesive layers, was pursued through the following tasks:

- Experimental mechanical characterization of the selected materials to compose the face layers (Maritime pine and Australian blackwood) and core layer (polyurethane rigid foam);
- Experimental characterization of the thermal insulation of the panels;
- Characterization of the adhesion between the wood materials and between the polyurethane foam material and Maritime pine, including the ageing effects.

The first task was developed through the collection of reference values found in the literature regarding Maritime pine and Australian blackwood solid wood. Australian blackwood lamellas were characterized through bending tests and the material to compose the core layer (polyurethane) was characterized, through compression, tension, shear, creep and ageing tests. The second task was dedicated to the experimental thermal characterization of the polyurethane foam material and cross-laminated timber panels made of Maritime pine wood, as well of the developed panel solution. The third task comprised the assessment of the bonding performance of the panels, including the face bonding of cross layers made of Maritime pine and Maritime pine with Australian blackwood, finger-joint connections between Maritime pine lamellas and face bonding of wood layers to the polyurethane foam.

The third objective, the mechanical characterization of the panels, was achieved through the following tasks:

- State-of-the-art review of experimental tests, as well as analytical and numerical models used to describe the mechanical behaviour of similar panels to the one developed in the thesis;
- Experimental assessment of the mechanical behaviour of the developed panels;
- Comparison of the experimental results with predictions from analytical models;
- Finite element modelling of the panels to simulate the mechanical behaviour of the panels in bending.

For the first task, a state-of-the-art review of experimental tests and analytical and numerical models used to describe the mechanical behaviour of SIP and CLT panels used as beam and column elements was made. In the second task, the experimental characterization of the mechanical behaviour of the developed panels was made through bending and compression (flexural buckling) tests. In the third task, a comparison of the experimental results with the one predicted by the analytical models available in the

literature was made. In the last task, due to the non-linear behaviour of the panels, finite element modèls were developed to simulate their bending response.

The fourth objective, the functional and economic optimization of the panels, was achieved through the following tasks:

- Identification of design requirements;
- Optimization of the panels.

In the first task, the design requirements regarding the structural and non-structural performance of the panels were identified from the current regulation. In the second task, a mathematical model was used to optimize the functionality and production cost of the panels.

The fifth objective, the evaluation of the environmental impact of the panels, was made through the following tasks:

- State-of-the-art review regarding the environmental impact of CLT and SIP;
- Life cycle assessment (LCA) of the developed panels.

The first task focused on the identification of the evaluation methods of the environmental impact of similar panels to the one developed in the thesis, namely SIP and CLT systems. The second task included the LCA of the developed panels, including some variations on the constituent materials, as well the comparison with other panel systems of similar performance.

The sixth objective, the acoustic characterization of the panels, encompassed the following tasks:

- State-of-the-art review regarding the analytical and experimental characterization of sound insulation of similar panels to the one developed in the thesis, namely SIP and CLT;
- Experimental campaign regarding the airborne and impact sound insulation of the developed panels.

For the first task, a state-of-the-art review of experimental tests and analytical and numerical models used to describe the acoustic behaviour of SIP and CLT panels was made. The second task comprised the experimental characterization of the airborne and impact sound insulation of the developed panels, as well their performance in comparison with other building solutions, including CLT panels, wood floors and concrete slab.

The seventh objective, the development of connection systems for the panels, was made through the following tasks:

- State-of-the-art review regarding CLT and SIP connections between panels and existing structural members and analytical design models;
- Development of connections for the developed panels;
- Experimental characterization of one of the developed connections.

In the first task, common CLT and SIP connections between panels and existing structural members (masonry or concrete foundations and walls) were identified to serve as a basis for the development of connection systems for the developed panels. In the second task, the connections systems for the developed panels were proposed and the advantages and drawbacks of each system were discussed. In the last task, one of the developed connections was experimentally tested to assess its mechanical performance.

1.4   Structure of the document

According to the described objectives, this document is organized in the following nine chapters:

- Chapter 1 – Introduction.
- Chapter 2 – Development of the panel concept – The basic layout and potential materials for the panels' development are presented. The materials include the wood species, insulation core materials and adhesive systems between layers.
- Chapter 3 – Characterization of polyurethane and wood materials – The information regarding the selected materials from the previous chapter and the results of experimental tests performed towards their characterization are presented.
- Chapter 4 – Characterization of adhesive layers – The results regarding the testing and optimization of the adhesive layers tested are presented.
- Chapter 5 – Mechanical characterization of the panels – Presents the results of the mechanical tests of the panels assessed through experimental tests and the comparison with analytical models.
- Chapter 6 – Design and optimization of the panels – To obtain functionally efficient and economically feasible solutions, the results from the optimization of the panel layers' thickness are presented, as well the comparison with CLT equivalent solutions.

- Chapter 7 – Life cycle assessment of the panels – Presents the results of the environmental impacts of the proposed panel and CLT equivalent solutions through a life cycle assessment methodology.
- Chapter 8 - Acoustic characterization of the panels - The results regarding the acoustic airborne and impact sound insulation performances of the panels assessed trough experimental tests are presented.
- Chapter 9 – Connections – Describes the idealization of different connection systems for the developed panels and presents results of tests on one of those connection systems.
- Chapter 10 – Conclusions and future developments.

2 DEVELOPMENT OF THE PANEL CONCEPT

2.1 Introduction

The production of an efficient panel solution requires the choice of the most appropriate constituent materials to obtain a product that guarantees the intended performance.

As referred to in the previous chapter, the target performance criteria include:

- Adequate structural capacity;
- Adequate thermal insulation;
- Optimized use of wood material;
- Low weight;
- Physical stability to hygrothermal variations.

As referred in Chapter 1, the developed panel has combined characteristics of Cross-Laminated Timber (CLT) and Structural Insulated Panel (SIP) systems, which resulted in an internal architecture similar to a sandwich type-panel. In a sandwich panel, the mechanical performance is assured by the faces composing the panel that are responsible for carrying most of the compression and tension stresses resulting either from axial forces (in-plane loads) or bending moments (out-of-plane loads), while the core material is mainly responsible for stabilizing the panel against buckling and resisting to shear forces (APA, 2014). Thus, the outer layers of the panel should be made of a rigid material with adequate properties in what concerns tension and compression, and the core layer should be made of a material with suitable shear and out-of-plane compressive/tensile properties. Regarding the thermal performance required for the panels, the core material should have low thermal conductivity, consequently presenting low density, and thus fulfilling the low weight requirement for the panels.

Regarding the physical stability due to hygrothermal variations, it is expected that one pair of cross wood layers at each side of the core is enough to ensure adequate performance. In wood boards, four basic types of wane can be considered: bow, spring, twist and cup (Figure 2-1) (FPL, 2010). Assuming the typical cross-section of the wood lamellas in CLT, (i.e. width larger than the depth), one can say that both the spring and cup wanes of one wood layer are restricted by the other wood layer disposed orthogonally. Concerning the bow and twist wanes that tend to appear in a wood layer, it is expected that they are restrained not only by the cross wood layer but also by the insulation layer.
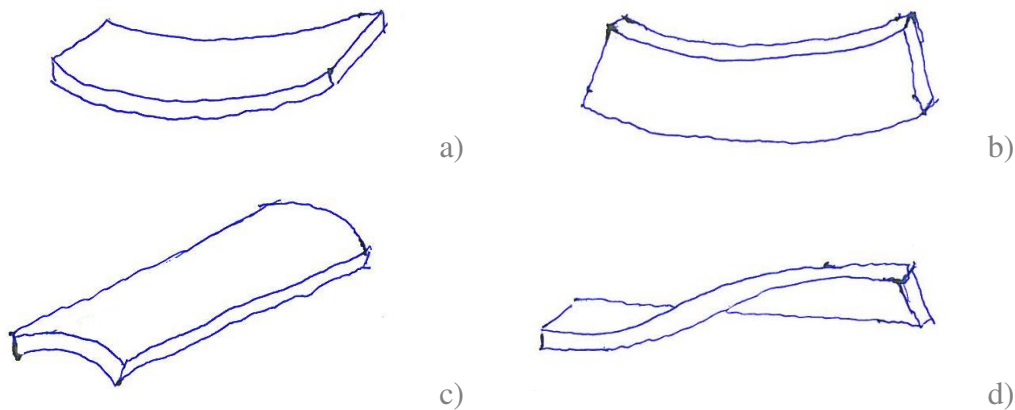
Figure 2-1 – Four basic types of wane in wood boards: a) bow; b) spring; c) cup; d) twist.

The use of more than two wood layers at each side of the panel would imply additional glue lines, with a consequent increase in production costs and loss of competitiveness compared to CLT current solutions. Besides considering a five-layer panel with two pairs of wood layers between an insulation layer, it would also be possible to consider the use of two insulation layers between three wood layers (Figure 2-2). In terms of mechanical behaviour, the differences between these options can be analysed taking a simple example, considering two cross-sections with the same volume of materials, but with different layouts (Figure 2-2). For the materials, let us consider that the wood layers correspond to C24 strength class (CEN, 2009) and the insulation layer is made of rigid polyurethane foam (ρ=40 kg/m^3).
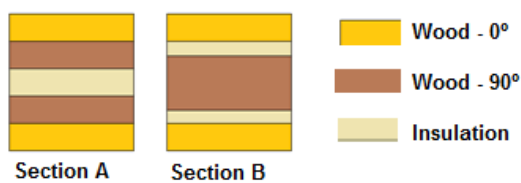
Figure 2-2 – Two options for the internal architecture of a five-layer panel using the same volume of raw material.
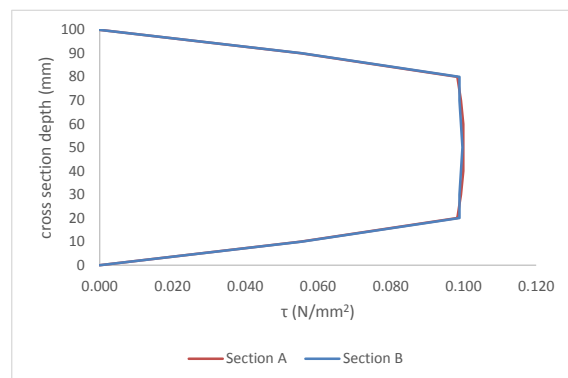
Figure 2-3 – Shear stress curves of both cross-sections for the same applied load.

As depicted in Figure 2-2, one layout has two pairs of wood cross layers and an inner core of insulation (section A), all with the same thickness. The other layout (section B) has two outer layers with the same grain direction (0º) and thickness of the outer layers of

section A, while the inner layer is made of a cross wood layer (90º) with twice of the thickness of one cross layer from section A, and is surrounded by two layers of insulation with half the thickness of the corresponding layer from section A. The geometry and properties of the two cross-sections are shown in Table 2-1. The values for the elasticity and shear modulus (E and G, respectively) listed in that table correspond to the C24 strength class of wood and experimental data (Chapter 3) for polyurethane foam.

Table 2-1 – Geometry and properties of the two cross-sections.

Section	Layer	h (mm)	b (mm)	E (N/mm^2)	G (N/mm^2)
A	1 and 5	20		11000	690
	2 and 4	20	100	370	69
	3	20		8	3
B	1 and 5	20		11000	690
	2 and 4	10	100	8	3
	3	40		370	69

It should be noticed that, according to the Timoshenko beam theory (presented in Chapter 5), the bending stiffness and the shear stress distribution over the cross-section are dependent on the composite layout geometry, as well as on the modulus of elasticity of the layers; the shear stiffness is additionally dependent on the shear modulus of the layers. It is important to mention that the ratio between the values of modulus of elasticity of the layers is about $E_{wood,0}=30\times E_{wood,90}$ and $E_{wood,90}=120\times E_{insulation}$. Using the Timoshenko beam theory, it is found that the bending and shear stiffness of both cross-sections are of the same order of magnitude ($EI_{section\_A}=7.25E+11$ kNm^2, $EI_{section\_B}=7.21E+11$ kNm^2, $GA_{section\_A}=9.04E+05$ kN and $GA_{section\_B}=9.22E+05$ kN), as well as the shear stress distributions (the governing stress for design) throughout the section height (Figure 2-3). It should be noticed that these results are valid for the material properties and geometries indicated before.

Although from the mechanical point of view no significant differences are found, the choice of section B may have some disadvantages compared to option A, namely:

- One is that the physical stability of the external wood layers may not be ensured, especially if the insulation material has a low modulus of elasticity or if it is crushable (e.g. polyurethane foam), allowing for the warping of the wood lamellas, either due to hygrothermal variations or punctual loads. This situation is even more likely to occur if the wood lamellas are not edge bonded laterally among themselves (Figure 2-4).

- The second is related to fire performance: in case of fire, the core material is much

more exposed to high temperature than if it is placed at the centre of the panel. It should be noticed that most of the insulation materials used in sandwich panels are combustible materials (typically, more combustible than timber), with temperature-dependent properties (also more critical than in timber).
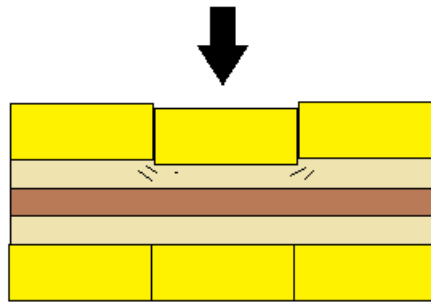
Figure 2-4 – Schematic representation of possible warping on a panel section of type B due to punctual loading.

Therefore, due to the reasons presented above, the placement of the insulation material at the inner layer of the panel between a pair of cross wood layers was found to be the most rational solution – this was the option followed for the panel development in the scope of the present thesis.

2.2 Materials definition

In the present section, the materials identified as having the potential to be used in the panel development are described, namely: (i) materials for the wood layers, (ii) materials for the insulation layer, and (iii) the adhesives.

2.2.1 Materials for wood layers

Regarding the definition of the materials, in CLT the layers are often made of solid wood laminations, with some manufacturers presenting alternative solutions that include other wood-based panels in the inner layers (e.g. Laminated Veneer Lumber (Leno, 2018)). In wood-based SIP, the faces are usually made of plywood or Oriented-Strand-Board (OSB) (APA, 2013), because with such layers it is possible to obtain uniform properties and stability in all the plane directions. However, the stiffness and strength of such wood-based panels are lower than those from solid wood. For this reason, solid wood was chosen as the basic material to constitute the wood layers.

2.2.1.1 Potential wood species identification

One of the objectives of this thesis is to assess and promote the use of Portuguese wood species for the proposed structural application. The focus was to identify which species have potential, in terms of functionality, to be used in the panels. Although not all the identified species could be feasible to use at this moment, due to their scarcity or/and elevated costs, it was deemed important to test them once the forest reality is changing fast, due to various factors, such as, for example, forest fires. Additionally, the assessment of invasive species with potential was considered to promote its logging with economical and ecological benefits. This phenomenon increased in recent years, leading to an opportunity to promote the reforesting of the burned areas with native species that in the future can be used in the panels' production.

Having these objectives in mind, information was collected about the characterization of the Portuguese forest and the relevant properties of the most common wood species identified. The most recent official data related to the global species distribution in the Portuguese forest by the *Institute for Conservation of Nature and Forestry* (*Instituto da Conservação da Natureza e das Florestas)* is found on two reports from this institution (ICNF, 2013a and ICNF, 2013b). The global distribution of species in the Portuguese forest is summarised in Figure 2-5.

The predominant species are Eucalyptus (including various sub-species), Maritime pine, Cork oak and Holm oak. It should be noticed that Cork oak and Holm oak are protected by a decree-law that forbids its logging. Based on the mentioned reports, a more detailed overview of the forest species is presented in Table 2-2.
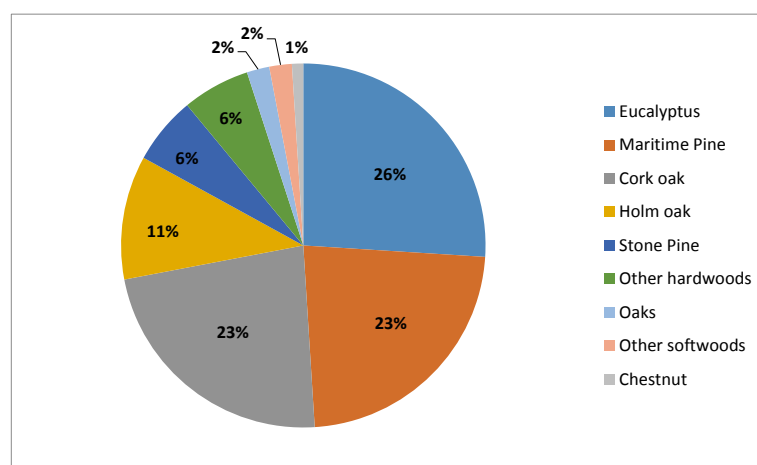
Figure 2-5 - Global distribution of species in the Portuguese forest according to (ICNF, 2013a).

Besides representing one of the predominant species in Portuguese forest, Maritime pine is one of the most used and studied species for structural applications in Portugal. Other species, such as Oak and Chestnut, have been widely applied in the past, but, nowadays, due to their scarcity, which leads to higher purchase costs, they are less used. Although Eucalyptus is the species with larger area, it still presents some issues associated with the industrial processing, namely related to the drying process after logging, which if not properly executed results in severe cracks and wanes in the wood pieces (Carvalho, 1997).

Table 2-2 – Most common forest species in Portugal based on the literature.

Type	Species		Portuguese name	Botanical name	Occurrence
Softwood	Pine	Maritime	Pinheiro Bravo	*Pinus pinaster*	P
		Stone	Pinheiro Manso	*Pinus pinea*	P
		Aleppo	Pinheiro de Alepo	*Pinus halepensis*	A
		Insinge	Pinheiro Insigne	*Pinus radiata*	F
	Cypress [1]	Buçaco	Cipestre do Buçaco	*Cupressus lusitanica*	F
	Pseudotsuga		Pseudotsuga	*Pseudotsuga menziesii*	A
Hardwood	Eucalyptus [1]	Southern Blue Gum	Eucalipto Vulgar (incl. Molar)	*Eucalyptus globulus*	P
	Acacia [1]	Australian Blackwood	Austrália	*Acacia melanoxylo*	A
	Alder		Amieiro	*Alnus glutinosa*	A
	Birch		Vidoeiro	*Betula pubescens*	A
	Poplar [1]	Hybrid	Choupo Híbrido	*Populus canadensis*	A
		White	Choupo Branco	*Populus alba*	F
		Black	Choupo Negro	*Populus nigra*	F
	Beech		Faia	*Fagus sylvatica*	F
	Ash [1]		Freixo	*Fraxinus angustifolia*	A
	Elm [1]	Scots elm	Ulmeiro	*Ulmus procera*	F
	Oak	Portuguese	Carvalho Português	*Quercus faginea*	P
		Pyrenean	Carvalho Negral ou Pardo	*Quercus pyrenaica*	P
		Roble	Carvalho Roble ou Alvarinho	*Quercus robur*	P
	Chestnut		Castanheiro	*Castanea sativa*	P

Notes: P - Predominant; A - Abundant; F - Frequent
[1] Other variants of the species exist

For the species listed in Table 2-2, the mean values of bending stiffness and strength of clear wood specimens were collected from (Carvalho, 1997), which gives much relevant information related to Portuguese woods. The natural durability of the species was taken from EN 350-2 (CEN, 1994) and for those not mentioned in the standard, complementary notes were taken from (Carvalho, 1997). This data is shown in Table 2-3.

Considering the information given in Table 2-3, in terms of mechanical properties, the following species may be highlighted as presenting the better performance: Maritime pine, Eucalyptus, Acacia, Ash, Elm and Oak. Concerning durability, all of the presented species are susceptible to biological degradation; despite this, the following are found to be the most durable ones: Buçaco cypress, Acacia, Roble oak and Chestnut.

Crossing data from mechanical and durability properties, it can be stated that Acacia and Roble oak are found as the most balanced ones. In Acacia, a complement to the excellent

natural durability of the heartwood is the high proportion in relation to the total volume of the tree found in Portuguese grown specimens (Knapic et al, 2006). This is an invasive species that is causing great concern due to its easy and fast propagation over the Portuguese forest (especially after fire forests), and for that reason, its planting is prohibited by decree-law (ICNF, 2013b). So, it is of great interest to find applications that promote its logging.

Table 2-3 – Reference mean values for the mechanical properties of clear wood and natural durability of the most common forest species in Portugal.

| Species | Botanical name | Mechanical Properties | | Natural Durability | | | | |
		C_{lf} [1]	f_m (N/mm^2)	Fungi	Hylotrupes	Anobium	Termites	Additional notes
Pine	*Pinus pinaster* [2]	26.0 - 31.0	132.3 - 148.9	3-4	S	S	S	-
	Pinus pinea	26.0	95.1	-	-	-	-	Slightly more durable than *Pinus pinaster.*
	Pinus halepensis	26.1	101.9	-	-	-	-	Slightly more durable than *Pinus pinaster.*
	Pinus radiata	30.0	97.0	4-5	S	SH	S	-
Cypress	*Cupressus lusitanica* [3]	29.0	93.1	-	-	-	-	Very durable to insects and fungus.
Pseudotsuga	*Pseudotsuga menziesii*	41.0	111.7	3-4	S	S	S	-
Eucalyptus	*Eucalyptus globulus* [4]	23.0 - 25.0	148.5 - 168.1	5	-	n/a	S	Thin sapwood susceptible to *Lyctus sp.*
Acacia	*Acacia melanoxylo*	24.0	153.9	-	-	-	-	Excelent durability of heartwood. Sapwood (small) susceptible to Anobium.
Alder	*Alnus glutinosa*	22.0	98.0	5	-	S	S	-
Birch	*Betula pubescens*	18.0	116.4	5	-	S	S	-
Poplar	*Populus canadensis*	28.0	67.1	5	-	S	S	-
	Populus alba	24.0	101.4	5	-	S	S	-
	Populus nigra	23.0	92.0	5	-	S	S	-
Beech	*Fagus sylvatica*	30.0	126.4	5	-	S	S	-
Ash	*Fraxinus angustifolia*	29.0	149.0	-	-	-	-	High vulnerability to xylophagous.
Elm	*Ulmus procera* [5]	30.0	132.3	4	-	S	S	-
Oak	*Quercus faginea*	22.0	149.5	-	-	-	-	High vulnerability to xylophagous.
	Quercus pyrenaica	30.0	137.5	-	-	-	-	Sapwood highly vulnerable to *Lyctus sp.* Heartwood durable.
	Quercus robur	26.0	134.8	2	-	S	M	-
Chestnut	*Castanea sativa* [6]	22.0	118.6	2	-	S	M	-

Notes:
1 = very durable; 2 = durable; 3 = moderately durable; 4 = slightly durable; 5 = not durable

D = durable; M = moderately durable; S = susceptible; SH - heartwood also susceptible; n/a = information not avaible

f_m - bending strength

[1] C_{lf} - stiffness quota = ratio between span and deflection at rupture according to (Carvalho, 1997)

[2] Including both variants from Leiria and Viana regions

[3] Including both variants "Dourado" and "Branco"

[4] Including both variants "Vulgar" and "Molar"

[5] Indicated values correspond to the species "*Ulmus glabra*"

[6] Variant "Bravo"

In Table 2-4, the density and shrinkage properties of the referred species taken from (Carvalho, 1997) are listed.

Density and shrinkage have great influence when orthogonally glueing different wood species (FPL, 2010) (CEN, 2015). It has also been stated that in CLT, the free swelling and shrinkage of adjacent layers usually differ by a maximum factor of 20 (Gereke et al,

2011). Not all the species listed in Table 2-4 verify this limit, especially the ones that present higher density, such as Eucalyptus or Oak.

Table 2-4 - Density and shrinkage properties of the Portuguese species according to (Carvalho, 1997).

Species	Botanical name	ρ_{12} (kg/m^3)	ϵ_v (%)	ϵ_t (%)	ϵ_r (%)	ϵ_a (%) [1]	α_v
Pine	*Pinus pinaster* [2]	565 - 640	14.6 - 16.7	9.0 - 10.1	6.0	0.27 - 0.28	0.52 - 0.57
	Pinus pinea	550.0	12.0	6.8	4.0	0.44	0.42
	Pinus halepensis	550.0	13.0	8.5	4.0	0.38	0.48
	Pinus radiata	500.0	11.5	6.2	4.0	0.46	0.40
Cypress	*Cupressus lusitanica* [3]	465.0	9.0	5.4	3.0	0.56	0.35
Pseudotsuga	*Pseudotsuga menziesii*	480.0	12.2	7.0	4.5	0.39	0.46
Eucalyptus	*Eucalyptus globulus* [4]	720 - 850	20.4 - 23.0	12.0 -13.2	6.0 - 8.3	0.21 - 0.28	0.60 - 0.62
Acacia	*Acacia melanoxylo*	650.0	12.1	8.0	3.4	0.44	0.48
Alder	*Alnus glutinosa*	460.0	11.4	7.1	4.2	0.38	0.25
Birch	*Betula pubescens*	580.0	14.7	8.6	5.1	0.34	0.47
Poplar	*Populus canadensis*	310.0	9.5	6.7	2.5	0.57	0.35
	Populus alba	510.0	16.3	10.2	5.2	0.31	0.49
	Populus nigra	445.0	12.6	8.3	3.7	0.41	0.40
Beech	*Fagus sylvatica*	675.0	19.0	13.0	5.0	0.29	0.60
Ash	*Fraxinus angustifolia*	700.0	15.1	8.8	5.3	0.32	0.50
Elm	*Ulmus procera* [5]	570.0	16.6	9.9	5.6	0.30	0.54
Oak	*Quercus faginea*	890.0	25.0	14.9	9.5	0.18	0.50
	Quercus pyrenaica	745.0	18.1	11.7	5.2	0.30	0.50
	Quercus robur	710.0	16.8	10.7	4.9	0.32	0.55
Chestnut	*Castanea sativa* [6]	600.0	12.5	7.9	4.1	0.39	0.42

Notes: ρ_{12} = density for H=12%; ϵ_v = total volumetric shrinkage; ϵ_t = total tangential shrinkage;

ϵ_r = total radial shrinkage; ϵ_a = total axial shrinkage; α_v = coefficient of volumetric shrinkage

[1] assuming that $\epsilon_v = \epsilon_t \cdot \epsilon_r \cdot \epsilon_a$

[2] Including both variants from Leiria and Viana regions

[3] Including both variants "Dourado" and "Branco"

[4] Including both variants "Vulgar" and "Molar"

[5] Indicated values correspond to the species "*Ulmus glabra* "

[6] Variant "Bravo"

Concerning costs of the sawn wood, these are related not only to the availability of the species, but also with the quality of the wood. It was not possible to collect costs for all the identified species; however, reference values for some of them are presented in Table 2-5.

Table 2-5 – Costs for sawn wood of different species.

Species	Cost (Eur/m^3)
Maritime pine, C24 strength class	350
Oak	2500
Chestnut	800
Beech	1400
Ash	2000

As expected, Maritime pine is the cheapest one due to its large availability, while other species, due to its scarcity, can exceed up to more than seven times the costs of the pine, as is the case of Oak.

From the collected information, it was decided to choose Maritime pine for the development of the panel solution. Besides, orthogonally glueing Maritime pine with Acacia (Australian blackwood) was also considered, as it presents excellent natural durability and thus is a potential species to be used in the external layers that are primarily exposed to biological degradation. Although it was not possible to collect information regarding its cost, this is an opportunity to assess the potential use of this undesirable invasive species in this kind of structural applications.

2.2.2   Insulation materials

As referred at the beginning of this chapter, the intended characteristics of the core insulation material include low weight, adequate shear stiffness and strength, and high thermal insulation. Other parameters, such as resistance to vapour transmission, creep and compatibility with adhesives, are also important (APA, 2013). Another relevant aspect is the environmental impact of the material during its life-cycle, as well as the fire performance. Although in sandwich-type panels the insulation core is covered by the outer layers, fire can reach the core through any critical point, such as the joints between panels. An example can be found in the work reported by (Hopkin et al, 2011) who performed full-scale fire tests on two-storey buildings made of engineered wood floors and SIP walls. The SIPs were made of OSB faces with expanded polystyrene (EPS) or polyurethane (PUR) core protected with gypsum boards designed to achieve 30 and 60 minutes of fire resistance. It was observed that in some cases OSB and plasterboard were intact; however, damage was found in EPS cores due to infiltration of hot gases through the insulation. At the end of the tests, it was observed either the melting of the EPS core or the combustion of the PUR core. As no collapse of the buildings was observed, it was concluded that an alternative load path was mobilized, probably by the solid timber elements connecting the panels. In the case of the developed panels, as in CLT, cracks due to moisture content variations may appear at the wood layers, thus creating direct openings from the outside to the core, which may be an issue.

For the core layer, plastic/polymeric foams are often used in sandwich panels, and the most common include EPS, extruded polystyrene (XPS) and PUR rigid foam, predominantly of the closed-cell type (APA, 2013). However, other materials, such as polyisocyanurates (PIR) rigid foams (Panjehpour et al, 2013) or wood fibres panels (Kawasaki et al, 2006) may also be used. It is found that in SIP, rigid plastic/polymeric

foams are often the most used material, and the most common include EPS, XPS, PUR and PIR, and phenolic resin (PR) rigid foams (APA, 2013; Panjehpour et al, 2013).

From the referred plastic-based options, EPS foam is the most common in SIPs due to its lower cost (Frechette, 1999) despite its limitations in terms of structural performance, with XPS being 10-30% more expensive (Schiavoni et al, 2016).

It should also be noticed that the mechanical and thermal properties of plastic foams are greatly dependent on temperature and humidity (Davies, 2008; Jelle, 2011; Garrido et al, 2016). An important issue for plastic foams is their combustibility. EPS and XPS, both thermoplastic materials, melt at temperatures slightly above 100 ℃ before their ignition, which occurs at nearly 300 ℃, while PUR, PIR and PR (thermosetting materials) do not melt when exposed to fire, but rather form a charred layer. PUR starts to decompose between 150-200 ℃ and ignites at nearly 300 ℃; PIR decomposes between 350-500 ℃ and ignites between 530-580 ℃, and PR starts to decompose at 350-500 ℃ and ignites between 530-580 ℃. EPS, XPS, PUR, PIR and PR release toxic substances when subjected to fire. EPS and XPS release mainly CO_2 and styrene; PUR and PIR release hydrogen cyanide and CO, while PR releases hydrocarbons and CO. The fire reaction behaviour of these materials can be improved by combining the plastic foams with other chemical components, such as fire retardants (Davies, 2008; Jelle, 2011; Schiavoni et al, 2016).

Also, wood based materials have applicability as core materials in sandwich panels with wood faces, such as panels of wood fibres (WF) (Kawasaki et al, 2006; Gebhardt and Blaß, 2010), agglomerated cork board (ACB) or expanded insulation corkboard (ICB) (Simonin, 2018).

Concerning some relevant properties, namely density (ρ), thermal conductivity (λ), shear strength (τ), shear modulus (G), creep coefficient (φ), fire reaction behaviour and water vapour diffusion resistance factor (μ-value), some reference values are found in the literature, which are summarized in Table 2-6 (Davies, 2008; Schiavoni et al, 2016). In what concerns fire reaction, EN 13501-1 (CEN, 2007) provides a set of classes (Euroclasses), from A1 (better behaviour) to F (worst behaviour). Table 2-6 indicates typical fire reaction classes for different core materials – it can be seen that most materials present poor performance (class E), with PIR and phenolic foams presenting much better fire reaction behaviour (classes C to B). For the water vapour diffusion resistance factor (μ), the lower the μ-value, the more breathable is the material. The creep values refer to a period of 100,000 hours (11.4 years), which according to EN 14509 (CEN, 2013) is adequate for permanent actions. Values for the creep coefficient were only found on that same document for EPS, XPS and PUR. It should be noticed that the values presented for

the different properties are only indicative; for example, PUR can be produced with higher densities and consequently present different properties, but this also leads to an increase in costs, which are proportional to density. According to (FERPFA, 2006), the current densities of PUR foams used in building construction are around 30-100 kg/m^3 but can reach up to 1150 kg/m^3 for extreme load situations or more demanding applications, such as bridge decks (Freitas, 2012). The thermal conductivity increases with density; however, according to (FERPFA, 2006), the variation of this parameter is small for current densities (30 to 100 kg/m^3).

Table 2-6 – Range of values for the relevant properties for the considered insulation materials.

Material	ρ (kg/m^3)	λ (W/m.ºC)	τ (N/mm^2)	G (N/mm^2)	φ (at 100,000 hours)	Fire reaction Euroclass according to EN 13501 -1	μ-value
Expanded Polystyrene (EPS)	15-35	0.031–0.038	0.05-0.15	2-6	7.0	E	20-70
Extruded Polystyrene (XPS)	32-50	0.032-0.037	0.18-0.50	3-8	7.0	E	80-150
Polyurethane (PUR)	15-45	0.022-0.040	0.08-0.18	2-5	7.0	E	30-170
Polyisocyanurate (PIR)	30-45	0.018-0.028	-	-	-	B	55-150
Phenolic Resin (PR)	40-160	0.018-0.024	-	-	-	B-C	35
Wood Fibres (WF) Board	50-350	0.038-0.050	0.10-1.40	10-220	-	E	1-5
Agglomerated Cork Board(ACB)	-	-	-	-	-	-	-
Insulation Cork Board (ICB)	110-170	0.037-0.050	0.06-0.07	0.98-1.27	-	E	5-30

From the data shown in Table 2-6, it can be concluded that regarding the mechanical behaviour, the different plastic materials present a range of values of the same magnitude, with XPS providing the best performance. Although no data was found for PIR, it is usually referred by manufacturers that it has similar properties to PUR. The wood fibres board shows the highest properties, while, on the other hand, insulation cork board is the most limited material, especially regarding its very low shear modulus.

Generally, the increase in mechanical properties is directly related to the foams' density. However, increasing density also means an increase in the raw material's costs (Davies, 2008) and a decrease in its thermal insulation capacity. Therefore, and depending on the required strength, sometimes it is preferable to add joists in the edges of the panels (Johansson et al, 2002) or to combine the core insulation with auxiliary internal structural members (ribs) for improved stiffness (Tuwair et al, 2015). Reference costs for the materials based on information collected from manufacturers are presented in Table 2-7.

As referred before, the EPS and XPS solutions are the cheapest, while PR, WF and ACB are the most expensive. For PUR, the cost increases proportionally to density; PIR is slightly more expensive than PUR of equivalent density.

Regarding sustainability, the environmental impact of wood-based materials, such as ICB, comparing to plastic ones, such as PUR, is expected to be lower, namely if accounting to the carbon sequestration of the former products. This aspect is evaluated in Chapter 7.

Table 2-7 – Cost of the different insulation materials.

	ρ (kg/m^3)	Cost (Eur/m^3)
EPS	35	120
XPS	50	160
PUR	35	260
	40	290
	70	520
	100	668
PIR	40	335
PR	35	405
WF	50	480
ACB	230	1760
ICB	115	350

From the collected information, it was decided to choose rigid PUR foam for the development of the panel solution, as it has a good balance between low density, mechanical properties, thermal insulation and cost.

2.2.3 Adhesive layers

The European standard EN 16351 (CEN, 2015) allows for the use of the following types of adhesives on CLT panels: phenolic and aminoplastic; moisture curing one-component (1C) polyurethane (PUR), and emulsion polymer isocyanate (EPI). The phenolic and aminoplastic adhesives include melamine-urea-formaldehyde (MUF), melamine-formaldehyde (MF), phenol-resorcinol-formaldehyde (PRF) and urea-formaldehyde (UF). According to FPInnovations (2013), the preferred adhesives are PRF, EPI or PUR types, because these are structural cold-set type, and thus avoid heating of the panels during pressing. However, according to Brandner (2013), the two most commonly used adhesives are MUF and 1C PUR, because both of them have a nearly uncoloured bond line, are resistant against sunlight exposure, humidity and hydrolysis. The main advantages of MUF include the increased resistance against elevated temperatures (e.g. fire), the gap-filling and penetration properties (easier for CLT production without previous manufacture of single layers, i.e. before the panel assembling) and the accelerated curing process (through high-frequency technology). Its disadvantages are the limited stored stability (1C systems), the strict mixing ratio of resin and hardener (two-

component (2C) systems) and the continuous emission of formaldehyde, which is known to be toxic and carcinogen (IARC, 2006). Particularly for the last reason, a great number of producers prefer 1C PUR adhesives. Although it is more vulnerable to elevated temperatures (above 60 ℃) if not properly modified, it has some advantages as the easy adaptation to reactivity and curing time or the provision of some internal pressure during curing (Brandner, 2013; Ansell, 2015).

According to FPL (2010), epoxy, PUR or isocyanate-based adhesives may be used to provide structural adhesion between wood and plastic materials. Davies (2008) states that 1C or 2C PUR adhesives are the most used in metal-faced sandwich panels.

From the collected information, it was decided (i) to test a 1C PUR adhesive for the glueing of wood elements, because it is a formaldehyde-free adhesive, and (ii) to test other types of adhesives only if the results obtained with such adhesive were not satisfactory regarding the EN 16351 standard requirements. For the same reason, 1C and 2C PUR adhesives were chosen to glue the surface between wood elements and the insulation material (polyurethane).

2.3   Concluding remarks

The current chapter presented an overview of the different potential materials to be used in the faces, core and adhesive of the panel to be developed.

The following conclusions were drawn:

-   The basic layout of the panels was defined as one insulation layer stacked between two pairs of cross wood layers (Figure 2-6). This layout was found to provide the best compromise between physical stability, fire safety and production costs.

Figure 2-6 – Description of the materials composing the developed panel.

- Solid wood was preferred to wood based panels for the outer layers due to its high strength and stiffness.

- Two species were identified from the Portuguese forest to be used in the panels: Maritime pine, due to its considerable presence in the forest and traditional use in structures, as well as its relative low-cost when compared to other species; and Australian blackwood, due to its similar properties, but higher natural durability than Maritime pine (making it suitable for use in the outer layers of the panels). Moreover, Australian blackwood's invasive behaviour in the Portuguese forest was taken into account, as this is an opportunity to promote its logging.

- For the insulation layer material, various options were identified, from plastic based materials to wood based materials.

- In terms of cost, EPS and XPS materials were found to be the cheapest ones; the cost of PUR increases proportionally to density; and cork materials were found to be the most expensive ones.

- Although some issues were found for the fire reaction of plastic foams, as they release toxic gases during combustion, PUR rigid foam was chosen for the core layer of the developed panel, accounting that the core is protected by the wood layers.

- The adhesives identified as being suitable to join the wood layers, as well as to connect the wood and polyurethane layers, were one- and two-component polyurethane adhesives, respectively, as they are formaldehyde-free.

3 CHARACTERIZATION OF POLYURETHANE AND WOOD MATERIALS

3.1 Introduction

To predict the panels' behaviour through analytical and/or numerical models, it is necessary to know the behaviour of the constituent materials, and therefore to characterize some of the physical and mechanical properties that are used as input in such models. Reference values for such properties may be provided by the materials' manufacturers or may need to be determined or even confirmed through additional experimental characterization tests.

The present chapter describes the material characterization tests performed in the constituent materials of the sandwich panels developed within the present thesis. One of the objectives of this task was to assess the performance of two possible manufacturing systems of the panels: the direct injection of polyurethane foam or the glueing of pre-manufactured polyurethane boards.

In terms of mechanical performance, in a sandwich panel subjected to in-plane compressive loads, the major axial stresses develop at the stiffer elements (outer layers or faces), while the core material is expected to stabilize the panel against buckling and other types of instability, such as wrinkling of the faces (which may also occur due to flatwise bending). When a sandwich panel is subjected to out-of-plane loads, substantial bending stresses are generated at the outer layers, while, in turn, the core material is subjected mostly to shear stresses. To avoid crushing of the foam core due to (i) concentrated compressive forces at the supports or load application points, (ii) distributed out-of-plane loads during the assembly of the panel (that may cause permanent deformation) or during its service life, the core compressive strength should also be taken into account. The mechanical behaviour of sandwich panels and their typical failure modes are analysed in more detail in Chapter 5.

Other important issues in polyurethane foam core include its creep behaviour when subjected to long-term loading and the loss of strength due to ageing (temperature). According to (FERPFA, 2006), PUR is resistant to most of the common chemical substances used in the building sector, including most solvents used in adhesives, bituminous, wood protection products or sealing compounds. According to the same source, it does not rot and resists to mould and decay; however, it is susceptible to

discolouration when exposed to UV radiation, which over time leads to a low-level sanding effect on the surface, but this is not considered as a technical drawback as in the developed panels the foam is covered by the wood layers.

Based on the information below, taking into account the application envisaged for the sandwich panels developed within the present thesis, the outer layers (in this case, the wood layers) should be characterized concerning their bending and in-plane compression behaviour, namely for the determination of the flexural modulus of elasticity and the bending strength. The inner layers, both insulation and inner wood layers, should be characterized with respect to shear, namely for the determination of the shear modulus and shear strength. The insulation layer should also be tested in compression and tension for the determination of the modulus of elasticity and strength (before and after accelerated ageing), and creep tests should also be performed to determine the creep coefficient required for long-term design.

Regarding the physical properties, the thermal conductivity is the main parameter to be determined, as it is the most influential one for the thermal behaviour (insulation) afforded by the sandwich panel. For acoustics, typical input parameters of airborne/impact insulation predictive models include the modulus of elasticity and mass of the composing layers.

The remainder of the chapter is organized as follows: section 3.2 presents the characterization of the wood materials, including the collection of reference values from the bibliography, bending tests of Australian blackwood boards and grading of the Maritime pine boards used to manufacture the beams and panels that were the target of subsequent experimental characterization; section 3.3 describes the characterization of the polyurethane foam material, including compression, tension, shear, creep and ageing tests; section 3.4 describes the thermal characterization of the polyurethane foam material as well of the developed panel solution; in the last section, 3.5, concluding remarks are made.

3.2 Wood layers - Maritime pine and Australian blackwood

Wood is an orthotropic material, which means that it has different mechanical properties along its three orthogonal axes: longitudinal (L), radial (R) and tangential (T). The longitudinal axis is taken as parallel to the fibres (grain), the radial axis is normal to the growth rings and perpendicular to the grain direction, and the tangential axis is tangent to the growth rings and perpendicular to the grain direction (Figure 3-1).
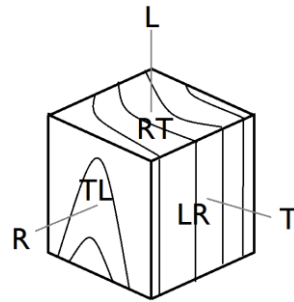
Figure 3-1 – Axes and shear planes in a solid wood piece.

For practical purposes in structural design, no distinction is made between the radial and tangential directions, because the properties in those two directions are quite similar, namely when compared with the longitudinal direction, and thus wood can be treated as a monotropic material, also known as transversal isotropic material (Silva, 2006).

This section presents the experimental tests on wood layers, which included bending tests on Australian blackwood and grading of Maritime pine boards, that would be used to manufacture the beams and panels (the results of tests in these structural members are reported in subsequent chapters).

3.2.1   Reference values for the mechanical properties

Reference values for relevant properties of Maritime pine and Australian blackwood (Figure 3-2) are found in bibliographic references, namely (Xavier et al, 2009; Machado et al, 2014; Bucur, 2016; Santos, 2017; Martins, 2018; Meier, 2020), from which mean values were collected and summarized in Table 3-1 for elasticity modulus (E), shear modulus (G), bending strength (f_m), tensile strength (f_t), compressive strength (f_c) and shear strength (f_v). Note that in that table, TR, LT and LR indexes mean tangential-radial, longitudinal-tangential longitudinal-radial planes, respectively. No reference values were found for the tensile strength of Australian blackwood, but do to similarities with Maritime pine (regarding the mechanical properties), close values are expected.

Figure 3-2 – Examples of Maritime pine (left) and Australian blackwood (right) boards after trimming operations.

As shown ahead in Chapter 6, for the typical spans of slab elements used in building floors, regarding the ultimate limit states design, the bending strength of the outer wood layers is not actually the limiting criteria, but rather the shear strength of the inner core layers. It should be noticed that for Maritime pine the mean value for the shear strength of the cross layers (TR plane) presented in Table 3-1 is much higher than the ones previously presented in Table 2-6 for the insulation materials, and thus the shear strength of the insulation layer is the limiting criteria in structural design.

Table 3-1 – Reference mean values of modulus of elasticity (E), shear modulus (G), bending strength (f_m), tensile strength (f_t), compressive strength (f_c) and shear strength (f_v) for Maritime pine and Australian blackwood.

Species	E (GPa)	G (MPa)			f_m (MPa)	f_t (MPa)	f_c (MPa)	f_v (MPa)		
		TR	LT	LR				TR	LT	LR
Maritime pine	11.2[d]	239[a]	1090[a]	1330[a]	120[d]	85[e]	40[e]	4.6[a]	11.7[a]	15.1[a]
Australian blackwood	14.1[b]	384[c]	1158[c]	1573[c]	139[b]	-	41[f]	-	-	-

Notes: a - (Xavier et al, 2009); b - (Machado et al, 2014); c - (Bucur, 2016); d - (Santos, 2017);e - (Martins, 2018); f - (Meier, 2020).

Despite the reference values presented in Table 3-1, some bending tests were performed on Australian blackwood boards, as the reference values (Table 2-3) correspond to small size cross-section specimens (20×20 mm^2). No tests were performed for Maritime pine; knowledge about the behaviour of this species stems from a series of bending tests performed in the past (Dias et al, 2014).

3.2.2 Bending tests on Australian blackwood

The bending tests on Australian blackwood boards were performed according to the procedure described in EN 408 standard (CEN, 2012a) for the determination of the modulus of elasticity and strength in bending. The test consists of applying an equal concentrated force at the thirds of the span of a simply supported beam and measuring the vertical deflection along the inner third of the span (i.e. the deflection due to pure bending) (Figure 3-3). To determine the elasticity modulus, the applied load during the test shall be less than 40% of the estimated maximum load.

a)
b)
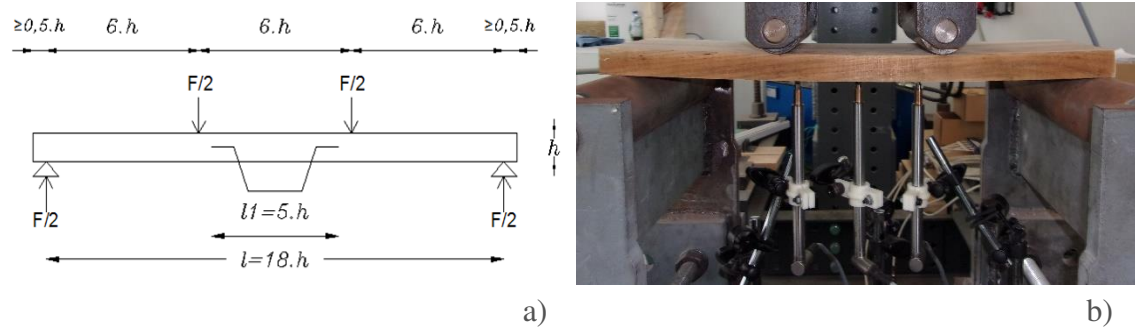
Figure 3-3 – Details of the bending tests: a) bending test apparatus according to EN 408 (CEN, 2012a); b) determination of the modulus of elasticity on an Australian blackwood board.

The modulus of elasticity due to pure bending was determined in accordance with Equation (3-1),

$$E = \frac{al_1(F_2 - F_1)}{16I(w_2 - w_1)} \qquad (3-1)$$

where: a – distance between a support and the closest loading point; l_1 – distance between the external deflection measurement points; I – second moment of area; F – applied force, and w – local deflection. The indexes 1 and 2 correspond to the extreme points of the longest portion of the force *vs.* deflection curve from which it is possible to obtain a linear regression with a correlation coefficient of at least 0.99.

The local deflection was determined by the difference between the deflection at mid-span and the mean deflections in the side points following Equation (3-2):

$$w = w_{central} - \left(w_{left} + w_{right}\right)/2 \qquad (3-2)$$

The bending strength was determined following Equation (3-3):

$$f_m = \frac{3F_{max}a}{bh^2} \qquad (3-3)$$

where: F_{max} – maximum applied force; b – width of the cross-section, and h – depth of the cross-section.

A total of 20 lamellas of Australian blackwood with dimensions of 23 mm × 130 mm × 440 mm, mean density of 593 kg/m³ and relative moisture content around 14-16% were tested on flatwise bending up to failure (Figure 3-4).

Figure 3-4 – Example of bending test up to failure of an Australian blackwood lamella.

The results of the (local) modulus of elasticity and bending strength are presented in Figures 3-5 and 3-6 using box plots. On each box, the central mark indicates the median, and the bottom and top edges of the box indicate the 25th and 75th percentiles, respectively. The whiskers extend to the most extreme data points not considered as outliers, and the outliers are plotted individually using the '+' symbol.
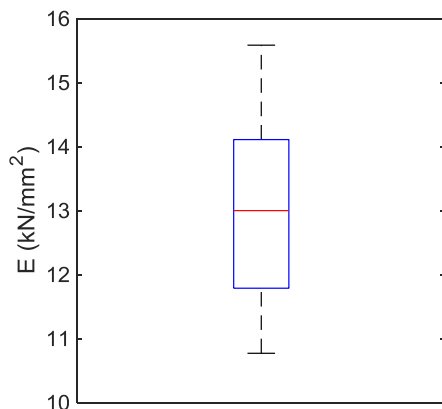
Figure 3-5 – Modulus of elasticity of Australian blackwood obtained in the tests.
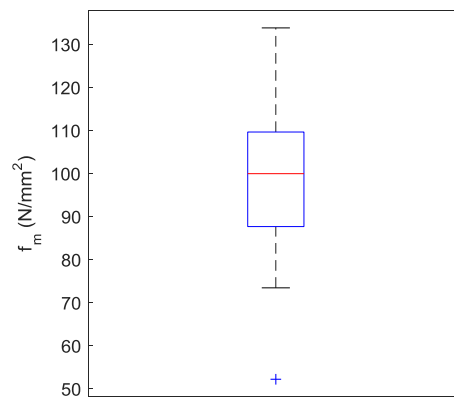
Figure 3-6 – Bending strength of Australian blackwood obtained in the tests.

The comparison of the obtained results with the reference values presented in Table 3-1 shows that the mean value for the modulus of elasticity (13028 N/mm^2) is quite in line with the reference value (14100 N/mm^2), while the bending strength (99.3 N/mm^2) is somehow lower compared to the reference one (139 N/mm^2). Mean values of both modulus of elasticity and bending strength obtained in the experiments are below the reference values of (Machado et al, 2014). The discrepancies may be explained by the fact that the tested specimens had greater moisture content, greater density, and greater dimensions than the ones tested by Machado et al (2014), whose specimens had a moisture content of 12%, mean density of 654 kg/m^3 and were probably were for clear wood (i.e. without defects). Thus, the increased moisture content, lower density and

presence of defects, which relate to wood properties (FPL, 2010), were probably responsible for the reduced mechanical properties obtained herein.

3.2.3 Grading of boards/lamellas used in the panels/beams' manufacture

The wood lamellas used to manufacture the beams and columns experimentally tested in Chapter 5 were subjected to experimental tests to determine the dynamic modulus of elasticity, which is found to have a high correlation with the static modulus of elasticity (Vries and Gard, 1998; Santos, 2012).

The tests were conducted using the Multi Timber Grader (MTG) device (Figure 3-7) that measures the fundamental frequency of a simply supported beam subjected to free longitudinal vibration. Together with the input information of the mass, dimensions and moisture content of the piece, the device delivers an estimate of the dynamic modulus of elasticity, E_{dyn}. If this information is complemented with the wood species (if this one is available in the database of MTG), grading of the timber into a strength class of EN 338 (CEN, 2009) is also possible.

Figure 3-7 – Dynamic test using the timber grader MTG.

The MTG device has the limitation of not delivering an estimate of the modulus of elasticity for pieces with thickness below 36 mm; however, it still identifies the fundamental frequency. As some of the lamellas used in the beams tested (Chapter 5) had 10 mm of thickness, in those cases, E_{dyn} was determined in accordance with Equation (3-4) (Clough and Penzien, 1993),

$$E_{dyn} = 4l^2 f^2 \rho \qquad (3-4)$$

where: l – length; f – fundamental frequency, and ρ – density.

The values of E_{dyn} used as input in the analytical models were corrected to the actual moisture (HR_{actual_test}) content of the beams used in the mechanical tests in accordance with Equation (3-6) based on the research from (Unterwieser and Schickhofer, 2011), which uses the HR and E_{dyn} at the time of the dynamic test ($dynamic\_test$) as input:

$$E_{dyn,actual\_test} = \frac{E_{dyn,dynamic\_test}}{1 - 0.00825(HR_{dynamic\_test} - HR_{actual\_test})} \tag{3-5}$$

The raw material boards (Figure 3-8) used to manufacture the panels tested in Chapter 5 were graded into a strength class using the referred procedure. The objective of this process was to achieve a more balanced distribution of quality among the panels, i.e., using the best quality boards for the outer layers and the lower quality ones in the inner layers, for improved mechanical performance. In the grading, two types of cross-sections were analysed - 15 mm × 145 mm (391 units) and 40 mm x 145 mm (286 units) - both with 2700 mm of length. The results obtained are shown in Table 3-2, including a combination of grades C40, C24 and C18. As can be seen, more than half of the material was assigned to the higher class.

Figure 3-8 – Maritime pine boards classified into strength classes using the timber grader MTG.

Table 3-2 – Percentage of boards of each cross-section classified into a specific grade.

Cross-section	C18	C24	C40
15 x 145	18	23	59
40 x 145	10	32	58

Table 3-3 – Mean modulus of elasticity (N/mmm^2) for the set of boards of each specific grade.

Cross-section	C18	C24	C40
15 x 145	7816	10279	15461
40 x 145	8259	10540	14564

3.3   Insulation layer - Polyurethane rigid foam

Rigid polyurethane (PUR) foam is an anisotropic closed-cell plastic material. It is produced through a chemical reaction between two base components (polyol and isocyanate) in liquid form and a low-boiling point blowing agent, typically pentane or carbon dioxide (Huber and Gibson, 1988; FERPFA, 2006).

There are two ways of manufacturing sandwich panels with PUR core: (i) directly injecting the foam between the layers in a continuous/discontinuous process, or (ii) glueing the faces to the pre-manufactured PUR core. In the first option, the reaction mixture is poured through a mixing head into the lower face, after which the mixture expands and consequently bonds to the panel faces. In the second option, the components are mixed in an agitator before being poured into a box mould, after which the mixture expands and forms the foam.

Initially, it was intended to use the first injection system for the panels' production. Taking into account the face material (wood), a specific chemical system was proposed by the chemical company *BASF*, namely *Elastopor H 1221/102/B – Iso PMDI 92140*. However, due to logistic issues, it was not possible to follow this option. Alternatively, and for the same production system, it was decided to test another chemical system (also provided by *BASF*) developed by a company specialized in polyurethane injection and used in various applications, such as brick wall insulation, silos, etc. (Figure 3-9 a)). However, from data sheets provided by the manufacturer, it was found that the bond (tensile) strength would be lower than the strength of the PUR foam itself – this was later confirmed in tests (Chapter 4). So, the glueing of pre-manufactured PUR boards was chosen for the consequent production and test of the developed panels (Figure 3-9 b)). However, both PUR materials (injected and pre-manufactured) were tested with respect to tension and compression. Additionally, for the pre-manufactured system, shear strength, creep and ageing tests were performed.

The manufacturers of PUR foam (both injected and pre-manufactured) only provided little or incomplete information related to its mechanical properties, most related to the compressive strength. Therefore, to fully characterize the relevant properties highlighted in Section 3.1, a set of experimental tests were conducted following procedures described in relevant standard or scientific works.

PUR foam is generally axisymmetric in its structure and properties due to the rise of gas during the foaming process (Huang and Gibson, 1991). Although injected PUR foam obtained from production lines is known to be an anisotropic material, the tested PUR foam was injected into small moulds (0.50 x 0.12 x 0.12 m^3). Such small dimensions may

have limited the gas expansion in a predominant direction and thus reduced the degree of anisotropy. Consequently, the specimens taken from the mould were, as a simplification, analysed without distinction between the edgewise and flatwise directions.

a)   b)
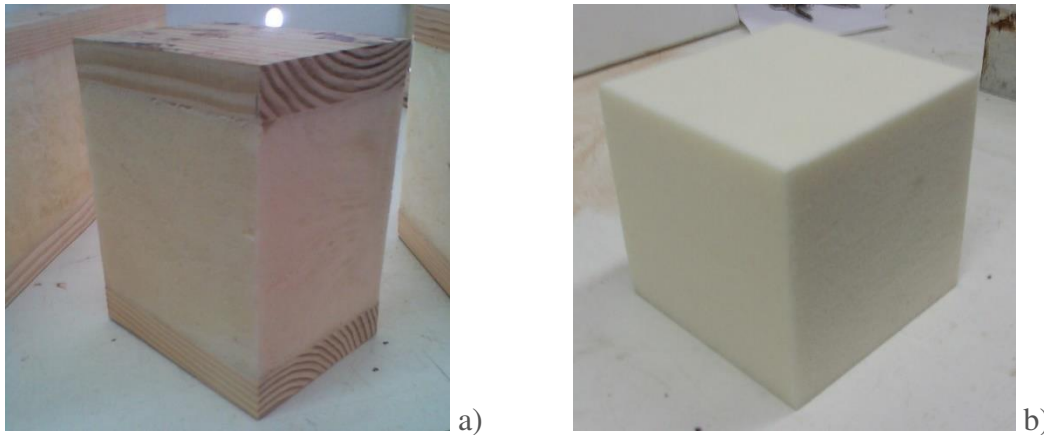
Figure 3-9 - Example of specimens obtained from: a) direct injection system; b) pre-manufactured board.

Concerning compressive tests, the PUR foam boards were tested only along two directions: one along the foam rising direction (flatwise) and the other along a direction normal to that one (edgewise) and parallel to one of the panel's edges (this one chosen randomly for the tested specimens). The option of randomly choosing the edgewise plane for testing was made attending to the reference stress-strain curves presented by (Huber and Gibson, 1988), who showed that the behaviour on those two directions is quite similar, and thus transversal isotropic behaviour may be assumed.

The declared coefficient of thermal conductivity (λ) at 10 ℃ of the injected PUR system is 0.021 W/(m.℃) and for the prefabricated boards it is 0.023 W/(m.℃).

3.3.1 Experimental procedures

As referred in Chapter 2, the properties of PUR foam strongly depend on the surrounding temperature. All the experimental tests were performed at temperatures ranging from 15 to 20 ℃. The mean densities of the tested specimens, determined as the mass/volume (width×heigth×length), were 43.0 kg/m^3 for PUR boards and 42.4 kg/m^3 for injected PUR.

Five types of tests were performed: compression, tension, shear, creep and ageing. It should be noted that these tests were always performed for PUR pre-manufactured specimens; however, for the PUR injected foam, only the compression and tension tests

were performed. The reason for this was, initially, the difficulty to obtain specimens with the dimensions required for the shear and creep tests. Despite that difficulty, from the conducted tests, a poorer performance was observed with the injected foam compared to the pre-manufactured system, with relatively lower values for compression/tension strength obtained with the former method. Additionally, also the adhesion (later analysed in Chapter 4) between the injected foam and the wood elements was found to be insufficient.

3.3.1.1 Compression test

The objective of this type of test is to determine the modulus of elasticity and strength in compression of the core material. The test principle, which is described in ETAG 016-1 (EOTA, 2003a), consists of applying a monotonically increasing compressive force normal to the specimen's faces together with the measurement of the relative displacement between the top and bottom edges of the specimen until its failure (Figure 3-10).

Polyurethane foams usually do not exhibit a well-defined ultimate load; in fact, due to the progressive collapse of the cell structure, at some point densification occurs and the stress generally increases (although this is more noticeable for high strains) – this is seen further ahead in the results. So, for practical purposes (i.e. structural design) the technical document defines such value at an extension of 10% (Figure 3-11).

According to the referred document, the specimens should have a square cross-section, with a width between 0.5 and 1.5 times the core thickness, but never less than 50 mm.

a)   b)
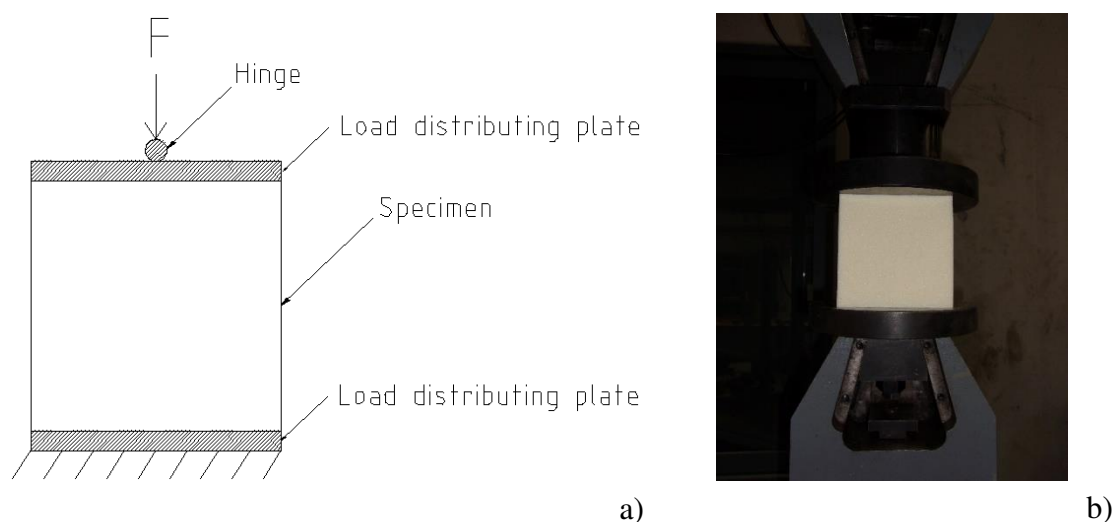
Figure 3-10 - Compression test: a) layout; b) specimen during a test.
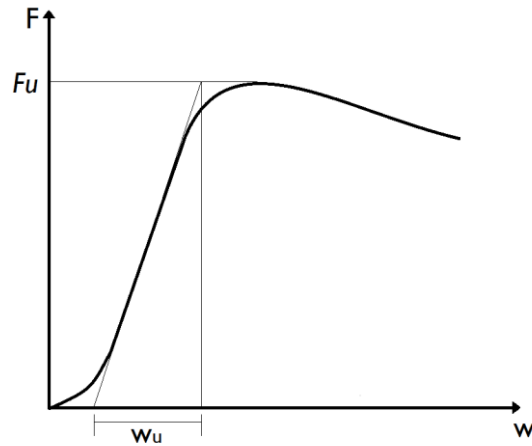
Figure 3-11 – Typical load vs. deflection curve of polyurethane foams in compression for low strains. Adapted from (EOTA, 2003a).

The elasticity modulus in compression (E_c) is obtained in accordance with Equation (3-5),

$$E_c = \frac{F_u d_c}{w_u b^2} \qquad (3\text{-}5)$$

where: F_u – ultimate load; d_c – core thickness; w_u - deflection at the ultimate load, calculated in the linear part of the load-deflection curve; b - specimen width.

The compressive strength (f_c) is obtained following Equation (3-6):

$$f_c = \frac{F_u}{b^2} \qquad (3\text{-}6)$$

In total, eight prefabricated PUR board specimens were tested in flatwise compression and six were tested in edgewise compression. It was decided to test more specimens in flatwise compression than in edgewise compression, as it was important to have a higher number of results in the former direction to estimate a characteristic value for the compressive strength to be used in the assembling of the panels. For the injected PUR, four specimens were tested in random directions.

The results of compression tests for the PUR board and injected PUR specimens, namely the modulus of elasticity and strength in compression, are shown using box plots in Figures 3-12 and 3-13, respectively. In these figures, "fw" stands for flatwise and "ew" for edgewise.

As referred before, the comparison of the edgewise and flatwise results is analysed to assess the anisotropic behaviour of the PUR boards. It should be noticed that no

distinction was made between the two orthogonal planes to the boards' plane from which the specimens were cut. Therefore, it was only possible to observe the "transversal isotropic behaviour" of the boards.
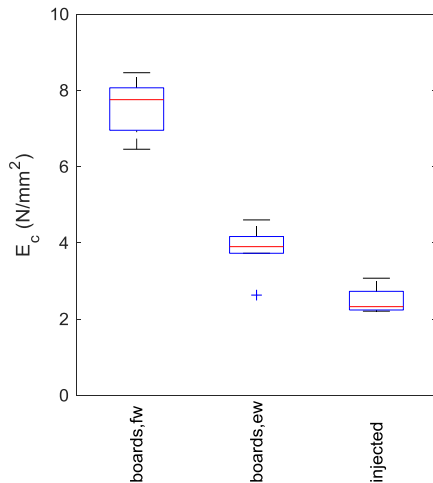
Figure 3-12 - Modulus of elasticity obtained in compression tests for PUR board and injected foam specimens.
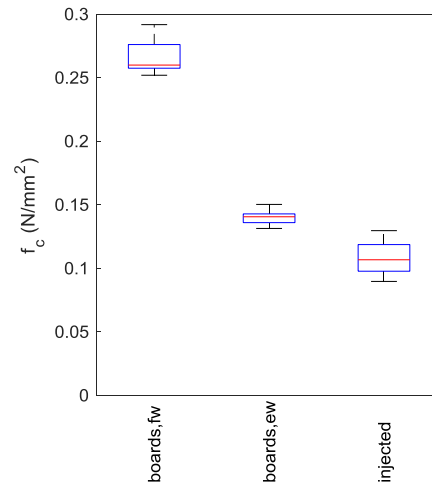
Figure 3-13 – Compression strength obtained in tests for PUR board and injected foam specimens.

The values of compression strength declared by the PUR boards manufacturer are 0.240+/-0.050 N/mm^2 and 0.120+/-0.030 N/mm^2 for flatwise and edgewise compression, respectively. The test results obtained here are thus within the range of the reference values, as shown in Figure 3-13.

PUR board specimens performed better than PUR injected specimens in terms of both modulus of elasticity (Figure 3-12) and strength (Figure 3-13). For the PUR boards, the significant difference between the edgewise and flatwise compression results confirms the transversal isotropic behaviour of the PUR boards.

Examples of stress-strain curves and corresponding failure modes for the three types of tests are shown in Figures 3-14 to 3-19. The constitutive behaviour obtained in the tests is much in line with the typical stress-strain curves presented by (Huber and Gibson, 1988) for compressive tests, for which the highest strength is found when applying the force along the rise direction of the foam.

After an initial toe region observed in all cases (due to adjustments in the components of the test setup), a linear elastic behaviour is observed, after which different behaviours can be found for the three types of tests. In the edgewise board specimen, a nonlinear softening is observed with significant ductility, during which deformations increase

plastically with a slight decrease in force. In the flatwise board specimen, after the initial linear behaviour, a nonlinear branch is also observed, but with smaller extension; at some point, an abrupt force reduction occurs, followed by a slight recovery in force, which then stabilizes in a plateau. The PUR injected foam specimen also exhibits an initial linear behaviour, followed by a nonlinear branch with decreasing stiffness, and, finally, it presents another linear behaviour branch, with lower stiffness than the initial one.
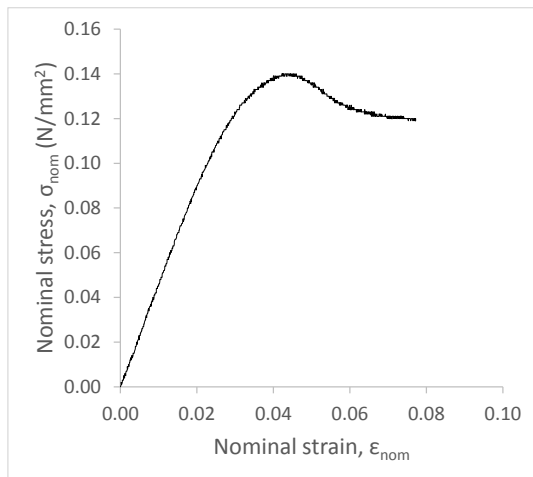
Figure 3-14 - Example of a stress-strain curve obtained in the edgewise compression tests of PUR boards.
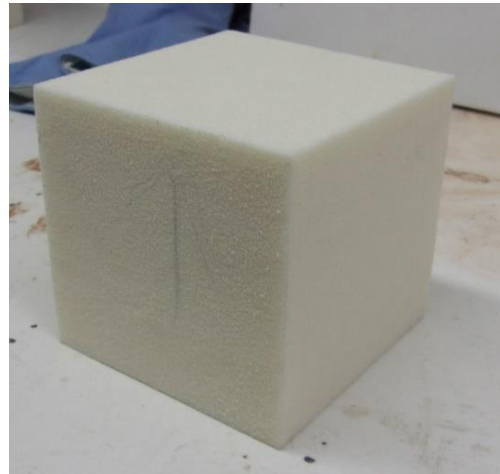
Figure 3-15 - Aspect of a PUR board specimen after an edgewise compression test.
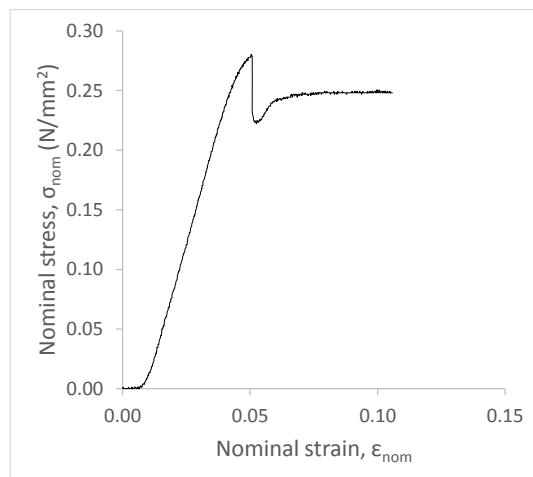
Figure 3-16 - Example of a stress-strain curve obtained in the flatwise compression tests of PUR boards.

Figure 3-17 - Aspect of a PUR board specimen after a flatwise compression test.

The observed failure modes are in line with the described behaviour of the force-displacement curves. Both the PUR injected specimens and the edgewise PUR board specimens, besides the lateral deflection due to Poisson' effect in the linear region,

showed no apparent failure line (Figures 3-15 and 3-19, respectively); however, the flatwise PUR board specimens showed a failure line at a surface almost perpendicular to the loading direction (Figure 3-16). This visible sign of failure seems to be advantageous, as during the panels' assembly (glueing of the core to the faces) it allows perceiving if the elastic limit of the foam material was exceeded due to excessive compression force.
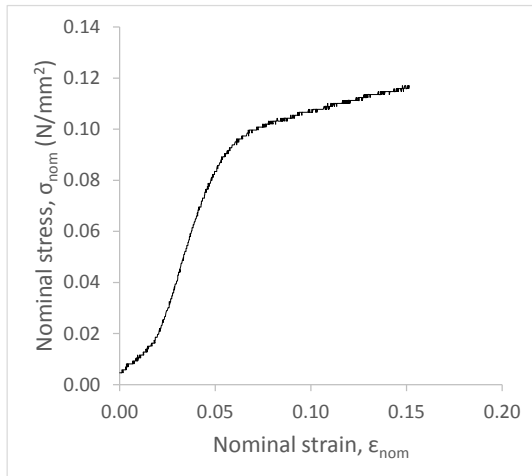
Figure 3-18 - Example of a stress-strain curve obtained in the compression tests of injected PUR.

Figure 3-19 - Aspect of an injected PUR specimen after a compression test.

Some of the PUR board specimens were loaded far beyond the initial failure, and two examples of stress-strain curves are shown in Figure 3-20 for edgewise compression and in Figure 3-21 for flatwise compression.
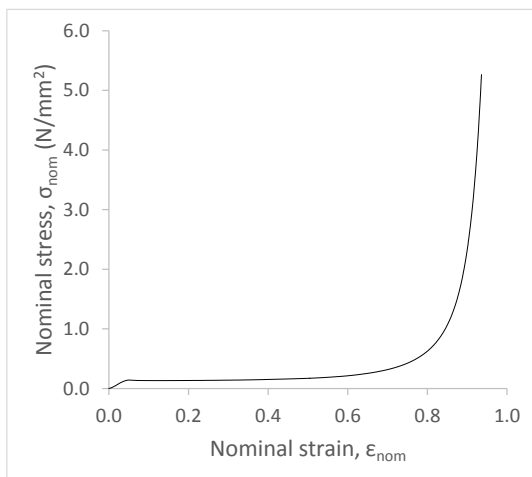
Figure 3-20 - Example of a stress-strain curve obtained in the edgewise compression tests of PUR board specimens (up to very high strains).
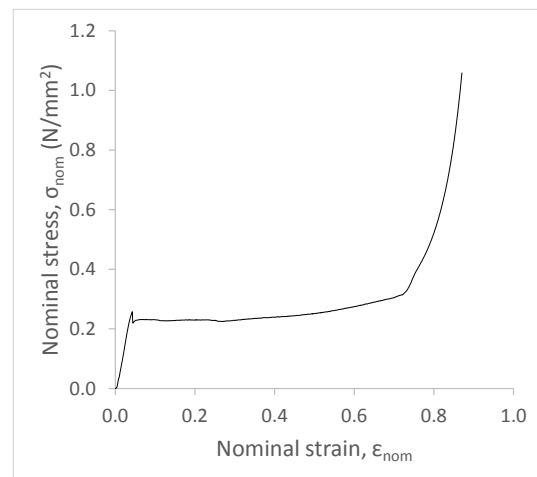
Figure 3-21 - Example of a stress-strain curve obtained in the flatwise compression tests of PUR board specimens (up to very high strains).

3.3.1.2 Tension test

The objective of this type of test is to determine the modulus of elasticity and strength in tension of the core material. The test principle, which is described in ETAG 016-1 (EOTA, 2003a), consists of applying a monotonically increasing tensile force normal to the specimen's faces alongside with the measurement of the relative displacement between the top and bottom of the specimen up to its failure (Figure 3-22).

a)   b)
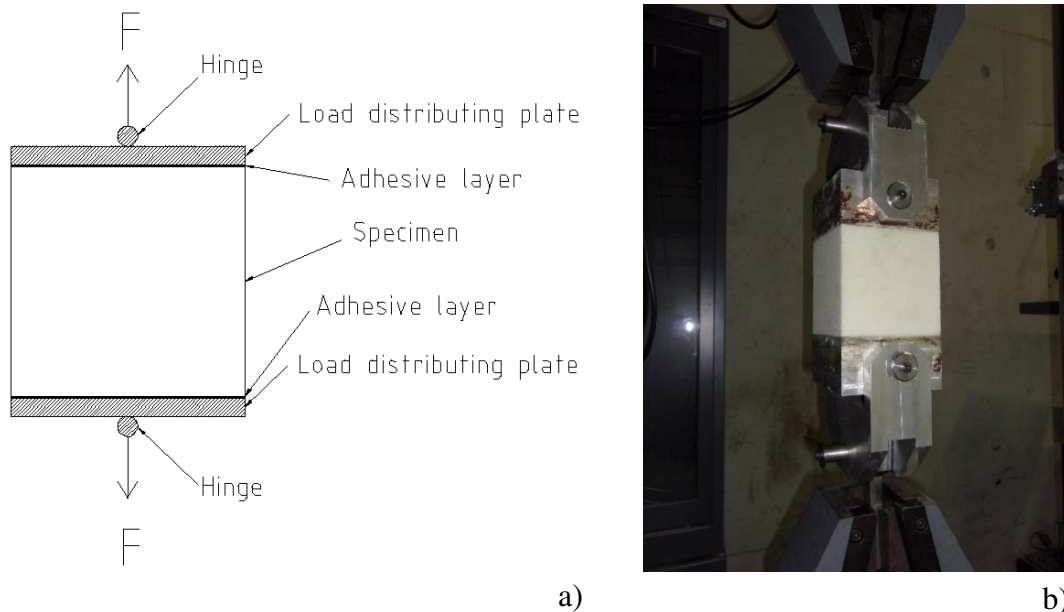
Figure 3-22 - Tension test: a) layout; b) specimen during test.

The PUR foam specimens were fixed to the test device using a 2C PUR adhesive developed for sandwich structures by Sika, the *SikaForce 7710 L100 + 7010*. According to the manufacturer product datasheet (Sika, 2012), the referred adhesive has an estimated modulus of elasticity in tension of 112.5 N/mm^2 and an adhesion strength of 9 N/mm^2, values that are much higher than the corresponding ones of the tested PUR foams; therefore, this ensures minimum interference of the adhesive layer on the measured behaviour of the PUR foam. According to the referred standard, the specimens should have a square cross-section, with a width between 0.5 and 1.5 times the core thickness, but never less than 50 mm.

The elasticity modulus in tension (E_t) is obtained following Equation (3-7):

$$E_t = \frac{F_u d_c}{w_u b^2} \tag{3-7}$$

The tensile strength (f_t) is obtained in accordance with Equation (3-8):

$$f_t = \frac{F_u}{b^2} \tag{3-8}$$

In total, two PUR board specimens (plus eighteen from the tension tests on bonded wood/PUR specimens, referred in Chapter 4, that failed within the PUR material) and three injected PUR specimens were tested, respectively.

The results of modulus of elasticity and strength in flatwise tension for the PUR board and injected PUR are shown in Figures 3-23 and 3-24 through box plots.
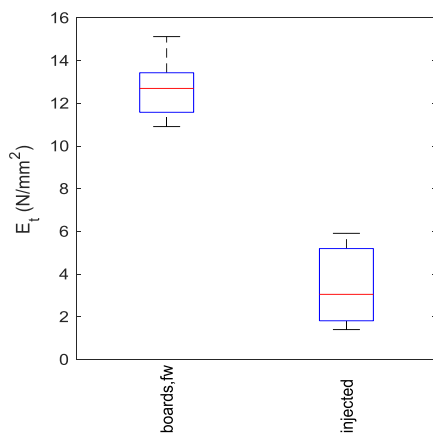
Figure 3-23 - Modulus of elasticity obtained in tension tests for PUR board and injected foam specimens.
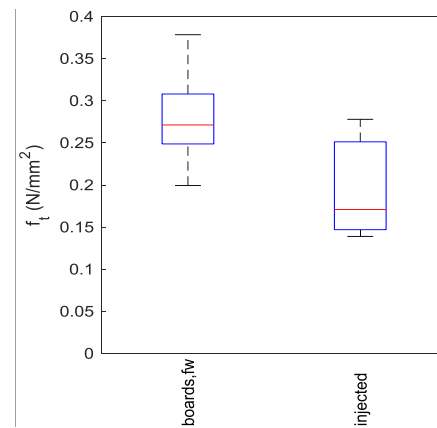
Figure 3-24 - Tensile strength obtained in tension tests for PUR board and injected foam specimens.

As shown in the compression tests, PUR board specimens performed better than PUR injected specimens in terms of both modulus of elasticity (Figure 3-23) and strength in tension (Figure 3-24) – the average values of the former specimens were 12.4 N/mm^2 and 0.28 N/mm^2, respectively, higher than the latter (2.5 N/mm^2 and 0.11 N/mm^2). As shown in the representative stress-strain curves depicted in Figures 3-25 and 3-27, both PUR board and injected PUR specimens showed linear elastic behaviour until failure, which occurred in a brittle manner.

In both cases, an initial toe region and a small discontinuity in the curves is observed in the stress-strain curves, which is associated to adjustments in the test setup, namely at the hinges of the steel fixtures. As shown in Figures 3-26 and 3-28, the failure modes always involved the PUR foam, with the failure surface being almost perpendicular to the loading direction, i.e. no failure was observed at the glue line.

From the compression and tension test results, it was possible to conclude that the PUR boards performed much better than the injected PUR. This better performance may be

attributed to the better quality control conditions in production that can be achieved in an industrial plant. Based on these results, it was decided to use the PUR boards for the panels' development.
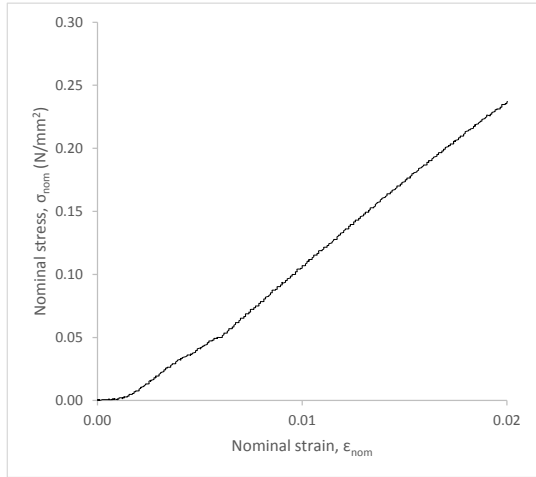
Figure 3-25 - Example of a stress-strain curve obtained in the flatwise tension tests of PUR board specimens.

Figure 3-26 - Aspect of PUR board specimen after flatwise tension test.
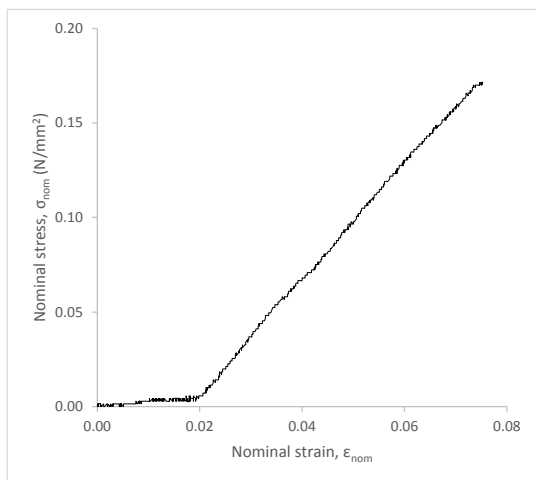
Figure 3-27 - Example of a stress-strain curve obtained in the tension tests of injected PUR specimens.

Figure 3-28 - Aspect of injected PUR specimen after tension test.

3.3.1.3 Shear test

The objective of this type of test is to determine the shear modulus and strength of the core material. The test setup used was the one developed by (Garrido, 2016), comprising a chamfered cubic specimen adhesively bonded to a set of test fixtures forming a corner

hinged quadrilateral frame. In this test, tension is applied along one of the frame's diagonals causing the quadrilateral frame to distort into a rhombic shape, thus subjecting the specimen to shear deformation (Figure 3-29). The applied force and the extensions of both diagonals are measured with displacement transducers.

a)   b)
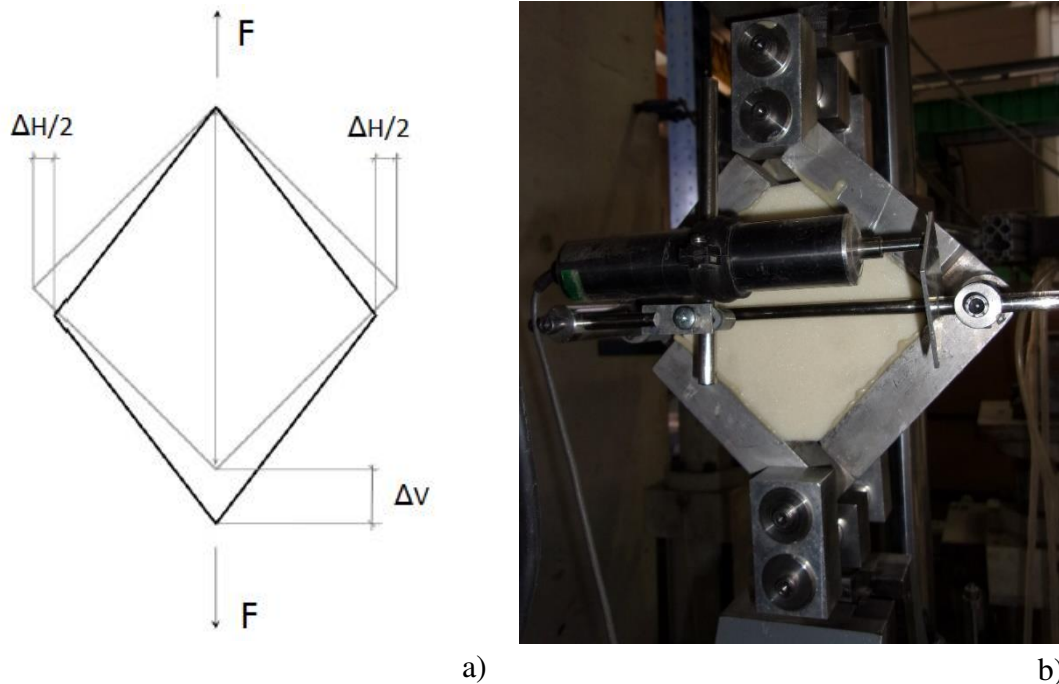
Figure 3-29 - Shear test: a) layout; b) specimen during a test.

The tested specimens had a width of 119 mm and a thickness of 120 mm. The PUR adhesive *SikaForce 7710 L100 + 7010* was used to fix the specimens to the test device.

The shear modulus (G) is obtained following Equation (3-9),

$$G = \frac{\Delta\tau}{\Delta\gamma} \qquad\qquad (3\text{-}9)$$

where: $\Delta\tau/\Delta\gamma$ - slope of the linear portion of the stress-distortion curve. The distortion is obtained in accordance with Equation (3-10),

$$\gamma = \frac{\Delta V + \Delta H}{\sqrt{2}b} \qquad\qquad (3\text{-}10)$$

where: ΔV - vertical extension; ΔH - horizontal shortening; b – specimen width.

The shear strength (f_v) is obtained in accordance to Equation (3-11),

$$f_v = \frac{\sqrt{2}}{2} \frac{F_u}{bt} \tag{3-11}$$

where: t – specimen thickness.

For the PUR injected foam it was not possible to obtain specimens with the required dimensions for the shear test, so the tests were only conducted on PUR boards specimens (five specimens were tested).

The results in terms of shear modulus and strength for the tested PUR board specimens are shown in Figures 3-30 and 3-31, respectively. A representative shear stress *vs.* distortion curve is depicted in Figure 3-32 and the failure mode is shown in Figure 3-33.

As shown in the representative shear stress *vs.* strain (distortion) curve depicted in Figure 3-32, after an initial toe region, due to adjustments in the test setup (at the hinges), a linear elastic behaviour is observed with a slight non-linear behaviour with stiffness reduction before failure, which occurred in a brittle way. The observed failure mode occurred at a surface almost perpendicular to the loading direction at the horizontal diagonal of the specimen, as expected (Figure 3-33).

The mean values of shear modulus and strength obtained in the tests, 3.01 N/mm^2 and 0.117 N/mm^2, respectively, are within the range of values identified in Chapter 2 for PUR foam with density between 15-45 kg/m^3 (Table 2-6), 2-5 N/mm^2 and 0.08-0.18 N/mm^2, respectively.
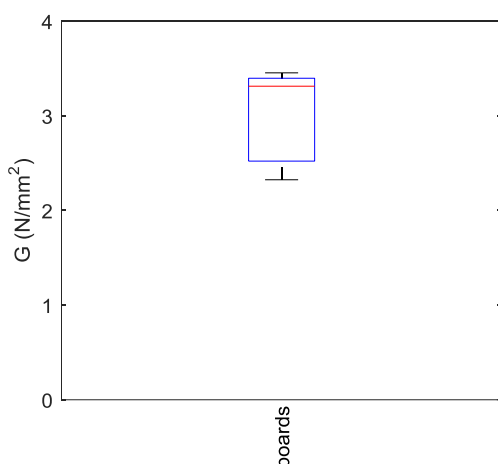
Figure 3-30 – Shear modulus obtained in DTS tests for PUR board specimens.
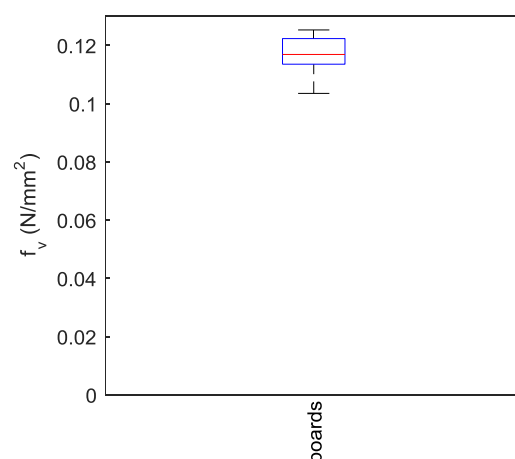
Figure 3-31 - Shear strength obtained in DTS tests for PUR board specimens.
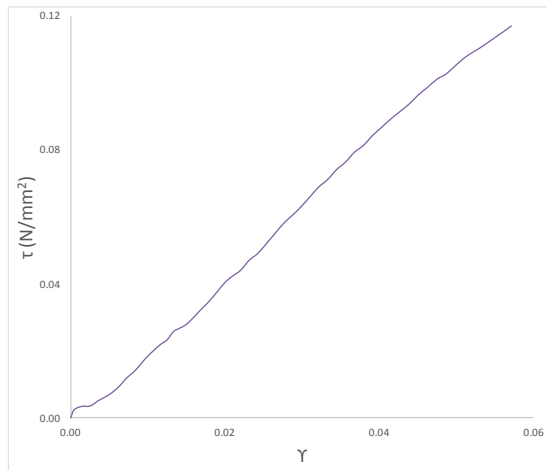
Figure 3-32 - Example of shear stress-strain curve obtained in the DTS tests of PUR board specimens.
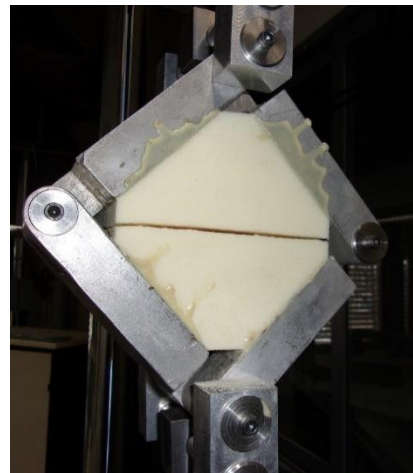
Figure 3-33 - Aspect of a PUR board specimen after a shear test.

3.3.1.4 Creep test

The objective of this type of test is to determine a creep coefficient for the core material that can be used in the design models to adjust the material properties at long-term. A test setup and procedure to obtain the creep coefficient for the core material of sandwich panels is provided in ETAG 016 -2 (EOTA, 2003b), which is based on the standard EN 14509 (CEN, 2013) for sandwich panels with metal faces.

The test layout consists of a single span simply supported beam under uniformly distributed load (kept constant over time), for which the mid-span deflections are measured (Figures 3-34 and 3-35).
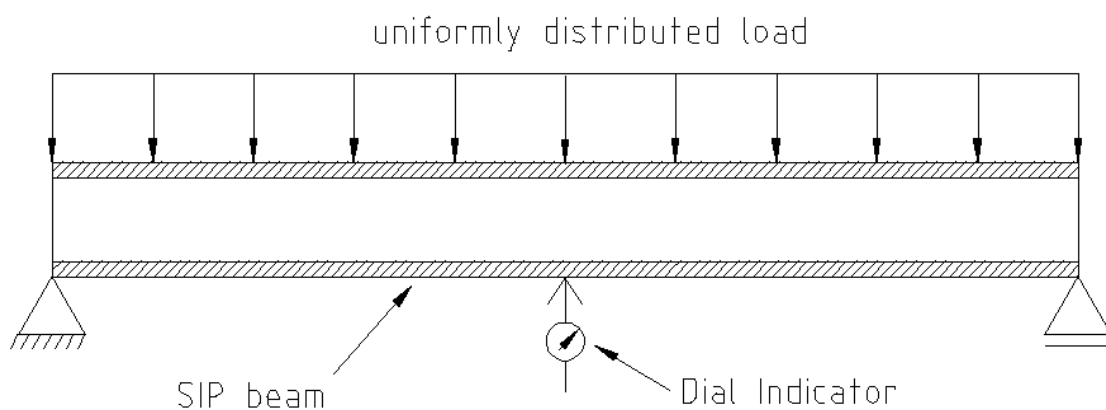
Figure 3-34 – Creep test layout.

The applied load shall be approximately 30% of the estimated core shear failure load;

however, EN 14509 states that the load is not unduly critical. The standard refers that just one test is enough and that when different core thicknesses are to be produced, the higher one shall be chosen for the test.

Figure 3-35 - Creep test of a structural insulated panel (SIP) beam.

The test is started by placing the panel over the two supports, subject only to its self-weight and setting the dial gauges at zero. Then, the panel should be propped from below on a minimum of two lines located at the third points of the span in such a way that the propping can be removed quickly and smoothly to initiate the test. For that purpose, in the tests, a pallet truck was used. With the props placed, the load is applied as quickly as possible, after which the props are removed and the test is initiated. The mid-span deflections are recorded regularly for the duration of the test (minimum of 2000 h), with deflections measured at 30 s, 1 h and 24 h after removal of the props and then at intervals of 24 h for the first week and 48 h thereafter. The graph of deflection versus time should be smoothly continuous for the duration of the test, otherwise the test shall be repeated. The creep coefficient of the core material, φ_t, at the time t is determined according to Equation (3-12),

$$\varphi_t = \frac{w_{T(t)} - w_{T(t=0)}}{w_{T(t=0)} - w_{B(t=0)}} \tag{3-12}$$

where $w_{T(t)}$ is the total deflection at instant t, and $w_{B(t)}$ is the deflection due to the elastic extension on the face. As referred before, this equation is based on the standard for sandwich panels with metal faces, and does not account for the creep on the faces. In the present case, it is found from the bibliography that for design purposes, the creep coefficient on solid wood is taken as 0.60 (CEN, 2004b), while for polyurethane it is 7.00 (EOTA, 2005), which indicates a ratio between coefficients of ~11.7. Based on that, it was assumed that the creep occurring in the test is mainly due to the core shear creep, and thus, as a simplification, the contribution from wood was actually accounted as from being from the core.

In parallel, a test setup based on measuring the total and local deflection as in EN 408 (CEN, 2004a) bending tests, was also used, aiming at measuring separately the creep due to the bending of the faces and that due to shear of the core (Figure 3-36 and 3-37).
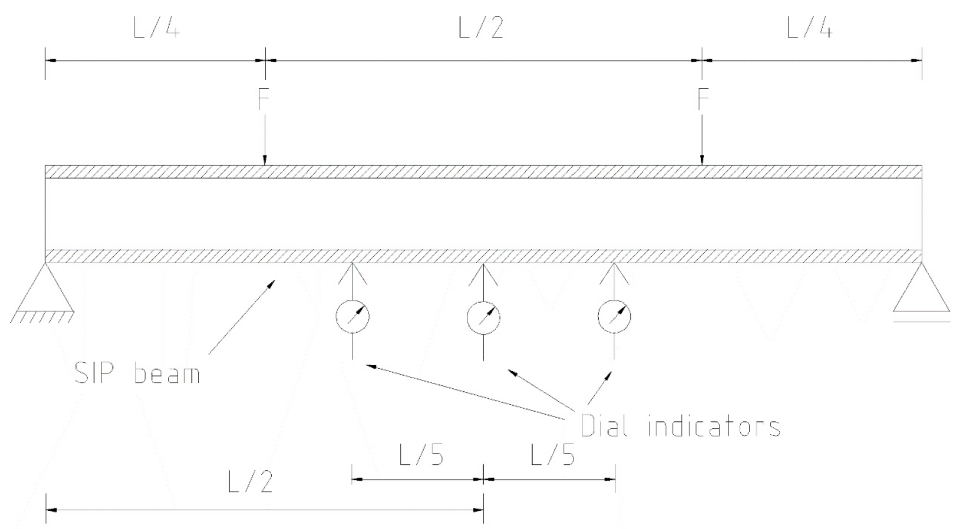
Figure 3-36 – Scheme for measuring the total and local deflection for more accurate determination of creep coefficient.

As mentioned, the alternative setup was defined to determine the local and global deflections measured on a four-point loading simply supported beam, and from those measurements, the creep coefficients were estimated as described below. From the measurement of local deflection ($w_{local(t)}$), which theoretically occurs only due to bending moment, one intended to determine the creep coefficient due to bending over time ($\varphi_{bending(t)}$) according to Equation (3-13). From structural mechanics, it can be assumed that the outer layers are the ones that essentially contributing to the bending stiffness, and thus this coefficient may be mainly attributed to the bending of the outer wood layers.

Figure 3-37 – SIP beam tested for measuring the total and local deflection for creep coefficient determination.

$$w_{local(t)} = w_{local,bending(t)} = \left(1 + \varphi_{bending(t)}\right) \cdot w_{local,bending(t=0)} \qquad (3\text{-}13)$$

Having determined the creep coefficient due to bending, and assuming that no significant variations on material properties occurs along the beam, from the global or total deflection ($w_{global(t)}$) the creep coefficient due to shear deformation ($\varphi_{shear(t)}$) can be estimated (assumed to be mainly due to the core) by Equation (3-14):

$$\begin{aligned} w_{global(t)} = w_{global,bending(t)} &+ w_{global,shear(t)} = \\ \left(1 + \varphi_{bending(t)}\right) &\cdot w_{global,bending(t=0)} \\ + \left(1 + \varphi_{shear(t)}\right) &\cdot w_{global,shear(t=0)} \end{aligned} \qquad (3\text{-}14)$$

For the determination of the referred coefficient, and using the value of $\varphi_{bending(t)}$ previously estimated, it was necessary to determine also the initial global deformations due to bending ($w_{global,bending(t=0)}$) and shear ($w_{global,shear(t=0)}$). The first value can be estimated from the bending stiffness (EI) calculated from the initial ($t = 0$) local deflection as in Equation (3-15),

$$w_{local(t=0)} = w_{local,bending(t=0)} = \frac{Fal_1^2}{16EI} \qquad (3\text{-}15)$$

where a – distance between a support and the load application section; and l_1 – distance between measuring points inside the central third of the span. Knowing the bending stiffness and the initial global deflection ($w_{global(t=0)}$), it is possible to obtain an estimate for the shear stiffness (GA), as in Equation (3-16).

$$w_{global(t=0)} = w_{bending(t=0)} + w_{shear(t=0)} = \frac{Fa}{48EI}\left(3l^2 - 4a^2\right) + \frac{Fa}{2GA} \qquad (3\text{-}16)$$

After having determined all the referred parameters, it is possible to obtain an estimate of $\varphi_{shear(t)}$.

From the experimental results, it was found that this method is unreliable for the type of panel (namely the combination of constituent materials) under study; in fact, at some point of the test, the $\varphi_{bending(t)}$ started to decrease, which is physically unrealistic. This situation is described in the analysis of results and attributed to the effects of environmental conditions. Based on this result, it was decided to rely on the test method described in ETAG 016 -2 (EOTA, 2003b), i.e. to consider only the creep due to the core (with the associated simplifying assumptions).

To determine the creep coefficient of the PUR foam in shear, a SIP beam was manufactured using the maximum PUR board foam thickness available (120 mm) and wood layers with 20 mm of thickness. The injected PUR foam was not tested, as it was found earlier that the adhesion between it and wood was not satisfactory. Dial gauges were used at each side of the bottom face of the beam to measure deflections. Cubic concrete weights were used to guarantee a total distributed load corresponding to 30% of the core shear failure stress. This load was estimated from the Timoshenko beam theory described in Chapter 5. The test was initiated using a hydraulic forklift to assure the propping, while cubic concrete weights were quickly disposed symmetrically over the beam, after which the hydraulic forklift was released and deflections started to be measured. The test was conducted in a room with nearly constant temperature and relative humidity conditions (20 ºC and 65% HR). The total duration of the test was 4698 hours (Figure 3-38).

Figure 3-39 shows the creep coefficient *vs*. time curve for the tested SIP beam under distributed load and the corresponding fitting curve (described ahead).

Various curve fit models were tested (linear, polynomial, power) to describe the creep coefficient over time. It was found that a 2-term power law (Findley's power law) following Equation (3-17) gave the best correlation among the fitting functions tested:

$$\varphi(t) = at^b + c \qquad\qquad (3\text{-}17)$$

The coefficients a, b and c, as well as the R-square value and the value of the creep coefficient φ after 100,000 hours (~11,4 years) are shown in Table 3-4. It should be noticed that for permanent actions the creep coefficient shall be estimated for 100,000 hours (CEN, 2013).

Figure 3-38 – Preparation of the creep test.
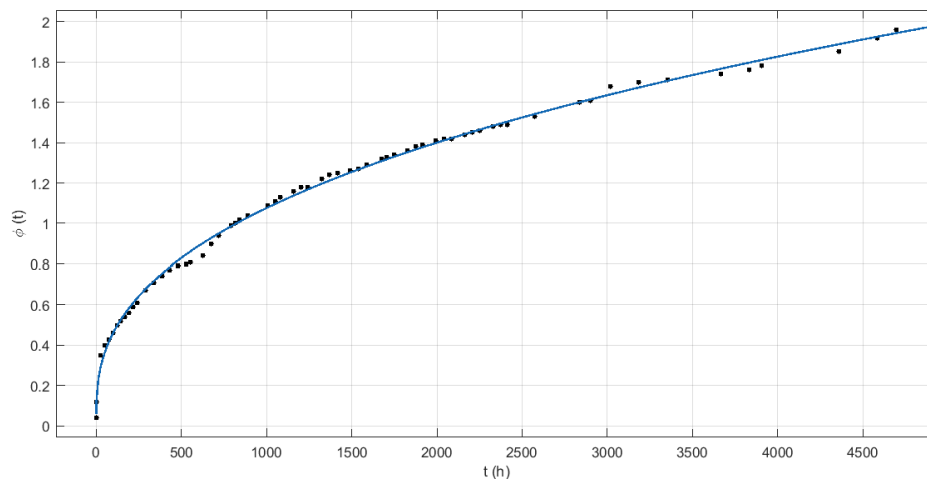
Figure 3-39 – Creep vs time curve response for the tested SIP beam and curve fit.

Table 3-4 – Coefficients of the 2-term power law curve used to describe the creep coefficient (φ), including the R-square and the prediction of φ for 100,000 hours.

	a	b	c	R^2	φ (t=100,000)
SIP	0.06656	0.396	0.04963	1.00	6.41

The obtained value of $\varphi(100,000 \text{ h}) = 6.41$ is quite close to the reference design value of 7.00 referred in the technical document TR 019 (EOTA, 2005). For comparison with other studies, one can refer to (Huang and Gibson, 1991), which reported a creep coefficient (100,000 h) of 9.59 (ρ=48 kg/m^3) calculated from tests at 23+/-1 ºC; and (Garrido, 2016) who reported a creep coefficient (100,000 h) of ~3.5 (ρ=87.4 kg/m^3) from tests at 20 ºC. These values reflect significant relative differences among the various studies.

As referred before, an alternative test setup was considered which accounts also for the creep of the faces. However, the results obtained were not satisfactory. Although the measured global deflection generally increased over time (Figure 3-40), the local deformation, at certain intervals showed significant variations, including deflection recovery (Figure 3-41). It was not possible to identify a clear reason for such inconsistent results, but it is believed that hygrothermal variations on the timber elements were responsible for such variations. It should also be noticed that before the end of the test (~200 h) the magnitude of such local deflections was less than 2 mm, which is quite small compared to the global deflections.
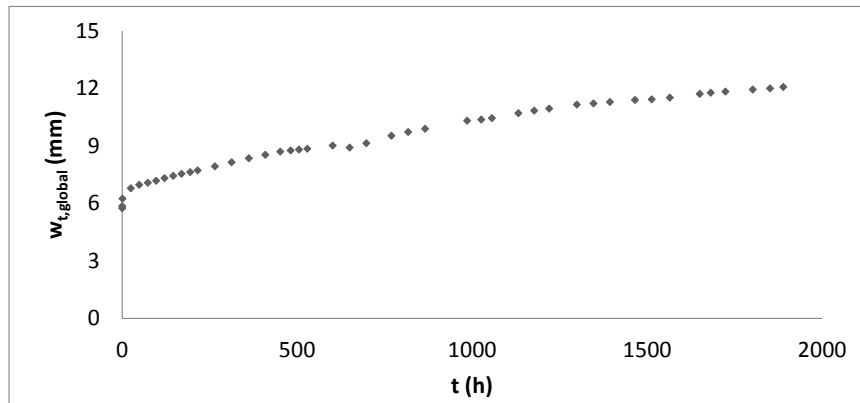
Figure 3-40 – Global deformation as a function of time for the alternative creep test.
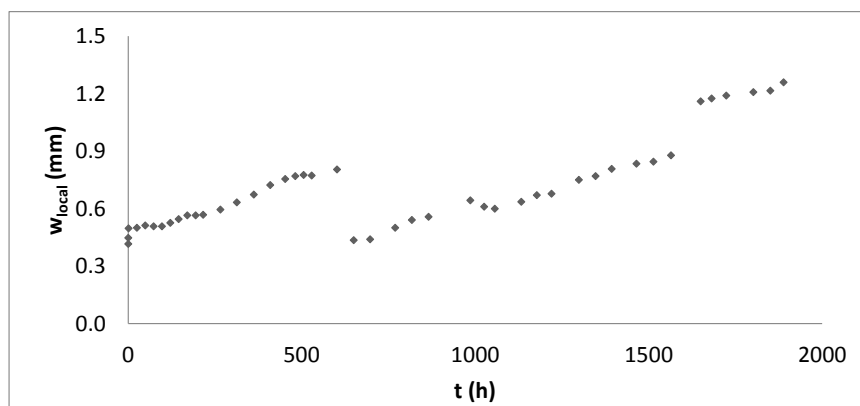
Figure 3-41 – Local deformation as a function of time for the alternative creep test.

3.3.1.5 Ageing

According to (FERPFA, 2006), and as referred in ETAG 016-2 (EOTA, 2003b), the temperature is the most relevant environmental agent for polyurethane rigid foam ageing. In the referred technical document, the effect of temperature should be assessed through tensile tests in specimens before and after the ageing test. The specimens shall be stored at a chamber with constant temperature (90+/-2 ºC) and relative humidity not greater than 15% for 24 weeks (Figure 3-42 and 3-44). Before the test, the specimens shall be stored for 24 hours at 24 ºC.

According to ETAG 016-2 (EOTA, 2003b), the tensile strength of the PUR foam after ageing shall be at least 50% of its initial tensile strength and the characteristic value of the tensile strength should be at least 0.04 N/mm^2.

During and after the ageing test, the specimens' thickness increases (Figure 3-44) and the standard imposes that such change shall not be greater than 5%.

Figure 3-42 – Ageing of specimens in a chamber at 90 ºC.
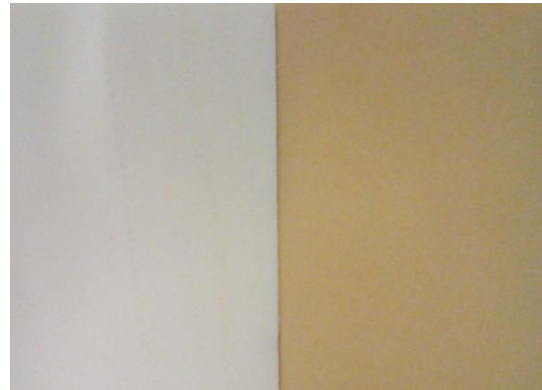
Figure 3-43 – Aspect of the foam before (left) and after (right) the ageing test.

Figure 3-44 – Thickness increase in PUR specimen glued between two wood layers during the ageing test (notice the bending of the foam).

The aspect of a PUR board specimen after the tension test is shown in Figure 3-45. Figures 3-46 and 3-47 compare the modulus of elasticity and strength in flatwise tension for the PUR board specimens with and without ageing using box plots.

Although the average values of the modulus of elasticity slightly decreased (4.2%) after ageing, the average values of tensile strength increased more noticeably (12.4%). Accordingly, the mean value of the tensile strength after ageing is much more than the minimum of 50% of the unaged value and its characteristic value is far above the threshold of 0.04 N/mm^2 required by ETAG 016-2. The slight decrease in the mean value of the modulus of elasticity can be explained by the own variability of the results, as a limited set of specimens were tested. The strength increase is referred by several authors as reported by (Tcharkhtchi et al, 2014), and may be explained by the additional cross-linking of the polymer, which, eventually, was not completely cured before ageing.

Figure 3-45 – Aspect of PUR board specimen after tension test.
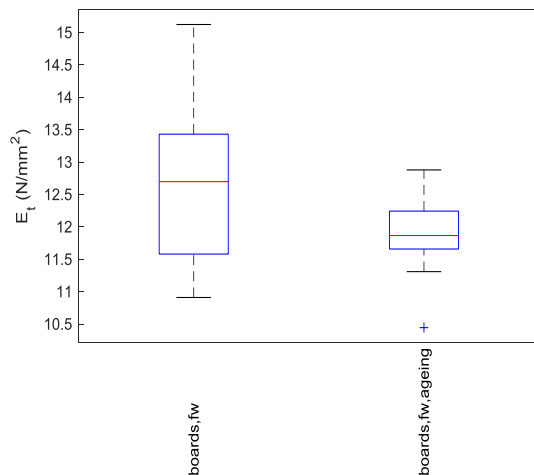
Figure 3-46 – Comparison of the modulus of elasticity obtained in tension tests for PUR board specimens with and without ageing.
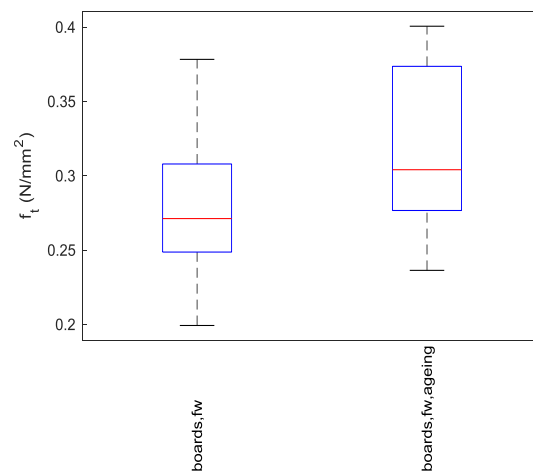
Figure 3-47 - Comparison of the tension strength obtained in tension tests for PUR board specimens with and without ageing.

The glass transition is defined as a reversible and/or irreversible change in an amorphous polymer or in amorphous regions of a partially crystalline polymer from (or to) a viscous or rubbery condition to (or from) a hard and relatively brittle one. The glass transition temperature (T_g) is the characteristic value of the temperature range over which the glass transition takes place (ISO, 2013b). Although it was not possible to obtain the T_g for the polyurethane used in the tests, reference values from other works with rigid polyurethane foam were found: 91 to 110 ºC for 118 and 42 kg/m^3, respectively (Thirumal et al, 2008) and 90 ºC for 68 kg/m^3 (Garrido, 2016). Based on the referred values it is estimated that the T_g for the tested foam (ρ=40 kg/m^3) should be not less than 100-110 ºC, which is slightly above the 90 ºC of the ageing test. This is in line with the fact that no significant loss of strength or increase in ductility was verified for the aged specimens, as the T_g was

not exceeded.

To some extent, the increase in tensile strength due to ageing was an unexpected result, as the test protocol aims at assessing the strength reduction due to ageing. According to the standard, the minimum strength should be reached at the latest after 24 weeks of thermal ageing. However, it was found that similar results were reported in other works, such as (Tcharkhtchi et al, 2014). In that work, tensile tests after thermal ageing at 85 ºC and 120 ºC were performed for different periods of ageing (between 3 to 62 weeks for 85 ºC and between 2 days to 13 weeks for 120 ºC). It was reported that for 85 ºC exposure, both modulus of elasticity and tensile strength had increased after 24 weeks with respect to the initial value (0 weeks), and after 52 weeks those properties had decreased to lower values compared to the unaged condition. For 120 ºC exposure, both modulus of elasticity and tensile strength had increased at day 2 with respect to the initial condition and started to decrease after 1 week to lower values than the unaged condition. These results thus indicate that either the test duration and/or the temperature prescribed by the technical document ETAG 016-2 may need to be adjusted to better reflect the complexity and the potentially competing phenomena involved in the thermal ageing of PUR foam. In fact, according to (Tcharkhtchi et al, 2014), during the thermal ageing of PUR, a competition between chain scission and cross-linking occurs. At the beginning of the ageing process, the effect of cross-linking will overcome the effect of chain scission, and, in consequence, the elastic modulus and strength tend to increase. Forward in time, the effects inverse, and the chain scission controls the ageing process, and, in consequence, the elastic modulus and strength decrease. On the other hand, regarding the ETAG procedure, it is questioned if the actual ageing process is representative of the degradation that the foam will undergo during its lifetime. If so, there is no need to increase the severity of the test.

3.4 Thermal characterization

To ensure an efficient solution in terms of thermal insulation, some specimens of the developed panels were used in an experimental campaign focusing on their thermal performance. Due to their structure made of cross wood layers and PUR, besides the panels, also PUR boards and CLT panels were tested to analyse the thermal properties of the individual components of the construction system proposed in the present thesis. Another objective of the experimental campaign was to compare the thermal conductivity coefficient of the materials obtained experimentally with the ones referred in the literature.

3.4.1 State-of-the-art

Few studies are found in the literature about the thermal performance of CLT and SIP solutions.

(AlSayegh, 2012) measured the thermal conductivity of three- and five-layer CLT specimens from different species and adhesives, including PUR and Emulsion Polymer Isocyanate (EPI), using a heat flow meter apparatus in accordance to ASTM C518 (ASTM, 2015). The results obtained were similar to other studies conducted on solid wood, allowing to conclude that no particular differences exist between CLT and solid wood. Probably for that reason, some manufacturers provide the thermal conductivity of CLT panels based on values for solid timber found in standards such as EN 12524 (CEN, 2000a).

(Wyss et al, 2015) performed thermal tests on a full-scale wall SIP system that includes panel-to-panel connections using an inverted test-hut setup (the exterior surfaces of the panels were faced to the interior of the hut subjected to lower temperatures than the exterior). The thermal effects at the panels and connections were modelled in a commercial software based on the method of explicit finite differences using 1D and 2D approaches. It was found that the 1D model could adequately predict the performance in the centre of the panels; however, for the connections, the 2D model was required as 2D heat transfer effects could not be captured by the 1D model, which is logical as the connection presents heterogeneities along the wall thickness.

Regarding the materials studied in the present thesis, for the polyurethane rigid foam, the thermal conductivity coefficient (λ) declared by the manufacturer at 10ºC is 0.023 W/(m.ºC). For solid wood, (Santos and Matias, 2006) indicate a value of 0.230 W/(m.ºC) for softwoods with densities higher than 610 kg/m^3, while (Gonçalves, 2010) refers a value of 0.120 W/(m.ºC) for Maritime pine (with no reference to the corresponding density range).

3.4.2 Experimental characterization of the thermal insulation of the panels

For the determination of the thermal resistance of the developed panels, an experimental test setup based on ASTM C1155 (ASTM, 1995) was adopted. The referred standard describes a method for the determination of the thermal resistance, in steady-state conditions, based on temperatures and heat fluxes on building envelopes. The *summation technique* prescribed in the standard was used, which is based on the accumulation of heat flux and differences in surface temperatures over time. For a rapid convergence, the

method requires a significant difference between temperatures at each side and constant temperature at one of the sides.

The thermal resistance of the element, R_e (m^2.ºC/W), for each defined time interval (k), starting from the beginning of the measurement, was calculated according to Equation (3-18),

$$R_e = \frac{\sum_{k=1}^{M}(\Delta T_{s,k})}{\sum_{k=1}^{M} q_k} \tag{3-18}$$

where $\Delta T_{s,k}$ is the difference between the surface temperatures on each side of the specimen measured at time interval k; q_k – is the heat flux (W/m^2) measured at time interval k, and M is the number of time intervals considered.

After a time period that starts n hours after the first data set, the convergence factor C (dimensionless) is calculated for each time moment, t (hours), as in Equation (3-19).

$$C = \frac{R_e(t) - R_e(t - n)}{R_e(t)} \tag{3-19}$$

The time interval from which R_e is determined for the tested solution is defined from the time where C remains below a certain threshold, which the standard requires to be no more than 0.10. A minimum of 24 hours is recommended for the test duration.

The experimental test setup was designed in a way that a steady-state heat flux perpendicular to the specimen plane was achieved. The test apparatus involved placing the specimen between two properly insulated chambers (Figure 3-48), each one with a rectangular opening of 80 cm × 80 cm. One of the chambers had a freezer that cooled the air to nearly 10ºC (Figure 3-49) and the other one had an electric resistance that heated the air to nearly 40ºC (Figure 3-50). One fan was also placed in each chamber to homogenise the air temperature. The air temperatures inside each chamber were monitored through three thermocouples: one placed near the bottom, another in the middle and the another near the top of the chamber.

To limit the heat loss to the surrounding environment and ensure that the heat flux developed essentially in the normal direction to the specimen's plane, the square-shape specimens tested (75 cm × 75 cm) were placed into a polyurethane rigid foam frame (of the same type of the one used to manufacture the panels). Also, the gaps between the specimen and the frame were bridged with low-density polyurethane expansive foam (ρ=32 kg/m^3) (Figure 3-51). The monitoring of the surface temperature at each side of the

specimen was made through four thermocouples placed over a 30 cm grid and the heat flow was measured at the centre on each side (Figure 3-52). The temperature values to calculate the thermal resistance were taken as the average of the thermocouples at each side of the specimen; the heat flow was taken as the average of the measurements at each heat flow meter.

Figure 3-48 – Experimental test apparatus - specimen mounted between the chambers.
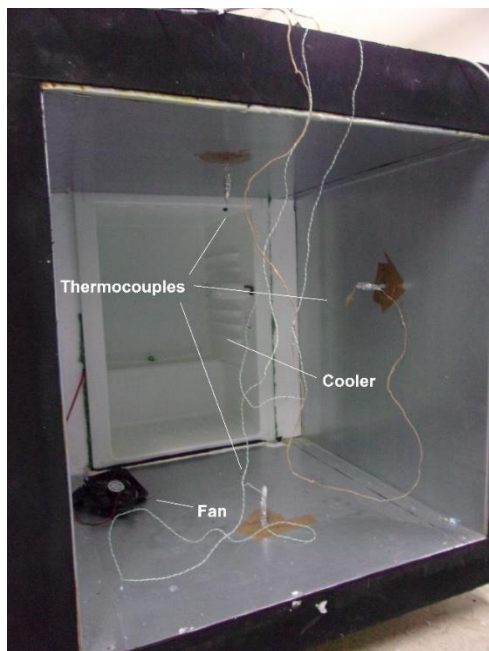
Figure 3-49 – Apparatus inside the cold chamber.
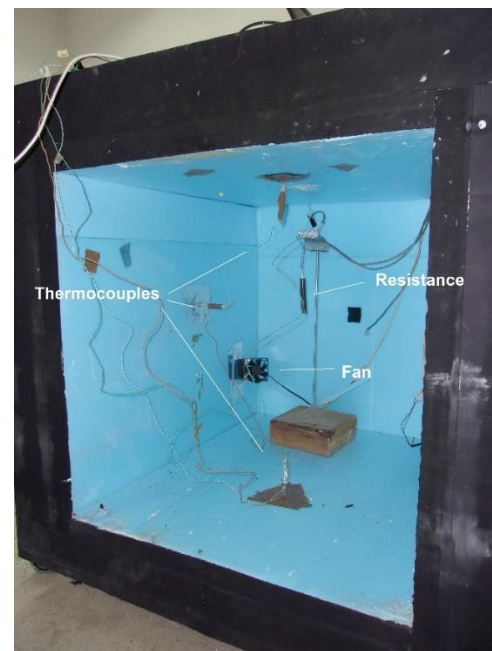
Figure 3-50 – Apparatus inside the hot chamber.

The acquisition of the electric signals from the transducers was made through two eight-channel thermocouple data loggers *PICO-TC08* and the data processed by the *PicoLog* software (Pico, 2019).
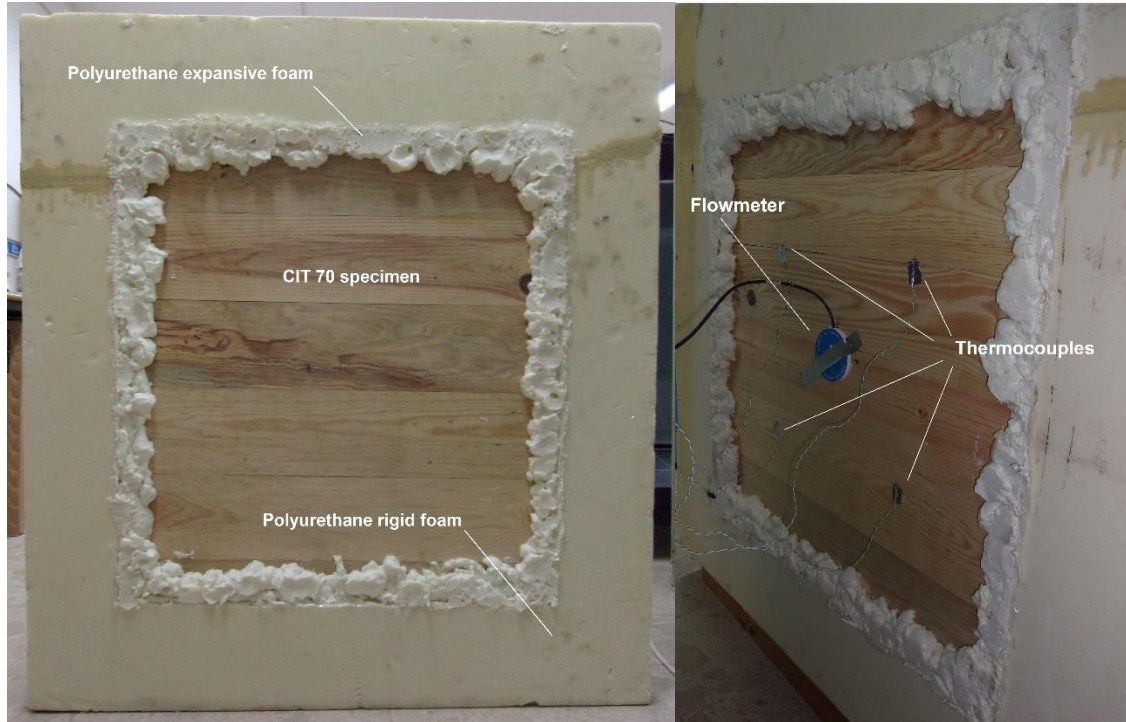
Figure 3-51 – Placement of one of the CIT specimens inside the rigid polyurethane foam frame and its bridging with rigid polyurethane expansive foam.

Figure 3-52 – Placement of the thermocouples and flowmeter at one of the sides of a CIT specimen.

Additionally to the CIT panels, PUR boards and CLT specimens were also tested. PUR boards were tested to compare the determined thermal conductivity coefficient with the one declared by the manufacturer; the same goal was set for CLT specimens, but in this case one aimed at comparing the results obtained with reference values found in the literature for Maritime pine solid wood. The characteristics and designation of the tested panels are shown in Table 3-5.

To compare the experimental results with the ones theoretically expected, the thermal resistance was calculated according to Equation (3-20),

$$R_e = \sum_{i=1}^{n} \frac{e_i}{\lambda_i}$$

(3-20)

where e_i and λ_i are the thickness and the coefficient of thermal conductivity, respectively, of the layer i of a n-layered panel.

It should be noticed that due to the insignificant thickness of the adhesive layers (less than 1 mm) in comparison to the wood/PUR layers, such layers were not accounted for in the

calculation. Also, as referred before, based on the conclusions of (AlSayegh, 2012), no significant differences were expected to exist between solid wood and CLT. In the calculation, the CLT specimens were thus accounted for as if they were made of solid wood.

Table 3-5 – Characteristics of the tested solutions.

Type	Thickness (mm)	no.	Designation	ρ_{PUR} (kg/m^3)	ρ_{wood} (kg/m^3)
CIT	70 (wood layers with 10 mm + polyurethane layer + 30 mm)	1	CIT 70-1	40	658
		2	CIT 70-2	40	648
		3	CIT 70-3	40	630
	170 (wood layers with 35 mm + polyurethane layer + 30 mm)	1	CIT 170-1	40	663
		2	CIT 170-2	40	643
		3	CIT 170-3	40	625
CLT	70 (wood layers with 10 mm; inner layer with 30 mm)	-	CLT 70	-	655
	170 (wood layers with 35 mm; inner layer with 30 mm)	-	CLT 170	-	614
PUR	30	-	PUR 30	40	-
	120	-	PUR 120	40	-

3.4.3 Results

As an example, for the CIT 70-1 specimen, the temperatures measured at the surfaces and the air temperature inside the chamber, at both cold and hot sides are presented in Figure 3-53 and the heat flows in Figure 3-54. From the analysis of the temperature curves, it is observed that the trend of the curves corresponding to the air temperature follows the ones of the surface temperatures in the corresponding side of the chamber, as expected. Also, it can be observed that for the hot side of the chamber, the average surface temperatures were more stable than on the cold side. The higher fluctuations observed for the cold side were caused by the freezing mechanism that does not work so constantly as the electric resistance on the hot side. The fact that one of the sides (hot) had an almost constant temperature, contributed to promote a quicker convergence for the calculus of R_e. Concerning the heat flow, after the initial period, the flow curves measured at each surface started to stabilize.

The thermal resistance *vs*. time plots, that are presented for each type of tested solution (Figure 3-55), confirm that the curves converged to a constant value. In general, it is observed that the R_e value stabilizes faster in the elements of lower insulation, as expected.
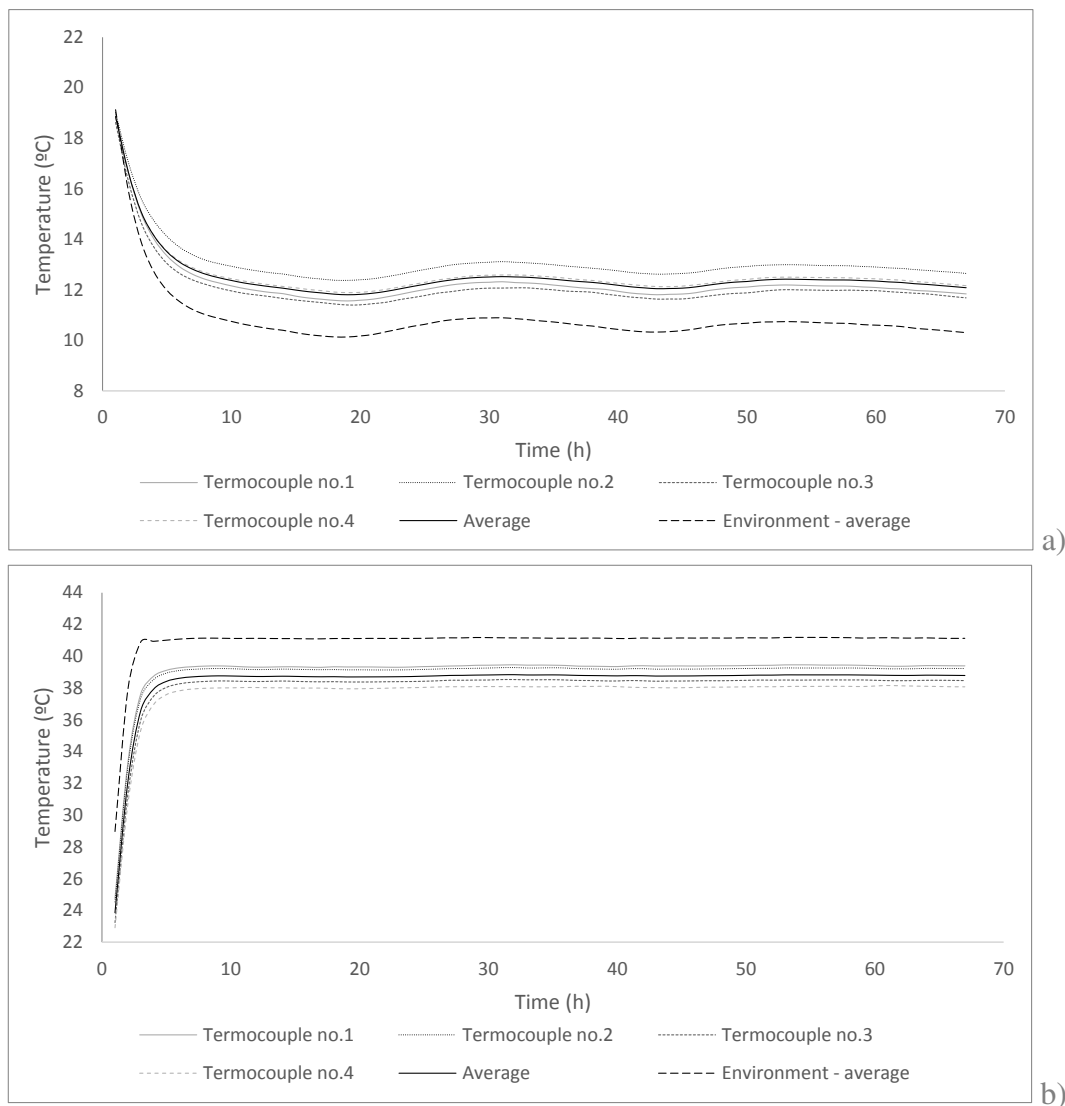
Figure 3-53 – Surface temperatures (including average) and average air temperature on the cold (a) and hot (b) side of the chamber – CIT 70-1.

Table 3-6 presents the values of the coefficients of thermal conductivity determined from the experimental data and their comparison with the reference values from (Santos and Matias, 2006) and (Gonçalves, 2010), and the corresponding relative difference (Δ).

From the comparison of the results, it is found that for the PUR foam the differences between values are quite reduced, with the thicker specimen (120 mm) matching the declared value and the smaller one (30 mm) performing even better. In the case of CLT, the differences considering the (Santos and Matias, 2006) reference λ values are significant, with the predictions being around 70% more conservative than the measured values. Such differences may be explained by the fact that such λ values refer to softwoods in general, and are probably characteristic values. Using the (Gonçalves, 2010) values,

which correspond to Maritime pine, the results are much closer (11-14%). It should be noticed that the experimental values lie between the predicted values from the two bibliographic references.
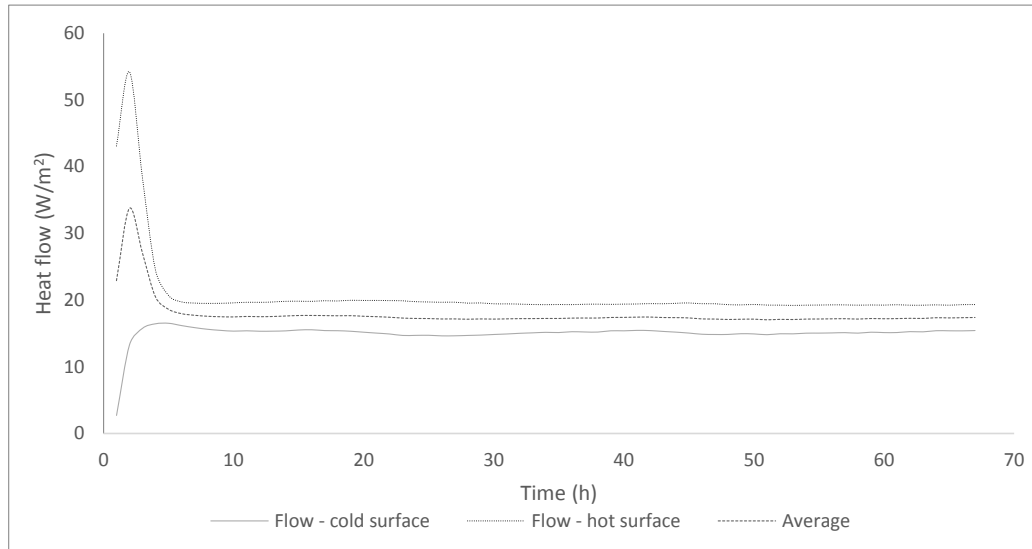
Figure 3-54 - Heat flows in hot and cold surfaces and average – CIT 70-1.
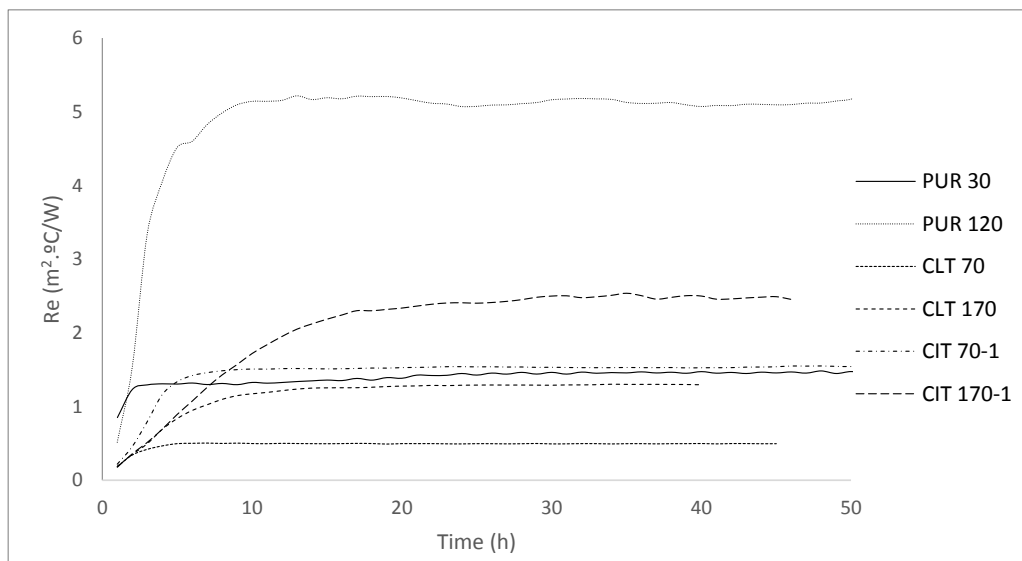
Figure 3-55 - Thermal resistance as a function of time for each type of tested solution.

In Table 3-7, values for the thermal resistance obtained experimentally for the CIT specimens and their comparison with the ones predicted by the analytical model are shown. For the analytical model, three different sets of input data (λ) were considered: two of them using the PUR manufacturer reference value and each of them using the values either from (Santos and Matias, 2006) and (Gonçalves, 2010); the other ones used

the average values for PUR and CLT obtained in the experimental tests (0.022 W/m.°C for PUR and 0.138 W/m.°C for wood).

Table 3-6 – Thermal conductivity coefficient obtained experimentally for the PUR and CLT specimens and comparison with expected values from the literature (percentage relative differences in square brackets).

Specimen	λ (W/m.°C) and [Δ (%)]						
	Experimental	Manufacturer		(Santos and Matias, 2006)		(Gonçalves, 2010)	
CLT 70	0.140	-		0.230	[-64]	0.120	[14]
CLT 170	0.135				[-70]		[11]
PUR 30	0.021	0.023	[-9]	-		-	
PUR 120	0.023		[0]				

Table 3-7 – Thermal resistance obtained experimentally for the CIT specimens and comparison with the one predicted by the analytical model (percentage relative differences in square brackets).

Specimen	R_e (m^2.°C/W) and [Δ (%)]							
	Experimental	Analytical						
		(Santos and Matias, 2006)		(Gonçalves, 2010)		Experimental		
CIT 70-1	1.530	1.478	[3]	1.638	[-7]	1.653	[-8]	
CIT 70-2	1.559		[5]		[-5]		[-6]	
CIT 70-3	1.640		[10]		[0]		[-1]	
CIT 170-1	2.318	1.913	[17]	2.471	[-7]	2.379	[-3]	
CIT 170-2	2.223		[14]		[-11]		[-7]	
CIT 170-3	2.045		[6]		[-21]		[-16]	

The experimental results show that within the same panel thickness some variability in the R_e exists, with values ranging from 1.530 to 1.640 m^2.°C/W (CIT 70) and from 2.045 to 2.318 m^2.°C/W (CIT 170). It should be noticed that no correlation between the wood density (Table 3-5) and R_e was found (R^2=0.01). The comparison of the experimental and analytical R_e values shows that the experimental ones lie between the models using input λ from (Santos and Matias, 2006) and (Gonçalves, 2010)/Experimental ones (from Table 3-6). Once again, such variability is attributed to the intrinsic variability of wood properties. Comparing the magnitude of the differences between the experimental and analytical values for R_e of CIT (Table 3-7) with the ones for λ of wood (Table 3-6), it is found that the first ones are less pronounced. This becomes clear looking at Equation (3-20), where R_e is dependent on the sum of the ratios between the layers' thickness and the corresponding λ. In the present case, PUR foam has a very small value of λ in comparison to that of wood, which, for the considered thickness, makes the PUR

contribution to the overall R_e being major. Thus, the potential influence of variation in λ of wood to the global value of R_e of the element is actually quite limited.

3.5   Concluding remarks

The following summarizes the main conclusions drawn from the investigations presented in the current chapter.

From bending tests in Australian blackwood, the modulus of elasticity was found to be similar to the reference value reported in the literature, while the bending strength was found to be lower; this was probably due to size effects.

The wood raw material was characterized through a non-destructive test method, to obtain the dynamic modulus of elasticity; this property is known to have a high correlation with the static modulus of elasticity.

The PUR board specimens performed better than the injected PUR ones in terms of compression and tension behaviour. Based on those results, it was decided to use the PUR boards for the development of the panels.

The mean values obtained for the shear properties (modulus and strength) of the PUR boards were within the range of values identified in Chapter 2 for foams with similar densities. In the same way, the compressive strength values of the PUR boards were also in line with the range of values declared by the manufacturer.

The anisotropic (at least transversal isotropic) behaviour of the PUR boards was confirmed by the different behaviour observed in the compression tests of the foam in the edgewise and flatwise directions.

In compression, the response of PUR was markedly non-linear and the failure mode was ductile. On the other hand, in tension, the response was linear up to failure, which occurred in a brittle way. The shear tests also revealed a general linear behaviour, with a slight non-linear response before failure, which was also brittle.

The creep coefficient obtained for the PUR board material (after 100,000 hours~11.4 years) is similar (slightly higher) to the reference value found in TR 019 (EOTA, 2005) technical document.

The exposure of polyurethane foam to elevated temperature (90 ºC) for 24 weeks of accelerated ageing has caused a slight reduction in the modulus of elasticity (4.2%), that could be attributed to the intrinsic variability of results, and an increase in the tensile strength (12.4%), which may be partly due to post-curing cross-linking effects. Similar results were found in the literature, reflecting (i) the complexity of the phenomena caused by thermal ageing of PUR foam and (ii) the possible need to adjust either the test duration and/or the temperature of the test protocol used.

The thermal conductivity coefficients determined experimentally for PUR were found to be similar to the one declared by the manufacturer; for CLT made of Maritime pine wood, the experimental values were found to be similar to the ones found in the literature for solid wood of that species.

Some variability was found on the determined thermal resistance of the CIT panels, which was attributed to the intrinsic variability in the material properties, namely for wood. Taking into account such material variability, it was found that the analytical model (conventional heat conduction) was able to predict the thermal resistance of the CIT panels, with good accuracy.

4   CHARACTERIZATION OF ADHESIVE LAYERS

4.1   Introduction

The adhesive layers are expected to ensure the efficient transmission of forces between the wood and insulation layers composing the panel, so that the panel can work as a composite member. The partial (or total) loss of efficiency of the adhesive layer may occur due to mechanical solicitations, physical/chemical degradation or a combination of both. Thus, to achieve an efficient and structurally safe solution, it is necessary to assess the bonding quality between the layers, namely through experimental testing.

When subjected to mechanical forces, the failure of the adhesive layer may occur by means of the following mechanisms: shear (Figure 4-1 a)), tension (Figure 4-1 b)), torsion (Figure 4-1 c)) or a combination thereof.

a)   b)   c)
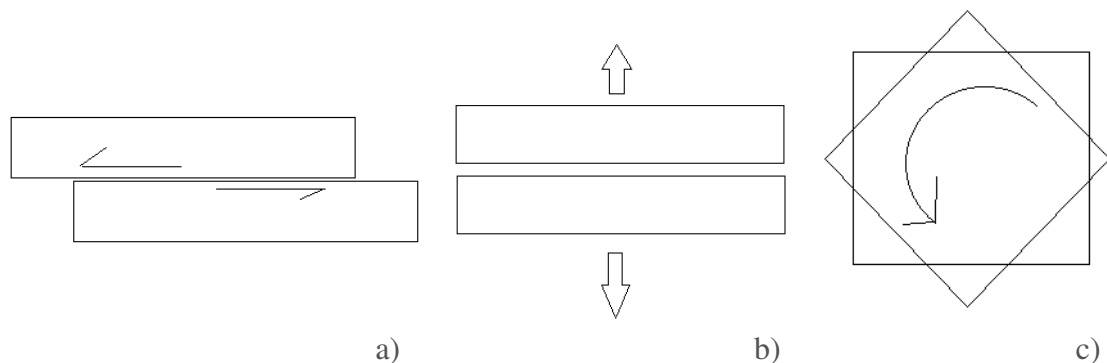
Figure 4-1 – Possible failure mechanisms of the glue line: a) shear; b) tension; c) torsion.

The shear failure mechanism is likely to occur in elements subjected to out of plane loading (e.g. beams), while in shear walls (i.e. with forces acting on the plane), in addition to the shear failure, the torsion mechanism is also likely to occur. The tension mechanism is likely to occur in elements subjected to in-plane loads (e.g. columns) when the wrinkling phenomenon occurs (described in Chapter 5). For a beam element with a cross-section such as that of the developed panel, according to the Timoshenko beam theory (described in Chapter 5), the shear stresses increase along the cross-section from the outer face of the outer layers towards the centre of the inner layer. An illustrative example of the shear stress distribution over the cross-section presented in Figure 4-2.

Based on the analysis of Figure 4-2, to ensure an optimized solution from the mechanical

point of view, it should be ensured that failure does not occur at the glue lines between layers 2 and 3, or between layers 3 and 4, but rather at the polyurethane layer where the shear stress reaches a maximum value. Similarly, a minimum shear strength of the glue line between layers 1 and 2 (or 4 and 5) should be ensured to avoid failure at that interface.
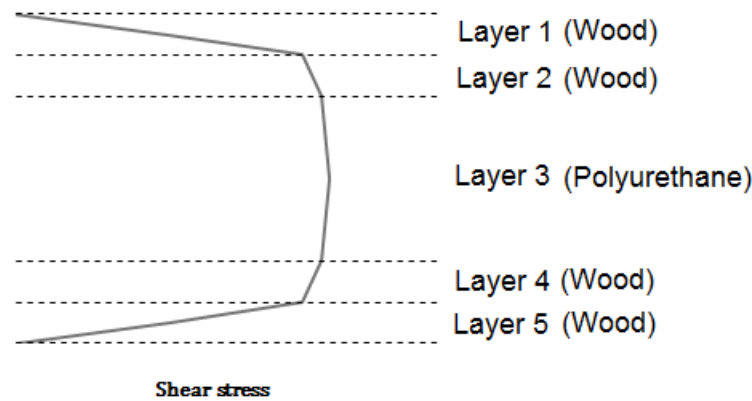
Figure 4-2 – Example of shear stress distribution along the cross-section of the developed panel.

In the case of sandwich-type panels, an efficient bonding is thus achieved if the failure occurs at the core material instead of at the adhesive layer itself. In such type of panels, usually the adhesive properties are higher than the strength of the core material, so usually they are not subjected to testing (Davies, 2008).

As referred, besides mechanical failure due to the above-mentioned mechanisms, failure may also occur due to degradation (ageing) of the material properties by physical/chemical agents, such as heat, moisture and other environmental agents.

For the mechanical testing of bonded cross-wood layers, the CLT dedicated standard EN 16351 (CEN, 2015), prescribes a shear test, while for accelerated ageing, a delamination test procedure is indicated.

For the mechanical testing of the wood/insulation layer, there are two alternative procedures: (i) a shear test, as per ASTM C273 (ASTM, 2011b), and (ii) a tension test, according to ETAG 016-1 (EOTA, 2003a). For durability assessment, a procedure is described in ETAG 016-2 (EOTA, 2003b).

The lengths in which the timber members (lamellas) are processed often do not allow the production of structural products with the necessary dimensions. To overcome this problem, longer members can be obtained through the use of finger-joints. For the panels tested in this thesis, due to limitations of the manufacturing press dimensions (maximum

length of 3 m), *a priori*, it was not necessary to rely on finger-joints. Even so, connections with finger-joints on Maritime pine were tested to validate the process for longer dimensions required in practice.

The main objectives of this chapter comprise the identification of the conditions that optimize the performance of the bonding layers, namely the bonding parameters, including the bonding pressure and the adhesive spread rate for both wood/wood and polyurethane/wood interfaces.

The remainder of the chapter is organized as follows: section 4.2 presents the results related to the adhesion between the wood materials, including the face bonding of cross layers made of Maritime pine and also of Maritime pine with Australian blackwood; section 4.3 presents the results related to the finger-joint connections between Maritime pine lamellas; section 4.4 describes the results related to the adhesion between the polyurethane foam material and Maritime pine, including the ageing effects; in the last section, 4.5, concluding remarks are made.

4.2 Adhesion between wood elements - Face bonding of cross layers

4.2.1 Introduction

In order to ensure a structurally safe and efficient solution, the bonding quality between the cross-wood layers has to be assessed. The developed panel is a lightweight panel made with two pairs of wood layers glued to a polyurethane core. The cross arrangement of the wood layers is similar to the one used on cross-laminated timber (CLT). For that reason, the state-of-art and the guidelines regarding the bonding quality assessment of CLT were followed for the assessment of the bonding performance of the wood layers of the panel.

The CLT harmonised product standard EN 16351 (CEN, 2015) establishes minimum requirements in terms of shear strength (the reference parameter) or delamination of the glue lines between the layers.

In the frame of the referred standard, the shear strength test can be considered as an unaged test procedure and the delamination test as an ageing test to evaluate the integrity of the bond line in the long-term. The last one consists of the introduction of internal stresses in the bond line due to the wood layers' shrinkage and swelling, which are generated by saturation with water and subsequent drying. The occurrence of delamination on the glue lines reflects inadequate bonding quality (Karacabeyli and Douglas, 2013; CEN, 2015).

The main objectives of the current section were to achieve an efficient bonding solution between the two-layered cross-wood elements of the CIT panels under development that fulfils the EN 16351 requirements.

4.2.2 State-of-the-art on CLT face-bonding

Some recent works can be found in the specialized literature regarding the evaluation of the bonding quality of CLT panels, mainly focusing on the influence of the bonding parameters on the shear strength and delamination of the glue lines, namely press time, bonding pressure or specimen shape.

(Betti et al, 2016) performed shear, delamination and combined delamination/shear tests on specimens from five-layer Spruce (*Picea abies L.*) CLT panels glued with a polyurethane (PUR) adhesive, using different sampling methods and testing methodologies. Based on the results obtained, shear tests on 40 x 40 mm^2 specimens (as in EN 16351), but with sides forming a 45 ° angle with respect to the grain direction, to avoid rolling shear failures, were proposed as standard.

(Sikora et al, 2016) performed shear and delamination tests according to the pre-standard version of EN 16351 on specimens taken from three-layer Irish Sitka Spruce (*Picea sitchensis*) CLT panels glued with two types of adhesive, one-component (1C) PUR and phenol resorcinol formaldehyde (PRF). They analyzed the effect of using different bonding pressures and concluded that shear strength of the glue lines was not particularly affected by the pressure variation; however, lower delamination and high wood failure percentages were found with a higher pressure.

(Knorz et al, 2017) performed delamination tests according to EN 16351 on specimens from three- and seven-layer CLT panels made of Spruce (*Picea abies L.*) glued with 1C PUR adhesive. They studied the influence of the number of layers, layers thickness, bonding pressure and specimen's shape (it should be noticed that EN 16351 prescribes two possible shapes, round or square) on delamination. They concluded that square specimens showed higher delamination, a result that was attributed to the higher top view area, as well as to the higher stresses at the corners of the square specimens compared to round specimens. No influence of layer thickness was found on the results. Concerning the number of layers, lower wood failure percentage was found for the seven-layer specimens, which was attributed to the glueing process, whose quality is time-dependent (i.e. increased number of layers means extended time between applying the glue and the beginning of the press stage). Regarding bonding pressure, lower values of delamination

were observed for increased pressure, but no influence was found with respect to wood failure percentage.

(Liao et al, 2017) performed shear and delamination tests on specimens from three-layered CLT made of Eucalyptus wood (*Eucalyptus urophylla x Eucalyptus grandis*) glued with 1C PUR adhesive. They evaluated the influence of pressure and press time on delamination, shear strength and wood failure percentage. The increase of bonding pressure led to lower delamination values, higher shear strength values, as well as higher wood failure percentage. They reported that increased press time led to a slight increase of shear strength and wood failure percentage, but to a significant decrease of delamination.

(Wang et al, 2018) performed shear and delamination tests on Western hemlock (*Tsuga heterophylla (Raf.) Sarg*) and Amabilis fir (*Abies amabilis (Dougl.) Forbes*) glued with 1C PUR and emulsion polymer isocyanate (EPI). They evaluated the influence of bonding pressure, for which they reported lower delamination and high wood failure percentage values for increased values, while shear strength was not noticeably affected.

Regarding the fulfilment of EN 16351 requirements for shear strength and delamination, some debate is found in the literature, as the limits for the first property are considered too lenient, while those for the second one have been considered too severe (Knorz et al, 2017). Another issue pointed by some authors is that no correlation could be found between shear and delamination results. Nonetheless, EN 16351 establishes that bonding quality is considered adequate if either shear strength or delamination test criteria are fulfilled, and the shear strength is referred as the reference method.

In some of the referred works (Betti et al. 2016; Sikora et al. 2016; Knorz et al. 2017) it is reported that a great part of the tested samples failed the delamination limits. One should notice that a common point in the referred works is the use of PUR adhesive. In a study on bonding of glued laminated timber (GLT) by (Luedtke et al, 2015), the use of a pre-treatment (primer) with a 1C PUR adhesive was found to be essential to enhance the bonding quality. For three different hardwood species that were tested, although shear strength was not noticeably affected, delamination decreased significantly with respect to un-primed specimens. Moreover, in recent work by (Lu et al, 2018), the effects on bonding quality of Eucalyptus (*Eucalyptus urophylla x E. grandis*) CLT glued with 1C PUR with pre-treatment with a hydroxymethylated resorcinol (HMR) primer were reported. From that work, it was found out that the pre-treatment of the wood surfaces with the primer reduced the delamination to almost zero, while shear strength and wood failure percentage increased.

Regarding the bonding of CLT composed of layers made on different wood species, just a few works were found, namely those by (Aicher et al, 2016) and (Wang et al, 2018), with only the last one focusing on the bonding quality assessment.

4.2.3 Materials and methods

The main objective of the current section was, besides, achieving an efficient bonding solution for the two-layered cross wood elements of the CIT panels under development, the optimization of the main bonding parameters (bonding, pressure and adhesive spread rate), as well the study of their influence on the bonding quality indicators (shear strength and delamination). It should be noticed that the influence of the adhesive spread rate was not investigated in the works reported in the state-of-the-art. Besides the bonding parameters, also the layer thickness influence was assessed. Based on the findings from other works, the use of 1C PUR primer on cross-wood layers was also considered due to the expected enhance of bonding quality. As referred in Chapter 2, for the CIT panel to be developed, Maritime pine (*Pinus pinaster* Ait.) was chosen, but also the combined layup of Maritime pine with Australian blackwood (*Acacia melanoxylo* R. Br.). As referred before, very few information was found regarding the bonding of CLT made of mixed wood species. In that context, another objective of this work was to check the possibility of obtaining a viable solution (as per the EN 16351 bonding requirements) of mixed two-layer species.

4.2.3.1 Overview of test programme

To fulfil the objectives mentioned above, shear and delamination tests according to EN 16351 (CEN, 2015) were performed. For the manufacturing of test specimens, the following parameters, and their variations in brackets, were considered:

- Bonding pressure (0.1, 0.6, 0.8 and 1.0 MPa);
- Adhesive spread rate (140, 160 and 180 g/m^2);
- Pre-treatment with primer (without or with primer, 20% concentration, spread rate of 20 g/m^2);
- Layer thickness (15 and 35 mm).

For bonding pressure and adhesive spread rate, the minimum, average and maximum values within the ranges recommended by the adhesive manufacturer were considered. For the bonding pressure, a lower value (0.1 MPa) was also considered as in practice some manufacturers produce CLT with pressures around such value. This bonding pressure was also used in the CIT panels to bond the wood layers to the PUR foam, and

so it was considered of interest to assess the possibility of bonding the entire panel at once and check the bonding strength and durability of the wood elements for such pressure.

Bonding pressure, adhesive spread rate and pre-treatment with primer were tested in all possible combinations; concerning wood layers thickness, 15 mm was chosen as reference, while 35 mm was only tested considering the pre-treatment and the minimum bonding pressure recommended by the adhesive manufacturer (0.6 MPa).

4.2.3.2 Materials

The adhesive system used in the tests was the 1C PUR LOCTITE PURBOND HB S709, which is formaldehyde-free and meets the requirements of adhesive type I according to standard EN 15425 (CEN, 2008). The primer used was the polyol-based LOCTITE PR 3105 PURBOND.

The mean densities of the wood species used to produce the test specimens were 669 kg/m^3 and 622 kg/m^3 for Maritime pine (*Pinus pinaster* Ait.) and Australian blackwood (*Acacia melanoxylo* R. Br.), respectively. The values were found to be in line with the reference values defined in the literature of 640 kg/m^3 and 650 kg/m^3, respectively (Carvalho, 1997).

4.2.3.3 Specimen preparation

As referred in Chapter 2, the developed panels were composed of two pairs of cross-wood layers with a PUR foam layer in the middle. As the PUR foam used ($\rho_{mean} = 40$ kg/m^3) has relatively low mechanical properties when compared to wood, in the delamination tests, one expected that the restriction imposed by the foam to swelling and shrinkage of wood on the delamination tests would have marginal influence. So, it was decided to test specimens composed of only two wood layers instead of a full cross-section (*i.e.* two pairs of wood layers plus the PUR inner layer).

As no industrial spread system was available for the manufacturing, the glue was applied manually using a notch trowel. To ensure the right spread rate of adhesive applied, a weighing scale was used to measure the effective adhesive weight spread over the wood layer. The primer was applied using a hand sprayer to both wood surfaces to be bonded, while the adhesive was applied only to one of the surfaces as recommended by the adhesive manufacturer. The room temperature and relative humidity conditions at the moment of bonding were 20ºC and 65%, and the wood mean moisture content was around 14.7%, all values in accordance to EN 16351 indications, as well as with the adhesive's

manufacturer recommendations. The pressure was applied through a hydraulic press system and all the periods concerned with the bonding process were defined according to the adhesive's manufacturer specifications: activation time of primer (minimum of 10 minutes), assembly time (maximum of 70 minutes) and curing time (minimum of 200 minutes). When using primer, a double-time press was used as required by the manufacturer (400 minutes).

To obtain the shear and delamination test specimens, a series of beam-type elements composed of two wood layers orthogonally arranged were produced following the previous indications. In general, the beams were composed of one layer with 140 mm x 420 mm and three cross layers with 140 mm x 140 mm. The delamination specimens that were cut from the produced beams had a square top view area of 100 ± 5 mm length and the shear specimens had 40 mm x 40 mm, all in accordance to EN 16351. The cutting scheme is presented in Figure 4-3 and examples of shear and delamination test specimens of Maritime pine and mixed Maritime pine/Australian blackwood are shown in Figure 4-4.
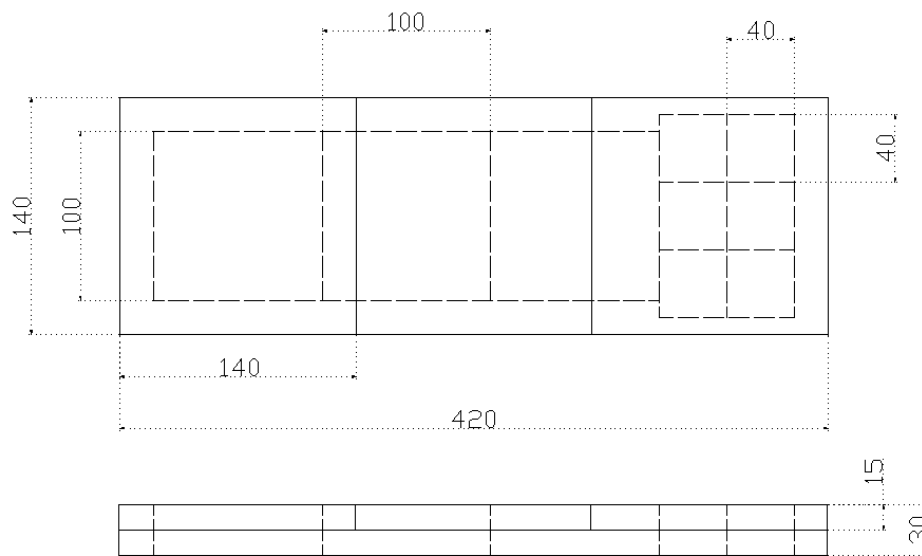
Figure 4-3 – Scheme of cut-outs (dashed) of specimens from the beam-type elements. (dimensions in mm).

To make it easier to refer, the different sets of test specimens (reflecting the studied parameter), the following nomenclature was used: Maritime pine (MP), Australian blackwood (AB), PR (primed) and 35 mm (e.g. 35 mm of thickness); the adhesive spread rate and the bonding pressure are referred in sequence (e.g., a spread rate of 180 g/m^2 and a pressure of 1.0 MPa, are referred to as '180 1.0'). The total numbers of tested specimens for the different sets are shown in Table 4-1. A total of 1418 specimens were produced and tested.
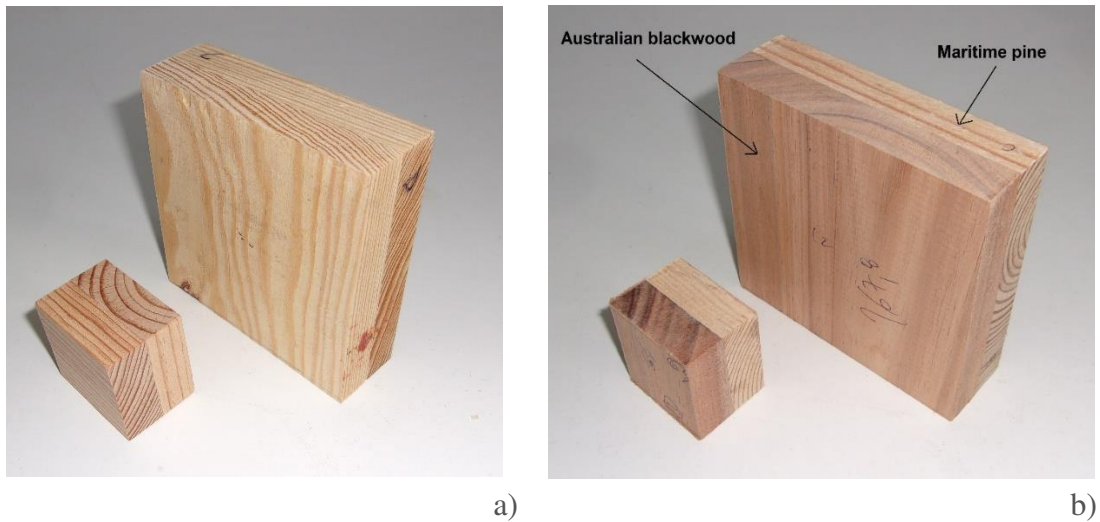
Figure 4-4 - Examples of specimens used in shear and delamination tests: a) Maritime pine solo; b) mixed Maritime pine/Australian blackwood.

Table 4-1 - Number of tested specimens for the different sets used in the delamination and shear tests.

Spread rate (g/m²)		180				160				140			
Pressure (MPa)		1.0	0.8	0.6	0.1	1.0	0.8	0.6	0.1	1.0	0.8	0.6	0.1
Delamination	MP	12	10	15	9	10	15	15	9	10	15	15	15
	MP - PR	18	45	10	9	20	30	10	9	10	15	10	15
	MP - PR - 35 mm	-	-	10	6	-	-	10	13	-	-	10	13
	MP + AB - PR	-	-	11	15	-	-	11	15	-	-	12	14
Shear	MP	33	30	30	12	30	30	30	12	30	30	30	30
	MP - PR	53	88	12	12	57	59	12	12	30	29	12	15
	MP - PR - 35 mm	-	-	10	8	-	-	10	12	-	-	10	12
	MP + AB - PR	-	-	27	20	-	-	27	19	-	-	18	36

4.2.3.4 Delamination tests

The delamination tests followed the guidelines of Annex C of EN 16351. The first stage of the test was the measurement of the mass and the total length of the glue lines in the perimeter of each specimen; specimens were previously conditioned in a room at 20 ºC and relative humidity of 65%. The specimens were then placed on a pressure vessel (Figure 4-5 a)), completely submerged, and a vacuum pressure of 70-85 kPa was applied for 30 minutes, after which the vacuum was released and a pressure of 500-600 kPa was applied for 2 hours. After the pressure was released, the specimens (Figure 4-5 b)) were placed on a drying duct (Figure 4-5 c) and d)) at a temperature of 65-75 ºC, relative humidity of 8-10% and air circulated at 2-3 m/s, during 10-15 hours, until the specimens reached between 100% to 110% of their original mass. The delamination lengths were

then measured, as well as the wood failure (WF) after opening the pieces with a metal wedge and hammer, as recommended by the standard. Delaminations caused by wood defects (e.g. knots) were ignored in the measurements in accordance with the standard.
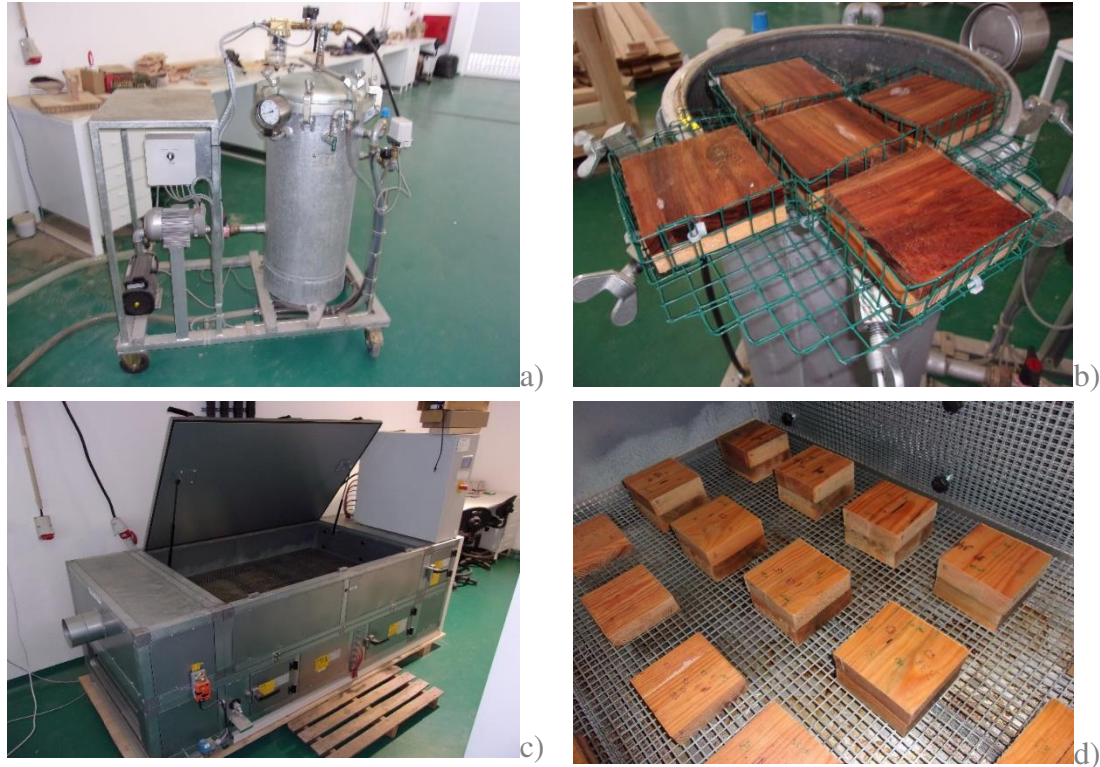
Figure 4-5 – Aspects of the delamination tests: a) pressure vessel used on the delamination tests; b) Maritime pine + Australian blackwood specimens after the vacuum-press stage; c) drying duct used on the delaminations tests; d) specimens placed on the drying duct before the drying stage.

EN 16351 establishes two parameters for evaluating the delamination of glue lines between layers on CLT, namely the maximum delamination (D_{max}) defined in Equation (4-1), and the total delamination (D_{tot}), defined in Equation (4-2):

$$D_{max} = \frac{l_{max,delam}}{l_{glue\ line}} \times 100\ (\%)$$ (4-1)

$$D_{tot} = \frac{l_{tot,delam}}{l_{tot,glue\ line}} \times 100\ (\%)$$ (4-2)

where $l_{tot,delam}$ is the total delamination length on a specimen, $l_{tot,glue\ line}$ is the sum of perimeters of all glue lines, $l_{max,delam}$ is the maximum delamination length, and $l_{glue\ line}$ is

the perimeter of one glue line. As the tested specimens had only a single glue line, in this case, $D_{max} = D_{tot}$.

EN 16351 requires that D_{tot} and D_{max} should be less or equal to 10% and 40%, respectively. In case any of the referred limits is not fulfilled, each glue line of the specimen must be split, and the wood failure percentage (WF) must be at least 50% for each split area ($WF_{glue\ line}$), and at least 70% for the sum of all split areas ($WF_{tot,glue\ line}$). However, no indications for the measurement of WF are provided in the above-mentioned standard.

In practice, it was found to be difficult and inaccurate to measure WF only by visual inspection, so a computational algorithm was developed for that specific propose using *MATLAB* software (Mathworks, 2018), following a similar process used by (Künniger, 2008). The whole process is described below:

- Each specimen is opened at the glue line using the metal wedge and hammer (Figure 4-6 a)) and the split areas are brushed with a chemical indicator solution (50% of phloroglucinol anhydrous solution at 2% + 50% of hydrochloric acid solution at 10%);
- The solution stains the wood fibres in pink (Figure 4-6 b)), while the PUR adhesive remains with its original colour (nearly white), thus generating a well-defined colour contrast;
- Each split area is photographed in a light environment over a white background for increased contrast with a digital camera;
- The pair of images is treated in the *MATLAB* software in a way that a rectangular frame is applied to the limits of the piece (Figure 4-6 b));
- One of the images is resized so that the framed pair of images has the same area (i.e. equal number of side pixels);
- One of the images is mirrored, so that the images can be later overlapped;
- The RGB images are converted to a black and white scale (Figure 4-6 c));
- The images are overlapped, in a way that if each corresponding pair of pixels is in black (meaning the presence of wood fibres), then the pixel remains in black, while in the other cases the pixel remains in white, meaning failure in the adhesive (Figure 4-6 d));
- The WF is then calculated by dividing the number of pixels in black by the total number of pixels of the image.

Although the referred method was found as a useful tool, it should be noticed that the referred method may be susceptible to some sources of inaccuracy, such as an imperfect fitting of the frames of the specimens or an imperfect overlap of images. For that reason,

in addition to a significant effort to minimize such sources of error, the algorithm results were always corroborated and eventually corrected with visual override.
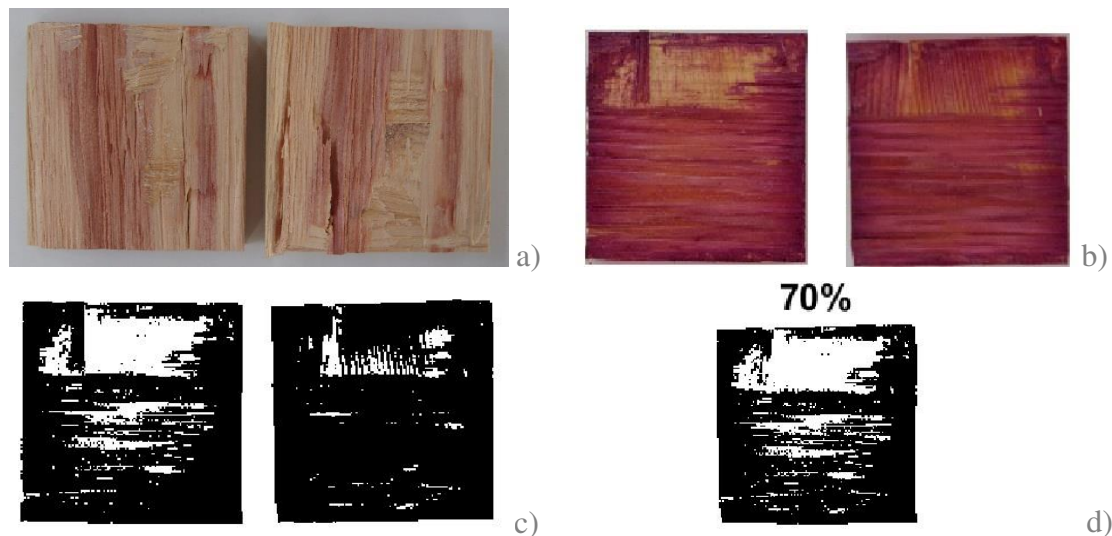
Figure 4-6 – Phases of the determination of the wood failure percentage: a) photograph of the split specimen; b) framing of each coloured piece; c) images converted to black and withe colour scale; d) wood failure percentage calculated (coloured in black).

An additional chemical indicator solution was used to stain Australian blackwood (0.25 g of methyl orange + 0.25 g of bromocresol green + 0.01 g of indigo carmine + 50 mL of ethanol + 50 mL + 25 mL of distilled water), because the original solution did not create enough colour contrast for this timber species with respect to the glue line. Even so, to observe clearly the glue line, it was necessary to resort to an ultraviolet light flashlight on a poor light room. Because a camera that could take photos with enough quality in such lighting conditions was not available, the wood failure percentage on the mixed specimens (both shear and delamination) was determined by an alternative visual method. Such method consisted of drawing a grillage on two glass plates with a ten-by-ten grid *(10 x 10 cm²)*, covering the standard test specimens top view area, so that when the glue line was visually identified in the grid in one of the faces it was manually marked. The process was then repeated in the other face, after which the glass plates were properly overlapped, the number of marked grids was counted, and the percentage of glued area failure determined.

4.2.3.5 Shear tests

Shear tests were performed using a shear tool (Figure 4-7) in accordance with Annex D of EN 16351.

Figure 4-7 – Maritime pine specimen under a shear test.

The specimens were placed in the testing device so that the wood layer at one side of the glue line was loaded in the direction of the grain and the glue line was positioned so that the distance between the shearing tool and the sheared plane nowhere exceeded 1 mm. The load was applied at a constant rate of deformation (0.06 mm/s) so that failure occurred after no less than 20 s, as required by the standard. The shear strength, f_v (MPa), was determined according to Equation (4-3):

$$f_v = k\frac{F_u}{A}$$

(4-3)

with k given by Equation (4-4),

$$k = 0.78 + 0.0044t$$

(4-4)

where F_u is the ultimate load (kN); A is the shear area (mm^2); t is the thickness (mm), in this case 40 mm in accordance to EN 16351. According to the standard, the bonding strength is considered sufficient if, for each individual glue line, a minimum strength of 1.00 MPa is achieved and if the characteristic value of all glue lines is at least 1.25 MPa. Although the above-mentioned standard specifies that WF shall be reported, no minimum limits are imposed for it.

4.2.3.6 Statistical analysis

For a clearer analysis of the influence of the different tested parameters in the results, the statistical technique Analysis of Variance (ANOVA) was used. The referred tool allows determining whether a variation in the response variable arises within or among different

population groups. The *MATLAB* (Mathworks, 2018) function *anovan()* was used to perform the ANOVA method, as it allows performing a multiway analysis of variance for testing the effects of multiple factors. It should be noticed that because the input data is unbalanced (i.e., there is a different number of observations within samples) it was not possible to estimate the interaction between parameters. Using the results from the ANOVA procedure, another *MATLAB* function, *multcompare*(), was used, which consists of a multiple comparison test. The referred function provides the differences between group means and a p-value for a hypothesis test that the corresponding mean difference is equal to zero. The function also enables to plot a graph of the estimates and comparison intervals, where each group mean is represented by a symbol (o), and the interval is represented by a line extending out from the symbol (-). Two group means are considered significantly different if their intervals are disjoint and are not significantly different if their intervals overlap.

Some results are also presented using box plots. In those plots, on each box, the central mark indicates the median, and the bottom and top edges of the box indicate the 25th and 75th percentiles, respectively. The whiskers extend to the most extreme data points not considered outliers, and the outliers are plotted individually using the '+' symbol.

4.2.4   Results and discussion

In the following section, the results regarding the delamination and shear tests on Maritime pine and mixed Maritime pine with Australian blackwood specimens are presented and discussed. In more detail, the effect in the bonding quality indicators (delamination, wood failure after delamination, shear strength and wood failure after shear) of the variation of each test parameter considered - bonding pressure, adhesive spread rate, use of primer and layer thickness - are analysed and discussed.

4.2.4.1   Analysis of the delamination and shear test results for the Maritime pine specimens

The results of the ANOVA and the multi-comparison regarding the Maritime pine samples are shown in Tables 4-2 and 4-3, respectively. In Table 4-2, 'Sum Sq.' stands for sum of squares due to each source (or parameter), 'd.f.' for degrees of freedom associated with each source (e.g. number of different adhesive spread rates minus one), 'Mean Sq.' for mean squares for each source, 'F' for F-statistic and 'Prob>F' for the p-values. The last one, p-value, represents the probability that the F-statistic can take a value larger than a computed test-statistic value. The probabilities were derived from the cumulative

distribution function of F-distribution. In Table 4-3 'Mean dif.' stands for differences between group means.

Table 4-2 – ANOVA results for the Maritime pine specimens.

	Source	Sum Sq.	d.f.	Mean Sq.	F	Prob>F
Delamination	Adhesive Spread Rate	1551.3	2	775.7	3.090	0.047
	Bonding Pressure	6588.9	3	2196.3	8.750	0.000
	Primer	9630.8	1	9630.8	38.390	0.000
	Thickness	384.9	1	384.9	1.530	0.216
	Error	101608.4	405	250.9	-	-
	Total	119792.7	412	-	-	-
WF Delamination	Adhesive Spread Rate	888.0	2	444.0	1.830	0.162
	Bonding Pressure	49018.8	3	16339.6	67.210	0.000
	Primer	50012.2	1	50012.2	205.710	0.000
	Thickness	1267.6	1	1267.6	5.210	0.023
	Error	98464.1	405	243.1	-	-
	Total	219502.7	412	-	-	-
Shear	Adhesive Spread Rate	5.9	2	3.0	1.880	0.154
	Bonding Pressure	5.6	3	1.9	1.190	0.314
	Primer	36.7	1	36.7	23.250	0.000
	Thickness	3.0	1	3.0	1.900	0.168
	Error	1218.5	772	1.6	-	-
	Total	1274.5	779	-	-	-
WF Shear	Adhesive Spread Rate	1471.6	2	735.8	3.110	0.045
	Bonding Pressure	79010.6	3	26336.9	111.450	0.000
	Primer	146331.6	1	146331.6	619.240	0.000
	Thickness	1034.6	1	1034.6	4.380	0.037
	Error	182431.4	772	236.3	-	-
	Total	453711.0	779	-	-	-

Table 4-3 - Multiple comparison test results for the Maritime pine specimens.

		Delamination (%)		$WF_{Delamination}$ (%)		Shear (N/mm^2)		WF_{Shear} (%)	
		Mean dif.	p-value	Mean dif.	p-value	Mean dif.	p-value	Mean dif.	p-value
Adhesive spread rate	140 vs. 160 g/m^2	-4.3	0.069	3.5	0.167	-0.19	0.226	1.6	0.490
	140 vs. 180 g/m^2	-4.2	0.080	0.9	0.892	0.00	0.996	3.5	0.035
	160 vs. 180 g/m^2	0.1	0.999	-2.6	0.340	0.18	0.212	1.9	0.336
Bonding pressure	0.1 vs. 0.6 MPa	8.8	0.001	-14.4	0.000	-0.04	0.992	-23.1	0.000
	0.1 vs. 0.8 MPa	9.4	0.000	-29.5	0.000	0.00	1.000	-27.6	0.000
	0.1 vs. 1.0 MPa	11.6	0.000	-30.2	0.000	-0.20	0.547	-32.6	0.000
	0.6 vs. 0.8 MPa	0.6	0.993	-15.0	0.000	0.04	0.990	-4.5	0.033
	0.6 vs. 1.0 MPa	2.9	0.652	-15.7	0.000	-0.15	0.675	-9.6	0.000
	0.8 vs. 1.0 MPa	2.3	0.748	-0.7	0.989	-0.20	0.303	-5.0	0.002
Primer	un-primed vs. Primed	10.9	0.000	-24.9	0.000	-0.48	0.000	-30.1	0.000
Thickness	15 vs. 35 mm	-3.2	0.216	-5.9	0.022	0.27	0.168	-4.9	0.036

From the analysis of the ANOVA results on Table 4-2, it is found that delamination was not visibly affected by the thickness (Prob>F = 0.216, which is a high value), while the other parameters apparently had some influence on delamination as they are closer to zero. From the multiple-comparison test results, it is found that for the lower adhesive spread rate (140 g/m^2) lower delamination values are found, as shown in Figure 4-8 (notice that in the figure 'ASR' stands for adhesive spread rate). However, as can be observed in the same figure, no trend is found concerning the other spread rates (i.e. an increase of delamination with an increase of the adhesive spread rate). Regarding the bonding pressure, from the multiple comparison test results, it is found that the lower Prob>F value (0.000) obtained in the ANOVA is actually due to the lower bonding pressure (0.1 MPa) for which the p-values between the other bonding pressures are quite low (Table 4-3) regarding delamination. This aspect is also illustrated in Figure 4-9 ('BP' stands for bonding pressure). In that figure, a trend of decreasing delamination with increasing pressure is also observed, although not quite significant between the bonding pressures above 0.1 MPa. In general, for all the bonding quality parameters, the mean differences in Table 4-3 regarding delamination are not quite significant with exception of the ones between the lower bonding pressure (0.1 MPa) and the other ones (ranging from 8.8% to 11.6%), and between the un-primed and primed samples (10.9%). The effect of primer in the enhancement of the delamination results, which reaches almost zero in all tested sets, (with exception of some of the lower bonding pressure samples), is shown in Figure 4-10.
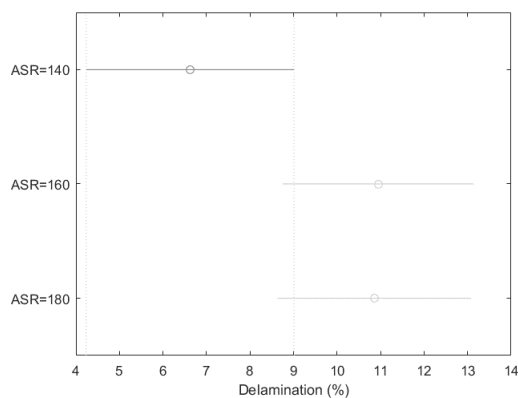
Figure 4-8 - Multiple comparison test results regarding the influence of the adhesive spread rate on delamination.
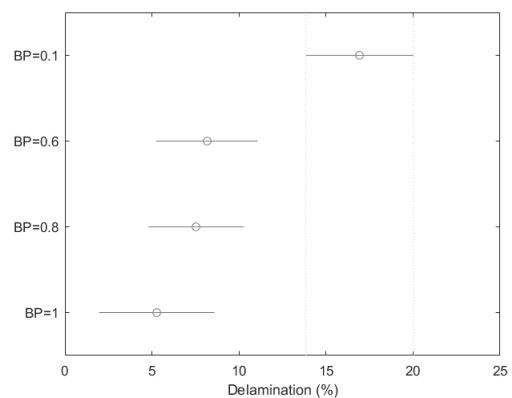
Figure 4-9 – Multiple comparison test results regarding the influence of bonding pressure on delamination.

Regarding the WF$_{delamination}$ results, from the ANOVA results, the adhesive spread rate is found to be the parameter with lower influence on results (Prob>F = 0.162), while the bonding pressure and primer (Prob>F = 0.000) are found to have influence (Table 4-2). More precisely, from the multiple comparison test, it is found that the increase of bonding pressure and use of primer enhance the WF$_{delamination}$ results (Table 4-3), which can be

observed in Figure 4-11. In Table 4-3, it is found that the mean differences between the lower and high bonding pressures (0.1 and 1.0 MPa) are about 30%; and between the un-primed and primed samples mean differences are about 25%. Although the thickness is found to have a low Prob>F value (0.023), from the multiple comparison test it is found that the mean values of $WF_{delamination}$ for the 35 mm thickness specimens are just 5.9% higher than the mean values for 15 mm thickness ones (Table 4-3), when compared to the magnitude of differences described for the bonding pressure and primer use.
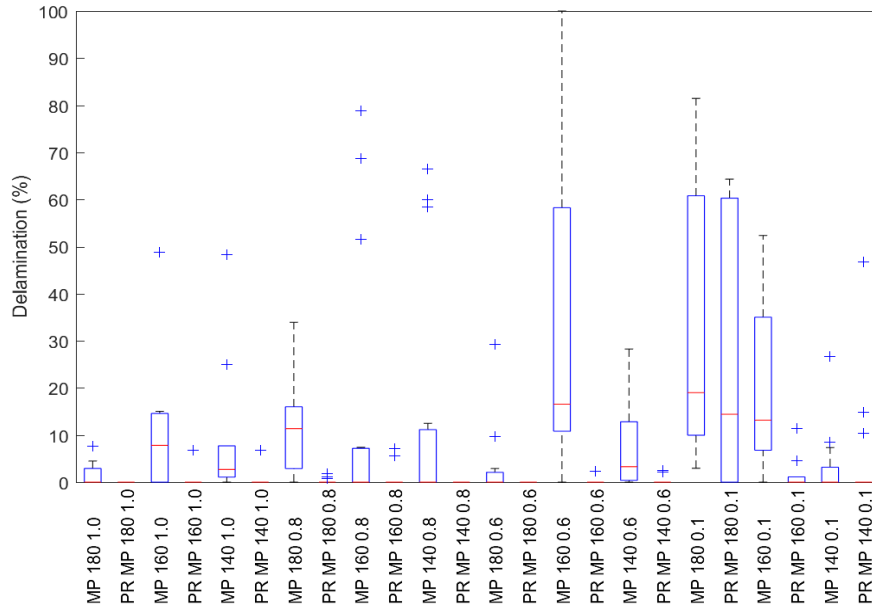
Figure 4-10 - Delamination results. Influence of pre-treatment with primer.
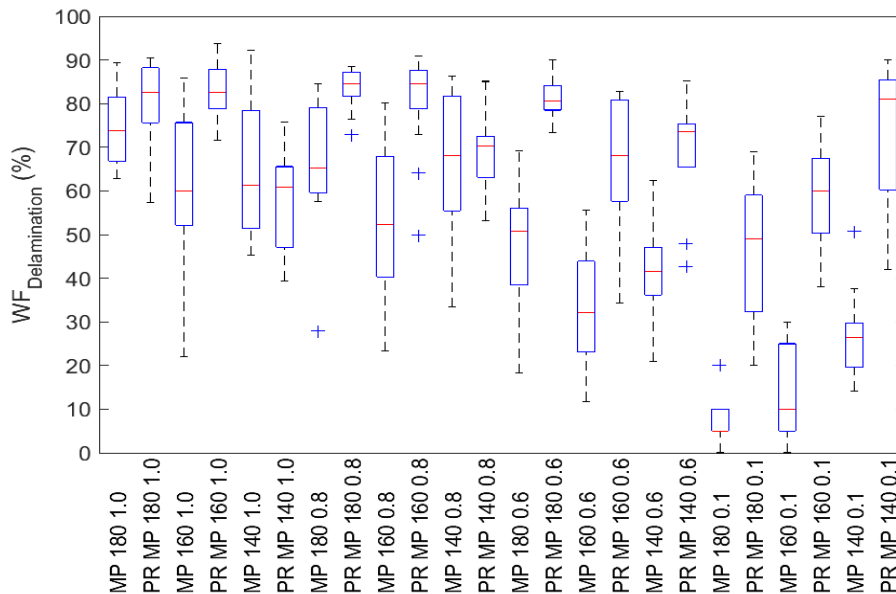
Figure 4-11 - Wood failure percentage (after delamination tests) results. Comparison of un-primed and primed specimens.

Regarding shear strength, it is found that it is essentially influenced by the primer use (Prob>F=0.000), while for the other parameters Prob>F ranged from 0.154 to 0.314. In a general way, the shear strength slightly increases due to primer application, with a mean difference of 0.48 N/mm^2 (Table 4-3). This tendency can be observed in the distribution of shear strength between un-primed and primed samples shown in Figure 4-12.
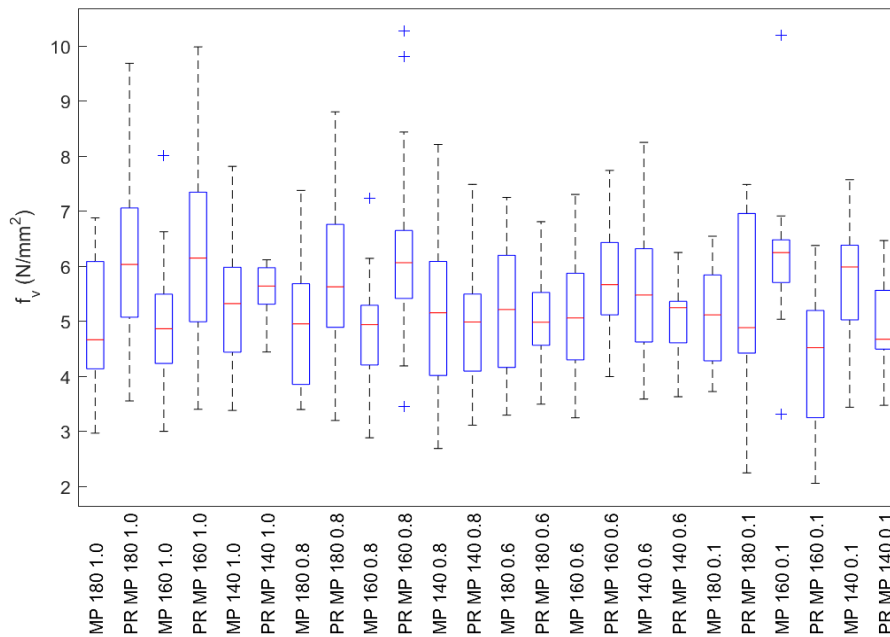
Figure 4-12 – Shear strength results. Comparison of un-primed and primed specimens.

In respect to WF$_{shear}$, from the ANOVA tests results, it seems that all the tested parameters had some influence as the Prob>F values, ranging from 0.000 to 0.045, are close to zero (Table 4-2). From a more detailed analysis using the multiple comparison test, it is found that the decrease on the adhesive spread rate, increase of bonding pressure, use of primer and increase of thickness would all increase WF$_{shear}$: for the adhesive spread rate the differences between group means (all positive values) are 3.5% (between 140 and 180 g/m^2), for the bonding pressure (all negative values) are -32.6% (between 0.1 and 1.0 MPa), for the primer use - 30.1% and for the thickness - 4.9% (Table 4-3). The comparison of those values shows that the use of primer and increase of bonding pressure are actually the most effective ways to enhance the WF$_{shear}$ results. The distribution of the wood failure percentage after the shear strength tests between the un-primed and primed samples is shown in Figure 4-13. It should be noticed that although the increase on the adhesive spread rate is found to slightly increase the WF$_{shear}$ results, such influence is very low (3.5 %) taking into account the scatter of the experimental data. Furthermore, observing Figure 4-13, it seems that 'MP 180 0.8' sample is out of trend. Excluding the referred sample from the input data of the ANOVA test, a Prob>F value of 0.435 is

obtained regarding the influence of the adhesive spread rate (the former was 0.045). Such result confirms the negligible influence of the adhesive spread rate on the WF_{shear} results.
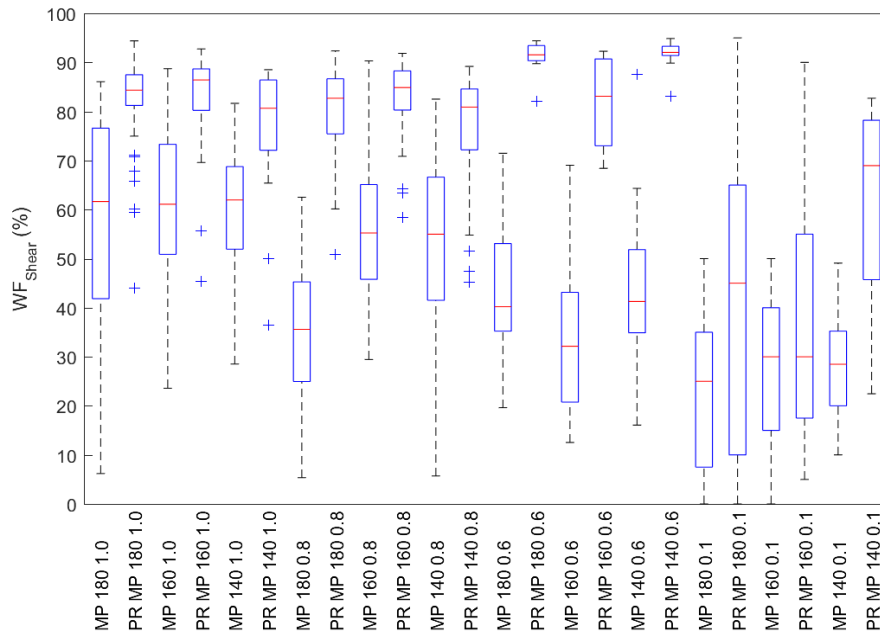
Figure 4-13 - Wood failure percentage (after shear tests) results. Influence of pre-treatment with primer.

From the analysis of Figure 4-13, a higher scatter is observed in the WF_{shear} results regarding the 0.1 MPa samples in comparison to the other samples. The same is also observed for the delamination results (Figure 4-10). The presence of wanes in lamellas, although slight, was pointed as the probable cause for such scattering. During the specimens' preparation, after cutting some shear specimens of the 0.1 MPa series from the beam elements, it was possible to clearly identify regions (within the same specimen) with different glue line thickness (Figure 4-14). That observation suggests that wanes, although slight, were present in the lamellas, allowing for some regions to have an excessively thick glue line due do the low pressure applied. It should be noticed, however, that such wanes should be present in all the tested series, including the ones produced with higher pressures, but in those cases the pressure level most likely has compensated the wanes. It should also be noticed that no surface irregularities were visually detected in the lamellas after planning and before bonding.

In sum, from the tests on Maritime pine specimens, the use of primer was found to be the parameter that most influences all the bonding quality indicators, with clear benefits resulting from its application. Such result is much in line with the findings of Luedtke et al (2015) for hardwood glulam and Lu et al (2018) for Eucalyptus CLT. The increase of bonding pressure was also found to enhance the performance of the bonding quality

indicators except for shear strength. The observed influence of bonding pressure on wood failure percentage and shear strength agrees with the findings from previous studies (Sikora et al, 2016; Knorz et al, 2017; Liao et al, 2017; Wang et al, 2018). Regarding the layer thickness, no clear influence was found regarding the delamination and shear strength. This is in line with the findings of Knorz et al (2017), who also reported no influence of the layer thickness on delamination for CLT spruce (*Picea abies* L.). Some influence was found in the wood failure percentages after both delamination and shear tests, with the thicker specimens performing better; however, the magnitude of the differences between samples when considering different thickness was much lower in comparison with the other tested parameters. Concerning the adhesive spread rate, it was found to be the less influent parameter on the bonding quality indicators.

Figure 4-14 – Aspect of glue line' thickness in one of the shear specimens produced with a bonding pressure of 0.1 MPa.

4.2.4.2 Analysis of the delamination and shear test results for the mixed species specimens

The results of the ANOVA and the multi comparison tests for the mixed Maritime pine/Australian blackwood samples are shown in Table 4-4 and Table 4-5.

From the analysis of Table 4-4, it is found that neither the adhesive spread rate (Prob>F=0.237) nor the bonding pressure (Prob>F=0.160) influenced the delamination results.

Regarding the $WF_{delamination}$ results, those were not influenced by the adhesive spread rate (Prob>F=0.779), but bonding pressure was found to enhance the results (Prob>F=0.000) - an increase on that parameter led to an enhancement of the results (mean difference of 24.9 %, Table 4-5).

Concerning shear strength, it was found to not be particularly affected by the bonding pressure (Prob>F=0.244), but by the adhesive spread rate (Prob>F=0.000). Looking at Table 4-5, a slight increase in performance is found for the lower rate of 140 g/m^2

compared to the other ones; however, no trend is found regarding the other spread rates (i.e. an increase of shear strength with a decrease of adhesive spread rate).

Table 4-4 - ANOVA results for the mixed Maritime pine/ Australian blackwood specimens.

	Source	Sum Sq.	d.f.	Mean Sq.	F	Prob>F
Delamination	Adhesive Spread Rate	268.2	2	134.1	1.470	0.237
	Bonding Pressure	184.0	1	184.0	2.010	0.160
	Error	6758.1	74	91.3	-	-
	Total	7220.8	77	-	-	-
WF Delamination	Adhesive Spread Rate	200.1	2	100.0	0.250	0.779
	Bonding Pressure	11844.6	1	11844.6	29.750	0.000
	Error	29466.2	74	398.2	-	-
	Total	41488.7	77	-	-	-
Shear	Adhesive Spread Rate	22.0	2	11.0	8.780	0.000
	Bonding Pressure	1.7	1	1.7	1.370	0.244
	Error	179.2	143	1.3	-	-
	Total	207.3	146	-	-	-
WF Shear	Adhesive Spread Rate	6297.3	2	3148.6	7.500	0.001
	Bonding Pressure	14843.4	1	14843.4	35.370	0.000
	Error	60017.7	143	419.7	-	-
	Total	77565.7	146	-	-	-

Table 4-5 - Multiple comparison test results for the mixed Maritime pine/ Australian blackwood specimens.

		Delamination (%)		$WF_{Delamination}$ (%)		Shear (N/mm^2)		WF_{Shear} (%)	
		Mean dif.	p-value	Mean dif.	p-value	Mean dif.	p-value	Mean dif.	p-value
Adhesive spread rate	140 vs. 160 g/m^2	-4.2	0.254	0.7	0.991	0.94	0.000	15.1	0.001
	140 vs. 180 g/m^2	-0.7	0.964	-3.0	0.851	0.63	0.016	12.6	0.007
	160 vs. 180 g/m^2	3.5	0.379	-3.7	0.783	-0.31	0.368	-2.5	0.828
Bonding pressure	0.1 vs. 0.6 MPa	3.1	0.160	-24.9	0.000	0.22	0.242	-20.7	0.000

The WF_{shear} results were found to be influenced by both the adhesive spread rate (Prob>F=0.001) and the bonding pressure (Prob>F=0.000). However, the influence of the adhesive spread rate, as occurred for the shear strength results, is not clear; indeed, a slight increase in performance is found for the lower rate of 140 g/m^2, but no clear trend is found regarding the other spread rates.

4.2.4.3 Fulfilment of EN 16351 requirements

The fulfilment of EN 16351 requirements for delamination and shear results are described and analysed in this sub-section.

The percentage of specimens that fulfilled the delamination criteria (D_{max} and D_{tot}) are presented in Table 4-6; the percentage that fulfilled the wood failure after delamination criteria ($WF_{glue\ line}$ and $WF_{tot,glue\ line}$) are presented in Table 4-7; the percentage that failed the $WF_{tot,glue\ line}$ criteria after failing D_{tot} criteria are presented in Table 4-8, and the characteristic values of shear strength are presented in Table 4-9.

Regarding the delamination criteria (Table 4-6), it is found that for the un-primed samples and for the higher adhesive spread rate, the D_{max} criteria is always fulfilled, while the most demanding criteria (D_{tot}) is only fulfilled for the higher bonding pressure and adhesive spread rate combination considered ('180 1.0'). In the works available in the literature, few specimens fulfilled such criteria: in (Sikora et al, 2016) both D_{tot} and D_{max} limits were never fulfilled; in (Knorz et al, 2017) about 44% of the samples failed D_{tot} and 15% failed D_{max}, with a total of 46% failing both limits; in (Betti et al, 2016) D_{max} was always fulfilled but D_{tot} failed in few specimens with 40 x 40 mm^2 and in more than half of the specimens with 75 x 75 mm^2 (however, it should be noticed that those were not the standard dimensions of specimens according to EN 16351). It should be noticed that in the referred works, the number of layers was odd and ranged from three to seven, while in the present work two-layer specimens were tested. In contrast, for the primed samples, looking at Table 4-6, D_{tot} was never exceeded for all the samples, an exception being made to 10% of the 'MP - PR - 35mm 0.6 MPa' sample and to the lower bonding pressure samples (0.1 MPa) for both layer thickness. Although some of the specimens of the 'MP - PR - 35mm 0.6 MPa' sample failed the wood failure percentage limits (Table 4-7), the specimens that did not fulfil the delamination criteria, fulfils the WF criteria, as seen in Table 4-8. The same did not happen for the 0.1 MPa samples, where only the 'MP+AB 140 0.1' one entirely fulfils such criteria (Table 4-8).

For the WF_{delam} criteria, it is found that the results are not consistent with the delamination ones: although some specimens fulfilled the delamination criteria, they failed the WF_{delam} requirements and vice-versa. Moreover, looking at Table 4-8, in the case of the primed specimens, apart from all the MP 0.1 MPa samples and the 160 and 180 g/m^2 MP+AB 0.1 MPa samples, none of the samples failed both criteria. This leads to question if maybe the opening method of the glue lines (with metal edge and hammer) is adequate, as it may possibly introduce additional damage at the glue line other than that caused by the delamination test itself. This potential situation has also been reported by Betti et al (2016).

Regarding the fulfilment of the minimum values for the shear strength, none of the specimens has a strength lower than 1.00 MPa and the characteristic value of all samples (Table 4-9) is well above the minimum of 1.25 MPa required by EN 16351. The minimum characteristic value obtained was 2.02 MPa for the 'MP+PR 160 0.1' sample. No correlation was found between delamination and shear tests, as all specimens fulfilled the shear criteria, but not all complied with the delamination requirements; this observation is in line with the work of Betti et al (2016).

As stated before, only for the higher pressure and higher adhesive spread rate combination ('MP 180 1.0') it was possible to fulfil all EN 16351 requirements regarding delamination without using primer. In contrast, when using primer, for both MP and MP + AB samples, the lower pressure and the lower adhesive spread rate recommended by the adhesive manufacturer (´140 0.6´) allowed complying with the minimum standard requirements. Regarding the lower pressure considered (0.1 MPa), although one of the mixed samples (MP+AB 140 0.1) fulfilled the referred criteria, some of the specimens composing the other samples failed the standard requirements. The worst results obtained, especially, from the delamination test (accelerated ageing) for the lower bonding pressure (0.1 MPa), shows that using such low pressure level for manufacturing is not adequate if the panels are to be exposed to severe ageing factors (e.g. moisture content variation). The minimum bonding pressure of 0.6 MPa, thus prevents the possibility of bonding the entire CIT panel at once, as it exceeds the bonding pressure defined for adhesion between the PUR foam and the wood layers (0.1 MPa).

The observations made above indicate two possible ways for cross glueing Maritime pine, which may be used depending on the manufacturing costs and conditions: (i) using higher bonding pressure (1.0 MPa) and higher adhesive spread rate (180 g/m^2) with lower press time (200 min); or (ii) using lower bonding pressure (0.6 MPa) and lower adhesive spread rate (140 g/m^2), but with pre-application of primer (20 g/m^2) and double of the press time (400 min).

Table 4-6 – Fulfilment of delamination limits for the different test series.

Spread rate (g/m²)		180				160				140			
Pressure (MPa)		1	0.8	0.6	0.1	1	0.8	0.6	0.1	1	0.8	0.6	0.1
$D_{max} < 40\%$ (% pass)	MP	100.0	100.0	100.0	66.7	90.0	80.0	60.0	77.8	90.0	80.0	100.0	100.0
	MP - PR	100.0	100.0	100.0	55.6	100.0	100.0	100.0	100.0	100.0	100.0	100.0	93.3
	MP - PR - 35mm	-	-	100.0	50.0	-	-	100.0	92.3	-	-	100.0	84.6
	MP + AB - PR	-	-	100.0	100.0	-	-	100.0	93.3	-	-	100.0	100.0
$D_{tot} < 10\%$ (% pass)	MP	100.0	50.0	93.3	22.2	70.0	80.0	20.0	33.3	80.0	73.3	73.3	93.3
	MP - PR	100.0	100.0	100.0	33.3	100.0	100.0	100.0	88.9	100.0	100.0	100.0	80.0
	MP - PR - 35mm	-	-	90.0	16.7	-	-	100.0	84.6	-	-	100.0	61.5
	MP + AB - PR	-	-	100.0	93.3	-	-	100.0	86.7	-	-	100.0	100.0

Table 4-7 - Fulfilment of wood failure percentage limits after delamination tests for the different test series.

Spread rate (g/m²)		180				160				140			
Pressure (MPa)		1	0.8	0.6	0.1	1	0.8	0.6	0.1	1	0.8	0.6	0.1
$WF_{glue\ line} > 50\%$ (% pass)	MP	100.0	90.0	53.3	0.0	80.0	60.0	13.3	0.0	80.0	80.0	13.3	6.7
	MP - PR	100.0	100.0	100.0	44.4	100.0	96.7	90.0	77.8	70.0	100.0	80.0	93.3
	MP - PR - 35mm	-	-	100.0	33.3	-	-	100.0	69.2	-	-	100.0	76.9
	MP + AB - PR	-	-	90.9	33.3	-	-	90.9	26.7	-	-	66.7	35.7
$WF_{tot,glue\ line} > 70\%$ (% pass)	MP	66.7	40.0	0.0	0.0	30.0	20.0	0.0	0.0	40.0	46.7	0.0	0.0
	MP - PR	83.3	100.0	100.0	0.0	100.0	93.3	50.0	22.2	10.0	53.3	70.0	73.3
	MP - PR - 35mm	-	-	60.0	16.7	-	-	50.0	46.2	-	-	90.0	69.2
	MP + AB - PR	-	-	54.5	13.3	-	-	54.5	0.0	-	-	33.3	14.3

Pedro Gil Girão dos Santos

Table 4-8 – Percentage of specimens that failed wood failure percentage limits after failing delamination limits.

Spread rate (g/m^2)		180				160				140			
Pressure (MPa)		1	0.8	0.6	0.1	1	0.8	0.6	0.1	1	0.8	0.6	0.1
D_{tot} & $WF_{tot,glue\ line}$ (% fail)	MP	0.0	50.0	6.7	77.8	30.0	20.0	80.0	66.7	20.0	26.7	26.7	6.7
	MP - PR	0.0	0.0	0.0	6.0	0.0	0.0	0.0	1.0	0.0	0.0	0.0	1.0
	MP - PR - 35mm	-	-	0.0	5.0	-	-	0.0	1.0	-	-	0.0	2.0
	MP + AB - PR	-	-	0.0	1.0	-	-	0.0	2.0	-	-	0.0	0.0

Table 4-9 – Characteristic value of shear strength for the different test series.

Spread rate (g/m^2)		180				160				140			
Pressure (MPa)		1	0.8	0.6	0.1	1	0.8	0.6	0.1	1	0.8	0.6	0.1
$f_{v,k}$ (N/mm^2)	MP	3.18	3.20	3.37	3.40	3.29	3.08	3.35	3.59	3.59	2.96	3.57	3.97
	MP - PR	3.83	3.67	3.32	2.54	3.61	4.22	3.88	2.02	4.67	3.29	3.67	3.47
	MP - PR - 35mm	-	-	3.39	2.72	-	-	2.75	3.94	-	-	3.72	4.61
	MP + AB - PR	-	-	4.03	3.72	-	-	3.99	3.61	-	-	3.45	4.53

4.3 Adhesion between wood elements - Finger-joint connections between Maritime pine lamellas

The finger-joint connection consists of an interlocking end joint formed by machining a number of similar, tapered, symmetrical fingers in the ends of timber components, which are formed by a finger joint cutter and then bonded together (CEN, 2015). This geometry enables an efficient connection due to the maximized bonded area and minimized timber volume loss. The finger-joints can be edgewise, which is common in glued-laminated timber (GLT), or flatwise (Figure 4-15).
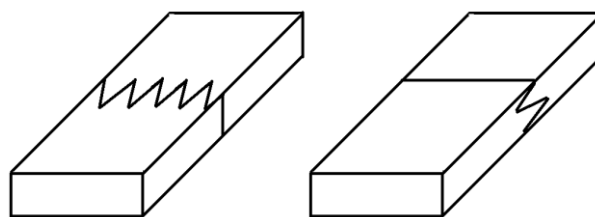
Figure 4-15 – Edgewise (left) and Flatwise (right) finger-joints.

4.3.1 Materials, specimen preparation, and experimental procedures

EN 16351 (CEN, 2015) provides some information regarding the finger-joint connections to be used in the laminations of cross-laminated timber panels. The basic parameters defining the geometry of a finger-joint are shown in Figure 4-16.
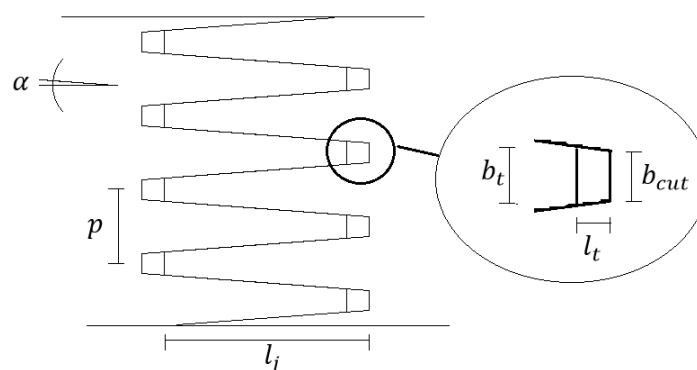
Figure 4-16 – Geometry of a finger-joint: l_j – finger length; l_t – tip gap; p – pitch; b_t – tip width; b_{cut} – tip width of the cutter. Adapted from (CEN, 2015).

EN 16351 recommends the following geometrical relation $1.1 \leq b_t/b_{cut} \leq 1.2$ and imposes the following ones: $l_j \geq 10$ mm; $0.01 \leq l_t/l_j \leq 0.08$; $b_t/p \leq 0.18$; $l_j \geq 4p(1 - 2\,b_t/p)$; $\alpha \leq 7.1°$. Although information related to the geometry is provided in

the standard, nothing is referred about the manufacturing process itself, namely regarding the magnitude and time of pressure applied to join the two profiled sections.

A set of 20 finger-joints on Maritime pine were manufactured by a sawmill factory at Soure, Portugal, but due to technical limitations of the manufacturing machine, it was not possible to know the value of the pressure applied during the manufacturing or even control the tip gap. Consequently, some variations were found in the produced specimens, with some having a very short tip gap (~ 0 mm), while others showed a considerable one (~ 1 mm). Due to the above-mentioned limitations, it was not possible to enhance the quality of manufacturing of the finger-joints, and consequently their performance. The overall dimensions of the manufactured finger-joint were thus: l_j+l_t= 20 + (0 to 1 mm); p= 6 mm; b_t= 1 mm.

Maritime pine timber from the strength class C24 (according to EN 338 (CEN, 2009)) was used to produce the test specimens. The same adhesive used for the face bonding (Loctite Purbond HS709) was used for the finger-joint connections. The finished lamellas (after finger-jointing and trimming) had a thickness of 35 mm, width of 140 mm and length of 700 mm. The manufactured specimens were tested in four-point bending in accordance with EN 408 (CEN, 2012a) to determine the modulus of elasticity and the bending strength (Figure 4-17).

a)   b)
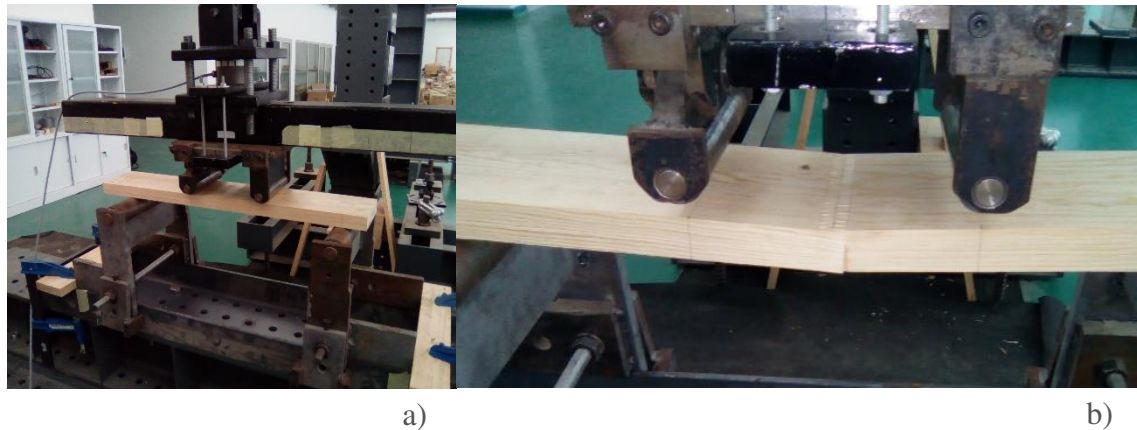
Figure 4-17 - Bending tests of finger-joint connections: a) setup; b) failure.

The modulus of elasticity (E) was determined from the global deflection (i.e. at mid-span) following Equation (4-5),

$$E = \frac{3al^2 - 4a^3}{2bh^3 \left(2\dfrac{w_2 - w_1}{F_2 - F_1} - \dfrac{6a}{5Gbh} \right)}$$
(4-5)

where: a – distance between a support and the closest loading point; b – width of the

cross-section; h – depth of the cross-section; G – shear modulus; F applied force, and w – global deflection. The indexes 1 and 2 correspond to the extreme points of the longest portion of the force *vs*. deflection linear regression for which it is possible to obtain a correlation coefficient of at least 0.99. In these calculations, the shear modulus was taken as 1210 N/mm^2 based on the information from Chapter 3.

The bending strength (f_m) was determined in accordance to Equation (4-6),

$$f_m = \frac{3F_{max}a}{bh^2}$$

(4-6)

where: F_{max} – maximum applied force.

4.3.2 Results

The mean and standard-deviation values for the modulus of elasticity and bending strength are presented in Table 4-10. The distribution of the modulus of elasticity and bending strength are presented in Figures 4-18 and 4-19.

Table 4-10 – Mean ($\bar{x}$) and standard-deviation (σ) values for the modulus of elasticity and bending strength obtained on the bending tests of finger-joint connections.

	E (N/mm^2)	f_m (N/mm^2)
$\bar{x}$	11202	41.7
σ	1602	8.0
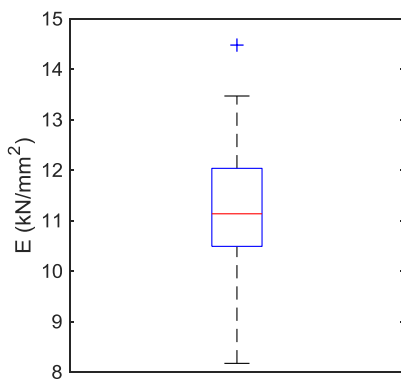
Figure 4-18 – Modulus of elasticity distribution from the tests on finger-joint.
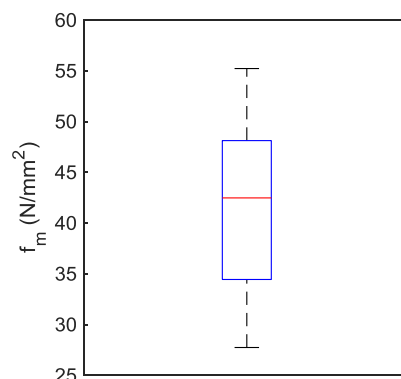
Figure 4-19 – Bending strength distribution from the tests on finger-joint.

The bending strength values obtained are all higher than the characteristic value of 24 N/mm^2 for C24 class, which means that the tested joints could be used to produce C24

lamellas (according to strength class standard EN 338). Despite this, the mean values of the modulus of elasticity (11202 N/mm^2) and bending strength (41.7 N/mm^2) are low when compared with the values obtained by (Balsa, 2013) for Maritime pine solid wood beams, respectively 15395 N/mm^2 and 59.0 N/mm^2. This is in accordance with the failure modes observed in the bending tests that include total or partial delamination at the finger-joint interface, with none of the specimens having presented total failure in wood. From the total sample, in 8 of the specimens the failure was mostly due to delamination at the finger (Mode I) (Figure 4-20 a)), while in 12 specimens a combined failure at wood and delamination at finger-joint (Mode II) was observed (Figure 4-20 b)).
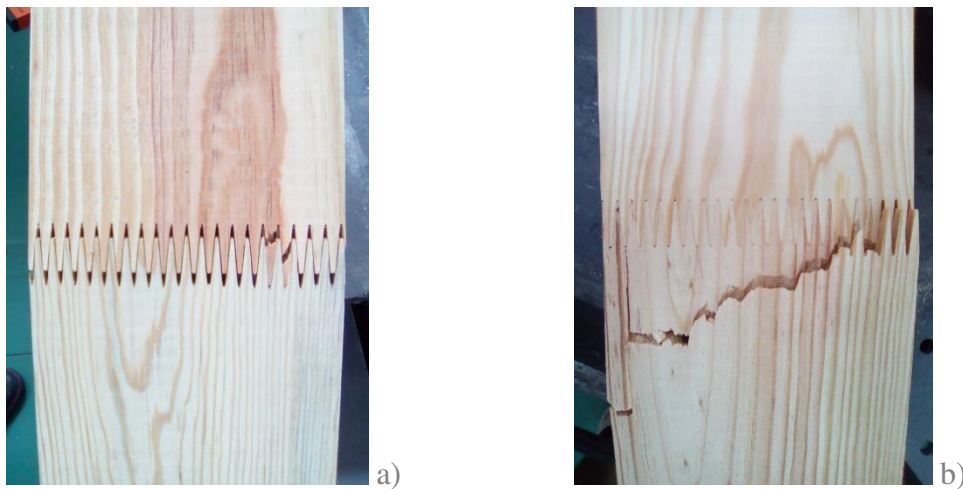
Figure 4-20 – Failures observed at the finger-joint tests: a) delamination at the finger-joint; b) combined failure at wood and delamination at finger-joint.

Furthermore, the square correlation between the bending strength value and the corresponding failure mode (values of 1 attributed to Mode I and 2 to Mode II) in Table 4-10 is 0.51, which confirms the observations made above: the lowest bending strength values correspond to specimens where failure was caused mostly by delamination at the finger-joint rather than wood fibre rupture. As expected, no correlation was found between the modulus of elasticity and the failure mode (R^2=0.00). It is also interesting to observe that some of the specimens in which Mode I failure occurred, although having a lower ultimate load, showed a slightly non-linear behaviour (attributed to the progressive delamination at the finger-joint) at the end of the bending test (Figure 4-21 a)). This behaviour was different from that of specimens where Mode II failure occurred, which presented a higher ultimate load and a brittle failure (Figure 4-21 b)).

a)
b)
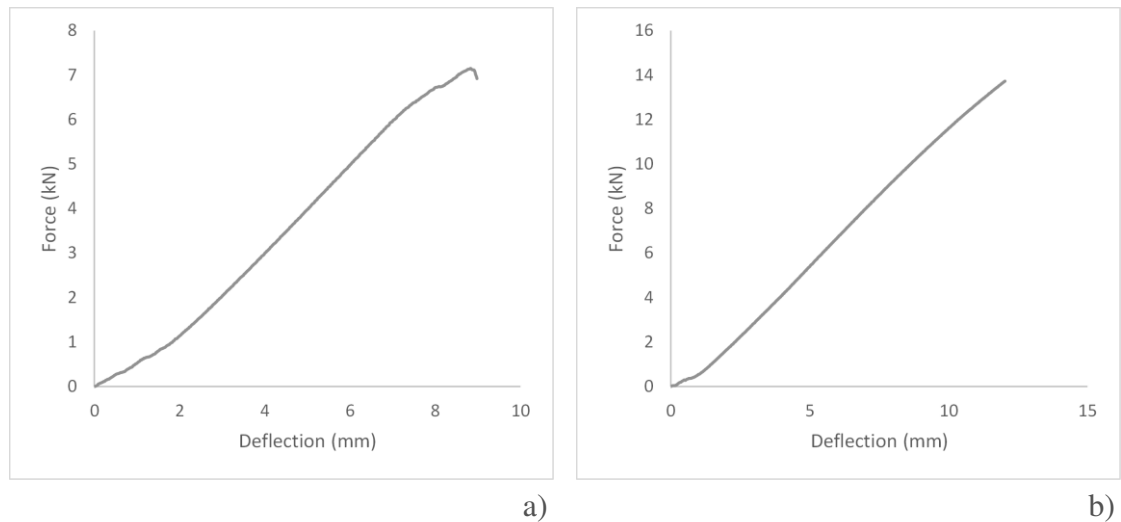
Figure 4-21 - Load-deflection curve of a specimen with failure caused by: a) delamination at the finger-joint interface; b) combined delamination and wood rupture at the finger-joint interface.

4.4 Adhesion between wood and polyurethane layers

The adhesion between the wood and polyurethane layers was assessed in a similar way to what was described before for the wood layers, *i.e.* by performing (i) short-term tests to obtain the initial strength and check the failure mode, and (ii) long-term tests to account for durability.

Durability was assessed by means of accelerated ageing, namely by determining the loss of strength/adhesion compared to the short-term tests.

The initial strength was assessed through tensile tests, as preconized in ETAG 016-2 (EOTA, 2003b), in a similar way to what was done for the material characterization. Although no correlation between shear and tensile strength was found in the bibliography, it was assumed that if the tensile adhesion between the wood and polyurethane layers was adequate, the same would happen for shear loading. The durability performance was checked by performing a previous ageing cycle on the specimens to be tested in tension. Both in terms of short- and long-term tests, the adhesion is found to be enough if a certain level of strength is achieved and if the failure mode of the specimens does not occur at the bond line, but rather at the materials that are connected (wood and polyurethane).

ETAG 016-2 (EOTA, 2003b) defines temperature as the degrading agent for the durability test of sandwich panels with a polyurethane foam core, either injected or bonded. It should be noted that the standard does not mention a reference period (i.e. real

conditions) to which the accelerated ageing results can be extrapolated. The test (defined in the standard as test cycle 1) consists of subjecting the test specimens to a constant temperature of 90 ℃ and relative humidity (RH) not greater than 15% for at least 24 weeks. The referred test cycle is actually based on metal-faced sandwich panels standard EN 14509 (CEN, 2013), which establishes three possible temperatures: 65, 75 and 90 ℃, as a function of the colour of the faces (the lowest temperature applies to lighter faces). For other types of core materials, other test cycles are proposed in ETAG 016-2 (also based on EN 14509). For mineral wool, expanded or extruded polystyrene cores, a test that consists of exposing the specimens to constant conditions of temperature (65 ℃) and relative humidity (100%) for 28 days is referred (test cycle 2). For other core materials, a cycle of 5 days at 70 ℃ and 90% RH followed by 1 day at 20 ℃ and 1 day at 90 ℃ is proposed.

Besides the test cycles defined in EN 14509, a procedure to test the durability of the adhesive bond between metal faces and prefabricated core material is presented in that standard (wedge test). The test consists of pressing a wedge between two strips made of the panels' faces (glued with the intended adhesive) that will cause an initial crack at the glue line, after which the wedge is loaded along the glue line and the specimen is immersed for 24 h in water heated to 70 °C, after which the final crack is measured. This procedure seems questionable, as only the adhesion to one of the materials (face) is being assessed; consequently, the adhesion between the adhesive and the foam material is not assessed. This test is also to be performed on metal facings with a thickness lower than 1 mm, and thus does not seem appropriate for wood-based faces.

Very few research works are found related to the durability of wood-based sandwich panels, especially with a focus on the adhesion between materials. Mateo et al (2011) performed ageing tests on sandwich panels made of two types of core materials (extruded polystyrene core bonded with polyurethane adhesive and injected polyurethane) to wood chipboard faces following the test cycle 2 of ETAG 016-2. They stated that the conditions (100% HR) were too aggressive for the tested panels which were to be applied in service class 2 of EN 1995 1-1 (CEN, 2004b), as the excessive humidification caused not only the severe degradation of the chipboard, but also the loss of cohesion of the adhesive. The first aspect, in some cases, made it impossible to perform the flatwise tension tests. It should be noticed that in service class 2, timber elements are expected to only overcome a moisture content of 20% occasionally, as the elements are to be applied protected from the direct contact with water. Estrada-Martínez et al (2015) also performed the same test cycle 2 of ETAG 016-2 on sandwich panels made of extruded polystyrene cores bonded with polyurethane adhesive to different wood-based face materials (including particleboard suitable for humid environment and solid wood). The specimens were tested in flatwise tension, a part of which after being subjected to the ageing cycle. Although

problems with degradation on the wood elements were not reported, failure at the glue line occurred in all the specimens not subjected to the ageing cycle, and thus it was not possible to conclude about the real effect of the ageing protocol on the cohesion of the adhesive layers. In both referred studies (Mateo et al, 2011 and Estrada-Martínez et al, 2015), a decrease of tensile strength was reported along the duration of the ageing tests.

The research presented in the previous paragraphs is not conclusive about the durability of the bond between wood and polyurethane adherents, namely regarding temperature being the unique degradation agent for bonded polyurethane foam cores; in fact, the humidity seems to affect the polyurethane adhesives cohesion. It is also not clear how the test cycle 2 of ETAG 016-2 may actually be suitable to assess the durability of the adhesion between materials. Therefore, a similar experiment to test cycles 2 and 3 of the same standard was defined in the present study. For that test, the guidelines of standard ISO 9142 (ISO, 2003b) addressing the selection of standard laboratory ageing conditions for testing bonded joints was followed. Additionally, the test cycle 1 of ETAG 016-2 was also considered (at least to evaluate the polyurethane degradation as a material itself, presented in Chapter 3). It was also decided to carry out an additional test protocol, the delamination test of EN 16351, which is indicated for the assessment of the bond between the wood layers.

4.4.1   Preparation of test specimens

As referred in Chapter 3, two types of adhesion systems were tested, foam-in-place and bonding of pre-manufactured materials. One- (1C) or two- (2C) component polyurethane adhesives applicable to sandwich panels were used, respectively *SikaForce 7110 L55* and *SikaForce 7710 L100 + 7010*.

For the bonding options, for both 1C and 2C systems, the following parameters, and their variations in brackets, were considered:

- Bonding pressure (0.02, 0.1 MPa);
- Adhesive spread rate (150, 250 and 350 g/m^2).

The minimum bonding pressure recommended by the manufacturer (0.02 MPa) was initially tested; however, it was found that such pressure was not enough to allow a perfect contact between the surface of the material layers during the pressing process, and thus a higher pressure of 0.1 MPa was considered. This value was defined based on the minimum flatwise strength of the polyurethane declared by the manufacturer, which was 0.19 MPa, and because it is in the linear range of the material behaviour in accordance to the results from the flatwise compression tests presented in Chapter 3. The minimum,

average and maximum values considered for the adhesive spread rate are within the range recommended by the adhesive manufacturer.

The test specimens were composed of one polyurethane layer with a thickness that varied from 60 mm to 120 mm (depending on the material available at the time) stacked between a pair of maritime pine trimmed boards (Figure 4-22).

Figure 4-22 – Example of glued polyurethane foam specimen for flatwise tension test.

It should be noticed that only one wood layer was used in each bonded face of the specimens instead of the cross-wood layers; yet, one did not expect this to affect the results, at least on the tests prior to ageing, as no severe humidity gradients would be introduced that would cause significant warping in wood. Just before bonding, pressurized air at low speed (to avoid damage in polyurethane) was used to remove the dust from the foam. As no industrial spread system was available, the glue was applied by hand using a notch trowel; to ensure the right spread rate, a weighing scale was used to measure the effective adhesive weight spread in the wood layers. The room temperature and relative humidity conditions were 20 ºC and 65% respectively, being in accordance with the recommendations of the adhesive manufacturer. The pressure was applied through a hydraulic press system (Figure 4-23) and all the periods concerned with the bonding process (assembly time and curing time) were defined according to the adhesive's manufacturer specifications. The specimens had a square top view area with a width between 90 to 120 mm.

Figure 4-23 – Manufacturing (press) of a beam from which specimens were taken from.

4.4.2 Experimental procedures

4.4.2.1 Flatwise tension test

The flatwise tension test (Figure 4-24) followed the ETAG 016-1 (EOTA, 2003a) procedure, as described in Chapter 3.

Figure 4-24 – Example of injected polyurethane foam specimen tested in flatwise tension.

4.4.2.2 Ageing tests – Cycle 1 according to ETAG 016 - 2

The cycle 1 of the ageing test of ETAG 016-2 (described in detail in chapter 3) was followed: storage of the specimens to test for 24 weeks at 90+/-2 ºC and relative humidity lower than 15%. After the ageing process, the specimens were tested in flatwise tension according to ETAG 016-1.

4.4.2.3 Ageing tests – Temperature and humidity according to ISO 9142

The guidelines of standard ISO 9142 (ISO, 2003b) related to the selection of standard laboratory ageing conditions for testing bonded joints were followed to test the bond lines between wood and polyurethane. The standard indicates a series of test conditions, each one including one or more climatic/chemical agents (including temperature and humidity), which are varied through a specific time interval (one cycle) that is repeated a certain number of times. The cycle D1 (heat and humidity) was selected, for being closest to the test conditions of cycles 2 and 3 from ETAG 016-2, as referred before. Due to limitations of the available equipment, it was not possible to achieve the maximum temperature of 55 ºC and the minimum relative humidity of 30 % defined - these values

were limited to 45 ºC and 40%, respectively. During one cycle (7 days), alternate periods of heating/drying and cooling/humidification were generated in accordance with Figures 4-25 and 4-26.
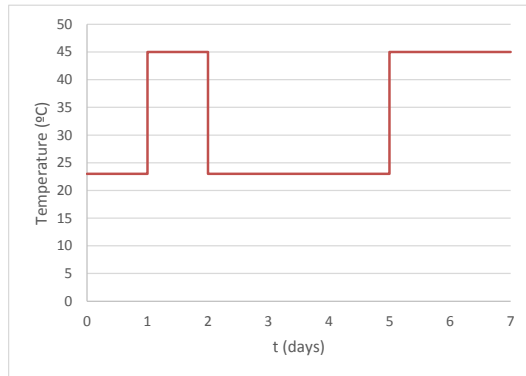
Figure 4-25 – Temperature profile imposed on test chamber during one cycle.
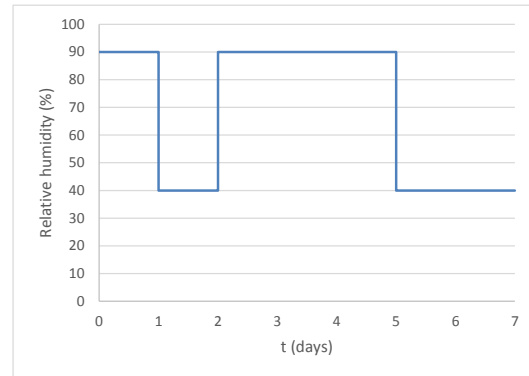
Figure 4-26 – Relative humidity profile imposed on test chamber during one cycle.

The standard does not impose a specific number of repetition cycles; it only defines a total duration of ageing exposure, from 1 to 52 weeks. To be consistent with the total duration of test cycle 1 defined in ETAG 016-1, it was decided to repeat the cycle 24 times, leading to a total test period of 24 weeks.

It should be noticed that before and after the ageing process, the specimens were conditioned for 24 h at 20 ºC and 65% HR. The ageing process was performed in a climatic chamber ARALAB FitoClima 12000 Pharma (Figure 4-27).

Figure 4-27 – Ageing of the specimens in the climatic chamber.

After the ageing process, tensile tests in accordance with ETAG 016 were performed. It

should be mentioned that the glue lines were examined after the ageing test, to identify possible delaminations that might have occurred.

4.4.2.4 Ageing tests – Delamination test according to EN 16351

The delamination tests were performed following EN 16351, following the procedure described before (cf. section 4.2.3.4). All the specimens had an inner foam element with 60 mm of thickness and two 15 mm thick wood elements (overall height of 90 mm), with a cross-section of 90x90 mm^2 (Figure 4-28).

Figure 4-28 – Specimens prepared for the delamination test.

4.4.3 Results and discussion

In this section, the results of the unaged and aged bonded wood/polyurethane specimens are presented and discussed.

4.4.3.1 Flatwise tension test

The failure modes of the polyurethane injected specimens all involved failure at the interface between the foam and the wood layers (Figure 4-29).

As a consequence of such type of failure, the (interface) tensile strength obtained in the test was in general much lower than the one obtained for the foam specimens tested in tension, whose results are presented in Chapter 3 and where failure occurred in the bulk of the core material (Figure 4-30).

It should be noticed that the chemical system of the polyurethane used was not the one recommended by the chemical company, which may explain the poor adhesion between

the materials. Due to this poor performance in terms of adhesion in an unaged condition, it was decided not to perform ageing tests for this system. Moreover, and for the same reason, it was decided to abandon this type of adhesion system for the development of the panels.

Figure 4-29 - Failure mode in a specimen produced with the injected foam technique: a) delamination at the wood/polyurethane interface; b) aspect of the interface.
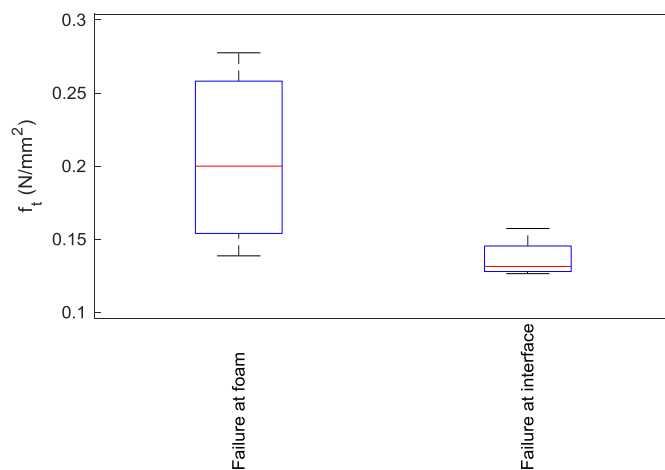
Figure 4-30 – Comparison between the tensile strength of the foam (left) and the tensile strength of the interface of specimens composed of foam injected between wood (right).

Concerning the pre-manufactured foam tests, the specimens manufactured with the lowest pressure recommended by the adhesive manufacturer (0.02 MPa), with both 1C

and 2C systems, showed mixed failures, i.e. with failure at the foam but also at the glue line (Figure 4-31).
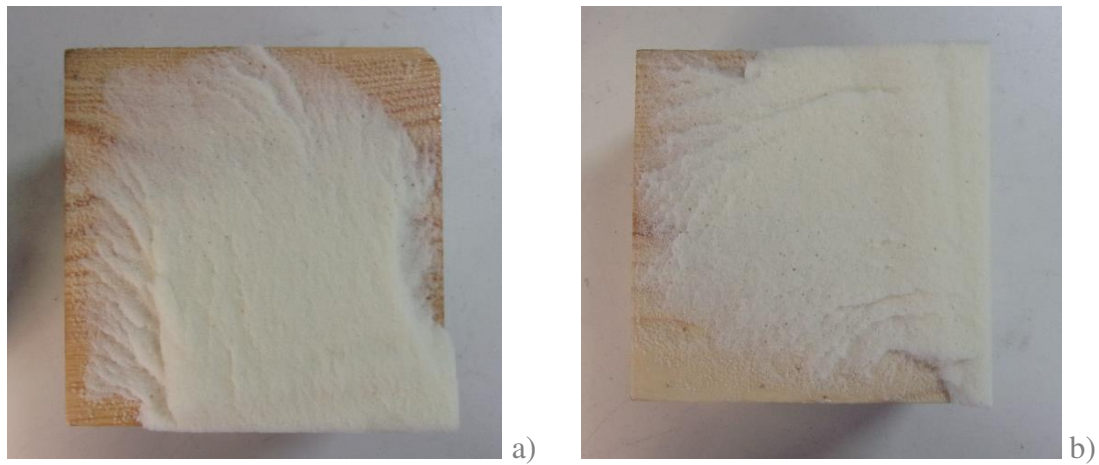
Figure 4-31 - Partial failure at the glue line observed in specimens bonded with a bonding pressure of 0.02 MPa: a) with 1C PUR adhesive; b) with 2C PUR adhesive.
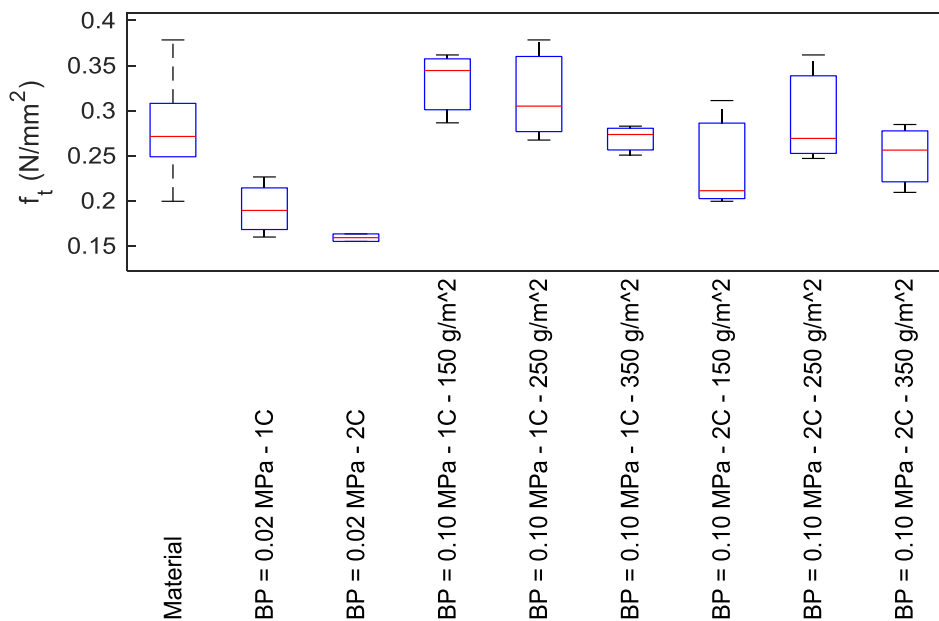
Figure 4-32 – Comparison between the tensile strength from the foam material with the glued specimens.

As shown in Figure 4-32, the tensile strength values for the lower bonding pressure (0.02 MPa) are much lower than the tensile strength of the foam as measured in the material characterization tests, which is in line with the failure modes observed. For the specimens produced with higher bonding pressure, both 1C and 2C specimens showed a similar range of values in comparison with the foam's tensile strength. This is in line with

the failure modes observed in the wood-PUR specimens, which occurred precisely within the foam (Figure 4-33).
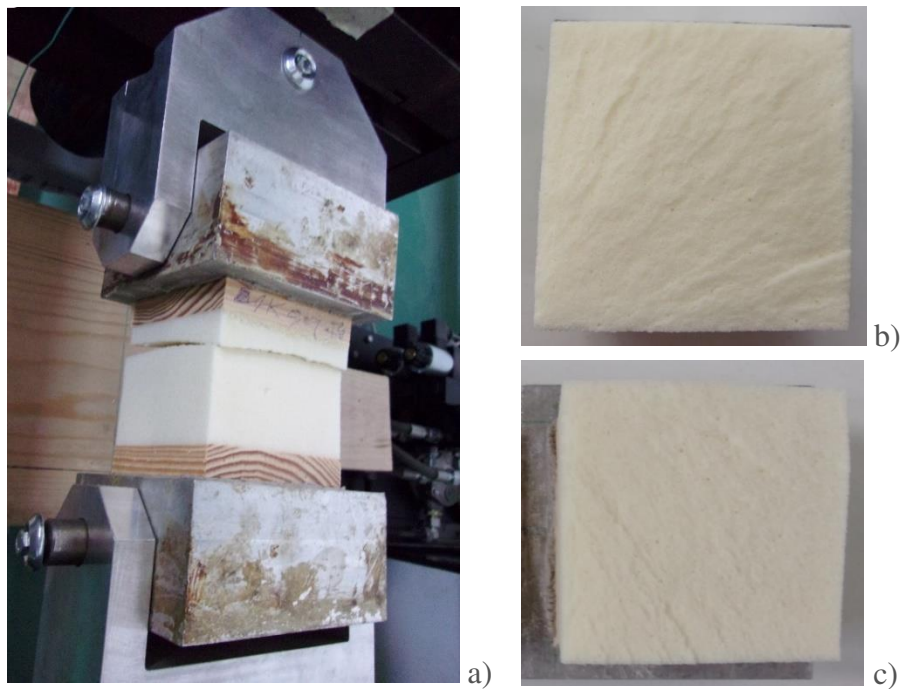
Figure 4-33 – Aspects of failure on the specimens bonded with a pressure of 0.10 MPa: a) failure at the foam in a 1C bonded specimen. Total failure at the foam in a: b) 1C specimen; 2C specimen.

It should be noted that some of the specimens failed apparently at the glue line (Figure 4-34 a)); however, a more careful inspection of the specimens allowed to verify that the failure was actually within the foam, with a thin layer of foam being visible (Figure 4-34 b)). This type of failure had occurred due to the stretching of the cross-section on some specimens, which was caused by the bending of the saw during the cutting of the specimens.
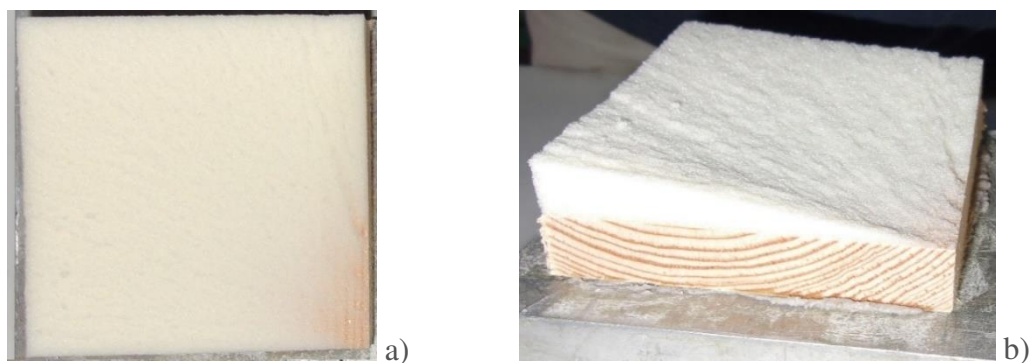
Figure 4-34 – Details of the failure in some of the bonded specimens: a) apparent failure of a specimen at glue line; b) detail of the failure that occurred close to the glue line, but where a thin layer of foam is still visible.

Although it was expected that the type of adhesive or the adhesive spread rate had no particular effect on the tensile strength (as the failure occurred within the foam), the Analysis of Variance (ANOVA) method was applied and the results obtained from such analysis are summarized in Table 4-11.

Table 4-11 – ANOVA results for the influence of adhesive type and spread rate on the tensile strength.

	Source	Sum Sq.	d.f.	Mean Sq.	F	Prob>F
Tensile strength	Adhesive Type	0.482	1	0.482	0.920	0.354
	Adhesive Spread Rate	1.108	2	0.554	1.050	0.375
	Error	7.359	14	0.526	-	-
	Total	8.949	17	-	-	-

As expected, the high values of Prob>F for both adhesive type and adhesive spread rate indicate that they have no significant influence on the tensile strength.

4.4.3.2 Ageing tests – Cycle 1 according to ETAG 016 – 2

The failure mode that occurred on the tensile tests after the ageing process was the failure within the foam material (Figure 4-35) for the 1C specimens. However, in some 2C specimens, a failure with some extension to the glue line was observed in the majority of specimens (Figure 4-36).

Figure 4-35 – Total failure at the foam observed in a specimen bonded with 1C PUR adhesive subjected to temperature ageing test.

Figure 4-36 – Partial failure at the foam observed in a specimen bonded with 2C PUR adhesive subjected to temperature ageing test.

The relative area where the failure at the glue line occurred with respect to the total area was determined to the nearest 5% by visual inspection. From all the specimens, a mean value of 14.4% with a standard-deviation of 11.2% was determined. No correlation between the area and the tensile strength (R^2=0.13), modulus of elasticity (R^2=0.34) or adhesive spread rate (R^2=0.10) was found as relevant.

The comparison between the tensile strength of the unaged and the aged (AG), according to cycle 1 of ETAG 016-2, specimens for the different adhesives (1C and 2C) and spread rates (150, 250 and 350 g/m^2) is shown in Figure 4-37.
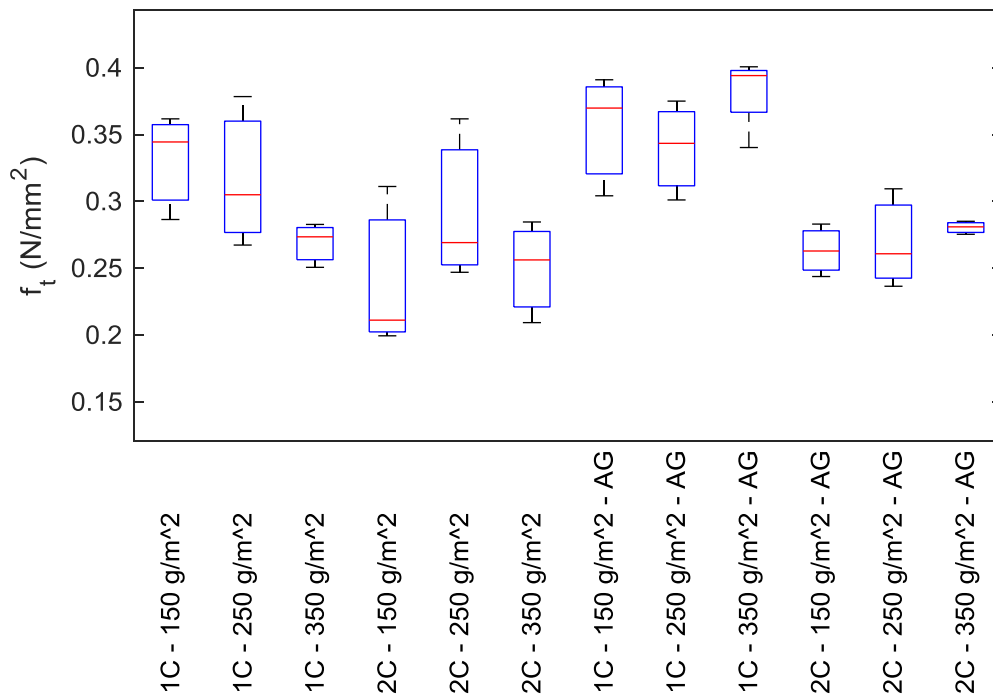
Figure 4-37 – Tensile strength of the unaged and the aged (according to cycle 1 of ETAG 016-2) specimens for the different adhesives and spread rates.

The results obtained show that the aged specimens, especially the 1C ones, presented higher values of tensile strength than the unaged specimens. As explained in Chapter 3, this increase on the strength of the polyurethane foam may be explained by the additional crosslinking of the polymer, which eventually was not completely fully cured before ageing. In the 1C specimens, as the failure occurred within the foam, it was not possible to perceive if post-curing also occurred in the adhesive. The fact that the increase in strength was more relevant in the 1C specimens, may indicate that the 2C adhesive was probably affected (i.e. degraded) by ageing, which may explain why part of the failures in this latter test series occurred at the glue lines.

The stress-strain curves of the 1C aged specimens showed a slightly non-linear behaviour

before failure (Figure 4-38 a)) in contrast to the unaged foam specimens (Figure 3-25) and the 2C aged specimens (Figure 4-38 b)), whose response was linear-elastic up to failure.

a)   b)
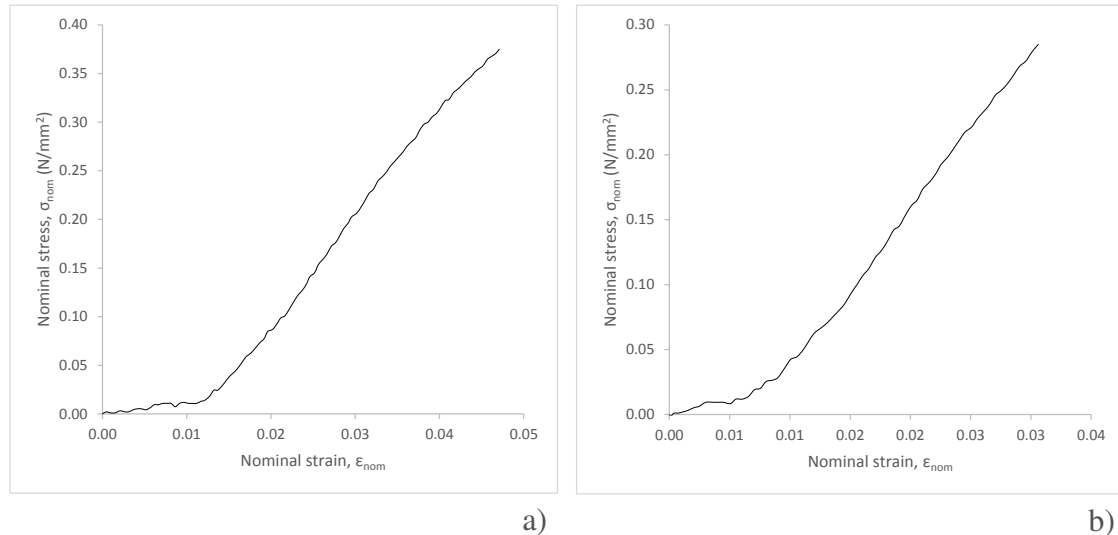
Figure 4-38 - Example of a stress-strain curve obtained in the flatwise tension tests of an aged: a) 1C specimen; b) 2C specimen.

The ANOVA method was applied to analyse the influence of the ageing, adhesive type and adhesive spread rate on the tensile strength before and after ageing. The results are listed in Table 4-12.

Table 4-12 - ANOVA results concerning the influence of ageing, adhesive type and adhesive spread rate on the tensile strength.

	Source	Sum Sq.	d.f.	Mean Sq.	F	Prob>F
Tensile strength	Ageing	0.033	1	0.033	27.230	0.000
	Adhesive Type x Ageing	0.003	1	0.003	2.600	0.112
	Adhesive Spread Rate x Ageing	0.012	2	0.006	4.830	0.011
	Error	0.073	60	0.001	-	-
	Total	0.219	71	-	-	-

In general, the results after ageing are significantly different than those obtained in unaged specimens (Prob>F=.000) – in particular, as mentioned, the tensile strength is higher in the former specimens most likely due to the aforementioned reasons. In a more detailed analysis, combining the effect of the adhesive type with ageing, the Prob>F value increases to 0.112. In a deeper analysis of this result, using the multi-comparison test function of *MATLAB*, it is found that it is only for the 1C adhesive that the results reflect a significant increase due to ageing with respect to the unaged specimens of the same adhesive type, while for the 2C adhesive few differences are observed (Figure 4-39).
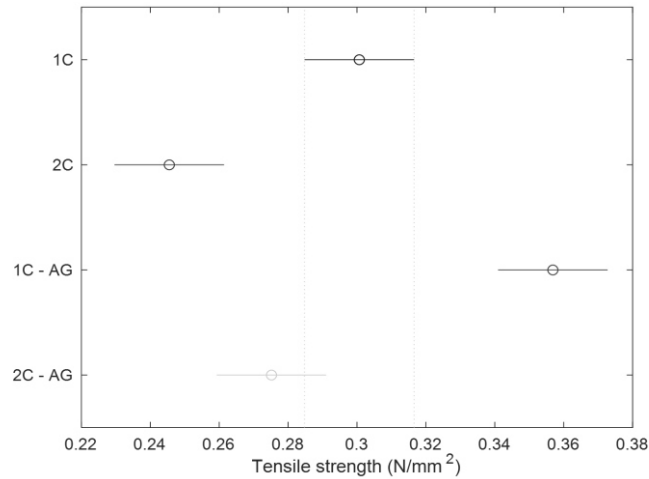
Figure 4-39 – Multiple comparison test results regarding the influence of adhesive type and ageing on the tensile strength.

This observation corroborates the previous comments: in both cases, the tensile strength increased due to the additional cross-linking of the polymeric foam. However, a more expressive increase of strength in the 1C specimens with respect to the unaged specimens is observed when compared to the 2C specimens; a fact that could be attributed to the degradation of the adhesive.

Also, the combined effect of the adhesive spread rate with ageing, which presented a low value of Prob>F=0.011, was analysed using the multiple-comparison test. In this case, it was found out that the differences between unaged and aged samples of equal spread rates is not significant, except for the higher spread rate of 350 g/m^2 (Figure 4-40). This means that the adhesive spread rate (since it is in the range recommended by the manufacturer) did not influence the ageing performance of the adhesive bonding.
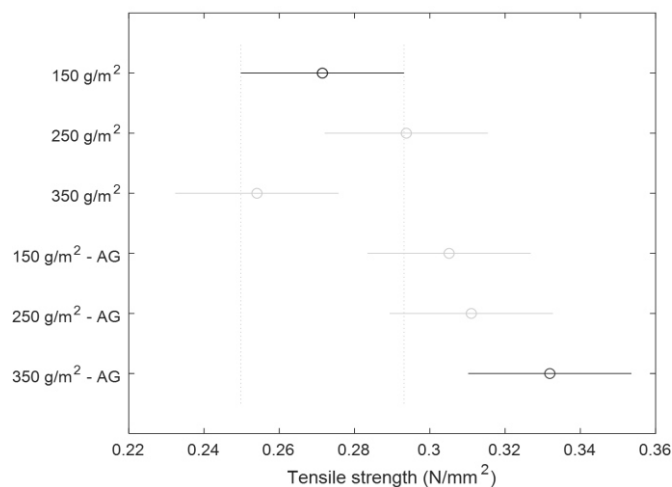
Figure 4-40 – Multiple comparison test results regarding the influence of adhesive spread rate and ageing on the tensile strength.

4.4.3.3 Ageing tests – Temperature and humidity according to ISO 9142

After the ageing process, the glue lines of the specimens were examined to identify possible delaminations that might have occurred; however, none was found in any of the specimens. From the tensile tests, the failure modes occurred mainly within the foam material, for both 1C and 2C specimens (Figure 4-41).
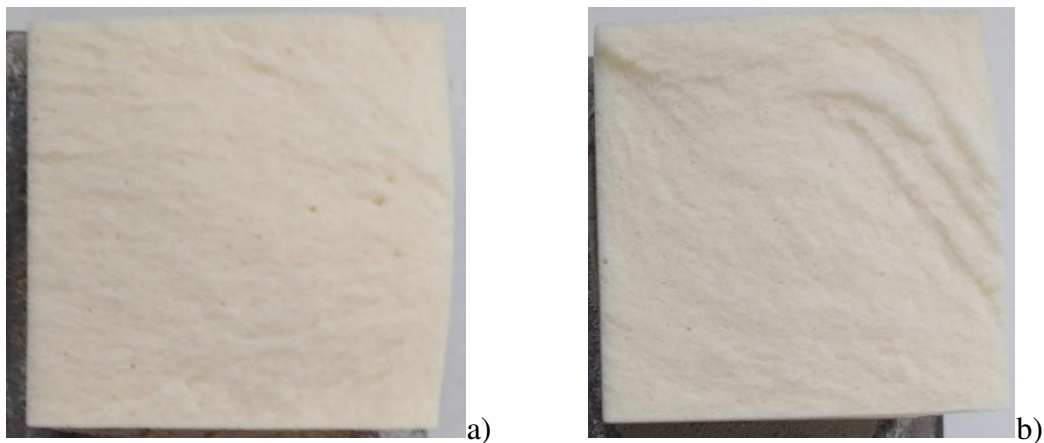
Figure 4-41 - Total failure at the foam observed in a specimen bonded with: a) 1C PUR; b) 2C PUR.

As occurred for the unaged specimens, some of the specimens failed apparently at the glue line (Figure 4-42 a)); however, a more careful inspection of the specimens allowed to verify that failure actually occurred within the foam, with a slight layer of foam being visible (Figure 4-42 b)). Once again, this type of failure occurred due to the stretching of the cross-section on some specimens, which was caused by the bending of the saw during the cutting of the specimens.
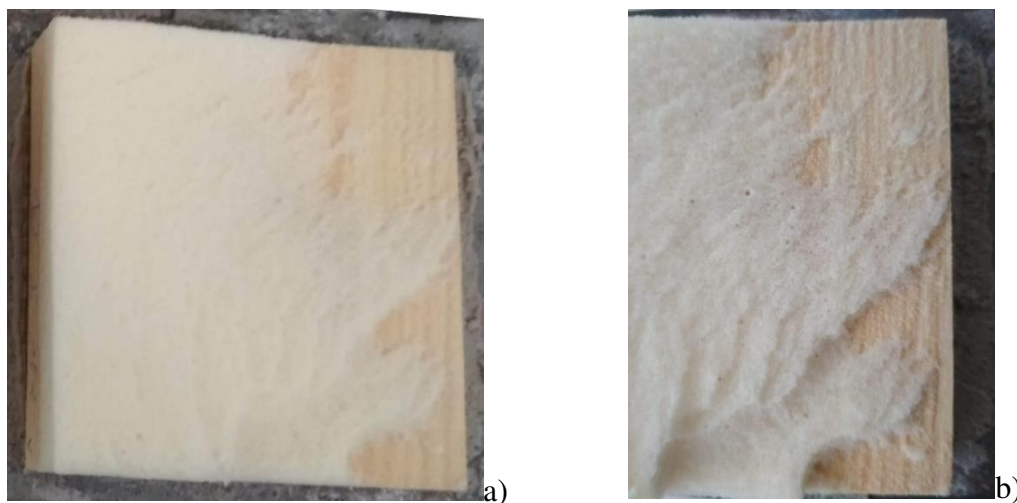
Figure 4-42 – a) Apparent failure of a specimen at glue line; b) detail of the failure that occurred close to the glue line, but where a thinner layer of foam is still visible.

The results regarding the comparison between the tensile strength obtained in the unaged and the aged (according to ISO 9142) specimens for the different adhesives (1C and 2C) and spread rates (150, 250 and 350 g/m^2) are shown in Figure 4-43.

The results obtained show that the aged specimens, especially the 1C ones, presented higher values of tensile strength than the unaged specimens. This was a similar result to the one obtained for the aged specimens exposed to a temperature of 90 ºC following the ETAG 016-2 procedure. As explained before for that protocol, also here the increase of tensile strength may be explained by the additional cross-linking of the polyurethane foam which, eventually, was not completely cured before ageing. Although the temperature was lower (45 º C) and alternated with a lower value (23 ºC), this was enough for the additional cross-linking of the foam to occur.

In the 1C specimens, as the failures occurred within the foam, it was not possible to perceive if a post-curing phenomenon also occurred in the adhesive. The fact that the strength increase was more significant in the 1C specimens may indicate that the 2C adhesive was probably affected by ageing (i.e. underwent degradation), which may explain why part of the failures occurred at the glue lines.
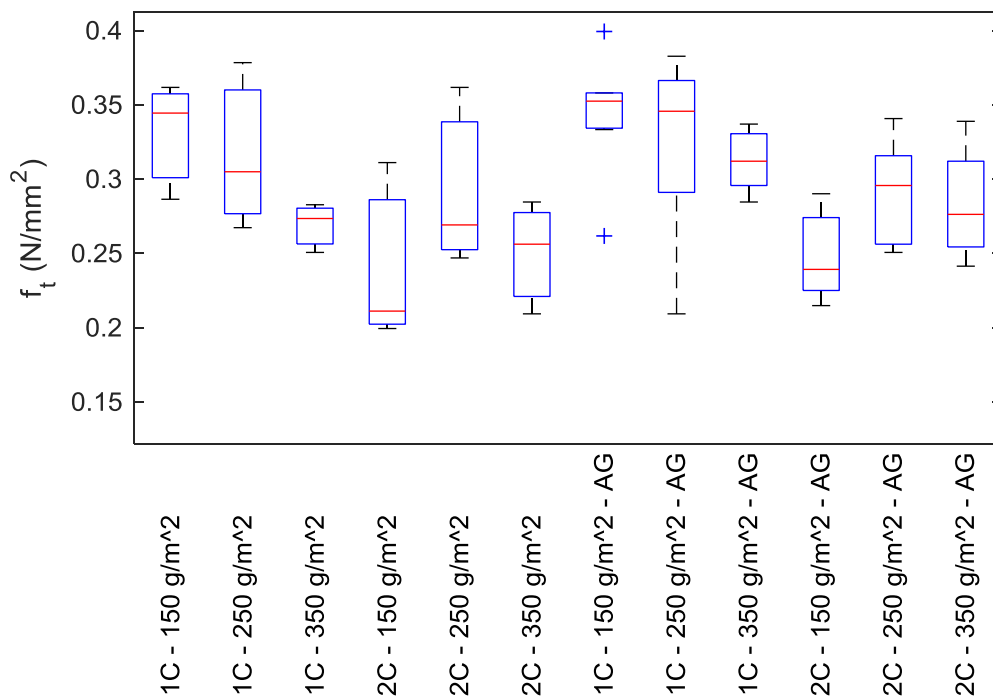
Figure 4-43 – Comparison between the tensile strength obtained in the unaged and the aged (according to ISO 9142) specimens for the different adhesives and spread rates.

The ANOVA method was once again applied to assess the influence of ageing, adhesive type and adhesive spread rate on the tensile strength before and after ageing. The results

are shown in Table 4-13.

Table 4-13 - ANOVA results for the influence of the ageing, adhesive type and adhesive spread rate on the tensile strength.

	Source	Sum Sq.	d.f.	Mean Sq.	F	Prob>F
Tensile strength	Ageing	0.029	1	0.029	23.000	0.000
	Adhesive Type x Ageing	0.001	1	0.001	0.430	0.511
	Adhesive Spread Rate x Ageing	0.007	2	0.004	2.850	0.061
	Error	0.240	192	0.001	-	-
	Total	0.467	203	-	-	-

In general, the results obtained after ageing are significantly different from the results obtained for unaged specimens (Prob>F=.000) – in particular, as mentioned, the tensile strength is higher in the former specimens, most likely due to the aforementioned reasons. Combining the effect of the adhesive type and ageing, the Prob>F value increases significantly (0.511), but using the multiple-comparison test function of *MATLAB*, it is found that for both 1C and 2C adhesives the tensile strength increases due to ageing with respect to their unaged state (Figure 4-44). This increase in tensile strength, which (despite the different ageing conditions) is consistent with results obtained after ageing according to cycle 1 of ETAG 016 – 2, may also be explained by the possible post-curing underwent by the adhesives.
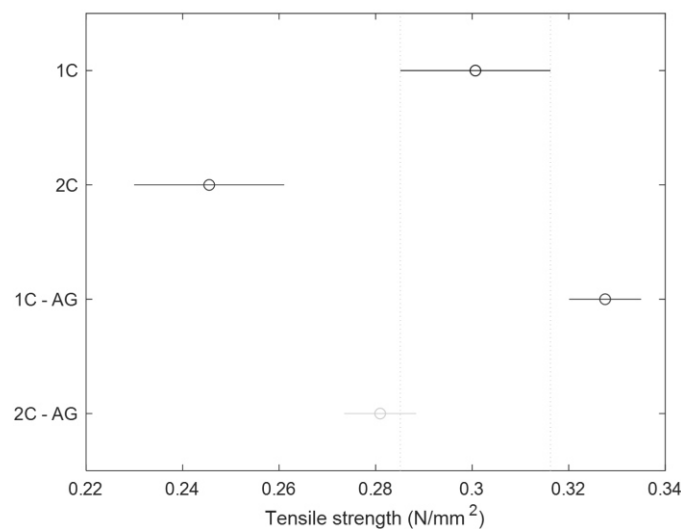
Figure 4-44 – Multi-comparison test results regarding the influence of adhesive type and ageing on the tensile strength.

The combined effect of the adhesive spread rate with ageing, which presented a low value of Prob>F=0.061, is also analysed using the multi-comparison test. It is found out that the differences between unaged and aged samples of equal spread rates are not significant,

except for the higher spread rate of 350 g/m^2 (Figure 4-45). This result is consistent with that obtained for the durability tests according to cycle 1 of ETAG 016 – 2.
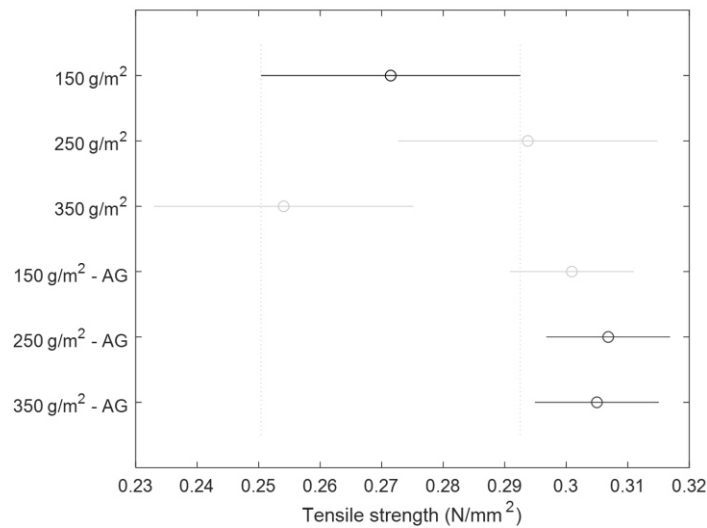
Figure 4-45 – Multi-comparison test results regarding the influence of adhesive spread rate and ageing on the tensile strength.

4.4.3.4   Ageing tests – Delamination test according to EN 16351

The aspect of the specimens in delamination tests after the vacuum-press stage and the after the drying stage is illustrated in Figure 4-46.
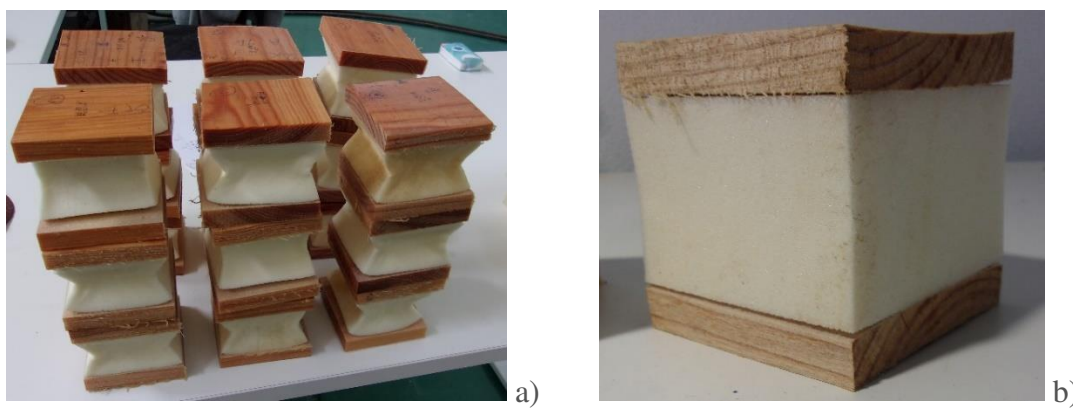
Figure 4-46 - Aspect of the specimens in delamination tests after: a) the vacuum-press stage; b) the drying stage.

It is clear that the induced pressure during the vacuum-press stage crushed the foam and caused it to separate from the wood faces; this is very clear in Figure 4-47 a), which depicts the aspect of the wood layers after the manual separation of the foam from the wood.
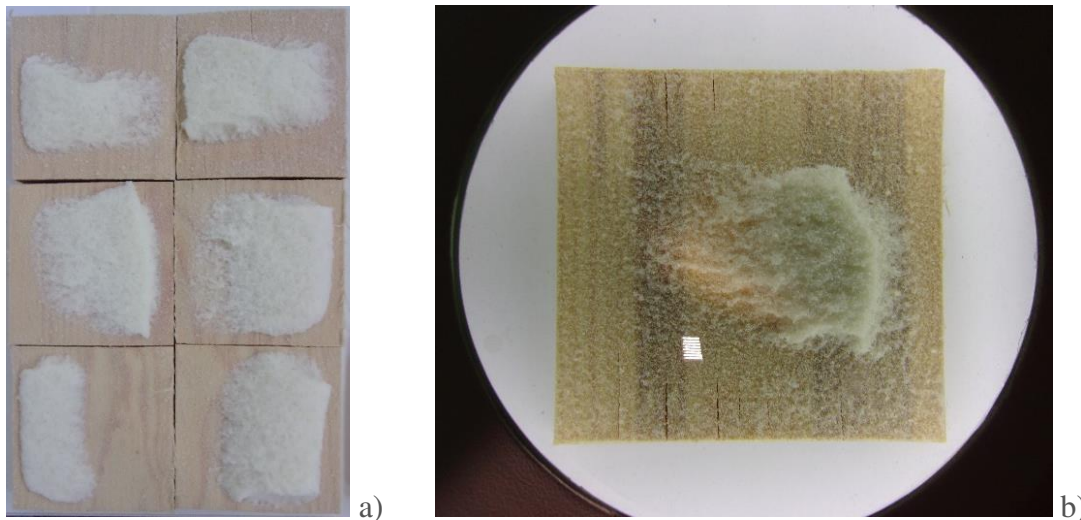
Figure 4-47 - Aspect of the polyurethane/adhesive/wood interface after the delamination test: a) series of specimens; b) zoomed image of one specimen.

Although it seems that a considerable area of the specimen failed at the glue line, a more detailed observation of the interface (Figure 4-47 b)) reveals that a thin layer of foam actually remained at the adhesive surface, which attests the efficiency of the bonding. However, it should be noticed that this is not a standard procedure, and thus these results are merely indicative.

4.5 Concluding remarks

This chapter presented a study about the adhesion performance between the materials composing the panels, namely between the wood lamellas, wood layers and wood/polyurethane layers. The following conclusions are drawn from the current chapter:

- Two possible bonding options for cross glueing of Maritime pine that fulfil both shear and delamination criteria of EN 16351 were defined: (i) using higher bonding pressure (1.0 MPa) and higher adhesive spread rate (180 g/m^2) with lower press time (200 min); or (ii) using lower bonding pressure (0.6 MPa) and lower adhesive spread rate (140 g/m^2), but with pre-application of primer (20 g/m^2) and double of the press time (400 min).

- From the adhesion between wood elements, it was found out that the increase in the bonding pressure ensures lower delamination and higher wood failure percentage, while the shear strength seems not to be particularly affected.

- Pre-treatment of the wood surfaces with primer prior to bonding noticeably enhances the bonding quality, providing almost zero delamination and higher

values of wood failure percentage and shear strength compared to un-primed specimens.

- The minimum requirements of EN 16351 for the reference test method (shear test) were always fulfilled; however, delamination was only fulfilled for the higher bonding pressure and adhesive spread rate considered (1.0 MPa and 180 g/m^2) for the un-primed specimens.

- The criteria used for the delamination analysis (delamination and corresponding wood failure percentage) were found to be inconsistent, as some specimens fulfilled the first one, but failed the second.

- The values of bending strength obtained from the finger-joint connections are much lower than the typical values of bending strength of Maritime pine solid wood. This is in line with the failure modes observed in the bending tests that involved the total or partial delamination at the finger-joint interface, with none of the specimens presenting total failure in wood.

- From the tensile tests on polyurethane/wood specimens, it was concluded that the foam injected technique was unfeasible for the chemical system used, as the failure occurred at the interface between the foam and the wood layers (*i.e.* at the glue line) and the tensile strength obtained was in general much lower than the one obtained from the characterisation of the material itself.

- Concerning the pre-manufactured foam specimens, the specimens manufactured with the lowest pressure recommended by the adhesive manufacturer (0.02 MPa), with both 1C and 2C systems, showed mixed failures, *i.e.* at the foam but also at the glue line, and the tensile strength obtained was also lower than the one obtained from the material characterisation tests. When the bonding pressure was increased (0.10 MPa), such results were improved, with failures at the foam and strength values in line with those from the material characterization tests.

- For the unaged tests, no influence on the tensile strength was found regarding the type of adhesive and adhesive spread rate.

- From the ageing tests following the Cycle 1 according to ETAG 016 – 2, an increase on the mean value of the tensile strength on both 1C and 2C specimens was observed. This increase was attributed to the additional cross-linking of the polyurethane foam polymer due to post-curing effects. In the 1C specimens, as the failure occurred within the foam, it was not possible to conclude if post-curing

also occurred in the adhesive; in the 2C specimens, as part of the failures occurred at the glue lines, the 2C adhesive was probably affected by the ageing (i.e. degradation).

- From the ageing tests following the temperature and humidity cycle according to ISO 9142, an increase of the mean value of the tensile strength on both 1C and 2C specimens was also observed. The same reason as for the strength increase on the specimens aged according to ETAG 016 – 2 was found: the additional cross-linking of the polyurethane polymer.

- From the ageing tests following the delamination test according to EN 16351, it was found that the induced pressure during the vacuum-press stage crushed the foam and caused it to separate from the wood faces; however, a thin layer of foam actually remained at the adhesive surface, indicating the occurrence of failure at the material and not at the glue line.

- In sum, from the results of the ageing tests, the bonding systems used (1C and 2C), performed quite well, although the 2C systems presented some failures at the glue line for the ETAG 016 – 2 protocol (temperature).

5   MECHANICAL CHARACTERIZATION OF THE PANELS

5.1   Introduction

The structural design of lightweight sandwich panels subjected to out-of-plane loads (i.e. beam type elements) is often governed by the serviceability limit states (deflection), for which the behaviour of the composing materials is within their linear elastic range; therefore, simple analytical models can be used to predict both deflections and stresses acting on the panels. However, in structural analysis for ultimate limit states design, the non-linear behaviour of the core material that may arise from the higher loads (and stresses) may require the use of numerical models to describe the non-linear behaviour of the panels. The assessment of the structural behaviour of sandwich panels is often made through experimental tests, whose results can then be used to validate analytical and/or numerical models used for the design of the panels. Due to their similarities with the developed panel, a review of the mechanical characterization of sandwich/structural insulated panels (SIP) and cross-laminated timber (CLT) is made and serves as a basis for an experimental campaign of characterization of the panels, as well for the validation of analytical models available in the literature, and the development of a numerical model.

The remainder of this chapter is organized as follows: section 5.2 presents a state-of-the-art review of experimental tests and analytical and numerical models used to describe the mechanical behaviour of both SIP and CLT panels used as beam and column elements; section 5.3 presents the experimental campaign conducted to characterize the mechanical behaviour of the developed panels and the results obtained in those tests; the comparison of the experimental results with the predictions from analytical models is also discussed; section 5.4 presents the finite element model developed to simulate the mechanical behaviour of the panels in bending, showing the comparison between numerical and test results; the last section 5.5 presents the concluding remarks.

5.2   Characterization of CLT and SIP - state-of-the-art

In the current section, a review of the experimental characterization of CLT and SIP panels used as beam or column elements is made. Also, a review of analytical and numerical models for such panels is presented.

5.2.1 Experimental characterization - Bending tests

Díaz et al (2008) performed bending tests on two-span SIPs made of wood-based faces and extruded polystyrene (XPS) core according to ETAG 016-1 (EOTA, 2003a) for the determination of the maximum bearing capacity.

Rungthonkit and Yang (2009) performed four-point bending tests on SIPs, made of oriented-strand-board (OSB) faces and polyurethane (PUR) injected foam core, following the guidelines of EN 14509 (CEN, 2013). All the tested specimens had timber beams glued and attached with nails at the ends of the panel, perpendicular to the span. Some of the specimens were composed of two panels connected (fastened with nails) along the span through either a smaller SIP beam (block spline) or a timber beam. The only-single panels failed due to either shearing of the core or debonding (at the core-face interface); the SIP connected panels failed due to debonding, and the timber beam connected' ones failed due to shear and flexure. For the three panel types, the analysis of the load-deflection curves revealed a linear elastic behaviour that slowly changed into a non-linear branch.

Fernandez-Cabo et al (2011) performed six-point bending tests on sandwich panels made of OSB faces glued to low-density wood fibre core (110-190 kg/m^3). A quasi-linear behaviour was observed in the load-displacement curve of the beams. The failure modes were mainly due to shear stress that started at the glued materials' interface.

Yang et al (2012) performed three-point bending tests on SIPs made with plywood faces and XPS core. They concluded that a significant amount of shear deformation occurred. A bilinear trend on the load-displacement curve was observed and the failure modes involved debonding at the interface between layers, starting from the edge, which was then followed by the failure of a plywood layer.

Srivaro et al (2015) performed three-point bending tests on sandwich panels made of oil palm wood core (200-450 kg/m^3) adhesively bonded to rubberwood veneer faces. The failure modes observed included face fracture and shear failure of the core, with the latter mode being predominant for specimens with low core density.

Jorissen et al (2016) performed bending tests on two-span sandwich panels made of expanded polystyrene (EPS) core and particle board faces, with some of the specimens featuring timber reinforcements along the faces. The shear stiffness was measured with the shear diagonal method, according to EN 408 (CEN, 2012a), and agreed well with the analytical result for the unreinforced specimen. From the load-displacement curves, for all the tested series, a linear elastic behaviour that slowly changed into a non-linear branch

was observed until brittle failure occurred. They concluded that, although the stiffness of the reinforced panels was higher than that of the unreinforced ones, the shear stress in the core panels of the reinforced panels was much higher, which resulted in core shear failure in some of the reinforced specimens.

Steiger et al (2012) performed bending tests on CLT made of Norway spruce. They tested full-width panels (2.50 m) and strips previously cut from the same panels (with a width of 100 and 300 mm). They concluded that the bending stiffness along a single panel can vary strongly due to wood defects, as well as the variation in mechanical properties of the lamellas. For quality control purposes, and to represent gross CLT panels acting as beam-like load-bearing elements, single tests on 300 mm strips from gross panels were considered as adequate; while 100 mm strips would require at least 5 to 6 specimens to achieve acceptable results.

Gu et al (2016) performed bending tests on three-layered CLT made of Southern pine glued with melamine-formaldehyde (MF) and PUR adhesives. Two different layups for the panels (orientation) were tested: one with the grain direction of the outer layers aligned with the beam length and the other one with the grain direction of the outer layers perpendicular to the length. For the first layup, they reported linear elastic behaviour until brittle failure occurred, which involved three phases: (i) appearance of rolling shear cracks in the inner layer, (ii) bending failure on the longitudinal layers, and (iii) progression of the rolling shear failure in the middle layer. Before failure, no signs of previous delamination on adhesive layers were detected. For the second layup, the authors reported failure to occur in three phases: (i) opening of a gap close to the mid-span section on the tension side (i.e. between the edges of the lamellas; notice that the edges were not glued), (ii) crack initiation at the gap in the inner layer, and (iii) bending failure in the inner layer.

Davids et al (2017) performed bending tests on hybrid three-layer CLT panels made with Spruce-Pine-Fir and/or laminated strand lumber layers for comparison of their bending stiffness and strength. For the grading classes used, they concluded that the use of laminated strand lumber as core layer prevented core shear failure (which occurred instead by flexural tension) and increased the mean bending stress at failure by 23% with respect to the Spruce-Pine-Fir all-made panels.

In sum, from the information collected, it is found that in sandwich beam-type elements, due to the low density of the core materials, a significant amount of shear deformation occurs; moreover, failure of the beams can occur either due to shearing of the core or debonding between the core and the faces, and significant non-linear behaviour can be expected. In CLT, bending stiffness can vary strongly due to wood defects, as well due

to the variation of properties between lamellas, and the failure modes are typically due to rolling shear on the inner layers.

5.2.2 Experimental characterization - Buckling tests

Kermani (2006) performed combined axial compression and combined axial compression-bending tests on SIP walls made of OSB faces and EPS core. Besides the bare panels, axial compression tests were also performed on bare panels with screwed header and footer at the ends (i.e. top and bottom of the column) and also that same solution plus screwed stiffeners (wood studs) placed along the panels' height. The combined axial compression-bending tests were only performed in panels that fitted with header and footer. From the axial compression tests, it was found out that, despite the inclusion of the header, footer and studs did not always decrease the mean deflection consistently for all cases; besides, the mean ultimate load always increased with respect to the bare panel's solutions. For those same tests, the failure modes included end bearing and/or buckling, while in the combined compression-bending tests, flexural failure occurred.

Mousa and Uddin (2011) performed concentric and eccentric compression tests on SIPs panels made of glass/polypropylene faces and EPS core bonded with a thermoplastic adhesive. Failure occurred due to global buckling and no debonding between layers was observed. Some differences between analytical buckling loads (described previously in this chapter) and experimental ones for the concentric (15%) and eccentric (11%) cases were reported, and attributed to the boundary conditions of the experimental test, which were not perfectly pinned as in the model.

Mousa and Uddin (2012) also reported the results for the same panel types but for full-scale walls tested with an eccentric compressive load. In those tests the failure mode was due to wrinkling of the faces in the compression side, which caused the debonding between the core and the faces. The load - lateral deflection curves were found to be linear until the onset of debonding, where a change in slope was observed.

Nakajima et al (2016) performed buckling tests on 3-, 5-, 7- and 9-layer CLT panels made of Japanese cedar. Two different layups for the panels (orientation) were tested: one with the grain direction of the outer layers aligned with the applied force and the other one with the grain direction of the outer layers perpendicular to the force. For both cases, they compared the buckling load obtained experimentally with the one predicted by Euler's formula and concluded about its suitability.

Wang et al (2016) performed concentric and eccentric load tests on 3-, 5-, 7-layer CLT panels. The main failure mechanism observed was buckling and besides the tension and compression failures observed in the outer layers, also rolling shear failures were observed in the inner layers.

From the information collected above, it is found that buckling is usually the typical failure mode of sandwich-type columns under axial loading, but other modes, such as wrinkling of the faces, may occur instead.

5.2.3 Analytical Models - Elements subjected to out-of-plane loads (beam-type elements)

Concerning CLT, according to Brandner et al (2016), design regulations are currently missing in European standards; however, some CLT manufacturers already refer to specific models in their European Technical Approvals (ETA). As for SIP, TR 019 (EOTA, 2005) prescribes some approaches to analyse sandwich panels acting as beam elements. Due to the high shear flexibility of the transverse layers in CLT (and core layer in SIP), the shear influence in their mechanical behaviour is very important (Brandner et al, 2016). Therefore, the classical beam theory (Euler-Bernoulli) has to be disregarded. Beam theories that consider the shear effects, such as Timoshenko beam theory (TBT) (Timoshenko, 1921), the gamma method (γ-method) (Möhler, 1962) or the shear analogy method (SAV) (Kreuzinger, 1999) are commonly deemed to be adequate for CLT design if the relation between the length and thickness of the panel is equal to or greater than 15 (Brandner et al, 2016). If such relation is not verified, shear flexible multilayer plate methods (e.g. (Guggenberger and Moosbrugger, 2006)) are recommended (Thiel, 2014). From the three analytical methods referred (TBT, γ-method and SAV), Christovasilis et al. (2016) found, by comparison with experimental results, that SAV provided the most reliable predictions for CLT, both in terms of stiffness and strength. SAV is also referred to in the technical document for sandwich panels, TR 019 (EOTA, 2005), as a recommended method for SIP. Díaz et al (2008) used that same method to predict the behaviour of experimentally tested SIPs (made of wood-based faces and XPS core), and found close values in terms of deflection and failure load. Another approach found in TR 019 (EOTA, 2005) adopts the classical beam theory, but takes into account the shear deformation of the core; that is actually the same formulation present in EN 14509 (CEN, 2013) for the elastic analysis of metal face sandwich panels. Indeed, in the study conducted by Díaz et al (2008), this method was applied to determine the displacements of a two-span continuous beam for various wood-based sandwich panel solutions, but since the experimental results were slightly different from the ones given by the method, some modifications were proposed.

In both TBT and SAV methodologies, the bending stiffness (EI) is given by Equation (5-1):

$$EI = EI_A + EI_B \qquad (5\text{-}1)$$

where:

$$EI_A = \sum_{i=1}^{n} E_i \cdot I_i \qquad (5\text{-}2)$$

$$EI_B = \sum_{i=1}^{n} E_i \cdot A_i \cdot E_i \cdot z_i{}^2 \qquad (5\text{-}3)$$

and where: n – number of layers in the cross-section; E_i – modulus of elasticity of layer i; I_i – moment of inertia of layer i with respect to its own neutral axis; A_i – cross-sectional area of layer i; z_i – distance between the centre of gravity of layer i and the full cross-section.

The shear stiffness (GA) for the TBT is given by Equation (5-4) and for SAV it is given by Equation (5-5):

$$GA = \frac{EI^2}{\int_h \dfrac{S\big(y, E_i(y)\big)^2}{G_i(y) \cdot b_i(y)} \, dy} \qquad (5\text{-}4)$$

$$GA = \frac{a^2}{\left[\dfrac{h_1}{2 \cdot G_1 \cdot b_1} + \left(\sum_{i=2}^{n-1} \dfrac{h_i}{G_i \cdot b_i} \right) + \dfrac{h_n}{2 \cdot G_n \cdot b_n} \right]} \qquad (5\text{-}5)$$

where: h – thickness of the cross-section; b – width of the cross-section; S – first moment of area; G – shear modulus; a – distance between the centres of gravity of layers 1 and n.

The normal stress due to bending at a normal distance y_0 from the neutral axis in layer i, $\sigma_i(y_0)$, is calculated for TBT in accordance with Equation (5-6), and for SAV it is determined from Equations (5-7) to (5-9).

$$\sigma_i(y_0) = \frac{M \cdot E_i(y_0)}{EI} \cdot y_0 \qquad (5\text{-}6)$$

$$\sigma_i(y_0) = \sigma_{A,i}(y_0) + \sigma_{B,i}(y_0) \tag{5-7}$$

$$\sigma_{A,i}(y_0) = \frac{M_A \cdot E_i(y_0)}{EI_A} \cdot y_0 \tag{5-8}$$

$$\sigma_{B,i}(y_0) = \frac{M_B \cdot E_i(y_0)}{EI_B} \cdot z_i(y_0) \tag{5-9}$$

The indexes A and B refer to two virtual beams that are coupled with infinitely rigid web members, the first with bending stiffness equal to EI_A and infinite shear stiffness, and the second with bending stiffness equal to EI_A and the shear stiffness obtained from Equation (5-5).

The shear stress at y_0 in layer i, $\tau_i(y_0)$, is calculated for TBT in accordance with Equation (5-10), and for SAV in accordance with Equations (5-11) to (5-13).

$$\tau_i(y_0) = \frac{V \cdot \int_{A_0} E_i(y) \cdot y \, dA}{EI \cdot b_i(y_0)} \tag{5-10}$$

$$\tau_i(y_0) = \tau_{A,i}(y_0) + \tau_{B,i,i+1}(y_0) \tag{5-11}$$

$$\tau_{A,i}(y_0) = \frac{V_A \cdot E_i(y_0)}{EI_A} \cdot \frac{1}{2} \cdot \left(\frac{h_i^2(y_0)}{4} - y_0^2 \right) \tag{5-12}$$

$$\tau_{B,i,i+1}(y_0) = \frac{V_B}{EI_B \cdot b_i(y_0)} \cdot \sum_{j=i+1}^{n} E_j \cdot A_j \cdot z_j \tag{5-13}$$

The bending moments (M) and shear forces (V) on the virtual beams may be obtained by applying for example the force method or using a finite element program.

Besides the referred analytical models, more advanced methods are required in special situations beyond small ratios between span to depth of CLT, such as point loads or supports (Thiel, 2014). In the case of the referred beam models, in order to achieve a two-way load transfer (as it occurs in plates supported in three or four sides), grid models may be used; however, this may result in a substantial modelling effort (Stürzenbecher et al, 2010). The same authors have numerically compared plate theories that included Mindlin (Mindlin, 1951) and Ren (Ren, 1986), and concluded that the latter proved to be the most effective one in estimating stresses and deformations in CLT. TR 019 (EOTA, 2005) also

recommends the use of differential equations or differential method solutions, such as finite element models.

Regardless of the analysis method in use, in CLT, the contribution of the transverse layers to normal stress is usually disregarded, either due to the high ratio of Young' modulus between the longitudinal and transversal layers, or the unavoidable appearance of cracks within layers. One issue that is still open in CLT design is the development of approaches that take into account stress interactions, i.e. a failure criterion (Brandner et al, 2016).

Indentation failure on sandwich panels may also occur when a load is applied to one of the faces over a small area, causing significant local deformation of the loaded face into the core, which results in an elastic-plastic stress state in the vicinity of the load (Figure 5-1). This type of crushing may occur due to punctual (or linear) loads acting normal to one of the faces or at the supports.
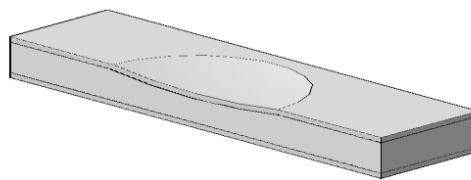
Figure 5-1 - Indentation failure.

For linear supports, in a simplified way, according to (CIB-W56, 2001), the distribution of the compressive stresses in the core may be assumed as uniformly distributed at mid-depth with a certain dispersion angle starting from the support length (the loading area) according to Equation (5-14).

$$\sigma_c = \frac{F}{b(l_s + k \cdot e)} \tag{5-14}$$

where: F – applied load; b – support width (direction transverse to cross-section); l_s – support length; e - distance between centroids of the faces and k – distribution parameter (taken as 0.5 for rigid plastic foams).

Equation (5-14) is valid for panels supported along the width, however it may be adapted for punctual supports by replacing b by $b_s + k \cdot e$, where b_s is the support width.

A more expeditious model that considers the face as an elastic beam resting on an elastic-plastic foundation (the core) was proposed by (Daniel et al, 2002). The beginning of the indentation failure is predicted by Equation (5-15).

$$F_{ind} = 1.7 \cdot \sigma_{c,core} \cdot b \cdot h_{skin} \sqrt[3]{\frac{E_{skin}}{E_{core}}} \qquad (5\text{-}15)$$

where $\sigma_{c,core}$ - core compressive strength to out-of plane loads; b – panel width; h_{skin} - thickness of the faces; E_{skin} - modulus of elasticity of the faces; E_{core} - modulus of elasticity of the core; F – force per unit length.

A priori, existing analytical models for sandwich/CLT panels, which account for shear effects, may be valid for the developed CIT panels, due to their similarities with the SIP and CLT concepts.

5.2.4 Analytical Models - Elements subjected to in-plane compressive loads (column-type elements)

When subjected to in-plane compressive loads, sandwich panels may fail due to several causes, namely: exceeding of the compressive strength (Figure 5-2 a)); buckling (Figure 5-2 b)); wrinkling of the faces (may also occur on the compressed face when subjected to out-of-plane loads) (Figure 5-2 c)); or shear crimping of the foam core (Figure 5-2 d)). It should be noticed that other types of failure exist, but some are specific for certain types of panels architectures, as for example the dimpling of faces in honeycomb core panels. The failure modes illustrated are detailed next.

a) b) c) d)
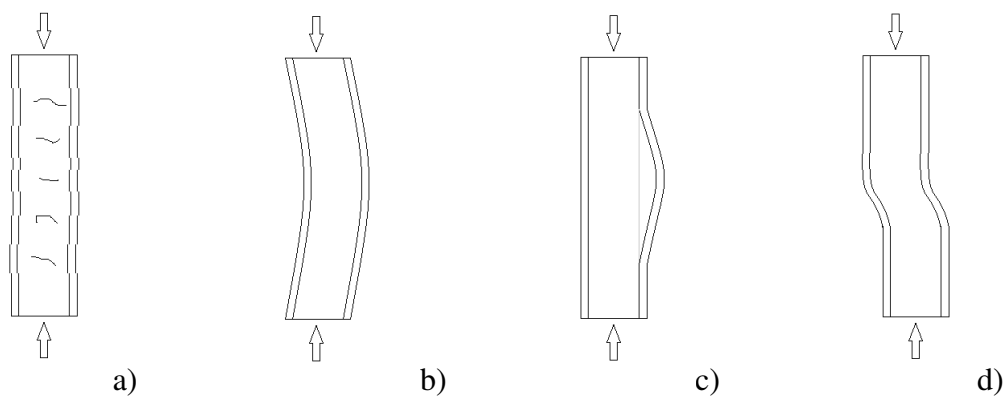
Figure 5-2 – Possible failure modes on subjected to in-plane compressive loads: a) exceeding of the compressive strength; b) buckling; c) wrinkling of the faces; d) shear crimping of the core.

5.2.4.1 Compressive failure

Considering that the strains on each layer of the composite element, subject to compression parallel to the layering, are equal, according to Hooke's law, the stress in each layer will be proportional to the respective modulus of elasticity, as given by Equation (5-16):

$$\sigma_i = \frac{F \cdot E_i}{\sum_{i=1}^{n} A_i \cdot E_i} \tag{5-16}$$

where F - applied force; E_i - modulus of elasticity of the layer i; A_i - cross-sectional area of layer i, and n - total number of layers.

In sandwich panels, as the modulus of elasticity of the core material is usually very low when compared to that of the faces, the resulting stress in the core is very low, which means that the load is almost fully resisted by the faces. In the same way, in CLT, according to Thiel (2014), for design purposes, only the layers compressed along the wood grain direction are considered to support the compressive loads.

5.2.4.2 Buckling

In slender elements subjected to in-plane compression, buckling has to be verified. Besides the traditional Euler column buckling formulation, a design approach directed to sandwich panel-type structures has been proposed by Allen (1969) for pin-pined columns, which includes the effects of shear stiffness. The Euler's buckling load for a pin-ended column is given by Equation (5-17).

$$P_{cr} = \frac{\pi^2 EI}{l^2} \tag{5-17}$$

According to Allen (1969), the buckling load for pin-ended sandwich panels is given by Equation (5-18):

$$P_{cr} = \frac{\pi^2 EI}{l^2} \frac{1}{\left(1 + \frac{\pi^2}{l^2} \cdot \frac{EI}{GA}\right)} \tag{5-18}$$

where EI is the bending stiffness; GA is the shear stiffness and l is the column length.

Besides this classical approach, based on Allen's approach, Mousa and Uddin (2011)

proposed a formula that accounts not only for the shear deformation of the core but also for the orthotropic behaviour of the faces and load eccentricity. Also, Tang et al (2015) proposed a formula that accounts for the core shear deformations, but for fixed-fixed boundary conditions; such formula showed good agreement with experimental results.

For CLT design purposes, a method based on Eurocode 5 methodology for buckling verification was presented by Thiel (2014), named Equivalent Beam Method (EBM), for which the buckling load is calculated according to (Allen, 1969) formula. In terms of timber elements design, according to Eurocode 5 (CEN, 2004b), when slenderness is found to be important, the stress on elements subjected to both compression and bending shall fulfil equation (5-19):

$$\frac{\sigma_{c,0,d}}{k_c \cdot f_{c,0,d}} + k_m \frac{\sigma_{m,d}}{f_{m,d}} \leq 1 \qquad (5\text{-}19)$$

where $\sigma_{c,0,d}$ is the design compressive stress on the parallel-to-grain loaded layers; $f_{c,0,d}$ is the corresponding design compressive strength; $\sigma_{m,d}$ is the design bending stress, $f_{m,d}$ is the design bending strength, k_m is a factor related to the type of wood product (taken conservatively as 1.0). The instability factor, k_c, that reduces the strength mainly due to slenderness, is given by Equations (5-20) and (5-21):

$$k_c = min \left\{ 1 \; ; \; \frac{1}{k + \sqrt{k^2 - \lambda_{rel}^2}} \right\} \qquad (5\text{-}20)$$

$$k = 0.5\left(1 + \beta_c(\lambda_{rel} - 0.3) + \lambda_{rel}^2\right) \qquad (5\text{-}21)$$

where $\beta_c = 0.2$ for solid wood. According to Thiel (2014), for CLT, the relative slenderness, λ_{rel}, is given by Equation (5-22):

$$\lambda_{rel} = \sqrt{\frac{A_0 \cdot f_{c,0,k}}{P_{cr}}} \qquad (5\text{-}22)$$

where A_0 is the cross-section area of the layers compressed parallel to the grain; $f_{c,0,k}$ is the respective characteristic compressive strength. The ideal elastic buckling load, P_{cr}, is given as in Equation (5-18) considering the 5% quartiles of the stiffness properties.

5.2.4.3 Wrinkling of the faces

The wrinkling of the faces is a phenomenon that consists of the formation of a (series of) buckling wave(s) on the faces of a sandwich panel subjected to compression and that converts into wrinkles with the load increase. The failure can either result in a local separation of a face from the core (if the adhesion between them is not adequate) or in local crushing of the skin into the core (Figure 5-2 c)). According to (CIB-W56, 2001), the wrinkling stress on the face of a sandwich panel can be predicted by Equation (5-23):

$$\sigma_{wr} = k^3 \sqrt{E_{core} G_{core} E_{skin}} \tag{5-23}$$

where k is a constant depending on the imperfections and quality of the face, core and bond, usually taken between 0.50 to 0.65; E_{core} is the average value of the flatwise tensile and compressive modulus of elasticity of the core material; G_{core} is the shear modulus of the core material, and E_{skin} is the modulus of elasticity of the face material. Other similar expressions have been proposed in the literature; a state-of-art is found in (Ley, 1999), where different values proposed for the constant k are given.

5.2.4.4 Shear crimping of the core

Shear crimping consists of a shear failure mechanism of the core of an edgewise compressed sandwich panel in which the faces remain undamaged. It occurs due to low sandwich shear stiffness (FPL, 1959). According to Mouritz and Gardiner (2002), the critical compressive force that causes shear crimping can be predicted by Equation (5-24):

$$F_{crimp} = \frac{G_c b (t_s + t_c)^2}{t_c} \tag{5-24}$$

where: t_s is the face thickness; t_c is the core thickness; b is the width of the panel; and G_c is the core shear modulus.

5.2.5 Numerical Models - Elements subjected to out-of-plane loads (beam type elements)

In terms of finite element models (FEM) using available commercial packages, some recent and relevant works were performed for sandwich panels and CLT.

Díaz et al (2008) performed a 2D plane strain analysis using the FEM software *ANSYS* of two-span continuous beams made of wood-based faces and XPS core. Both faces and

core parts were modelled with bi-dimensional plane elements (PLANE42) with orthotropic material models. Each element had four nodes with two degrees of freedom at each node (translations). Friction between the panels and supports was considered. The results of the simulation regarding the displacement agreed reasonably well with the test results (ratios between results of experiments and simulation around ~1.00 to ~1.25).

Mostafa et al (2013) performed a 3D FEM analysis using *ABAQUS* software to predict the shear behaviour and failure modes of sandwich panels made of glass fibre reinforced polymer (GFRP) skins and polyvinyl chloride (PVC) core (100 kg/m^3). The faces and the foam were modelled using continuum linear brick elements C3D8R. The faces were modelled assuming linear elastic and isotropic behaviour and the PVC foam was modelled using the crushable foam plasticity model from *ABAQUS*. For this material model, the isotropic hardening sub-option was selected and geometric non-linear analysis was considered. The authors reported the impossibility of reproducing the exact behaviour of the PVC foam material in the model. In fact, the real response of the material is quite different in tension and compression, but the (custom) plasticity model available in the software considered equal behaviour in compression and tension. The interaction between layers was modelled using node-to-surface interaction and assuming a cohesive property interaction to represent the debonding behaviour between layers (traction-separation model). The debonding was considered to initiate based on a maximum contact stress ratio criterion that was dependent on the maximum tensile and shear strength of the PVC material obtained from tests. The comparison between the shear stress-strain response of the experimental vs. numerical results showed good modelling accuracy and the FEM model was also able to predict the damage initiation (face-core debonding).

Mohamed et al (2015) performed a 3D non-linear FEM analysis of the flexural behaviour of sandwich panels made of glass fibre/polyurethane faces with high density PUR foam core (96 kg/m^3) for comparison with experimental results. The faces were modelled with three-layer eight-node quadrilateral reduced-integration continuum shell elements and the core was modelled with eight-node linear reduced-integration hexahedral elements. The face material was modelled as linear elastic and the foam as non-linear. The overlap of the experimental/numerical force-displacement curves showed good agreement.

Jorissen et al (2016) performed 3D linear elastic FEM analysis of two-span sandwich panels made of EPS core and particle board faces with timber reinforcements attached to the faces using *ABAQUS*. They used shell elements (S4R) for the faces and solid elements for the core (C3D20R), but no details on material models were given. The comparison with the experimental results showed that the model slightly over predicted the stiffness and was not able to describe the non-linear behaviour of the load-displacement curve.

The FEM has also been used to model the torsional behaviour of CLT panels experimentally tested in a 3D analysis using *ANSYS* (Sebera et al, 2015). The layers were modelled with quadratic finite elements (SOLID95) and the material behaviour as orthotropic. As the lamellas composing the experimentally tested CLT panels were not edge bonded, two FEM models were considered: one with 1 mm gap between lamellas and the other without gaps (to simulate edge bonding). A good agreement was found for the load-deflection curves' comparison between numerical and experimental results, with a better agreement for the FEM gapped models.

From the information collected above, it is found that different approaches have been used for the modelling of sandwich or CLT beam elements, using either 2D or 3D approaches and using different elements, either with solid elements for both face and core, or with solid elements for the core combined with shell elements for the faces (3D models). Depending on the materials used, the face materials are modelled as linear elastic, while the core is modelled using a non-linear material model, such as plasticity or crushable foam. A reported difficulty is the exact modelling of materials behaviour, such as plastic foams, as they usually have different behaviour in tension and compression (which is the case of the polyurethane foam used on the developed panels), and the plasticity models available in FEM software consider equal behaviour in compression and tension.

5.2.6 Elements subjected to in-plane compressive loads (column-type elements) - Numerical Models

Veedu and Carlsson (2005) used *ANSYS* to model the buckling behaviour of sandwich panels made of glass/vinylester faces and PVC core that included previous face/core debonding. Both faces and core parts were modelled with 2D plane elements (PLANE42), each one with four nodes having two degrees of freedom at each node (translations) and considering plane strain analysis. A 2D linear analysis was conducted to obtain the buckling loads and modes, which were used as input to define the shape of the initial imperfection for non-linear analysis. They concluded that the buckling loads determined from the eigenvalue analysis exceeded the ones from the experiments and from the non-linear FEM simulations, while the latter were in good agreement with the experimental ones.

Mousa and Uddin (2012) used *ANSYS* to model the buckling behaviour of SIPS made of glass/polypropylene faces and EPS core. Both faces and core parts were modelled with 3D solid elements (SOLID45). The faces were modelled as an orthotropic material and the core as an isotropic one. A non-linear static analysis was performed to simulate the

behaviour of the SIP under in-plane eccentric load. The comparison of the predicted load-deflection and load-strains curves with the experimental results showed good agreement.

Tang et al (2015) used *ABAQUS* to model the buckling behaviour of SIPs made of calcium silicate faces and polyurethane core. Both faces and core parts were modelled with 3D solid elements (C3D20R) with linear elastic material models. As the adhesion between the core and faces was considered to be sufficiently strong (the panels were produced on a continuous foaming line), the interaction between layers was modelled with tie contacts in the FEM model. The eigenvalue linear geometric analysis was performed using the Lanczos eigensolver. From the obtained buckling loads and modes, a non-linear analysis was performed using the Riks method (STATIC, RIKS), assuming an initial perturbation (IMPERFECTION) of 1 ‰ of the length. The comparison of the predicted buckling load with the experimental results showed good agreement.

Perret et al (2016) performed a 3D linear buckling analysis of CLT walls with different numbers and geometries of layers using *ABAQUS* with timber modelled as an orthotropic material and using quadratic 3D brick-elements (C3D20R). From the simulations, they concluded that the critical buckling load was close to the one that causes the exceeding of the material strength.

The details reported above from FEM models of SIP and CLT using FEM software for buckling analysis show that similar material models and elements to the ones used for beam analysis are employed.

Regarding the developed panels, from the state-of-the-art review, it is found that such solution (two pairs of cross-wood layers between a low-density foam layer) has never been experimentally tested, either as beam or column element. For the experimental characterization of the developed panels, it is expected that similar aspects found on the behaviour of CLT and SIP panels may be observed in the experiments, namely significant shear deformation and shear failure of the core in bending tests. Moreover, due to the similarities with SIP and CLT, it is expected that the same analytical models and similar numerical models will be able to describe the behaviour of the developed panels with adequate accuracy.

5.3 Experimental campaign

5.3.1 Overview

To assess the mechanical behaviour of the developed panels when subjected to either out-of-plane loads (floors) or in-plane loads (walls), and to validate the analytical/numerical

models to describe such behaviour, an experimental campaign was carried out. The experimental campaign included bending tests on both beams and panels, performed according to ASTM C393 (ASTM, 2011a) and EN 408 (CEN, 2012a) guidelines, and buckling tests were performed on column type-elements as per ASTM E1803 (ASTM, 2014).

5.3.2 Materials and specimen preparation

Besides the developed CIT beam/panels, it was also decided to perform some tests on CLT and SIP beams, for which the analytical models referred on the state-of-the-art were referred to as being valid.

The tested beam/column specimens were produced at the *Centro de Inovação e Competências da Floresta (SerQ)*, while the panels were produced by a third party (*Pedrosa & Irmãos, Lda*). The production and assembling of the wood parts, and the assembling of the wood parts to the polyurethane foam was done in the same way as for the specimens presented in Chapter 4. An adhesive spread rate of 180 g/m^2, a primer spread rate of 20 g/m^2 and a bonding pressure of 0.6 MPa were considered for the manufacturing of the cross-wood layers. To assemble the wood parts to the polyurethane foam, an adhesive spread rate of 350 g/m^2 and a bonding pressure of 0.1 MPa were considered. The beam specimens, unlike the panels, were not edge bonded, as no lateral press system was available. Depending on the available materials, different layer thicknesses for the wood and polyurethane elements were considered, which for wood ranged from 10 to 35 mm, and for polyurethane from 30 to 120 mm. It should be noticed that such values were not defined with basis on design, as the main purpose here was to validate the prediction models. It was also a way to verify if different thickness and ratios between the thickness of the wood and polyurethane layers had any particular influence on the observed mechanical behaviour.

To abbreviate the reference of the different sets of test specimens, the following nomenclature was used: for the identification of the materials composing the layers - Maritime pine (MP), Australian blackwood (AB) and polyurethane (PUR); element type: beam (B) and panel (P); and to identify the layer thickness structure - (wood_thickness/foam_thickness). So, for example, one of the CIT beams composed of 20 mm thick wood layers and 120 mm thick foam is identified as CIT-20/120-B1. The description of the structure and dimensions of the tested beams and panels are described in Tables 5-1 and 5-2, respectively.

As referred in Chapter 3, the modulus of elasticity/grade class of the boards used to

manufacture the beams and panels was determined individually with the MTG device. In the case of the beams, it was possible to identify its location in each beam, as only four wood lamellas were used per beam. For the panels, since it was not possible to identify the location of each board inside the panel, but only the grade that it belongs to, the mean modulus of elasticity determined for the corresponding class was considered. For some of the panels, it was decided to perform a grade combination between the outer and inner wood layers, in such a way that the outer layers belonged to a class equal to or higher than the inner ones. The mean values for the boards used in the beams are shown in Table 5-3 and the grade classes of the panels are listed in Table 5-4.

Table 5-1 – Type, composing materials and overall dimensions of the tested beams.

Type	Materials	Layers thickness (mm)	Designation	Depth (mm)	Width (mm)	Length (m)
CLT	MP/MP/MP	20-20-20	CLT3-B1	60	110	2.2
			CLT3-B2		123	2.2
	AB/MP/AB	20-20-20	CLT3-B3	60	122	2.1
	MP/MP/MP/MP/MP	20-20-20-20-20	CLT5-B1	100	127	2.2
SIP	MP/PUR/MP	10-40-10	SIP-10/40-B1	60	127	2.5
			SIP-10/40-B2		121	2.5
		20-120-20	SIP-20/120-B1	160	136	2.5
			SIP-20/120-B2		127	2.3
CIT	MP/MP/PUR/MP/MP	10-10-40-10-10	CIT-10/40-B1	80	131	2.3
			CIT-10/40-B2		131	2.3
			CIT-10/40-B3		129	2.3
		20-20-40-20-20	CIT-20/40-B1	120	130	2.4
		20-20-120-20-20	CIT-20/120-B1	200	108	2.3
			CIT-20/120-B2		137	2.2
			CIT-20/120-B3		127	2.2
	AB/MP/PUR/MP/AB	20-20-120-20-20	CIT-20/120-B4	200	126	2.1

Table 5-2 – Type, composing materials and overall dimensions of the tested CIT panels.

Type	Materials	Layers thickness (mm)	Designation	Depth (mm)	Width (mm)	Length (m)
CIT	MP/MP/PUR/MP/MP	10-10-30-10-10	CIT-10/30-P1	70	740	3.0
			CIT-10/30-P2	70	735	3.0
			CIT-10/30-P3	70	740	3.0
		35-35-30-35-35	CIT-35/30-P1	170	375	3.0
			CIT-35/30-P2			3.0
			CIT-35/30-P3			3.0
			CIT-35/30-P4			3.0
			CIT-35/30-P5			3.0
			CIT-35/30-P6			3.0

Table 5-3 – Mean modulus of elasticity of the wood layers composing the beams.

Designation	E (kN/mm²)
CLT3-B1	14.0
CLT3-B2	14.0
CLT3-B3	16.4
CLT5-B1	18.9
SIP-10/40-B1	17.2
SIP-10/40-B2	16.8
SIP-20/120-B1	16.9
SIP-20/120-B2	19.5
CIT-10/40-B1	17.1
CIT-10/40-B2	18.3
CIT-10/40-B3	19.3
CIT-20/40-B1	18.6
CIT-20/120-B1	17.6
CIT-20/120-B2	16.5
CIT-20/120-B3	16.7
CIT-20/120-B4	14.6

Table 5-4 – Grade combinations considered on the panels.

Designation	Grade Combination
CIT-10/30-P1	C24 - C24
CIT-10/30-P2	C40 - C40
CIT-10/30-P3	C40 - C40
CIT-35/30-P1	C24 - C18
CIT-35/30-P2	C24 - C18
CIT-35/30-P3	C24 - C24
CIT-35/30-P4	C24 - C24
CIT-35/30-P5	C40 - C40
CIT-35/30-P6	C40 - C40

Table 5-5 – Type of tests performed in each specimen.

Designation	Bending		Buckling
	Stiffness	Failure	
CLT3-B1	✓	-	-
CLT3-B2	✓	-	-
CLT3-B3	✓	-	-
CLT5-B1	✓	-	-
SIP-10/40-B1	✓	✓	✓
SIP-10/40-B2	✓	✓	✓
SIP-20/120-B1	✓	✓	-
SIP-20/120-B2	✓	✓	-
CIT-10/40-B1	✓	✓	✓
CIT-10/40-B2	✓	✓	✓
CIT-10/40-B3	✓	✓	✓
CIT-20/40-B1	✓	✓	-
CIT-20/120-B1	✓	✓	-
CIT-20/120-B2	✓	✓	-
CIT-20/120-B3	✓	✓	-
CIT-20/120-B4	✓	✓	-
CIT-10/30-P1	✓	✓	-
CIT-10/30-P2	✓	✓	-
CIT-10/30-P3	✓	✓	-
CIT-35/30-P1	✓	✓	-
CIT-35/30-P2	✓	✓	-
CIT-35/30-P3	✓	✓	-
CIT-35/30-P4	✓	✓	-
CIT-35/30-P5	✓	✓	-
CIT-35/30-P6	✓	✓	-

As mentioned, two types of tests were performed: (i) bending tests, involving either relatively low loading levels (to assess stiffness) or loading up to failure, and (ii) buckling tests. The types of tests performed in each type of specimens are described in Table 5-5. Note that due to the limitations in material to produce the specimens, some of the tests could only be performed for one specimen of a certain layer thickness (e.g. CIT 20/40-B1). The testing of all specimens with the same layer thicknesses (e.g. CIT 20/120) was performed to assess the replicability of the results.

5.3.3 Bending tests

In the current section, the details regarding the experimental setup and test results of the specimens in bending are described and discussed.

5.3.3.1 Experimental setup

The bending tests were performed with the aim to determine the global stiffness of the beams/panels, as well as their behaviour up to failure (in part of the specimens). The obtained data was then used to validate the analytical models from the literature and to develop a numerical model in a FE software package.

The bending tests were performed using a four-point loading configuration (Figure 5-3), one of the test configurations prescribed for sandwich panels in ASTM C393 (ASTM, 2011a), as well as in EN 408 (CEN, 2012a) for wood products. To obtain an important contribution of shear to the total deflection, in addition to a short span in relation to the beams' depth, the distance between the loading heads to the supports was kept short (between one-quarter and one-third of the span), so that the bending moment was reduced.
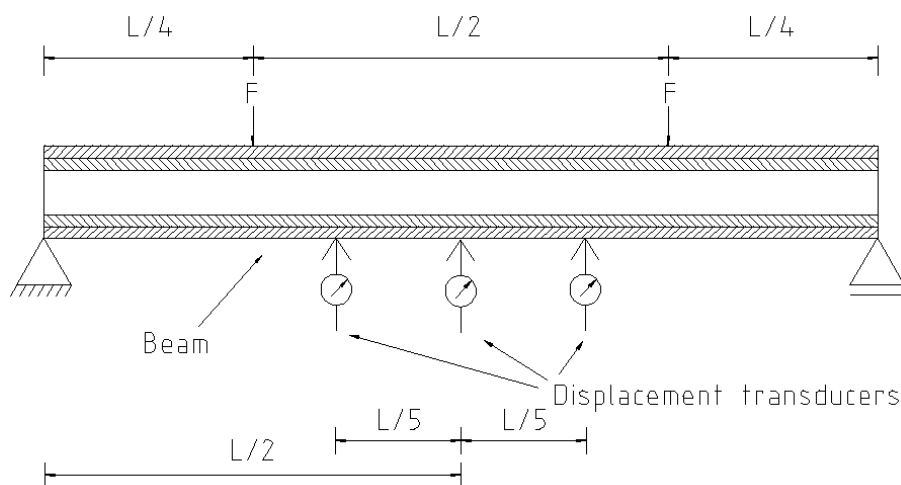
Figure 5-3 - Scheme of the bending tests.

For the determination of the flexural stiffness, the test comprised the application of an equal concentrated force at the thirds of the span of the test specimen, which were simply supported. The experimental assessment included the global and local deflection in the inner third of the span. The global deflection refers to the deflection at mid-span with reference to the supports, while the local deflection refers to the same mid-span deflection but now with reference to two equally spaced points within the inner third of the span (subjected to pure bending). The beams/panels were loaded to 40% of the estimated maximum load causing failure. For the estimation of such load, the Timoshenko beam theory was applied and linear elastic behaviour was considered. For the determination of the failure load, the same setup was used, but only the load and mid-span deflection were measured. In both tests, to determine stiffness and failure load, the load was applied at a rate of 0.0005× h mm/s, where h is the panel depth, a sufficiently slow speed to guarantee a static test.

A load cell (*HBM C6A*) with a capacity of 200 kN and precision of 0.01 kN was used to measure the force, and displacement transducers (from *HBM* and *TML*) with a minimum capacity of 20 mm and precision of 0.01 mm were used to measure the displacement.

The deflections were measured in three points (one at mid-span and the other two equally spaced from the first and between each other by a distance equal to one-third of the span, i.e. between the loading points) and at each side of the bottom face, thus resulting in a total of six measurement points (Figure 5-4). The local deflection was determined by the difference between the deflection at mid-span and the mean deflections in the side points in accordance with Equation (5-25).
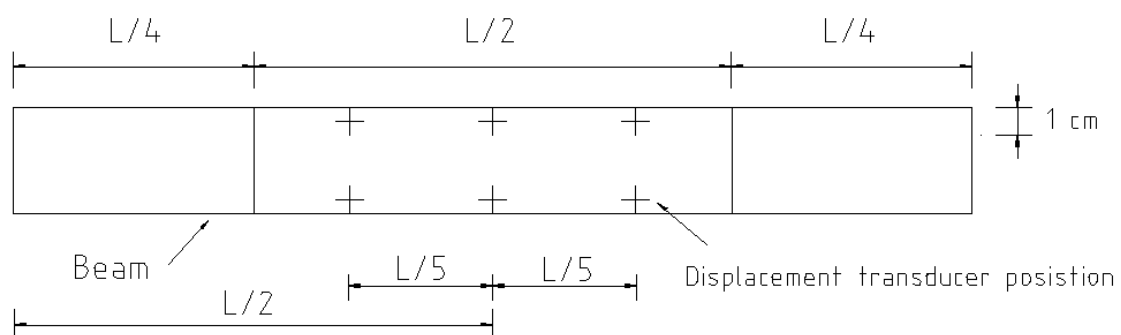
Figure 5-4 – Position of the displacement transducers on the beams.

$$w = w_{central} - \left(w_{left} + w_{right}\right)/2 \qquad (5\text{-}25)$$

One aimed at obtaining the bending stiffness of the beams from the measured local

deflection, as theoretically the deflection in that zone is only due to bending; subsequently, from the measured global deflection, using that same estimate of bending stiffness, one would then determine an estimate of the shear stiffness. However, as shown ahead, from the results obtained, it was found out that the estimated bending stiffness for the tested beams only gave reasonable approximations for the CLT specimens, while it failed to deliver reliable values for the SIP and CIT specimens.

In the initial tests, to evaluate if the compression in the foam layer could have some influence on the measured deflection (in the linear branch of the behaviour), both the local and global deflections were additionally measured at the top face of one of CIT-20/120-B1 specimen (Figure 5-5). As shown in Figure 5-6, the differences between the global deflections measured at the top and bottom of the beam specimen were less than 1%; therefore, after that test, for the remaining tests, the beam's deflections were only measured at the bottom face.
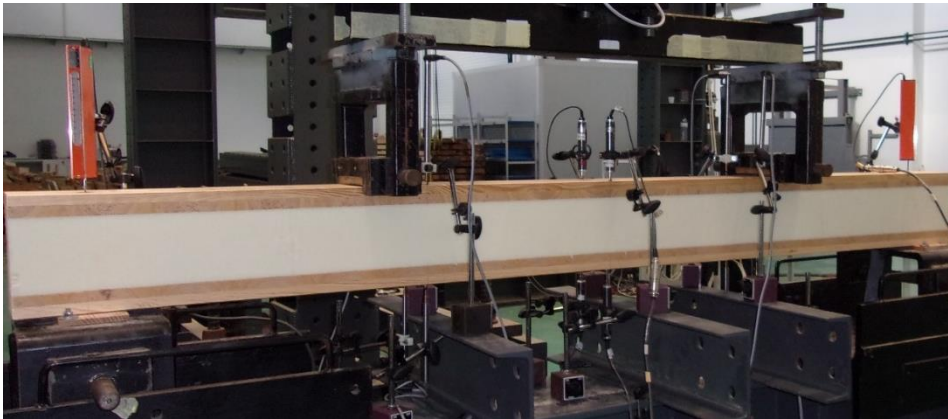
Figure 5-5 – Initial measurement setup.
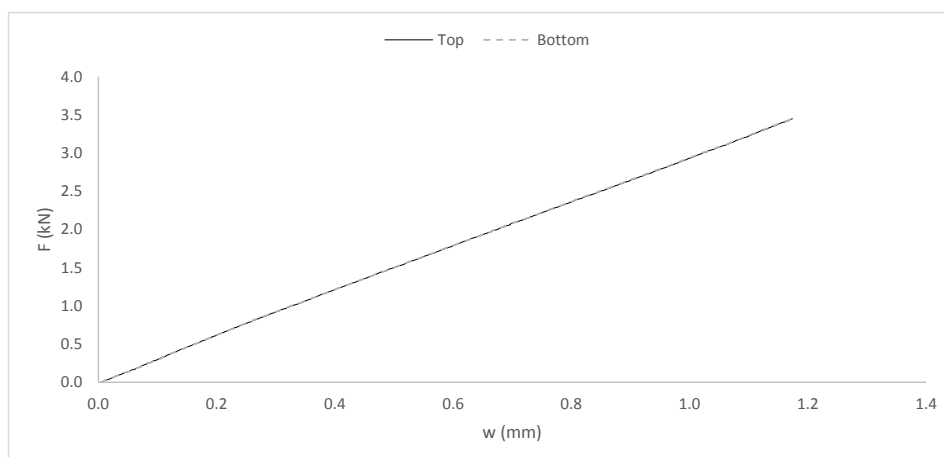
Figure 5-6 – Comparison of the measured global deflection at the top and bottom surface of beam specimen CIT-20/120-B1.

The total deflection (d_T) is obtained from the sum of the deflection caused by bending (d_M) and that caused by shear (d_V), according to Equation (5-26):

$$d_T = d_M + d_V = \frac{Fa}{48EI}(3l^2 + 4a^2) + \frac{Fa}{2G\Omega_r} \tag{5-26}$$

where F is the applied force; a is the distance between the support to the closest load point; l is the span; EI is the bending stiffness, and $G\Omega_r$ is the effective shear stiffness.

From the local deflection measurement, it is possible to obtain the bending stiffness, as in EN 408, according to Equation (5-27):

$$d_{local} = \frac{Fal_1^2}{16EI} \tag{5-27}$$

where l_1 is the distance between the reference points for the local deflection measurement.

Using the bending stiffness calculated from the local deflection measurement as an input in Equation (5-26), it is possible to obtain an estimate of the effective shear stiffness.

5.3.3.2 Results and discussion

Table 5-6 presents the bending stiffness (EI) obtained from the local deflection measurements and the one estimated by the analytical models (Equation (5-28)), as well as the corresponding relative difference (Δ). Based on the information collected from the state-of-the-art review, from the referred analytical approaches, it was decided to use the Timoshenko Beam Theory (TBT) and Shear Analogy (SAV) approaches for the comparison with the results from the experimental campaign. For the calculations, the modulus of elasticity from Table 5-3 and the ones corresponding to the class shown in Table 5-4 were used. For the shear modulus of the wood layers, the mean values of Table 3-1 (Chapter 3) were used. Notice that for the inner wood layers, the shear modulus was taken as the mean value between the ones for the Longitudinal-Tangential and Longitudinal-Radial directions. The shear modulus and strength values for the PUR foam properties were taken as the mean values obtained from the characterization tests (Chapter 3). The comparison between the experimental bending stiffness and that calculated from both analytical approaches is presented in Table 5-6, where Δ was obtained according to Equation (5-28):

$$\Delta = \frac{Experimental - Analytical}{Experimental} \times 100 \ (\%) \tag{5-28}$$

Table 5-6 – Comparison between the bending stiffness calculated from the local deflection with that predicted by the Kreuzinger/Timoshenko models.

Designation	EI (N/mm^2)		Δ (%)
	Experimental	Kreuzinger/Timoshenko	
CLT3-B1	2.59E+10	2.67E+10	-3
CLT3-B2	3.49E+10	2.99E+10	14
CLT3-B3	3.24E+10	3.42E+10	-6
CLT5-B1	1.62E+11	1.47E+11	9
SIP-10/40-B1	1.31E+10	2.98E+10	-127
SIP-10/40-B2	1.32E+10	2.83E+10	-115
SIP-20/120-B1	4.57E+10	4.63E+11	-914
SIP-20/120-B2	3.95E+10	4.59E+11	-1062
CIT-10/40-B1	3.20E+10	6.56E+10	-105
CIT-10/40-B2	3.55E+10	7.60E+10	-114
CIT-10/40-B3	2.71E+10	6.25E+10	-131
CIT-20/40-B1	3.06E+09	2.44E+11	-7892
CIT-20/120-B1	7.73E+09	5.37E+11	-6849
CIT-20/120-B2	4.87E+10	7.37E+11	-1414
CIT-20/120-B3	9.07E+09	5.90E+11	-6398
CIT-20/120-B4	4.58E+10	6.04E+11	-1219
CIT-10/30-P1	1.02E+10	1.38E+11	-1251
CIT-10/30-P2	1.36E+10	2.08E+11	-1432
CIT-10/30-P3	1.36E+10	2.06E+11	-1422
CIT-35/30-P1	3.28E+10	1.26E+12	-3729
CIT-35/30-P2	3.34E+10	1.26E+12	-3659
CIT-35/30-P3	3.81E+10	1.29E+12	-3285
CIT-35/30-P4	3.41E+10	1.29E+12	-3679
CIT-35/30-P5	4.18E+10	1.78E+12	-4157
CIT-35/30-P6	4.05E+10	1.78E+12	-4297

Within the specimens of the same type (e.g. CIT), it is found that some variation on the experimental EI exists, which was expected, as the layers composing the beams, especially the wood ones, had some variation on the elastic properties. Even in CIT, some of the deeper cross-sections present lower stiffness than the smaller ones (e.g. 20/120-B1 vs. 10/40-B1), which is in contradiction with the analytical predictions (deeper cross-section should have higher stiffness). From the analysis of the table, a good agreement is found between the measured and predicted EI for the CLT specimens, with Δ ranging from 3% to 14%. However, for the SIP and CIT specimens, the values are incongruent. It should be mentioned that the procedure of measuring the local deflection for the determination of the bending stiffness is found not only in EN 408, but also, for example, in the technical document TR 002 (EOTA, 2000) for light composite wood-based beams (e.g. I-joists). In such cases of wood products, the differences between the mechanical properties of the core and face materials is not as high as in the tested panels made of wood and PUR. The great differences between those materials, which results in higher

differences between bending and shear stiffnesses, is the possible reason for the inaccuracy of the applied procedure. As an example, considering the analytical estimates of the bending and shear stiffnesses for the CLT 3 and CIT 10/40 beams, it is found that the ratio between EI/GA is around 13E+03 for the first and 13E+05 for the second, which results in a difference of magnitude of around 100 times.

Table 5-7 shows the comparison between the shear stiffness calculated from experimental data with that predicted using the Kreuzinger/Timoshenko models.

Table 5-7 – Comparison between the shear stiffness calculated from experimental data with the predicted by the Kreuzinger/Timoshenko models.

Designation	GA (N/mm²)			$\Delta_{Kreuzinger}$ (%)	$\Delta_{Timoshenko}$ (%)
	Experimental	Kreuzinger	Timoshenko		
CLT3-B1	4.52E+07	2.54E+06	2.11E+06	94	95
CLT3-B2	5.25E+05	2.83E+06	2.36E+06	-440	-349
CLT3-B3	1.13E+07	2.81E+06	2.35E+06	75	79
CLT5-B1	1.69E+06	3.95E+06	4.25E+06	-134	-151

From the analysis of Table 5-7, it is found that the differences between the analytical models (either from Timoshenko and Kreuzinger theories) and the experimental values for the shear stiffness are very different (ranging from 75% to 440%), with the differences being positive in two cases (CLT3-B1 and CLT5-B3) and negative in the other two (CLT3-B2 and CLT5-B1). This may indicate that the procedure used is not adequate to determine the shear stiffness for CLT. The reason for that may be the high relative difference between the mechanical properties between the wood layers, which results in a higher difference between the bending and shear stiffness, much higher than the one that would correspond to glued-laminated timber for example, which has the wood fibres of all layers aligned in the same direction. However, it is also possible that the mean value of the shear modulus considered in the analytical calculation, especially for the cross layers, can be different from the actual value. Part of these differences could also be due to the influence of possible gaps, as the layers were not edge bonded.

The comparison of the measured global deflection with the one estimated by the analytical models (corresponding to 40% of the estimated maximum load causing failure) is presented in Table 5-8.

From the analysis of the results, it is shown that a good agreement was obtained between the analytical models and the experimental values for all types of tested beams/panels. For the CLT, Δ ranged from 1% to 9%; for SIP, Δ ranged from 1% to 12%; for CIT beams, Δ ranged from 0% to 9%; and for the CIT panels, Δ ranged from 1% to 13 %. Both

Timoshenko and Kreuzinger theories gave accurate and comparable predictions. Higher relative differences were obtained for the CIT panels compared to the CIT beams; this result was expected, as the modulus of elasticity of the wood boards composing such panels was not known (only its grade and the corresponding mean value), in contrast to that of the beams.

Table 5-8 – Relative error on the estimation of the mid-span deflection using the Kreuzinger and Timoshenko models.

Designation	$\Delta_{Kreuzinger}$ (%)	$\Delta_{Timoshenko}$ (%)
CLT3-B1	-1	-2
CLT3-B2	-3	-1
CLT3-B3	-2	-1
CLT5-B1	-9	-3
SIP-10/40-B1	-12	-10
SIP-10/40-B2	-5	-3
SIP-20/120-B1	-11	-10
SIP-20/120-B2	-1	1
CIT-10/40-B1	-5	-4
CIT-10/40-B2	-8	-7
CIT-10/40-B3	-1	0
CIT-20/40-B1	-4	-1
CIT-20/120-B1	1	1
CIT-20/120-B2	3	4
CIT-20/120-B3	-8	-7
CIT-20/120-B4	5	6
CIT-10/30-P1	8	9
CIT-10/30-P2	6	7
CIT-10/30-P3	3	4
CIT-35/30-P1	7	10
CIT-35/30-P2	7	9
CIT-35/30-P3	-4	-1
CIT-35/30-P4	11	13
CIT-35/30-P5	-5	-1
CIT-35/30-P6	-3	1

The mid-deflection vs force (per width) curves measured in the failure tests for each beam/panel type are presented next, in Figures 5-7 to 5-13. As the beams had different widths, the force per width is presented instead of the force, to allow for a comparison between beams of the same type.

The thinnest SIPs (10/40) initially presented a linear response, which for a load/width of ~20 N/mm started to present a non-linear behaviour, with progressive stiffness reduction. In the thickest ones (20/120), one of the specimens showed linear behaviour up to failure, while in the other ones the initial linear response was followed by a non-linear variation that resulted in a loss of stiffness, which was then followed by a new linear branch. The CIT beams and the thicker panels (35/30) presented similar curves to the ones of the thickest SIPs, i.e. with an initial linear response followed by a non-linear variation that

stabilized into an almost linear branch. Instead, the thinnest CIT panels (10/30) presented linear behaviour with a slight non-linearity before failure.

All tested specimens presented a similar failure mode: shear failure of the foam layer. Examples of the shear failure in the different specimens tested are shown for SIP (Figures 5-14 and 5-15), CIT beams (Figures 5-16 to 5-18) and CIT panels (Figures 5-19 and 5-20). However, it is worth mentioning that a noticeable deformation of the polyurethane foam was observed in the brink of collapse (between the supports and loading sections), especially in the specimens with the 120 mm thick foam (Figure 5-21).
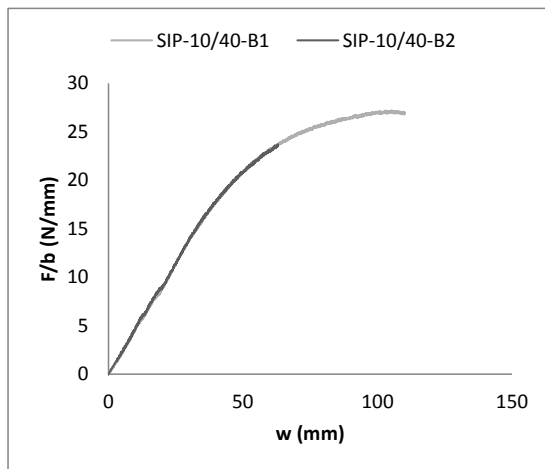
Figure 5-7 – Deflection vs Force per width for the 10/40 SIP beams.
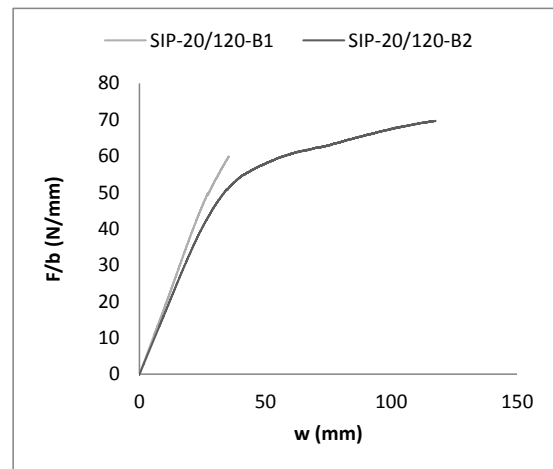
Figure 5-8 – Deflection vs Force per width for the 20/120 SIP beams.
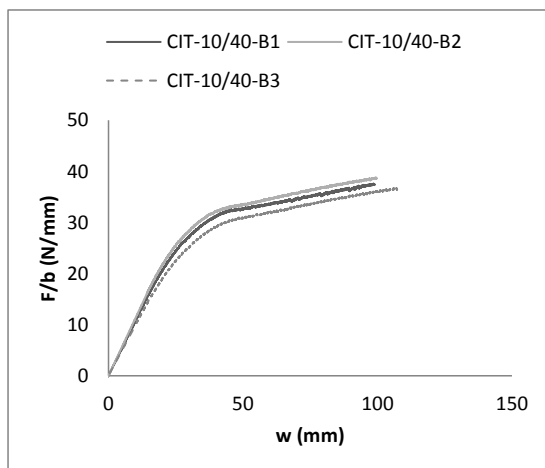
Figure 5-9 – Deflection vs Force per width for the 10/40 CIT beams.
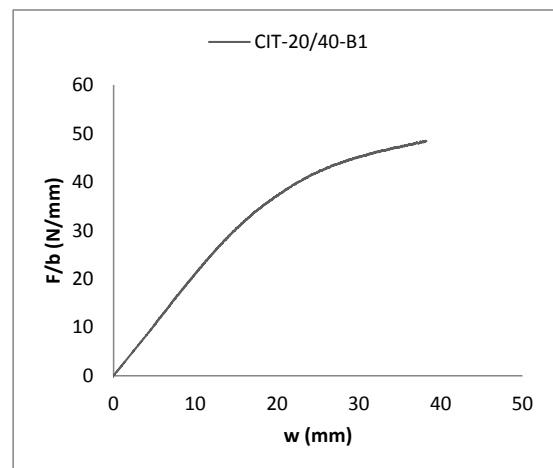
Figure 5-10 – Deflection vs Force per width for the 20/40 CIT beam.
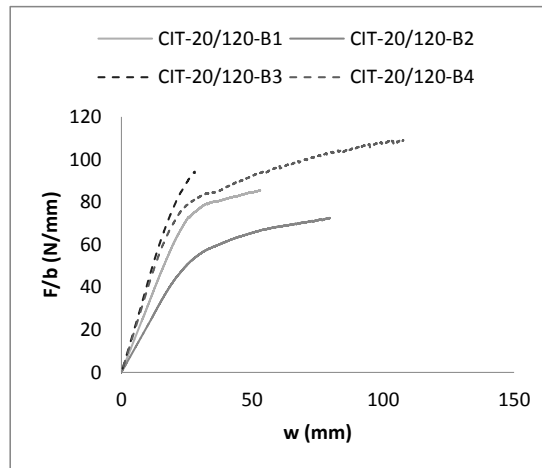
Figure 5-11 – Deflection vs Force per width for the 20/120 CIT beam.
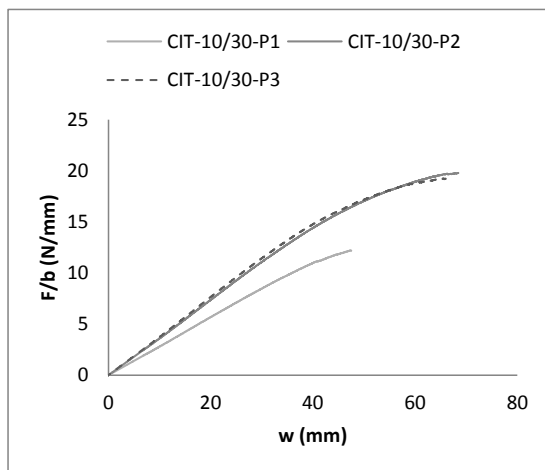
Figure 5-12 – Deflection vs Force per width for the 10/30 CIT panels.
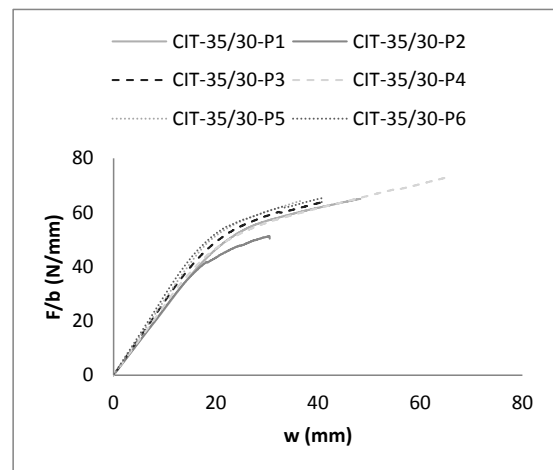
Figure 5-13 – Deflection vs Force per width for the 35/30 CIT panels.

Figure 5-14 – Failure of SIP-10/40-B1.

Figure 5-15 – Failure of SIP-20/120-B1.

Figure 5-16 – Failure of CIT-10/40-B1.

Figure 5-17 – Failure of CIT-20/120-B1.

Figure 5-18 - CIT-20/40-B1.

Figure 5-19 - Failure of CIT-10/30-P1

Figure 5-20 - Failure of CIT-35/30-P1

Figure 5-21 – Detail of the deformation of the polyurethane foam during the failure test.

The maximum load (F_{max}) reached in the bending tests and the corresponding shear stress values (τ) calculated with analytical models (assuming that the behaviour was linear up to failure) are presented in Table 5-9. Notice that both Timoshenko and Kreuzinger models gave the same values of shear stress for the analysed beams, so in the referred table, only one column is shown for the analytical results.

Table 5-9 - Maximum load (F_{max}) reached on the bending tests and corresponding shear stress (f_v) calculated with the analytical models.

Specimen	F_{max} (kN) Experimental	τ (N/mm^2) Analytical
SIP-10/40-B1	3.5	0.27
SIP-10/40-B2	2.9	0.23
SIP-20/120-B1	8.1	0.21
SIP-20/120-B2	8.9	0.25
CIT-10/40-B1	4.9	0.26
CIT-10/40-B2	5.1	0.26
CIT-10/40-B3	4.7	0.26
CIT-20/40-B1	6.3	0.24
CIT-20/120-B1	11.2	0.29
CIT-20/120-B2	11.6	0.23
CIT-20/120-B3	12.0	0.27
CIT-20/120-B4	14.1	0.31
CIT-10/30-P1	9.0	0.10
CIT-10/30-P2	14.6	0.16
CIT-10/30-P3	14.1	0.16
CIT-35/30-P1	24.4	0.24
CIT-35/30-P2	19.2	0.19
CIT-35/30-P3	24.1	0.23
CIT-35/30-P4	27.3	0.26
CIT-35/30-P5	24.2	0.23
CIT-35/30-P6	24.5	0.24

Within each type of panel (e.g. SIP), as expected, the maximum loads reached are higher

on the deeper beams/panels. The same is verified within SIP and the closest CIT solutions (i.e. with the same layer thickness, but with two extra wood layers, like SIP-10/40 and CIT 10/40): the CIT solutions had higher failure loads.

The comparison of the shear stress values calculated using the analytical models (considering the maximum load reached in the tests) with the mean value of shear strength of the polyurethane foam determined in Chapter 3 (0.12 N/mm^2) shows that the analytical models are not accurate in the prediction of the ultimate strength. This overestimation was not unexpected, as non-linear behaviour was clearly observed in the load-displacement curves.

5.3.4 Buckling tests

In the current section, the details regarding the experimental setup and test results of the specimens tested to buckling are described and discussed.

5.3.4.1 Experimental setup

The buckling tests were performed to determine the buckling load of the tested columns and compare it with the one predicted by the analytical models described earlier.

The tests were performed using a simply supported configuration of columns subjected to centred loading. To reproduce as closely as possible an idealized pinned support, following the indications of (Nunes et al, 2016), a support system composed of two steel plates, one with a deep chamfer and the other with a triangular shaped wedge (Figure 5-22), was manufactured (Figure 5-23 a)).
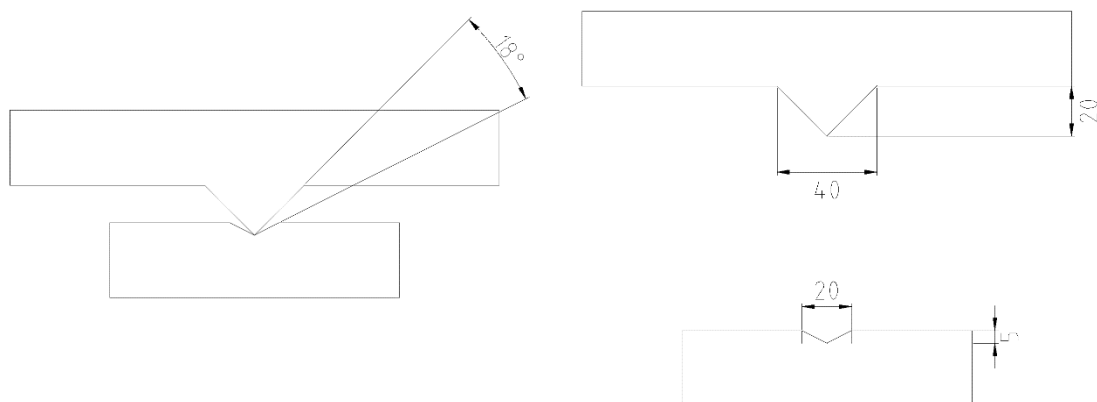
Figure 5-22 – Dimensions (in mm) of chamfer and wedge of the profiled steel plates used to reproduce a pin support.

To connect the end sections of the tested specimens to the steel supports, steel brackets were attached to a eucalyptus wood board, which in turn was connected to one of the steel supporting plates (Figure 5-23 b)). The brackets were attached in a way that the sides were in contact with the specimen and thus restraining the rotation at that point; however, they were not attached to the specimen (e.g. with screws) in order to allow for the sandwich structure to deform freely along the axis direction during the tests. The distance between the base of the plate in contact with the test specimen and the axis of rotation between the steel plates was 21.6 cm.

a)   b)
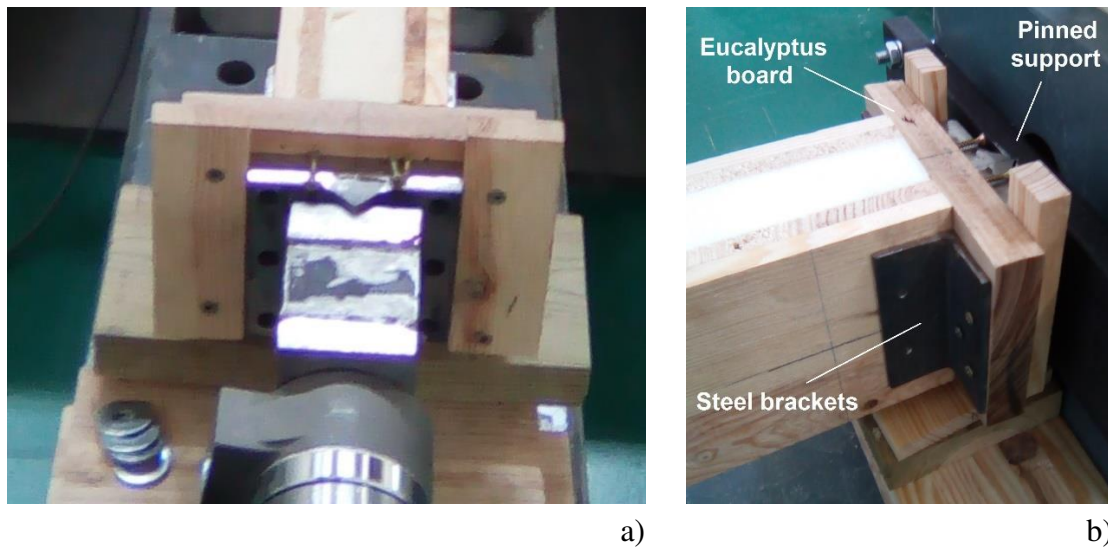
Figure 5-23 - Details of the supports: a) pinned support at the steel plates; b) connection between the test specimen and the steel support.

For the determination of the buckling load, the Southwell method (Southwell, 1932) was used. Since the axial load *vs*. mid-span deflection curve resembles a rectangular hyperbola passing through the origin of the coordinates, then the deflection/load ratio plotted against the deflection will fall closely on a straight line. The inverse of the slope of such line gives an estimate of the least critical buckling load; the intersection of the line with the vertical axis relates the initial imperfection with the least critical buckling load.

The experimental test setup (Figure 5-24 a)) thus included the measurement of the axial load (and axial displacement), as well as the lateral deflection. As the first buckling shape of a simply supported column corresponds to a half-sine wave, the lateral deflection was measured at the mid-span (and at the middle) of both outer layers of the specimens where the amplitude of out-of-plane displacements was expected to be higher (Figure 5-24 b)). A load cell (*HBM C6A*) with a capacity of 200 kN and precision of 0.01 kN was used to measure the applied load, and displacement transducers (from *TML*) with a capacity of

100 mm and precision of 0.01 mm were used to measure the lateral displacements. The axial displacement was measured by the sensor of the hydraulic actuator responsible for the load head movement (precision of 0.01 mm).
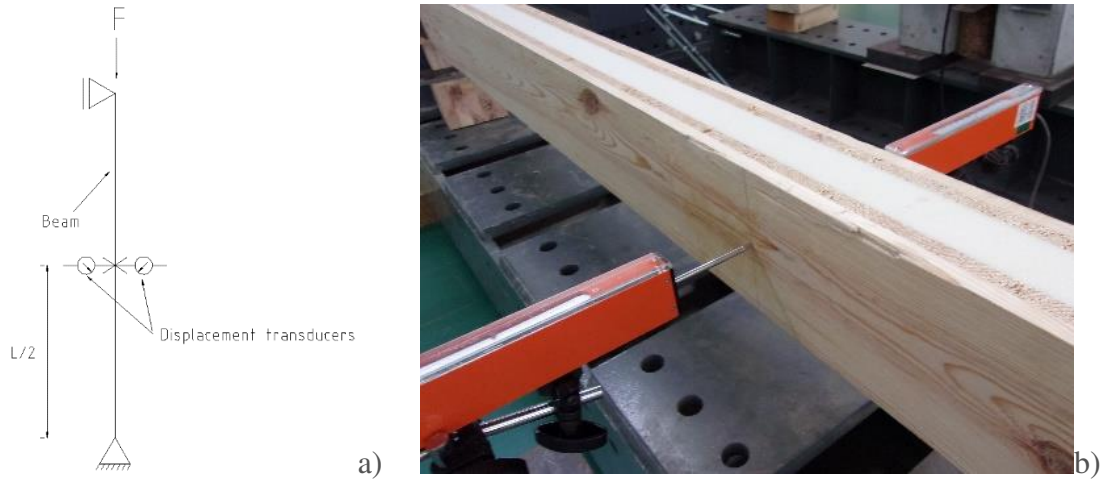
Figure 5-24 – Details of the buckling tests: a) setup; b) measurement of lateral deflection.

The columns were loaded (i) to a value close to the one estimated by Equation (5-20), which according to (Allen, 1969), causes the buckling of a pin-ended sandwich panel or (ii) until approaching the stroke of the displacement transducers. In the tests, the load was applied at a rate of 0.05 kN/s, which was deemed as being slow enough to guarantee a static test. Examples of buckling tests performed in SIP and CIT columns are shown in Figure 5-25.
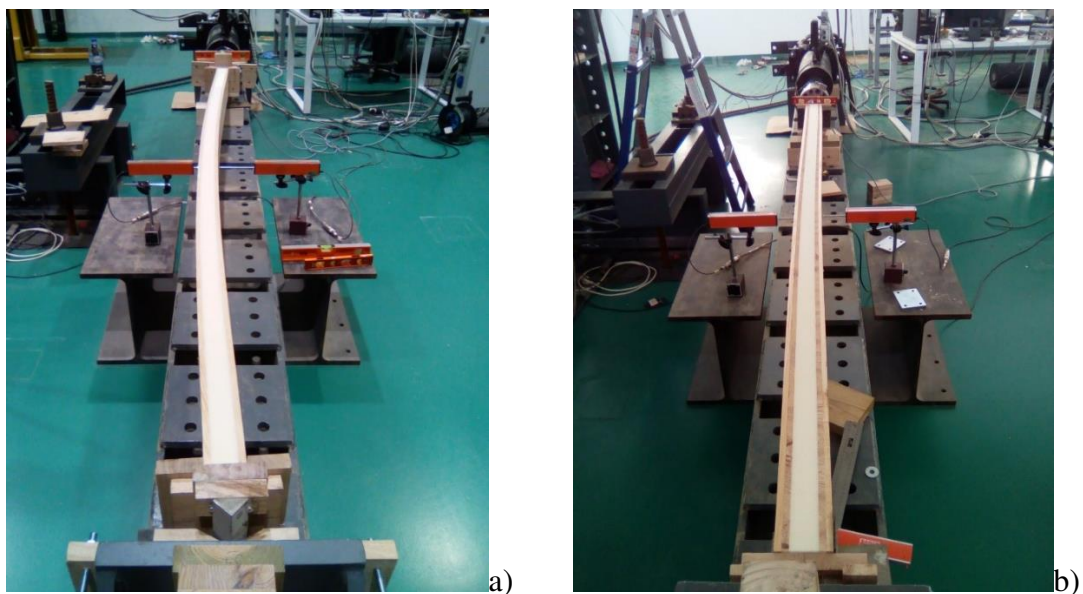
Figure 5-25 - Buckling test of: a) SIP specimen; b) CIT specimen.

5.3.4.2 Results and discussion

The load *vs.* axial displacement curves obtained for the SIP and CIT specimens are shown in Figures 5-26 and 5-27, respectively.
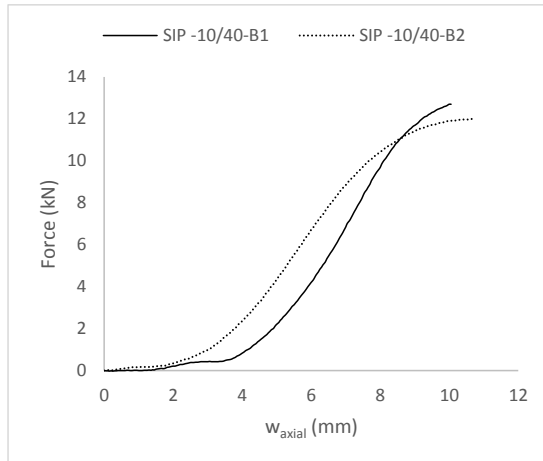
Figure 5-26 – Load *vs.* axial displacement curves for the SIP-10/40 specimens.
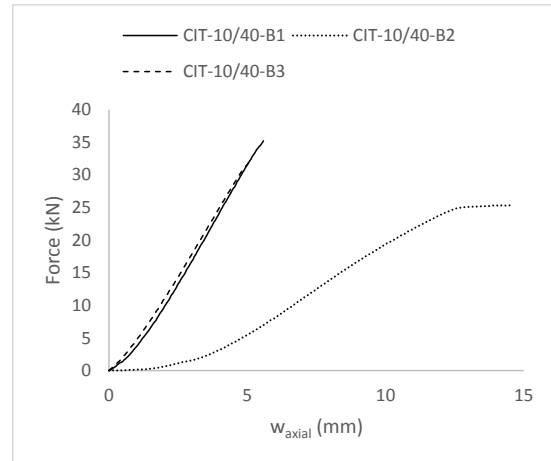
Figure 5-27 – Load *vs.* axial displacement curves for the CIT-10/40 specimens.

From the analysis of the figures, it is found that the SIPs curves had, after the initial toe region, a nearly linear branch, followed by a non-linear phase. In the CIT specimens, a similar linear part is better defined; in one of the specimens from that series (B2), at some point, the response became non-linear with an almost constant force plateau with an increase of axial displacement, which is related to the bending of the specimens associated to the triggering of flexural buckling.

The load *vs.* lateral displacement curves for the SIP and CIT specimens are shown in Figures 5-28 and 5-29, respectively.

As a general comment, all the specimens showed a curve that can be approximated to a rectangular hyperbola, thus allowing to apply the Southwell method. The two SIP specimens showed a very similar response, and so did two of the CIT specimens (B1 and B3). The CIT B2 specimen showed a slightly different response, with higher initial lateral displacements and reaching a significantly lower load compared to the other two specimens of the same series.

The lateral displacement/load *vs.* lateral displacement curves used for the determination of the buckling load for the SIP and CIT specimens are shown in Figures 5-30 and 5-31, respectively.

The limits for the linear regression (marked with dots in the figures) were chosen in a way that the square correlation obtained for that portion was equal to or higher than 0.99. From the analysis of the figures, it is found that similar slopes are observed between the SIP specimens and the same applies to the CIT ones. This indicates that few differences would exist between the buckling loads of the same type of specimens.
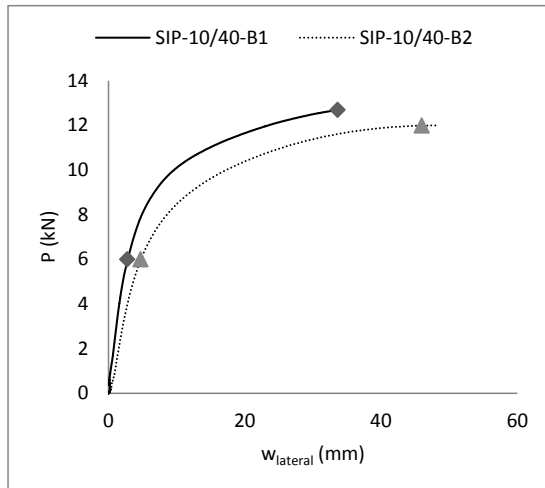
Figure 5-28 – Load *vs.* lateral displacement curve for the SIP-10/40 specimens.
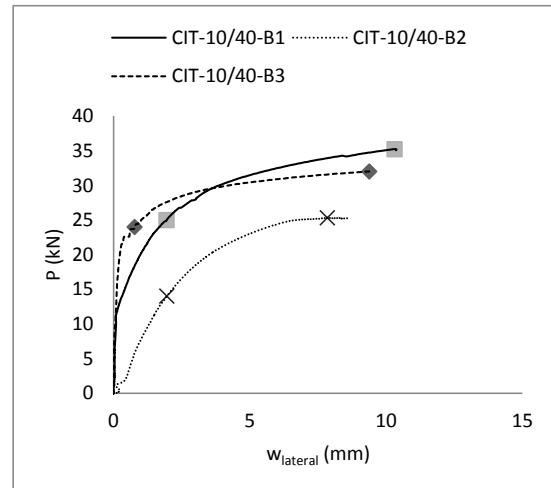
Figure 5-29 – Load *vs.* lateral displacement curve for the CIT-10/40 specimens.
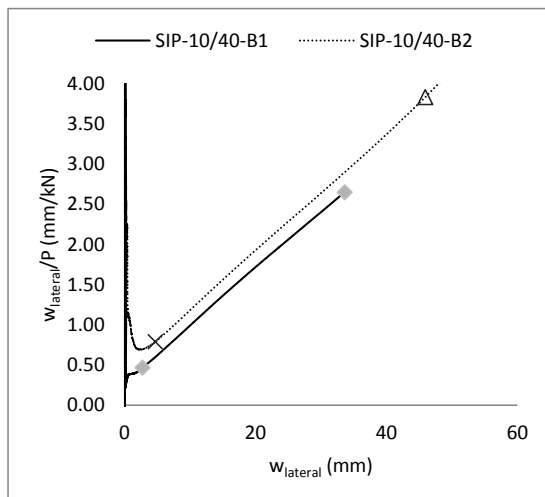
Figure 5-30 – Lateral displacement /load *vs.* lateral displacement curve for the SIP-10/40 specimens.
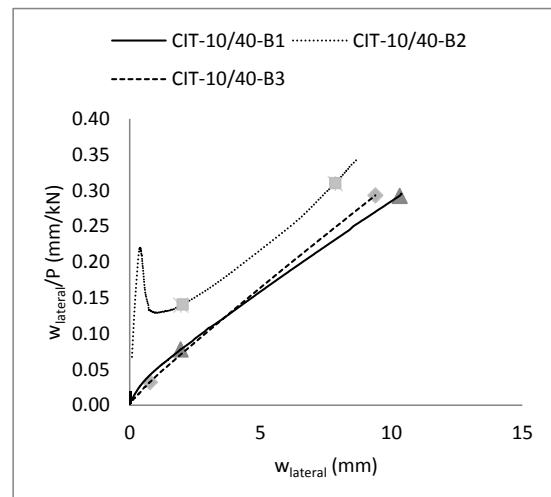
Figure 5-31 – Lateral displacement /load *vs.* lateral displacement curve for the CIT-10/40 specimens.

The comparison between the buckling loads obtained from the experimental results and the ones predicted using the analytical model of (Allen, 1969) are shown in Table 5-10. It should be noticed that in the calculation of the theoretical buckling load, the column

length was taken as the length of the specimen plus the distance to the axis of rotation of each support. The consideration of the actual length of the specimen would provide higher buckling values than the ones listed in Table 5-10. The relative difference between the estimates of the buckling load with the experimental values was calculated in accordance with Equation (5-18).

Table 5-10 – Comparison between the buckling loads predicted using the analytical model of (Allen, 1969) and the experimental ones, and corresponding percentage relative difference (Δ).

| Specimen | Buckling load (kN) | | Δ (%) |
	(Allen, 1969)	Experimental	
SIP-10/40-B1	15.5	14.0	-11
SIP-10/40-B2	14.7	13.6	-8
CIT-10/40-B1	35.7	38.8	8
CIT-10/40-B2	36.5	33.3	-10
CIT-10/40-B3	32.8	32.9	0

The analysis of the results shown in Table 5-10 confirms that the analytical model of (Allen, 1969) provides accurate predictions for the buckling load for both SIP and CIT specimens. In what comprises the experimental loads, it is found that few differences exist between the equivalent series, with SIP ranging from 13.6-14.0 kN and CIT between 32.9 to 38.8 kN. As expected, due to the higher axial stiffness, the CIT beams present higher buckling loads than the SIP ones.

5.4 Finite element modelling of the beam-type elements

5.4.1 Introduction

For the simulation of the load-displacement behaviour of the beams tested in bending, numerical models were developed and implemented in the finite element software *ABAQUS* (Simulia, 2014). Two options for the modelling of the foam material were considered: the plastic model and the crushable foam model from *ABAQUS* library. According to the *ABAQUS* manual, the crushable model can describe the foam material deformation in compression due to the cell wall buckling process and can be used to model the difference between a foam material's compressive strength and the much smaller tensile bearing capacity resulting from cell wall breakage in tension. The crushable foam option is limited to 3D models, while the plastic one can be used in both 2D and 3D models. For the last one, the two types of modelling were considered in order to check the accuracy of using a 2D model instead of a 3D model to simulate the response

of the beams, which would improve the computational costs involved in this type of simulations.

5.4.2 Description of the FE model

5.4.2.1 Selection of finite element type

For the 3D models, the type of finite element used was the "C3D8R" - a three-dimensional, continuum hexahedral, eight-node linear brick with reduced integration, hourglass control and first-order interpolation. For the 2D model, the type of finite element used was the "CPS4R" - a four-node bilinear plane stress quadrilateral element with reduced integration, hourglass control. (Simulia, 2014).

5.4.2.2 Material modelling

For the modelling of the wood parts, two material options were considered: linear isotropic and linear orthotropic. In the case of the compressed wood layer (top layer) plastic behaviour was also considered. Although the orthotropic model is the closest to the real behaviour of wood, it was decided to check if the simpler one (isotropic) was able to deliver accurate results too. For the definition of the modulus of elasticity on the isotropic option, the mean values obtained from the experimental tests shown in Table 5-3 and 5-4 were considered. The Poisson's coefficient was taken as 0.3, based on previous works with FE models (Santos et al, 2015).

For the orthotropic modelling in *ABAQUS*, nine constants were required: the modulus of elasticity in the three orthogonal directions (longitudinal-L, tangential-T and radial-R), the shear modulus in the three planes (LT, TR and LR) and the three corresponding Poisson's coefficients (v_{LT}, v_{TR} and v_{LR}). Reference values of the referred parameters for Maritime pine were found in (Xavier et al, 2004). The considered relations between the modulus of elasticity and shear modulus with the longitudinal modulus of elasticity and the Poisson's ratios are shown in Table 5-11. As no differentiation between the tangential and radial directions was made, the values for the shear modulus and Poisson's ratio related to those directions were assumed as mean values of the two directions.

Regarding the definition of the plasticity for the compressed wood layers, the information collected from (Martins, 2018) for Maritime pine was used and is shown in Table 5-12. Due to lack of data related with these properties for Australian blackwood, the same plasticity model was used, which was expected to be a good approximation since the

compressive strength of both species were found to be quite close from the state-of-art review (Chapter 3).

Table 5-11 - Relations between the modulus of elasticity and shear modulus on the three orthogonal directions with the longitudinal modulus of elasticity and the corresponding Poisson's ratios.

E_R/E_L (%)	E_T/E_L (%)	G_{LR}/E_L (%)	G_{LT}/E_L (%)	G_{RT}/E_L (%)	v_{LR}	v_{LT}	v_{RT}
12.6	6.7	9.3	8.1	1.9	0.47	0.051	0.59

Table 5-12 - Nominal stress and nominal strain used on the plastic model of the wood layers.

$\varepsilon_{nominal}$	$\sigma_{nominal}$ (MPa)
0.005	39.8
0.024	40.0

The comparison between the load-displacement curve obtained with the 3D model considering the orthotropic and the isotropic behaviour of the wood layers is shown in Figure 5-32 for CIT-10/40-B1. The material model considered for the foam was the linear plasticity.
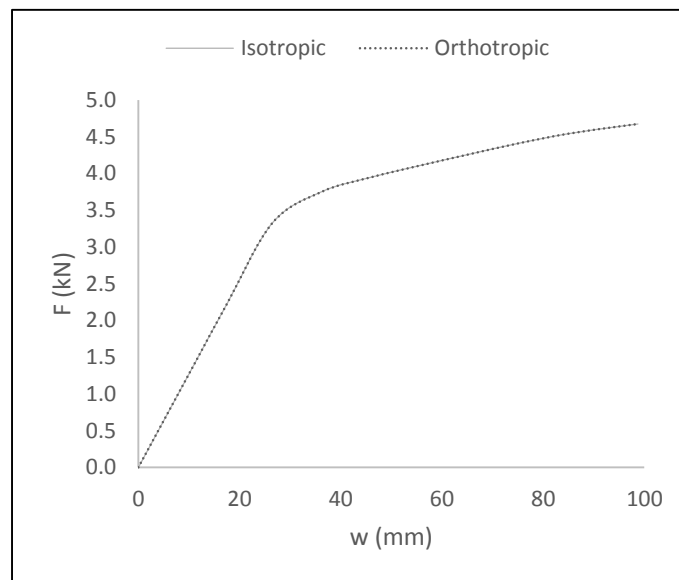
Figure 5-32 – Comparison between the load-displacement curves for the CIT-10/40-B1 beam calculated using the 3D model and assuming either the isotropic or orthotropic material model for wood.

From the analysis of the figure, it is found that the two curves are very similar, which indicates that the simplification of assuming wood as a linear isotropic material can be

used in the models. In further simulations, the isotropic model was used.

As referred earlier, the polyurethane foam was modelled assuming two different models: the plastic and the crushable foam models, both of them in combination with a linear elastic material model to describe the initial behaviour of the foam. For the definition of the plasticity of the material (or the foam hardening), *ABAQUS* requires the true-stress/true-plastic strain curve. The conversion of the nominal strain ($\varepsilon_{nominal}$) to true strain (ε_{true}) is made in accordance to Equation (5-29) and the conversion of the nominal stress ($\varepsilon_{nominal}$) to true stress (ε_{true}) is made in accordance to Equation (5-30).

$$\varepsilon_{true} = \ln(1 + \varepsilon_{nominal}) \tag{5-29}$$

$$\sigma_{true} = \sigma_{nominal}(1 + \varepsilon_{nominal}) \tag{5-30}$$

From the subtraction of the elastic strain ($\varepsilon_{true,elastic}$) as in Equation (5-31) from ε_{true}, which represents the total strain, the plastic strain is obtained as in Equation (5-32).

$$\varepsilon_{true,elastic} = \sigma/E \tag{5-31}$$

$$\varepsilon_{true,plastic} = \varepsilon_{true} - \varepsilon_{true,elastic} \tag{5-32}$$

In *ABAQUS*, the plasticity model is only valid for isotropic materials, so it was necessary to simplify the behaviour of the polyurethane foam and assume it as isotropic. This resulted in assuming that the material has the same mechanical properties in all the symmetry planes; moreover, the response in tension and compression was also assumed to be equal. In fact, polyurethane was found to be anisotropic (or at least transversal isotropic from the experimental characterization tests, Chapter 3) with a linear elastic response in tension and an elastoplastic response in compression.

For the definition of the stress-strain curve, *ABAQUS* requires that the input is strictly increasing or constant. However, the nominal stress-strain curves obtained in the flatwise and edgewise compression tests for the polyurethane foam (see Chapter 3, sub-section 3.3.1.1) were not strictly increasing or constant. Both the flatwise and edgewise curves had an initial yield point from which the stress decreased to a nearly constant value, after which, for large very strains, it increased again and significantly due to densification of the foam. Based on this fact, for the definition of the input nominal stress-strain curve on the software, the following assumptions were made:

- The Poisson's ratio was taken as 0.3 based in (Mohamed et al, 2015).
- For the definition of the initial linear elastic region, the modulus of elasticity was defined with basis on the mean shear modulus (3.0 N/mm^2) (obtained in the experimental tests presented in Chapter 3) and the Poisson's ratio, for which a value of 7.8 N/mm^2 was calculated assuming the material as isotropic;
- For the definition of the yield stress, the mean value for the maximum stress reached at low strains (<0.1) obtained in the flatwise and edgewise compression tests were considered (0.267 and 0.140 N/mm^2, respectively) plus a mean value of those (0.204 N/mm^2). The reason for considering a "mean" curve, was to get a possible approximation to the real behaviour of the foam, as in reality it is an anisotropic material, but as referred before, the plasticity model considers an isotropic material;
- After the yield point, the strains were assumed as constant until $\varepsilon_{nominal} = 0.15$ (a value which was found enough on the numerical simulations to describe accurately the experimental results).

The nominal stress-strain curves used as input data in the FE models is shown in Figure 5-33 and the corresponding true stress-plastic strain curve in depicted in Figure 5-34.
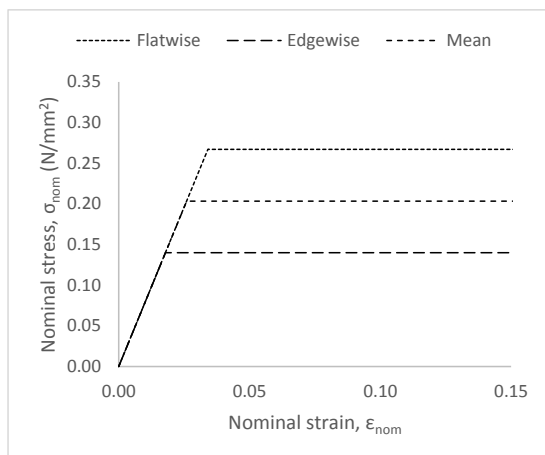
Figure 5-33 – Nominal stress-strain curves adapted to use as input data in the FE model.
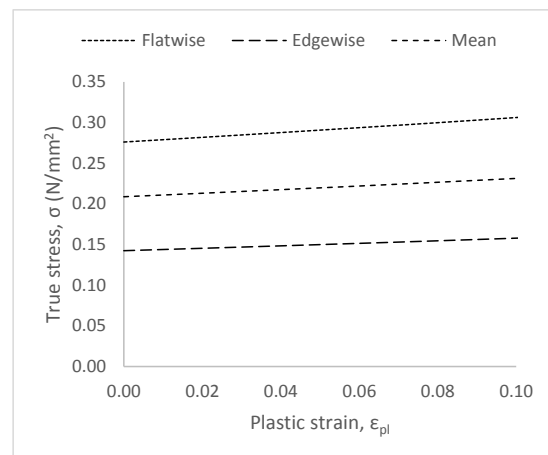
Figure 5-34 - True stress-plastic strain curve used as input in the FE model.

The crushable foam material model presents two options for the hardening: isotropic or volumetric. Both of them require the definition of the compression yield stress ratio (k), which is given by the ratio between initial yield stress in uniaxial compression to initial yield stress in hydrostatic compression of the material. As no hydrostatic tests were performed, this parameter was estimated following another method. According to the

ABAQUS manual, the compression yield stress ratio can be estimated from the plastic Poisson's ratio according to Equation (5-33),

$$k = \sqrt{3(1 - 2v_p)} \qquad (5\text{-}33)$$

where v_p is the plastic Poisson's ratio. The *ABAQUS* manual indicates that for low-density foams the plastic Poisson's ratio is nearly zero, so zero was assumed for the simulations, which corresponds to $k = 1.73$. For the volumetric foam hardening model, also the hydrostatic yield stress ratio (k_t), that represents the ratio of the yield stress in hydrostatic tension to initial yield stress in hydrostatic compression is required. If no data is available, a value between 0.05 to 0.10 is recommended, and 0.05 was considered in the simulations. However, due to lack of convergence on simulations when using the volumetric hardening option, only the isotropic hardening option was considered for the crushable foam model simulations presented ahead.

The adhesive layers connecting the wood layers and the wood layers to the polyurethane foam layer were modelled as tie constraints, as from the characterization results from Chapter 4 and the experimental test results presented in this chapter, it was found that no failure on those elements was expected. For the interaction between the outer wood layers with the adjacent inner wood layers, the outer layers were considered as master surfaces and the inner ones as slave surfaces. Similarly, for the interaction between the inner wood layers and the foam core, the wood was considered as a master surface and the foam core as slave surface.

5.4.2.3 Loading and boundary conditions

For the boundary conditions, in the 3D model, the supports were modelled as a linear constraint along the width of the beam, while in the 2D model they were simulated as a punctual constraint. To simulate a simply supported beam, one of the supports had all the degrees of freedom blocked and only the rotation along the axis parallel to the beam width was allowed; in the other one, the horizontal sliding along the beam length was also allowed.

As in the experimental tests the load was applied using a displacement rate per time, the load application in the model was simulated by imposing a gradual displacement at the point loads.

5.4.2.4 Mesh

It should be noticed that the definition of the mesh elements in the 3D models was often limited due to the maximum number of nodes allowed in the used version of the software (250,000). For the 3D models, one aimed at having at least three elements along the depth of each layer. However, due to the referred limitations, it was only possible to have two elements along the depth of the outer wood layers, while for the inner part layers three elements were considered or six for the beams with the deepest core (Figure 5-35).

a)   b)
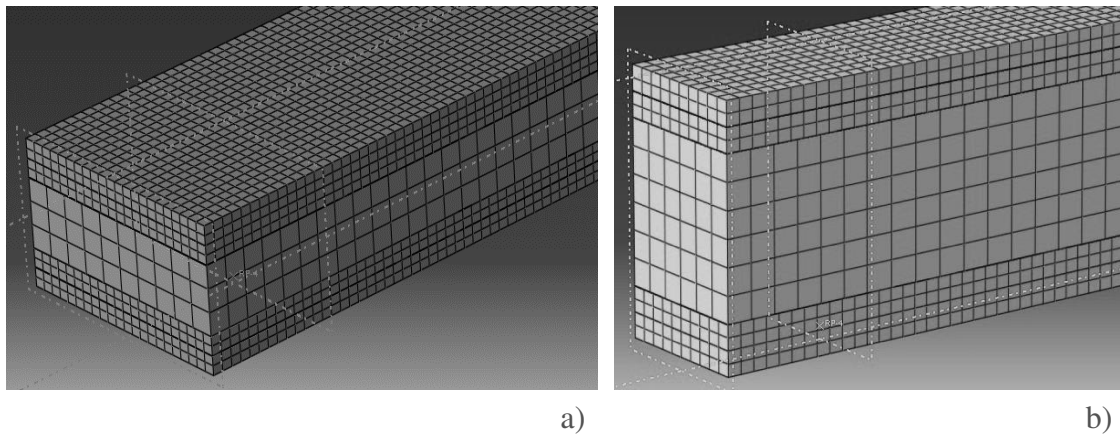
Figure 5-35 - Details of the 3D model mesh: a) CIT-10/40-B1; b) CIT-20/120-B1.

For the definition of the mesh in the 2D models, due to the use of node-to-node tie constraints between layers, *ABAQUS* requires that the element size of the mesh is smaller at the master surfaces than at the slave surfaces. For that reason, the outer wood layers were modelled with a finer mesh than the inner wood layers. The same principle was applied for the mesh of the foam layer with respect to the inner wood layer (Figure 5-36).

a)   b)
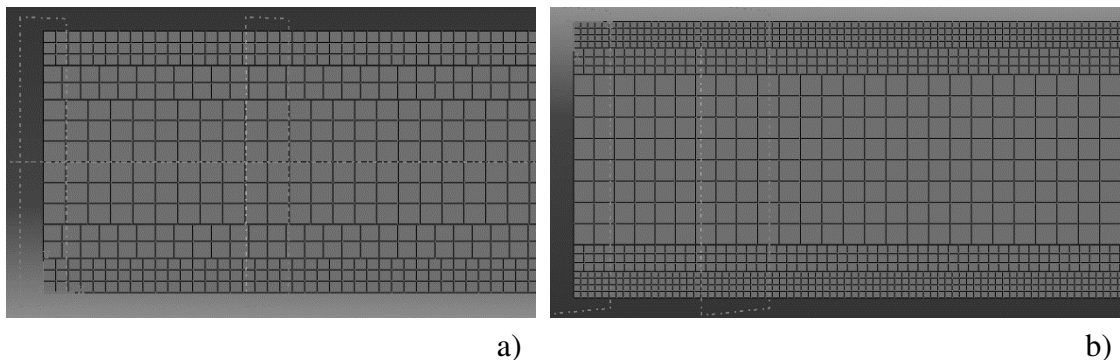
Figure 5-36 - Details of the 2D model mesh: a) CIT-10/40-B1; b) CIT-20/120-B1.

A sensitivity analysis was carried out considering the three different meshes (Table 5-13)

applied to two types of CIT beams: the thinner CIT-10/40-B1 and the deeper CIT-20/120-B1.

Table 5-13 – Discretization of the mesh as a function of the number of elements along the depth of each layer for the 2D models.

Name	Elements along the depth		
	Outer wood	Inner wood	Foam
Ref 1	3	2	6
Ref 2	4	3	8
Ref 3	6	5	12

The comparison between the load-displacement curves obtained with the different mesh discretizations is shown in Figure 5-37 for CIT-10/40-B1 and CIT-20/120-B1. Notice that the referred curves correspond to models that used the plasticity material model (and flatwise compression curve) for the foam layer. For crushable foam models, the results were similar.

a)   b)
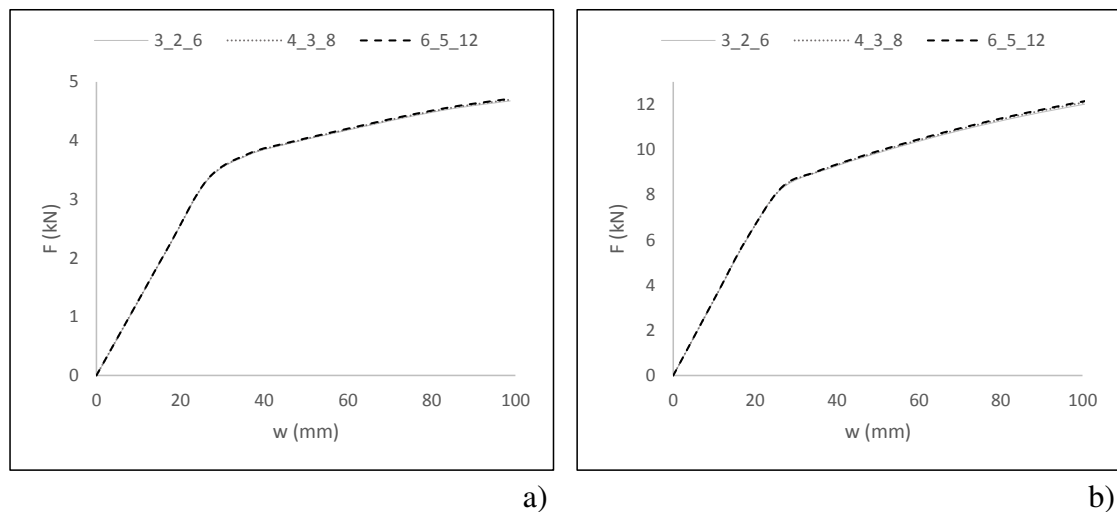
Figure 5-37 - Load-displacement curve calculated using different mesh discretization for: a) CIT-10/40-B1; b) CIT-20/120-B1.

From the analysis of the referred figure, it is found that for both cases, the different meshes delivered very similar curves, indicating that the less refined mesh "Ref 1" could be used in the numerical simulations.

5.4.3 Preliminary studies

In the current section, results regarding initial studies about different modelling options

are compared and discussed, namely the consideration of non-linear geometrical effects and the use of 2D vs. 3D models. For the stress-strain curves of the models, the one corresponding to flatwise compression curve (Figure 5-34) was considered.

5.4.3.1 Effect of the non-linear geometrical effects on the results

The consideration of the non-linear geometrical effects on the results was tested for two types of CIT beams: the thinner CIT-10/40-B1 and the deeper CIT-20/120-B1 (Figure 5-38). Notice that the referred curves correspond to models that used the plasticity material model for the foam layer. For crushable foam models, it was not possible to consider the non-linear geometrical effects due to convergence problems.

a)   b)
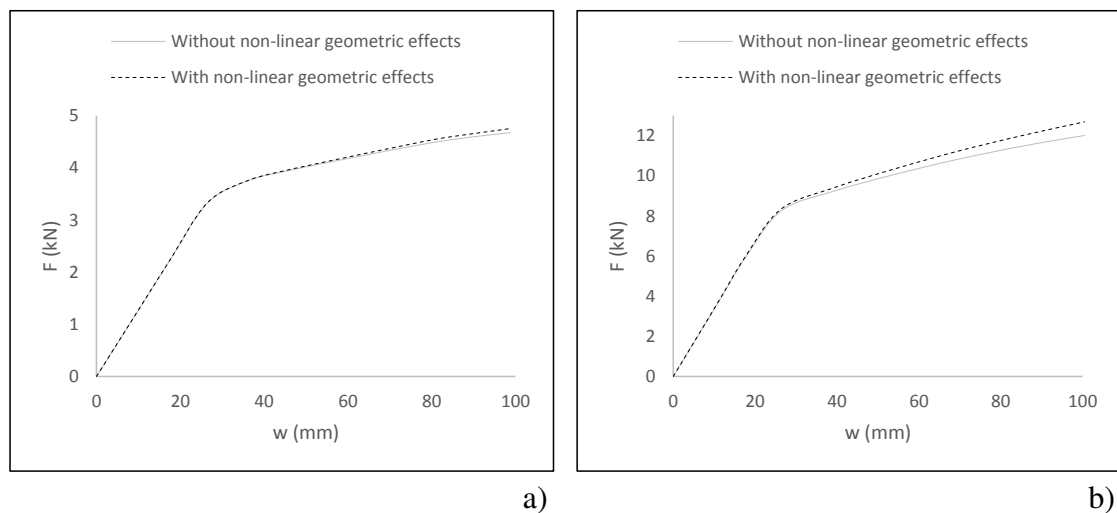
Figure 5-38 - Load-displacement curve calculated in the FEM model with and without the consideration of geometrical non-linear effects for: a) CIT-10/40-B1; b) CIT-20/120-B1.

The results show that for the thinner beam (CIT-10/40-B1) the influence is almost negligible; however, for the deeper beam (CIT-20/120-B1) a significant increase of the load in the plastic region is observed. The reason behind such difference may be related to the different thickness of the polyurethane foam, whose plastic deformations would increase for higher thicknesses. This aspect can be observed in a simulated compression test (as the one presented in Chapter 3) in the FE software for two parallelepiped foam specimens: both with 120×120 mm^2 of area, one with 40 mm of depth and the other with 120 mm. Both specimens had the material properties defined for the polyurethane foam and were loaded in the larger plane (120×120 mm^2) up to 4 kN, a load level corresponding to the plastic region of the material. From the simulation results, total deformations of 1.3 mm and 4.7 mm were obtained for the 40 mm and 120 mm specimens, respectively. This shows that for the same load level, the deformation occurring at the

thicker foam is higher and thus the geometry of the cross-section on the thicker beams would actually vary more.

5.4.3.2 Comparison between the 2D and 3D models

Figure 5-39 a) and b) present a comparison between the numerical load-displacement curves for the CIT-10/40-B1 and 20/120-B1 beams, respectively, obtained from 2D and 3D models, where the plasticity model for the foam layer was considered.

a)   b)
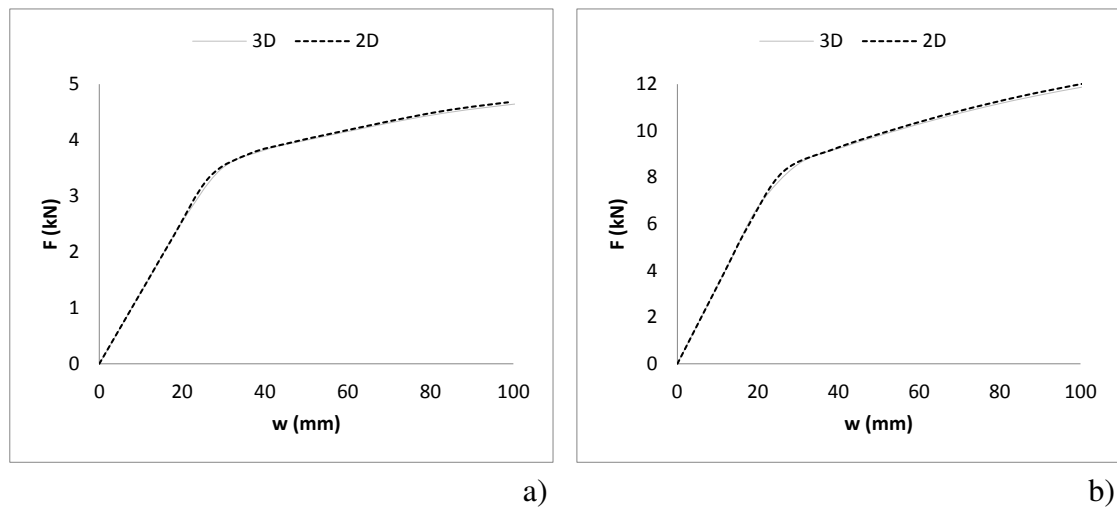
Figure 5-39 - Comparison between the load-displacement curves obtained from the 2D and 3D models: a) CIT-10/40-B1; b) CIT-20/120-B1.

From the analysis of the figures, it is found out that, for both beams, the outputs of the 2D models are almost similar to the ones obtained from the corresponding 3D models. Thus, it is found that the 2D model can be used for the simulations, as it provides similar levels of accuracy at a much lower computational cost.

5.4.4 Study of the experimental setup

The FE model was used to ascertain the experimental methodology for determining the bending and shear stiffness from the local and global deflections, in particular, to conclude about its viability/precision. For that purpose, and using the geometry of the SIP 10/40-B1 and the plasticity model for the foam layer, three beams were modelled using distinct material properties: one assuming all layers made of wood with the inner layer crossed as in CLT; another one with the inner layer made of polyurethane as in SIP and the third with two additional wood layers, i.e. a CIT beam. The same span and load positions of SIP 10/40-B1 were considered. For the local deflection points, besides the

setup used in the experiments, i.e. outer points spaced at L/2.5 from each other, other relative distances between the outer points, namely L/10 and L/20, were considered to check for some possible influence on the position of measurement. The material properties considered in the models are presented in Table 5-14.

The material properties in conjunction with the beam geometry were used to calculate the analytical bending and shear stiffnesses according to the Timoshenko beam theory. To obtain the stiffness from the FE model results, the methodology presented in section 5.3.3.1 was used. For the variations considered, the bending and shear stiffnesses calculated from the FE models are compared to the reference solution (Timoshenko) and the relative differences shown in Figure 5-40 (bending) and Figure 5-41 (shear).

Table 5-14 – Material properties assumed in the model.

Material	E (N/mm^2)	v
Wood	14000	0.3
Wood - cross layer	470	0.3
PUR	8	0.3
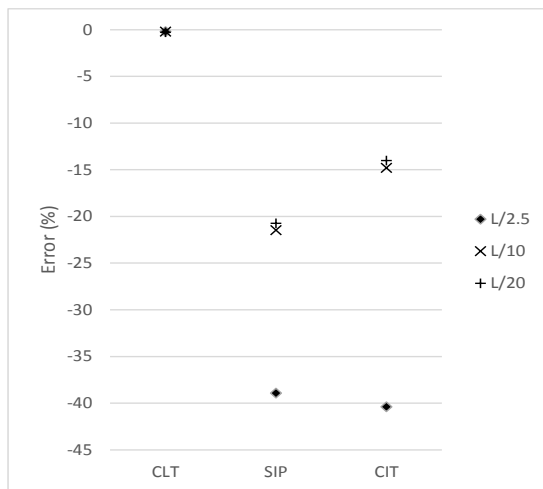
Figure 5-40 – Relative differences between the bending stiffness calculated according to the Timoshenko beam theory and the ones calculated from the FE model from different measuring points of the local deflection.
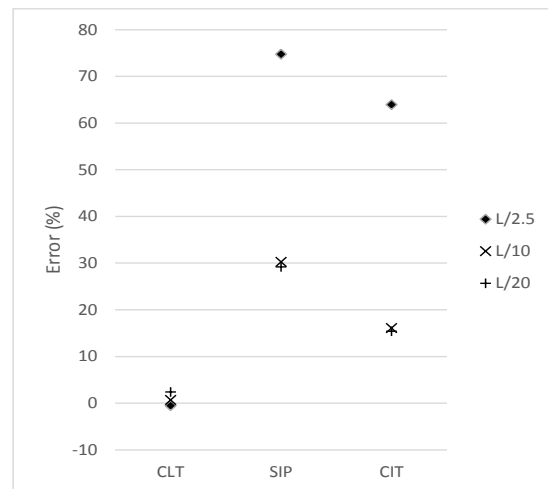
Figure 5-41 – Relative differences between the shear stiffness calculated according to the Timoshenko beam theory and the ones calculated from the FE model from different measuring points of the local deflection.

Overall, it is found out that the bending stiffness calculated from the FE model for the CLT solution matches the analytical value and it is independent of the position of measurement of the local deflection. In the same way, the determined shear stiffness approaches quite well the analytical value for CLT. However, for both SIP and CIT, there

is a significant error, with the bending stiffness presenting relative differences of ~20-40% for SIP and ~15-40% for CIT. For both cases, it is also found out that the error is smaller for the measurements taken closer to the middle of the beam. As a consequence of the error on the calculus of the bending stiffness, also the shear stiffness values are inconsistent with the analytical ones (Figure 5-41). In sum, the FEM simulations confirmed that the experimental procedure of measuring the local deflection for the determination of the bending stiffness is not a viable method for SIP or CIT beams, while for CLT it is expected to deliver accurate results.

5.4.5   Results and discussion

This section presents the comparison of the experimental and numerical load-displacement curves. The 2D model assuming isotropic materials, with the plastic model for the foam layer, without non-linear geometric analysis and mesh 'Ref 1' was used. For the crushable foam, the 3D model (2D is not available for such material model) with isotropic hardening, without non-linear geometric analysis and mesh 'Ref 1' was considered. As no failure criterion was defined, the simulations were run until the displacement on the simulations was at least equal to the one measured on the experimental tests. Due to limitations in the maximum number of nodes allowed for the software license (250,000) and the requirement of a 3D analysis, the crushable foam model was not considered for modelling the CIT panels.

The comparison between experimental and numerical load-displacement curves for the SIP beams for two types of cross-section tested, 10/40 (B1) and 20/120 (B2), are presented in Figures 5-42 and 5-43, respectively. The results for the remaining beams, which were generically similar, are presented in Appendix A, section A.1.
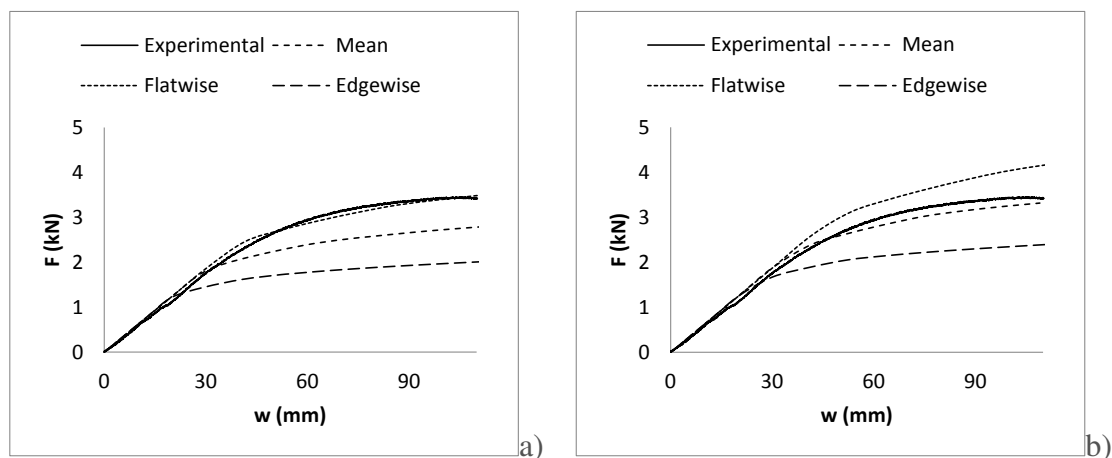
Figure 5-42 - Comparison of the experimental and numerical load-displacement curves for SIP-10/40-B1: a) Plastic model; b) Crushable foam model.
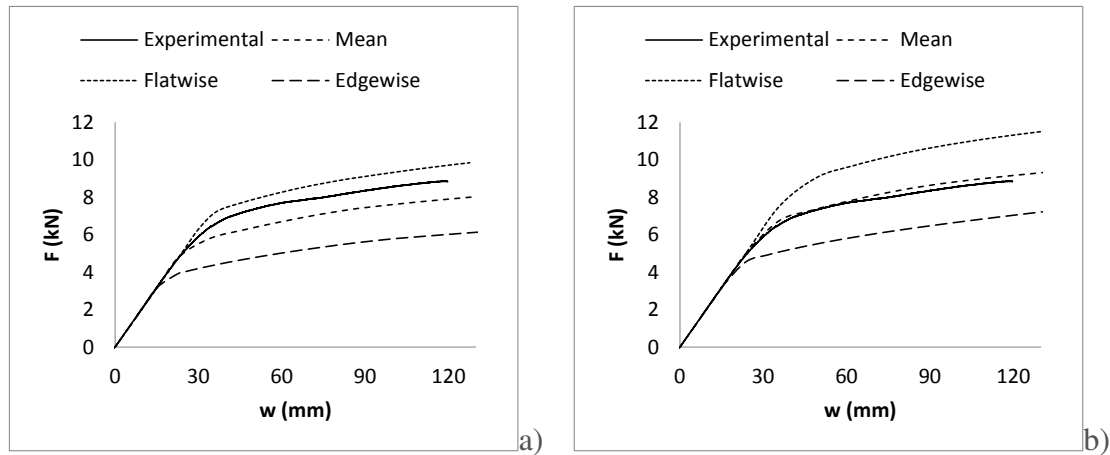
Figure 5-43 - Comparison of the experimental and numerical load-displacement curves for SIP-20/120-B2: a) Plastic model; b) Crushable foam model.

Regarding the 2D plastic model, from the analysis of the referred figures, in general, a good agreement between experimental results and numerical simulations is found, when considering the flatwise compression curve as input, especially for the smaller section SIPs (10/40). Regarding the SIP-20/120-B2, the model overestimates the load capacity on the plastic region. Even so for that same beam, it is observed that the stiffness in the plastic region in the experimental curve (around 21.4 N/mm) is quite close to the numerical one (around 20.8 N/mm). Regarding the numerical curves corresponding to the edgewise compression, they are clearly above the experimental ones. Regarding the 3D crushable foam model, the best match for all specimens is found when considering the mean curve of flatwise and edgewise data as input for the material model. In terms of precision, in general, 2D plasticity assuming the flatwise compression data and the 3D crushable foam assuming mean values for data delivers similar levels of precision.

The comparison between experimental and numerical load-displacement curves for the CIT beams for the different types of cross-section tested, 10/40 (B1), 20/40 (B1) and 20/120 (B1), are presented from Figures 5-44 to 5-46, respectively. The results for the remaining beams, which were quite similar, are presented in Appendix A, section A.2.

From the analysis of the referred figures, and similarly to what was observed for the SIP beams, regarding the plastic model, a good agreement was found for the smaller (thinner) CIT sections (10/40 and 20/40) when assuming the flatwise compression data as input for the material; however, for the deeper 20/120 cross-section, the same model overestimated the load capacity in the plastic region, and the model considering the mean curve of flatwise and edgewise data as input for the material model delivered a better approach. Regarding the crushable foam model results, the differences to the experimental curves seem higher than the ones found for the plasticity model. However, for the thicker beams,
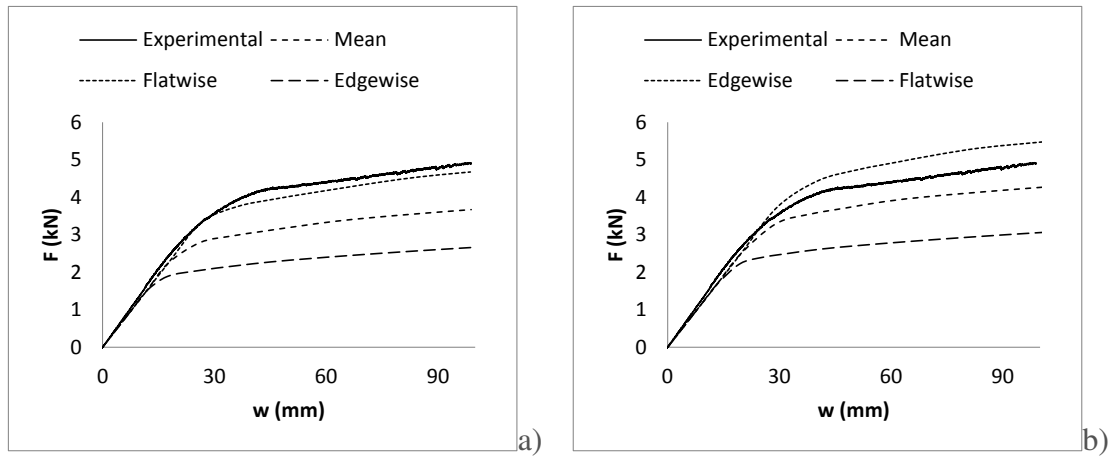
Figure 5-44 - Comparison of the experimental and numerical load-displacement curves for CIT-10/40-B1: a) Plastic model; b) Crushable foam model.
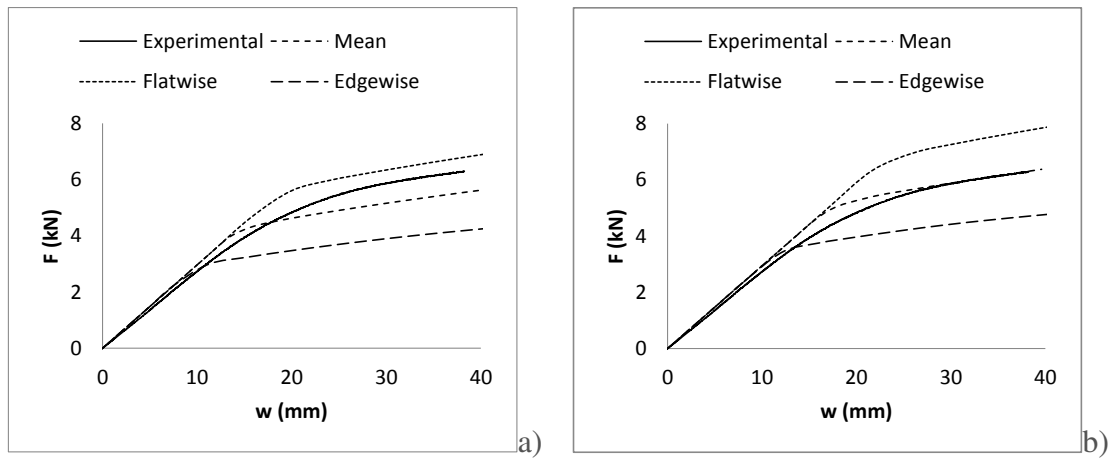
Figure 5-45 - Comparison of the experimental and numerical load-displacement curves for CIT-20/40-B1: a) Plastic model; b) Crushable foam model.
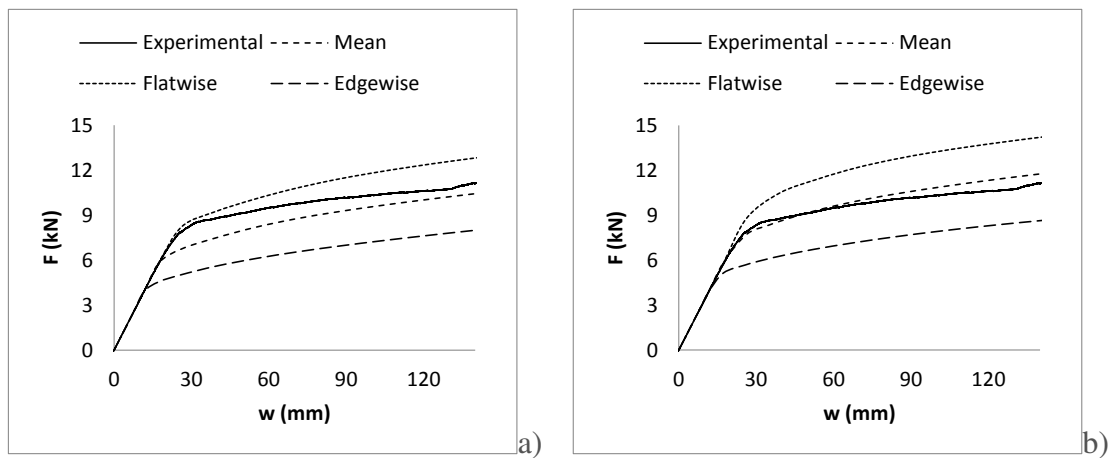
Figure 5-46 - Comparison of the experimental and numerical load-displacement curves for CIT-20/120-B1: a) Plastic model; b) Crushable foam model.

the crushable foam model that considered the mean curve of flatwise and edgewise as input for the material presented the best match possible.

The comparison between experimental and numerical load-displacement curves for the CIT panels for the two types of cross-section tested, 10/30 (P2) and 35/30 (P2), are presented in Figure 5-47. The results for the remaining panels, which were quite similar, are presented in Appendix A, section A.3.
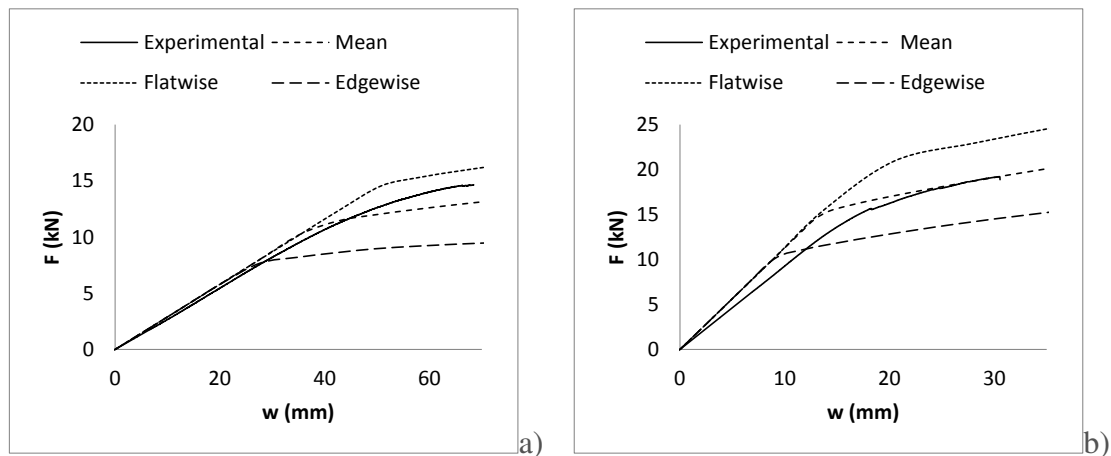
Figure 5-47 - Comparison of the experimental and numerical load-displacement curves for: a) CIT-10/30 P2 and b) CIT-35/30 P2.

From the analysis of the referred figures, in general, a good agreement between numerical and experimental curves is found for both 10/30 and 35/30 cross-sections. More significant differences are found in some cases: as an example, just at the beginning of the experimental curve for CIT-35/30-P2 (Figure 5-47 b)), the linear part presents quite different slopes than the numerical one. This can be explained by the consideration of a mean modulus of elasticity of the wood layers (assumed as a mean value for all the boards classified on that strength class). Despite that, in general, one can say that the accuracy of the results is much in line with the observations made for the CIT beams with the smaller (thinner) cross-sections.

To compare the stress levels computed by the numerical model with the ones from the analytical model for the same load level during the elastic phase, the maximum shear stresses occurring on the foam layer in the FE model are compared with those expected according to the Timoshenko beam theory for the plastic model considering the flatwise compression curve. To this end, the stress level corresponding to the mean value of the shear strength of the foam (0.117 N/mm^2) was considered. From that value, the corresponding applied load was calculated with the Timoshenko beam theory and the same load level used to determine the stress in the FE model. The results are presented in Table 5-15 for one specimen of each type and cross-section of beam.

Table 5-15 – Comparison of the maximum shear stress levels on the foam layer during the elastic phase between the analytical and numerical models for the same load level.

| Specimen | F (kN) | τ (N/mm²) | | Err (%) |
		Timoshenko	FEM	
SIP-10/40-B1	1.5	0.117	0.106	9
SIP-20/120-B1	4.5	0.117	0.095	19
CIT-10/40-B1	2.3	0.117	0.111	5
CIT-20/40-B1	3.1	0.117	0.097	17
CIT-20/120-B1	4.4	0.117	0.095	19
CIT-10/30-P1	10.5	0.117	0.118	-1
CIT-35/30-P1	12.1	0.117	0.102	12

From the analysis of the values, it is found that the stress levels on the FE model are generally lower than the ones of the analytical model. This discrepancy may be related with the fact that the FE model reproduces more precisely the real position of the loading points and supports, but also the total length of the beams (that is smaller than the span) that would also contribute to the global stiffness of the beams. In any case, the stress estimates obtained from both methods are of the same order of magnitude and the relative differences are low (overall average relative difference of 12%).

The evolution of the principal normal stress in the outer layers and shear stress in the inner layers are analysed as a function of the loading level. The stress curves were collected from the FE models in different points, where they reached a maximum: the normal stress on an external point of the tensioned outer layer above a load point; the shear stress on the inner part of the lower wood cross layer close to the support and on the middle of the foam layer between a support and a loading point (Figure 5-48).
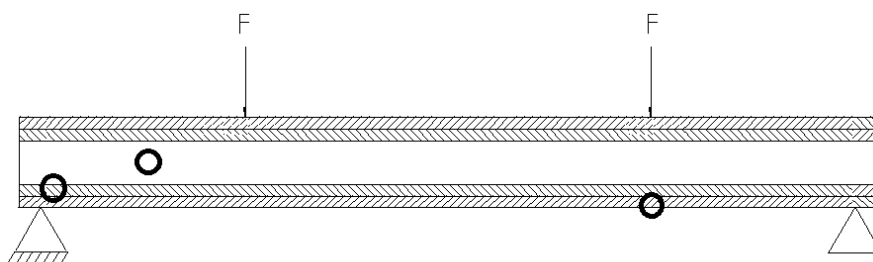
Figure 5-48 – Locations where the principal stresses were collected from the FE models.

The maximum principal stress as a function of the loading level is shown in Figure 5-49 (normal stress on the tensioned outer wood layer), Figure 5-50 (normal stress on the compressed outer wood layer), Figure 5-51 (shear stress on foam layer) and Figure 5-52 (shear stress on the wood cross layer). Figure 5-53 plots the Von Mises stress (taken on

the same location where the shear stress on the foam layer were taken). As the shear stress curves from both wood cross layers were similar, only the lower one is shown.

Figure 5-49 shows that the evolution of the normal stress in the tensioned layer with the applied load was linear up to a point where the slope of the curve changes. That same point coincides with the one where the shear stress curves on the foam (Figure 5-51) and cross wood layers (Figure 5-52) also changed their slopes. The analysis of the Von Mises stress (Figure 5-53) shows that the referred point is when the plastification of the foam layer starts to occur at some regions of the foam, at yield stress of 0.267 N/mm^2 as defined on the material model (Figure 5-33). The maximum normal stress reached on the wood tensioned layers (around 47 N/mm^2) is above the mean strength value expected for Maritime pine sawn wood, which is around 85.3 N/mm^2 (Martins, 2018). For Australian blackwood (CIT 20/120-B4) the maximum stress value was around 53 MPa, which is also expected to be above the tensile strength for that species (note that no reference value was found in bibliography, but similar strength to Maritime pine is expected). So, it is not surprising that no tensile failure of the wood layers was observed in the experimental tests. The normal stress in the compressed wood layers, followed, in general, a similar pattern to the one of the tensioned layers, with some of the specimens (e.g. CIT 20/120-B1) reaching the yield stress defined in the material model (39.8 N/mm^2). The shear stresses on the cross-wood layers were found to be higher than the ones in the foam layer, which may be a result of the former stresses being taken from the vicinities of the supports – these were modelled as punctual elements in the 2D models, which increased the stresses calculated on their vicinity (stress concentration effect, Figure 5-54).
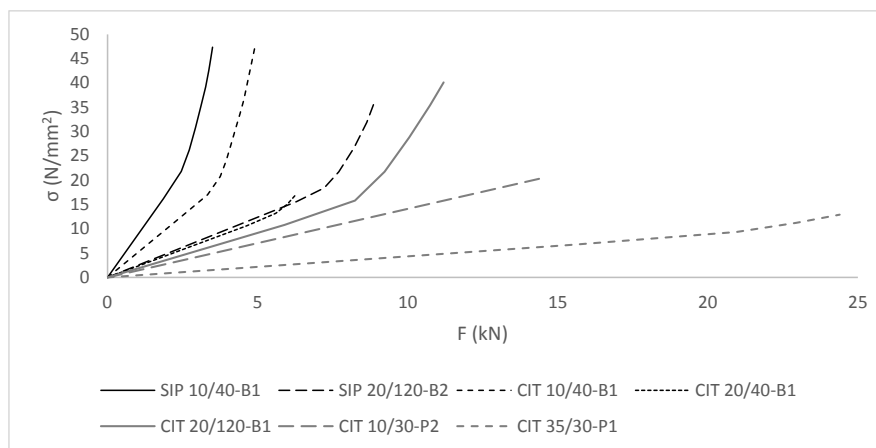
Figure 5-49 - Maximum principal normal stress on the tensioned outer wood layer *vs.* total vertical load on supports for one specimen of each type/configuration modelled.
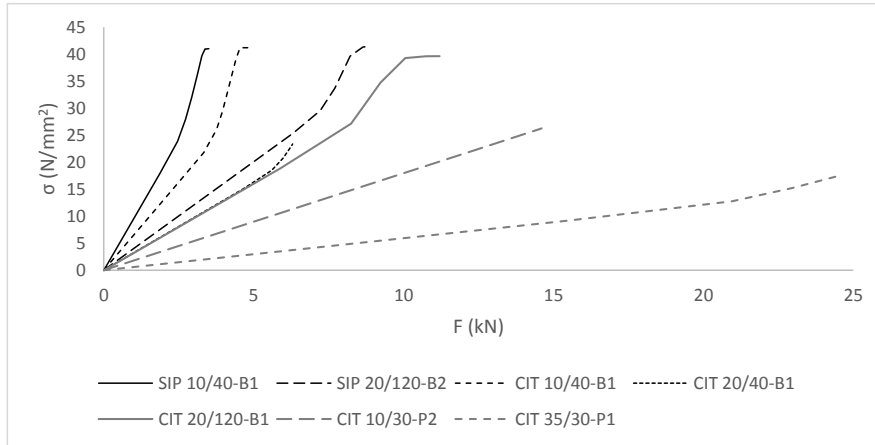
Figure 5-50 - Maximum principal normal stress on the compressed outer wood layer *vs*. total vertical load on supports for one specimen of each type/configuration modelled.
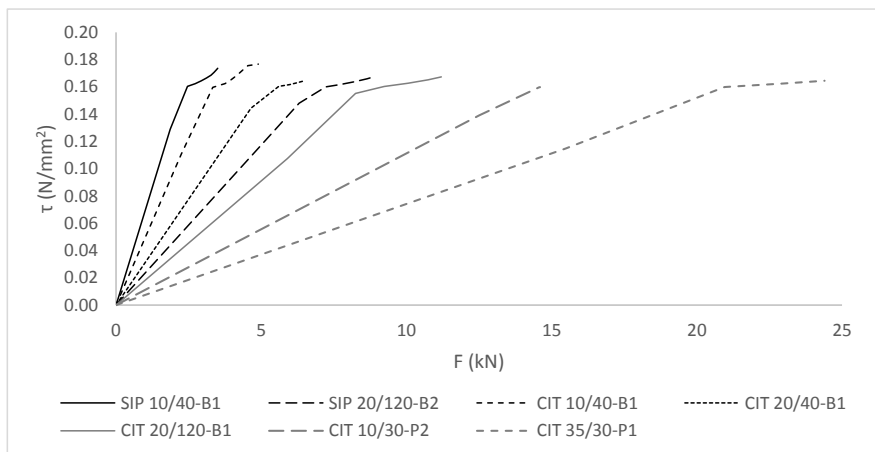
Figure 5-51 - Maximum principal shear stress on the foam layer *vs*. total vertical load on supports for one specimen of each type/configuration modelled.
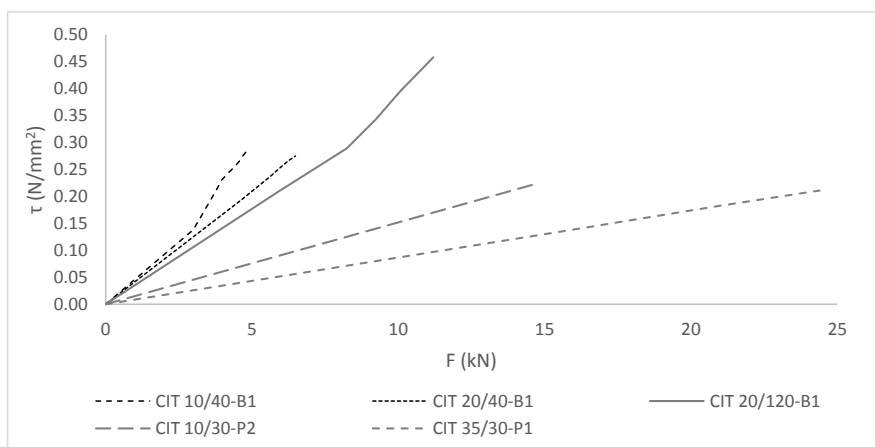
Figure 5-52 - Maximum principal shear stress on the lower cross-wood layer *vs*. total vertical load on supports for one specimen of each type/configuration modelled.
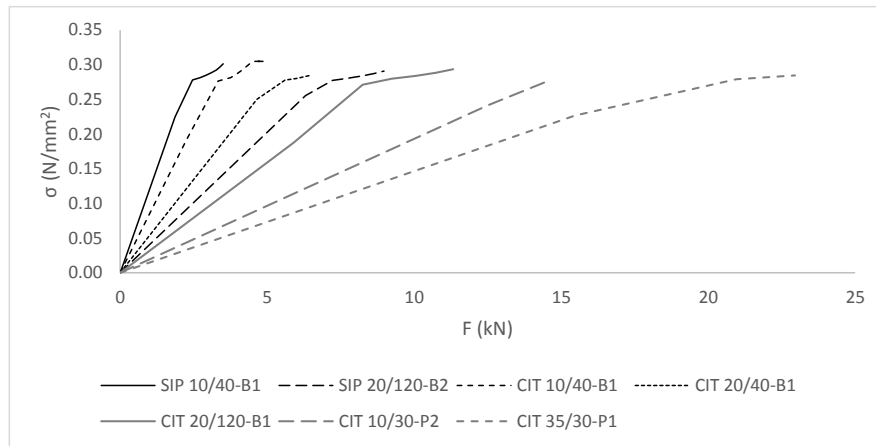
Figure 5-53 - Maximum Von Mises stress *vs*. total vertical load on supports for one specimen of each type/configuration modelled.
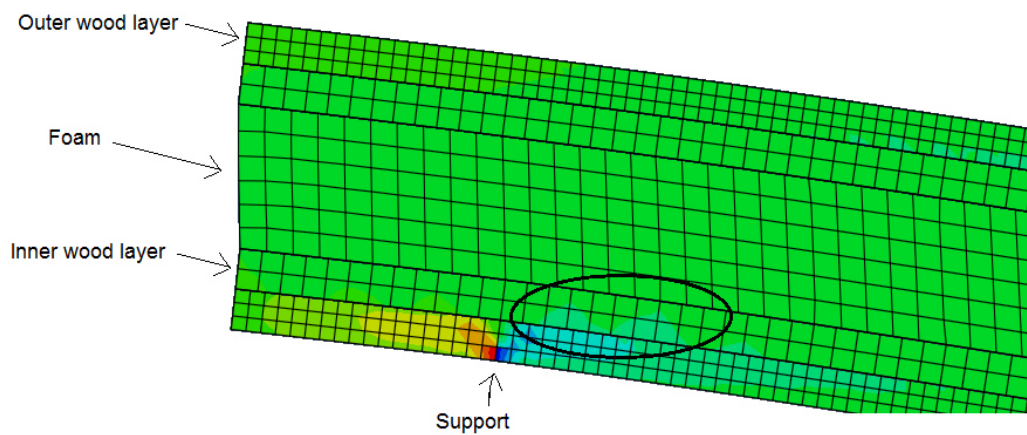
Figure 5-54 – Shear stress distribution on the inner wood layer in the vicinity of the supports in the FE model for the on the CIT 10/40-B1 specimen.

Even so, the maximum value reached (around 0.45 N/mm^2) is much lower than the characteristic value for rolling shear on Maritime pine, which is 4.6 N/mm^2 (see Chapter 3, Table 3-1). From the analysis of Figure 5-51, it is observed that the maximum shear stress reached in the foam layer has a close value for all the specimens, which as referred previously, was the failure mode observed in the experimental tests. The maximum shear stress in the foam layer determined in the FE model corresponding to the maximum displacement measured on the experimental tests is shown in Table 5-16.

As it can be seen, the values do not vary significantly with respect to the beam type or layer thickness. The maximum shear stress values are within the interval of 0.123-0.176 N/mm^2 with a mean value of 0.168 N/mm^2. The referred values are actually significantly higher than the mean or even maximum shear strength values determined in Chapter 3, 0.117 and 0.125 N/mm^2, respectively. These differences may be related to the densification of the foam, which may have caused an increase of the shear strength.

Table 5-16 – Maximum shear stress in the foam layer determined in the FE model corresponding to the maximum displacement measured on the experimental tests.

Specimen	τ (N/mm²)
SIP-10/40-B1	0.174
SIP-10/40-B2	0.165
SIP-20/120-B1	0.160
SIP-20/120-B2	0.175
CIT-10/40-B1	0.176
CIT-10/40-B2	0.176
CIT-10/40-B3	0.176
CIT-20/40-B1	0.168
CIT-20/120-B1	0.175
CIT-20/120-B2	0.176
CIT-20/120-B3	0.162
CIT-20/120-B4	0.171
CIT-10/30-P1	0.123
CIT-10/30-P2	0.164
CIT-10/30-P3	0.163
CIT-35/30-P1	0.175
CIT-35/30-P2	0.166
CIT-35/30-P3	0.172
CIT-35/30-P4	0.176
CIT-35/30-P5	0.170
CIT-35/30-P6	0.172

Overall, the results indicate that the FE model developed may be suitable for describing the beams/panels, especially the ones with smaller foam thickness (up to 40 mm). For the beams with thicker foam (120 mm), the higher differences may be attributed to the complex nature of the foam densification and cell crushing (see Figure 5-21), and also to the difficulty in modelling the orthotropic behaviour of the foam with consideration of plasticity.

5.5 Concluding remarks

This chapter presented a study about the mechanical performance of the developed panels. Analytical and numerical models presented earlier were initially reviewed. The panels were tested to assess their mechanical behaviour when used as beam and column elements. The results from those tests were used to validate analytical models and to develop a numerical model to describe the non-linear behaviour of the panels tested in bending. A finite element model was implemented using a commercial software package

to describe the structural (non-linear) behaviour of the panels tested in bending. The following conclusions were drawn from the current chapter:

- Due to the high shear flexibility of the transverse layers in cross-laminated timber (and core layer in sandwich panels), the shear influence in the mechanical behaviour is very important.
- Beam theories that consider the shear effects, such as Timoshenko beam theory or the Kreuzinger shear analogy method, are referred as design models for both cross-laminated timber and sandwich panels.
- When subjected to in-plane compressive loads, sandwich panels may fail due to other mechanisms than the exceeding of the compressive strength or buckling, namely the wrinkling of the faces or the shear crimping of the core.
- An experimental campaign was carried out to assess the mechanical performance of beam and column type elements. In addition to the developed panels, also CLT and SIP beam elements were tested. From the behaviour observed in the bending tests, it was found that the shear failure at the polyurethane foam was the governing failure mode. Additionally, a noticeable deformation of the polyurethane foam before failure was observed, an aspect more notorious in the specimens with thicker foam (120 mm).
- For both SIP and CIT, the comparison of the experimental results of the buckling tests with the analytical model showed a reasonable correlation.
- The comparison of the experimental results of the bending tests with the analytical models showed a good correlation for the linear part of the behaviour for all the types of tested panels/beams.
- A 2D FE model considering a plastic model for the foam was found to describe with accuracy the experimental results for specimens with thinner foam using the flatwise compression curve as input data; however, it provided slightly non-conservative strength predictions for the specimens with thicker foam layers, for which the simulated responses in the non-linear branch of the behaviour tended to deviate from the test data. For those cases, the model considering the mean curve of flatwise and edgewise tests as input for the material model delivered better approaches. A 3D crushable model for the foam that considered the mean curve of flatwise and edgewise tests as input for the material model delivered also reasonable approaches, especially for the thicker beams.
- The maximum shear stress at the foam layer computed by the FE plastic models, corresponding to the maximum displacement on the experimental tests, exceeded significantly the range of shear strength values determined in the characterization of the polyurethane foam. These differences were attributed to the densification of the foam, which may have caused an increase in the shear strength.

6 DESIGN AND OPTIMIZATION OF THE PANELS

6.1 Introduction

Besides the optimization of the adhesive connection between the panel's layers to ensure a minimum acceptable level of efficiency and durability, also the optimization of the layers' thickness is rather relevant. This aims not only at ensuring the fulfilment of structural and non-structural design requirements, but also to guarantee the maximum efficiency at the minimum cost.

With that purpose in mind, analytical models were considered for the design of the developed panels together with a mathematical model to perform the cost optimization. The same panel type was also optimized considering a different adhesion system between the polyurethane core and the wood elements, i.e. direct injection. Also, other optimized solutions were also developed considering additional restrictions, such as different ratios between the thicknesses of wood layers. The optimized panel solutions were compared with equivalent cross-laminated timber (CLT) solutions to assess the potential competitiveness of the proposed panel solution when compared to those, namely in terms of costs. This optimization study comprised another iteration, which involved the consideration of a layup of combined wood layers with different strength classes, an optimization exercise typically made in the manufacturing of glued laminated timber and CLT.

For the design of the panels, requirements were defined and accounted for the following aspects:

- Structural behaviour;
- Fire safety;
- Thermal comfort.

Although acoustic requirements are also important for the envisaged application, they were not considered in the present optimization study as the developed panels are expected to present poor acoustic performance due to the high ratio between stiffness and mass. Notice that CLT panels, that are a massive solution, usually require non-structural elements to fulfil acoustic insulation requirements (referred later in Chapter 8). So, to fulfil acoustic requirements on the developed panels, non-structural elements are also expected to be necessary (mitigation measures).

In the next sections of this chapter, the various aspects of the optimization are presented, namely: the design requirements regarding each behaviour aspect (section 6.2); the optimization model together with the load definition considered in the optimization (section 6.3); the presentation and discussion of results (section 6.4); the concluding remarks (section 6.5).

6.2   Design requirements

In this section, the design requirements regarding the various performance aspects - structural behaviour, fire resistance and thermal comfort - are described.

6.2.1   Structural behaviour requirements

For the structural design of the panels, the "Partial Factor Method" as described in NP EN 1990 (IPQ, 2009) was considered. The overall ultimate limit states (ULS) requirements defined in the standard were considered for the design, namely regarding the stresses acting in the panels. Moreover, the serviceability limit states (SLS) requirements were also considered for the design, regarding the instantaneous and final (long-term) deflection.

As the panels include wood in their constitution, most of the design provisions were obtained from EN 1995-1-1 (CEN, 2004b), as well as those indicated in the technical document TR 019 (EOTA, 2005), which provides some information regarding the properties of polyurethane (PUR) foam and assumptions in terms of creep and modification factors.

6.2.1.1   Ultimate limit states

For ULS design, the fundamental load combination defined in NP EN 1990, is considered as in (Equation (6-1),

$$\sum_{j \geq 1} \gamma_{G,j} G_{k,j} " + " \gamma_{Q,1} Q_{k,1} " + " \sum_{i > 1} \gamma_{Q,i} \psi_{0,i} Q_{k,i} \tag{6-1}$$

where $\gamma_{G,j}$ – partial factor for the permanent action j; $\gamma_{Q,1}$ – partial factor for the base variable action; $\gamma_{Q,i}$ – partial factor for other variable action i; $G_{k,j}$ – characteristic value of the permanent action j; $Q_{k,1}$ – characteristic value of the base variable action; $Q_{k,i}$ –

characteristic value of the other variable action i; $\psi_{0,i}$ – coefficient to determine the combination value of the variable action i.

The partial factors according to the referred standard are listed in Table 6-1 as a function of the load type, and the coefficients ψ_0 as a function of the type of action are listed in Table 6-2.

Table 6-1 – Partial factors according to NP EN 1990 (IPQ, 2009).

Load Type	Permanent	Base variable	Other variables
Favourable	1.00	0.00	0.00
Unfavourable	1.35	1.50	1.50

Table 6-2 - Coefficients ψ_0 , ψ_1 and ψ_2 according to NP EN 1990 (IPQ, 2009).

Action		ψ_0	ψ_1	ψ_2
Live load	Category A: residential area	0.7	0.5	0.3
	Category H: roofs	0.0	0.0	0.0
Snow	H>1000 m from the sea level	0.7	0.5	0.2
Wind		0.6	0.2	0.0

According to EN 1995-1-1, when checking ULS based on a first-order linear elastic analysis for composite members containing materials with different time-dependent properties (which is the case, as the cross layers have different creep behaviour than the outer layers, as well as the PUR layer), final mean values of such properties adjusted to the load component causing the largest stress in relation to strength shall be used. The final mean values of modulus of elasticity ($E_{mean,fin}$) and shear modulus ($G_{mean,fin}$) were thus calculated according to Equations (6-2) and (6-3),

$$E_{mean,fin} = \frac{E_{mean}}{(1 + \psi_2 k_{def})} \tag{6-2}$$

$$G_{mean,fin} = \frac{G_{mean}}{(1 + \psi_2 k_{def})} \tag{6-3}$$

where E_{mean} – mean value of modulus of elasticity; G_{mean} – mean value of shear modulus; k_{def} - deformation factor.

According to the referred standard, ψ_2 should correspond to the action (e.g. permanent or variable) that causes the largest stress in relation to strength. If the action is permanent, the value should be taken as 1.0.

The values for k_{def}, which actually corresponds to the creep coefficient, are found in EN 1995-1-1 for solid timber (load duration of 10 years or more) and in TR 019 for PUR rigid foam (load duration of 100,000 hours ~11.4 years). As no information is found in the standards related to the k_{def} value to be used on the wood cross-layers, a conservative value of 2.30 for service class 1 (load duration of 10 years) was considered based on the information available in (Jöbstl and Schickhofer, 2007). Although the design of the panels was made considering a service life of 50 years, the referred creep factors for PUR and wood cross-layers corresponding to ~11.4 and 10 years were assumed in the calculations, as at the time of optimization task no standardized/experimental values were available for a reference period of 50 years, either for the wood cross-layers or for the polyurethane foam used to manufacture the panels (density of 40kg/m^3). In the case of PUR, values for other densities were available (e.g. 5.0 at 20ºC for 50 years, (Garrido, 2016)), which are lower than the value reported in TR 019 for the 11.4 years time period. Although later, after performing the creep tests, it was possible to obtain an estimate of the creep coefficient for PUR from (Chapter 3), because no estimate was obtained for the wood cross-layers for that same period, it was decided to maintain the reference values from TR 019 and (Jöbstl and Schickhofer, 2007) in the design, as it would not be logical to consider very different times for the creep coefficient of PUR for (50 years) and the wood cross layers (10 years), especially for comparison of the CIT and CLT solutions.

As the external faces of the panels are planned to be protected from the direct action of environment agents, according to EN 1995-1-1, service class 1 is considered. The summary of the creep coefficients considered herein is presented in Table 6-3.

Table 6-3 – Creep coefficients considered for the different layers of the panels.

Material	k_{def} (for service class 1)
Solid wood	0.60
Solid wood (cross layers)	2.30
PUR	7.00

The design strength of the materials, X_d, was defined in accordance to NP EN 1990, as given in Equation (6-4),

$$X_d = \eta \frac{X_k}{\gamma_m} \tag{6-4}$$

where X_k – characteristic value of the property; η – conversion factor; γ_m – partial coefficient.

Note that in accordance with EN 1995-1-1 and TR 019, $\gamma_m = \gamma_M = 1.25$ for glued

laminated timber and PUR, and $\eta = k_{mod}$. From the referred documents, k_{mod} values are as shown in Table 6-4.

Table 6-4 – Modification factors (k_{mod}) for wood and PUR.

Material	Load-duration class (for service class 1)				
	Permanent action	Long term action	Medium term action	Short term action	Instantaneous action
Solid timber/GLT	0.60	0.70	0.80	0.90	1.10
PUR	0.25	0.50	0.75	1.00	1.00

If the load combination consists of actions belonging to different load-duration classes, k_{mod} from the shortest duration action shall be considered.

6.2.1.2 Serviceability limit states

For serviceability limit states (SLS) design, according to EN 1995-1-1, the instantaneous deformation should be calculated for the characteristic combination of actions, referred in NP EN 1990 and given by Equation (6-5):

$$\sum_{j \geq 1} G_{k,j}" + "Q_{k,1}" + " \sum_{i > 1} \psi_{0,i} Q_{k,i} \tag{6-5}$$

The final deformation should be calculated for the quasi-permanent combination of actions in accordance to Equation (6-6):

$$\sum_{j \geq 1} G_{k,j}" + " \sum_{i \geq 1} \psi_{2,i} Q_{k,i} \tag{6-6}$$

According to EN 1995-1-1, for a structure consisting of members or components having different creep behaviour (which is the case), the final deformation should be calculated using final mean values of the modulus of elasticity ($E_{mean,fin}$) and shear modulus ($G_{mean,fin}$), obtained according to Equations (6-7) and (6-8):

$$E_{mean,fin} = \frac{E_{mean}}{(1 + k_{def})} \tag{6-7}$$

$$G_{mean,fin} = \frac{G_{mean}}{(1 + k_{def})} \tag{6-8}$$

For simply supported beam elements, according to EN 1995-1-1, the maximum instantaneous and final deformation limits should be in the range $L/300$ to $L/500$ and $L/150$ to $L/300$, respectively. For both situations, the most demanding limits were considered in the present optimization study.

6.2.2 Fire resistance requirements

In accordance to the Portuguese Decree-Law nº 220/2008 (DR, 2008a), residential buildings up to 9 m high (utilization-type I according to the document) correspond to the 1st risk category. For those conditions, according to *Portaria nº 1532/2008* (DR, 2008b) the structural elements should have a minimum standard fire resistance of R30 or REI30. Note that 'R' stands for structural resistance, 'E' to tightness to flames and inflammable gases and I to thermal insulation; R applies to elements with structural function, while REI applies to those elements where fire resistance compartmentation is also required. This was the type of buildings considered in the present study, as the panels are mainly intended not only for new construction but also, due their low-weight in comparison to other materials (e.g. concrete or steel), to be used in rehabilitation of old masonry buildings, which are usually low-rise buildings and mainly used for residential purposes.

6.2.3 Thermal requirements

The thermal performance requirements for the external envelope of building wall and floor elements were taken from the Portuguese ordinance *nº 379-A 2015* (DR, 2015), which indicates the maximum coefficients of thermal transmission (U_{max}) as a function of the country thermal zone, as depicted in Table 6-5.

Table 6-5 – Maximum heat transfer coefficient in Portugal.

Element	U_{max} [W/(m².°C)]		
	Zone		
	I1	I2	I3
Walls	0.50	0.40	0.35
Floors	0.40	0.35	0.30

6.3 Optimization of the panels' layout

The main objective of the optimization task was to achieve efficient panel solutions with minimized production costs. The basis of the optimization model was defined as:

- The target: optimize the cost of the panels;
- Variables: the layers' thickness;
- Restrictions: structural, fire and thermal design requirements;
- Additional restrictions: maximum panels' height, minimum and maximum layers' thickness and symmetry of the cross-section.

Besides the panels system produced by glueing pre-manufactured polyurethane boards to wood layers (which was experimentally tested and validated, see Chapter 4), also the alternative system of direct injection of polyurethane between wood layers was considered. The consideration of such alternative is justified as it entails different mechanical properties and costs compared to the pre-manufactured system. Although the referred system was not actually tested using the chemical system recommended by the manufacturer, it was assumed that it would be able to fulfil the bonding requirements referred in Chapter 4. Besides the referred comparison, also the comparison with equivalent three-layered CLT panels was considered.

A parallel goal of the study was to assess the impact on the panels' costs of imposing different relations between the wood layers' thickness. This was considered an important issue, as the optimized solution in terms of the structural performance of the member *per se* could not be necessarily the best option for connection purposes (e.g. due to loads applied perpendicularly to the grain). Having different relations between wood layers' thickness would also imply changes in both wood and polyurethane layers' thickness, thus affecting the environmental impact, an issue that is analysed in Chapter 7.

It should be noticed that only the costs of raw materials were considered in the optimization process, i.e. costs with the manufacturing process (press, labour, etc.) were not considered.

6.3.1 Optimization model

For the optimization process, it was decided to resort to an algorithm implemented in the *MATLAB* software (Mathworks, 2018), the *fmincon* function. This function is based on a nonlinear programming solver that finds the minimum of a problem specified by the Equation (6-9),

$$\min_{x} f(x) \text{ such that } \begin{cases} c(x) \le 0 \\ ceq(x) = 0 \\ A \cdot x \le b \\ Aeq \cdot x = beq \\ lb \le x \le ub \end{cases} \tag{6-9}$$

where: x – matrix of the solution; $f(x)$ - function to minimize; $c(x) \leq 0$ - nonlinear inequalities; $ceq(x) = 0$ - nonlinear equalities; $A \cdot x \leq b$ - linear inequalities; $Aeq \cdot x = beq$ - linear equalities; lb - lower bound for the solution; ub – upper bound for the solution.

The routine starts by the definition of an initial solution, x_0, and the solver then iteratively attempts to find a minimizer solution x of the function subjected to the linear/nonlinear (in)equalities and imposed bounds.

The function to minimize is given by Equation (6-10),

$$f(x) = \sum_{i=1}^{n} x_i cost_i \qquad (6\text{-}10)$$

where: x_i - height of layer i; $cost_i$ – cost of the material composing layer i by unit volume.

In all cases a geometrical restriction was imposed: the cross-section layers should be symmetric in relation to the geometric centre of the cross-section. Besides the general optimized solution, other optimized solutions were considered when imposing specific ratios between thicknesses of consecutive wood layers, namely 1, 1/2 and 2.

6.3.2 Costs

Although EN 16351 (CEN, 2015) imposes restrictions to the thickness of the wood layers (between 6 and 45 mm), as the developed panels are not CLT, different limits were considered. For the direct injection system, the thickness of the PUR foam is usually limited to a maximum of 200 mm, while for the pre-manufactured boards higher thickness can be achieved. To evaluate the influence of each layer on the panels' performance and cost, minimum and maximum limits of 1 and 200 mm were set for both wood and PUR layers.

Notice that after computing the costs from Equation (6-10), the costs of the adhesive layers were added by considering the results from Chapter 4 regarding the optimization of the bonding system, namely regarding the adhesive spread rate. The costs of wood and PUR foams were collected from the manufacturers (*Pedrosa & Irmãos, Lda* and *Poliuretanos. SA*) that provided the raw materials used in the tests. The costs of the different raw materials are shown in Table 6-6 and Table 6-7. For the sandwich bonding, only the 2C-PUR adhesive system was considered in the optimization process, due to the lower costs.

Table 6-6 – Cost of wood and PUR rigid foam materials.

Material layer	Cost (€/m³)
Maritime pine sawn timber, C24 class	350
PUR injected, 40 kg/m³ density	100
PUR board, 40 kg/m³ density	260

Table 6-7 - Cost of the adhesive materials.

Adhesive layer material	Cost (€/kg)	Spread rate (g/m²)	Cost (€/m²)
1C PUR wood adhesive	7.70	140	1.08
Primer	14.35	4	0.06
1C PUR sandwich panel adhesive	10.08	150	1.51
2C PUR sandwich panel adhesive – Comp. A	8.19	126	1.03
2C PUR sandwich panel adhesive – Comp. B	12.04	24	0.29

6.3.3 Design models

The analytical models used for the structural analysis were the Shear Analogy Method (SAV) (Kreuzinger, 1999) for the floor elements and the Equivalent Beam Method (EBM) (Thiel, 2014) for the wall elements, described in Chapter 5. The expressions for wrinkling of the faces and shear crimping described in the same chapter were also considered. Both wall and floor elements were treated as simply supported members.

Regarding the fire resistance, from the literature about the fire performance of CLT bonded with polyurethane adhesive (Frangi et al, 2008; Frangi et al, 2009), it is expected that external layers of unprotected CIT panels may fall off prior to their total charring. Therefore, it was decided to assume that the bare panels would be protected by an air box and gypsum plasterboard to ensure the required 30 min of structural integrity. According to EN 1995-1-2 (CEN, 2004c), with such protection, the time for the start of charring (t_{ch}) in minutes is given by Equation (6-11),

$$t_{ch} = 2.8h_p - 14 \qquad (6\text{-}11)$$

where h_p is the gypsum plasterboard thickness.

So, to fulfil the fire resistance criteria, and for all the types of panels, the same protective system was considered: an 18 mm thick gypsum plasterboard (type A), which according to Equation (6-11) allows achieving 36 min, which is more than the required 30 min defined previously. Thus, it should be noticed that the thickness of the gypsum

plasterboard was not considered as an optimization variable.

The gypsum plasterboard thermal conductivity and costs (including the constructive accessories) obtained from a manufacturer (*Gyptec Ibéria, SA*) are shown in Table 6-8.

Table 6-8 - Thermal conductivity coefficient (λ) of gypsum plasterboard and cost the additional constructive systems for wall and floor.

Parameter	Element		
	Gypsum plasterboard - Type A - 18 mm	Floor accessories	Wall accessories
λ (W/(m.°C))	0.20	-	-
Cost (€/m²)	5.21	3.37	3.23

The coefficient of thermal transmission was determined from Equation (3-20),

$$U = \frac{1}{R_{se} + \sum R_i + R_{si}}$$

(6-12)

where R_{se} is the superficial external thermal resistance; R_{si} is the superficial internal thermal resistance, and R_i is the thermal resistance of the layer i.

For the definition of R_{se} and R_{si}, the values found in the Portuguese Dispatch No. 15793-K / 2013 (DR, 2013) were considered – they are presented in Table 6-9.

Table 6-9 – Values for the superficial thermal resistances considered in the design.

Parameter	vertical flux	horizontal flux
R$_{si}$ (m².°C/W)	0.10	0.13
R$_{se}$ (m².°C/W)	0.04	0.04

In the case of CLT, for the external elements design, the panels themselves were optimized, excluding the thermal requirements; otherwise, this would result in exaggerated thicknesses due to the thermal conductivity coefficient of wood. The value of this coefficient was taken as the mean value from the reference values of (Santos and Matias, 2006; Gonçalves, 2010), 0.18 W/(m.°C) (see section 3.4.1). For the verification of the referred requirements, it was decided to add to the CLT panels a system composed of (i) mineral wool with 30 kg/m³ of density (whose thickness was also a variable in the optimization process), (ii) an air box (between 15 to 100 mm for floor and 25 to 100 mm for wall), and (iii) gypsum plasterboard with 18 mm of thickness, as commonly used in practice and found in CLT manufacturers' catalogues. Mineral wool was chosen for the insulation as it was found to be cheaper and thermally more efficient than other current

materials, such as EPS or XPS. The thermal conductivity coefficient and cost considered for mineral wool are shown in Table 6-10.

Table 6-10 – Thermal conductivity coefficient (λ) and cost of mineral wool insulation.

Parameter	Mineral wool - ρ=30 kg/m^3
λ (W/(m.°C))	0.037
Cost (€/m^3)	45.0

The following values for the thermal and mechanical properties of the PUR for the direct injection system were assumed: λ=0.021 W/(m.°C), G_{mean}=3.00 N/mm^2 and $f_{v,k}$=0.07 N/mm^2. These values were based/estimated on information collected from a manufacturer and data from some experimental tests performed.

6.3.4 Definition of spans and imposed loads

Different spans ranging from 3.0 m to 5.0 m in steps of 0.5 m were considered for the floors, while for the walls a height of 3.0 m was considered, which leaves enough space for introducing the necessary non-structural elements (e.g. air-box + gypsum board, etc.), thus ensuring the minimum height between floors of 2.70 m and the free ceiling height of 2.40 m according to (RGEU, 1951).

For the load definition, the live loads for floors and roofs were based on NP EN 1991. For interior floors, the category A (residential area) was assumed, and for exterior floors (roof) the category H was assumed. As a simplification, wind loads were considered as being uniformly distributed along the length of the panels: load values of 0.5 kN/m^2 and 1.0 kN/m^2 were assumed for roofs and walls, respectively. Although residential buildings up to 9 m high (3-storey) and maximum spans of 5 m were assumed as case-study in the design (which results in vertical loads acting in the top of the bottom walls of around 8 kN/m and 15 kN/m for permanent and live loads, respectively), for the definition of the loads, a range of values typically found on pre-design tables of CLT manufacturers were considered ranging from 10 to 60 kN/m (which is beyond the previous range). The permanent and live loads were combined only once for the considered range, assuming the same value for both loads (e.g. $"G_k" + "Q_k"$ = 40 kN/m +40 kN/m). The summary of the loads considered in the design of the panels is shown in Table 6-11.

The basic scheme of the panels considered in the optimization process is shown in Figure 6-1 for the different floor and wall solutions. Notice that the mineral wool is only considered for the exterior elements.

Table 6-11 – Load definition for the different panel types.

Load type	Floor		Wall	
	Interior	Exterior	Interior	Exterior
Self-weight	✓	✓	✓	✓
Permanent load	1.0 kN/m²	1.0 kN/m²	10.0; 20.0; 30.0; 40.0; 50.0; 60.0 kN/m	
Live load	category A: residential area – 2.0 kN/m²	category H: roofs – 0.4 kN/m²	10.0; 20.0; 30.0; 40.0; 50.0; 60.0 kN/m	
Snow load	-	1.0 kN/m²	-	
Wind load	-	0.5 kN/m²	-	1.0 kN/m²
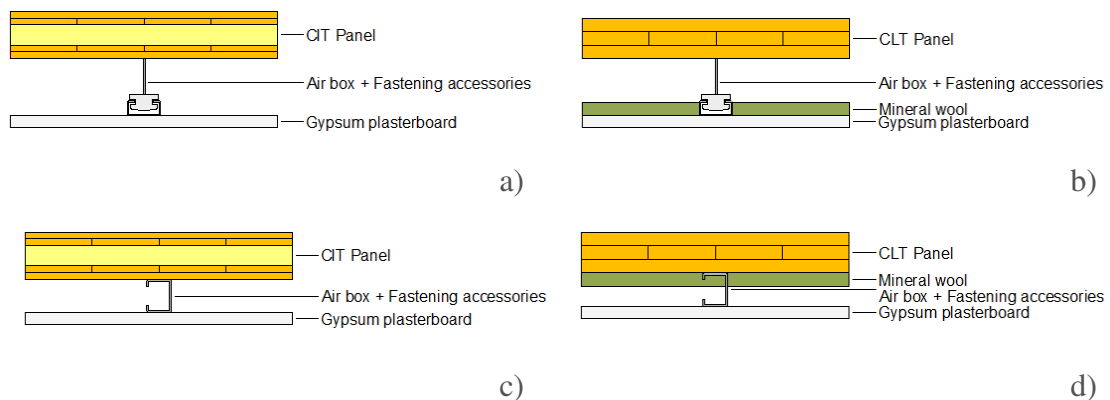
Figure 6-1 - Building scheme for the different panel solutions: a) CIT floor; b) CLT floor; c) CIT wall; d) CLT wall.

6.4 Results

In the current section, the results for the different applications (interior and exterior, including the three thermal zones considered), type of elements (floor and wall) and type of panels (CIT with pre-manufactured core, CIT with injected core and CLT) are presented. The optimized solution, i.e. with no specification of the ratio between the thicknesses of the wood layers is referred to as 'no spec'. The thickness of the outer wood layer is referred to as (h_1) and that of the inner wood layer as (h_2), so the corresponding panel solutions with imposed ratios between thicknesses of wood layers are referred to as half ($h_1 = h_2/2$), equal ($h_1 = h_2$) and double $h_1 = h_2 \times 2$.

The results are presented through (i) span *vs.* cost plots (floors) or load *vs.* cost plots (walls), (ii) figures illustrating the cross-section arrangement, and (iii) span *vs.* ratio of utilization (e.g. applied stress *vs.* maximum allowed stress) plots. For the ratio of utilization, in the case of floors, the shear strength, instantaneous and final deflections and thermal transmission coefficient were considered. For the case of walls, the axial

strength, stability, shear crimping and thermal transmission coefficient were considered. It should be noticed that in the case of floors, the shear stresses in the core were always the limiting factor regarding ultimate limit states. It is also worth referring that the wrinkling stress in the faces calculated according to Equation (5-23) (Chapter 5) for ULS for both PUR foam systems (29.7 MPa for PUR boards and 37.2 MPa for PUR foam) are higher than the characteristic bending strength of the C24 timber class (24 MPa), so wrinkling was not a limiting criterion on the optimization process.

6.4.1   Interior floor

The optimization results for the interior floor solutions are shown in Figures 6-2 to 6-4. It is important to note that in the cross-section figures, for each span, the 1st column represents the 'no spec' solution, and the 2nd, 3rd and 4th columns represent respectively solutions '$h_1=h_2/2$', '$h_1=h_2$', and '$h_1=h_2\times2$'.
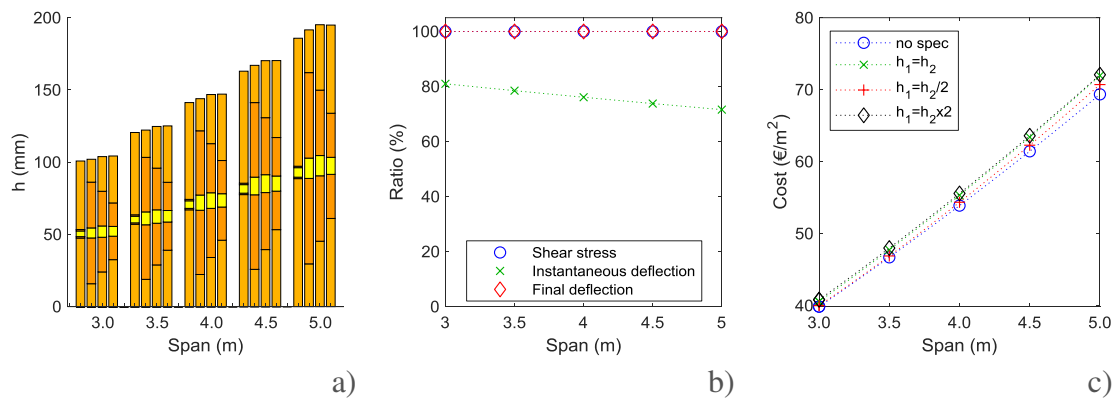
Figure 6-2 – Results of the optimization as a function of span for the CIT board's interior floor solution: a) cross-sections; b) ratios of utilization; c) costs.
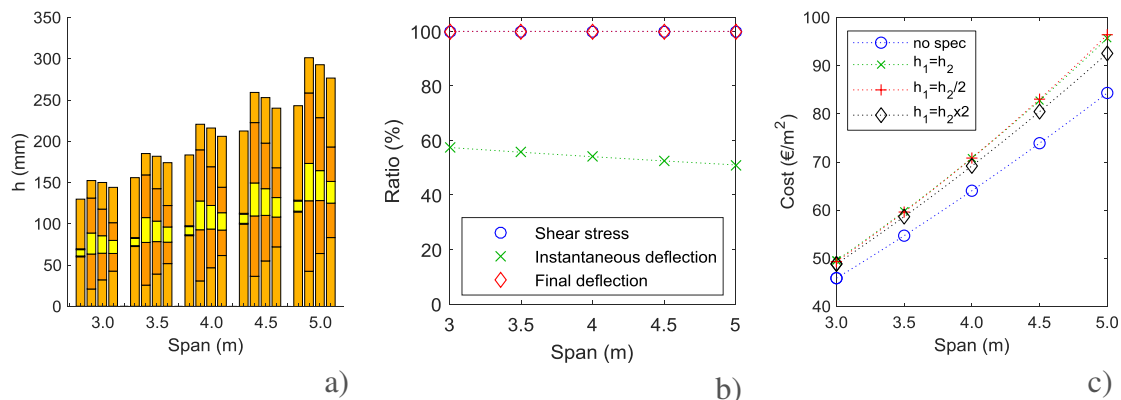
Figure 6-3 – Results of the optimization as a function of span for the CIT injected floor solution: a) cross-sections; b) ratios of utilization; c) costs.
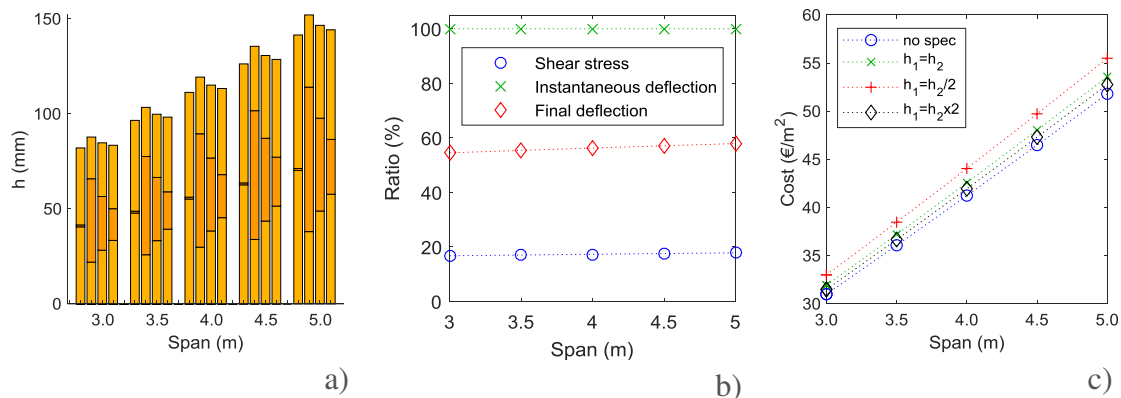
Figure 6-4 – Results of the optimization as a function of span for the CLT interior floor solution: a) cross-sections; b) ratios of utilization; c) costs.

Analysing the cross-section figures, a common point is identified in the three panel solutions: the thickness of the inner wood layers is close to the minimum value allowed (1 mm) for the optimized solution ('no spec'). This logical result indicates that, from the point of view of the mechanical behaviour of the panels as beam-type elements, the presence of these layers is not truly beneficial in terms of one-way load distribution. However, when imposing specific ratios between wood layers thickness, the costs only slightly increase with respect to the optimized solution. It is also interesting to see that for both CIT solutions the thickness of the PUR foam layer is relatively small with respect to that of the wood layers, which is also in line with the observations above.

In terms of utilization ratios, the most limiting criteria in the CIT solutions are the instantaneous and final deflections, while in CLT only the instantaneous deflection is found to be the most critical. The increase on the final deflections in the former solutions stems from the higher creep coefficient of PUR foam compared to the one for the cross-wood layers. The shear stresses are found to be more critical in CIT solutions than in CLT, which is in line with the lower shear strength of the PUR foam cores.

Since three-layered CLT panels with layers of equal thickness are usually commercialized by CLT manufacturers, the costs of the three solutions having equal wood layer thickness are compared in Figure 6-5.

For all the considered spans, the costs of the CLT solutions are about one- and two-thirds cheaper than the CIT ones with boards and injected cores, respectively. In addition to the small PUR thickness with respect to the wood layers, the results clearly show that the presence of the foam layer is not truly advantageous when only structural requirements are considered in floor solutions – this result is also logical.
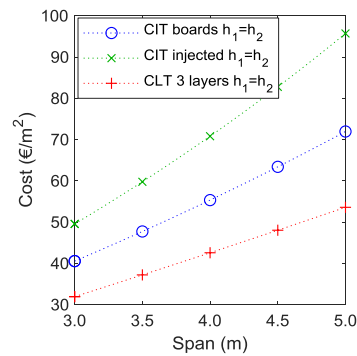
Figure 6-5 - Comparative costs for different interior floor solutions.

To achieve more optimized solutions, an additional study was conducted by replacing the inner wood layers of C24 class by layers of C18 class, as done in combined layups of CLT. This study was carried out for the case of wood layers with an equal thickness ($h_1=h_2$). As a simplification, the cost of C18 class wood was kept equal to that of C24 class. Figure 6-6 presents the comparison between the cross-sections made of C24 layers with the ones made of combined C24/C18 layers for the different panel solutions.
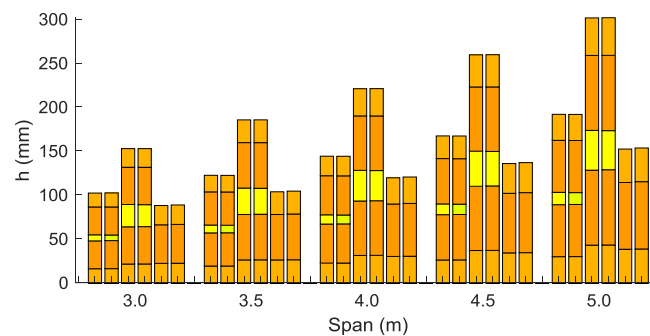
Figure 6-6 – Comparison between cross-sections for homogeneous and combined wood class layups. For each span, the 1st pair of columns correspond to CIT boards, the 2nd to CIT injected core and the 3rd to CLT. For each pair, the 1st corresponds to C24 class and the 2nd to C24/C18 combined layup.

As can be seen, almost no difference is found between homogenized and combined solutions, which indicates that it is possible to optimize the wood quality distribution over the panels cross-section. It should be noticed, however, that the characteristic value of the rolling shear strength (i.e. shear strength of the cross layers) was assumed to be equal for both C24 and C18 classes (i.e. 1.1 kN/mm^2) as in EN 16351 (CEN, 2015), which assumes that unique value independently of the strength class.

6.4.2 Exterior floor

The results of the optimization study for exterior floor solutions are shown in Figures 6-7 to 6-9 for U=0.30 W/(m^2.ºC). For U=0.35 and U=0.40 W/(m^2.ºC), the results are shown in Appendix A, sections A.1 and A.2, respectively.

In CIT solutions, it is observed that the thickness of the PUR layer decreases with the maximum coefficient of thermal transmission allowed – this result is logical. This is much in line with the previous remarks about the interior floor, namely the inefficiency of the PUR layer for structural purposes; however, when thermal requirements become more demanding, it is more economical to increase the PUR thickness than that of the wood layers.

a)   b)   c)
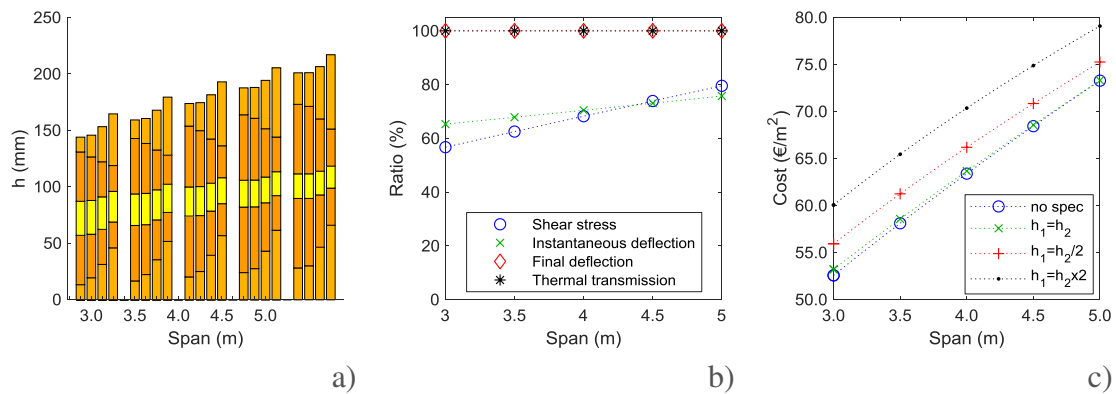
Figure 6-7 – Results of the optimization in function of span for the CIT board's exterior floor solution with U≤0.30 W/(m^2.ºC): a) cross-sections; b) ratios of utilization; c) costs.

a)   b)   c)

Figure 6-8 – Results of the optimization in function of span for the CIT injected exterior floor solution with U≤0.30 W/(m^2.ºC): a) cross-sections; b) ratios of utilization; c) costs.

Figure 6-9 – Results of the optimization as a function of span for the CLT exterior floor solution with U≤0.30 W/(m^2.°C): a) cross-sections; b) ratios of utilization and c) costs.

When imposing specific ratios between the thickness of wood layers, for the CIT boards, the costs compared to the optimized solution are not much different for the specific case of '$h_1=h_2$', while for the other cases the costs increase more significantly. For the CIT injected and CLT cases, all the solutions with a specific ratio between h_1 and h_2 are generally slightly more expensive than the optimized one.

Looking at the figures that illustrate the ratios of utilization, the most limiting criterion for both CIT solutions is the final deflection, while in some cases the other parameters also tend to be critical.

As for interior floors, the costs of the three solutions having equal wood layer thickness are compared in Figure 6-10 for the different thermal zones considered.
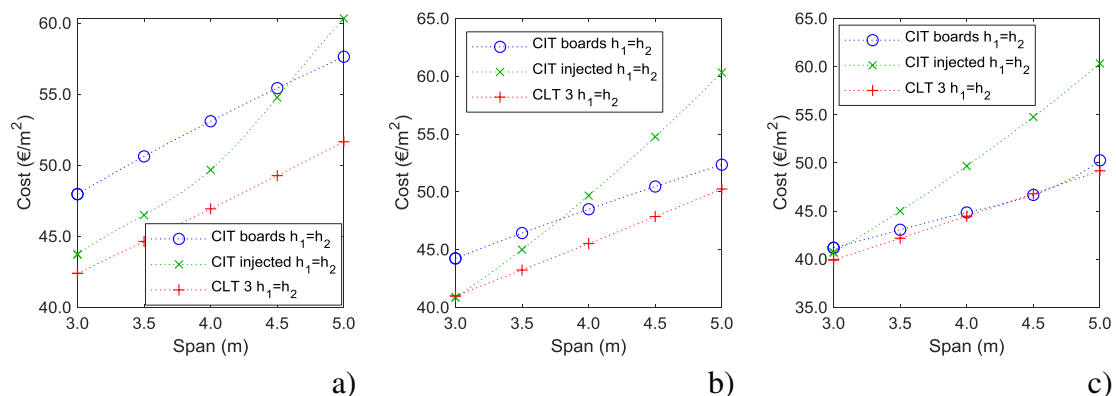
Figure 6-10 - Comparative costs for different exterior floor solutions: a) U=0.30 W/(m^2.°C); b) U=0.35 W/(m^2.°C); c) U=0.40 W/(m^2.°C).

The figures above show that the costs of the CIT injected solutions tend to exceed the

Pedro Gil Girão dos Santos

ones for CIT boards for longer spans and when the thermal resistance requirements are less demanding. The CLT solutions generally present the lowest costs; however, when the thermal requirements are less demanding, the CIT board solutions become more competitive, with a very similar cost for the U=0.40 W/(m^2.°C) requirement.

6.4.3 Interior wall

The results of the optimization study for interior wall solutions are shown in Figures 6-11 to 6-13. For the CLT solution, due to the relatively high value for the shear modulus of the inner cross-layer (239 N/mm^2), the shear crimping is not a relevant failure mode as in CIT, see Equation (5-24), Chapter 5, and so the results concerning the utilization ratios of that failure mode are not shown in the figures for CLT.
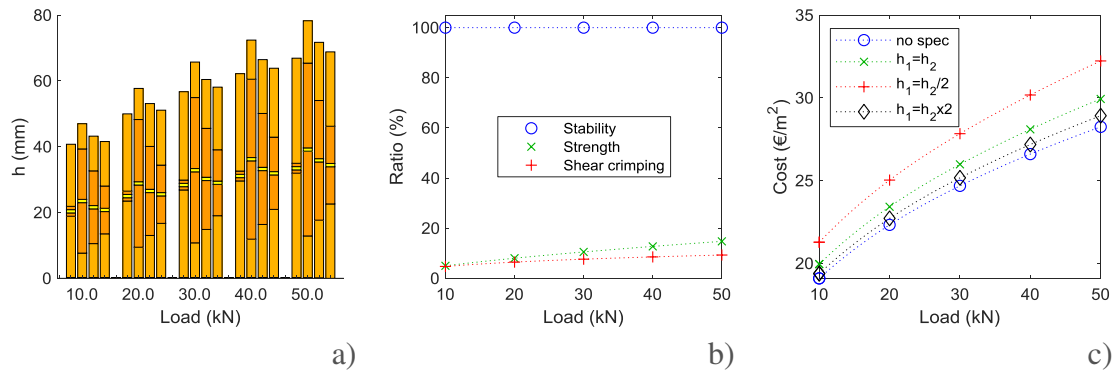
Figure 6-11 – Results of the optimization as a function of span for the CIT board's interior wall solution: a) cross-sections; b) ratios of utilization; c) costs.
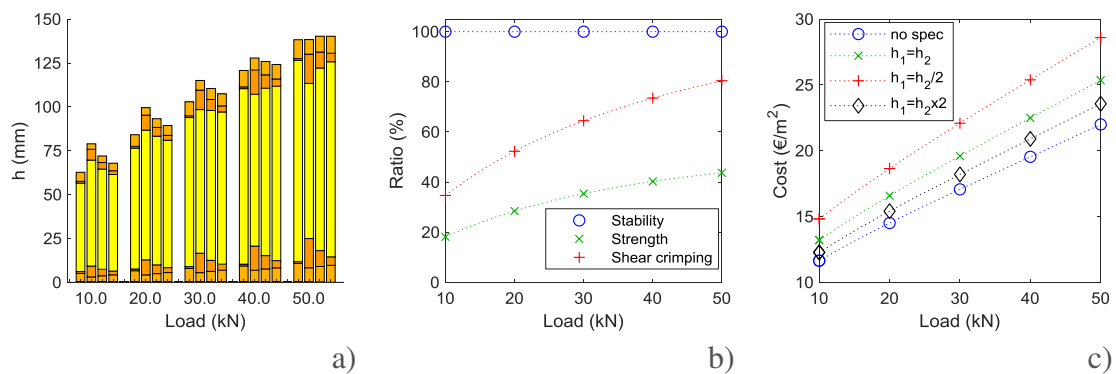
Figure 6-12 – Results of the optimization as a function of span for the CIT injected interior wall solution: a) cross-sections; b) ratios of utilization; c) costs.
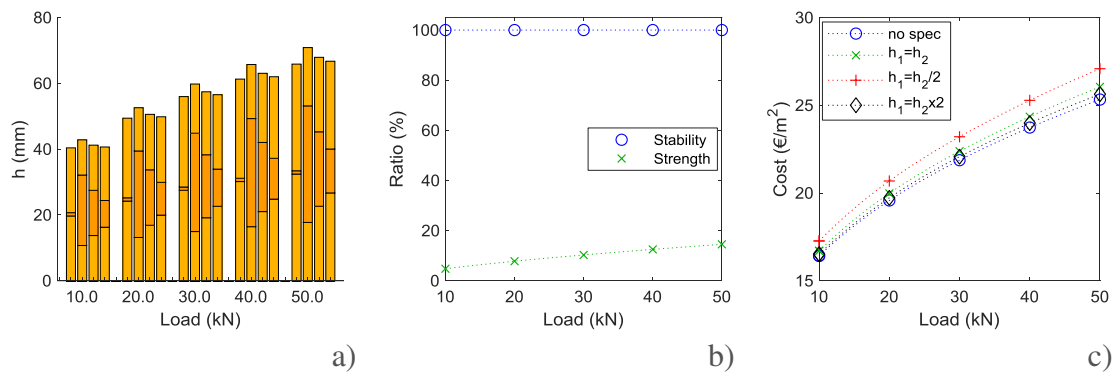
Figure 6-13 – Results of the optimization as a function of span for the CLT interior wall solution: a) cross-sections; b) ratios of utilization; c) costs.

As observed for the interior floor solutions, in the optimized solutions for interior walls, the thickness of the inner wood layers tends to the minimum value allowed (1 mm), indicating that it impairs the mechanical performance as a vertical member.

When imposing different ratios between the thickness of the wood layers, the costs slightly increase for the '$h_1=h_2$' and '$h_1=h_2\times2$' options, while for the '$h_1=h_2/2$' option, the cost increases more significantly, especially for the CIT solutions. It is also interesting to highlight that the thickness of the PUR foam layer is smaller in the CIT boards than in the CIT injected solutions, which can be explained by the great difference between the corresponding material costs (260 €/m^3 – PUR boards vs. 100 €/m^3 – PUR injected). The most limiting criterion in all solutions is stability, while strength and shear crimping criteria are largely fulfilled.

Since three-layered CLT with layers of equal thickness is usually commercialized by CLT manufacturers, the costs of the three solutions having equal wood layer thickness are compared in Figure 6-14.
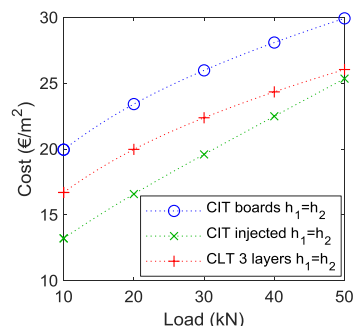
Figure 6-14 - Comparative costs for different interior wall solutions.

For all the considered loads, although the CIT injected solution presents the thicker cross-

sections, it involves lower costs than the CLT solution, while the CIT board's solution is the most expensive one.

6.4.4 Exterior wall

The results of the optimization study for exterior wall solutions are shown in Figures 6-15 to 6-17 for U=0.35 W/(m^2.ºC). For U=0.40 and U=0.50 W/(m^2.ºC), the results are shown in Appendix A, sections A.3 and A.4, respectively.

As for the interior wall solutions, in the optimized solutions for exterior walls, the thickness of the inner wood layers tends to the minimum value allowed (1 mm) in most of the cases. Also, as for the interior wall solutions, the ratio between foam and wood thicknesses is higher in the injected CIT solutions than in the CIT boards. Imposing different ratios for the wood layer thicknesses increases the costs, especially for the CIT solutions. In the CIT board solutions, when the thermal requirements become more stringent, it is found that the thickness of the PUR foam layer increases more than that of the wood layers. In the CIT injected solution, when the thermal requirements become more severe, the variation in the PUR thickness is not pronounced.

When imposing specific ratios of wood layers thickness, the costs of the optimized CIT solutions are generally higher than those of the optimized solutions for both 'boards' and 'injected' systems. For the CLT case, except for the '$h_1=h_2/2$' ratio, the solutions with other wood layer ratios present quite similar costs to the optimized solution.

In what concerns the utilization ratios, it is shown that for all solutions the most limiting criterion is stability.
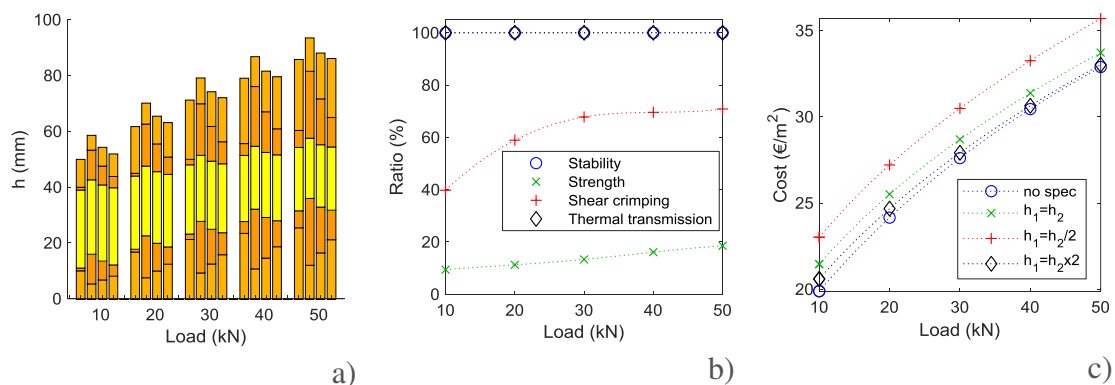
Figure 6-15 – Results of the optimization as a function of load for the CIT board's exterior wall solution with U≤0.35 W/(m^2.ºC): a) cross-sections; b) ratios of utilization; c) costs.
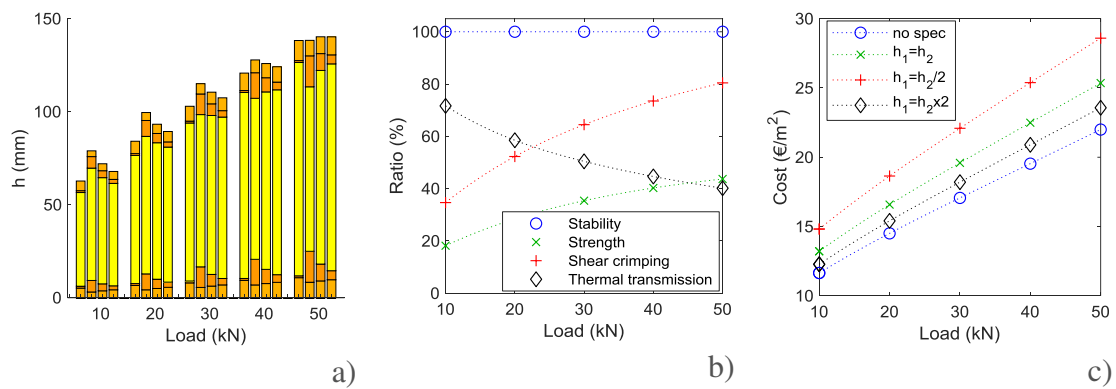
Figure 6-16 – Results of the optimization as a function of load for the CIT injected exterior wall solution with U≤0.35 W/(m^2.°C): a) cross-sections; b) ratios of utilization; c) costs.
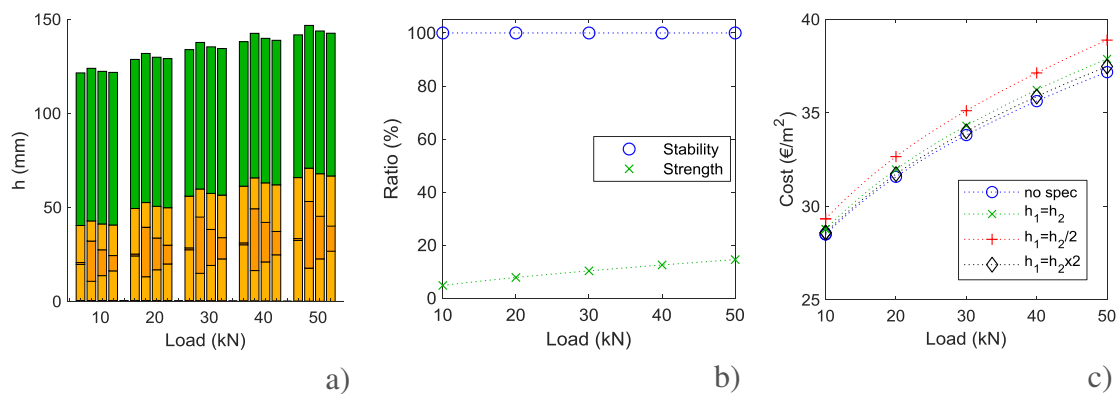
Figure 6-17 – Results of the optimization as a function of load for the CLT exterior wall solution with U≤0.35 W/(m^2.°C): a) cross-sections; b) ratios of utilization; c) costs.

The comparison of the costs of the three different panel solutions accounting for $h_1=h_2$ is presented in Figure 6-18 for the considered thermal zones.
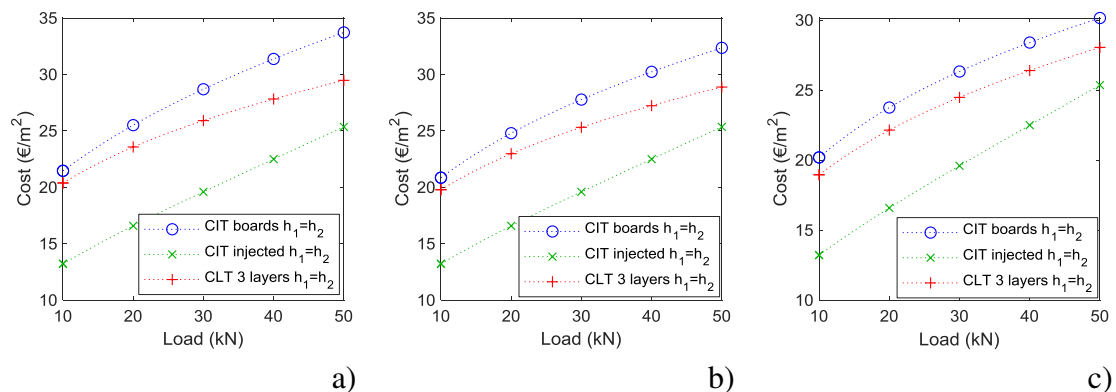
Figure 6-18 - Comparative costs for different exterior wall solutions: a) U=0.35 W/(m^2.°C); b) U=0.40 W/(m^2.°C); c) U=0.50 W/(m^2.°C).

For all the considered loads, the CIT injected solution presents the lowest costs. The CIT board solution is slightly more expensive than the CLT solution, which presents intermediate costs for all load levels considered in the study.

6.5 Concluding remarks

This chapter presented the results of a study aiming at the optimization of the costs of the developed panels. The study included the identification of design models and performance criteria to be fulfilled, as well as the definition of the optimization model. Besides the developed panel with PUR boards, also an alternative system using direct injection of the foam between the wood layers was considered, as well as equivalent CLT solutions. Additionally, besides the overall optimized solutions, alternative optimized solutions were also determined by considering additional restrictions, namely by imposing different ratios between the thicknesses of the wood layers or by considering combinations of wood strength classes. The study focused on floor and wall elements for both interior and exterior conditions (i.e. with and without thermal requirements). The following conclusions were drawn from the optimization study:

- For the interior floor supported in two opposite sides and for interior wall elements, in the optimized solutions for all types of systems (CIT boards, CIT injected and CLT), the thickness of the inner wood layers tended to the minimum value allowed; similarly, in the CIT solutions, the PUR layer tended to relatively small values. This indicates that from the point of view of the structural behaviour of the panels as beam-type elements, as expected, the presence of the PUR layers impairs their performance.

- When imposing specific ratios for the thickness of the wood layers, for the CIT interior floor solutions, the costs only slightly increase with respect to the optimized solution; for CIT interior wall solutions, the costs for the solutions with '$h_1=h_2$' and '$h_1=h_2\times2$' slightly increase; for exterior floor solutions, the costs for the specific case of '$h_1=h_2$' for the CIT boards are quite similar to those of the corresponding optimized solutions, while for the injected option, they increase more significantly; regarding the exterior wall solutions, for ratios different than the optimized ones, the costs in the CIT solutions increase significantly.

- In terms of utilization ratios, for the interior floor solutions, the most limiting criteria for CIT are the instantaneous and final deflections; for CIT exterior floor

solutions, generally, the final deflection governs design; and for both interior and exterior CIT walls, stability was found to be the most limiting criterion.

- No relevant performance differences were found between using homogenized or combined wood strength classes; this seems to indicate that it is possible to optimize the wood quality distribution over the panel's cross-section.

- For the interior floor solutions, the costs of CLT were always lower than the CIT ones; for exterior floors, the CLT solutions generally presented the lowest costs; however, while decreasing the thermal requirements, the CIT board solutions become more competitive, with very similar costs to CLT; for the interior wall solutions, the CIT injected solution presented lower costs than the CLT solution, while the CIT board solution was the most expensive one; for exterior walls, the CIT injected solution presented the lowest costs, while the CIT board solution was found to be slightly more expensive than the CLT solution.

- For the CIT exterior floor and wall solutions, it was observed that the PUR layer thickness decreases with the maximum coefficient of thermal transmission; this shows that when thermal requirements become more demanding, it is more economical to increase the thickness of the PUR layer than that of the wood layers.

In summary, the results showed that the presence of the foam layer is not truly advantageous when only structural requirements are set, but it becomes more relevant when thermal demands exist, which makes this type of panels a more interesting solution to be used as an exterior element. Thus, the panels can be considered as an alternative solution to CLT construction, by replacing those panels in elements that are used in the external envelope of the building, keeping the conventional CLT for the inner elements.

7 LIFE CYCLE ASSESSMENT OF THE PANELS

7.1 Introduction

The standards ISO 14040 (ISO, 2006a) and ISO 14044 (ISO, 2006b) define Life Cycle Assessment (LCA) as the compilation and evaluation of the inputs, outputs and the potential environmental impacts of a product system through its life cycle. The entire life cycle includes raw material extraction and acquisition, energy and material production, manufacturing, use, end of life treatment and final disposal. LCA is thus a tool that allows modelling the environmental impacts of a product system, and can be used to compare two or more products, to assess which one is more or less beneficial in certain aspects. According to this philosophy, LCA is used in the present work to assess the environmental impacts of the developed panel, but also to compare it with other solutions of equivalent functional performance, using either alternative core materials or even CLT.

The following chapter is organized as follows: a description of basic concepts and methodology associated to life cycle assessment is provided in section 7.2; next, the state-of-art regarding LCA of CLT and SIP is presented in section 7.3; in sections 7.4 to 7.6 the LCA study assumptions are presented; in section 7.7 the results are presented and discussed and, finally in section 7.8 the concluding remarks of the study are made.

7.2 Description of LCA methodology

According to the standards ISO 14040 (ISO, 2006a) and ISO 14044 (ISO, 2006b), LCA studies are composed of four main inter-related phases (Figure 7-1):

  I.   Goal and scope definition;
 II.   Inventory analysis;
III.   Impact assessment;
IV.   Interpretation.
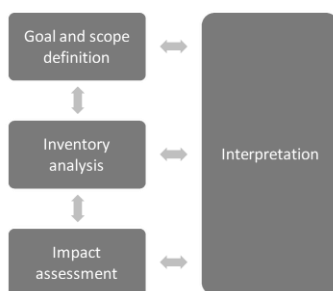
Figure 7-1 – Life cycle assessment phases.

In the first phase of LCA, referred as the goal and scope definition, one states the intended application and the reasons for carrying out the LCA study. The scope definition includes the following items:

- The product system to be studied;
- The functions of the product system;
- The functional unit;
- The system boundary;
- The allocation procedures;
- The selected impact categories and methodology of impact assessment.

The product system is defined as the collection of unit processes performing one or more defined functions, which models the life cycle of a product. Such unit processes are linked to each other by intermediate flows (and/or waste to treatment), to other product systems by product flows and to the system environment by elementary flows. A schematic example is shown in Figure 7-2.
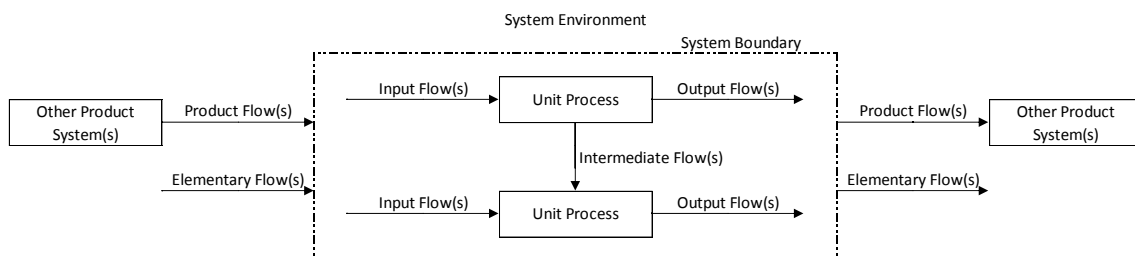
Figure 7-2 – Product system example.

A unit process is the smallest element for which input and output data (product, material or energy flow) are quantified. The boundary of each unit process is determined as a function of the modelling detail that is required to achieve the goal of the study. An example of a unit process is *"packaging"*.

The intermediate flow(s) may be either a product, material or energy between unit processes. An example of intermediate flow is *"basic materials and subassemblies"*.

The product flow(s) represents product(s) entering from or leaving to another product system. An example of product flow is *"recycled materials for reuse"*.

The elementary flow(s) represents material or energy entering the system that has been drawn from the environment without previous human transformation (i.e. natural resources) or leaving the system that has been released into the environment without

subsequent human transformation (releases to air, water and land). Examples of elementary flows entering/ leaving the system are *"crude oil from the ground"* and *"discharges to water"*.

The function(s) is defined as the performance characteristic(s) of the product. An example of a function is *"beam that supports a distributed load of 2 kN/m^2"*.

The functional unit defines the quantification of the identified function(s). This provides a reference to which the inputs and outputs are related and ensures the comparability of LCA results, including those from different systems. An example of a functional unit is *"1 m^2 of CLT panel"*.

The system boundary defines the unit processes to be included in the product system, i.e. it represents the separation between the product system and the environment. Ideally, the product system should be modelled in a way that the inputs and outputs at the boundary are elementary flows. However, factors such as the goal and scope definition, assumptions made, data constraints or cut-off criteria, limit that choice. Unit processes and flows when setting the system boundary usually include the following:

- Acquisition of raw materials;
- Inputs and outputs in the main manufacturing/processing sequence;
- Distribution/transportation;
- Production and use of fuels, electricity and heat;
- Use and maintenance of products;
- Disposal of process wastes and products;
- Recovery of used products (including reuse, recycling and energy recovery);
- Manufacture of ancillary materials;
- Manufacture, maintenance and decommissioning of capital equipment;
- Additional operations, such as lighting and heating.

Some of the input flows may not be considered in the LCA study by applying cut-off criteria that is the specification of the minimum amount of material/energy flow or level of environmental significance associated with unit processes or product system to be considered in the study. In the case of material (mass) and energy, the flows are considered if the cumulative contribution to the input of the system is above a defined percentage in relation to the product system.

The second phase of LCA, referred as Life Cycle Inventory Analysis (LCI), involves the data collection and calculation procedure to quantify relevant inputs and outputs through the life cycle of the product. The process itself is iterative as while data is collected, new

data requirements or limitations are identified. Regarding the data collection, each unit process is classified under major headings:

- Energy, raw materials, ancillary and other inputs;
- Products, co-products and waste;
- Emissions to air, discharges to water and soil;
- Other environmental aspects.

During the data collection, it is important to verify if those are consistent not only among them but in relation to other database sources (Ferrão, 2009). After the data collection, the calculation procedures include the relation of the data to the unit process and to the reference flow of the functional unit.

As referred in ISO 14040, most of the industrial processes yield more than one product (co-products) and recycle intermediate or discarded products as raw materials, which may imply allocation procedures. The standard recommends to avoid allocation, wherever it is possible, but if it cannot be avoided, the input and output data might be allocated between the co-products in proportion to their economic value.

The third phase of LCA, referred as Life Cycle Impact Assessment (LCIA), is aimed at evaluating the magnitude and significance of the potential environmental impacts of a product system. This is done through an environmental mechanism that is a system of physical, chemical and biological processes for a given impact category, that links the life cycle inventory analysis results (LCI results) to (impact) category indicators and in some cases to category endpoints.

The first step of the process is the definition of a set of impact categories. An impact category is defined as a class that represents environmental issues of concern to which LCI results (*e.g. SO_2*) may be assigned (*e.g. Climate change*). A (impact) category indicator corresponds to a quantifiable representation of that impact category (*e.g. infrared radiative forcing (W/m^2)*). The process of converting impact categories to category indicators is made through a characterization model. The characterization model is used to derive the characterization factors that allow the conversion of an assigned LCI result to the common unit of the category indicator (classification phase) (*e.g. the contribution of 1 kg of CH_4 to the impact category "greenhouse effect", which has as common unit kg CO_2, is converted to 42 kg CO_2 equivalents*). The converted LCI results are then aggregated within the same impact category giving the category indicator results (characterization phase) (*e.g. total of kg CO_2 equivalents per functional unit*).

ISO 14044 does not require the calculation of the category endpoint(s), which is defined

as an attribute or aspect of the natural environment, human health, or resources, identifying an environmental issue giving cause for concern. Instead, it suggests that the category indicator can be chosen anywhere along the environmental mechanism between the LCI results and the category endpoint(s). This approach is usually referred as Midpoint indicator (Goedkoop et al, 2016).

According to (Ferrão, 2009), there are two types of characterization models: (i) Problem-oriented approach – methods that are based on midpoint indicators directly related to the environmental interventions; and (ii) Environmental damage approach – methods that are related to the ultimate environmental consequences, and thus more related to endpoint indicators.

Optional elements on LCIA, include normalization, grouping, weighting and data quality analysis. Normalization is the calculation of the magnitude of the category indicator results relative to some reference information. Grouping is the sorting and possibly ranking of the impact categories. Weighting is the conversion and possibly aggregation of the indicator results across impact categories using numerical factors based on value-choices.

The last phase of LCA is the Interpretation, which comprises:

- the identification of issues based on the results of the previous phases;
- the evaluation that considers completeness, sensitivity and consistency checks;
- drafting of conclusions, limitations and recommendations.

Depending on the covered stages (Figure 7-3), LCA can be classified into cradle-to-cradle (from A1 to D), cradle-to-grave (from A1 to C4) or cradle-to-gate (from A1 to A3). The last option is mandatory when manufacturers intend to issue an Environmental Product Declaration (EPD) according to the European standard EN 15804 (CEN, 2012c).

Production stage			Construction process stage		Usage stage							End-of-life stage				Benefits and loads beyond the system boundary
A1	A2	A3	A4	A5	B1	B2	B3	B4	B5	B6	B7	C1	C2	C3	C4	D
Raw material supply	Transport	Manufacturing	Transport	Construction installation process	Use	Maintenance	Repair	Replacement	Refurbishment	Operational energy use	Operational water use	Deconstruction/demolition	Transport	Waste processing	Disposal	Reuse, recovery or recycling potential

Figure 7-3 – Stages of a life cycle assessment (CEN, 2012c).

7.3   State-of-the-art on LCA of CLT and SIP

There is still disagreement concerning on how to deal with carbon sequestration in timber products, however most of the studies related to timber products refer that carbon sequestration shall be included in LCA (Symons et al, 2013). The sequestered carbon, referred as biogenic carbon is removed from the atmosphere during the tree growth and will be stored as long as the wood product is in use or fully recycled. Potential scenarios for the end-of-life of CLT include re-use (in the existing form), re-engineering (cutting the panels in smaller sections for re-use), recycling, incineration (preferably with energy recovery) or landfill disposal (preferably with gas recovery for energy production). Darby et al (2013) who performed an LCA of a CLT building assuming the different end-of-life scenarios mentioned above (with exception of recycling) concluded that re-use is the best option and the worst is incineration without energy recovery in terms of CO_2 emissions. For end-of-life scenarios, such as incineration, the CO_2 is fully restored to the atmosphere (Cadorel and Crawford, 2018). Concerning wood degradation in a landfill, there is still a lot of uncertainty regarding the CO_2 emissions, as this is dependent on the rate of timber that actually rots and turns into CO_2 and methane (CH_4), in the case that the process is anaerobic. According to Weight (2011), it has been assumed that all, or nearly all, of the CO_2 sequestrated during the tree growth will be released. Besides CO_2, also methane (CH_4) is released, which has a high impact on global warming - the Intergovernmental Panel on Climate Change estimates its impact to be 25 times worse than CO_2 over 100 years (IPCC, 2007). This means that the effects on global warming for the landfill scenario are potentially worse than the ones due to incineration. However, in practice, a series of studies reported in (Weight, 2011) refer that wood degradation in landfill presents relatively low levels of CO_2 emissions, ranging from 0-17% of the carbon content in wood.

In bonded wood products, such as CLT, it is not possible to separate the wood elements from the adhesive at a large scale. Instead, it is possible to chop the panels into smaller parts, such as chips, that could then be used as raw material to manufacture composite panels, such as OSB or fibreboards (Scalet, 2015).

Due to the subjectivity and specificity of the construction process and usage stages, CLT manufacturers have supplied EPD based mostly on the production stage (e.g. (Structurlam, 2013)), and sometimes including the sub-stages from C2 to D (see Figure 7-3). Regarding the LCA of CLT panels, some studies are found, which are enumerated next.

Durlinger et al (2013) performed a cradle-to-grave LCA between a CLT multi-storey building and an equivalent reinforced concrete solution for a life span of 50 years. Some

limitations were found, such as limited data related to CLT production, the uncertainty related to CLT degradation in a landfill, or the omission of impacts from the non-timber components of the building. From the results, it was concluded that the CLT solution had lower environmental impacts on all assessed categories, with the exception of renewable energy demand. It should be noticed that the operation phase, for both building solutions, contributed between 75% to 96% to the environmental impacts depending on the impact category. Concerning the global warming potential (GWP), it was shown that if carbon sequestration is considered, the impacts of the CLT solution are 22% lower when compared to the reinforced concrete solution. Even so, if the sequestration is not considered, the impacts of the CLT solution are still 13% lower than the reinforced concrete one. Focusing only on the building materials, the GWP impacts, at the end of the cradle-to-gate stage, are 30% lower for the CLT building's materials compared to the reinforced concrete ones. Including the remaining stages, the impacts are 52% higher or 15% lower depending on if the carbon sequestration is considered or not, respectively.

Liu et al (2016) performed a cradle-to-grave LCA between a reference seven-storey building made on reinforced concrete and an equivalent solution made of CLT considering a life span of 50 years. Two locals for the building implementation were considered: a cold region and a severe cold region. For the end-of-life scenario of the reference reinforced concrete building, it was assumed that the concrete and steel materials go to landfill, while for the bricks a recycling ratio of 60% was assumed. For the CLT building, a recycling ratio of 60% was considered for timber with the remaining material being used for biomass energy. The carbon sequestration of timber was assumed as 800 kg CO_2 per cubic meter of wood. From the results obtained, the authors concluded that, for both locations considered, the one with CLT would lead to a reduction of the energy consumption of more than 30%, while the CO_2 emissions would reduce by more than 40% when compared to the reinforced concrete solution.

Chen et al (2019) performed a cradle-to-gate LCA of CLT produced in Western Washington, USA. In the analysis, they compared transportation logistics, mill location and wood species mix. From the results, they concluded that the location of the lumber suppliers with respect to the CLT factory and the wood species mix are important factors that affect the total environmental impacts of the panels' production. The local sourcing of lumber and the use of lighter species instead of heavier ones were pointed out as factors that could significantly reduce the global warming potential of CLT products.

Cadorel and Crawford (2018) presented a review of studies related to the environmental performance of CLT buildings. They referred that most of the analysed studies conclude that CLT buildings have lower greenhouse gas emissions than reinforced concrete solutions.

Unlike CLT, few studies related to LCA of SIP buildings were found in the technical literature.

Du et al (2013) presented a dual-index evaluation model of economic efficiency and carbon emission (based on LCA) for SIPs. The comparison of the results from the model applied to SIPs and masonry-concrete house has shown benefits in favour of SIP.

Cárdenas et al (2015) performed a very simplified LCA of SIP houses assuming a lifespan of 50 years. They concluded that the operation stage was the most demanding in terms of energy, with the embodied energy representing 11% of the total energy. The energy contained on the construction process, transport, loading and unloading represented about 2% of the embodied energy.

7.4 LCA analysis - Goal and scope definition

For the assessment of the environmental impacts of the developed panels, the following goals were defined:

- Identification of the process(es) that contributes the most for the environmental impact of the CIT panel solutions;
- Comparison of the environmental impacts of the CIT panel solutions, for both exterior walls and floors, regarding the specification of different thicknesses of wood layers compared to the ones resulting from the optimization study (presented in Chapter 6);
- Comparison of the environmental impacts of using an un-primed solution for the wood layers' bonding instead of one that uses primer (from the results of Chapter 4);
- Comparison of the environmental impacts of the CIT panel solutions for exterior walls and floors using an alternative core material instead of rigid polyurethane, namely insulation cork board (ICB) and with equivalent three-layered CLT solutions (which include insulation material).

The CLT equivalent solutions were designed to fulfil the same structural and thermal requirements of the corresponding CIT panels (according to Chapter 6). For the additional insulation material used on the CLT panels, three commonly used materials were considered, namely ICB, extruded polystyrene (XPS) and rock wool (RW).

The optimized CIT panel solution using an ICB core instead of PUR foam was obtained using the algorithm described in Chapter 6. Reference values for the ICB properties were

collected from an EPD (Amorim Isolamentos, 2016), while other parameters necessary for the design were kindly provided by *Amorim Isolamentos, SA*. No reference values for the shear creep coefficient (φ) of ICB were available, so a value of 5.4 was assumed based on the equation proposed by (Dias et al, 2018) for the compressive creep coefficient of cork estimated for 100,000 hours. The properties and material cost considered in the optimization design are shown in Table 7-1. In this table, the density (ρ), Young's (E) and shear (G) moduli are mean values, while the shear strength (f_v) is an estimated characteristic value (5% percentile).

Table 7-1 - Insulation cork board (ICB) material properties and cost considered in the optimization of the panel layout.

	ρ (kg/m^3)	E (N/mm^2)	G (N/mm^2)	f_v (N/mm^2)	λ (W/mºC)	φ	Cost (Eur/m^3)
Expanded corkboard (ICB)	115	1.5	1.148	0.063	0.040	5.4	350

The unit processes associated with the ICB production were modelled with basis on the EPD data from (Amorim Isolamentos, 2016). It was assumed that the same adhesive used on PUR foam' core panels would be used for the ICB ones, with the same adhesive spread rates.

To avoid an extended description for all the considered loads/spans/requirements of the optimization chapter, the study was conducted only for two specific cases of external wall and floor, with the following characteristics:

- Panels designed for 3 m of span/height by 1 m of width;
- Exterior floor (roof) requirements corresponding to a permanent load (g_k) of 1.0 kN/m, imposed load (q_k) of 1.0 kN/m and a maximum thermal transmission coefficient (U) of 0.40 W/mºC;
- Exterior wall requirements corresponding to g_k=30.0 kN/m, q_k=30.0 kN/m and U=0.35 W/mºC;
- Adhesive spread rates based on the results from the previous chapters.

For the conditions described above, the layer thicknesses for each panel solution are presented in Table 7-2 (floor) and Table 7-3 (wall). In the referred tables 'Optimized' refers to the optimized solution; '$h_1=h_2/2$' corresponds to the solution where the outer wood layer's thickness (h_1) is half of the inner wood layer thickness (h_2) and so on.

The product system studied is the panels, with the functions described above, and the defined functional unit is 1 m^2 of panel. The system boundaries for each panel type, CIT

and CLT, were initially defined with basis on EPDs from CLT manufactures, as well as on others studies referred in the state-of-art.

Table 7-2 – Layer thickness for each analysed solution of an exterior floor panel.

Panel Type	Wood layers' ratio	Thickness (mm)					
		h_1	h_2	h_3	h_4	h_5	$h_{insulation}$
CIT with PUR core	Optimized	13	44	30	44	13	-
	$h_1=h_2/2$	19	39	30	39	19	-
	$h_1=h_2$	31	31	29	31	31	-
	$h_1=h_2x2$	46	23	27	23	46	-
CIT with ICB core	Optimized	11	86	35	86	11	-
CLT + RW insulation	$h_1=h_2$	26	26	26	-	-	93
CLT + XPS insulation	$h_1=h_2$	26	26	26	-	-	70
CLT + ICB insulation	$h_1=h_2$	26	26	26	-	-	100

Table 7-3 - Layer thickness for each analysed solution of an exterior wall panel.

Panel Type	Wood layers' ratio	Thickness (mm)					
		h_1	h_2	h_3	h_4	h_5	$h_{insulation}$
CIT with PUR core	Optimized	21	2	25	2	21	-
	$h_1=h_2/2$	9	18	24	18	9	-
	$h_1=h_2$	12	12	24	12	12	-
	$h_1=h_2x2$	16	8	25	8	16	-
CIT with ICB core	$h_1=h_2$	22	22	34	22	22	-
CLT + RW insulation	$h_1=h_2$	19	19	19	-	-	88
CLT + XPS insulation	$h_1=h_2$	19	19	19	-	-	59
CLT + ICB insulation	$h_1=h_2$	19	19	19	-	-	84

The bonding solution for the wood layers considered as standard in the LCA study was the one that uses primer (20 g/m²), an adhesive spread rate of 140 g/m² and a bonding pressure of 0.6 MPa applied during 400 minutes, values based on the information of Chapter 4. The un-primed bonding solution used for comparison consisted of the following parameters: adhesive spread rate of 180 g/m² and a bonding pressure of 0.6 MPa applied during 200 minutes. For the bonding solution between the wood/polyurethane layers, a bonding pressure of 0.1 MPa applied during 90 minutes was considered. Due to lack of information regarding the LCI of the sandwich adhesives (either 1C or 2C), its production was considered as an input material to the product system. It is also expected that its production process is not too different from the one-component polyurethane adhesive used for the bonding of the wood layers. Taking that into account and due to the low quantity involved (300 g/m² of panel), a low impact on the results was expected (as discussed ahead in the results section, this hypothesis was

confirmed through the one-component polyurethane adhesive).

The construction process, use stage and de-construction process were not included in the study. Concerning the construction and de-construction processes, it was expected that few differences would exist between applying the CIT and CLT systems, probably with some advantages of CIT due to the lower weight, at lifting operations. Even so, it was not possible to collect accurate information regarding the construction/deconstruction processes. For the referred reasons, only the transport from the panels' factory to the construction site and from there to the waste treatment plant were considered, as the difference between the CIT and CLT panels' weight will certainly influence the transportation impacts. For the use stage, a service life of 50 years was assumed and that no refurbishment would be required during that period. The operational energy during that period was not considered, as both CIT and CLT systems were designed to have similar thermal performance.

For the end-of-life stage, six scenarios were considered

- Incineration;
- Incineration with energy recovery;
- Landfill assuming partial rot of timber;
- Landfill assuming partial rot of timber and energy recovery;
- Landfill assuming total rot of timber;
- Landfill assuming total rot of timber and energy recovery.

For the incineration option, full combustion was assumed. Thus, a quantity of CO_2 equal to the one stored during the tree growth is released to the atmosphere. For the estimation of the CO_2 stored in wood, the rules from EN 16449 (CEN, 2012b) were followed, which assumes that 50% of the dry mass of wood ($m_{0\%}$) is transformed into carbon, that in turn combines with oxygen (1 part carbon to 2.67 parts oxygen) to produce CO_2 according to Equation (7-1).

$$CO_{2,sequestred} = \frac{m_{0\%}}{2} \times 3.67 \tag{7-1}$$

For maritime pine, considering a mean dry density of 532 kg/m^3, the amount of storage CO_2 is 976 kg/m^3 (or 1.73 kg CO_2/kg). For the ICB, considering a mean dry density of 108 kg/m^3, the amount of storage CO_2 is 200 kg/m^3 (or 1.74 kg CO_2/kg).

To calculate the energy recovered from the incineration process, the calorific values of the materials were taken as: 5.1 kWh/kg for dry timber (Weight, 2011); 6.7 kWh/kg for PUR (Wittbecker et al, 2011); 8.2 kWh/kg for ICB (Nunes, 2015) and 11.1 kWh/kg for

XPS (Santos, 2016). The adhesives were not accounted for such calculation due to lack of information regarding their calorific value and also the low quantities required for the manufacturing.

The efficiency of production of electricity from the incineration process was taken as 20% according to (Symons et al, 2013).

A CO_2 credit can be taken if the energy is used in a national grid system with a dominant fossil fuel source, as the energy recovered is, therefore, reducing the amount of fossil fuel being consumed; and the credit is equal to the marginal (offset) emissions that would otherwise have been made. The CO_2 emissions from the grid electricity that are being offset are assumed to be 0.436 kg CO_2/kWh (Weight, 2011).

As referred in the state-o-the-art, there is still a lot of uncertainty regarding the CO_2 equivalent emissions from wood decomposition at landfill. Weight (2011) and Symons (2013) considered that 20% of wood degrades into carbon, from which 40% turns into CO_2 and 60% into CH_4. The same values were considered for the landfill with partial rot scenario, but also that 100% of wood degrades into carbon (landfill with total rot scenario). The efficiency of the capture of CH_4 was assumed to be 50% and the efficiency of generating electricity from methane was taken as 34% (Weight, 2011) (Symons et al, 2013).

As referred before, the recycling option of CLT type-elements is possible, by chopping them into wood chips that in turn may be used to produce wood fibre insulation or wood-based panel. However, in the CIT case, due to the presence of the insulation layer, such option would imply either the separation of the PUR layer from the remaining components or the presence of PUR foam in the chips. Due to the lack of information on these aspects, it was decided to not consider the recycling option on the LCA study.

The defined system boundary for the CIT PUR foam' core panel is shown in Figure 7-4. The system boundary for the CIT with ICB core is similar, with the difference that the PUR foam production is replaced by the ICB one. In the case of the CLT panel, the system boundary is depicted in Figure 7-5.

In the schematized system boundaries, some processes were excluded, namely:

- Fixed capital equipment and facilities (manufacturing and construction were ignored, i.e. assuming that they already took place);
- Land use (not relevant for the impact categories considered);
- Packaging (low quantity involved);

- Processes associated with the construction, use and deconstruction/demolition stages;
- Fixings of the insulation materials to the CLT panels (low quantity involved);
- Gypsum boards applied as a complement to the CIT/CLT panels (impacts are the same for both panels);
- Primer used for the wood bonding (low quantity).
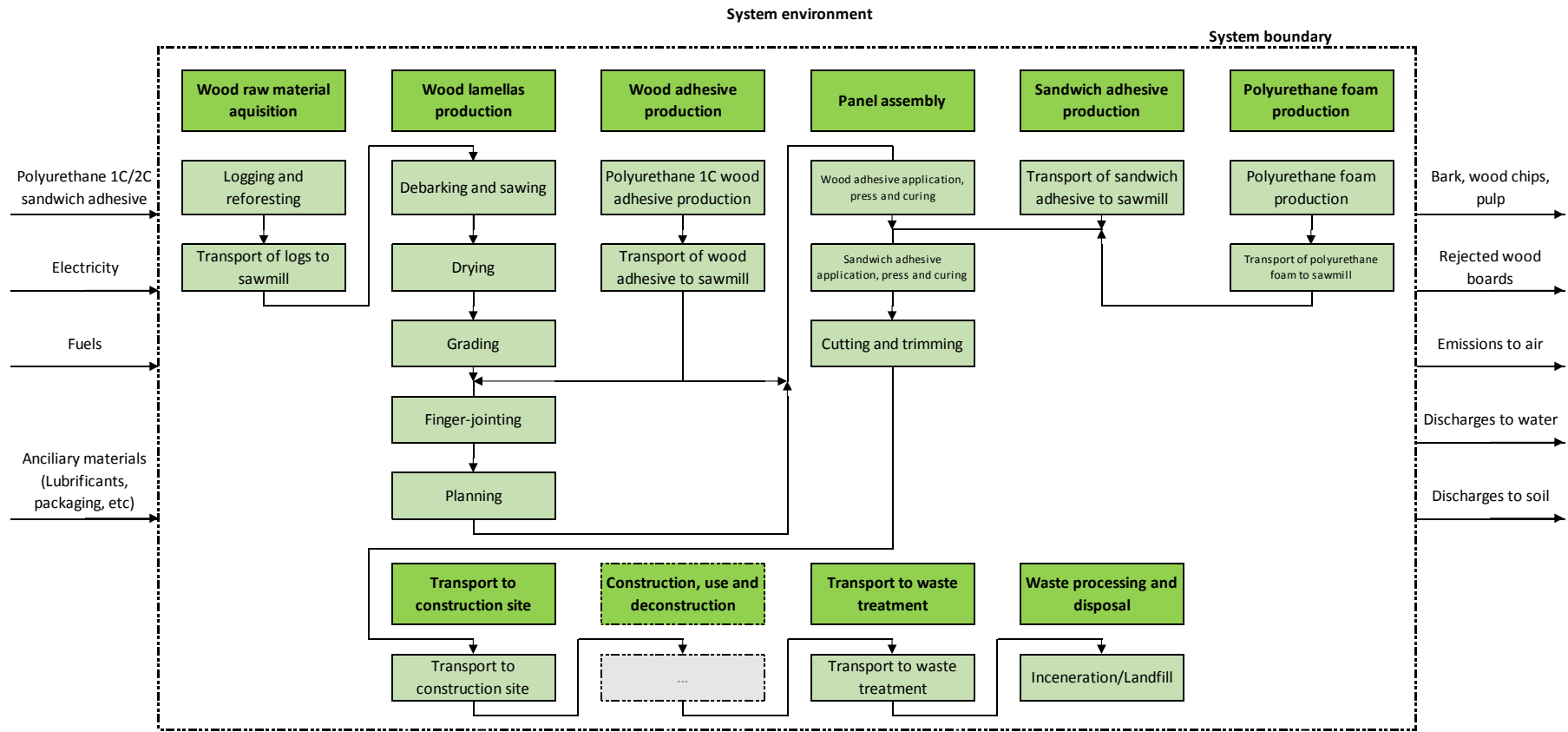
Figure 7-4 – System boundary defined for the CIT with PUR foam core panel solution.
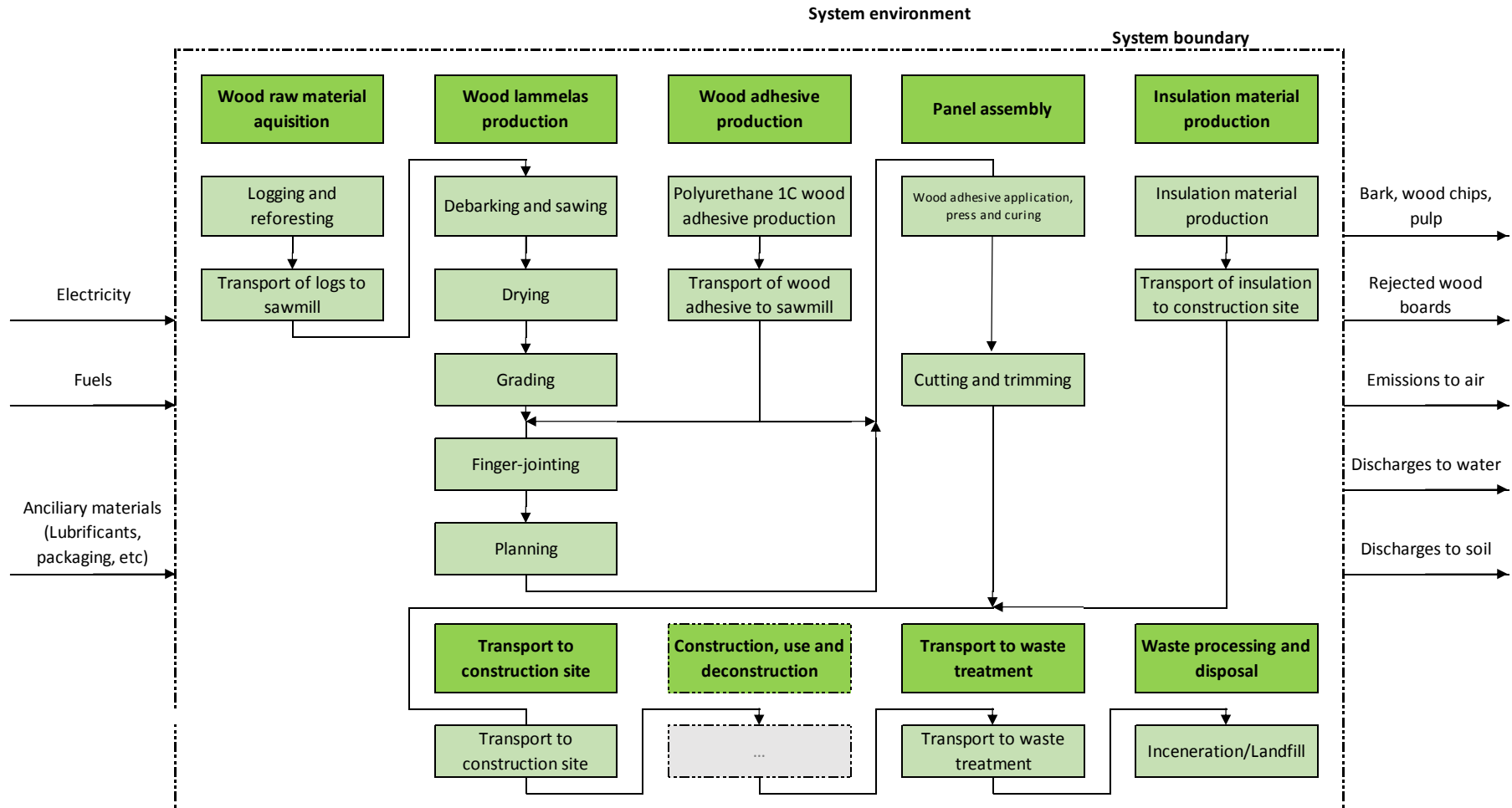
Figure 7-5 – System boundary defined for the CLT panel solution.

7.5 Life cycle inventory analysis

The inventory of processes to model the LCA of the panels was mainly based in pre-defined processes included in Ecoinvent 2.2 database (Ecoinvent, 2010), with most of them being adapted to the Portuguese situation (e.g. the electric energy production). Other processes were created with basis on other works: the logging and reforesting processes applicable to Maritime pine wood were collected from the information found in (Dias and Arroja, 2012); some processes regarding the CLT production were based on (Mapelli, 2012), namely the finger-jointing and press operations; the 1C PUR wood adhesive process was collected from (Messmer, 2015) and the ICB production from (Amorim Isolamentos, 2016).

The database sources, outputs, sub-products, allocation type and corresponding percentages for each unit process modelled for the CIT panels are shown in Table 7-4, while for the CLT panels they are shown in Table 7-5.

In some processes, it was necessary to proceed to allocations, as they delivered more than one product. For example in the unit process "Debarking and sawing", the outputs (boards, wood chips, sawdust and bark) are all economic, but one cannot split the process into a part that is responsible for the boards and one that is responsible for the sawdust. So, in the referred process, the mass criterion was used for the allocation.

Table 7-4 – Database sources, outputs, sub-products, allocation type and corresponding percentages for each unit process modelled for the CIT panels.

Unit Process	Database source(s)	Outputs	Sub-products	Allocation type	Percentage of allocation
Logging and reforesting (Transport of logs to sawmill)	(Dias and Arroja, 2012) Ecoinvent 2.2	Maritime pine logs	-	-	-
Debarking and sawing	Ecoinvent 2.2	Wood boards, green	Sawdust, pulp chips	Mass	61/39
Drying	Ecoinvent 2.2	Wood boards, dried	-	-	-
Classification	-	Selected boards	Rejected boards	Mass	90/10
Fingerjointing	(Mappelli, 2011)	Selected boards fingerjointed	Sawdust, pulp chips	Mass	95/5
Planning	(Mappelli, 2011)	Lamellas	Waste (Wood) Waste (Adhesive)	Mass	99/1
Polyurethane 1C wood adhesive production (Transport of wood adhesive to sawmill)	(Messmer, A. 2015) Ecoinvent 2.2	PUR 1C wood adhesive	-	-	-
(Polyurethane 1C/2C sandwich adhesive production) (Transport of sandwich adhesive to sawmill)	- Ecoinvent 2.2	1C/2C sandwich adhesive	-	-	-
Insulation material production (Transport of insulation material to sawmill)	Ecoinvent 2.2 / (Amorim Isolamentos, 2016) Ecoinvent 2.2	Insulation material	-	-	-
Wood adhesive application, press and curing	(Mappelli, 2011)	Wood layers	-	-	-
Sandwich adhesive application, press and curing	-	Panel unfinished	-	-	-
Cutting and trimming	-	Panel finished	Waste (Wood) Waste (PUR Foam / Adhesives)	Mass	99/1
(Transport to construction site)	Ecoinvent 2.2	-	-	-	-
(Transport to waste treatment)	Ecoinvent 2.2	-	-	-	-
Inceneration/Landfill	Ecoinvent 2.2	-	-	-	-

Table 7-5 – Database sources, outputs, sub-products, allocation type and corresponding percentages for each unit process modelled for the CLT panels.

Unit Process	Database source(s)	Outputs	Sub-products	Allocation type	Percentage of allocation
Logging and reforesting (Transport of logs to sawmill)	(Dias and Arroja, 2012) Ecoinvent 2.2	Maritime pine logs	-	-	-
Debarking and sawing	Ecoinvent 2.2	Wood boards, green	Sawdust, pulp chips	Mass	61/39
Drying	Ecoinvent 2.2	Wood boards, dried	-	-	-
Classification	-	Selected boards	Rejected boards	Mass	90/10
Fingerjointing	(Mappelli, 2011)	Selected boards fingerjointed	Sawdust, pulp chips	Mass	95/5
Planning	(Mappelli, 2011)	Lamellas	Waste (Wood) Waste (Adhesive)	Mass	99/1
Polyurethane 1C wood adhesive production (Transport of wood adhesive to sawmill)	(Messmer, A. 2015) Ecoinvent 2.2	PUR 1C wood adhesive	-	-	-
Insulation material production (Transport of insulation material to construction site)	Ecoinvent 2.2 / (Amorim Isolamentos, 2016) Ecoinvent 2.2	Insulation material	-	-	-
Wood adhesive application, press and curing	(Mappelli, 2011)	Panel unfinished	-	-	-
Cutting and trimming	-	Panel finished	Waste (Wood) Waste (Adhesive)	Mass	99/1
(Transport to construction site)	Ecoinvent 2.2	-	-	-	-
(Transport to waste treatment)	Ecoinvent 2.2	-	-	-	-
Inceneration/Landfill	Ecoinvent 2.2	-	-	-	-

Concerning the waste generated in some of the production processes (e.g. wood and polyurethane foam wastes from planning), it was assumed that such wastes were used as fuel for energy production at the manufacturing facilities. The adhesives were not accounted for in such processes due to lack of information regarding their calorific value and the low quantities employed.

According to the European List of Waste (CE, 2000), wood, cork, polyurethane, extruded polystyrene, rock wool, and cured adhesives may be treated as non-dangerous wastes, so they can be delivered on a non-dangerous waste landfill. The landfill facilities were assumed to be located at Trouxemil, Coimbra, Portugal, which according to (APA, 2016), can receive the referred materials (APA, 2017).

For the unit process for which transportation is required, a 16-ton lorry was assumed and the following distances were considered:

- 100 km between the forest and the sawmill (Leiria, Portugal);
- 2014 km between the wood adhesive factory (Neuenkirch, Switzerland) and the sawmill;
- 2198 km between the sandwich adhesive factory (Stuttgart, Germany) and the sawmill;
- 287 km between the polyurethane foam factory (Galiza, Spain) and the sawmill;
- 180 km between the insulation cork board factory (Vendas Novas, Portugal) and the sawmill;
- 158 km between the rock wool factory (Vila das Aves, Portugal) and the construction site;

- 97 km between the extruded polystyrene factory (Ovar, Portugal) and the construction site;
- 100 km between the sawmill and the construction site (Coimbra, Portugal);
- 20 km between the construction site and the incineration facilities (Souselas, Coimbra, Portugal);
- 20 km between the construction site and the landfill facilities (Trouxemil, Coimbra, Portugal).

It should be noticed that in the transportation, the total distance is assumed to be travelled twice (round trip), and that in one of the trips, the truck is empty. This is already assumed in the unit process from Ecoinvent, where the truck travels with 50% of the load for the defined distance of one trip.

7.6   Life cycle impact assessment

From the EPDs and published works related to CLT, it was found out that the most common impact category indicators used in LCA include:

- Depletion of abiotic resources – is concerned with the protection of human welfare, human health and ecosystem health. It is related to the extraction of minerals and fossil fuels due to inputs in the system;
- Climate change - represents possible adverse effects on ecosystem health, human health and material welfare; it is related to emissions of greenhouse gases to air;
- Stratospheric ozone depletion – represents the harmful effects upon human health, animal health, terrestrial and aquatic ecosystems, biochemical cycles and on materials due to the stratospheric ozone depletion;
- Photo-oxidant formation - represents the formation of reactive substances (mainly ozone), which are injurious to human health and ecosystems and that may also damage crops;
- Acidification - concerns with impacts on soil, groundwater, surface water, organisms, ecosystems and materials (buildings) by acidifying substances;
- Eutrophication - considers all impacts due to excessive levels of macronutrients in the environment caused by emissions of nutrients to air, water and soil.

The midpoint method CML 2 baseline 2000 V2.05 / West Europe, 1995 (Goedkoop et al, 2010) was chosen to perform the LCIA. For that method, the correspondence between the above-mentioned impact categories and category indicators (results), as well as the corresponding characterization model, time horizon and geographical scale are presented in Table 7-6.

Table 7-6 – Correspondence between impact categories, category indicators (results) and respective characterization models considered in CML 2 baseline 2000 V2.05 method. Note: Eq. stands for equivalents.

Impact category	Category indicator	Category indicator result	Characterization model		
			Designation	Time horizon	Geographical scale
Acidification	Acidification potentials (AP)	kg SO_2 eq./ kg emission	Adapted RAINS 10 model	∞	Local/continental
Climate change	Global warning potential (GWP_{100})	kg CO_2/kg emission	Intergovernmental Panel on Climate Change (IPCC) model	100 years	Global
Depletion of abiotic resources	Abiotic depletion potential (ADP)	kg Sb eq. /kg extraction	Model based on concentration reserves and rate of de-accumulation	-	Global
Eutrophication	Eutrophication potential (EP)	kg PO_4 eq./ kg emission	Stoichiometric procedure of Heijungs	∞	Local/continental
Photo-oxidant formation	Photochemical ozone creation potential (POCP)	kg C_2H_4 eq./kg emission	UNECE Trajectory model	5 days	Local/continental
Stratospheric ozone depletion	Ozone depletion potential (ODP)	kg CFC-11 eq./ kg emission	World Meteorological Organisation (WMO) model	∞	Global

7.7 Results and discussion

In the current section, for each of the considered categories, the results are presented in terms of absolute values in a set of tables. In complementary figures, the results are presented in terms of relative percentage, by dividing the process value by the absolute maximum value on each category indicator.

7.7.1 Analysis of the contribution of each process on the environmental impact of the CIT panel floor

The contribution of each process on each category indicator considered for the CIT floor is presented in Table 7-7. The relative contribution of each process on the different environmental impacts considered is shown in Figures 7-6 to 7-11 for the CIT floor. In the referred figures, each process is identified by its corresponding stage of LCA as in Figure 7-3.

Table 7-7 – Contribution of each process on each category indicator considered for the CIT floor.

Process/Stage	Abiotic depletion (ADP) kg Sb eq.	Acidification (AP) kg SO$_2$ eq.	Eutrophication (EP) kg PO$_4$ eq.	Ozone layer depletion (ODP) kg CFC-11 eq.	Photochemical oxidation (POCP) kg C$_2$H$_4$ eq.	Global warming (GWP100) kg CO$_2$ eq.
Logging and reforesting [with CO$_2$ seq.]	2.24E-02	2.46E-02	1.34E-02	4.18E-07	7.77E-04	3.3 [-235.8]
Transport of logs to sawmill	1.18E-02	8.86E-03	2.35E-03	2.63E-07	2.65E-04	1.6
Debarking and sawing	2.24E-02	2.63E-02	4.53E-03	1.77E-07	9.83E-04	2.9
Drying	1.84E-02	2.81E-02	6.51E-03	1.58E-07	1.07E-03	2.6
Grading	1.60E-07	1.95E-07	5.71E-08	2.07E-12	6.98E-09	0.0
Finger-jointing	2.92E-02	3.43E-02	5.55E-03	2.20E-07	1.29E-03	3.6
Planning	2.63E-02	3.10E-02	5.52E-03	2.10E-07	1.16E-03	3.7
Polyurethane 1C wood adhesive production	5.74E-04	4.08E-04	2.38E-05	1.38E-09	2.61E-05	0.1
Transport of wood adhesive to sawmill	1.07E-02	7.62E-03	5.30E-04	3.67E-08	4.74E-04	1.0
Transport of sandwich adhesive to sawmill	6.44E-04	4.82E-04	1.28E-04	1.43E-08	1.44E-05	0.1
Polyurethane foam production	5.17E-02	2.11E-02	4.31E-03	2.18E-08	2.45E-03	5.1
Transport of polyurethane foam to sawmill	3.36E-04	2.52E-04	6.67E-05	7.45E-09	7.52E-06	0.0
Wood adhesive application, press and curing	6.57E-02	7.73E-02	1.33E-02	5.21E-07	2.89E-03	8.6
Sandwich adhesive application, press and curing	1.49E-02	1.76E-02	3.03E-03	1.19E-07	6.57E-04	2.0
Cutting and trimming	1.36E-04	1.90E-04	7.43E-04	2.62E-09	7.38E-06	-0.2
Transport to construction site (A4)	6.40E-03	4.79E-03	1.27E-03	1.42E-07	1.43E-04	0.9
Transport to waste treatment (C2)	1.28E-03	9.57E-04	2.54E-04	2.84E-08	2.86E-05	0.2
Incineration [with energy recovery] (C3/C4)	7.00E-03	1.66E-02	2.09E-02	1.11E-07	6.05E-04	115.7 [89.5]
Landfill with partial rot [with energy recovery] (C3/C4)	1.02E-02	5.73E-03	1.85E-01	2.33E-07	1.20E-03	128.0 [71.5]
Landfill with total rot [with energy recovery] (C3/C4)	1.02E-02	5.73E-03	1.85E-01	2.33E-07	1.20E-03	621.8 [339.0]
A1 [with CO$_2$ seq.]	7.47E-02	4.60E-02	1.77E-02	4.41E-07	3.26E-03	8.4 [-230.7]
A2	2.35E-02	1.72E-02	3.07E-03	3.21E-07	7.61E-04	2.8
A3	1.77E-01	2.15E-01	3.92E-02	1.41E-06	8.05E-03	23.2
A1-A3	2.75E-01	2.78E-01	5.99E-02	2.17E-06	1.21E-02	34.4 [-204.7]

Pedro Gil Girão dos Santos
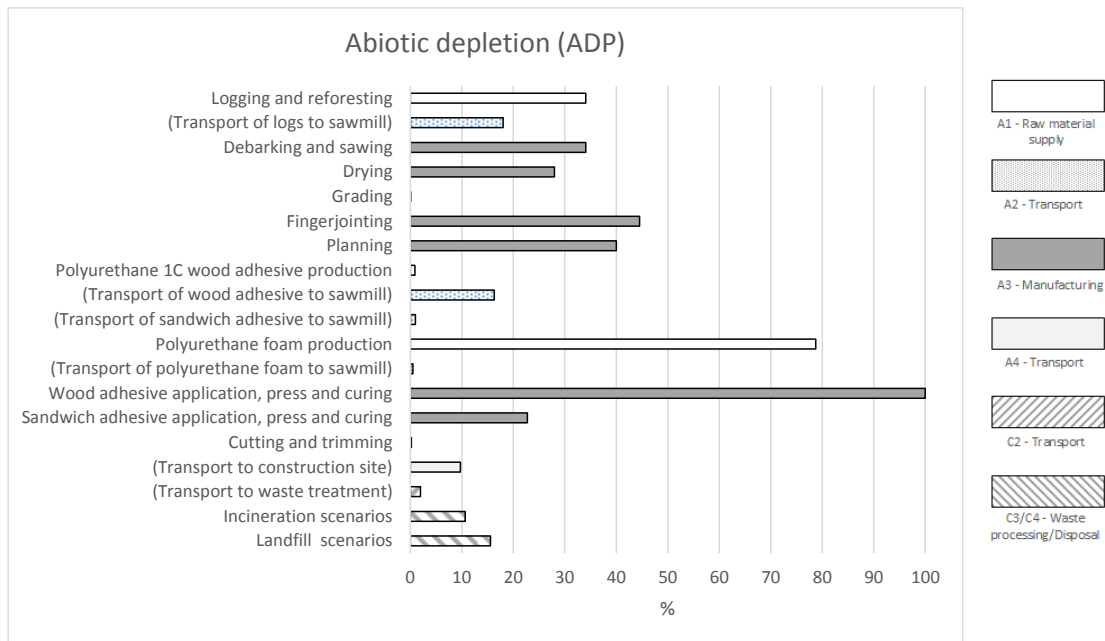
Figure 7-6 – Relative contribution of each process on the environmental impact (Abiotic depletion) of the CIT floor.
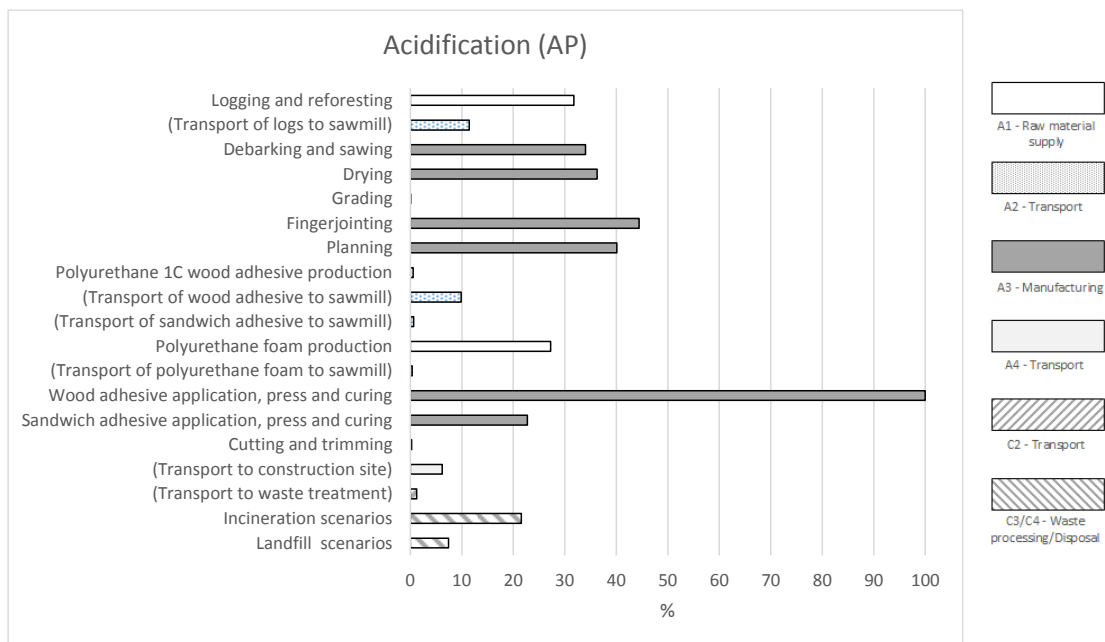
Figure 7-7 – Relative contribution of each process on the environmental impact (Acidification) of the CIT floor.
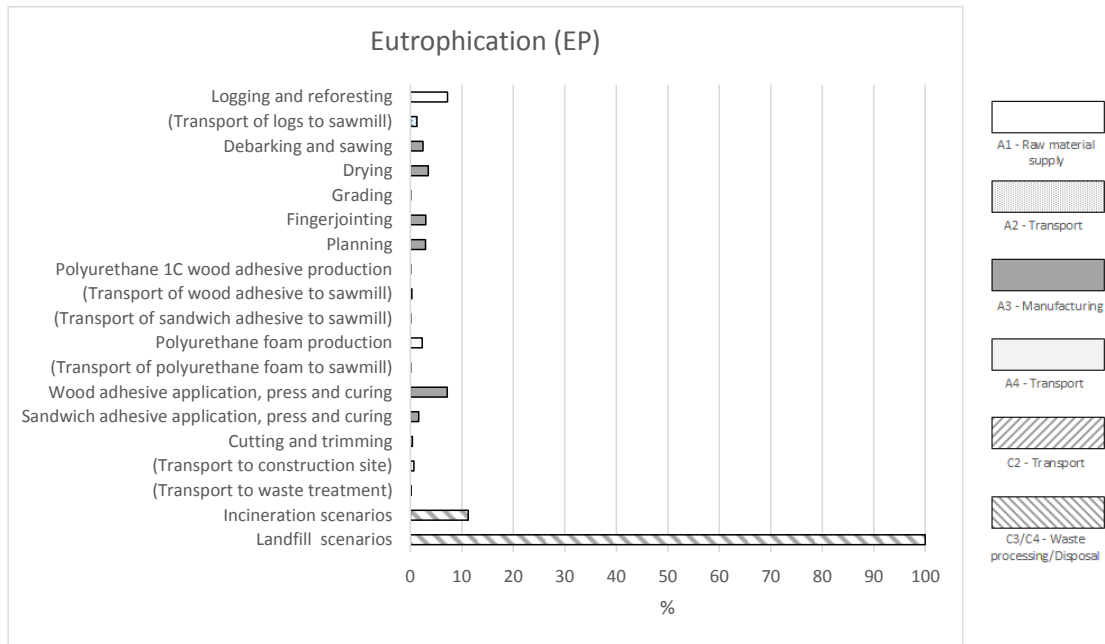
Figure 7-8 - Relative contribution of each process on the environmental impact (Eutrophication) of the CIT floor.
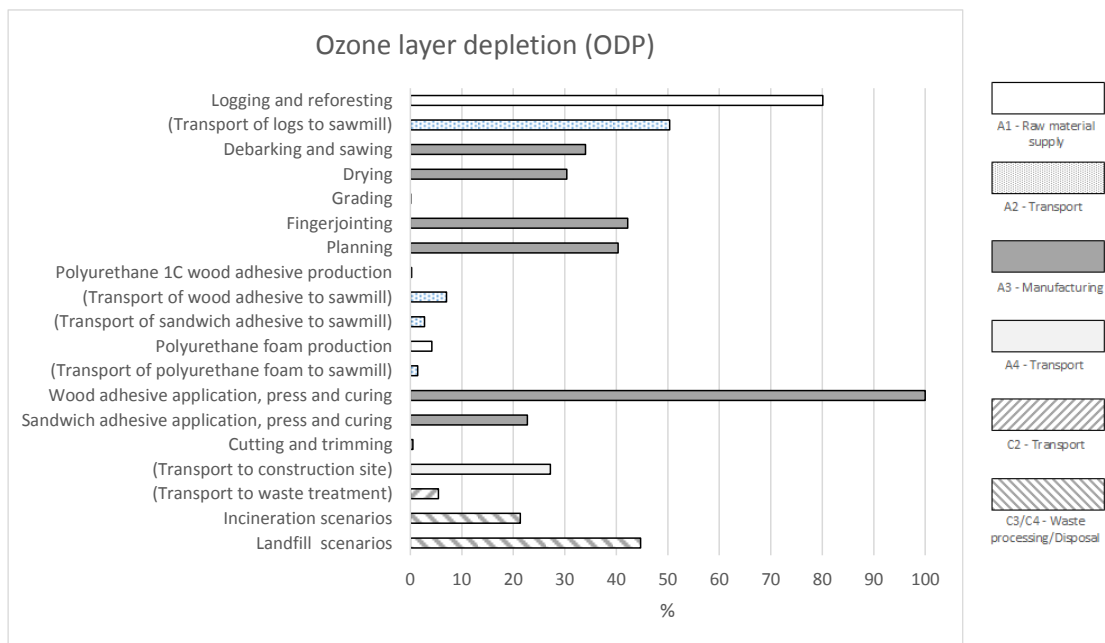
Figure 7-9 - Relative contribution of each process on the environmental impact (Ozone layer depletion) of the CIT floor.
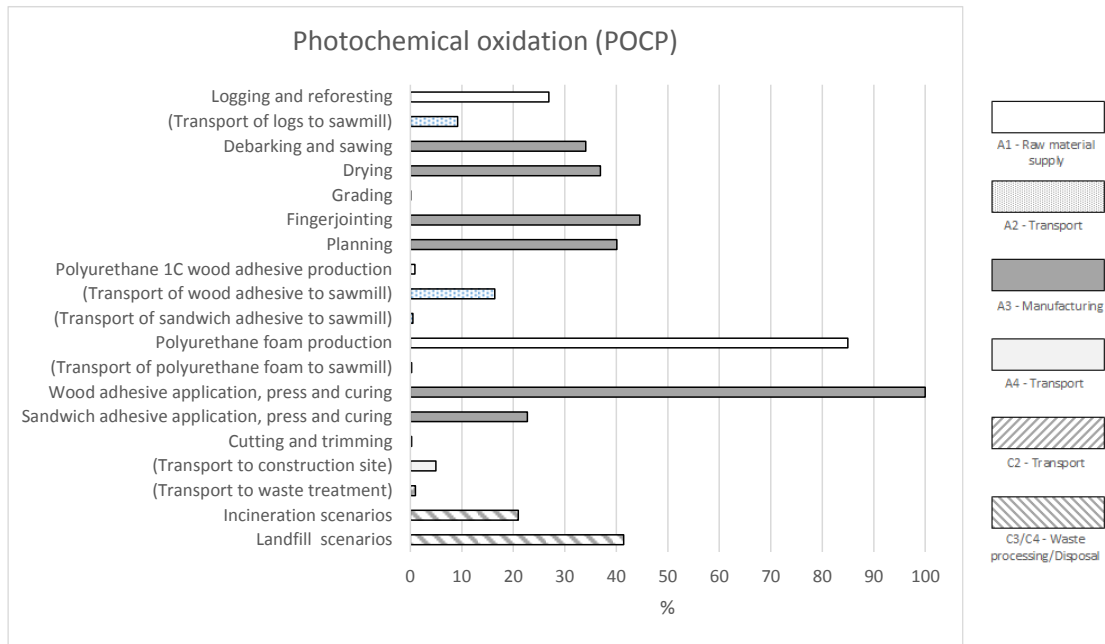
Figure 7-10 - Relative contribution of each process on the environmental impact (Photochemical oxidation) of the CIT floor.
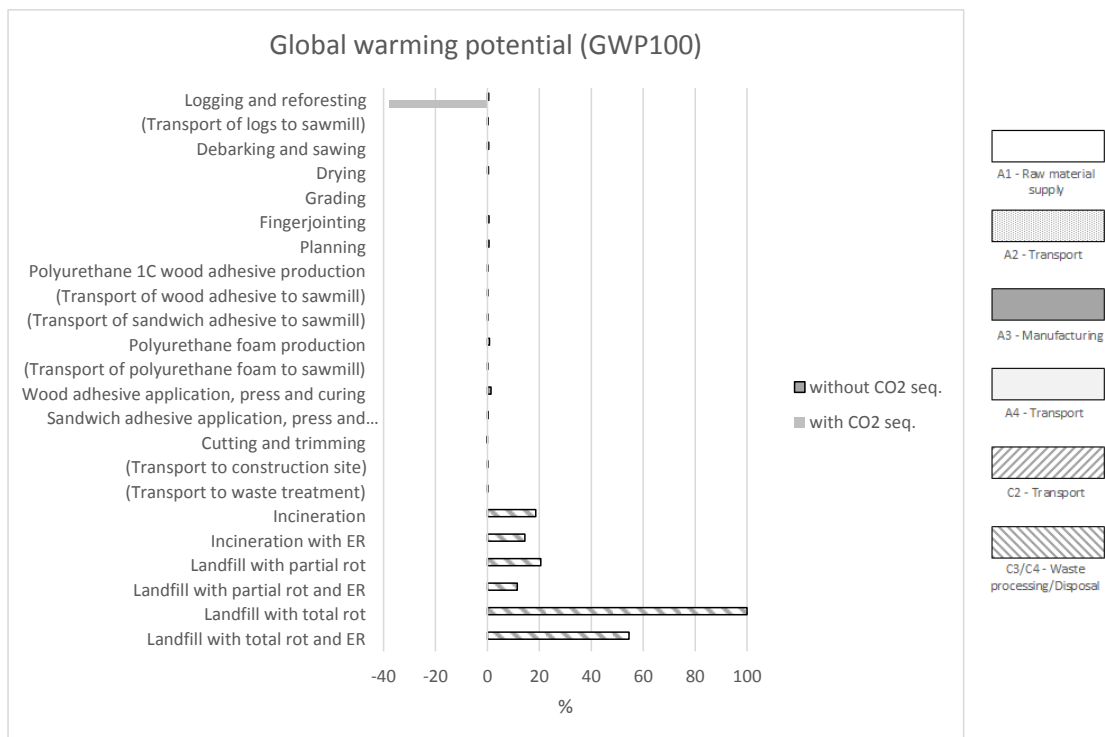
Figure 7-11 - Relative contribution of each process on the environmental impact (Global warming potential) of the CIT floor.

Notice that in Table 7-7, the value (-0.2 kg CO_2 eq.) regarding the global warming potential (GWP100) of the 'cutting and trimming' process is actually negative; this is due

to the energy recovery benefit (CO_2 credit) obtained from the incineration of the residues of the process.

From the analysis of the previous figures, one can say that, regarding the LCA's stages, the ones that contribute the most for each impact category are: the raw material supply (A1) and manufacturing (A3) to abiotic depletion (ADP); A3 to acidification (AP); waste processing/disposal (C3/C4) to eutrophication (EP); A3 to ozone layer depletion (ODP); A1 and A3 to photochemical oxidation (POCP) and C3/C4 to global warming potential (GWP100).

Regarding the individual processes, from the analysis of the same figures, it is found that the 'wood adhesive, press and curing' is the one that produces the highest impacts regarding four of the six categories: ADP, AP, ODP and POCP. With close impacts to those is the 'polyurethane foam production' for the ADP and POCP categories and the 'logging and reforesting' for ODP.

Concerning the end-of-life scenarios, all the landfill scenarios present similar results in all categories with the exception of GWP100. The same occurs between the two possible incineration scenarios. For EP, those processes are clearly the ones responsible for the highest emissions. If instead of landfill, the incineration is considered as the end-of-life scenario, those processes and the logging and reforesting operations become the main contributions to the EP.

Some processes have low or even negligible impact in all categories, such as the grading – this result is logical, which was considered to proceed to an allocation process (i.e. accepted wood for the panels or rejected wood for the panels). Also, the transport of the polyurethane foam has low impacts in all categories, due to the small amount that has to be transported to produce 1 m^2 of panel (1.2 kg). As expected, due to the low quantity involved (280 g/m^2), the one-component polyurethane adhesive used for bonding the wood layers produced almost negligible impacts in all categories. Therefore, as referred, it was also expected that the two-component polyurethane adhesive used to bond the wood layers to the polyurethane foam (not modelled due to lack of data) would also produce residual impacts.

Regarding GWP100, it should be noticed that the quantity of CO_2 eq. that is released at the incineration process (115.7 kg) is actually smaller than the biogenic CO_2 absorbed during the tree growth (235.8 kg CO_2 eq.). This is because part of the wood raw material is allocated to other sub-products (that were considered out of the boundary system). From the analysis of Figure 7-11, it is clear that the most substantial part of the gases that contribute to the GWP is released at the end-of-life stage. From the scenarios considered,

the less harmful is landfill with partial rot and energy recovery (71.5 kg CO_2 eq.). However, as there is still a lot of uncertainty about the behaviour of wood in landfill, this scenario can turn into the most harmful one if total rot occurs; in that case, the CO_2 eq. emitted will become about 2.6 times higher than the sequestered CO_2 (621.8 kg with no energy recovery or 339.0 with energy recovery). In both cases, the formation of CH_4 is responsible for the substantial part of the emissions. In the first case, from the total 621.8 kg eq. emissions, 575.1 kg corresponds to CH_4 (it should be noticed that a conversion factor of CH_4 to CO_2 eq. of 25 is considered). In the second case (for a total of 339.0 kg CO_2 eq.), although part of CH_4 is captured and burnt for energy recovery (the combustion of each kg of CH_4 delivers 2.75 kg of CO_2), the remaining 50% of CH_4 is still released resulting in a total 311.3 kg CO_2 eq.. It should be noticed that if an efficiency of 100% on the CH_4 collection on the landfill was possible, the GWP would be just 56.2 kg CO_2 eq. (assuming total rot and energy recover). However, that is just a hypothetical scenario that would be very difficult to obtain in practice, as there are always leaks in landfills through where the gases can escape.

Not quite different in terms of the magnitude of emissions with respect to the landfill option with partial rot and energy recovery is the incineration scenario with energy recovery (89.5 kg CO_2 eq.). Also, the GWP impacts of the same scenario without energy recovery (115.7 kg CO_2 eq.) is quite close to the ones of the landfill with partial rot and no energy recovery (128.0 kg CO_2 eq.).

In sum, due to the uncertainty about wood degradation in landfill, the incineration option with energy recovery seems to be the best option.

7.7.2 Analysis of the contribution of each process on the environmental impact of the CIT panel wall

The results regarding the contribution of each process on the environmental impact of the CIT panel wall are presented in Appendix C, section C.1, namely:

- the contribution of each process on each category indicator considered for the CIT wall - Table C.1;
- the relative contribution of each process for the different environmental impacts considered – Figures C.1 to C.6.

From the analysis of the results, similar conclusions to those obtained for the floor solutions can be drawn:

- for the LCA's stages, it is found that for each impact category, the ones that contribute the most for each one are the following: A1 and A3 to ADP; A3 to AP; C3/C4 to EP; A3 to ODP; A1 and A3 to POCP and C3/C4 to GWP100;

- regarding the individual analysis of the processes, it is found that the 'wood adhesive application, press and curing' process is the one that produces the highest impacts regarding the ADP, AP, ODP and POCP categories, with the 'polyurethane foam production' process being also standing out for the ADP and POCP categories. For EP, the landfill end-of-life scenario is responsible for the highest impact; however, if instead of landfill, incineration is considered, both incineration and 'wood adhesive application, press and curing' are the main contributors;

- concerning the end-of-life scenarios, once more and as occurred for the floor case, all the landfill scenarios present similar results between them regarding the AD, AP, EP, ODP and POCP. The same occurs between the two possible incineration scenarios;

- in general, the landfill scenarios have the highest impacts in all categories with the exception of AP;

- the quantity of CO_2 eq. that is released at the incineration process (48.2 kg) is smaller than the biogenic CO_2 absorbed during the tree growth (95.2 kg CO_2 eq.), because of the allocation of wood to other sub-products;

- any of the end-of-life processes is responsible for the most substantial contribution to the GWP in comparison to the other processes;

- the magnitude of emissions that contribute to GWP from the landfill option with partial rot and energy recovery (29.0 kg CO_2 eq.) is quite similar to the incineration scenario with energy recovery (37.3 kg CO_2 eq.). Also, the incineration scenario without energy recovery (48.2 kg CO_2 eq.) is found to be quite similar to landfill with partial rot and no energy recovery (51.9 kg CO_2 eq.).

7.7.3 Comparison of the impacts between using different parameters for the bonding of wood layers

For the comparison of the impacts obtained when considering a different bonding system for the wood layers (i.e., with or without primer), the CIT floor case was used for the

study. It should be noticed that for the wall application, the results would be similar DUE to the same adhesive spread rates and pressing times applied.

The relative contribution of each process directly related to the wood layers' bonding, namely the production, transport and application are shown in Figures 7-12 to 7-17. In the figures, the bonding process with primer (adhesive spread rate of 140 kg/m^3 and 400 min of press time) is identified as 'A', and the bonding process without primer (adhesive spread rate of 180 kg/m^3 and 200 min of press time) as 'B'. Notice that some processes (e.g. cutting and trimming), including the end-of-life scenarios, are not presented because the adhesives were not accounted for in those process due to the lack of data, as well the low quantities involved, as explained previously.
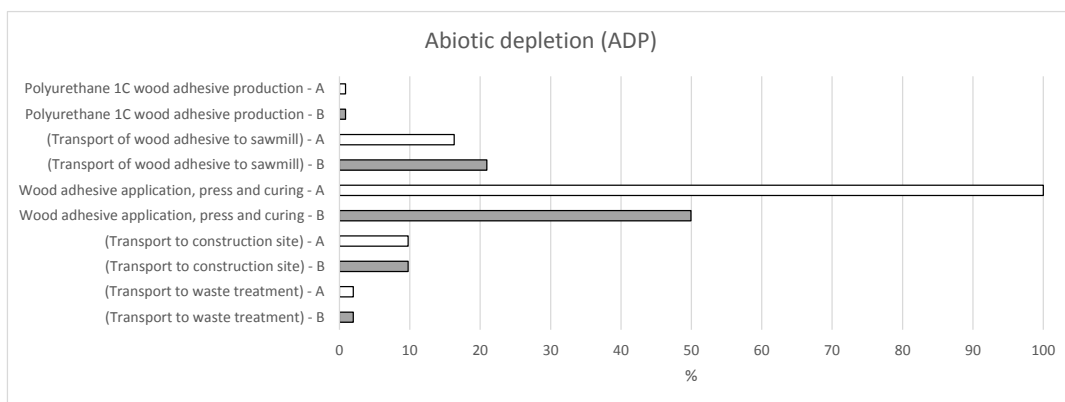
Figure 7-12 – Relative contribution of each process directly related to the wood layers' bonding on the environmental impact (Abiotic depletion) of the CIT floor.
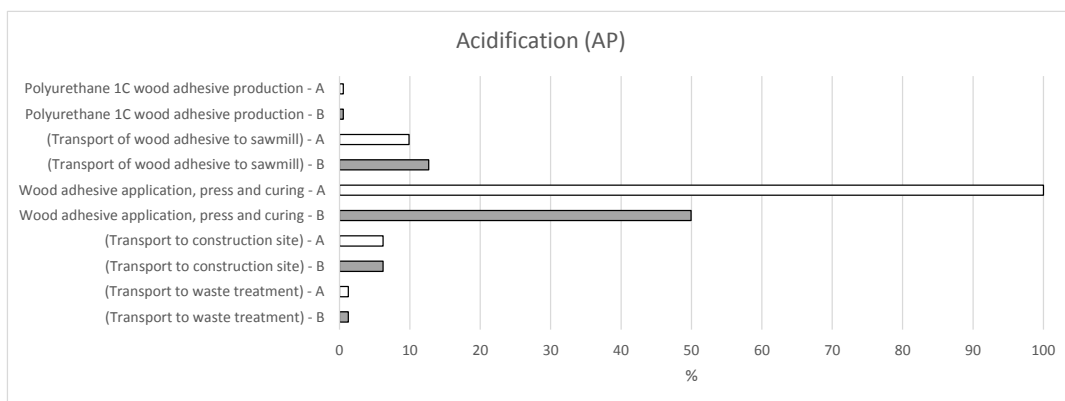
Figure 7-13 – Relative contribution of each process directly related to the wood layers' bonding on the environmental impact (Acidification) of the CIT floor.
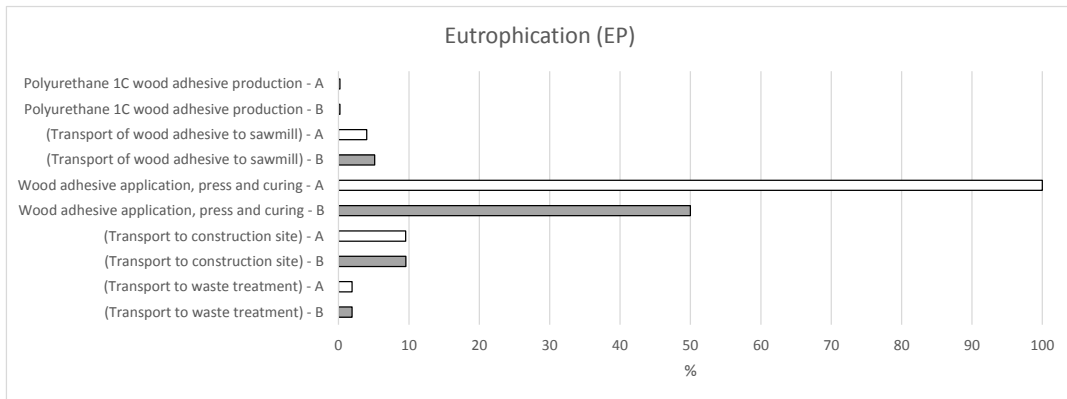
Figure 7-14 – Relative contribution of each process directly related to the wood layers' bonding on the environmental impact (Eutrophication) of the CIT floor.
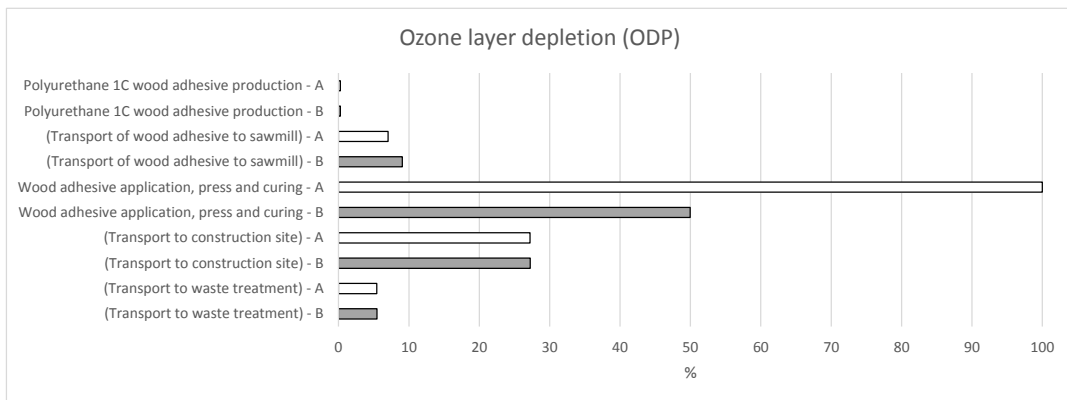
Figure 7-15 – Relative contribution of each process directly related to the wood layers' bonding on the environmental impact (Ozone layer depletion) of the CIT floor.
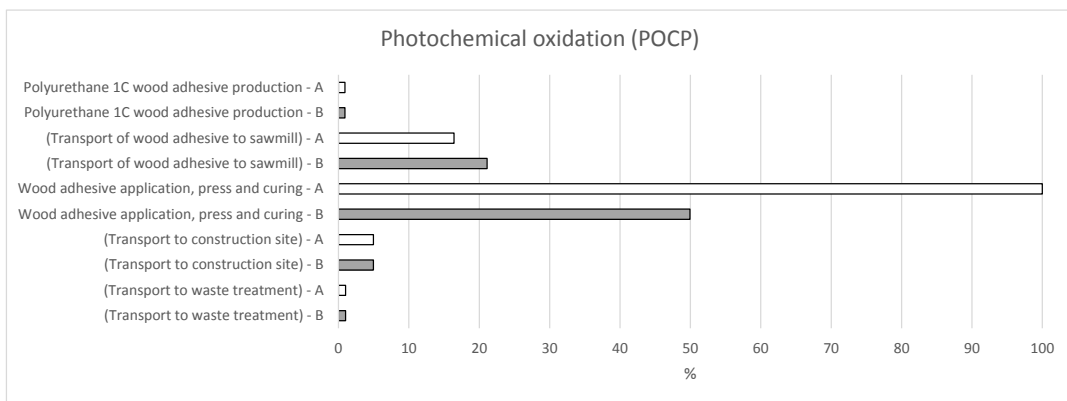
Figure 7-16 – Relative contribution of each process directly related to the wood layers' bonding on the environmental impact (Photochemical oxidation) of the CIT floor.
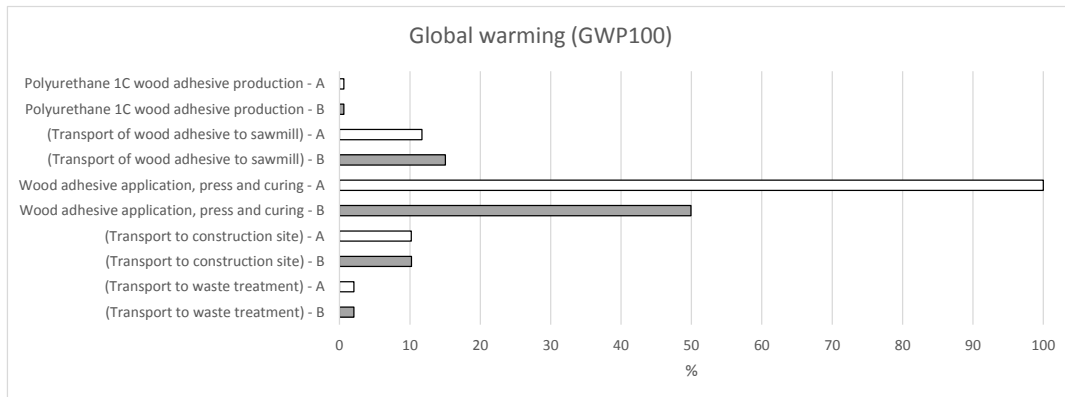
Figure 7-17 – Relative contribution of each process directly related to the wood layers' bonding on the environmental impact (Global warming) of the CIT floor.

From the analysis of the figures above, it is found that in all the considered categories, the major difference between the two bonding options occurs for the 'wood adhesive press and curing' process. This is explained by the double of electric energy required for the press for the primed case (A), which consequently doubles the impacts compared to the un-primed case (B). Regarding the other categories, which are directly related to the adhesive production and transport, it is found (as expected) that the low difference in the spread rate between the two options (40 g/m^2) results in an insignificant difference between impacts.

The results regarding the impacts of using the two different bonding options for the CIT floor solution at the end-of-life as a function of the end-of-life scenario are presented in Table 7-8 and the relative impacts are shown in Figures 7-18 to 7-21. Notice that in that table 'ER' stands for energy recovery.

From the analysis of the table and figures presented, it is found that the bonding option without primer has always lower impacts than the solution that uses primer. Looking at Table 7-8, and calculating the difference between the corresponding GWP100 values for both adhesive systems of any of the end-of-life scenarios (e.g. Incineration, 35.9 minus 31.9) results in a constant value of around 4.0 kg CO_2 eq., which is the amount of emissions that are avoided when adopting the un-primed system. This means that although the primed solution was clearly better in terms of mechanical performance (see Chapter 4) it was slightly worse in an environmental perspective than the un-primed one.

Table 7-8 – Impacts at the end-of-life as a function of the end-of-life scenario considered on floor solution regarding the use of different wood layers' bonding parameters.

Adhesive system	End-of-life scenario	Abiotic depletion (ADP)	Acidification (AP)	Eutrophication (EP)	Ozone layer depletion (ODP)	Photochemical oxidation (POCP)	Global warming (GWP100)	Global warming (GWP100) with CO_2 seq.
		kg Sb eq.	kg SO_2 eq.	kg PO_4 eq.	kg CFC-11 eq.	kg C_2H_4 eq.	kg CO_2 eq.	kg CO_2 eq.
with primer	Incineration [w/ ER]	0.269	0.072	2.02E-06	0.012	0.269	147.2 [121.0]	35.9 [9.7]
	Landfill with partial rot [w/ ER]	0.259	0.237	2.14E-06	0.012	0.259	159.5 [102.9]	48.2 [-8.3]
	Landfill with total rot [w/ ER]	0.259	0.237	2.14E-06	0.012	0.259	653.3 [370.5]	542.0 [259.2]
without primer	Incineration [w/ ER]	0.233	0.066	1.77E-06	0.010	0.233	143.2 [117.0]	31.9 [5.7]
	Landfill with partial rot [w/ ER]	0.222	0.230	1.89E-06	0.011	0.222	155.5 [98.9]	44.2 [-12.3]
	Landfill with total rot [w/ ER]	0.222	0.230	1.89E-06	0.011	0.222	649.3 [366.5]	538.1 [255.2]
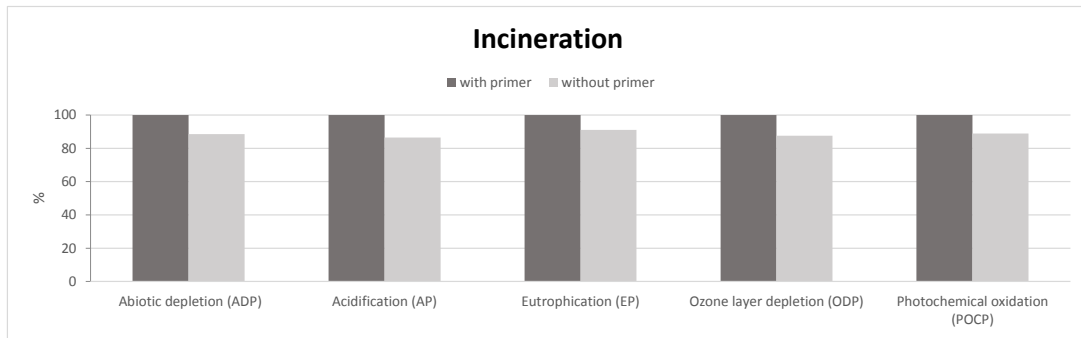
Figure 7-18 – Relative impacts (at the end-of-life) of using different wood layers' bonding parameters for the incineration end-of-life scenario (CIT floor).
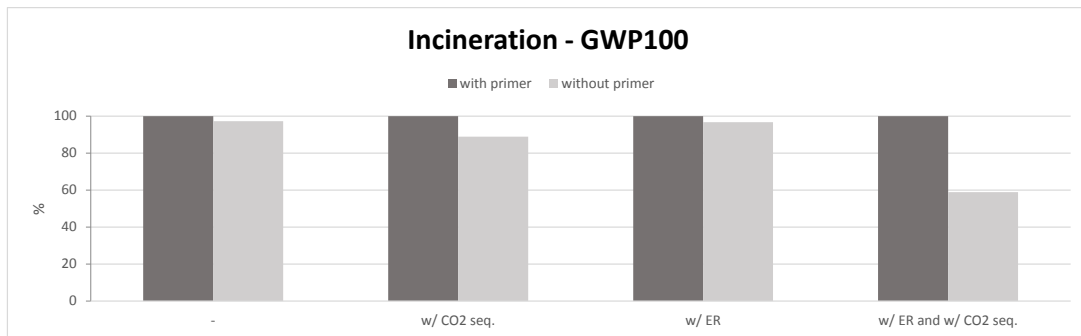
Figure 7-19 – Relative impacts (at the end-of-life) on GWP100 of using different wood layers' bonding parameters for the incineration end-of-life scenario (CIT floor).
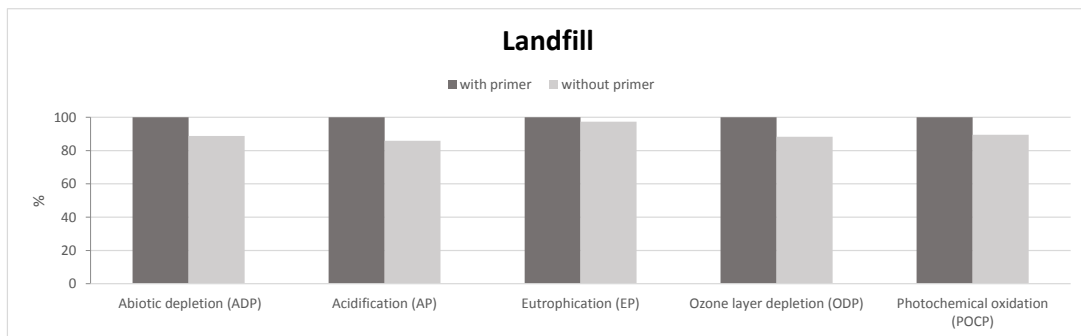
Figure 7-20 – Relative impacts (at the end-of-life) of using different wood layers' bonding parameters for the landfill end-of-life scenario (CIT floor).
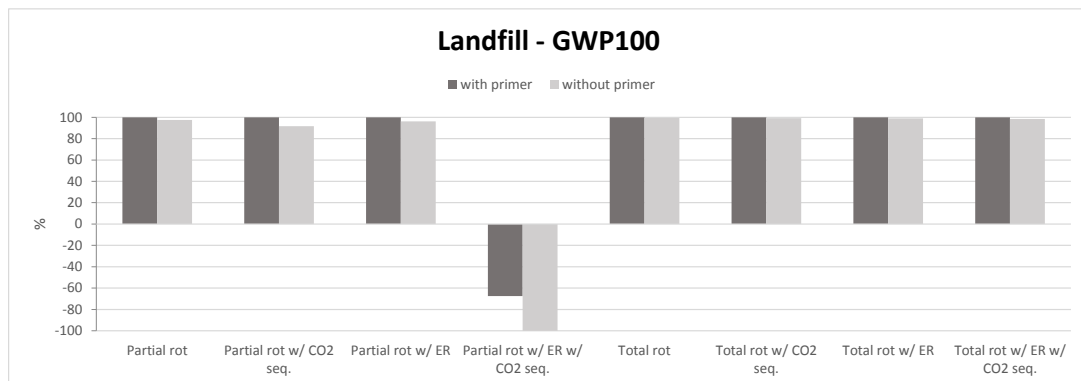
Figure 7-21 – Relative impacts (at the end-of-life) on GWP100 of using different wood layers' bonding parameters for the landfill end-of-life scenario (CIT floor).

7.7.4 LCA results for different thicknesses of wood layers compared to the optimized one for the CIT floor

The results regarding the impacts of each CIT floor solution regarding the wood layer thickness for the cradle-to-gate stage (A1-A3) are presented in Table 7-9. The comparison of the relative impacts is shown in Figure 7-22.

Table 7-9 - Impacts of each floor solution regarding the wood layer thickness for the cradle-to-gate stage (A1-A3).

Wood layers' ratio	Abiotic depletion (ADP)	Acidification (AP)	Eutrophication (EP)	Ozone layer depletion (ODP)	Photochemical oxidation (POCP)	Global warming (GWP100)	Global warming (GWP100) w/ CO_2 seq.
	kg Sb eq.	kg SO_2 eq.	kg PO_4 eq.	kg CFC-11 eq.	kg C_2H_4 eq.	kg CO_2 eq.	kg CO_2 eq.
Optimized	2.75E-01	2.78E-01	5.99E-02	2.17E-06	1.21E-02	34.4	-204.7
$h_1=h_2/2$	2.77E-01	2.80E-01	6.05E-02	2.19E-06	1.22E-02	34.7	-208.6
$h_1=h_2$	2.85E-01	2.90E-01	6.31E-02	2.29E-06	1.25E-02	35.7	-224.3
$h_1=h_2 x2$	2.97E-01	3.08E-01	6.75E-02	2.47E-06	1.30E-02	37.5	-251.9
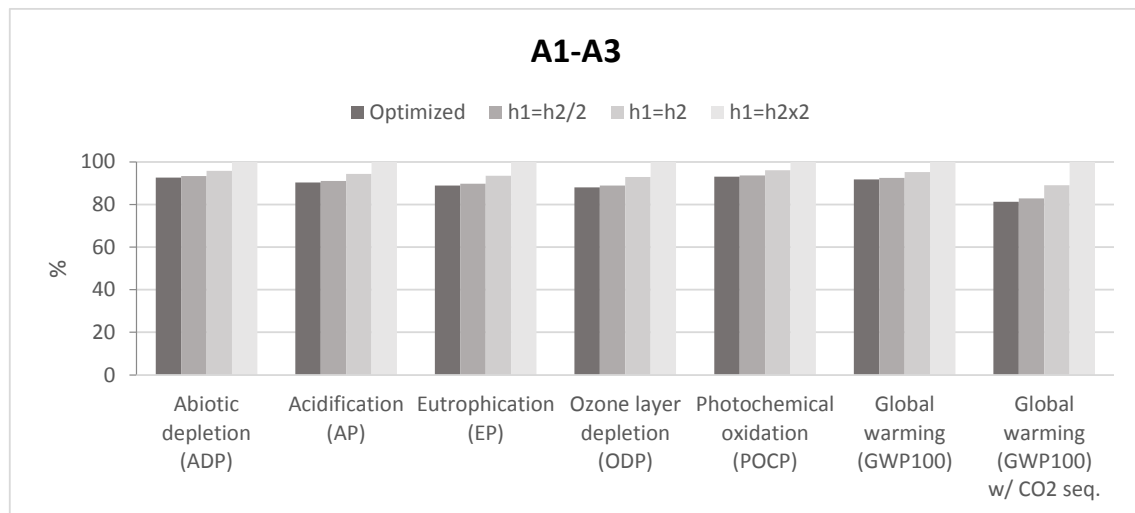
Figure 7-22 - Relative impacts of each floor solution regarding the wood layer thickness for the cradle-to-gate stage (A1-A3).

The analysis of Table 7-9 and Figure 7-22 shows that at the cradle-to-gate stage, the impacts of all the alternative solutions to the optimized one has higher impacts, with exception of the GWP100 indicator when carbon sequestration is included, which is logical since those alternative solutions make use of more wood than the optimized one (Table 7-2). Even so, the impacts for the $h_1=h_2/2$ solution are very close to the ones of the optimized solution, while the ones for the $h_1 \times h_2$ solution deviate the most from the optimized ones.

Pedro Gil Girão dos Santos

The results regarding the impacts at the end-of-life of each CIT floor solution regarding the wood layer thickness as a function of the end-of-life scenario considered are presented in Table 7-10.

The comparison of the results at the end-of-life obtained for the different thicknesses of wood layers for each of the considered categories is shown in Figures 7-23 a 7-26 for the considered end-of-life scenarios.

From the analysis of the figures above, it is concluded that the consideration of ratios between wood layers thickness different from the optimized one leads to an increase in all the impact categories. Only when considering the energy recovery and biogenic CO_2 sequestration (for the incineration and landfill with partial rot scenarios) it is possible to obtain a benefit in the global warming potential. This is because the energy obtained from the incineration/burning processes (that is converted to CO_2 emissions from the grid electricity that are being offset) is higher due to higher wood volume used in the non-optimized solutions. In the case when CO_2 sequestration is considered, it is even possible to obtain a negative GWP100.

Indeed, in general, the differences in terms of impacts between the optimized solution and the one considering $h_1 = h_2/2$ are quite reduced. For example, the differences between the relative impacts for the incineration with energy recovery end-of-life scenario are as follows: 4% for GWP100 with CO_2 seq., 1% for the ADP, EP and GWP100 without CO_2 seq. and 0% for AP, ODP and POCP. In contrast, the $h_1 = h_2 \times 2$ solution is the one that produces higher impacts in all categories, with the exception of GWP100 with CO_2 seq. (29%): 15% for GWP100 without CO_2 seq., 12% for EP and ODP, 9% for AP and 7% for ADP and POCP.

Table 7-10 – Impacts at the end-of-life of each floor solution regarding the wood layer thickness as a function of the end-of-life scenario considered.

Wood layers' ratio	End-of-life scenario	Abiotic depletion (ADP) kg Sb eq.	Acidification (AP) kg SO$_2$ eq.	Eutrophication (EP) kg PO$_4$ eq.	Ozone layer depletion (ODP) kg CFC-11 eq.	Photochemical oxidation (POCP) kg C$_2$H$_4$ eq.	Global warming (GWP100) kg CO$_2$ eq.	Global warming (GWP100) w/ CO$_2$ seq. kg CO$_2$ eq.
Optimized	Incineration [with ER]	0.261	0.269	0.072	2.02E-06	0.012	147.2 [121.0]	35.9 [9.7]
	Landfill with partial rot [with ER]	0.264	0.259	0.237	2.14E-06	0.012	159.5 [102.9]	48.2 [-8.3]
	Landfill with total rot [with ER]	0.264	0.259	0.237	2.14E-06	0.012	653.3 [370.5]	542.0 [259.2]
$h_1=h_2/2$	Incineration [with ER]	0.263	0.271	0.073	2.01E-06	0.012	149.2 [122.6]	36.0 [9.4]
	Landfill with partial rot [with ER]	0.266	0.261	0.240	2.16E-06	0.012	162.0 [104.4]	48.8 [-8.8]
	Landfill with total rot [with ER]	0.266	0.261	0.240	2.16E-06	0.012	664.5 [376.7]	551.2 [263.4]
$h_1=h_2$	Incineration [with ER]	0.269	0.280	0.076	2.10E-06	0.012	157.9 [129.5]	36.8 [8.4]
	Landfill with partial rot [with ER]	0.273	0.270	0.253	2.26E-06	0.013	171.8 [110.3]	50.8 [-10.8]
	Landfill with total rot [with ER]	0.273	0.270	0.253	2.26E-06	0.013	708.9 [401.3]	587.9 [280.3]
$h_1=h_2 \times 2$	Incineration [with ER]	0.280	0.297	0.082	2.28E-06	0.013	173.1 [141.6]	38.4 [6.9]
	Landfill with partial rot [with ER]	0.284	0.285	0.277	2.43E-06	0.013	188.9 [120.4]	54.2 [-14.3]
	Landfill with total rot [with ER]	0.284	0.285	0.277	2.43E-06	0.013	786.7 [444.3]	652.0 [309.6]
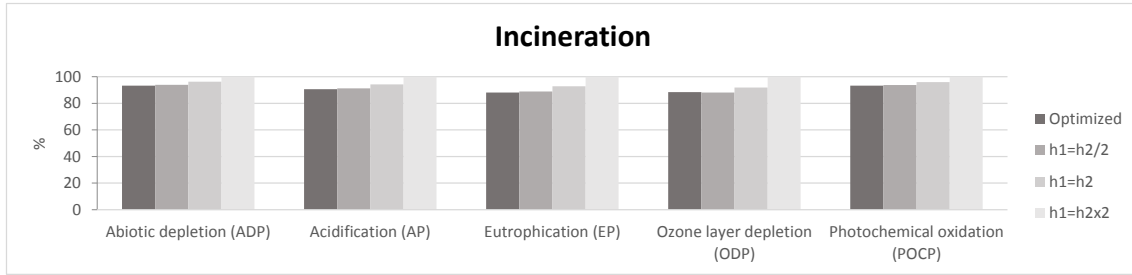
Figure 7-23 – Relative impacts (at the end-of-life) of using different thicknesses of wood layers compared to the optimized one for the CIT floor, for the incineration end-of-life scenario.
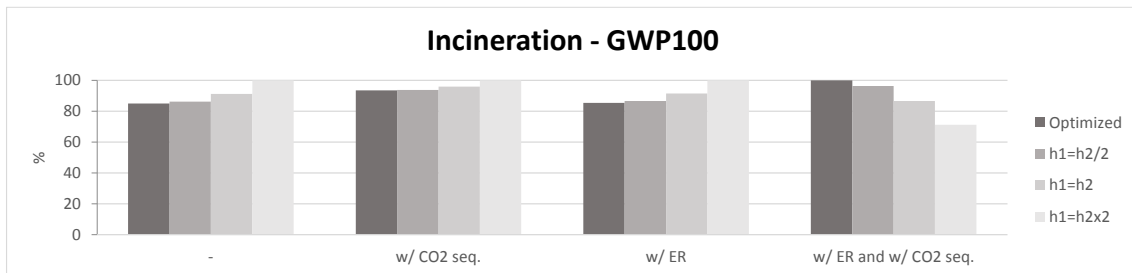
Figure 7-24 – Relative impacts (at the end-of-life) on GWP100 regarding the use of different thicknesses of wood layers compared to the optimized one for the CIT floor, for the incineration end-of-life scenario.
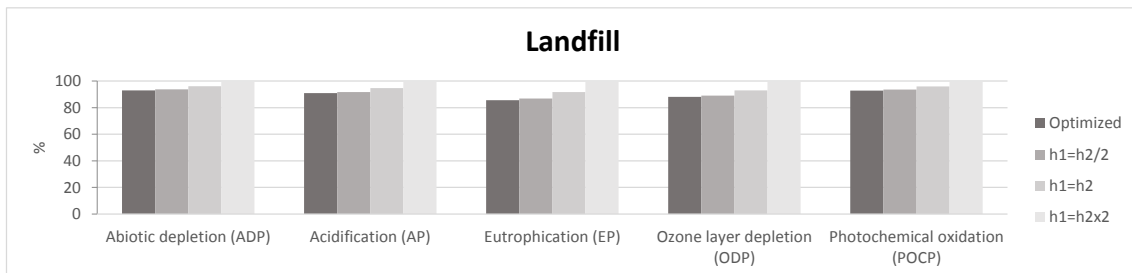
Figure 7-25 – Relative impacts (at the end-of-life) of using different thicknesses of wood layers compared to the optimized one for the CIT floor, for the landfill end-of-life scenario.
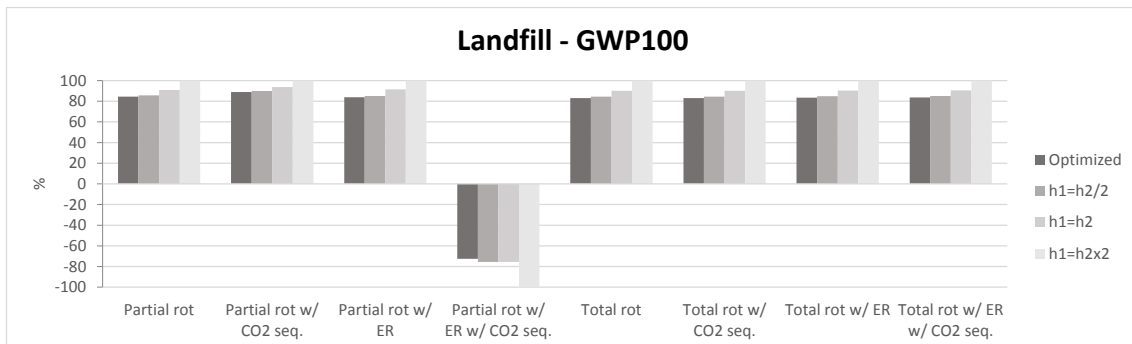
Figure 7-26 – Relative impacts (at the end-of-life) on GWP100 regarding the use of different thicknesses of wood layers compared to the optimized one for the CIT floor, for the landfill end-of-life scenario.

7.7.5 LCA results for different thicknesses of wood layers compared to the optimized one for the CIT wall

The results regarding the impacts of each CIT wall solution regarding the wood layer thickness are presented in Appendix C, section C.2, namely:

- for the cradle-to-gate stage (A1-A3), in Table C.2 and Figure C.7;
- as a function of the end-of-life scenario, in Table C.3 and Figures C.8 to C.11.

The results show that, for the wall case, at the cradle-to-gate stage, the impacts of the $h_1=h_2$ and $h_1=h_2\times2$ solutions are very close to the ones of the optimized solution, with the $h_1=h_2$ solution showing the closest approximation to the results of the optimized solution. On the other hand, the $h_1=h_2/2$ solution shows the highest impacts in all categories, with the exception of GWP with CO_2 sequestration. For that same category, when considering the carbon sequestration in timber, all the alternative solutions to the optimized one have lower impacts, due to the higher wood volume of those solutions.

Similarly to the floor results, it is concluded that the consideration of ratios between wood layer thicknesses different than the optimized one, leads, in general, to an increase in all the impact categories. Only when considering the incineration with energy recovery and biogenic CO_2 sequestration as end-of-life scenario, it is possible to reduce the GWP indicator.

7.7.6 Comparison between LCA results for the CIT floor panels with CIT with ICB core and CLT with different insulation materials

The impacts per category of each floor solution (CIT with PUR or ICB core, and CLT solutions with different insulation materials, namely RW, XPS and ICB) for the cradle-to-gate stage (A1-A3) are presented in Table 7-11 and the comparison of the relative impacts is shown in Figure 7-27.

Table 7-11 - Impacts of each floor solution for the cradle-to-gate stage (A1-A3).

Solution	Abiotic depletion (ADP)	Acidification (AP)	Eutrophication (EP)	Ozone layer depletion (ODP)	Photochemical oxidation (POCP	Global warming (GWP100)	Global warming (GWP100) w/ CO2 seq.
	kg Sb eq.	kg SO2 eq.	kg PO4 eq.	kg CFC-11 eq.	kg C2H4 eq.	kg CO2 eq.	kg CO2 eq.
CIT w/PUR	2.75E-01	2.78E-01	5.99E-02	2.17E-06	1.21E-02	34.4	-204.7
CIT w/ICB	3.16E-01	4.13E-01	9.56E-02	3.17E-06	1.77E-02	41.6	-365.3
CLT + RW	1.60E-01	1.75E-01	3.99E-02	1.45E-06	6.91E-03	20.6	-143.1
CLT + XPS	2.24E-01	1.76E-01	4.04E-02	1.43E-06	8.91E-03	25.3	-138.3
CLT + ICB	1.23E-01	2.82E-01	6.98E-02	1.26E-06	1.71E-02	16.4	-147.2
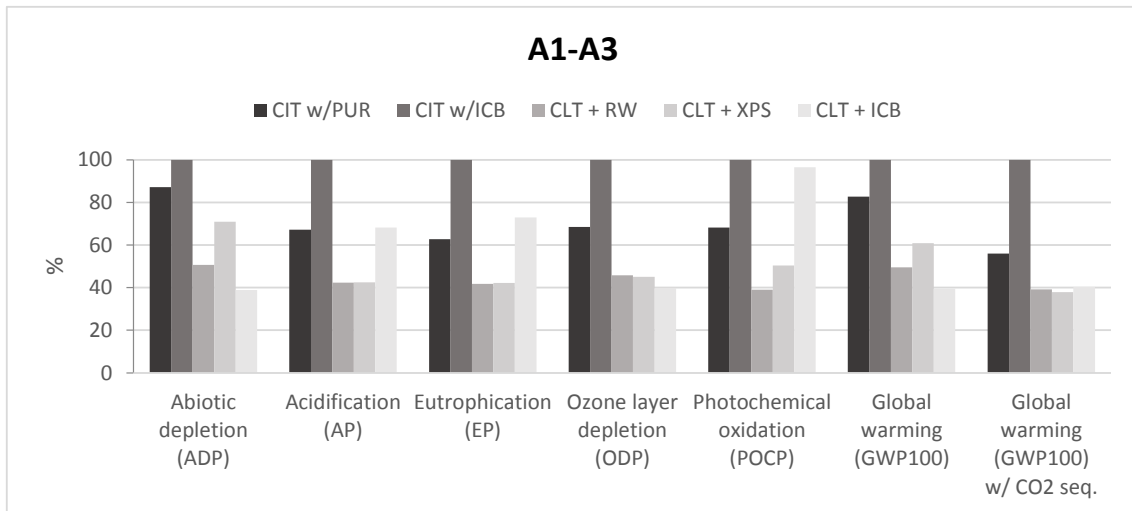
Figure 7-27 – Relative impacts of each floor solution for the cradle-to-gate stage (A1-A3).

The analysis of Table 7-11 and Figure 7-27 shows that at the cradle-to-gate stage, the impacts of the CIT with ICB core solution, apart from the GWP category including carbon sequestration (of both timber and cork) are the highest, with some expressive differences (e.g. ~60 % difference compared with CLT+RW regarding POCP). Also, the CIT solution with PUR core presents higher impacts in some categories when compared to the CLT solutions, namely in ADP, ODP and GWP100. Both CLT+RW and CLT+XPS solutions present similar results and are in general the solutions with fewer impacts.

The results regarding the impacts at the end-of-life of the CIT floor solution with an ICB core and CLT solutions with different insulation materials, namely RW, XPS and ICB, are presented in Table 7-12 for each of the considered categories depending on the end-of life scenario. The comparison of the relative impacts of those same results is shown in Figures 7-28 to 7-31.

Table 7-12 – Impacts at the end-of-life of each floor solution depending on the end-of-life scenario considered.

Panel Type	Wood layers' ratio	End-of-life scenario	Abiotic depletion (ADP)	Acidification (AP)	Eutrophication (EP)	Ozone layer depletion (ODP)	Photochemical oxidation (POCP)	Global warming (GWP100)	Global warming (GWP100) w/ CO_2 seq.
			kg Sb eq.	kg SO_2 eq.	kg PO_4 eq.	kg CFC-11 eq.	kg C_2H_4 eq.	kg CO_2 eq.	kg CO_2 eq.
CIT w/ PUR core	Optimized	Incineration [with ER]	0.261	0.269	0.072	2.02E-06	0.012	147.2 [121.0]	35.9 [9.7]
		Landfill with partial rot [with ER]	0.264	0.259	0.237	2.14E-06	0.012	159.5 [102.9]	48.2 [-8.3]
		Landfill with total rot [with ER]	0.264	0.259	0.237	2.14E-06	0.012	653.3 [370.5]	542.0 [259.2]
CIT w/ ICB core	Optimized	Incineration [with ER]	0.291	0.397	0.115	2.91E-06	0.017	235.5 [189.2]	39.0 [-7.2]
		Landfill with partial rot [with ER]	0.298	0.381	0.380	3.13E-06	0.018	262.1 [162.3]	65.7 [-34.1]
		Landfill with total rot [with ER]	0.298	0.381	0.380	3.13E-06	0.018	1133.3 [634.3]	936.9 [437.9]
CLT + RW insulation	$h_1=h_2$	Incineration [with ER]	0.161	0.177	0.050	1.39E-06	0.007	28.9 [11.4]	22.4 [5.0]
		Landfill with partial rot [with ER]	0.164	0.170	0.160	1.48E-06	0.008	108.7 [70.0]	102.3 [63.6]
		Landfill with total rot [with ER]	0.164	0.170	0.160	1.48E-06	0.008	446.6 [253.1]	440.1 [246.6]
CLT + XPS insulation	$h_1=h_2$	Incineration [with ER]	0.225	0.177	0.050	1.35E-06	0.009	30.6 [10.8]	26.4 [6.7]
		Landfill with partial rot [with ER]	0.227	0.170	0.157	1.44E-06	0.010	112.8 [74.1]	108.7 [70.0]
		Landfill with total rot [with ER]	0.227	0.170	0.157	1.44E-06	0.010	450.7 [257.2]	446.6 [253.0]
CLT + ICB insulation	$h_1=h_2$	Incineration [with ER]	0.127	0.287	0.085	1.26E-06	0.018	42.4 [16.7]	22.4 [-3.3]
		Landfill with partial rot [with ER]	0.129	0.279	0.210	1.35E-06	0.019	108.9 [69.9]	88.9 [49.9]
		Landfill with total rot [with ER]	0.129	0.279	0.210	1.35E-06	0.019	449.0 [254.2]	429.0 [234.2]

Pedro Gil Girão dos Santos
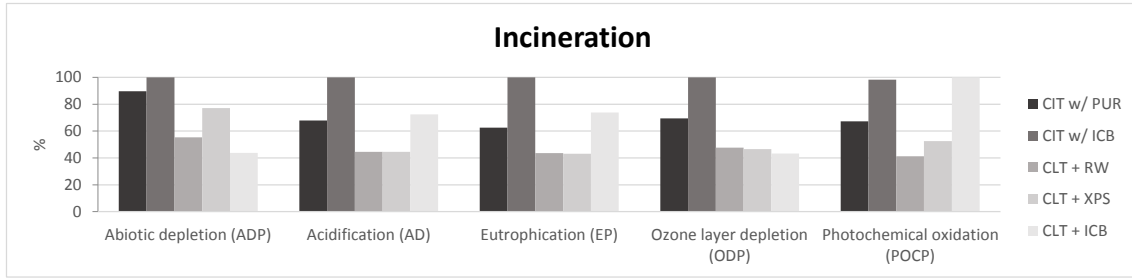
Figure 7-28 – Comparison of the relative impacts (at the end-of-life) between the different CIT and CLT floor solutions for the incineration scenario.
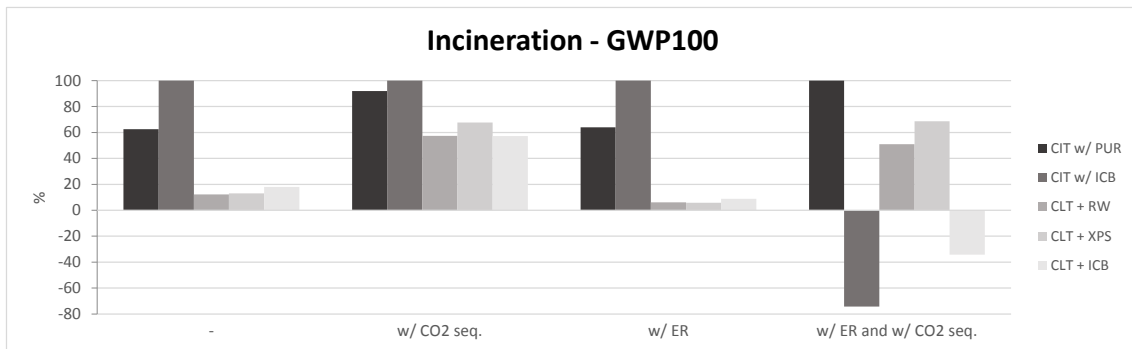
Figure 7-29 – Comparison of the relative impacts (at the end-of-life) between the different CIT and CLT floor solutions for the incineration scenario regarding GWP100.
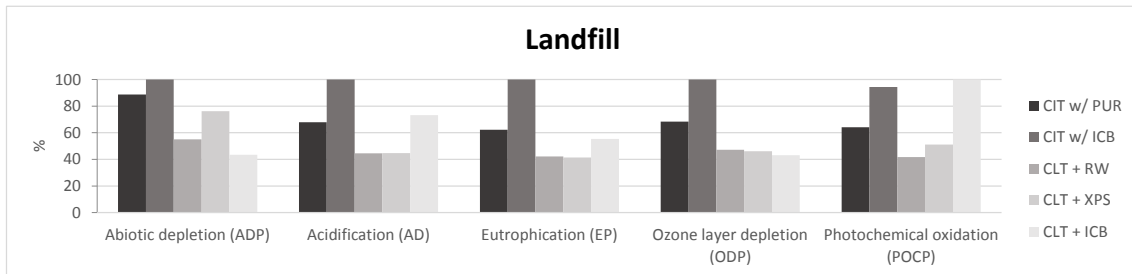
Figure 7-30 – Comparison of the relative impacts (at the end-of-life) between the different CIT and CLT floor solutions for the landfill scenario.
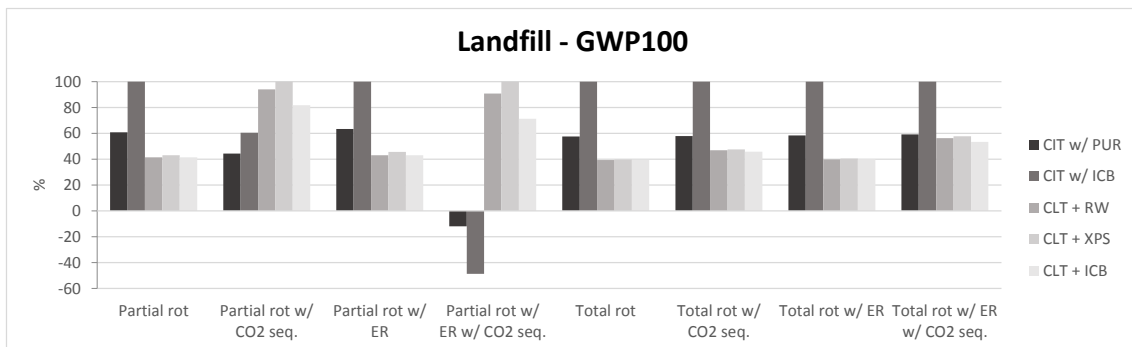
Figure 7-31 – Comparison of the relative impacts (at the end-of-life) between the different CIT and CLT floor solutions for the landfill scenario regarding GWP100.

From the analysis of the figures above, and for all of the end-of-life scenarios with exception to the energy recovery at the incineration and landfill with partial rot scenarios and CO_2 sequestration, the CIT with ICB core solution is the one that presents the highest impacts in all categories, as happened for the cradle-to-gate stage. To some point, this was an unexpected result, as cork is usually referred to as a very sustainable material. To analyse this result in further depth, the comparison of the relative impacts between ICB and PUR production (cradle-to-gate stage) for the same quantity of material (1 kg) is shown in Figure 7-32.
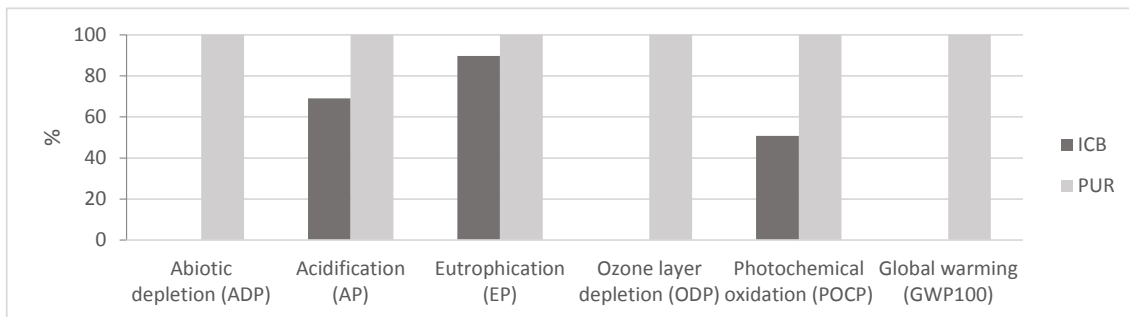
Figure 7-32 – Comparison of the relative impacts (at the cradle-to-gate stage) between 1 kg of PUR and 1kg ICB.

It is clear that the impacts of ICB are significantly lower in the majority of the categories. If for the same mass, ICB has fewer impacts than PUR, thus, the explanation for the differences between panel solutions lies not only in the material itself but also in the required quantity for each panel solution. In fact, the lower shear properties of ICB (Table 7-1) in comparison to the ones of PUR determined in Chapter 3 explain such differences; also, 5 mm of additional thickness are required for the cork layer compared to the PUR solution and the ICB density is 115 kg/m^3, which is almost three times the one of PUR (40 kg/m^3); moreover, the required wood thickness for the ICB core solution is 80 mm more than that for the PUR core solution (see Table 7-2).

Comparing the CLT solutions with the CIT ones, the former have clearly less impact than the latter and especially in the cases when RW or XPS cores are used. In these cases, and for some categories, the differences to the CIT impact reach more than 50% of difference. The reasons for such differences are the same as previously pointed out for the CIT with ICB core: although in the CLT solutions the additional insulation is thicker than the PUR core of the CIT panel, the required wood thickness is lower and, consequently, the impacts are more reduced.

7.7.7 Comparison between LCA results for the CIT wall panels with CIT with ICB core and CLT solutions with different insulation materials

The results regarding the environmental impact for the CIT wall panels with CIT with ICB core and CLT solutions with different insulation materials are presented in Appendix C, section C.3, namely:

- for the cradle-to-gate stage (A1-A3), in Table C.4 and Figure C.12;
- as a function of the end-of-life scenario, in Table C.5 and Figures C.13 to C.16.

As for the floor case, the results for the wall, show that at the cradle-to-gate stage, the impacts of the CIT solution with ICB core, apart from the GWP category including carbon sequestration, are higher than the ones from the CIT solution with PUR core, with some expressive differences (e.g. ~40 % difference for EP).

The CLT solution with ICB core presents higher impacts than the CIT solution with PUR core in some of the categories (AP, EP and POCP), but less impacts in the remaining ones (ADP, ODP, GW100 and GWP with CO_2 seq.). The CLT solutions with RW and XPS insulations present lower impacts than the CIT solution with PUR core in all the categories.

For all of the end-of-life scenarios, the CIT with ICB core has, in general, the highest impacts regarding AP, EP, ODP and GWP100 categories. Regarding ADP, it is the CLT+XPS solution that has the highest impacts, and regarding POCP, the CLT+ICB solution is the one that has the highest impacts.

In terms of GWP100, when considering the CO_2 sequestration and incineration with energy recovery as end-of-life scenario, the CIT and CLT solutions that include ICB core present lower impacts. Also, for the partial landfill with energy recovery, the CIT solution with ICB core has the lowest impacts.

7.8 Concluding remarks

This chapter presented the results regarding the LCA of the developed panels. The study included the identification of processes/life-cycle-stages that contribute the most for each of the impact categories considered and for different end-of-life scenarios. The influence of an alternative bonding system (without primer) for the wood layers was also assessed. The comparison between the developed panel with the same panel but with an alternative

core material and equivalent CLT solutions was also performed. The following conclusions were drawn from the current chapter:

- The results regarding the contribution of each process for the environmental impact are quite similar for both floor and wall solutions analysed.

- Polyurethane foam production and wood application, press and curing processes are the ones that produce the highest impacts.

- Considering the life cycle stages, the ones found to be more relevant to the environmental impacts are the raw material supply, manufacturing and waste processing/disposal.

- All the landfill scenarios present similar results regarding all the impact categories, with the exception of the global warming potential. The same occurs for the two possible incineration scenarios.

- Some processes have low or even negligible impact in all the categories, such as grading.

- A substantial part of the gases that contribute to the global warming potential are released at the end-of-life stage. From the scenarios considered, the less harmful one is landfill with partial rot and energy recovery, but, since there is still a lot of uncertainty about the behaviour of wood in landfill, this scenario can turn into the most harmful one if total rot occurs.

- The global warming potential impact of the incineration scenario with energy recovery is quite similar to the landfill option when partial rot and energy recovery is assumed; the same happens for those scenarios without energy recovery.

- Due to the uncertainty about wood degradation in landfill, the incineration option with energy recovery is considered the best option.

- The use of the bonding system for the wood layers that does not require the use of primer was found to produce fewer impacts than the one that uses primer. The reason beyond such performance relies on the required press time. Although a larger amount of adhesive is required, the press time is reduced to half, and thus half of the electric energy is needed. So, although the solution with primer is more efficient in terms of bonding performance (see Chapter 4), it is less interesting from an LCA perspective.

- Using thicknesses of wood layers different from the optimized ones leads, in general, to an increase in all the impact categories.

- Only when considering the energy recovery and biogenic CO_2 sequestration (for the incineration and landfill with partial rot scenarios) it is possible to obtain a benefit in the global warming potential, due to the CO_2 emissions from the grid electricity that are being offset.

- Even so, the differences in terms of impacts between the optimized solutions and the ones considering $h_1=h_2/2$ (floor) and $h_1=h_2$ (wall) are quite reduced.

- The comparisons of the CIT floor with equivalent solutions (CIT with ICB core) and three-layered CLT plus insulation (RW, XPS or ICB) revealed that the CIT with ICB core solution is the one that presents the highest impacts in all categories, while CLT solutions have considerably lower impacts, especially in the cases where RW or XPS cores are used. Despite ICB being a sustainable material (as attested by the comparison between the same mass of ICB and PUR), the reason for the worse performance of the ICB core panel is its lower shear properties when compared to PUR. This requires an increased thickness of the wood layers to fulfil the design purposes, and thus the environmental performance is impaired.

- For the wall solutions, from the results obtained, it is not fully clear which solution is the best performing one, as a variation between categories and end-of-life scenarios was observed. However, the CIT solution with ICB core leads, in general, to the highest impacts regarding AP, EP, ODP and GWP100 categories.

8 ACOUSTIC CHARACTERIZATION OF THE PANELS

8.1 Introduction

This chapter deals with the acoustic performance of the developed panels, regarding their airborne and impact sound insulation. The performance of the panels is assessed through an experimental campaign using a reduced size-chamber, as well as an adaptation of the standardized procedures. Additionally, other current solutions, including cross-laminated timber (CLT) or concrete slabs, are also tested to compare the relative performance of the developed panels with those conventional solutions. The analytical models with the potential to describe the acoustic insulation behaviour of the developed panels are identified, taking into account the information reported in the literature about their suitability to describe structural insulated panels (SIP) and CLT systems. The experimental results are then compared with the predictions of those models, and an empirical model to describe the panels' behaviour is proposed.

The current chapter is organized as follows: in section 8.2, considerations related to the acoustic behaviour of sandwich lightweight panels are presented; in section 8.3, a summary of the analytical and numerical models suitable for the prediction of the sound insulation of CLT and SIP is presented; subsequently, standard tests or experiments reported in the literature for the evaluation of the acoustic performance of CLT and SIP solutions are presented; in section 8.4, the details and results of the experimental campaign developed in this thesis are presented and discussed; finally, in section 8.5, the comparisons between experimental results and predictions from analytical models are presented and discussed.

8.2 Considerations on the sound insulation of lightweight panels

In building acoustics, the airborne sound insulation of a partition element can be defined as the amount of sound reduction that the element imparts to a transmitted wave when subjected to an incident field on the opposite side. When subjected to such field (incident wave), part of the same wave is reflected back from the surface of the element, another part is absorbed by the own element and the remaining part is transmitted to the other side (Figure 8-1).

An indicator, such as the sound transmission loss (TL), usually defines the airborne sound insulation. The (sound) transmission loss or sound reduction index corresponds to the

difference between the incident and transmitted sound levels, as defined by Equation (8-1),

$$\text{TL} = 10 \log_{10} \left(\frac{|p_{inc}|^2}{|p_{tr}|^2} \right) = 10 \log_{10} \left(\left| \frac{1}{\tau} \right| \right) \tag{8-1}$$

where p_{inc} and p_{tr} correspond to the incident and transmitted sound pressures, and τ is the sound transmission coefficient.
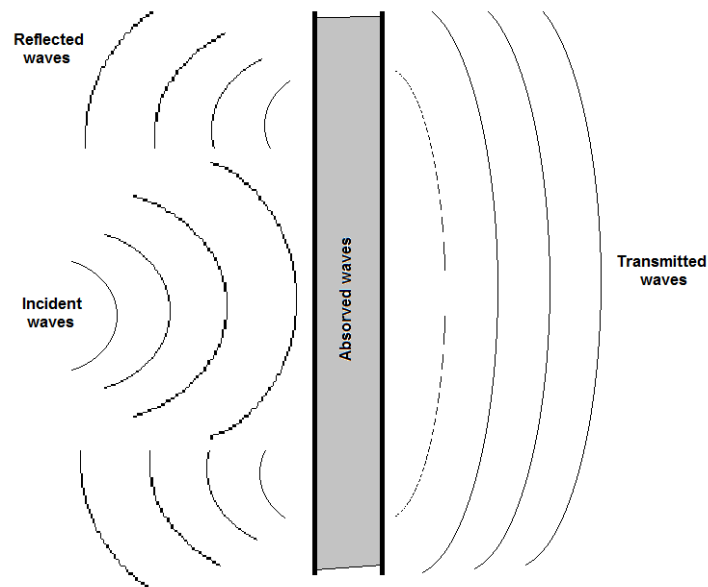
Figure 8-1 – Schematic representation of the sound waves' distribution in the presence of a partition element when subjected to an incident field.

Lightweight sandwich panels made of strong thin faces and low-density core with relative high thickness tend to perform poorly in terms of acoustic insulation when compared with other common building solutions. Their low-mass nature, high stiffness-to-mass ratio and internal architecture are the main causes of such poor performance. To better understand these aspects, a generic airborne sound reduction (or transmission loss) curve of a typical sandwich panel (D'Alessandro et al, 2013) is presented in Figure 8-2.

The curve can be divided into four regions, wherein one of the following parameters mainly governs it: stiffness, resonance, mass or coincidence.

The first region, that is valid until the occurrence of the first natural frequency, is often controlled by the stiffness of the panel, with the transmission loss decreasing with frequency by 6 dB per octave. In the second region, where the lowest structural resonances of the panel appear, major variations occur, whose magnitude is dependent on

the damping capacity of the panel. For a rectangular plate simply supported at all edges, the fundamental frequency, f_{11} (Hz), can be expressed by Equation (8-2),

$$f_{11} = \frac{\pi}{2} \sqrt{\frac{EI}{m}} \left[\left(\frac{1}{l_x}\right)^2 + \left(\frac{1}{l_y}\right)^2 \right] \tag{8-2}$$

where l_x and l_y are the plate dimensions (m); m is the surface mass (kg/m^2), and EI is the bending stiffness (N/m^2).
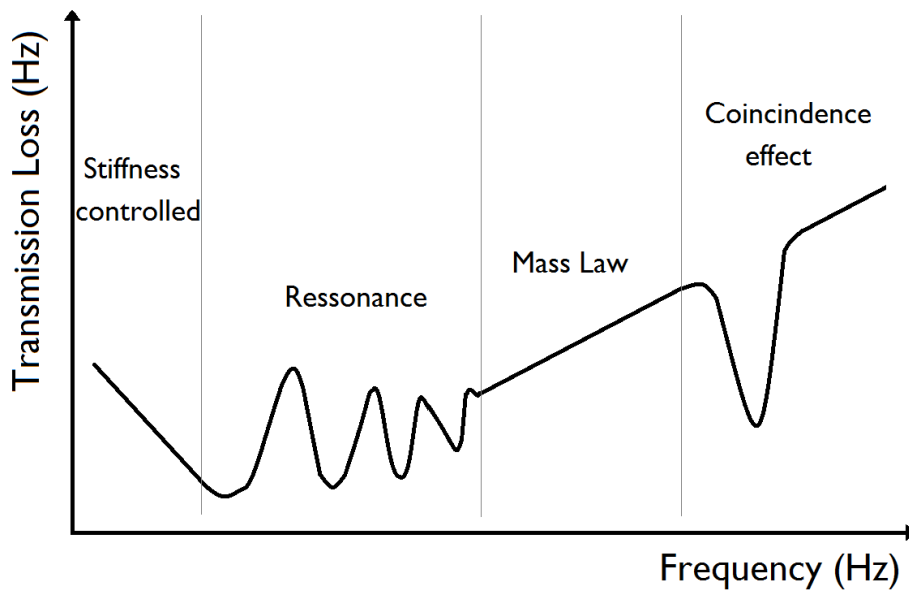
Figure 8-2 – Airborne sound transmission loss. Adapted from (D'Alessandro et al, 2013).

In the third region, governed by mass, an increase of TL of 6 dB (or even less) occurs for each octave band or by doubling the mass. This region typically may extend from two or three times the lowest resonance frequency to the coincidence frequency, where the last region is defined. The coincidence frequency corresponds to the frequency at which the bending wavelength of the panel equals the wavelength of the radiated acoustic wave in the air. In such condition, the amplitude of vibration of the panel is almost the same as that of incident waves, thus allowing a great part of the energy to pass through the panel. The first coincidence frequency that occurs is designated as the critical frequency and occurs for grazing incident sound. According to Wawrzynowicz et al (2014), the critical frequency, f_c (Hz), can be defined by Equation (8-3),

$$f_c = \frac{c_0^2}{2\pi} \sqrt{\frac{m}{EI}} \tag{8-3}$$

where c_0 is the speed of sound in air (m/s); m is the surface mass (kg/m^2) and EI is the bending stiffness (N/m^2).

As referred before, besides their low mass, the internal architecture of the panels also contributes to a loss of performance compared to homogeneous panels, as it is responsible for the presence of more than one coincidence frequency. Indeed, in a three-layer sandwich panel, two coincidence frequencies occur, rather than one as in homogeneous panels (D'Alessandro et al, 2013). As for a single-layer homogeneous panel, in sandwich panels, one of the coincidence frequencies occurs due to bending deformation of the whole section following an anti-symmetric pattern (Figure 8-3 a)). Also, due to thickness deformation of the core, a dilatational motion occurs following a symmetric pattern (Figure 8-3 b)).

a)   b)
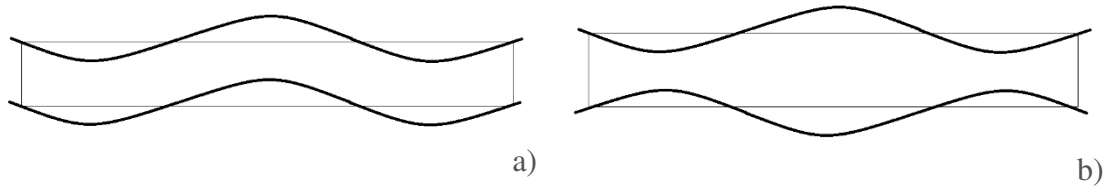
Figure 8-3 – Deformation patterns: a) anti-symmetric; b) symmetric.

According to Ballagh (2010), in a three-layer sandwich panel, the faces act as masses and the core acts as a spring, and thus the symmetric resonant frequency, f_{dil} (Hz), can be predicted by Equation (8-4),

$$f_{dil} = \frac{1}{2\pi}\sqrt{\frac{2m_f E_c}{h_c m_f^2}} \qquad (8\text{-}4)$$

where E_c is the modulus of elasticity of the core (N/m^2); m_f is the surface mass of one face (kg/m^2) and h_c is the core thickness (m).

Other alternative expressions can be found in (Krakers, 2009), Equation (8-5), and (Wawrzynowicz et al, 2014), Equation (8-6):

$$f_{dil} = \frac{1}{2\pi}\sqrt{\frac{4E_c}{h_c\left(2m_f + m_c/3\right)}} \qquad (8\text{-}5)$$

where m_c is the surface mass of the core (kg/m^2),

$$f_{dil} = \frac{1}{2\pi}\sqrt{\frac{2K_c}{h_c\left(\rho_f h_f + \rho_c h_c/6\right)}} \tag{8-6}$$

with

$$K_c = \frac{E_c(1 - \nu_c)}{(1 - 2\nu_c)(1 + \nu_c)} \tag{8-7}$$

where h_f is the thickness of one face (m); ρ_f is the face density (kg/m^3); ρ_c is the core density (kg/m^3) and ν_c is the Poisson ratio of the core (kg/m^3).

As can be seen in the equations given above, the anti-symmetric coincidence frequency is governed by the flexural stiffness, as well as by the overall mass, while the symmetric one is mostly controlled by the compressive stiffness, as well as the overall mass of the panel (D'Alessandro et al, 2013; Tadeu et al, 2010; Wang et al, 2009).

8.3 Characterization of the sound insulation of SIP and CLT – state-of-the-art

8.3.1   SIP and sandwich panels

Few studies related to the acoustic characterization of wood-based SIPs are available in the literature. Garay and Pino (2019) performed laboratory measurements for the determination of the airborne sound reduction index (R_w) of SIPs made of expanded polystyrene (EPS) core and 10 mm thick oriented-strand board (OSB) faces (total thickness of 64 mm), with an overall density of 97 kg/m^3. For the tested specimen, a R_w value of 39 dB was obtained.

Other works are reported for non-wood faces, such as Wawrzynowicz et al (2014), who analysed the airborne acoustic sound insulation of a composite SIP made of magnesium-cement faces and EPS core in the range of 100-5000 Hz. They conducted experimental tests using an experimental setup composed of two reverberation chambers: the setup, which included the acoustic laboratory, was modelled on a commercial software package using a 2D model with two approaches, steady-state and transient Finite Element (FE) analysis. Also, an analytical expression was used to predict the sound reduction curve. The comparison with test results revealed a very good agreement of the FE models, especially for steady-state conditions, while the analytical model provided accurate predictions until 1600 Hz.

An extensive review of theoretical and numerical models for acoustic analysis of sandwich panels is presented by D'Alessandro et al (2013). Besides theoretical models, numerical methods, such as the Finite Element Method (FEM), the Boundary Element Method (BEM) or Statistical Energy Analysis (SEA), are referred. FEM and BEM are mostly used for the analysis of the low- and medium-frequency regions, but for high frequencies, as the minimum element size has to be much smaller than the minimum wavelength considered, SEA is the most used method due to lower computational costs (D'Alessandro et al, 2013).

Besides the referred advanced models, simpler analytical/empirical models for sandwich-type panels were proposed by different authors, such as (Wang et al, 2005; Krakers, 2009) and Ballagh, 2010).

The formulation by Wang et al (2005) is presented next. According to these authors, the average diffuse field sound transmission coefficient ($\bar{\tau}$) is calculated as in Equation (8-8),

$$\bar{\tau} = \frac{\int_{-\pi}^{\pi} \int_{0}^{\theta_0} \tau \sin\theta \cos\theta \, d\theta d\phi}{\int_{-\pi}^{\pi} \int_{0}^{\theta_0} \sin\theta \cos\theta \, d\theta d\phi} \tag{8-8}$$

where θ_0 is the empirically determined upper bound of the incident angle (78º).

The sound transmission coefficient for normal incidence (τ) is calculated as in Equation (8-9):

$$\tau = \left| \frac{\frac{Z_a}{2Z_0} - \frac{Z_s}{2Z_0}}{\left(1 + \frac{Z_a}{2Z_0}\right)\left(1 + \frac{Z_s}{2Z_0}\right)} \right|^2 \tag{8-9}$$

The symmetric and anti-symmetric impedances, Z_s and Z_a are calculated as follows,

$$Z_s = \frac{-2i\left(Tk^2 + EI_f k^4 - \rho_f A\omega^2 + 2K - M_0\omega^2\right)}{\omega} \tag{8-10}$$

$$Z_a = \frac{-2i\left(EI_f k^4 - \rho_f A\omega^2 + 3Tk^2 - 3M_0\omega^2\right)}{\omega} \tag{8-11}$$

where

$$M_0 = \frac{\rho_c b h_c}{6} \tag{8-12}$$

$$E_0 = \frac{E_c}{(1 - v_c^2)} \tag{8-13}$$

$$K = \frac{E_0 b}{h_c(1 - v_0^2)} \tag{8-14}$$

$$v_0 = \frac{v_c}{(1 - v_c)} \tag{8-15}$$

$$k = k_0 \sin\theta \tag{8-16}$$

$$k_0 = \frac{\omega}{c_0} \tag{8-17}$$

Additionally, EI_f (N.m^2) is the bending stiffness of one face; A is the cross-section area of one face (m^2); b is the panel's width (m); ω is the angular frequency (Hz).

Krakers (2009) calculates the sound reduction according to Equation (8-18),

$$R = R_0 - 10\log_{10}\left[\frac{2\sigma_{radd}}{\left(1 - \left(\frac{f_{11}}{f}\right)^2\right)^2\left(1 - \left(\frac{f}{f_c}\right)^2\right)^2 + \eta_{eq}^2} + \frac{\pi\sigma^2 f_c}{2\eta_c f}\right] \tag{8-18}$$
$$+ 10\log_{10}\left[\left(1 - \left(\frac{f}{f_{dil}}\right)^2\right)^2 + \eta_{eq}^2\right]$$

$$R_0 = 20\log_{10}(f \cdot m) - 42 \tag{8-19}$$

$$\sigma_{rad} = \begin{cases} \dfrac{Uc_0}{\pi^2 S f_c^{3/2}}\sqrt{f} & f \ll f_c \\[2mm] 0.45\sqrt{\dfrac{Uf_c}{c_0}} & f = f_c \\[2mm] 1 & f \gg f_c \end{cases} \tag{8-20}$$

$$\sigma_{radd} \cong \frac{1}{2}\left(0.2 + \ln\left(2\pi\frac{f}{c_0}\sqrt{S}\right)\right) \tag{8-21}$$

$$\eta_{eq} \cong \sqrt{\eta_c^2 + 0.1\eta_c} \tag{8-22}$$

where U is the panel perimeter (m); S is the panel area (m^2); η_c is the loss factor of the core material.

In the analytical formulation proposed by Ballagh (2010), the TL curve is obtained from the mass law (Equation (8-23) minus the transmissibility curve, Equation (8-24)),

$$TL = 20\log_{10}(f \cdot m) - 47 \tag{8-23}$$

$$\Delta R = 10\log_{10} \frac{1 + \left(2\zeta\dfrac{f}{f_{dil}}\right)^2}{\left(1 - \left(\dfrac{f}{f_{dil}}\right)^2\right)^2 + \left(2\zeta\dfrac{f}{f_{dil}}\right)^2} \tag{8-24}$$

where f is the frequency (Hz) and ζ is the fraction of critical damping.

8.3.2 CLT

Some CLT manufacturers already include in their European Technical Approvals (ETA) information about airborne and impact sound insulation values for their products, based either on (i) predictive methods from EN 12354-1 (CEN, 2000b), or (ii) laboratory tests, based on standards ISO 10140-2 (ISO, 2010a) and ISO 10140-3 (ISO, 2010b), such as Artuso (ETA, 2010), KLH (ETA, 2011) or Stora Enso (OIB, 2014). A series of experimental tests to evaluate the acoustic performance of single or multiple CLT panels are also found in the literature.

Pérez and Fuente (2013) evaluated the acoustic performance of CLT panels made by EGO (Egoin, 2015). They followed the ISO 10140-2 and ISO 10140-3 standards for the evaluation of the airborne and impact sound insulations. The floor elements included panels with 135 mm of thickness, which provided in the bare solution 37 dBA for the Sound Reduction Index A-weighted (R_A) and 89 dB for the Weighted Normalized Impact Sound Pressure Level ($L_{n,w}$). The same solution with the addition of a floor covering with an anti-impact element, plasterboard and a suspended ceiling resulted in R_A=58 dBA and $L_{n,w}$=52 dB. Wall elements were also tested, like a bare CLT panel of 80 mm of depth, with a result of R_A=30 dBA, and the same solution with the addition of plasterboard, mineral wool and gypsum board, which resulted in R_A=49 dBA.

Schoenwald et al (2014) evaluated the flanking transmissions between double walls and

continuous CLT floors and concluded that the flanking path through a continuous floor in a double-wall junction is much more critical than a path through wall-to-wall.

Pagnoncelli et al (2014) referred that the predictive models from EN 12354-1 and EN 12354-2 (CEN, 2000c) are not adequate for CLT systems because they were developed for masonry and concrete structures, which have different damping and junction details. The authors conducted a series of impact and airborne sound insulation tests between dwellings in three-storey residential building entirely made of CLT according to field measurement standards ISO 140-7 (ISO, 1998) and ISO 16283-1 (ISO, 2014), and concluded that the addition of stone wool (50 kg/m^3 of density and 50 mm of thickness) in the ceiling cavity of the floor elements improves the acoustic performance by around 3-5 dB. The placement of dry floating screeds in conjunction with a high-density filling layer (marble granulate) over the CLT floors gave a better performance than cement and lightweight infill. Also, the use of low dynamic stiffness materials, such as polyester and stone wool, between the screeds and the marble granulate offered better performance in comparison to stiffer materials. Concerning the walls, they concluded that applying a lining system, such as a cavity filled with stone wool and finishing material, is a proper option to fulfil normative requirements. They also stated that discontinuous walls between stories and resilient elements in wall-to-floor connections help to improve flanking transmissions.

Zeitler et al (2014) evaluated the impact sound insulation of bare CLT floors covered with concrete toppings following the ISO 10140-3 and obtained improvements in $L_{n,w}$ from 6 dB (without intermediate resilient layer) to 13 to 21 dB (with an intermediate resilient layer).

Also, Marini et al (2015) assessed the applicability of the predictive acoustic model from EN 12354-2 and stated that the application of this method without proper corrections overestimates the impact sound insulation for CLT floor elements (between 4 and 6 dB in the tested floors).

(Bella et al, 2016) proposed a reference curve to rate the impact sound insulation of bare CLT floors based on the results of laboratory tests. A predictive formula for the weighted normalised impact sound pressure level ($L_{n,w}$) valid to five-layer CLT panels with thickness between 140-275 mm and mass per area between 70-130 kg/m^2 was proposed as in Equation (8-25),

$$L_{n,w} = 128 - 22 \log_{10}(m) \ [\text{dB}] \qquad (8\text{-}25)$$

where m is the mass per area (kg/m^2).

It should be kept in mind that in most European countries, requirements for the Weighted Apparent Sound Reduction Index (R'_w) are around 50-55 dB and requirements for the Weighted Normalized Impact Sound Pressure Level ($L'_{n,w}$) are around 47-64 dB (Martins et al, 2015). It should be noted that different descriptors are used depending on the country (Rasmussen, 2010), and for this reason, the referred values are just an approximation. For example, in Portugal, the applicable requirements are the Weighted Standardized Level Difference ($D_{nT,w}$) ≥ 50 dB and the Weighted Standardized Impact Sound Pressure Level ($L'_{nT,w}$) ≤ 60 dB. To meet the normative requirements, bare CLT panels generally have to be combined with other elements, such as toppings, suspended ceilings or floating floors (Pérez and Fuente, 2013).

8.4   Experimental characterization of the panels

8.4.1   Materials and test specimens

Two types of CIT panels were manufactured for the tests, with the thickness of the wood layers of either 10 mm or 35 mm, while both types had a 30 mm thick polyurethane core (Figure 8-4). For the airborne tests, a set of three CIT panels of each type were produced.

a)   b)
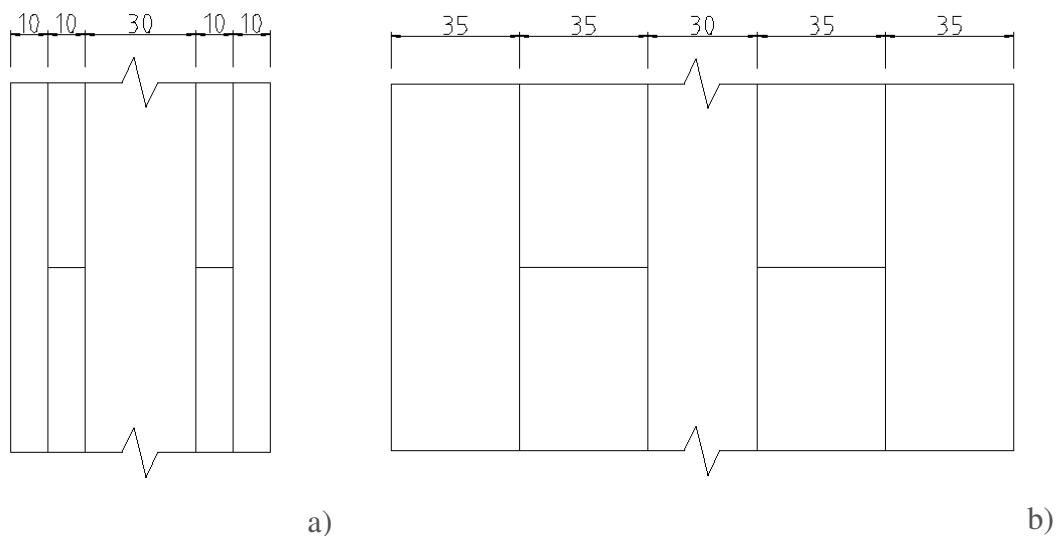
Figure 8-4 - Cross-section of the tested panels: a) CIT with 70 mm thickness; b) CIT with 170 mm thickness.

For comparison purposes, besides the CIT panels (Figure 8-5), CLT panels (*i.e.* massive wood) with equivalent layer thickness were also tested (Figure 8-6). For easier reference, the panels are named by the type and thickness (e.g. CIT 70). Additionally, for the airborne sound insulation tests, also the performance of a sandwich panel made of steel faces (0.5 mm thick) and polyurethane core (38 mm thick and $\rho = 40$ kg/m^3) was assessed (Figure 8-7). Such type of panel was tested to assess the suitability of analytical models
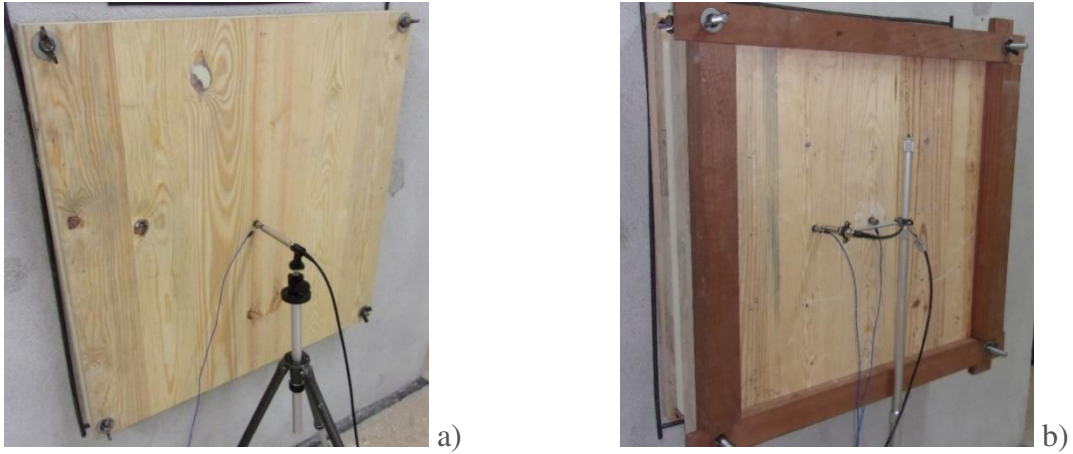
Figure 8-5 - Simplified airborne sound insulation test of: a) CIT 70 panel; b) CIT 170 panel.

Figure 8-6 - Simplified airborne sound insulation test of: a) CLT 70 panel; b) CIT 170 panel.

Figure 8-7 – Simplified airborne sound insulation test of the sandwich panel.

from the literature (*i.e.* developed assuming thin faces and thick core) to describe its behaviour.

In the impact sound insulation tests, besides the CLT (Figure 8-8) and CIT panels (Figure 8-9), a traditional wooden floor and a reinforced concrete slab (Figure 8-10) were tested for performance comparison purposes.

a)   b)
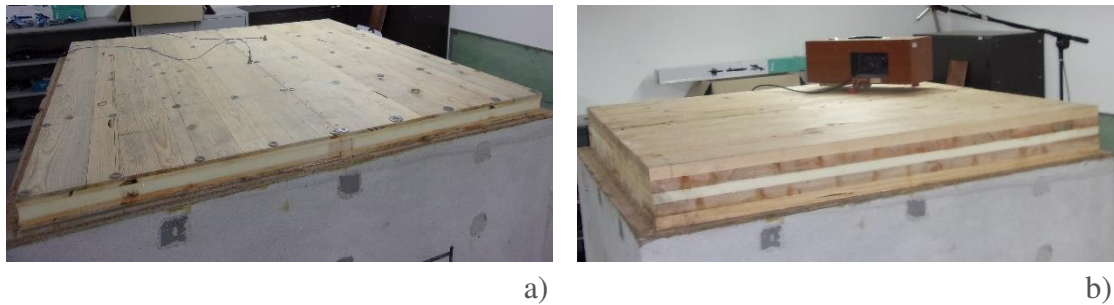
Figure 8-8 – Simplified impact sound insulation test of: a) CIT 70 floor; b) CIT 170 floor.

a)   b)
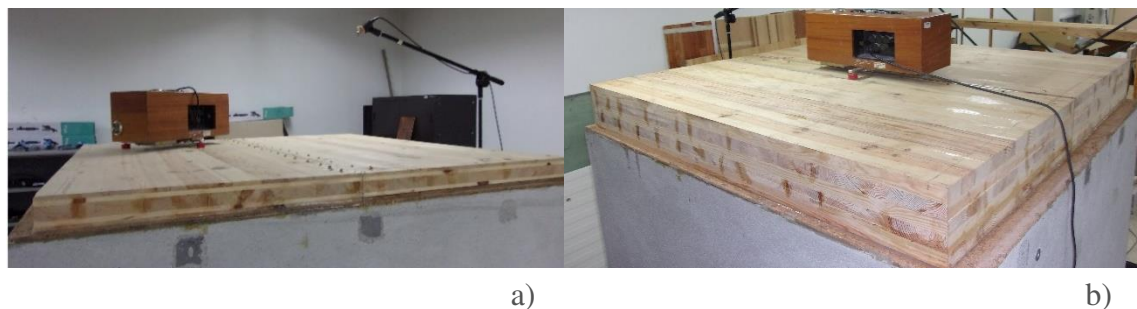
Figure 8-9 – Simplified impact sound insulation test of: a) CLT 70 floor; b) CLT 170 floor.

a)   b)
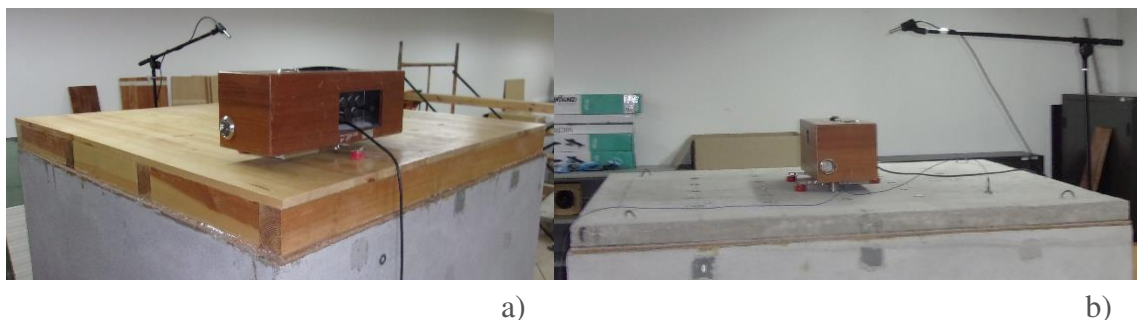
Figure 8-10 – Simplified impact sound insulation test of: a) traditional wood floor; b) 60 mm reinforced concrete floor.

The reinforced concrete slab had overall plan dimensions of 1.5×1.6 m^2, a thickness of 6 cm and mean density of 2400 kg/m^3. The wood floor was made of Maritime pine and

its dimensions are shown in Figure 8-11. Based on the visual characteristics of wood, its mean density was estimated as 650 kg/m^3.

Figure 8-11 – Wood floor dimensions (mm).

The characteristics of the panels tested for airborne and impact sound insulation are presented in Tables 8-1 and 8-2. It should be noted that the mass per area for the wood floor (30.0 kg/m^2) is an approximate value, as in practice the mass is not equally distributed per area due to the floor configuration (deck supported in evenly spaced beams).

Table 8-1 – Characteristics of the panels used in the airborne sound insulation tests.

Type	Thickness (layers' thickness)	no.	m_S (kg/m^2)
CIT	70 mm (10/10/30/10/10)	1	27.6
		2	27.1
		3	26.4
	170 mm (35/35/30/35/35)	1	94.0
		2	91.3
		3	88.7
CLT	70 mm (10/10/30/10/10)	-	45.9
	170 mm (35/35/30/35/35)	-	104.4
Sandwich	40 mm (0.5/39/0.5)	-	8.5

Table 8-2 – Characteristics of the panels used in the impact sound insulation tests.

Type	Thickness (layers' thickness)	m_S (kg/m^2)
CIT	70 mm (10/10/30/10/10)	24.7
	170 mm (35/35/30/35/35)	90.2
CLT	70 mm (10/10/30/10/10)	42.1
	170 mm (35/35/30/35/35)	112.7
Wood floor	21 mm deck + 70 mm beams	30.0
Concrete	60 mm	144.0

Due to manufacturing constraints, the CIT and CLT panels used for the impact tests had plan dimensions of 1.5 m x 0.75 m. Therefore, it was necessary to connect two panels to fill the 1.4 x 1.3 m^2 top opening of the chamber. To this end, connection systems developed and presented in Chapter 9 were used. The CIT 70 panels were connected with a Spruce (*Picea abies*) spline with a cross-section of 66 x 27 mm^2 (Figure 8-12). The spline was inserted between a pre-drilled channel on the polyurethane foam layer at one side of each panel, and then it was fixed with 3 mm diameter screws (with 40 mm of length) spaced at 100 mm at each side and face of the panels (Figure 8-13). For the 170 mm CIT and CLT panels, connections with crossed 5 mm diameter (and 90 mm length) screws spaced at 100 mm in one face of the panels were used (Figure 8-14).

a)   b)

c)   d)
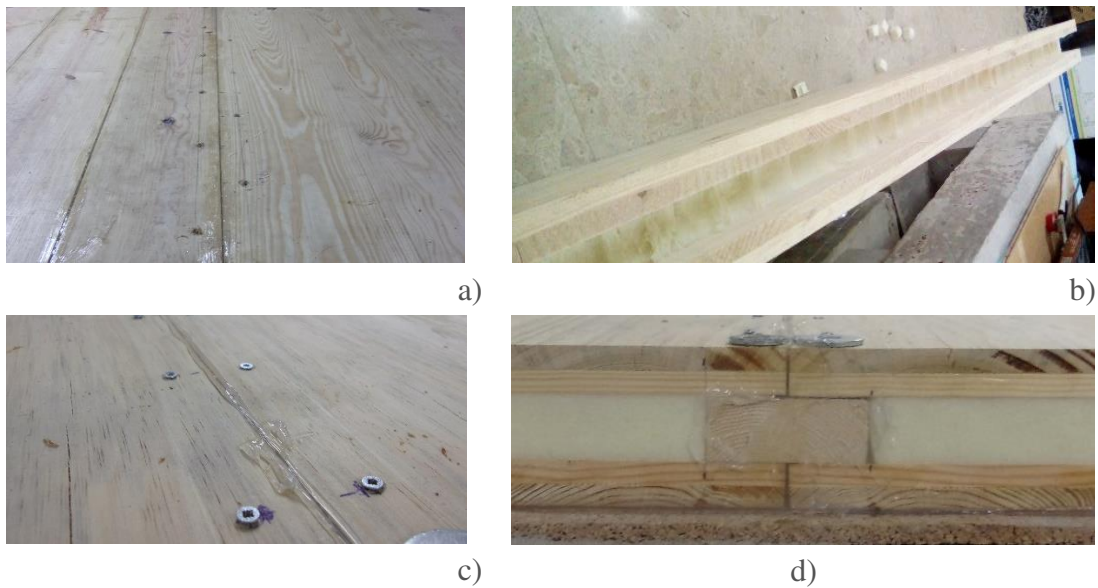
Figure 8-12 – Details of the connections used to assemble the panels: a) Crossed-screws in the CLT 70, 170 and CIT 170 panels; b), c) and d) Spline in the CIT 70 panels.
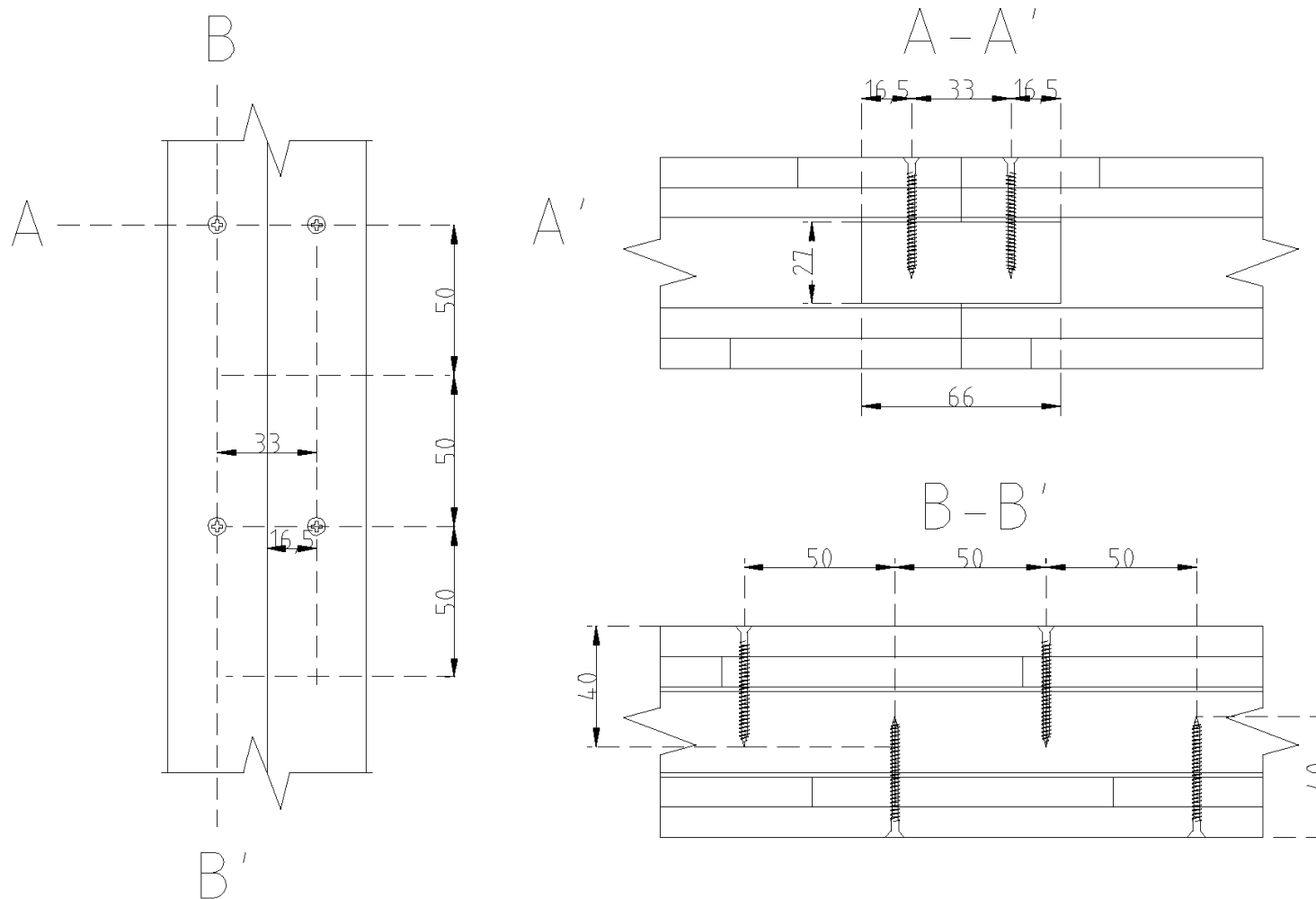
Figure 8-13 – Scheme of the connections used in the CIT 70 panels. Dimensions in mm.
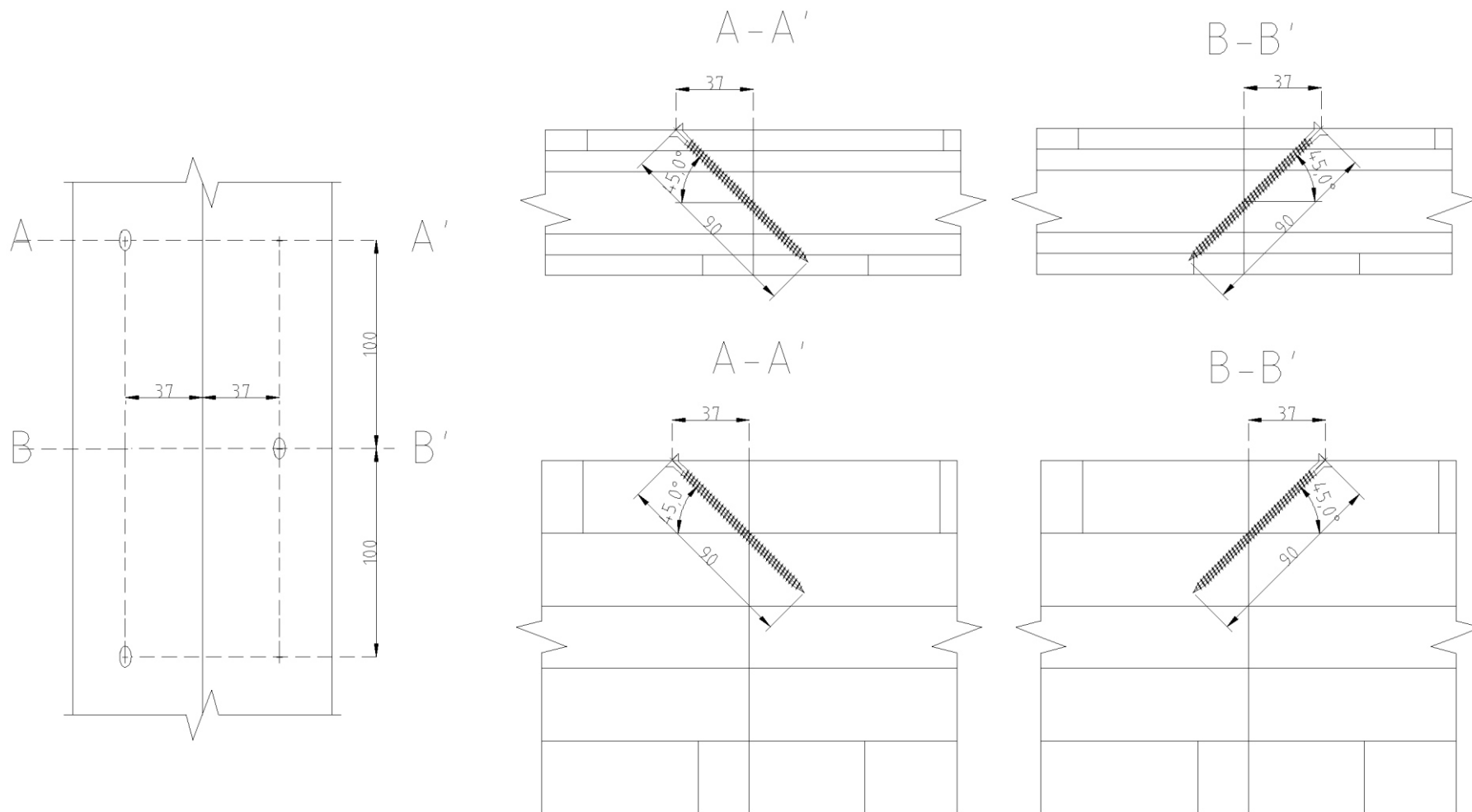
Figure 8-14 - Scheme of the connections used in the CLT 70 and CIT/CLT 170 panels. Dimensions in mm.

8.4.2 Airborne sound insulation

The standard procedure according to ISO 10140-2 (ISO, 2010a) involves placing the element to be tested between two adjacent rooms. In one of the rooms, a diffuse sound field is generated by a source (that is moved in turn between a series of different positions) and the average sound pressure level is measured at both the source and receiving rooms. The difference between the sound pressure levels of the two rooms, taking into account the equivalent absorption area and the size of the tested element, gives the airborne sound insulation of the element.

The normalized test requires facilities that are in accordance with ISO 140-1 (ISO, 1997), *i.e.* reverberant chambers with a volume larger than 50 m^3, while in turn the element to test should have preferably the reference area of 10 m^2. Smaller areas can be tested; however, the wavelength of free flexural (bending) waves at the lowest frequency considered has to be smaller than half of the minimum dimension of the test element. Even so, the standard refers that the smaller the test element, the more sensitive the results tend to be to edge constraint conditions and local variations in the sound field.

Although in the facilities of UC a chamber with the referred characteristics is available, due to difficulties in producing larger test specimens, and to have better control over the test conditions, it was decided to adapt the ISO 10140-2 test to a reduced size-chamber (Figure 8-15).

Figure 8-15 – Reduced size-chamber used in the acoustic tests.

Such chamber, whose characterization can be found in (Godinho et al, 2010) and (Colaço

et al, 2018), consists of a parallelepiped structure made of reinforced concrete with an internal volume of 2.73 m³. To avoid coincidence between the frequencies of the internal normal modes along the three orthogonal directions, the internal height, width and length are different: 1.50 m x 1.30 m x 1.40 m. To ensure proper airborne sound insulation, the walls are 10 cm thick, which according to reference values corresponds to a weighted sound reduction index (R_w) of around 40 dB. In turn, the top of the chamber is sealed by a 6 cm thick concrete slab over a resilient material (5 mm thick natural cork agglomerate). In one of the walls, an opening with 55 x 55 cm² was left for the installation of the element to test (Figure 8-16). The whole chamber was placed on the ground above a rubber agglomerate with a thickness between 5 to 10 mm to avoid vibration transmissions from external sources.

Figure 8-16 – CLT 70 specimen placed on the chamber's opening.

The specimens had dimensions around 75 cm × 75 cm, so that the opening of the test chamber was completely filled; near the edges of the opening, a draught stopper tape was applied and the specimen was tightened to the chamber through four threaded rods near the corners. In the case of the CIT specimens, the polyurethane layer was sealed with an insulation adhesive tape.

In accordance with ISO 10140-2, when a reduced-size opening is used instead of a full 10 m² opening, the element-normalized level difference ($D_{n,e}$) is determined instead of the sound reduction (R), according to Equation (8-26),

$$D_{n,e} = L_1 - L_2 + 10 \log_{10} \left(\frac{A_0}{A} \right) \text{ [dB]} \tag{8-26}$$

where L_1 is the energy average sound pressure level in the source room (dB); L_2 is the energy average sound pressure level in the receiving room (dB); A is the equivalent absorption area in the receiving room (m²) and A_0 =10 m².

In the adapted test, the receiving room is considered as an open field (assuming that the reverberant field will have a negligible influence on the registered signal), and thus the contribution of the equivalent absorption area is taken as zero in Equation (8-26). As a consequence, the level difference (D) is calculated as in Equation (8-27).

$$D = L_1 - L_2 \ [\text{dB}] \tag{8-27}$$

To ensure that the measurements in the receiving room are not significantly contaminated by background noise, the background noise level (L_b) has to be at least 6 dB below the level of the signal from the source combined with the background noise (L_{sb}). If this is not the case, then for each frequency band considered where such a limit is not fulfilled, a 1.3 dB correction has to be made. If the difference is greater than 6 dB but smaller than 15 dB, the correction shown in Equation (8-28) should be made to the sound pressure level,

$$L = 10 \log_{10} \left(10^{\frac{L_{sb}}{10}} - 10^{\frac{L_b}{10}} \right) \ [\text{dB}] \tag{8-28}$$

where L_{sb} is the sound pressure level due to combined source and background noise (dB), and L_b is the sound pressure level due to background noise (dB).

In accordance with ISO 10140-4 (ISO, 2010c), the energy average sound pressure level in room i (L_i) for n measurement positions is obtained as in Equation (8-29),

$$L_i = 10 \log_{10} \left(\frac{1}{n} \sum_{j=1}^{n} 10^{\frac{L_j}{10}} \right) \ [\text{dB}] \tag{8-29}$$

where L_j is the sound pressure level (dB) at position j.

Due to the reduced chamber dimensions, a reverberant field is assumed, and thus only one microphone was used at the inside of the chamber placed at about 0.4 m from the walls/floor and outside the direct sound field of the source (Figure 8-17). It should be noted that five microphone positions and a minimum distance of 0.7 m from any room boundary and 1.0 m from the source are recommended for a standard chamber in ISO 10140-4. Although at least two source positions are prescribed by the standard, also due to the small dimensions of the test chamber, only one source position was used, at one of the corners.

Figure 8-17 – Position of the microphone and sound source inside the chamber.

The sound pressure levels at the outside of the chamber were measured by placing a microphone close to the surface of the element being tested (Figure 8-18). To confirm that the measured sound pressure levels outside the chamber corresponded to the energy radiated from the panel, additional measurements at the outside of the chamber were performed using an accelerometer (fixed at the specimen surface), for the determination of the sound pressure level radiated per unit area (Figure 8-18). For the thicker elements, it was expected that the insulation of such elements was significantly higher than the one of the chamber, and thus some contamination would reach the microphone measurements. For both microphone and accelerometer, the measurements were performed over a grid of 25 points equally spaced over an area of 0.54 m x 0.54 m centred with the opening of the chamber.

Figure 8-18 – Placement of the microphone and accelerometer.

The acquisition of signals was made through an *NI USB 4431 DAQ* device, two *G.R.A.S. 46AE* model microphones and a *PCB 352C33* model accelerometer. Before the tests, both the microphones and the accelerometer were calibrated. A white noise signal was

generated through the NI device that connected to an *interM model M700* power amplifier that in turn connected to the three-speakers sound source inside the chamber. The generation, acquisition and manipulation of the signals was done through *MATLAB* software (Mathworks, 2018). The acquisition time for each measurement was 10 s, which is above the minimum of 6 s imposed by ISO 10140-4.

The conversion of the electric signal from the microphone to sound pressure was made through the methodology depicted in Figure 8-19.
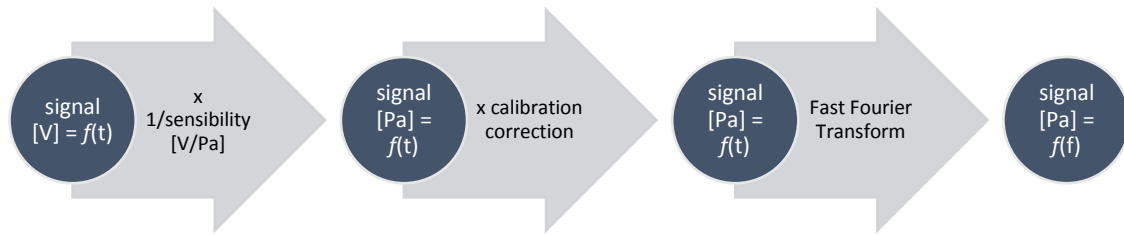
Figure 8-19 – Workflow adopted for the determination of the sound pressure from test data.

The sound pressure (p) was then converted to sound level (L), according to Equation (8-30),

$$L = 20 \log_{10}\left(\left|\frac{p}{p_0}\right|\right) \text{ [dB]}$$

$$(8\text{-}30)$$

where p_0 corresponds to the reference pressure (2×10^{-5} Pa).

A similar procedure was adopted for the conversion of the electric signal from the accelerometers to acceleration as a function of frequency, as depicted in Figure 8-20.
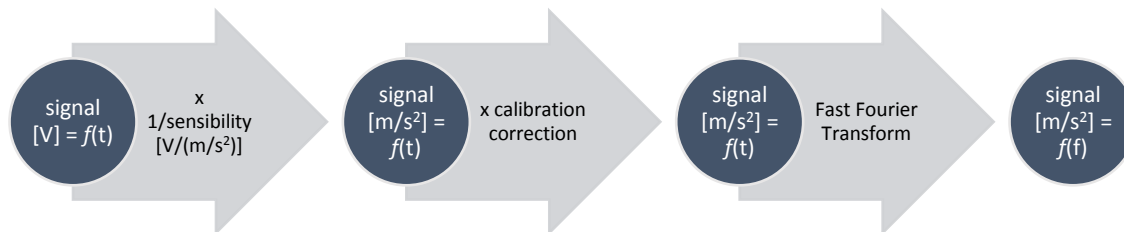
Figure 8-20 – Workflow adopted for the determination of the acceleration from test data.

The conversion of the acceleration to sound level radiated per unit area (L_w) was made according to Equation (8-31),

$$L_w = 20 \log_{10} \left(\frac{\rho c a}{\omega p_0} \right) \text{ [dB/m}^2] \tag{8-31}$$

where a is the acceleration (m/s^2); ω is the angular frequency (Hz); ρc is the characteristic impedance of air (415 Ns/m^3) and p_0 is the reference pressure (2×10^{-5} Pa).

For comparison purposes between the sound insulation (D) calculated using the data from both microphones placed inside and outside the chamber (as by Equation (8-27)) *vs*. the sound insulation calculated using the data from the accelerometer fixed at the specimen' surface and the microphone placed inside the chamber, the last one was calculated from L_w for an area of 1 m^2 (and thus L_w units were converts to dB), following Equation (8-32):

$$D = L_1 - L_w \text{ [dB]} \tag{8-32}$$

8.4.3 Impact sound insulation

The standard procedure according to ISO 10140-3 (ISO, 2010b) involves placing the element to be tested between two vertical adjacent rooms. In the top room, over the element to test, an impact source is placed (that is moved between a series of different positions) and the average sound pressure level is measured at the bottom room. The impact sound insulation of the element is obtained from the sound pressure level corrected taking into account the equivalent absorption area of the receiving room and the background noise.

As described for the airborne sound tests, the normalized impact test requires facilities that are in accordance with the guidelines of ISO 140-1 (ISO, 1997). In this work, the test procedure was adapted for the small-sized chamber previously described. The chamber's door was sealed by closing a 15 mm thick OSB door at the inside (Figure 8-21), and at the outside by a sandwich panel made of two plasterboard layers each with a thickness of 12.5 mm (density of 1050 kg/m^3) and a 4 mm thick inner bituminous layer tight to the threaded rods (Figure 8-22).

Following ISO 10140-3, the normalized impact sound pressure level (L_n) is determined according to Equation (8-33),

$$L_n = L_i + 10 \log_{10} \left(\frac{A}{A_0} \right) \text{ [dB]} \tag{8-33}$$

where L_i is the energy average sound pressure level in a one-third octave band in the

receiving room (dB).

Figure 8-21 – OSB door at the inside of the chamber.

Figure 8-22 – Outside panel for the chamber's closing.

The equivalent sound absorption area (A) in the receiving room is calculated according to ISO 10140-4 (ISO, 2010c) using Sabine's formula as in Equation (8-34),

$$A = \frac{0.16V}{T} \tag{8-34}$$

where V is the volume of the receiving room (m^3) and T is the reverberation time (s).

Corrections were introduced to reduce the contamination of the measured sound pressure level inside the chamber by airborne transmission. Indeed, it is known that in impact tests airborne transmission through weak elements of the test chamber may influence the final results; in the present case, these elements include the lateral door and also the tested floor specimen.

The sound pressure level due to the airborne sound generated by the impact source that crosses the floor and door elements ($L_{i\_airborne}$) is calculated from the energy average sound pressure level measured in the front of the door (L_{out_door}) and the floor (L_{out_floor}), according to Equation (8-35),

$$L_{i\_airborne} = 10 \log_{10} \left(\frac{1}{2} \left(10^{\frac{L_{out\_door} - D_{door}}{10}} + 10^{\frac{L_{out\_floor} - D_{floor}}{10}} \right) \right) \text{ [dB]} \tag{8-35}$$

where D_{door} and D_{floor} are the uncorrected airborne sound insulation of the door and

floor, respectively.

If $L_i - L_{i_{airborne}} < 10$dB, then L_i is replaced by L_{i_impact} that corresponds to the sound pressure level due to impact sound, calculated according to Equation (8-36).

$$L_{i\_impact} = 10 \log_{10} \left(10^{\frac{L_i}{10}} - 10^{\frac{L_{i\_airborne}}{10}} \right) \text{ [dB]} \tag{8-36}$$

The correction due to background noise is performed in the same way as it was described for the airborne sound tests, according to Equation (8-28).

According to ISO 10140-4, the number of microphone positions shall be equal to the number of tapping machine positions, which should be not less than four. Five microphone positions and five source positions were considered in the tests: four near the corners and one at the centre (Figure 8-23). As for the airborne sound tests, in the impact tests, due to the reduced chamber dimensions, it was not possible to simultaneously fulfil the minimum distances between the microphone positions (0.7 m), between the microphones and the chamber boundaries (0.7 m), and between the microphones and the test element (1.0 m). Taking into account results from previous works (Godinho et al, 2010), it was decided to place the microphones 0.30 m apart from the inner walls' surface (with exception of the microphone at the central position) and 0.40 m apart from the floor's surface. Simultaneously to the microphone measurements, measurements with accelerometers were also performed, by placing the transducers below the tested specimen on the vertical alignment of the microphones (Figure 8-24).
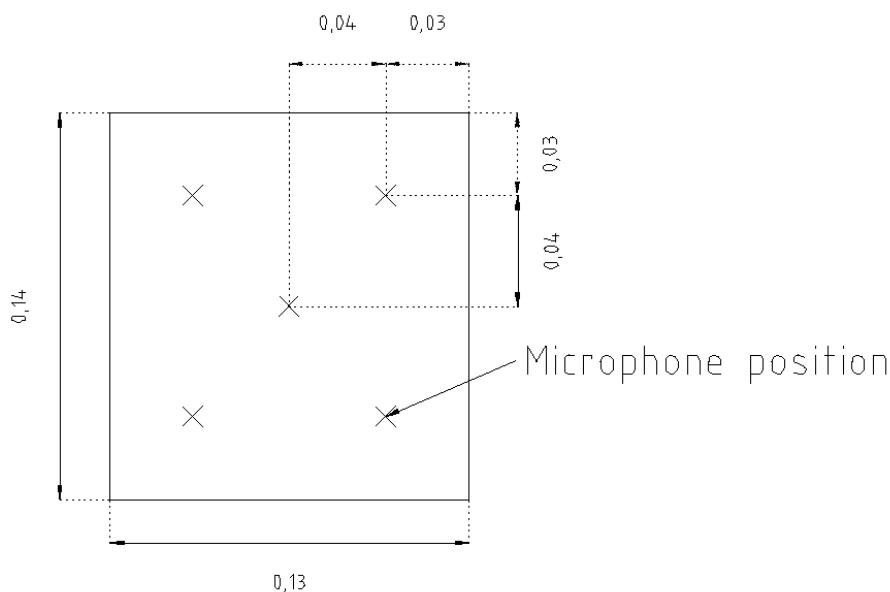
Figure 8-23 – Microphone positions inside the chamber (plan).
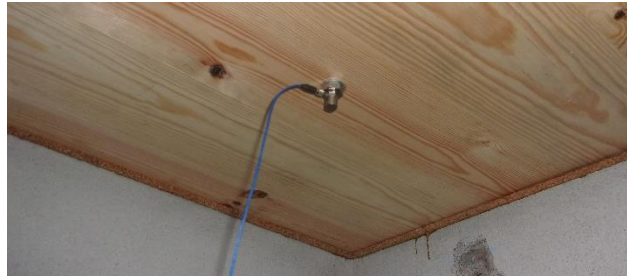
Figure 8-24 – Placement of accelerometer at the surface of the specimen for the impact tests.

A normalized tapping machine, *Brüel & Kjær model 3204*, was used in the tests. The machine was placed close to the vertical alignment of the microphone positions, with care to avoid the hammers to fall in the alignment of the chamber walls. For each combination of microphone/source position, the test was repeated five times, by changing the source position over the same place (Figure 8-25).
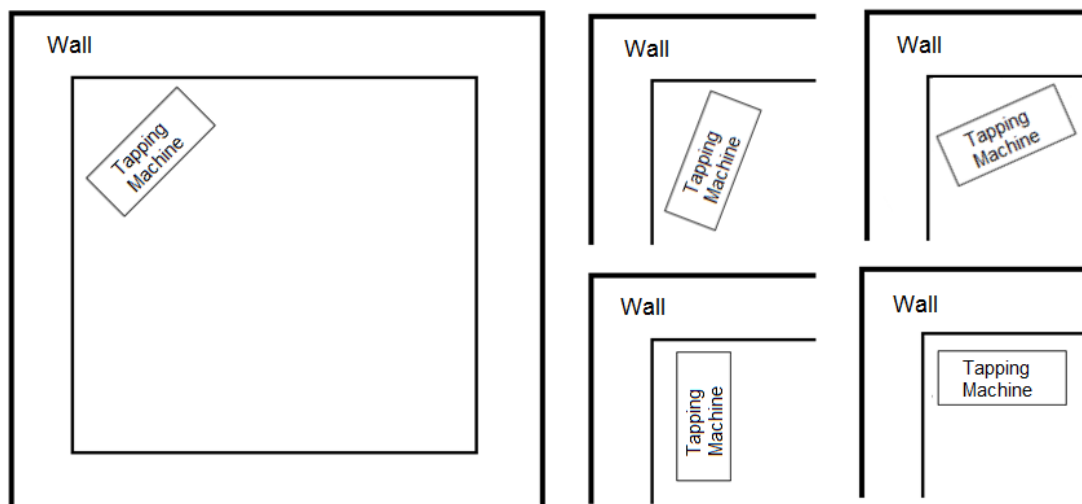
Figure 8-25 – Scheme of variation of the orientation for one of the tapping machine positions.

The same equipment used for the airborne sound tests was used in the impact tests, namely the acquisition device, microphones and accelerometers. The acquisition and manipulation of the signals was done once again with *MATLAB*. The acquisition time for each measurement was 10 s, which is above the minimum of 6 s defined in ISO 10140-4.

For the determination of the airborne sound insulation of the floor and door elements, a directional sound source *Brüel & Kjær Type 4224* was placed outside the chamber. The procedure of measuring the uncorrected airborne sound insulation was the one described earlier for the airborne tests, but with the sound source emitting from the outside to the inside of the chamber. One of the outside microphones was placed about 1 m from the

front of the door aligned with its centre and the other one at half-height (~0.5 m) between the top slab and the ceiling of the room (Figure 8-26). In total five measurements were taken, one for each inner microphone position.

a)   b)
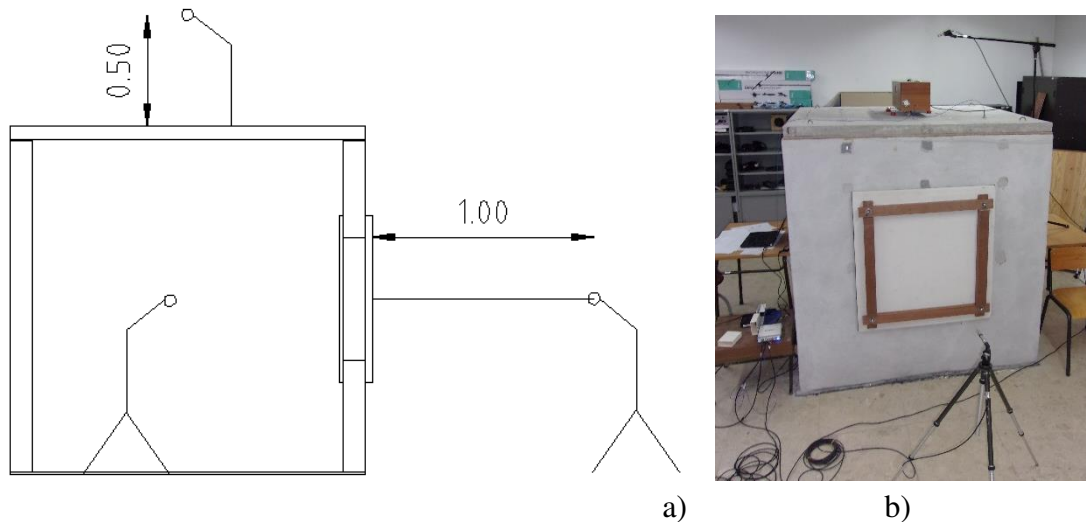
Figure 8-26 – Microphones positions: a) scheme; b) test apparatus.

For the determination of the reverberation times, the guidelines of ISO 354 (ISO, 2003a) were followed. It was not possible to fulfil the minimum distances between the sound source and the walls. The source was placed at one of the corners of the chamber (as in Figure 8-17) and four microphone positions were considered (the same that were used in the impact tests, except the one closest to the sound source). For each tested specimen, the reverberation time was determined as the mean value of the four measurements.

Each test specimen was placed over the cork layer on the top of the chamber (after the removal of the concrete slab used in the airborne sound insulation tests). To avoid marginal transmissions, the gaps between panels (at the connection) and between the panels and the chamber were sealed with silicone (Figure 8-27).

a)   b)
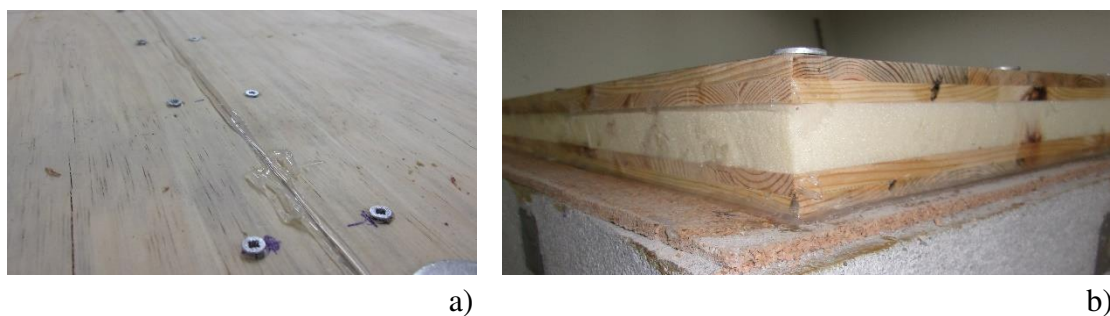
Figure 8-27 - Aspect of the sealing: a) between two panels; b) between a panel and the cork layer.

8.5 Results and discussion

8.5.1 Airborne sound insulation

8.5.1.1 Analysis of the experimental results

Some initial tests were conducted to check the insulation at the specimen/chamber interface. Besides the insulation with adhesive tape along the foam of the CIT specimens, the specimens were tested by surrounding that perimeter with mineral wool (Figure 8-28). From the comparison of the sound reduction curves, some visible differences were found, as shown in the examples of CIT 70 no1 and CIT 70 (Figure 8-29), so it was decided to apply such insulation in all the subsequent tests, to avoid marginal transmissions.
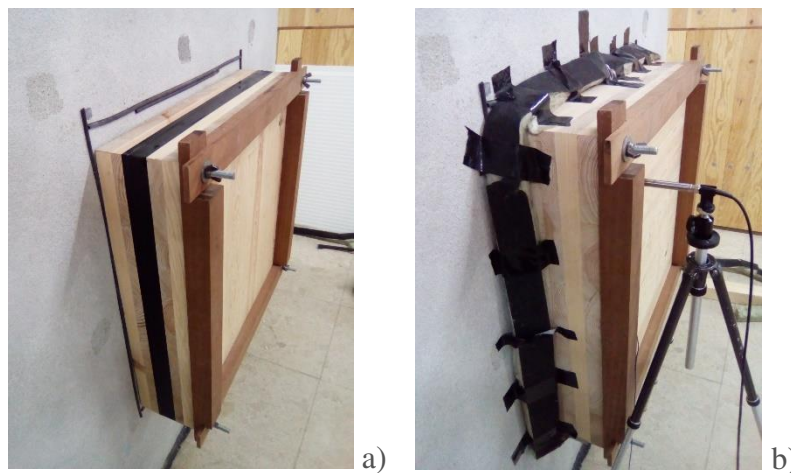
Figure 8-28 - Insulation of: a) the inner layer with adhesive tape; b) the specimen/chamber interface.
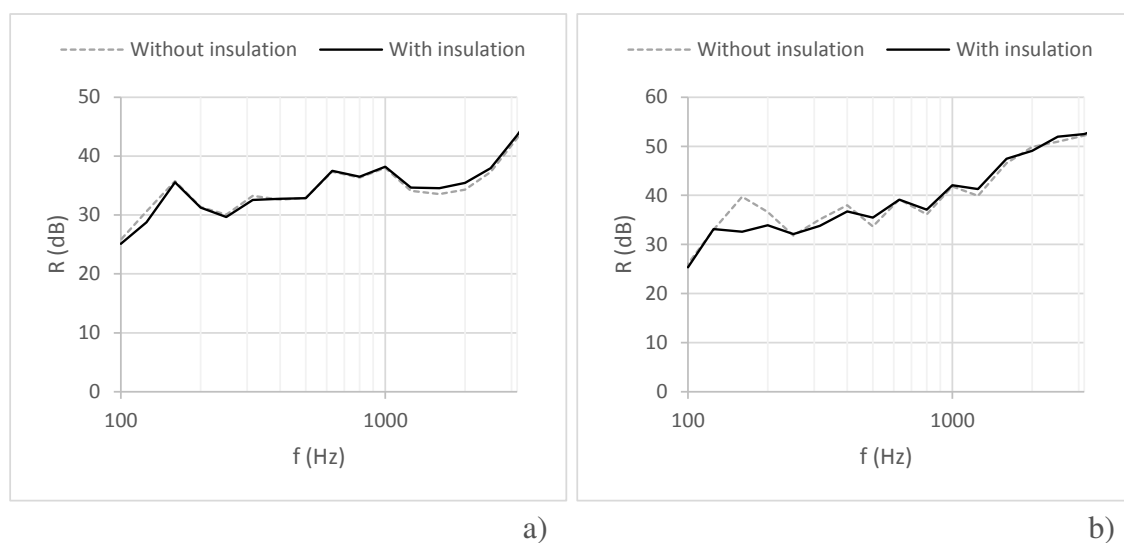
Figure 8-29 - Comparison of the airborne sound insulation curves with and without insulation at the interface specimen/chamber: a) CIT 70 no1; b) CLT 70.

The results regarding the uncorrected airborne sound insulation curves (D), calculated from the microphones $(L_1 - L_2)$ and microphones/accelerometers $(L_1 - L_w)$ for the different panels solutions are presented in Figures 8-30 and 8-31.

a)   b)
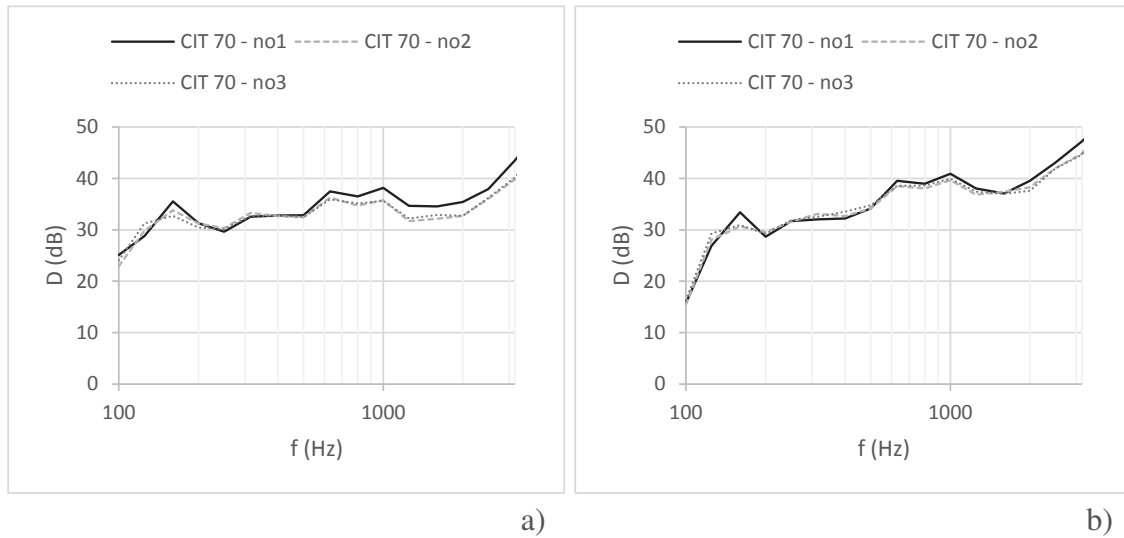
Figure 8-30 - Uncorrected airborne sound insulation curves for the CIT 70 panels calculated from: a) the microphones' data; b) accelerometers' data.

a)   b)
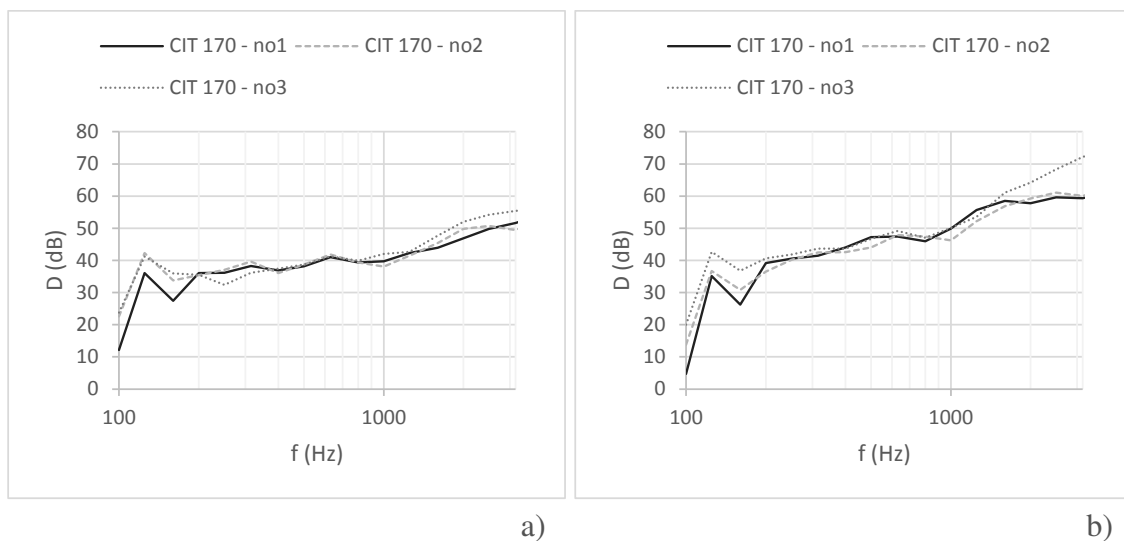
Figure 8-31 - Uncorrected airborne sound insulation curves for the CIT 170 panels calculated from: a) the microphones' data; b) accelerometers' data.

As a general comment, for the CIT 70 panels, the sound insulation curves of the three panels overlap very well, especially in the case of the measurements with accelerometers. Regarding the CIT 170 panels, although some overlap is still visible, especially in the 400-900 Hz range for the microphone measurements and 200-1000 Hz for the accelerometer measurements, higher variations are observed for the lower and highest

frequency bands considered, although the trend of the curves is still quite similar.

The comparison of the uncorrected airborne sound insulation curves obtained from the measurements of the outside level with microphone *vs.* accelerometer for the CLT and CIT panels tested is shown in Figures 8-32 to 8.33.

a)   b)
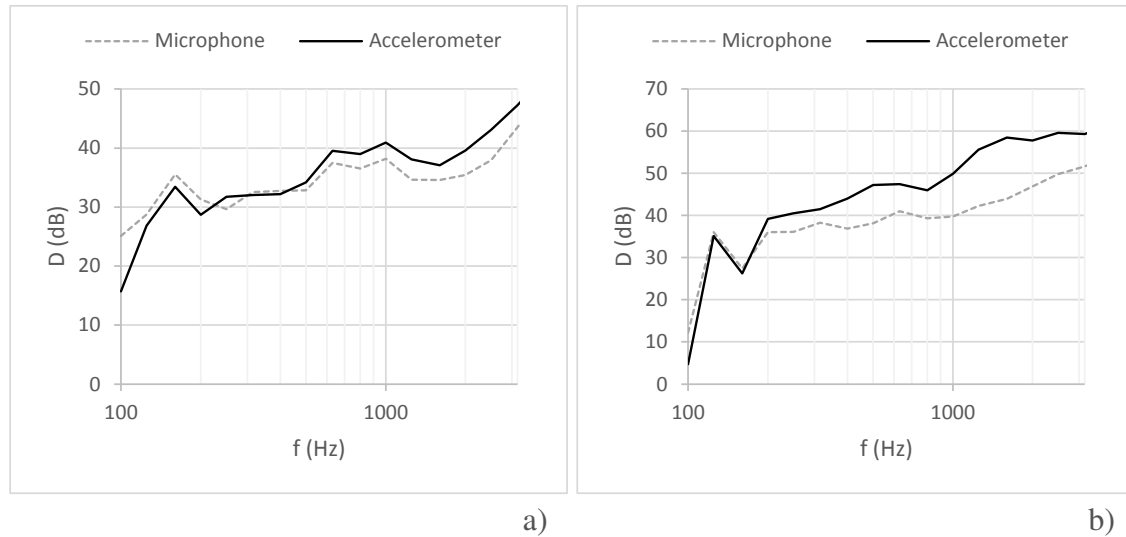
Figure 8-32 - Comparison between the uncorrected airborne sound insulation curve calculated from the outside microphone data and from the accelerometer for: a) CIT 70 panel no1; b) CIT 170 no1.

a)   b)
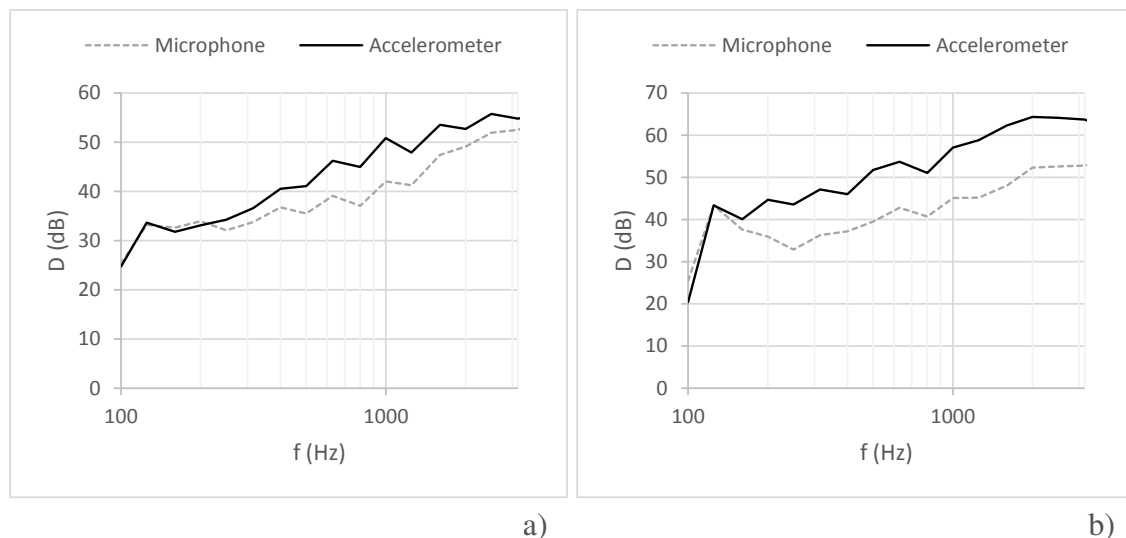
Figure 8-33 - Comparison between the uncorrected airborne sound insulation curve calculated from the outside microphone data and from the accelerometer for: a) CLT 70 panel; b) CLT 170.

From the analysis of the figures, it is possible to observe that few differences exist between the two curves for the lighter (and with less sound insulation) CIT 70 panel.

These differences increase when increasing the mass (and sound insulation) of the panel - in fact, an increasing difference can be observed between the microphone and the accelerometer curves for the remaining panels sorted by mass: CLT 70, CIT 170 and CLT 170. This aspect indicates that, after a certain point, the sound insulation of the tested panel exceeds the one provided by the test chamber composed of a 6 cm thick slab and 10 cm thick concrete walls, and thus the energy that is being radiated from the chamber to the outside through those elements will contaminate the signal measured by the outside microphone. In such case, the microphone results are unreliable for the calculation of the sound insulation of the tested element, so the curve has to be obtained from the acceleration measurements on the surface of the tested element. For that reason, all the results regarding the airborne sound insulation that are presented next are based on the acceleration measurements.

The comparison of the uncorrected airborne sound insulation curves for the four panel types obtained from the accelerometers is shown in Figure 8-34. In this figure, the CIT 70 and 170 curves represent the arithmetic mean values obtained from the individual tested elements.
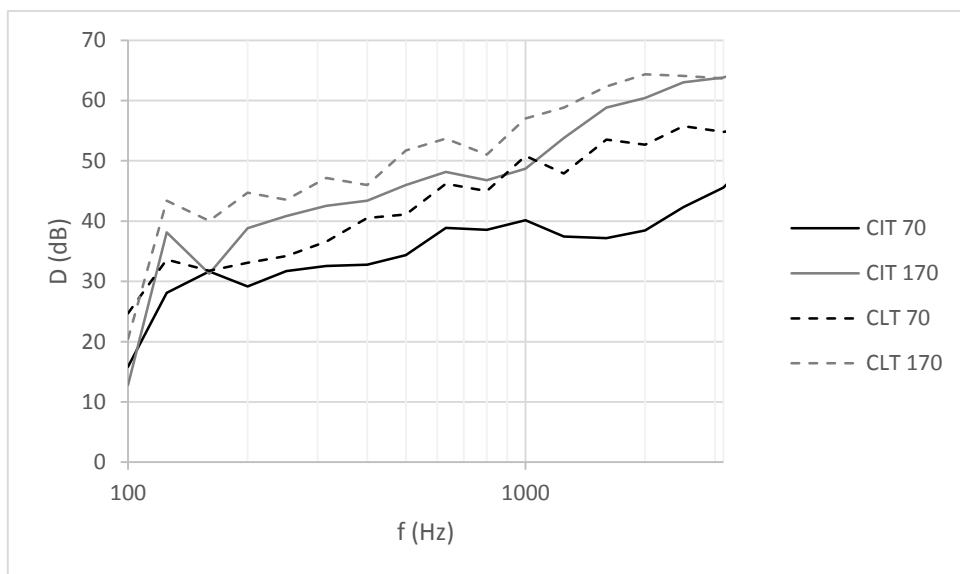
Figure 8-34 – Comparison between the uncorrected airborne sound insulation curves calculated from the accelerometer data for the different panel solutions.

As referred, in the figure above it is possible to observe that the heavier panels had increased sound insulation in almost all the frequency 1/3 octave bands considered in relation to the lightest panels. The CLT solution curves had a very similar trend, with a difference between curves around 4-6 dB.

For the tested panels, the weighted sound reduction index (R_w) was calculated from the

uncorrected airborne sound insulation curves calculated from the accelerometer data, according to ISO 717-1 (ISO, 2014). The results obtained are shown in Table 8-3.

Table 8-3 – Weighted sound reduction index for the panels tested.

	R_w (dB)
Sandwich	26
CLT 70	46
CLT 170	53
CIT 70 no1	38
CIT 70 no2	38
CIT 70 no3	38
CIT 170 no1	45
CIT 170 no2	47
CIT 170 no3	49

From the analysis of the table, it is observed that the R_w value for the CIT 70 panels is consistent among the three specimens (38 dB); in the CIT 170 panels, some variations are observed with a mean value of 47 dB. As expected, thicker and heavier panels provided better overall performance in terms of insulation to airborne sounds.

Regarding the CLT panels, some reference values from the literature regarding the airborne sound insulation are presented in Table 8-4.

Table 8-4 – Reference airborne sound insulation values for CLT panels.

Panel	Source	Thickness (mm)	Mass per unit area (kg/m^2)	Airborne Sound Insulation	
				Parameter	Value
EGO CLT 80	(Pérez and Fuente, 2013)	80	-	R_A	30 (dBA)
EGO CLT 135		135	-	R_A	37 (dBA)
Stora Enso CLT 100	(Enso, 2015)	100	37	R_W	34 (dB)
Stora Enso CLT 120		120	45	R_W	36 (dB)

Comparing the values in the table with the ones obtained for the CLT 70 panel (m_s=46 kg/m^2) it is found that the insulation of the tested panel (R_w=46dB) is somehow higher than the ones of panels with similar thicknesses (e.g. CLT 80, R_A=30dBA) or mass (e.g. CLT 120, R_w=46dB and m_s=45 kg/m^2) reported in the literature. No clear reasons could be identified for such difference between the tested solution and the similar reference CLT panels.

8.5.1.2 Comparison of experimental results with analytical prediction models

To assess which prediction models would describe better the experimental results, a series of models, including the ones referred before from (Wang et al, 2005), (Krakers, 2009) and (Ballagh, 2010) were considered. Initially, such models were used to predict the behaviour of the tested sandwich panel made of metal faces, which fits on the type of cross-section for which such models were developed, i.e. with thin stiff faces and low-density tick core. Besides the surface mass that was determined experimentally for each specimen, some parameters used as input in the models were estimated based on the information from Chapter 3 - they are shown in Table 8-5. The comparison of the experimental and predicted sound reduction curves for the reference sandwich panel is illustrated in Figure 8-35.

Table 8-5 – Input data used in the analytical models.

Layer	E (N/mm²)	v (-)	η (-)	ρ (kg/m³)
Steel	210000	-	-	7800
Wood 0º	12905	-	-	-
Wood 90º	239	-	-	-
Polyurethane	7.83	0.3	0.05	40

Figure 8-35 – Comparison between the airborne sound reduction obtained experimentally *vs.* the analytical models for the sandwich panel with metal faces.

Figure 8-35 shows that, from the considered models, the one proposed by (Ballagh, 2010) fits very well the test results, apart from the low frequency regions (up to 200 Hz 1/3 octave band), where all models fail to simulate the experimental results. The model from (Wang et al, 2005) also fits quite well the experimental curve approximately up to the dip

corresponding to the dilatational frequency between 1k and 2k 1/3 octave bands, but the prediction of the dip zone from both (Wang et al, 2005) and (Krakers, 2009) deviate from the experimental one. In particular, the curve from (Krakers, 2009) model deviates quite significantly before the dip region.

The comparison of the experimental and predicted sound reduction curves for the CIT panels is shown in Figure 8-36 and Figure 8-37. Only one of the specimens (no1) is shown for each case, as the experimental results within the same thickness were quite similar.

Figure 8-36 - Comparison between the airborne sound reduction obtained experimentally *vs*. the analytical models for the CIT 70 no1 panel.
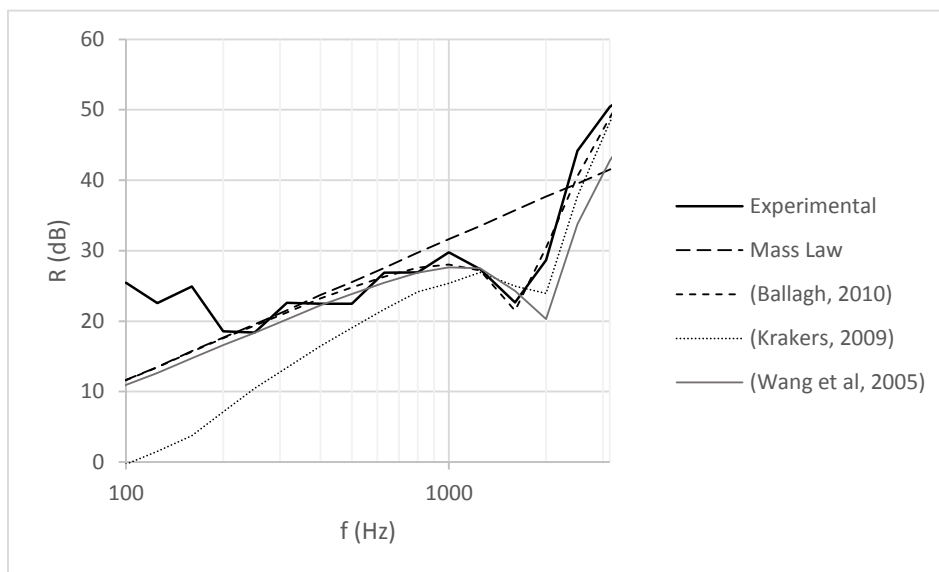

Figure 8-37 – Comparison between the airborne sound reduction obtained experimentally *vs*. the analytical models for the CIT 170 no1 panel.

Figure 8-36 and Figure 8-37 show that, for both the CIT 70 and 170 panels, up to the low frequency region (200 Hz 1/3 octave band), none of the models matches the experimental results. For the 70 mm panel, after that region and until 500 Hz, the Mass Law and the models from (Krakers, 2009) and (Ballagh, 2010) fit well the experimental results; subsequently, none of them delivers satisfactory results. Concerning the CIT 170 mm panel, the Mass Law fits quite well the experimental results, which is expected since this element has a surface mass of 94.0 kg/m². All the other models failed to predict the sound insulation behaviour of this panel.

It should be noticed that due to the reduced dimensions of the test specimens (75 × 75 cm²) and the high ratio between the thickness (70 and 170 mm) and the panel area, the wavelengths corresponding to the zone where the coincidence effect occurs could not fully develop. Thus, such an effect is less pronounced in the CIT panels than in the sandwich one. The coincidence effect will be more visible if the standard dimensions of the test opening of ISO 10140-2 (ISO, 2010a) would have been adopted (10 m²).

As it can be seen from the results above, the models that can predict the sound insulation of the sandwich panel with metal faces failed to predict the sound insulation of the CIT panels, particularly for the thicker 170 mm panels, whose wood layers (35 mm) are thicker than the core (30 mm). This is probably because those models were developed for sandwich panels with very thin faces with respect to the core thickness, which is not the case of the developed panels. Other models were assessed regarding their ability to simulate the experimental curves, namely the Beshenkov and Mechel models (Mechel, 2001), but none of them gave satisfactory results.

The model proposed by Sharp for homogeneous isotropic elements (Tadeu et al, 2010), which accounts for the mass, loss factor and critical frequency, as in Equation (8-37), was also tested.

$$
R = \begin{cases}
20 \log_{10}(fm) - 47 & if\ f < 0.5 f_c \\[2mm]
20 \log_{10}(f_c m) - 53 + [26.58 + 33.22 \log_{10}(\eta)] \log_{10} \dfrac{2f}{f_c} & if\ 0.5 f_c < f \le f_c \\[2mm]
20 \log_{10}(fm) - 44.4 + 10 \log_{10}\left(\dfrac{\eta f}{f_c}\right) & if\ f_c \le f \le 0.443 \dfrac{f_c}{\eta} \\[2mm]
20 \log_{10}(fm) - 47 & if\ f > 0.443 \dfrac{f_c}{\eta}
\end{cases}
\tag{8-37}
$$

Although it delivered good approximations for the heavier panel CIT 170 (Figure 8-39), it failed to match the experimental results for the CIT 70 panel (Figure 8-38) – in these figures, the predictions from this model are labelled as "Sharp-f_c". This model was then modified by replacing the critical frequency due to bending, by the dilatational frequency ("Sharp-f_{dil}") calculated according to Equation (8-6). In all cases, a core loss factor of

0.05 (Table 8-5) was considered, and the loss factor was determined according to Equation (8-22).
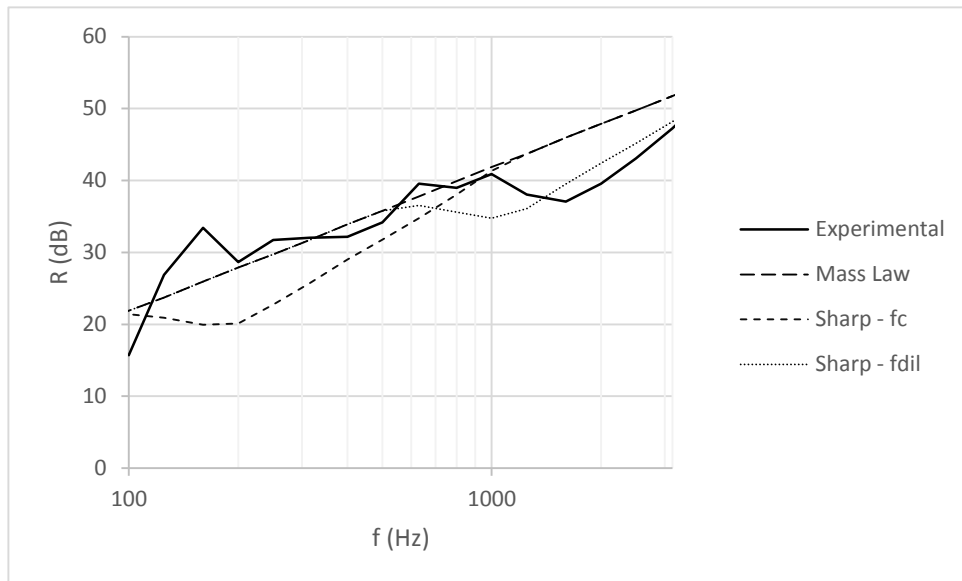
Figure 8-38 – Comparison between the airborne sound reduction obtained experimentally *vs.* the proposed model (adapted from Sharp) for the CIT 70 no1 panel.
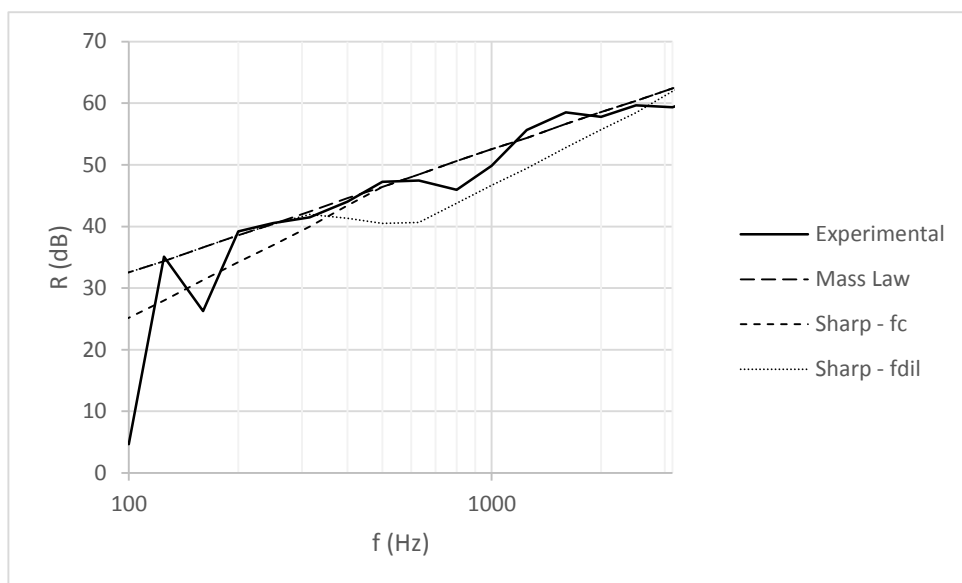
Figure 8-39 – Comparison between the airborne sound reduction obtained experimentally *vs.* the proposed model (adapted from Sharp) for the CIT 170 no1 panel.

As it can be seen from the results above, the original model by Sharp provides a reasonable fit to the experimental results for the 170 mm panel, with exception of the low frequency region, up to 200 Hz 1/3 octave band. However, for the 70 mm panel, such

model deviates significantly from the experimental results, while the modified Sharp model provides much more accurate predictions.

For the CLT panels, as they are massive elements, it is found that the Mass Law fits well the experimental results (Figure 8-40 and Figure 8-41).
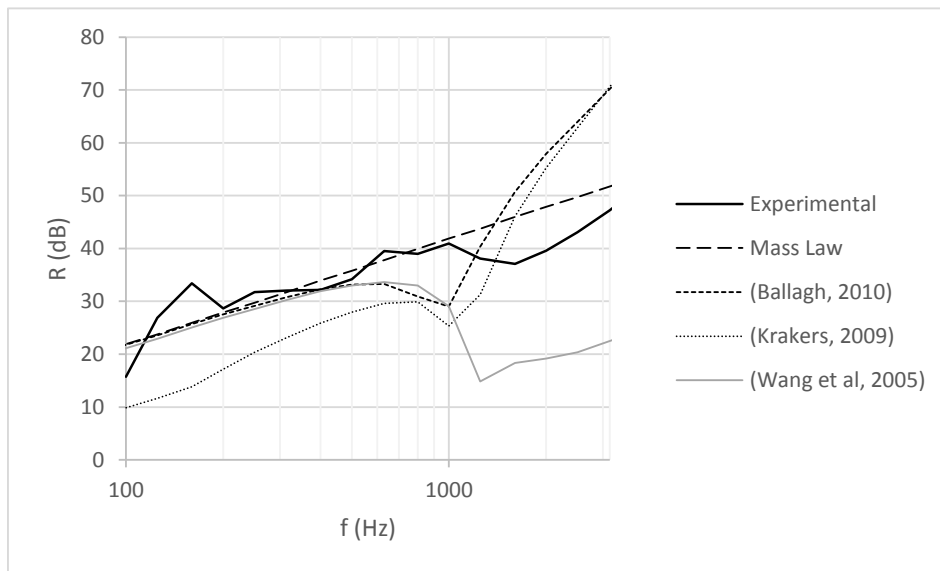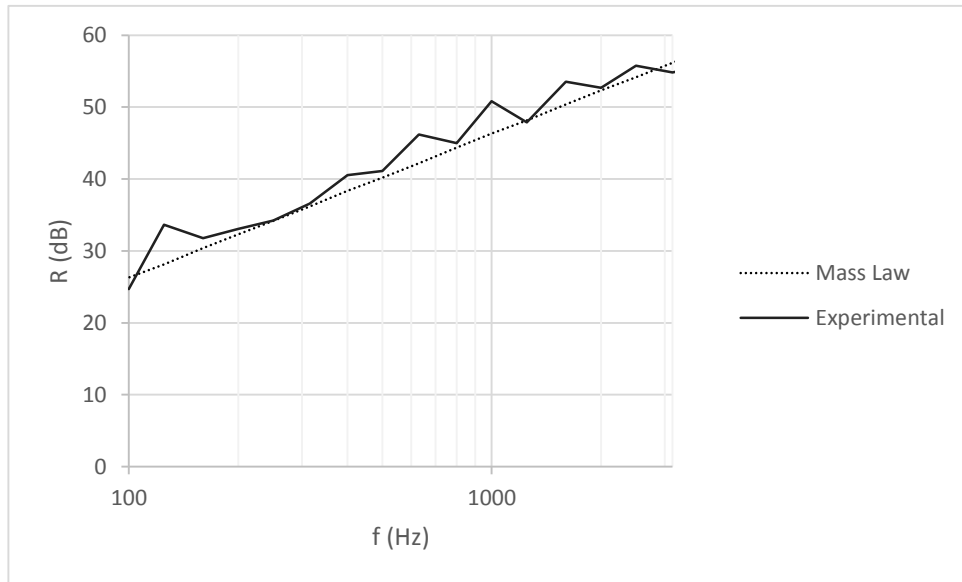

Figure 8-40 – Comparison between the airborne sound reduction obtained experimentally *vs*. the Mass Law model for the CLT 70 panel.
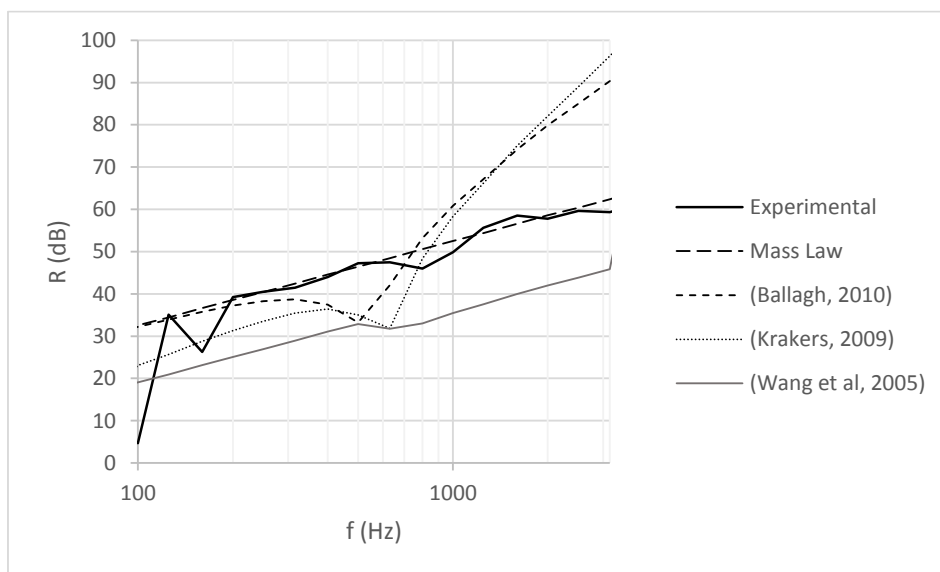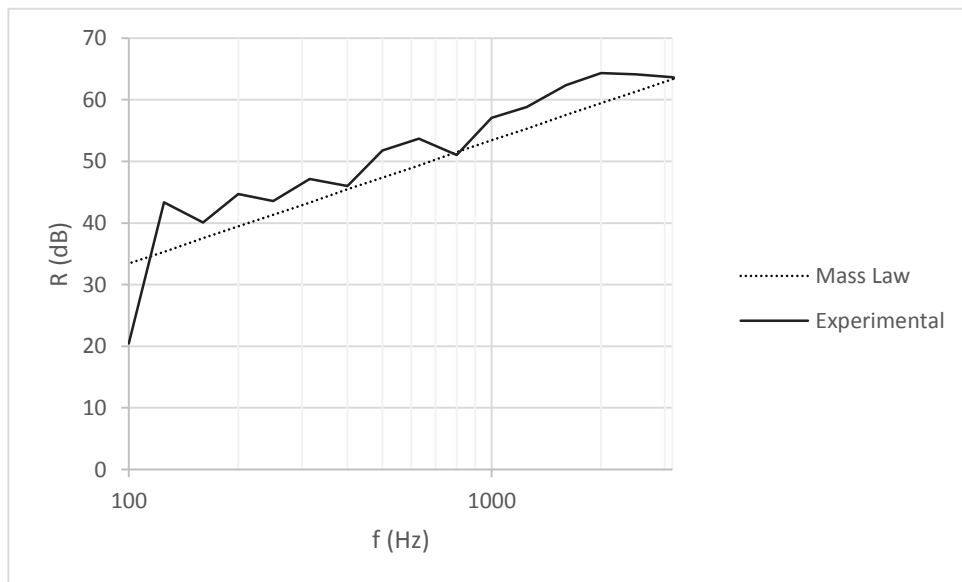

Figure 8-41 – Comparison between the airborne sound reduction obtained experimentally *vs*. the Mass Law model for the CLT 170 panel.

8.5.2 Impact sound insulation

8.5.2.1 Analysis of the experimental results

Figures 8-42 to 8-44 present the results obtained for the normalized impact sound level curve (L_n) and radiated sound pressure level (L_w) for the different panel solutions.

a)   b)
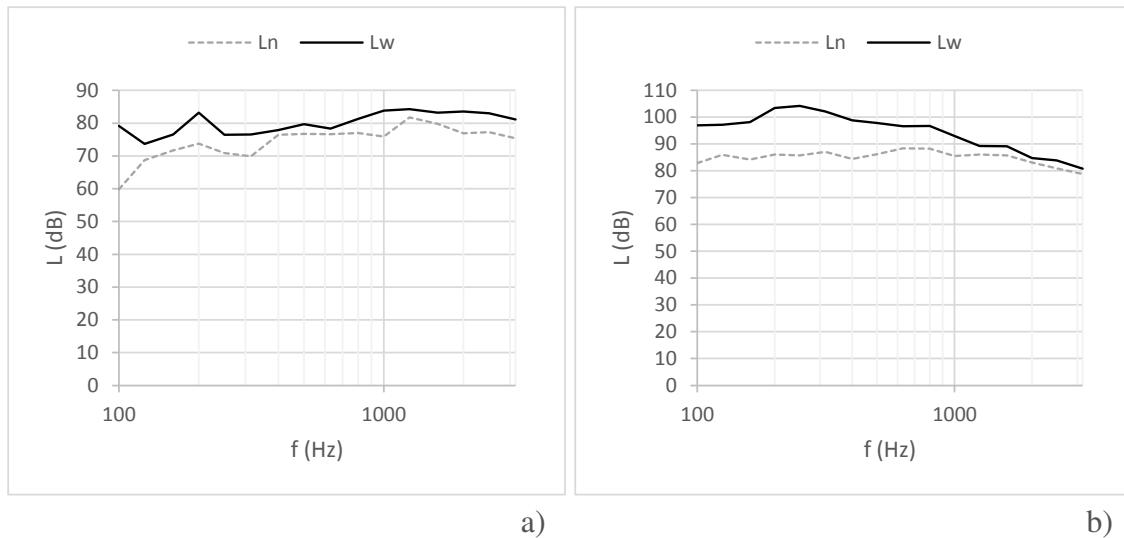
Figure 8-42 - Normalized impact sound level curve (L_n) and radiated sound pressure levels (L_w) (for 1 m^2) for: a) 60 mm concrete slab; b) traditional wood floor.

a)   b)
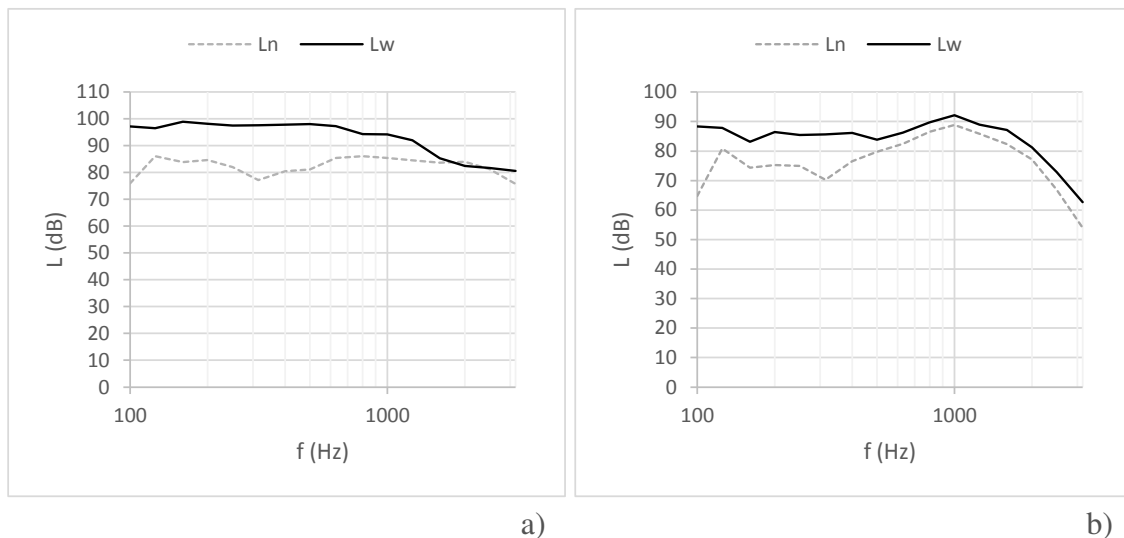
Figure 8-43 - Normalized impact sound level curve (L_n) and radiated sound pressure levels (L_w) (for 1 m^2) for: a) CIT 70; b) CIT 170.

a)   b)
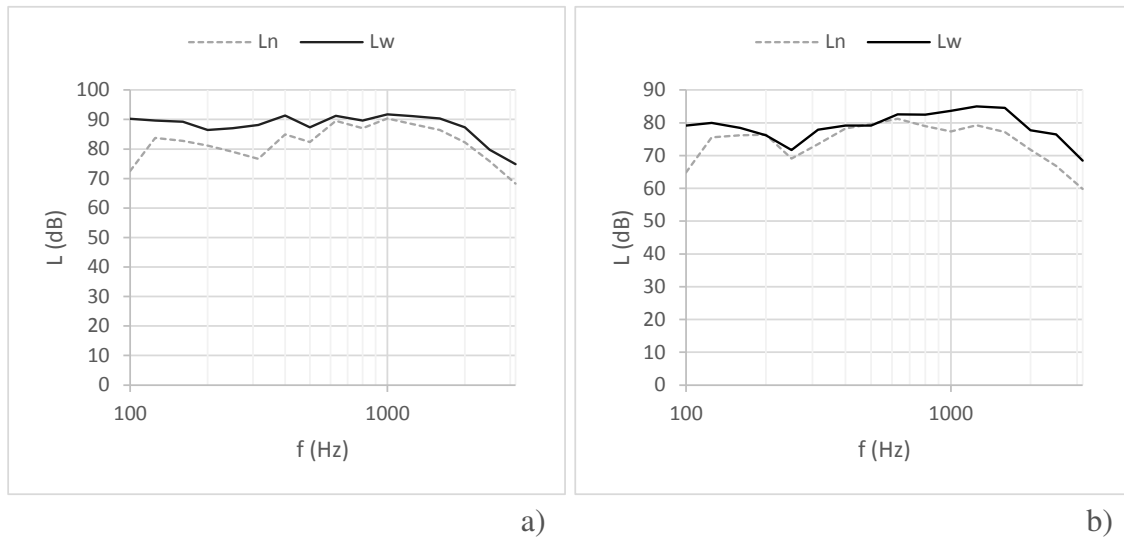
Figure 8-44 - Normalized impact sound level curve (L_n) and radiated sound pressure
levels (L_w) (for 1 m^2) for: a) CLT 70; b) CLT 170.

It is noted that for the lighter elements (CIT 70 and wood floor), major differences between L_n and L_w curves are found up to 1.6 kHz - in some regions, these differences are around 20 dB. Also, in the heavier CIT 170 panels, in some frequency bands, this difference can be around 15 dB. In the heavier elements (concrete slab and CLT 170) the differences between the L_n and L_w curves are less pronounced than the ones found in lighter floors.

Figure 8-45 presents a comparison between the radiated sound pressure levels for the different solutions that were tested in the experimental campaign.
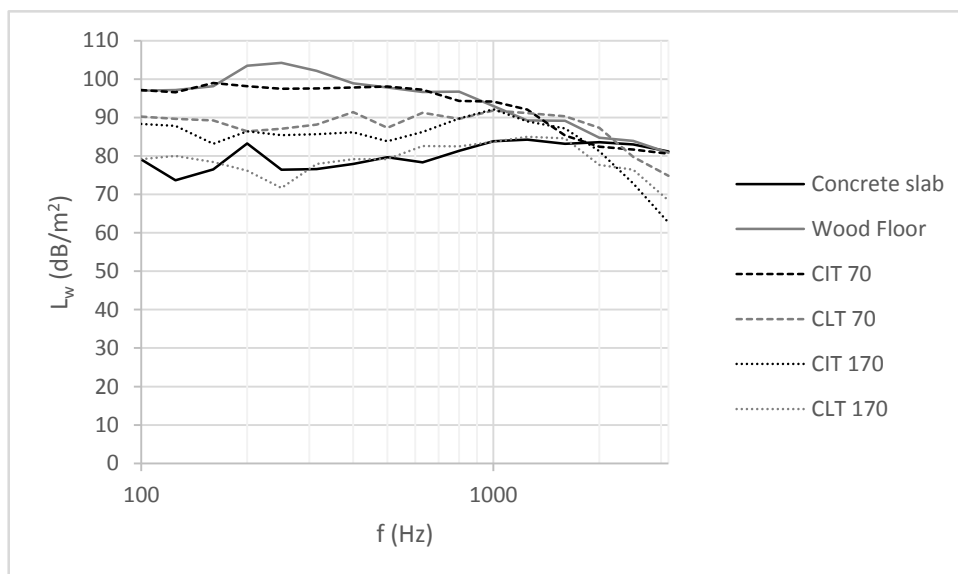
Figure 8-45 – Comparison between the radiated sound pressure levels for the different solutions tested.

It should be noted that the lighter solutions, CIT 70 (24.7 kg/m^2) and Wood Floor (30.0 kg/m^2), are the ones that show poorer performance in terms of insulation to impact sounds. The two curves had a quite similar trend, except for the 200-400 Hz range, where the performance of the Wood Floor is clearly worse. As referred, it should be noted that the mass per area for the CIT 70 floor (30.0 kg/m^2) is an approximate value, as in practice the mass is not equally distributed per area, due to the floor configuration (deck supported in evenly spaced beams). This may explain the fact that despite the difference of 5.3 kg/m^2 between the mass per area of the two solutions, the curves are quite similar. The trend of the CIT 170 curve is quite close to the one for the CLT 70, with a slightly better performance of the former starting from 200 Hz up to 3.15 kHz. Also, the trend between the concrete slab and the CLT 170 panel is very similar, with the CLT solution performing even better for the frequency range between 200-300 Hz and 1700-3.15 kHz.

For the tested panels, the weighted normalised impact sound pressure level ($L_{n,w}$) was calculated from the radiated sound pressure level curve according to ISO 717-2 (ISO, 2013a). The results are shown in Table 8-6.

Table 8-6 - Weighted normalised impact sound pressure level ($L_{n,w}$) obtained for the different floor solutions with varying mass per area (m_s).

Solution	$L_{n,w}$ (dB)	m_S (kg/m^2)
Concrete slab	89	144.0
Wooden floor	97	30.0
CLT 70	92	42.1
CLT 170	85	112.7
CIT 70	95	24.7
CIT 170	88	90.2

From the results above, it is observed that the insulation to impact sounds provided by the CLT 170 panel (which has the second higher value of mass per area) is the highest (85 dB), followed by the CIT 170 panel (88 dB) and the concrete slab (89 dB). The lighter elements, namely the CIT 70 panel and the wooden floor, afford the lowest acoustic insulation to impact sounds, with 95 dB and 97 dB, respectively.

8.5.2.2 Comparison of the experimental results with analytical prediction models

Based on the values of R_w obtained from the airborne sound insulation tests and the values of $L_{n,w}$ obtained from the impact sound insulation tests, the invariant law (Tadeu et al, 2010) was applied according to Equation (8-38). The results obtained are presented in Table 8-7.

$$L_{n,w} + R_w = constant\_value \qquad (8\text{-}38)$$

Table 8-7 – Application of the invariant law to the measured values of $L_{n,w}$ and R_w.

	$L_{n,w}$ (dB)		R_w (dB)	$L_{n,w} + R_w$ (dB)
CLT 70	92	CLT 70	46	138
CLT 170	85	CLT 170	53	138
CIT 70	95	CIT 70 no1	38	133
		CIT 70 no2	38	133
		CIT 70 no3	38	133
CIT 170	88	CIT 170 no1	45	133
		CIT 170 no2	47	135
		CIT 170 no3	49	137

For the CLT solutions, a consistent value (138 dB) is obtained for the sum of $L_{n,w}+R_w$ for the two tested thicknesses. Also, for the CIT solutions, a consistent value of 133 dB is obtained for all the 70 mm specimens and for the specimen no1 from the 170 mm series. For specimens no2 and no3, due to variations of R_w, values of 135 and 137 dB are obtained, respectively.

The experimental results of the CIT and CLT panels were also compared with the prediction by the empirical Equation (8-25) proposed by Bella et al (2016) for CLT panels. It should be noted that in the mass per area used in the calculus, the mass of the tapping machine (16 kg) was also accounted for. The results are shown in Table 8-8.

Table 8-8 – Application of the (Bella et al, 2016) model.

	$L_{n,w}$ Predicted (dB)	$L_{n,w}$ - $L_{n,w}$ Predicted (dB)
CLT 70	91	1
CLT 170	82	3
CIT 70	94	1
CIT 170	84	4

Although for the CIT 70 and CLT 70 cases the approximation is quite good (1 dB difference), for the other two cases, the differences are not negligible, with 3 and 4 dB for the CLT 170 and CIT 170, respectively. It should be noted that the tested floors were composed of two panels mechanically connected to each other, which may have caused the panels to behave in a different way than if they were monolithic.

Regarding the CLT panels, some reference values from the literature regarding the impact sound insulation are presented in Table 8-9.

Table 8-9 – Reference impact sound insulation values for CLT panels.

Panel	Source	Thickness (mm)	Mass per unit area (kg/m²)	Impact Sound Insulation	
				Parameter	Value (dB)
EGO CLT 135	(Pérez and Fuente, 2013)	135	-	$L_{n,w}$	89
Stora Enso CLT 140	(Enso, 2015)	140	60	$L_{n,w}$	88
CLT 5-layer 140	(Bella et al 2016)	140	70	$L_{n,w}$	87-88
CLT 5-layer 175		175	90	$L_{n,w}$	85
CLT 7-layer 245		245	130	$L_{n,w}$	80
CLT	(Homb et al, 2017)	-	51	$L_{n,w}$	86
		-	58	$L_{n,w}$	86
		-	68	$L_{n,w}$	85
		-	80	$L_{n,w}$	83
		-	85	$L_{n,w}$	87
		-	89	$L_{n,w}$	85

Comparing the values in the table with the one obtained for the CLT 70 panel ($L_{n,w}$=92 dB) it is found that the insulation of the tested panel is slightly poorer than the ones found in the literature (the worse insulation is 89 dB for a 135 mm panel). This result is not unexpected since the thickness (70 mm), as well as the mass per area (m_s=42.1 kg/m2) of the panel tested, are above the values reported on those previous studies. A good agreement is found for the CLT 170 panel (m_s=112.7 kg/m^2 and $L_{n,w}$=85 dB), which compares well with CLT panels with similar thickness and mass per area (e.g. CLT 5-layer 175 mm and m_s=90 kg/m^2, $L_{n,w}$=85 dB or CLT with m_s=89 kg/m^2, $L_{n,w}$=85 dB).

8.5.3 Concluding remarks

This chapter presented an experimental and analytical study related to the acoustic performance of the developed panels concerning their airborne and impact sound insulation. The results obtained allow drawing the following conclusions:

- Regarding the airborne sound insulation, for panels containing an elastic core, additionally to the critical frequency due to bending, another critical frequency due to dilatation of the core appears;

- The airborne sound insulation of the CIT panels was found to be lower than that of CLT panels with equivalent thickness – this result is logical being due to the lower mass of the former panels;

- The impact sound insulation of the CIT 70 floor was found to be lower when compared to that of the CLT 70 panel; the same happened with the CIT 170 panel compared to the CLT 170 panel; however, in the high frequency region considered, the CIT panel performed better;

- Analytical models developed to describe the airborne sound insulation of typical sandwich panels (*i.e.* with thin rigid faces and thick soft core) were able to reproduce the experimental behaviour of the metal-faces sandwich panel tested corresponding to those characteristics, but failed to describe the behaviour of the CIT panels;

- The Sharp model for homogeneous isotropic elements was able to describe well the airborne sound insulation behaviour of the thicker CIT 170; however, it failed to describe the behaviour of the CIT 70 specimen. An adaptation of such a model, by replacing the typical critical frequency due to bending by the dilatational frequency, enhanced the predictions;

- The invariant law can be used to estimate the impact sound insulation of both CIT and CLT panels.

9 CONNECTIONS

9.1 Introduction

The use of connections in prefabricated construction with wood-based panels, like cross-laminated timber (CLT), structural-insulated panels (SIP), as well the developed panels - cross-insulated timber (CIT), requires a proper design to provide structures with adequate strength, stiffness, stability and ductility. At the same time, the structural efficiency of floor and wall systems acting as diaphragms in their plane in resisting lateral loads depends on the efficiency of the fastening systems and connection details, both the one used to connect the panels at the same plane, and also the one used to connect the panel to the surrounding structural elements.

This chapter presents a review of the most common types of connections found for CLT and SIP systems, which were the basis for the solutions proposed for the developed panels. The state-of-art regarding analytical models for the prediction of the strength of CLT-type connections is also presented, due to their similarity with some of the developed connections for CIT. The chapter presents also the results of experimental tests on one of the developed connections.

The following chapter is organized as follows: first, the most common CLT and SIP connections between panels and existing structural members (masonry or concrete foundations and walls) are presented in section 9.2; proposed connections for the developed panels are presented and described in section 9.3; analytical design models found to describe the strength of CLT-type connections are presented in sections 9.4 to 9.6; experimental results on one of the developed connections are presented and discussed in section 9.7; in the last section 9.8, conclusions are presented.

9.2 Common types of CLT and SIP connections

The common ways to join CLT and SIP panels involve the use of additional wood elements and/or metal parts, including the use of fasteners. When using such type of connections (fasteners), minimum fastener spacing and end/edge distances are required to avoid premature and brittle failures due to splitting or shear stresses on the wood elements, whose general rules are described in EN 1995 1-1 (CEN, 2004b).

In CLT structures, two main typologies of building construction are used in practice: the 'platform' and the 'balloon'. The first consists of building each storey in turn (i.e. one after another), in a way that the floor panels rest directly on the top of the walls composing that storey, which consequently forms a platform for the subsequent stories. In the second option, the walls are continuous for more than one storey and, therefore, the intermediary floor elements are laterally attached to those walls. Due to the limitations in the length of the (wall) panels, this system is more likely to be applied in low-rise buildings. The platform type construction has the advantages that simple connection systems can be used and the erection of upper stories is made more easily, and for those reasons it is often most used in practice than the balloon one (Karacabeyli and Douglas, 2013).
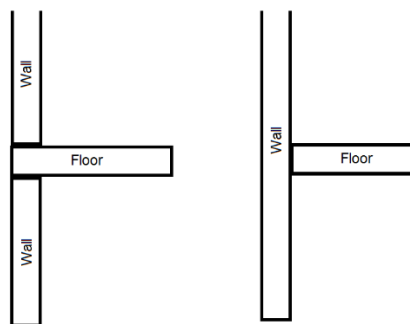
Figure 9-1 – Platform (left) and balloon (right) building construction typologies.

In a typical building made of wood panels, the following connections are usually required:

- Wall panels in the same plane (aligned wall-to-wall or lateral floor-to-floor);
- Wall panels positioned at angle (corner walls);
- Wall-to-floor or wall-to-roof panels;
- Floor-to-masonry/concrete wall;
- Wall-to-masonry/concrete foundation.

Most of the times, the same connection system or part(s) of it can be used in different situations (e.g. aligned wall-to-wall or lateral floor-to-floor).

The most representative connections systems found in practice for CLT and SIP systems are presented next.

9.2.1 Single or double internal or external spline in CLT connections

This type of connection is achieved by profiling the panels to be connected and then inserting a wood stripe (spline) attached by metal connectors (wood screws, self-tapping

screws or nails) to the panels. For a five-layered panel, common solutions include the use of one or two splines that may be applied at the outer or inner layers (Figure 9-2). The spline is usually made of laminated veneer lumber (LVL), thin CLT or plywood.
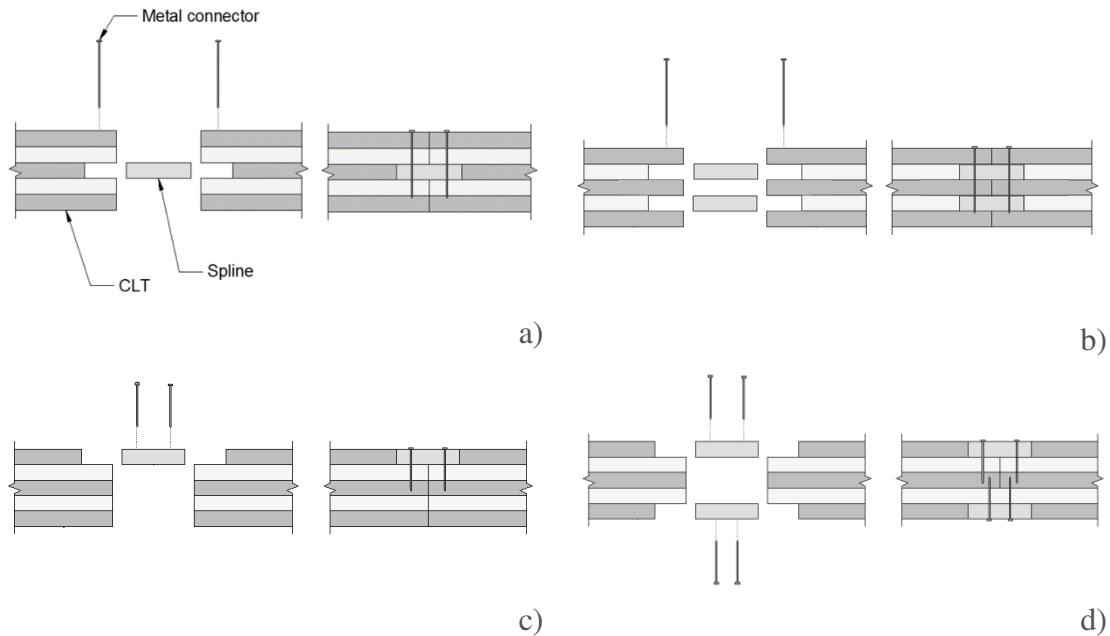
Figure 9-2 – Spline connections between five-layered CLT panels: a) single internal spline; b) double internal spline; c) single external spline; d) double external spline.

This type of connection is used to connect wall panels, and thus it should resist in-plane shear loads; however, according to Karacabeyli and Douglas (2013), some studies indicate that the external double spline connection can also be designed to resist out-of-plane loads.

From the four types of connections presented in Figure 9-2, the single external spline connection has the lowest strength and stiffness as it is a single shear connection; however, it requires less machining and work time.

9.2.2 Half-lapped joint in CLT connections

The half-lapped joint type of connection is obtained by profiling the panels to connect at opposite sides and then attaching directly the panels by metal connectors, usually self-tapping screws (Figure 9-3).

This type of connection is used to connect wall panels as it can resist normal and transverse loads. It is also used to connect floor elements, although it is more limited to resist bending moments. An advantage of this connection is that it is simple to assemble;

however, the concentration of tensile stresses perpendicular to the grain increases the risk of splitting (e.g. where loading on the adjacent floor elements is uneven) (Karacabeyli and Douglas, 2013).
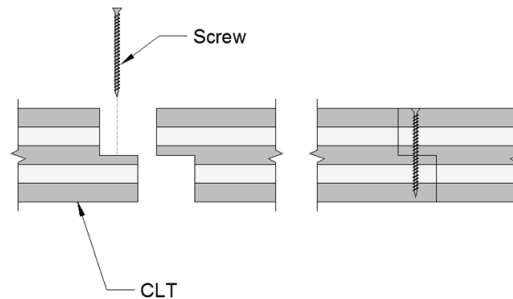
Figure 9-3 – Half-lapped joint connection in five-layered CLT panels.

9.2.3 Self-tapping screws in corner CLT elements

The connection using self-tapping screws for corner wall or wall-to-floor elements is achieved by joining the panels to be connected by using self-tapping screws (Figure 9-4).
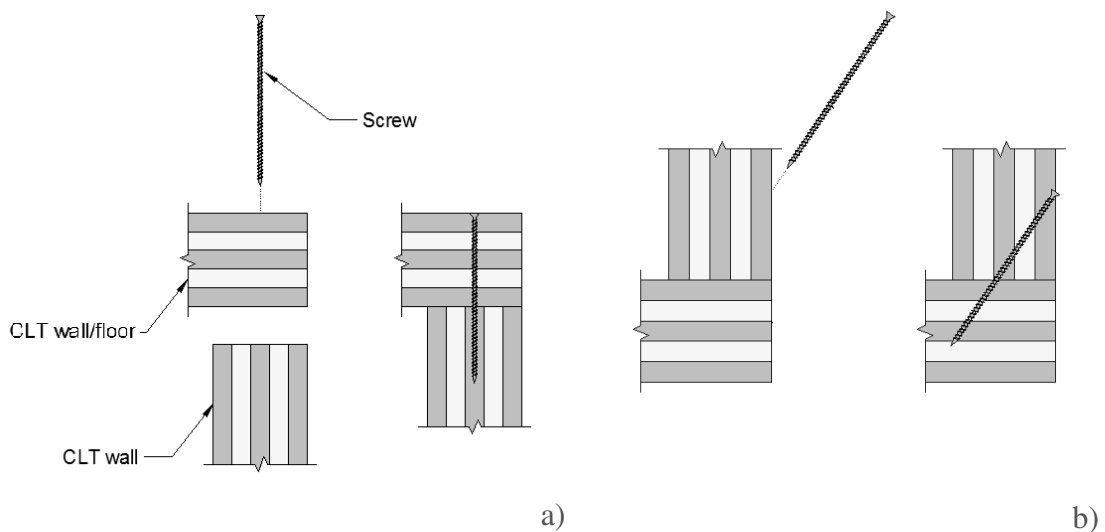
Figure 9-4 – Self-tapping screws connections between CLT panels: a) normally inserted; b) at angle.

This connection system has the advantage of being quite simple to execute. However, as the screws are driven in the narrow side of the panels, especially if they are installed in the end grain of the cross layers as in Figure 9-4 a), the load-carrying capacity is limited. For this reason, the screws may be driven at an angle as in Figure 9-4 b), optimizing the performance of the connection (Karacabeyli and Douglas, 2013).

9.2.4 Wood beam – balloon construction typologies – CLT elements

The use of a wood beam for a floor-to-wall assembly is mainly used in balloon type construction; this connection system comprises the use of a wooden beam attached to the panels through metal connectors to provide continuous bearing support to the CLT floor panels (Figure 9-5). The beam is usually made of solid composite lumber, but CLT could also be used for this purpose.
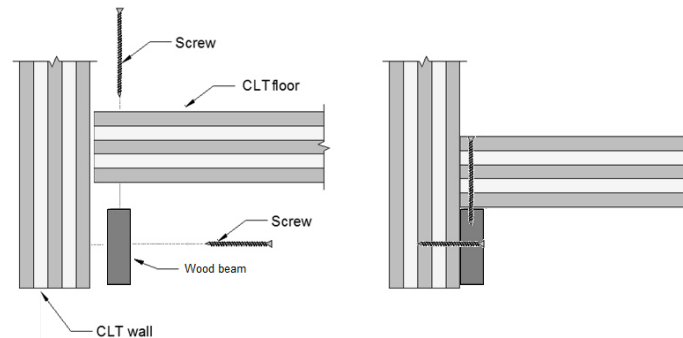
Figure 9-5 – Connection between a wall and floor CLT panels with wood beam.

This connection has the advantage that if an entire floor element needs to be removed for some reason (e.g. degradation), it can be disassembled with minimum interference with the wall structure and other floor elements.

9.2.5 Angle bracket – CLT elements

This type of connection is achieved by joining the panels with an angular metal bracket that in turn is connected to the panels by wood screws or nails (Figure 9-6).
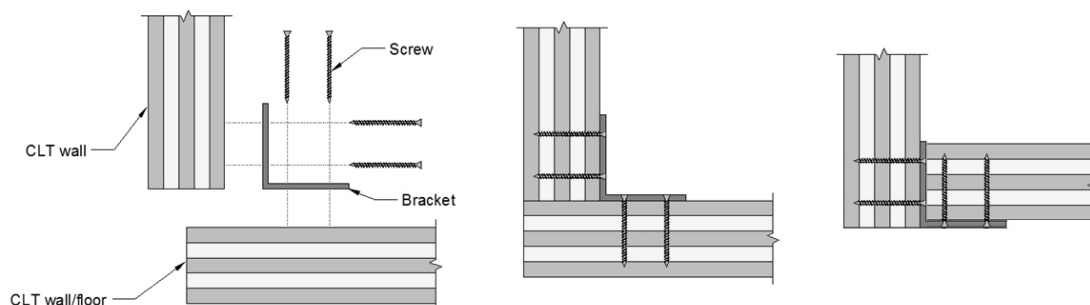
Figure 9-6 – Angle bracket connection between CLT panels.

With this connection, it is possible to achieve considerable strength once the fastening is

done in the direction perpendicular to the plane of the panels. It has the disadvantage that it requires a protective coating for fire resistance purposes (Karacabeyli and Douglas, 2013). When a floor element is to be connected to a wall element, hold-down connectors may be used instead of angle brackets, especially at the ends of the walls, where the tensile forces due to uplifting are higher.

9.2.6 Concealed plate - CLT

This type of connection is achieved by joining the panels with T-shape metal profiles. The bottom plate of the profile is attached to one of the panels through screws, while the other is inserted to the other panel (profiled) and fixed through dowels or screws (Figure 9-7). Regarding fire safety, this system is efficient as the metal plate is less exposed to elevated temperatures (Karacabeyli and Douglas, 2013).
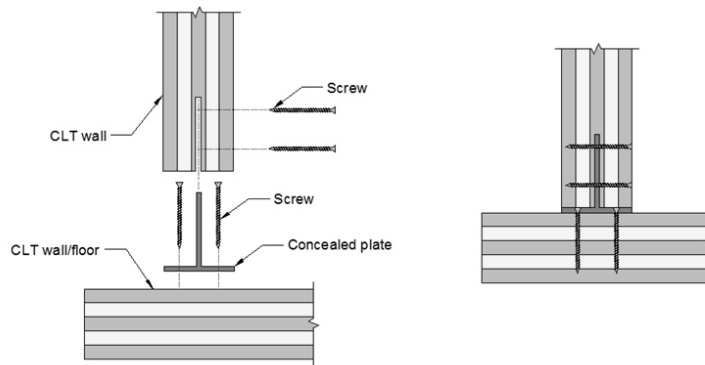
Figure 9-7 – Concealed plate connection between CLT panels.

9.2.7 Connections between wall and foundations: angle bracket or hold-down - CLT

This type of connection is similar to the one used for panel-to-panel connections; the only difference lies in the fixing elements of the bracket to the foundation (usually concrete), which are substituted by anchor bolts (Figure 9-8). In this connection type, an intermediate layer between wood and concrete should be provided to avoid transmission of moisture between the foundation and the panel, and thus to improve the durability of the panel (Karacabeyli and Douglas, 2013).
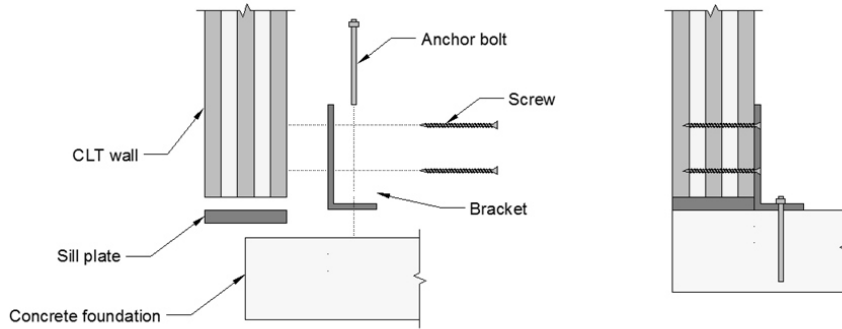
Figure 9-8 – Angle bracket connection between foundation and CLT wall.

9.2.8 Connections between wall and foundations: straight plate - CLT

This type of connection consists of a metal plate that is attached to the sides of the panel and the foundation. The attachment to the wood panel is usually made through lag or self-tapping screws, while in concrete foundation lag screws, powder-actuated fasteners or anchor bolts are used (Figure 9-9).
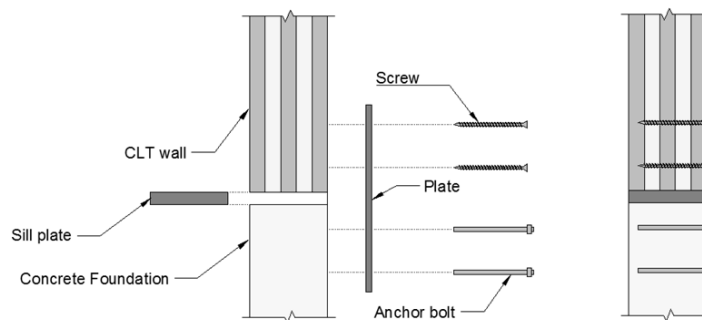
Figure 9-9 – Straight plate connection between foundation and CLT wall.

9.2.9 Connections between wall and foundations: concealed plate - CLT

This type of connection is similar to the one used for panel-to-panel connections; the only difference refers to the fixing elements of the plate to the foundation (usually concrete) that are substituted by anchor bolts (Figure 9-10).
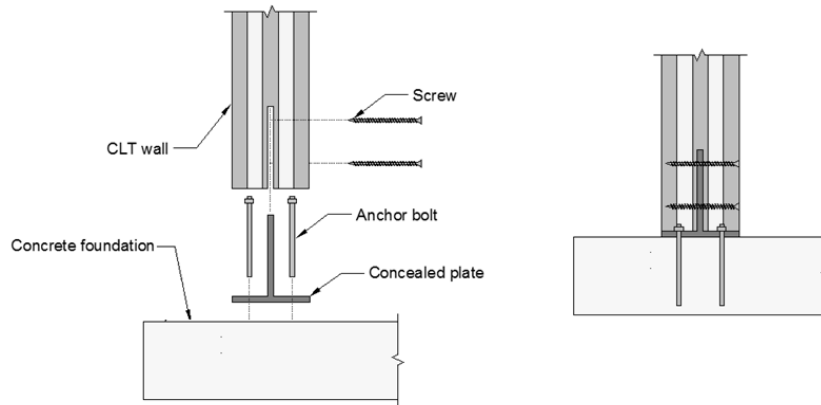
Figure 9-10 – Concealed plate connection between foundation and CLT wall.

Different connection systems were developed for SIPs (SIPS, 2016). The most common types of connections include vertical wall-to-wall in the same plane, panel-to-panel in intersecting planes (e.g. wall-to-floor and wall-to-wall) and wall-to-foundation.

9.2.10 Spline - SIP

This type of connection is achieved by profiling the core of the SIP at the interfaces to be connected and then inserting a SIP block, wood strip or wood block, which is attached through metal connectors (screws, staples or nails) to the panels (Figure 9-11). The wood layer can be made of solid wood or composite material (e.g. orientated strand board).
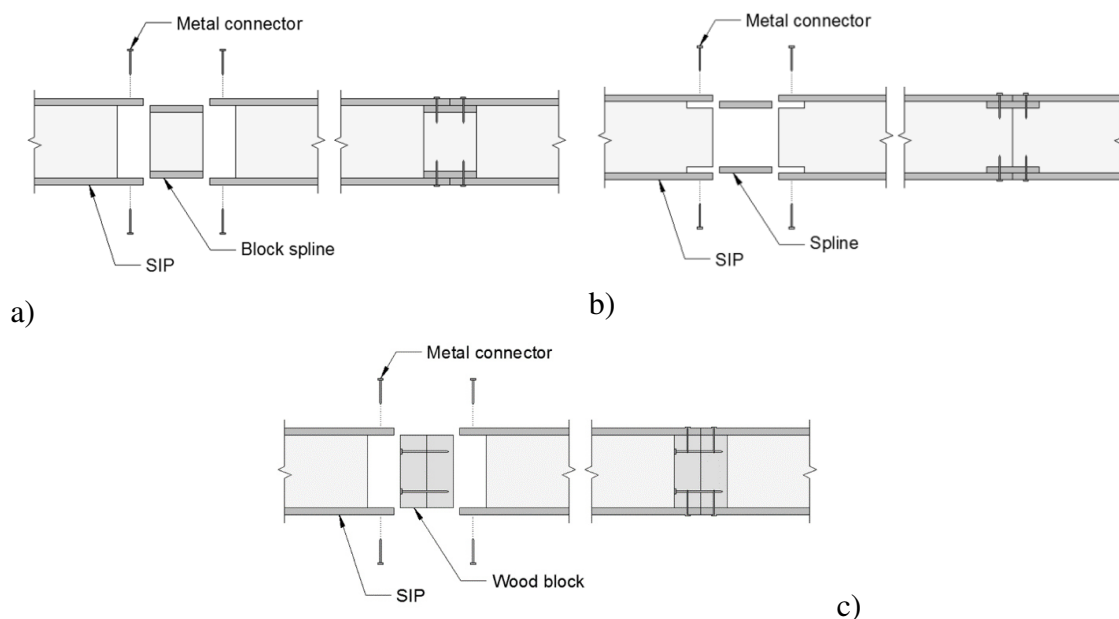
Figure 9-11 – Spline connection between SIP panels: a) SIP block; b) wood layer; c) wood block.

The main advantage of this connection when using a SIP block or wood strip as spline is the minimization of thermal bridging; however, it is structurally more limited than using a wood block due to the lower penetration depth of the connectors.

9.2.11 Corner wall connection with screws and wood stripes - SIP

This type of connection, used to join SIP walls, is achieved by profiling the cores of the wall panels and filling them with a wood stripe attached by metal connectors. The panels are then connected to each other through screws (Figure 9-12).
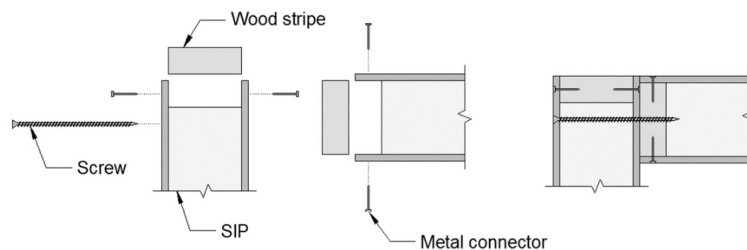
Figure 9-12 - Corner wall connection with screws and wood stripes between SIPs.

9.2.12 Wall-to-floor-to-wall connection with screws and wood stripes - SIP

This type of connection is similar to the one described previously (section 9.2.11): the panels are profiled and wood stripes/blocks are inserted, and the joints are ensured by metal connectors (Figure 9-13).
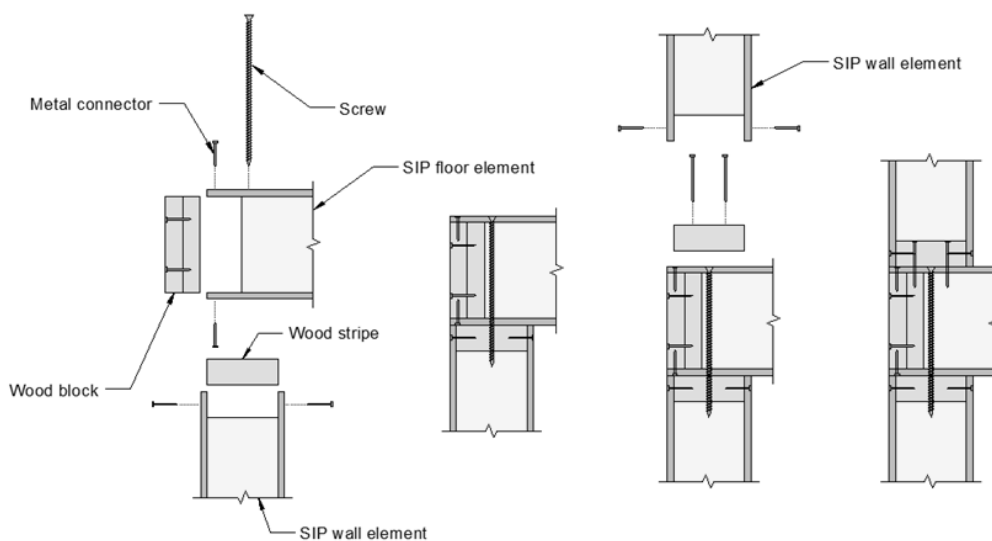
Figure 9-13 - Wall-to-floor-to-wall connection with screws and wood stripes between SIPs.

9.2.13 Wall-to-foundation bolted connection - SIP

This type of connection is achieved by fixing a treated sill plate with an anchor bolt to the concrete foundation. The wall panel, previously profiled in the core, is then placed over the plate and is laterally fixed to it through metal connectors (Figure 9-14).
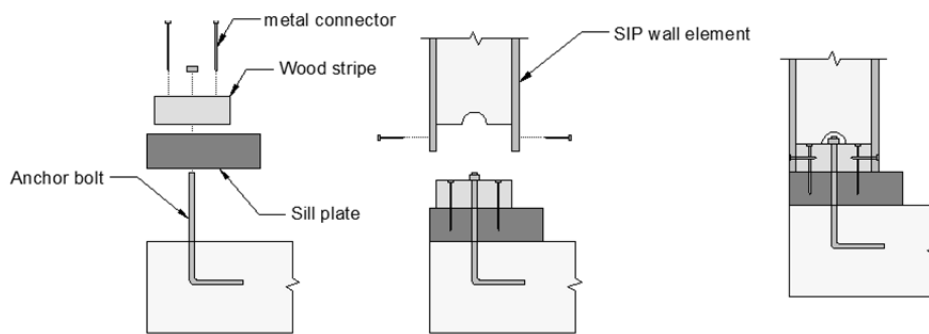
Figure 9-14 – SIP wall-to-foundation bolted connection.

9.3 Proposed connections systems

In this section, a series of conceptualized connection systems to connect the developed panels, (i) among them and (ii) to existing masonry or concrete structures are presented.

The connections developed and further described including the following:

- Screws driven in angle;
- Half-lapped joint;
- Single internal spline;
- Double internal spline;
- Single external spline;
- Double external spline;
- Multiple spline;
- Internal SIP spline;
- Hybrid spline and SIP beam;
- Screws, nails and splines for angle connections;
- Angle bracket;
- Beam and screws;
- Concealed plate;
- 45º profiled panels with angle brackets;
- Wall-to-concrete foundation – anchor bolt;

- Wall-to-concrete/masonry foundation or wall-to-concrete/masonry wall – angle bracket;
- Wall-to-concrete/masonry foundation or wall-to-concrete/masonry wall – concealed plate;
- Wall-to-concrete/masonry foundation or wall-to-concrete/masonry wall – straight plate;
- Floor-to-concrete/masonry wall – angle bracket.

Notice that in some cases, the developed connections to join CIT panels can also be used to join CIT panels to CLT panels, due to the similarities of the two panel systems.

9.3.1 Screws driven in angle

This connection is made through the use of screws driven in angle into the surface of the panels and can be applied to wall-to-wall or lateral floor-to-floor connections (Figure 9-15), and also to corner wall-to-wall or wall-to-floor connections (Figure 9-16).
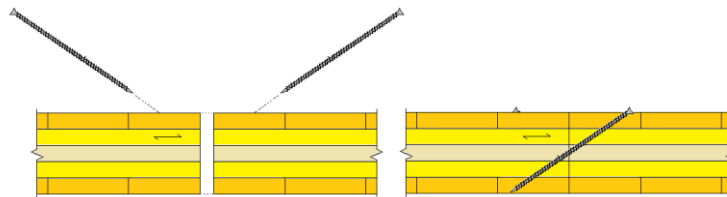
Figure 9-15 – Screws driven in angle solution for aligned wall-to-wall or lateral floor-to-floor connections.
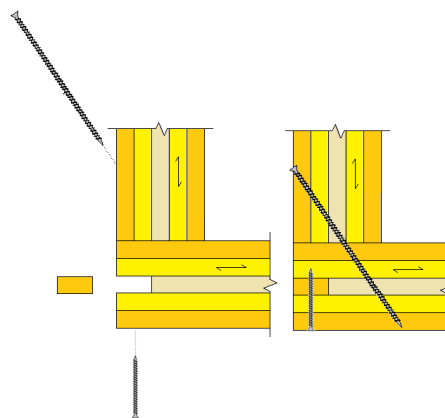
Figure 9-16 – Screws driven in angle solution for corner wall-to-wall or wall-to-floor connections.

This type of connections has the advantage that they are easy to produce and only require

screws/nails, besides the timber spline in the corner wall-to-wall or wall-to-floor connections.

In both the corner wall-to-wall and wall-to-floor connections, a timber spline is placed along the edge of the panel where the insulation layer would be visible, so that fire protection of such layer is achieved. In the case of the wall-to-floor connection, that same timber piece is also used to transmit the vertical load along the cross-section of the floor through wood elements (that are stiffer than the insulation), thus avoiding local deformation (including creep) of the foam. It should be noticed that the width of the spline depicted in Figure 9-16 can be extended up to the limit of the right wood layer so that maximum stiffness is reached. However, such an option means less thermal efficiency due to increased thermal bridging.

9.3.2 Half-lapped joint

To produce the half-lapped joint connections, the profiling of the panel edges is necessary (Figure 9-17). The connection is then ensured by screws (floor-to-floor connection) or also by nails (in the case of wall-to-wall connections).

To avoid the premature formation of plastic hinges on the wall-to-wall connections (subjected to shear), an inner timber spline is placed to avoid such issue (Figure 9-18); however, this detail affects negatively the thermal insulation. Also, in the case of floor-to-floor connections, a similar solution can be used to avoid an increase of the lapped area and the corresponding stress concentration in the foam (that would result in excessive deformation of the foam).
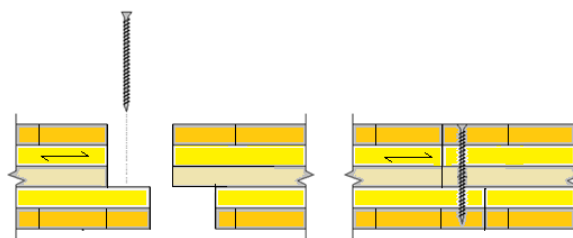
Figure 9-17 – Half-lapped joint for aligned wall-to-wall or floor-to-floor connections.
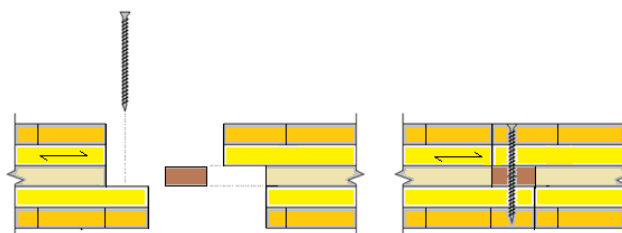
Figure 9-18 – Half-lapped joint with inner timber lath for wall-to-wall or lateral floor-to-floor connection.

9.3.3 Single internal spline

This system can be used for wall-to-wall or lateral floor-to-floor connections (Figure 9-19).

Figure 9-19 – Single internal spline solutions for aligned wall-to-wall or lateral floor-to-floor connections: a) spline with a thickness equal to the corresponding layer's one and full-length fasteners; b) same solution with alternate single-shear planes; c) spline with larger thickness and full-length fasteners; d) same solution with alternate single-shear planes.

Four variations of this connection are proposed: a) and b), which are made through the use of a timber spline in place of the insulation layer, differing only in the placement of the fasteners; and c) and d), which are made through the use of a timber spline in place of the insulation layer and part of the inner wood layers. The last configurations, c) and d), may be advantageous when more thickness for the spline is required for the shear

connection (wall-to-wall connection). Depending on the load requirements, the option of using alternate and partial-length fasteners (one-shear plane), as in variations b) or d), may be more economical than using the full-length fasteners, as in variations a) and c), which correspond to double shear plane solutions.

In general, this system has the advantage of being a stiff connection; however, in this system thermal bridges cannot be avoided.

9.3.4   Double internal spline

This solution is intended to connect aligned wall panels or floor elements (Figure 9-20) using either long fasteners through the whole section (solution a)) or smaller fasteners connecting only the wood elements (solution b)).
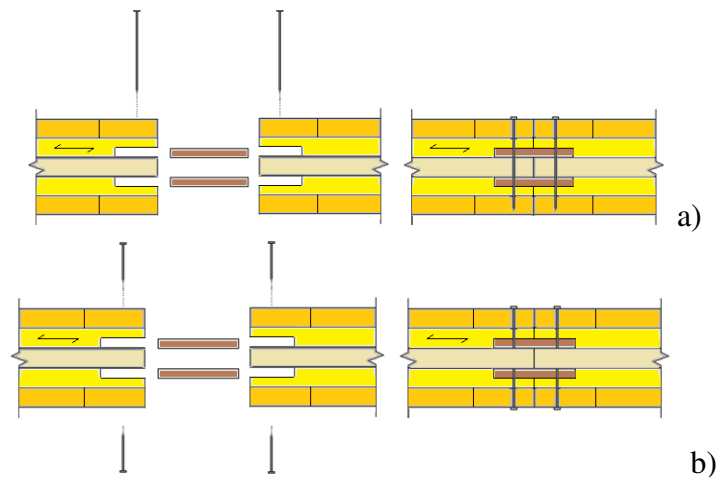
Figure 9-20 – Double internal spline solution for aligned wall-to-wall or lateral floor-to-floor connections: a) with full length fasteners; b) with partial length fasteners (single shear planes).

The advantage of this connection, especially of solution b), is that thermal bridging is avoided. Instead, solution a) may be easier to produce in practice, when there is access only to one of the sides of the panels to mount. In the case of the floor-to-floor connection, to increase the stiffness of the connection, an extended profiled area may be necessary to either increase the width of the spline, to increase the diameter of the connectors (which also would require larger distances to the spline edges to avoid splitting) or even to add another row of connections on each panel.

The disadvantage of this connection is that it may be difficult to process. To obtain the profiled shape of the panels to connect, it is often necessary to leave *a priori* the 'empty

spaces' (which the splines would then fill) during the panel assembly. In this case, the profiling by milling operations on the finished panels would not be feasible, as the polyurethane foam is glued to the wood, and thus it would not be possible to keep the polyurethane layer intact.

9.3.5   Single external spline

The single external spline solution can be used to connect aligned wall-to-wall connections, and in this case, four variations are proposed (Figure 9-21). The use of fasteners through the whole cross-section (solutions b) and d)) is justified if higher contact area between the connectors and the wood layers whose grain direction is parallel to the shear plane is required to resist higher solicitations (it should be noticed that the wood strength along the grain direction is much higher than in a normal direction). For the same reason, the spline with a thickness smaller than the one of the layer where it is inserted (solutions c) and d)) may be used.
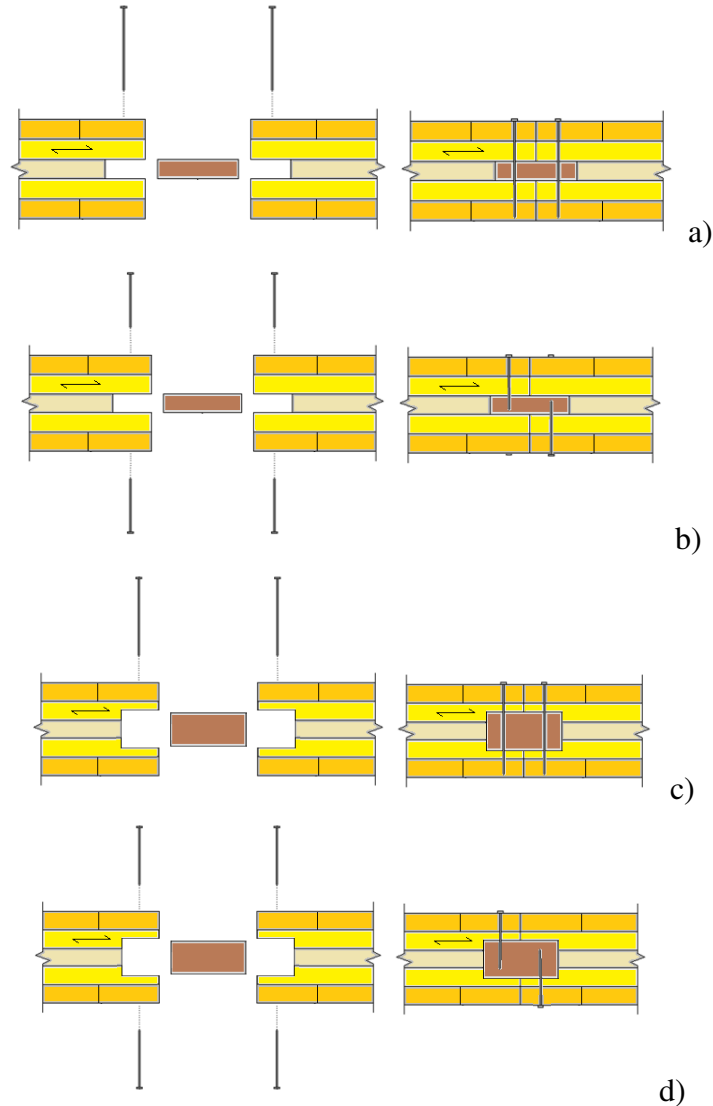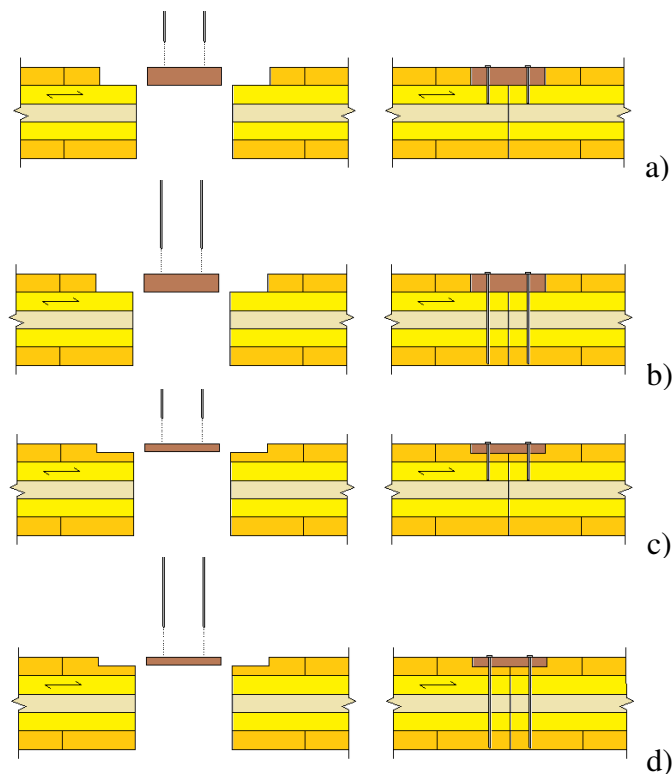

Figure 9-21 – Single external spline solution for aligned wall-to-wall connection: a) spline with a thickness equal to the one of the layer where it is inserted and partial-length fasteners; b) same solution with full length fasteners; c) spline with a thickness smaller than the one of the layer where it is inserted and partial-length fasteners; d) same solution with full length fasteners.

The advantages of this connection are that only few and simple profiling of the panels is required and thermal bridging is avoided in the case of solutions a) or c). The main disadvantage is related to the fact that it has only one shear plane per panel, and consequently this connection is less resistant than a double spline connection.

9.3.6   Double external spline

This connection system is similar to the previous one, but has one spline at each side of the panels (Figure 9-22).
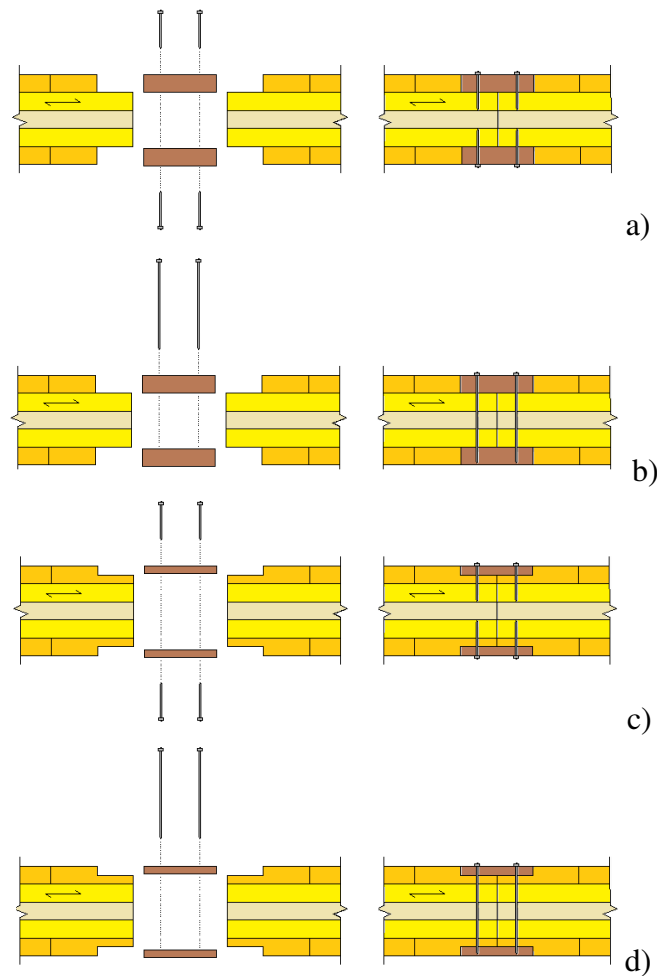
Figure 9-22 – Double external spline solution for aligned wall-to-wall or lateral floor-to-floor connections: a) splines with thicknesses equal to the ones of the layers where they are inserted and partial-length fasteners; b) same solution with full length fasteners; c) splines with thicknesses smaller than the ones of the layers where they are inserted and partial-length fasteners; d) same solution with full length fasteners.

Four alternative connection layouts (a) to d)) are proposed. The choice of using partial length fasteners (single shear planes, solutions a) and c)) or full length fasteners (double

shear planes, solutions b) and d)), in practice may depend on whether there is access to only one of the sides of the panels to mount. The solutions with a spline with thickness smaller than the one of the layer where they are inserted (solutions c) and d)) may be justified if higher contact area between the connectors and the wood layers whose grain direction is parallel to the shear plane is required to resist higher load demands.

Besides the thermal efficiency of solutions a) and c), the advantage of this connection when compared to the single spline is that increased strength and stiffness are obtained because the connection system offers a double shear plane. As a disadvantage, it requires more machining for the additional profile.

9.3.7 Multiple spline

This connection system (Figure 9-23) is intended to increase the number of shear planes with respect to the double spline connection, and can make use of full-length connectors (solution a)) or smaller connectors that only penetrate on the wood layers. Solution a) may be preferable when, in practice, there is access to only one of the sides of the panels to mount.

a)

b)
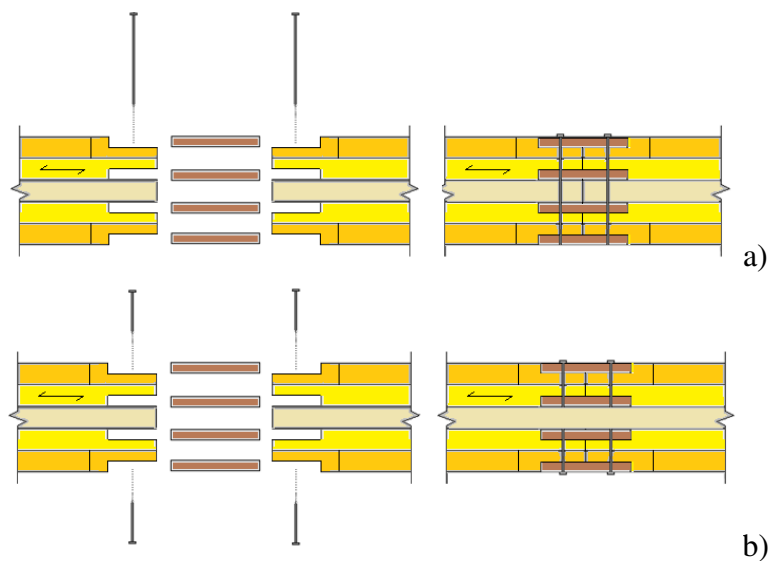
Figure 9-23 – Multiple spline solution for aligned wall-to-wall or lateral floor-to-floor connections: a) with full-length fasteners; b) with partial length fasteners (double shear planes).

Besides its structural capability, this connection system has the same advantages of the previous systems, but it was the disadvantage that more complex profiling of the panels is required.

9.3.8 Internal SIP spline

The internal SIP spline connection (Figure 9-24) is similar to the previously presented single spline connection, but it has the advantage of having an insulation layer embedded in the spline piece. Additionally, fully (a)) or partially (b)) inserted connectors can be used. Solution a) may be preferable when, in practice, there is access to only one of the sides of the panels to mount.
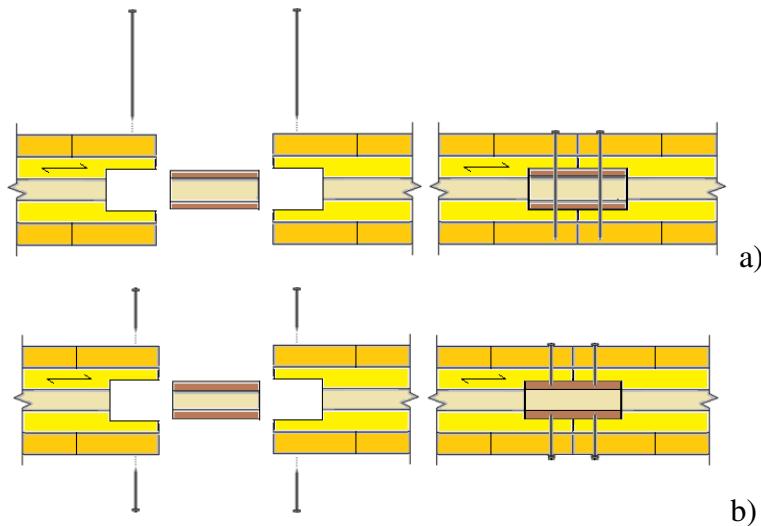
Figure 9-24 - Internal SIP spline solution for aligned wall-to-wall or lateral floor-to-floor connection: a) with full-length fasteners (double shear planes); b) with partial length fasteners (single shear planes).

The advantage of this system is that thermal bridging is limited (solution a)) or even avoided (solution b)).

9.3.9 Hybrid spline and SIP beam

The proposed system (Figure 9-25) is a combination of the multiple spline and internal SIP spline connection systems. Fully (a)) or partially (b)) inserted connectors can be used. Solution a) may be preferable when, in practice, there is access to only one of the sides of the panels to mount.

This system has the same advantages of the multiple spline solution and it involves easier profiling of the panels, as no insulation "tongue" needs to be created.
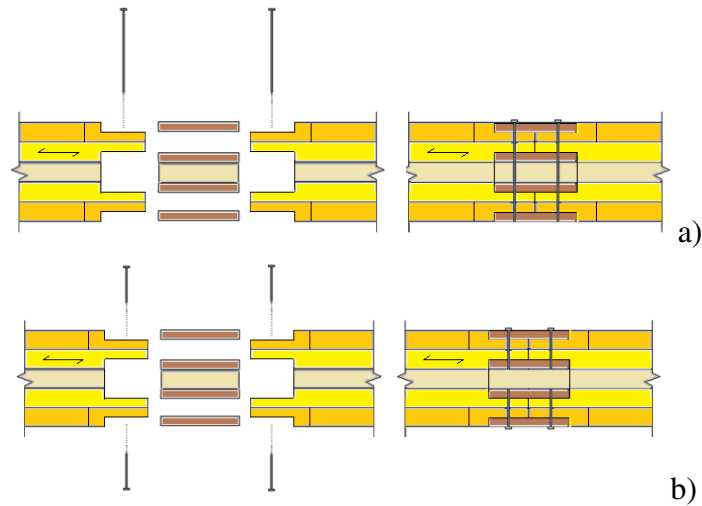
Figure 9-25 – Hybrid spline and SIP beam solution for aligned wall-to-wall or lateral floor-to-floor connections: a) with full-length fasteners; b) with partial length fasteners (double shear planes).

9.3.10 Screws, nails and splines for angle connections

A solution that makes use of screws, nails and splines for angle connections is proposed either for corner wall-to-wall or floor-to-wall connections (Figure 9-26).
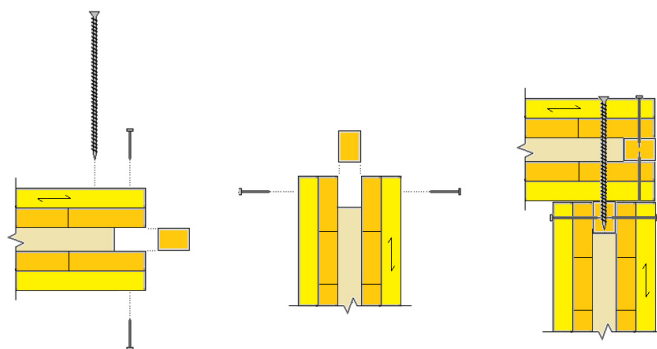
Figure 9-26 – Screws, nails and splines solution for corner wall-to-wall or floor-to-wall connections.

This type of connection has as main advantages its easy production and the fact that it only requires screws/nails, besides the timber spline.

9.3.11 Angle bracket

Metal angle brackets can be used to connect corner wall-to-wall or wall-to-floor elements

(Figure 9-27).
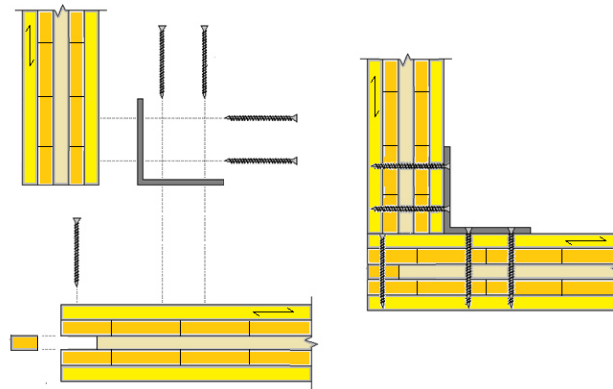
Figure 9-27 – Angle bracket solution for corner wall-to-wall or wall-to-floor connection.

In the case that both walls are end elements or the floor is not continuous, a wood spline is used along the edge of the profiled panel for increased fire safety, as shown in Figure 9-27. The screws are driven until the external wood layers; however, they can also be driven only until the inner wood layers of the panels, avoiding thermal bridging. However, such a solution is structurally more limited due to the increased stress that results from the smaller wood area mobilized.

A similar connection system can be used to connect a corner wall-to-wall intersection, or, in the case of balloon type construction, a floor-to-wall according to the scheme of Figure 9-28.
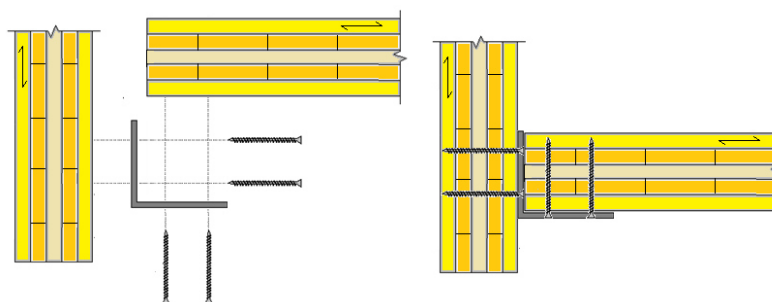
Figure 9-28 – Angle bracket solution for wall-to-wall intersection or wall-to-floor connections.

The main advantage of this last system is that if a replacement of the floor element is needed (e.g. due to deterioration from a biological attack), the floor element can be entirely removed without interfering with the remaining structure (which would occur in the platform type construction).

9.3.12 Beam and screws

This system is quite similar to the previous one, with the difference that a wood beam is used instead of a metal bracket (Figure 9-29).
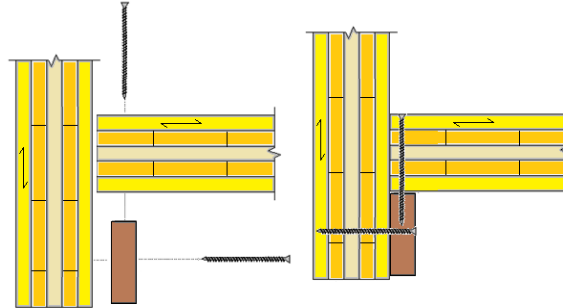
Figure 9-29 – Beam and screws solution for wall-to-floor connection.

The horizontal screws can also be driven only until the inner wood layers of the panels, thus avoiding thermal bridging, but in that case reducing stiffness and strength. An advantage of this system is its simplicity and, moreover, it only requires wood beams and screw fasteners.

9.3.13 Concealed plate

This solution could be used to connect a wall-to-wall intersection (Figure 9-30) or a wall-to-floor (Figure 9-31). An advantage of this system is that the metal plate is fully covered by wood in a fire situation (with exception of the base perimeter). As a disadvantage, this system requires the use of intermediary wood elements between the steel plate and the panel to ensure perfect fit. Another relevant disadvantage is related to the thermal bridging that might occur through the screws that cross the insulation layer.
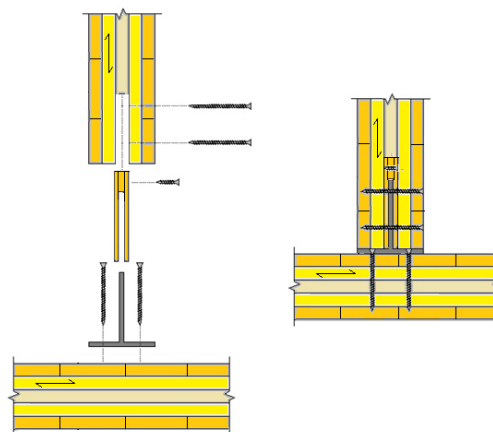
Figure 9-30 – Concealed plate solution for wall-to-wall intersection connection.
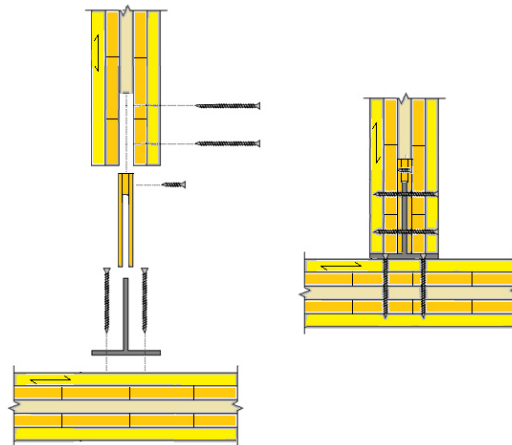
Figure 9-31 – Concealed plate solution for wall-to-floor connection.

9.3.14 45º profiled panels with angle brackets

This solution could be used to connect walls at angle (corner walls) (Figure 9-32).
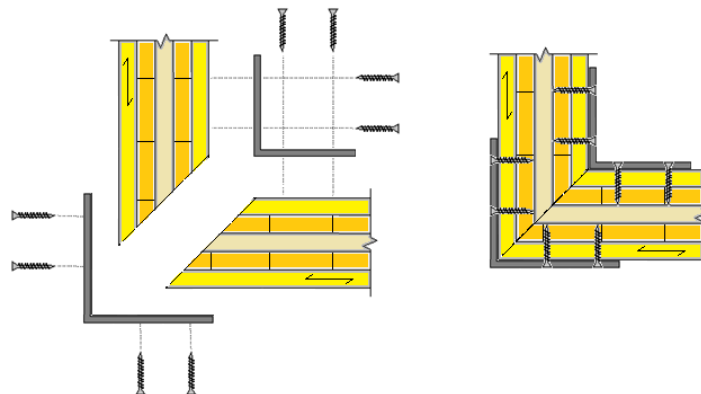
Figure 9-32 - 45º profiled panels with angle brackets

The advantage of this connection is that thermal bridging is significantly reduced (even avoided if in practice no gaps are left between the panels). A possible disadvantage of this connection is that it requires precision on the placement at the building site so that the panels fit on each other (i.e. with no gaps); otherwise, they would need to be rectified *in situ*.

9.3.15 Wall-to-concrete foundation - Anchor bolt

This type of connection (Figure 9-33) is the same previously presented for SIP-to-

foundation connections, but instead of the SIP panel, a CIT panel is used.
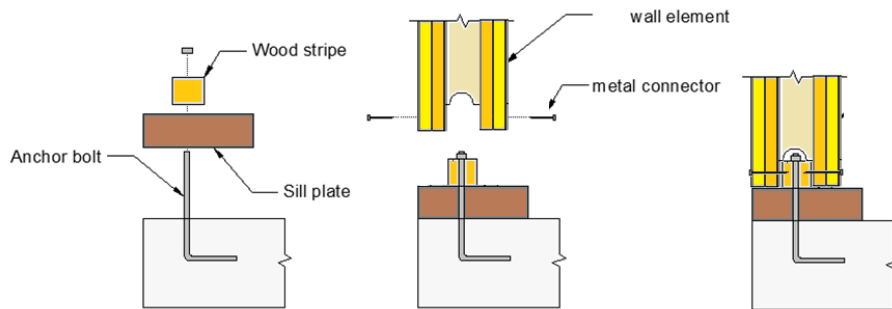
Figure 9-33 – Anchor bolt connection for wall-to-concrete foundation.

Due to the use of a wood stripe as bottom rail, this solution may be structurally more limited than other solutions due to the risk of splitting, as stresses perpendicular to grain occur at the timber element.

9.3.16 Wall-to-concrete/masonry foundation or wall-to-concrete/masonry wall – Angle bracket

This type of connection (Figure 9-34) is the same previously presented for CLT-to-foundation connection using an angle bracket, but instead of the CLT panel, a CIT panel is used.
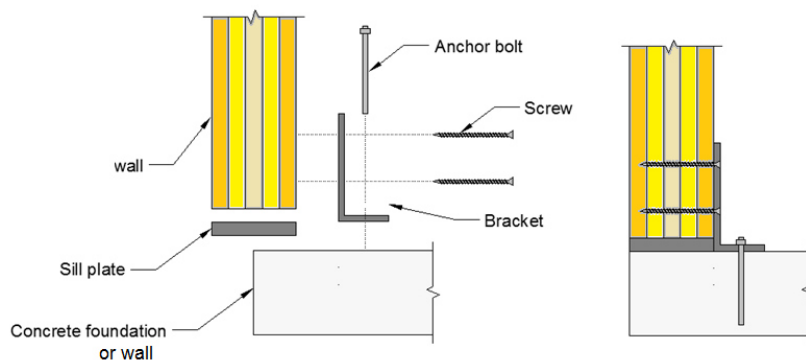
Figure 9-34 – Angle bracket connection for wall-to-concrete/masonry foundation or wall-to-concrete/masonry wall.

9.3.17 Wall-to-concrete/masonry foundation or wall-to-concrete/masonry wall – concealed plate

This type of connection (Figure 9-35) is the same previously presented for CLT-to-foundation connections using a concealed plate, but instead of the CLT panel, a CIT panel is used. This system requires the use of intermediary wood elements between the steel plate and the panel to ensure a perfect fit.
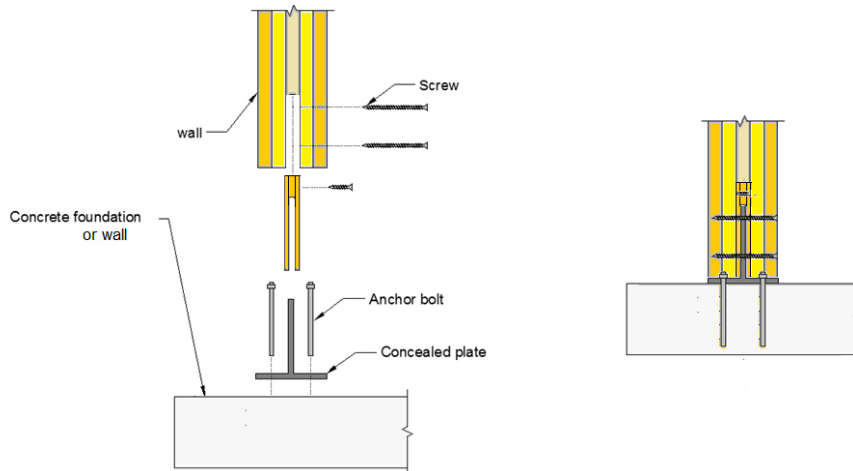
Figure 9-35 – Concealed plate bracket connection for wall-to-concrete/masonry foundation or wall-to-concrete/masonry wall.

9.3.18 Wall-to-concrete/masonry foundation or wall-to-concrete/masonry wall – straight plate

This type of connection (Figure 9-36) is the same previously presented for CLT-to-foundation connection using a straight plate, but instead of the CLT panel, a CIT panel is used.
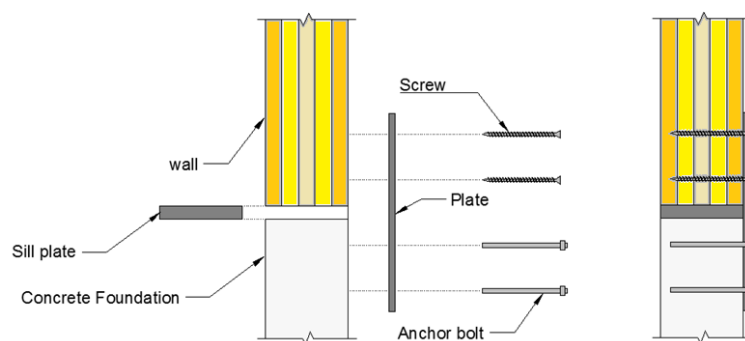
Figure 9-36 - Straight plate connection for wall-to-concrete/masonry foundation or wall-to-concrete/masonry wall.

9.3.19 Floor-to-concrete/masonry wall – angle bracket

This type of connection (Figure 9-37) is equal to the one presented for wall-to-concrete/masonry foundation or wall-to-concrete/masonry wall connections with an angle bracket.
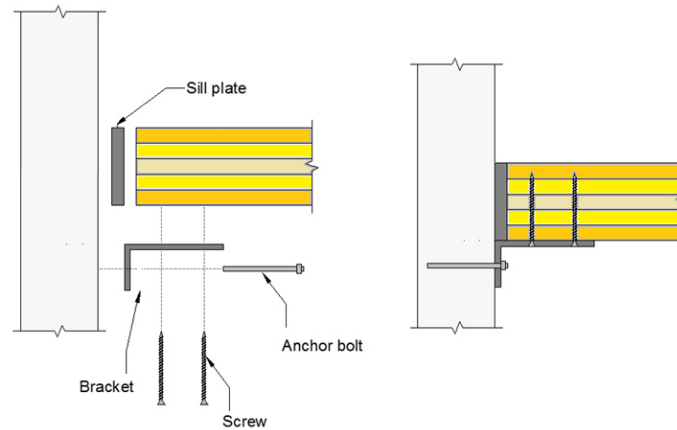
Figure 9-37 – Angle bracket connection for floor-to-concrete/masonry wall.

9.4 Lateral load-carrying capacity of metal dowel-type fasteners

Regarding the definition of the failure modes of hybrid-layer panels like CLT, two approaches can be used: (i) the derivation of load carrying capacity formulas by taking into account the layered structure of the panels, according to Johansen's yield theory (Johansen, 1949); or (ii) the use of load carrying capacity formulas derived for homogeneous timber elements, as in Eurocode 5 (CEN, 2004b), but where the embedment strength and withdrawal capacity values are estimated for the multi-layered CLT, instead of solid wood. According to (Uibel and Blass, 2006), the first option results in a complex calculation, even just for three-layer panels; moreover, the resulting models do not account for the variability of the density among the CLT layers, as well for the gaps between lamellas. So, based on that, the second option is of easy application for practical purposes; in the literature, a series of empirical formulas for the estimation of the embedment strength and withdrawal capacity of CLT-type elements have been proposed.

According to Johansen's yield theory (Johansen, 1949), and depending on the failure mode, the load-carrying capacity ($F_{v,R}$) of timber-to-timber or steel-to-timber connections depends on the following parameters: the diameter of the connector (d), the thickness of the timber (t_1 or t_2) and/or steel (t) element(s), the embedment strength of the timber element(s) ($f_{h,1}$ or $f_{h,2}$), the withdrawal capacity of the fastener ($F_{ax,R}$) and the yield

moment of the fastener ($M_{y,R}$). The characteristic lateral load-carrying capacity ($F_{v,Rk}$) for timber-to-timber and timber-to-steel connections according to Eurocode 5 are presented in Table 9-1 and Table 9-2. Notice that $\beta = f_{h,2}/f_{h,1}$. In the referred tables, the element filled in blank corresponds to the member 1 and the element filled with dashes corresponds to element 2.

Table 9-1 - Characteristic lateral load carrying capacity ($F_{v,Rk}$) for timber-to-timber connections.
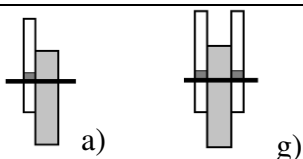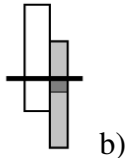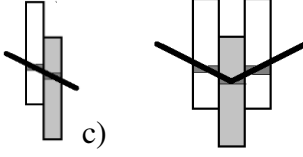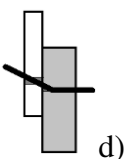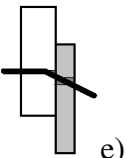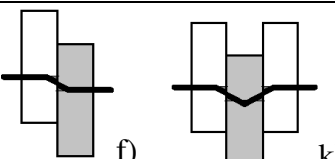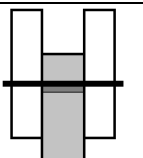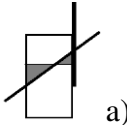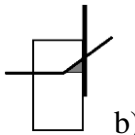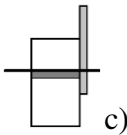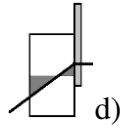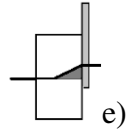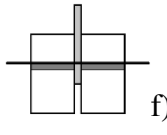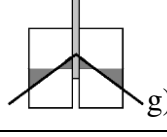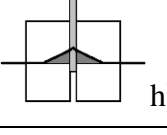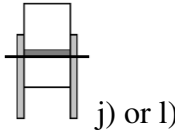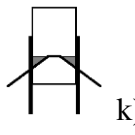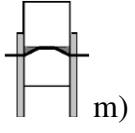
$F_{v,Rk}$	Failure mode
$f_{h,1,k} t_1 d$	a) g)
$f_{h,2,k} t_2 d$	b)
$\dfrac{f_{h,1,k} t_1 d}{1+\beta}\left[\sqrt{\beta + 2\beta^2\left[1+\dfrac{t_2}{t_1}+\left(\dfrac{t_2}{t_1}\right)^2\right] + \beta^3\left(\dfrac{t_2}{t_1}\right)^2} - \beta\left(1+\dfrac{t_2}{t_1}\right)\right] + \dfrac{F_{ax,Rk}}{4}$	c) j)
$1.05\dfrac{f_{h,1,k} t_1 d}{2+\beta}\left[\sqrt{2\beta(1+\beta) + \dfrac{4\beta(2+\beta)M_{y,Rk}}{f_{h,1,k} t_1^2 d}} - \beta\right] + \dfrac{F_{ax,Rk}}{4}$	d)
$1.05\dfrac{f_{h,1,k} t_2 d}{1+2\beta}\left[\sqrt{2\beta^2(1+\beta) + \dfrac{4\beta(1+2\beta)M_{y,Rk}}{f_{h,1,k} t_2^2 d}} - \beta\right] + \dfrac{F_{ax,Rk}}{4}$	e)
$1.15\sqrt{\dfrac{2\beta}{1+\beta}}\sqrt{2M_{y,Rk} f_{h,1,k} d} + \dfrac{F_{ax,Rk}}{4}$	f) k)
$0.5 f_{h,2,k} t_2 d$	h)

Table 9-2 - Characteristic lateral load carrying capacity ($F_{v,Rk}$) for steel-to-timber connections.

$F_{v,Rk}$	Failure mode
$0.4 f_{h,k} t_1 d,$ if $t \leq 0.5d$	a)
$1.15\sqrt{2M_{y,Rk} f_{h,k} d} + \frac{F_{ax,Rk}}{4},$ if $t \leq 0.5d$	b)
$f_{h,k} t_1 d,$ if $t \geq d$	c)
$f_{h,k} t_1 d \left[\sqrt{2 + \frac{4M_{y,Rk}}{f_{h,k} t_1^2 d}} - 1 \right] + \frac{F_{ax,Rk}}{4},$ if $t \geq d$	d)
$2.3\sqrt{M_{y,Rk} f_{h,k} d} + \frac{F_{ax,Rk}}{4},$ if $t \geq d$	e)
$f_{h,1,k} t_1 d$	f)
$f_{h,1,k} t_1 d \left[\sqrt{2 + \frac{4M_{y,Rk}}{f_{h,1,k} t_1^2 d}} - 1 \right] + \frac{F_{ax,Rk}}{4}$	g)
$2.3\sqrt{M_{y,Rk} f_{h,1,k} d} + \frac{F_{ax,Rk}}{4}$	h)
$0.5 f_{h,2,k} t_2 d$	j) or l)
$1.15\sqrt{2M_{y,Rk} f_{h,2,k} d} + \frac{F_{ax,Rk}}{4},$ if $t \leq 0.5d$	k)
$2.3\sqrt{M_{y,Rk} f_{h,2,k} d} + \frac{F_{ax,Rk}}{4},$ if $t \geq d$	m)

As referred before, the adaptation of the EC5 load-carrying capacity formulas (which are valid for homogeneous timber elements) to CLT is made through the replacement of the embedment strength (f_h) and withdrawal capacity ($F_{ax,R}$) for homogeneous solid wood by corresponding values for the multi-layered CLT structure. Regarding such parameters, empirical models that are found in the state-of-the-art are presented in the next section.

9.5   Embedment strength of dowels, nails and screws in CLT panels

9.5.1   Fasteners inserted perpendicular to grain and to CLT panels' surface (plane joint)

Two models were presented by (Uibel and Blass, 2013) for the determination of the embedment strength (f_h) of dowels inserted perpendicularly to the grain and to CLT panels' surface, also known as plane joint (Figure 9-38). One of the models is independent of the build-up of the panels, Equations (9-1) and (9-2); while the other accounts for the layup of a multi-layered panel, Equation

(9-3). Notice that some of the equations are presented considering the mean value (f_h), while others indicate the design (characteristic) value ($f_{h,k}$).
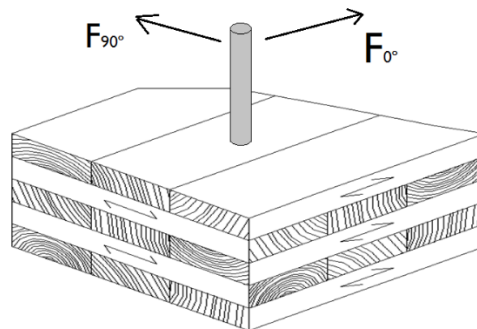
Figure 9-38 – Plane joint in CLT panel: dowel inserted perpendicularly to grain and normal to the panels' surface. Adapted from (Uibel and Blass, 2013).

$$f_h = \frac{0.035(1 - 0.015d)\rho^{1.16}}{1.1 \sin^2(\alpha) + \cos^2(\alpha)} \tag{9-1}$$

$$f_{h,k} = \frac{0.031(1 - 0.015d)\rho_k^{1.16}}{1.1 \sin^2(\alpha) + \cos^2(\alpha)} \tag{9-2}$$

$$f_h = 0.032(1 - 0.015d)\rho^{1.20} \left[\frac{\sum_{i=1}^{n} t_{0,i}}{t(1.6\sin^2(\alpha) + \cos^2(\alpha))} + \frac{\sum_{j=1}^{n-1} t_{90,j}}{t(1.6\cos^2(\alpha) + \sin^2(\alpha))} \right]$$

(9-3)

In Equations (9-1) to

(9-3) the index k represents the characteristic value; f_h is the embedment strength (N/mm^2); d is the dowel diameter (mm); ρ is the wood panel density (kg/m^3); α is the angle between the load and the grain direction of the outer layer (º); t is the panel thickness; $\sum_{i=1}^{n} t_{0,i}$ is the sum of the thickness of the layers with the same grain direction of the outer layers (mm); $\sum_{j=1}^{n-1} t_{90,j}$ is the sum of the thickness of the layers with the grain direction in the orthogonal direction to the outer layers (mm). According to Uibel and Blass (2006), the referred equations are valid for panels with a maximum layer thickness of 40 mm and for $0.95 < \sum_{i=1}^{n} t_{0,i}/\sum_{j=1}^{n-1} t_{90,j} < 2.10$.

A model to predict the embedment strength of threaded fasteners (lag and self-drilling screws with diameters between 6 and 19 mm) inserted in CLT, independent of the build layup, was proposed by Kennedy et al (2014) and is shown in Equation (9-4).

$$f_h = \frac{80(\rho - 0.12)^{1.11}}{1.07(\rho - 0.12)^{-0.07}\sin^2\alpha + \cos^2\alpha}$$

(9-4)

A model for the determination of the embedment strength of nails/screws in CLT plane joints was proposed by Uibel and Blass (2006) and is shown in Equations (9-5) and (9-6):

$$f_h = 0.13d^{-0.53}\rho^{1.05}$$

(9-5)

$$f_{h,k} = 0.112d^{-0.5}\rho_k^{1.05}$$

(9-6)

where f_h is the embedment strength (N/mm^2); d is the nail/screw diameter (mm). The equation is referred to be valid for panels with layers thickness up to 7 mm.

Dong et al (2019) proposed an expression that is dependent on the ratio between the thickness of the transverse and longitudinal layers (r), in addition to the density, diameter and loading angle - Equations (9-7) and (9-8).

$$f_h = 0.3364(0.4541 - 0.0205d)\rho \left(\cfrac{r}{1.4101 \cos^2 \alpha + \sin^2 \alpha} + \cfrac{1-r}{1.4101 \sin^2 \alpha + \cos^2 \alpha} \right) \tag{9-7}$$

$$f_{h,k} = 0.2575(0.4541 - 0.0205d)\rho_k \left(\cfrac{r}{1.4101 \cos^2 \alpha + \sin^2 \alpha} + \cfrac{1-r}{1.4101 \sin^2 \alpha + \cos^2 \alpha} \right) \tag{9-8}$$

9.5.2 Fasteners inserted parallel to the grain in the edges of CLT panels (edge joint)

For the determination of the embedment strength of dowels inserted in parallel to the grain in the edges of CLT panels or edge joints (Figure 9-39), Uibel and Blass (2007) proposed a model described by Equations (9-9) and (9-10).
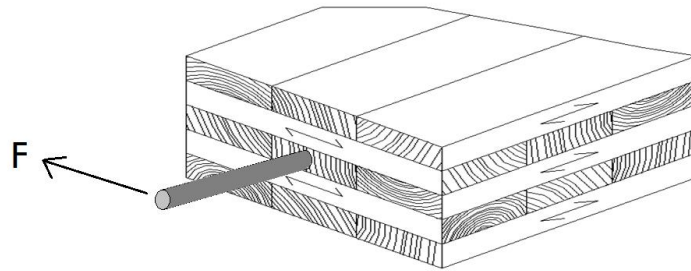
Figure 9-39 - Edge joint in CLT panel: dowel inserted in parallel to the grain in the edge of a CLT panel. Adapetd from (Uibel and Blass, 2007).

$$f_h = 0.049(1 - 0.017d)\rho_{layer}^{0.91} \tag{9-9}$$

$$f_{h,k} = 0.0435(1 - 0.017d)\rho_{layer,k}^{0.91} \tag{9-10}$$

In Equations (9-9) and (9-10), ρ_{layer} is the density of the layer(s) in which the dowel is applied (kg/m³) and $\rho_{layer,k}$ is the corresponding characteristic value.

As for dowels, also a model for nails/screws was proposed by Uibel and Blass (2007) for the determination of the embedment strength of CLT edge joints, which is described by Equations (9-11) and (9-12).

$$f_h = 0.8622d^{-0.46}\rho_{layer}^{0.56} \tag{9-11}$$

$$f_{h,k} = 0.862d^{-0.5}\rho_{layer,k}^{0.56}$$ (9-12)

9.6 Withdrawal strength of self-tapping screws in CLT

A model for the determination of the withdrawal capacity of self-tapping screws ($F_{ax,R}$) inserted perpendicularly to the grain and to the panels' surface as well in edge joints of CLT (Figure 9-40) was proposed by Uibel and Blass (2007) and is described by Equations (9-13) and (9-14).

a)   b)   c)
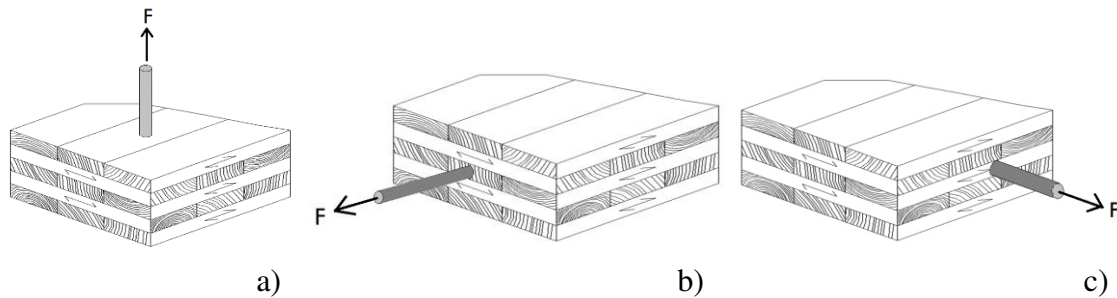
Figure 9-40 – Screws inserted in CLT panels: a) perpendicular to grain and to panels' surface; b) edge joint with screw inserted parallel to grain c) edge joint with screw inserted perpendicularly to grain. Adapted from (Uibel and Blass, 2007).

$$F_{ax,R} = \frac{0.44d^{0.8}l_{ef}^{0.9}\rho^{0.75}}{1.25\cos^2\beta + \sin^2\beta}$$ (9-13)

$$F_{ax,Rk} = \frac{0.35d^{0.8}l_{ef}^{0.9}\rho_k^{0.75}}{1.5\cos^2\beta + \sin^2\beta}$$ (9-14)

In Equations (9-13) and (9-14) the index k represents the characteristic value; $F_{ax,R}$ is in (N); d is the nominal screw diameter (mm); l_{ef} is the effective point-side penetration length (mm); β is the angle between the screw axis and the grain direction; ρ is the density either of the whole panel (case a) of Figure 9-40) or of the edge joints (cases b) and c) of Figure 9-40).

9.7 Experimental tests on wall-to-wall connections

9.7.1 Introduction

The single internal spline solution, variation b) of (Figure 9-19) was experimentally tested in shear, using a test setup based on standards EN 408 (CEN, 2012a) and EN 16351 (CEN, 2015). This connection was chosen due to its simplicity of execution and because it is a common solution to join CLT or SIP walls. The test setup is described next.

9.7.2 Materials and specimen preparation

For the tested connections, small-sized specimens were produced using two pairs of orthogonally glued wood layers (each layer with 10 mm thickness) that were connected to an inner spline made of Maritime pine solid wood (30 mm thickness) with metal screws (Figure 9-41). The wood material was visually inspected according to NP 4305 (IPQ, 1995), so that the strength class of the wood used to produce the specimens was at least C18. The layer thicknesses were defined based on one of the configurations tested in the mechanical tests of the panels (Chapter 5). For each connection between an orthogonal pair of wood layers and the spline (single shear plane), one line composed of three screws was used (all with 50 mm of length), resulting in a total of 4 shear planes and 12 connectors per specimen.
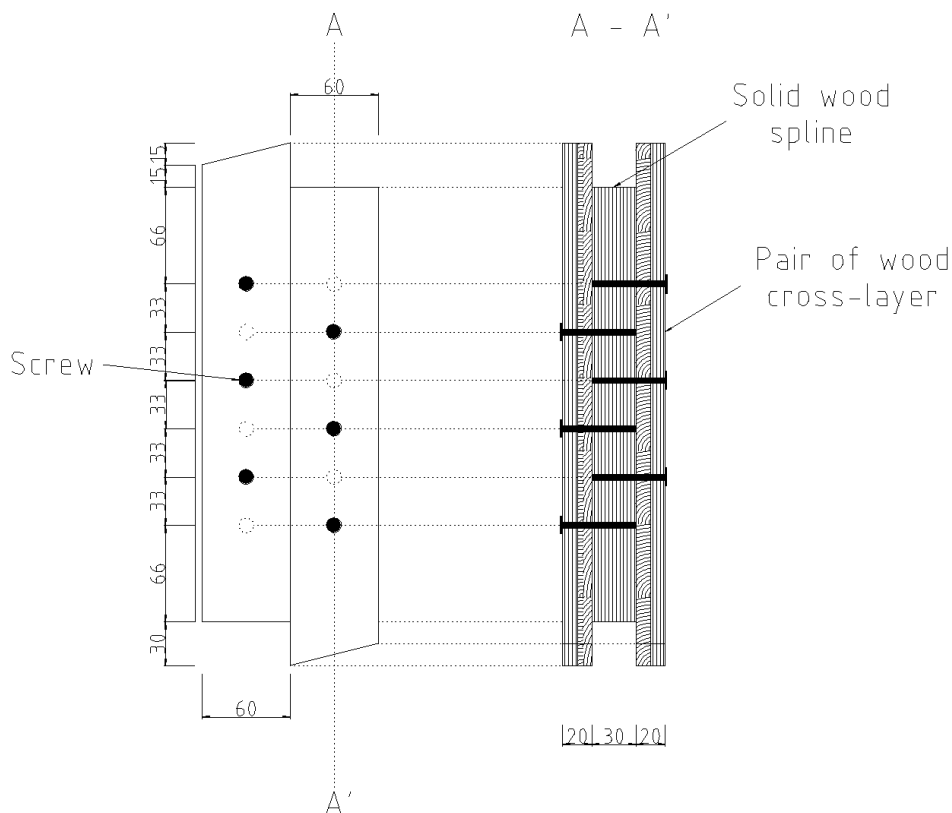
Figure 9-41 – Specimen layout and dimensions (in mm) of the single internal spline wall-to-wall connection.

Four nominal diameters were considered for the fasteners used in the connections between specimens: 3.5, 4.0, 4.5 and 5.0 mm. These diameters were defined based on typical diameters found for SIP wall assemblies. The screws were fully threaded and had a characteristic yield strength of 1000 N/mm^2. As required by EN 1995-1-1 (CEN, 2004b), the pre-drilling was performed on wood for the 4.0, 4.5 and 5.0 mm screws, with pre-diameter holes of 2.5 mm for the first and 3.0 mm for the last two. The screws were disposed in the specimens in a way that the minimum spacing between connectors and between connectors and edges of wood elements according to EN 1995 1-1 were fulfilled for the highest diameter of 5.0 mm (limiting one). Three specimens were tested for each screw diameter considered.

9.7.3 Experimental setup

The test setup was designed to simulate as close as possible the shear flow between two aligned CIT panels connected with an internal solid wood spline (Figure 9-42).
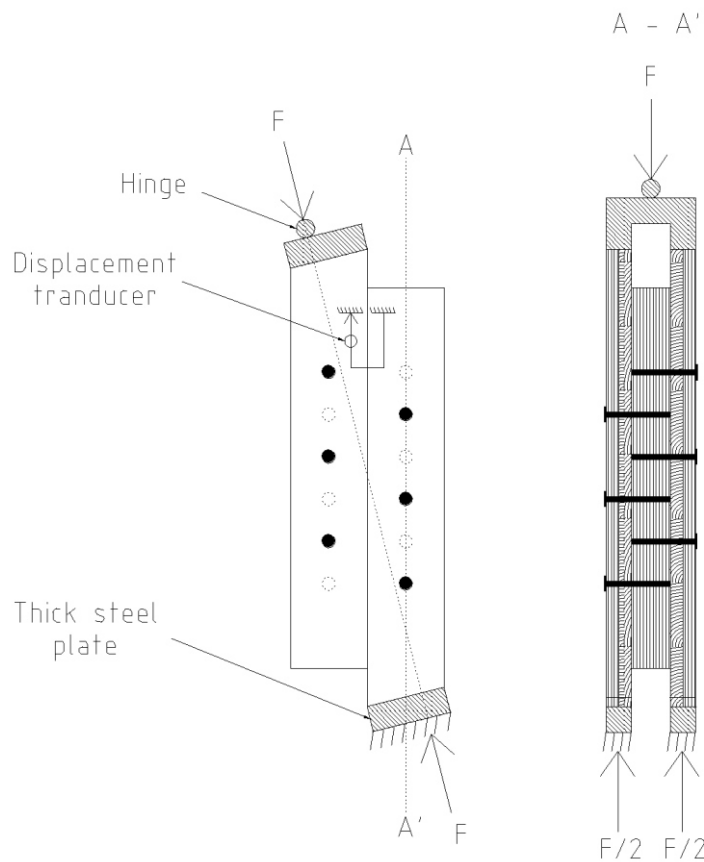
Figure 9-42 – Test layout for the developed connection system.

The force (F) was applied at a 14° angle to the vertical plane of the CIT panels. The shear force (F_v) per shear plane was calculated according to Equation (9-15).

$$F_v = \frac{F \cos(14°)}{2} \tag{9-15}$$

The force resisted by each connector was determined by dividing F_v by the effective number of connectors per line, according to EN 1995-1-1 indications.

The load was applied according to the EN 26891 (CEN, 1991) quasi-static protocol (Figure 9-43) and measured with a load cell with a capacity of 100 kN and precision of 0.01 kN.
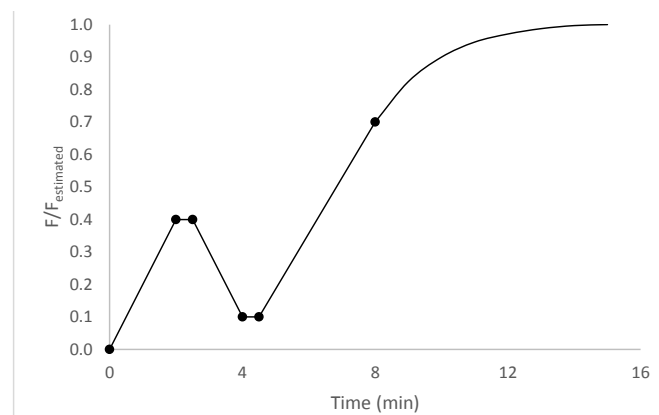
Figure 9-43 – Load protocol according to EN 26891 (CEN, 1991).

According to the referred standard, the maximum load is taken at a slip of 15 mm, if it does not occur before that value. The relative displacement between the adjacent cross-wood layers in each side was measured using *HBM* displacement transducers with a maximum capacity of 50 mm and a precision of 0.01 mm (Figure 9-44).
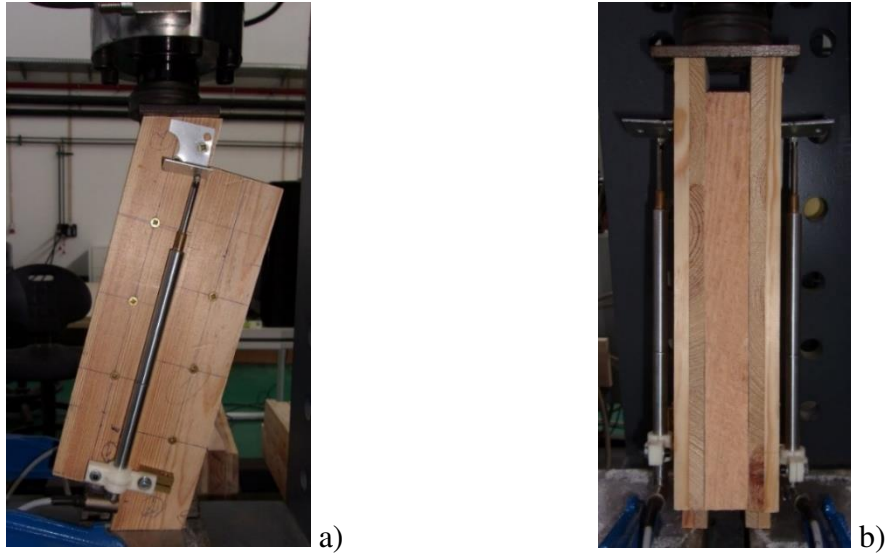
Figure 9-44 – Test apparatus of the connection: a) lateral view; b) side view

The slip modulus (K_s) at the elastic stage (until 40% of the maximum estimated load) was determined according to the EN 26891 procedure. The slip modulus was obtained according to Equation (9-16),

$$K_s = \frac{0.4 F_{est}}{v_{i,mod}} \tag{9-16}$$

where F_{est} is the estimated maximum force and $v_{i,mod}$ is the modified elastic slip modulus given by Equation (9-17),

$$v_{i,mod} = \frac{4}{3}(v_{04} - v_{01}) \tag{9-17}$$

where v_{01} and v_{04} correspond to the slip at 10% and 40% of F_{est}, respectively.

9.7.4   Results and discussion

Figure 9-45 shows the mean relative displacement between adjacent cross-layers *vs.* the shear force per screw for each diameter tested. The slip modulus is shown in Figure 9-46 and the maximum shear force obtained at a slip of 15 mm (according to EN 26891), as well as the maximum shear force measured in the tests are shown in Figure 9-47 and Figure 9-48, respectively. It should be noted that due to limitations of the test setup, it was not possible to reach more than 30 mm of relative displacement, and for that reason, some of the maximum loads presented correspond to that slip value (i.e. the specimens still had additional load capacity).

In general, a relation between the increase of the screw diameter and the increase of the shear force and slip modulus (although the maximum shear force was not achieved in some specimens) is observed, as expected according to the Johansen's yield theory. However, the highest diameters (4.5 and 5.0 mm), especially the last one, showed lower strength values than the others. For both diameters, the mean value regarding the maximum shear force according to EN 26891 was lower than the one corresponding to the 3.5 mm diameter. Regarding the maximum shear force measured, the mean value for the 5.0 mm diameter was even lower than the one for the lowest diameter (3.5 mm). Although a reduced number of specimens was tested, observing Figure 9-45 d), two of the specimens with 5.0 mm diameter screws presented more brittle failure in comparison to the other diameters, which in general presented more marked non-linear load-slip curves.
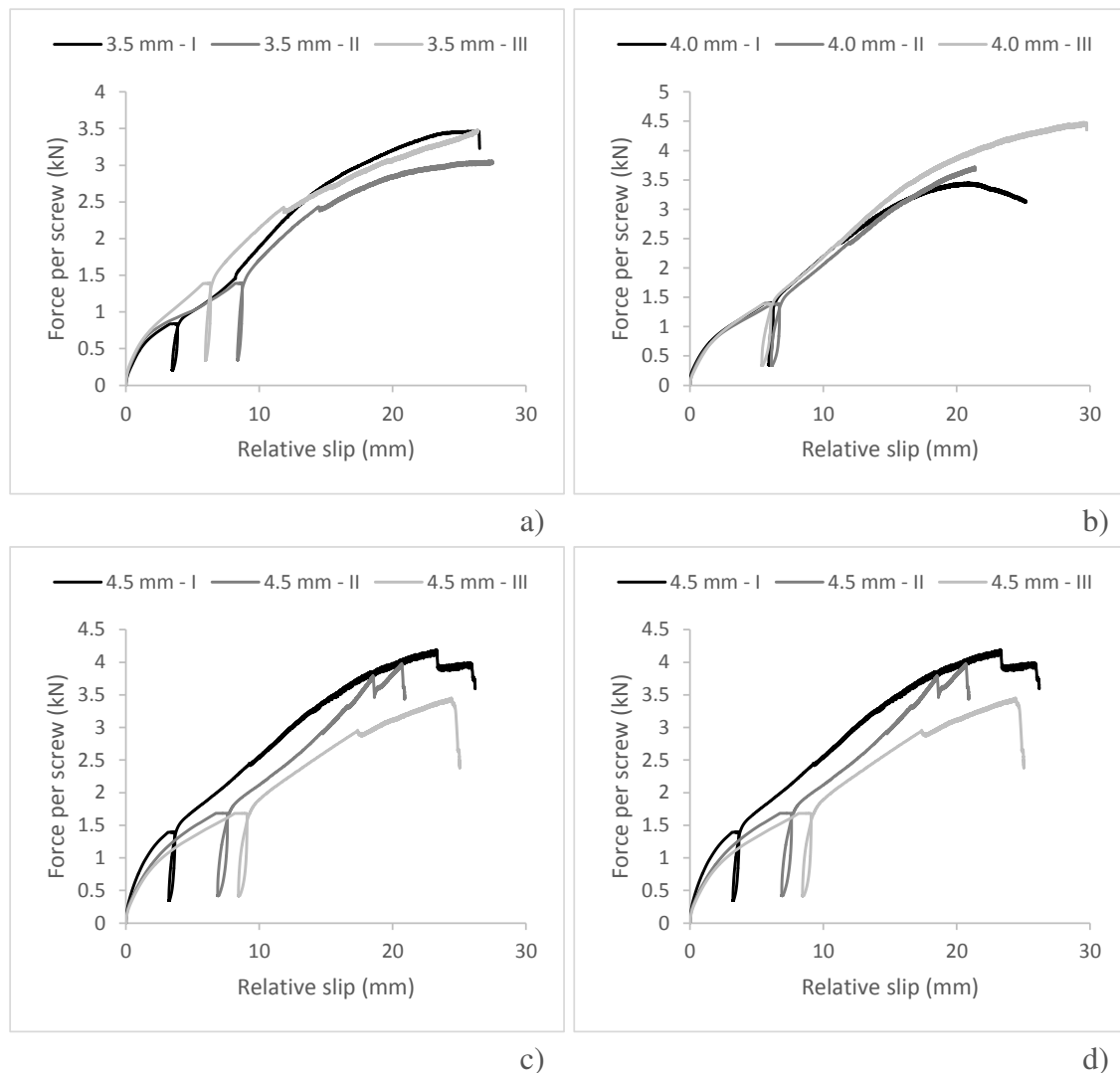
Figure 9-45 – Relative slip *vs.* force per screw: a) d=3.5 mm; b) d=4.0 mm; c) d=4.5 mm; d) d=5.0 mm.
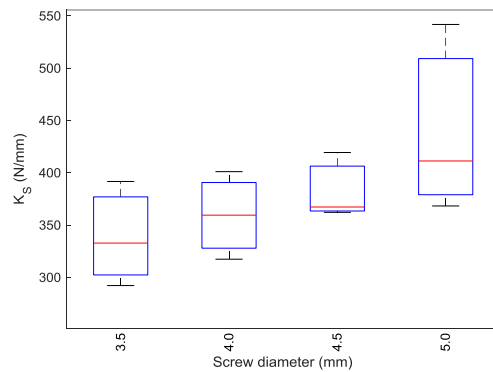
Figure 9-46 – Slip modulus obtained per connector in the tests.

An explanation for the more brittle failure modes observed with the higher diameters (4.5 and 5.0 mm) compared to the lower diameters, could be the fact that in the wood spline (which was made on solid wood), significant stresses perpendicular to the grain direction of the fibres develop during the test. Such increased stresses (due to the higher diameter) may have caused that wood element to split prematurely. Other cause that can be pointed, is that the spacing between the screws were taken equally for all the diameters; thus the higher diameters are more prone to splitting.
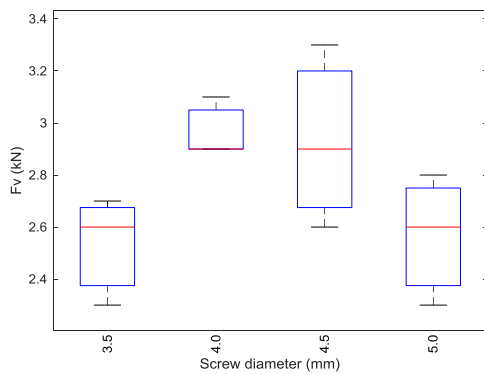
Figure 9-47 – Maximum shear force according to EN 26891 (slip of 15 mm) per connector obtained in the tests.
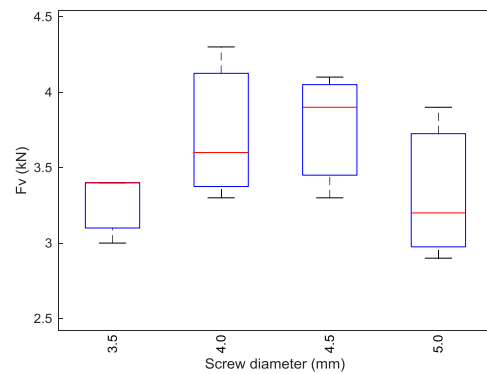
Figure 9-48 - Maximum shear force obtained per connector in the tests.

A comparison between the characteristic values of the maximum shear force measured experimentally according to EN 26891, *i.e.* at a slip of 15 mm, and the design ones (Table 9-4) is given in Table 9-3. In Figure 9-49, the comparison of the experimental values with the minimum values of Table 9-4 is shown. Notice that due to practical issues in inspecting the tested specimens to identify the failure modes, all possible failure modes in single shear (Table 9-1) are shown in Table 9-4. The practical issues are related to the

method of inspection, which would imply splitting the specimen, which in consequence could add additional damage to the one caused by the test. Other non-destructive methods that could be used (e.g. x-ray) were not available. Besides that, mixed failure modes could also occur in practice.

Table 9-3 – Characteristic-values of the maximum shear force ($F_{v,k}$) according to EN 26891 (slip of 15 mm) obtained in the experimental tests for different screw diameters (d).

d (mm)	3.5	4.0	4.5	5.0
$F_{v,k}$ (kN)	2.4	2.9	2.6	2.4
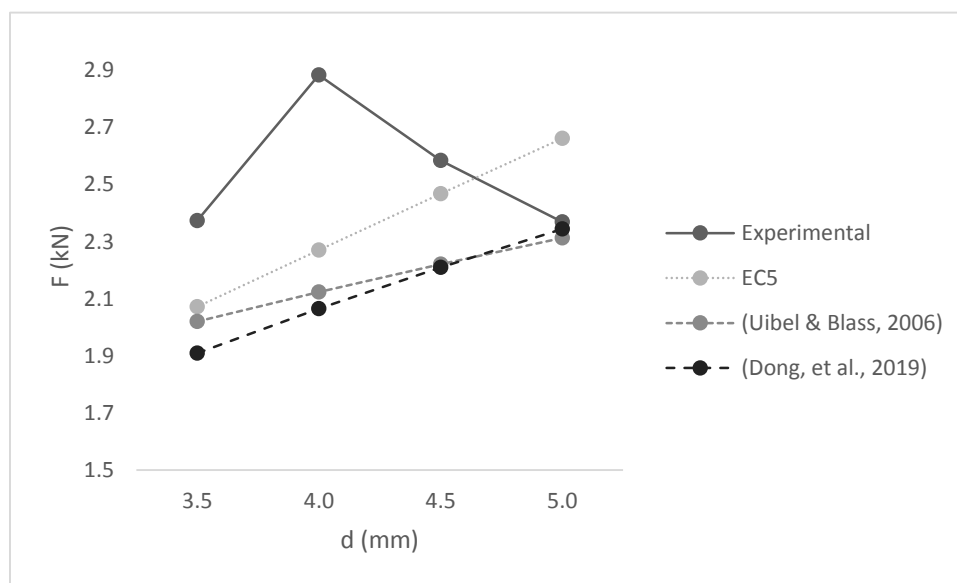
Figure 9-49 – Comparison between the shear force per connector obtained experimentally *vs.* the minimum one determined by the analytical models.

Table 9-4 - Characteristic-values of the design shear force according to different prediction models.

Model	Mode	d (mm) 3.5	4.0	4.5	5.0
Eurocode 5	(a)	2.7	3.1	3.5	3.8
	(b)	4.1	4.6	5.2	5.7
	(c)	2.1	2.3	2.5	2.7
	(d)	2.1	2.4	2.8	3.2
	(e)	2.4	2.8	3.1	3.5
	(f)	2.7	3.2	3.8	4.5
(Uibel & Blass, 2006)	(a)	2.8	3.0	3.2	3.3
	(b)	4.2	4.5	4.8	5.0
	(c)	2.0	2.1	2.2	2.3

	(d)	<u>2.0</u>	2.3	2.6	2.9
	(e)	2.4	2.6	2.9	3.2
	(f)	2.6	3.1	3.6	4.1
(Dong, et al., 2019)	(a)	2.6	2.9	3.2	3.4
	(b)	<u>3.9</u>	<u>4.3</u>	<u>4.7</u>	<u>5.1</u>
	(c)	<u>1.9</u>	<u>2.1</u>	<u>2.2</u>	<u>2.3</u>
	(d)	2.0	2.3	2.6	2.9
	(e)	2.3	2.6	2.9	3.2
	(f)	2.5	3.0	3.6	4.2

Notes: Rope effect formula from (Uibel & Blass, 2006) model considered on (Dong, et al., 2019) model. The maximum and minimum values for each diameter are underlined.

As expected, in all the prediction models, the design force increases with the diameter. It should be noticed that from the minimum to the maximum predictions (underlined in the table), all design values are considered, as the failure mode is greatly dependent on the variability of the material, particularly relevant for wood. From the comparison of the design and experimental values, it is found that the experimental values are within the range of the design values for all the models and diameters, with exception of d=5.0 mm for the Eurocode 5 model. This discrepancy can be explained either by the reduced number of specimens tested or to the premature split on the wood spline member. To avoid such loss of performance, a CLT spline could be used instead of a solid wood one, so that the stresses perpendicular to the grain direction were limited due to the cross-layering.

9.8   Concluding remarks

This chapter first presented a review of the most common types of connections for CLT and SIP solutions, including a discussion of their main advantages and disadvantages.

Based on such connection systems, several solutions were proposed for the developed CIT panels, namely for connections between panels, as well as between these and masonry/concrete elements. The most relevant benefits and handicaps of such proposed systems were analysed and discussed.

Due to the similarity of some parts of the developed connections, a review of design models for CLT-type connections was also made.

An experimental campaign to assess the behaviour of one of the developed connections was carried out. The results revealed that for the higher screw diameters tested, some of the failure modes were brittle, which was believed to occur due to tensile stresses

developing in the central wood spline member. It was found out that the measured shear force was in general within the range of values provided by the design predictive models.

10 CONCLUSIONS AND FUTURE DEVELOPMENTS

10.1 Conclusions

The present work aimed to develop, test and simulate the behaviour of a new type of structural panel that could be an alternative or at least a complement to the modern trend in wood construction, cross-laminated timber (CLT).

The reason for the development of such an alternative was to optimize the wood volume that is currently employed in CLT, which is a massive system. With the proposed panel, one aimed not only at reducing the wood volume, but also at increasing the thermal insulation efficiency and ensuring a lightweight solution. With that purpose in mind, and despite other solutions found in the literature to optimize CLT making use of other concepts, a new solution was defined in Chapter 1: a sandwich panel combining CLT and structural insulated panel (SIP) concepts, which was named cross-insulated timber (CIT).

The concept of the panel itself and its composing materials were then defined in **Chapter 2**. The basic layout of the panel was defined as one insulation layer stacked between two pairs of cross-wood layers, similar to a five-layer CLT panel where the inner wood layer was replaced by an insulation core. This layout was found to provide the best compromise between physical stability, fire safety and production costs.

Solid wood was defined for the outer layers due to its high strength and stiffness in comparison to other wood-based materials, and two species from the Portuguese forest were considered: Maritime pine and Australian blackwood, the former due to its abundance and use in structures, and the latter due to its higher natural durability and the fact that it is an invasive species. For the insulation layer material, polyurethane (PUR) rigid foam was chosen, and for the adhesive layers, one- and two-component polyurethane adhesives were selected.

In **Chapter 3**, the constituent materials of the different layers of the CIT panels, solid wood and polyurethane foam, were characterized to obtain the relevant properties for the design of the panels, and also to allow validating the selected analytical/numerical models through comparison with experimental results.

From the mechanical characterization tests performed on two possible PUR systems, injected *in situ* or pre-manufactured, the last one performed clearly better. Also regarding

the adhesion between the foam and wood, the injected PUR system revealed low adhesion: failure occurred at the interface between the foam and the wood layers, and the interfacial tensile strength was in general much lower than the tensile strength of the PUR material itself.

The anisotropic (at least transversal isotropic) behaviour of the PUR boards was confirmed by the different responses observed in the compression tests of the foam in the edgewise and flatwise plans. In compression, the response was markedly non-linear and the failure mode was ductile, while in tension (and also in shear), the response was linear up to failure, which occurred in a brittle way.

The accelerated ageing test due to temperature (90 ℃ for 24 weeks) performed on polyurethane foam showed that prolonged exposure to elevated temperature caused a slight reduction in the modulus of elasticity, which was attributed to the intrinsic variability of results, and an increase in the tensile strength, which was partly attributed to cross-linking effects on the polymer.

Taking into account some material variability, namely in wood, it was found out that the analytical model used to simulate the thermal resistance of the CIT panels (conventional heat conduction) was able to predict its behaviour with good accuracy.

In **Chapter 4**, the adhesive layers were experimentally characterized for normal and accelerated ageing conditions.

Two possible bonding options for cross-glueing Maritime pine were found to be valid, according to both shear and delamination criteria of EN 16351: (i) using higher bonding pressure and higher adhesive spread rate (with lower press time), or (ii) using lower bonding pressure and lower adhesive spread rate, but with pre-application of primer and double of the press time.

It was found out that the increase in the bonding pressure ensures lower delamination and higher wood failure percentage, while the shear strength does not seem to be particularly affected; results also showed that the pre-treatment of the wood surfaces with primer before bonding noticeably enhances the bonding quality, providing almost zero delamination and higher values of wood failure percentage, and shear strength compared to un-primed specimens.

Regarding the minimum requirements of EN 16351 for bonding quality, they were always fulfilled for the reference method (shear test); however, regarding delamination, for the un-primed specimens, those requirements were only fulfilled for the higher bonding

pressure and adhesive spread rate considered. The criteria used for the delamination analysis (delamination and corresponding wood failure percentage) were found to be inconsistent, as some specimens fulfilled the first one, but failed to comply with the second one.

The strength values obtained from the bending tests of finger-joint Maritime pine connections were found to be much lower than the typical values found for solid wood, as the failure modes involved the total or partial delamination at the finger-joint interface.

Regarding the adhesion between the pre-manufactured PUR boards and wood, a bonding pressure five times higher than the one recommended by the adhesive manufacturer was found to be enough, namely to ensure that failure in the tensile tests would occur in the material instead of at the glue line. The type of adhesive and adhesive spread rate showed no influence on the tensile strength.

From both ageing tests performed on PUR/wood specimens following the ETAG 016 – 2 (temperature) and ISO 9142 (temperature and humidity) protocols, an increase on the mean value of the tensile strength on both 1C and 2C specimens was observed, which was attributed to the additional cross-linking of the polyurethane foam due to post-curing. In the 1C specimens tested with the ETAG protocol, as the failure occurred within the foam, it was not possible to conclude if post-curing also occurred in the adhesive; in the 2C specimens, the fact that part of the failures occurred at the glue lines may indicate that the 2C adhesive was probably affected by the ageing (*i.e.* degradation). From the ageing tests following the delamination test according to EN 16351, it was found out that the induced pressure during the vacuum-press stage crushed the foam and caused it to separate from the wood faces; however, a thin layer of foam actually remained at the adhesive surface, indicating the occurrence of failure in the material and not in the glue line.

In **Chapter 5**, full-scale beams/columns and panels were produced and experimentally tested. The results were then used to validate analytical models available in the literature. From the experimental campaign carried out to assess the mechanical performance of beam/floor panels and column type elements, it was found out that the comparison of the experimental results from both bending and buckling tests with the corresponding analytical models showed a reasonable correlation. In both cases, as expected, the shear deformability of the core was relevant for the global behaviour observed.

For the description of the non-linear behaviour of the beams, a finite element model was implemented in a commercial software package. A 2D plastic model of the PUR foam, considering its flatwise compression curve as input data, was found out to describe well

the experimental results, especially for the specimens with thinner foam, while for the thicker ones more noticeable relative differences to test data were found, which were attributed to the difficulty in modelling the complex behaviour of the polyurethane foam (anisotropic and crushable). A 3D crushable model considering the mean curve of flatwise and edgewise tests as input for the material model also delivered reasonable predictions, especially for the thicker beams.

In **Chapter 6**, an optimization study about the panel layers thickness was presented and the costs were compared with equivalent CLT solutions. From this optimization study, it was found out that the presence of the foam layer is not truly advantageous when only structural requirements are set. However, when thermal demands exist, it does become more relevant; in this case, CIT panels become a more interesting solution to be used in exterior elements, being competitive when compared to CLT solutions.

In **Chapter 7**, a life-cycle assessment was performed for the panels; this analysis also considered (i) the effect of adopting an alternative core material solution and (ii) CLT solutions of equivalent performance.

From the life-cycle assessment, it was concluded that the "polyurethane foam production" and "the wood application, press and curing processes" are the processes that produce the highest impacts. Considering the life cycle stages, the "raw material supply", "manufacturing" and "waste processing/disposal" processes are the ones that produce the highest impacts.

From the end-of-life scenarios considered, the less harmful one is the landfill with partial rot and energy recovery; however, since there is still a lot of uncertainty about the behaviour of wood in landfill, this scenario can turn into the most harmful one if total rot occurs, and thus the incineration option with energy recovery is considered to be the best option.

The use of the bonding system for the wood layers that does not require the use of primer was found to produce fewer impacts than the one that uses primer. The reason beyond such performance relies on the required press time: although more quantity of adhesive is required, the press time is reduced to half, and thus half of the electric energy is needed. So, although the solution with primer is more efficient in terms of bonding performance, it is less interesting from an LCA perspective.

The comparisons of the CIT solution developed in this thesis (with PUR foam) with equivalent CIT solution with insulation corkboard core (ICB) and three-layered CLT plus insulation revealed that the CIT with ICB core solution is the one that presents the highest

impacts in all categories, while CLT solutions have considerably lower impacts. Despite ICB being a sustainable material (as attested by the comparison between the same mass of ICB and PUR), the reason for the worse performance of the ICB core panel is its lower shear properties when compared to PUR, which requires an increased thickness of the wood layers to fulfil the design requirements.

In **Chapter 8**, small-sized panel specimens were acoustically tested, regarding both airborne and impact sound insulation, and the results were compared with CLT solutions of equivalent thickness.

The airborne sound insulation of the CIT panels was lower than that of CLT panels with equivalent thickness; this result was expected due to the lower mass of the former panels.

The analytical models developed to describe the airborne sound insulation of typical sandwich-type panels failed to describe the behaviour of the CIT panels; however, the Sharp model for homogeneous isotropic elements was found to be able to describe well the behaviour of the thicker CIT 170 mm panels. That same model failed to describe the CIT 70 mm specimens; an adaptation of the model, by replacing the typical critical frequency due to bending, by the dilatational frequency (due to the core elasticity), enhanced the results. It was found out that the invariant law could be used to estimate the impact sound insulation of the CIT panels.

In **Chapter 9**, connection systems between the panels and other structural components were developed, and one of the connections was experimentally tested.

Several connection solutions were proposed for the developed panels, namely connections between panels and masonry/concrete elements, by analysing the most relevant advantages and limitations of such proposed systems.

From the experimental campaign developed to assess the behaviour of one of the developed connections, wall-to-wall connections with inner spline, it was found out that for the higher screw diameters tested, some of the failure modes were more brittle than when using smaller diameters; this was attributed to the development of tensile stresses that caused the solid wood spline member to split. Despite that, the measured shear force was in general within the range of expected values predicted by the design models for similar connections with CLT.

Overall, the study conducted in this thesis showed that the developed panels have the potential to, at least, complement or in some cases replace the CLT panels. The use of native species, such as Maritime pine and the invasive Australian blackwood, were found

as feasible for the intended application, which confirmed the objective of promoting the use of wood species found in the Portuguese forest. The effectiveness and durability of the adhesion between the materials to ensure the integrity of the panels during its life-span was proven from the results of a series of accelerated ageing protocols. From the observed mechanical performance, it was found that analytical models found in the bibliography can be used for design purposes, as serviceability limit states (deflection) govern the design. The comparison of production costs of the developed panels with CLT showed that the former panels have potential to be competitive when used as elements of the external envelope; this competitiveness has potential to be enhanced if a direct injection system of the polyurethane foam between the wood layers would be implemented. The developed connections are expected to ensure the integration of the developed panels with CLT and other current building structures. This means that both CIT and CLT systems may be used in the same structure, with CIT being preferred for applications in external elements and CLT in inner elements.

10.2 Future developments

From the work conducted, it was possible to identify some aspects that could be the object of additional investigations in the future, as well some other topics that were not addressed in this thesis and are worth being pursued.

Regarding the materials characterization, from the ageing tests on PUR foam (temperature) according to ETAG 016-2, it was not possible to conclude if the protocol test is too severe or lenient, or if it is even representative of the degradation that the material will suffer during its lifetime. Even so, it would be of interest to perform ageing tests on PUR foam (temperature) for other conditions than the ones prescribed in ETAG 016-2, namely higher duration or higher temperature, or a combination thereof, to observe the materials' behaviour and compare with results from other works. It would also be interesting to compare the effects of such ageing protocols with different real long-term exposure conditions.

Regarding the assessment of the creep behaviour of the panels, it was not possible to determine separately the creep due to bending of the faces and that due to shear of the core. To obtain those coefficients for the species of wood used (Maritime pine and Australian blackwood), creep tests on beam types for those species are of interest. Also, shear creep tests of cross-wood layers would be important, as little information was found regarding this aspect.

Regarding the mechanical behaviour of the panels, besides the bare panels that were tested in the thesis, it would also be of interest to perform tests on the panels that include certain types of elements that result from connections, namely splines along the edges of the panels, as those elements will certainly affect the behaviour of the panels. Furthermore, analytical and numerical models will need to be identified/or developed to describe the mechanical behaviour of such elements.

Regarding the finite element modelling of the panels and despite the good agreement between experimental and numerical results, due to identified limitations on the modelling, namely the definition of a material model that can be representative of the complex behaviour of the PUR foam, some enhancements are needed; for instance, the crushable foam model with volumetric hardening from *ABAQUS* software. Another important aspect worth analysing in further depth is why the failure at the foam (according to the FE models) occurred for shear stresses much higher than the predictions from the experimental characterization of the PUR foam - this is believed to have occurred due to the foam densification. For this reason, a type of test that could determine the shear strength for a certain level of densification of the foam would be of interest.

An important issue not addressed in this work is the fire resistance of the developed panels. Due to the combustible nature of the materials involved in the panels (wood, polyurethane and adhesives) and the reduction of their mechanical properties with temperature, experimental tests should be performed to assess the panels' behaviour in fire, when used as wall or floor elements. Furthermore, also the influence of the connections (and corresponding details) between panels on the structural performance in a fire situation is of interest.

Regarding the optimization of the panels, a requirement that was not considered was the acoustic insulation. Based on the results from the acoustic characterization that identified analytical models to describe the behaviour of the panels, new optimization calculations could be performed to include these aspects. As referred in the optimization chapter, those requirements would not probably be fulfilled without additional non-structural components that need to be account for, eventually through additional experimental characterization tests.

Another issue identified in the optimization chapter was the consideration of creep coefficients for a reference period of ~11.4 years, which is smaller than the one considered for the typical service life of buildings (50 years). Thus, using creep values extrapolated for 50 years is of interest to obtain more realistic deformation predictions for such reference period.

An aspect that was not considered in the LCA study was the comparison of the method used to manufacture the panels (pre-manufactured PUR boards) and the direct injection of the foam at the panels manufacturing plant. This should be analysed in future studies.

One of the limitations of the LCA study was the exclusion of the use stage. Another one is that the study was performed for specific elements (walls or floors), and not for a whole building made with the constructive solution proposed. So, performing a full LCA (including the construction, use and deconstruction stages) of a building using the panels, including the developed connection systems, as well as additional constructive elements, such as coatings would be of interest, as well as the comparison of such results with an equivalent reinforced-concrete building.

To compare and understand the advantages and limitations of using a reduced-size chamber and adapted test protocols for the acoustic insulation characterization of the panels, it would be of interest to perform full–size acoustic tests according to applicable standards. This would also allow understanding if some of the limitations of the tests carried out in this thesis, namely the observation of the coincidence effect on the airborne sound insulation curves, would not be so unpronounced in a normalized test.

Regarding the connection system that was experimentally tested, in order to avoid splitting in wood, it would be of interest to test a similar connection, but using an internal spline made of CLT instead of solid wood; with this change, it would be relevant to check if the premature brittle failure observed in the specimens with higher screws diameter was in fact caused by the tensile stress acting normal to the wood fibres. Besides that, additional experimental tests on the other proposed connections systems would also be of interest. Another aspect deserving attention would be to perform 2D numerical simulations of the panels' assembly, using each type of connection, and compare the thermal bridging of those solutions.

BIBLIOGRAPHIC REFERENCES

Abbasi, H. (2014). "Structural behaviour of insulated foam-timber panels under gravity and lateral loading". PhD Thesis. Ryerson University, Toronto.

Aicher, S., Hirsch, M. and Christian, Z. (2016). "Hybrid cross-laminated timber plates with beech wood cross-layers". Construction and Building Materials, Vol. 124, pp. 1007–1018.

Allen, H. (1969). "Analysis and Design of Structural Sandwich Panels". Pergamon Press, London.

AlSayegh, G. (2012). "Hygrothermal Properties of Cross Laminated Timber and Moisture Response of Wood at High Relative Humidity". MSc Thesis. Carleton University, Ottawa.

Amorim Isolamentos, Sa. (2016). "Aglomerado de cortiça Expandida (ICB) - Declaração Ambiental de Produto". DAP habitat, Vendas Novas.

Ansell, M. (2015). "Wood Composites: Engineering with Wood - From Nanocellulose to Superstructures". Woodhead Publishing, Cambridge.

APA. (2013). "Standard for Performance-Rated Structural Insulated Panels in Wall Applications". ANSI/APA PR S 610.1-2013, APA – The Engineered Wood Association, Tacoma.

APA. (2014). "Design and Fabrication of Sandwich Panels". APA The Engineered Wood Association, Washigton.

APA. (2016). "Lista de aterros em exploração 2016". Agência Portuguesa do Ambiente.

APA. (2017). "Guia de Classificação de Resíduos". Agência Portuguesa do Ambiente.

ASTM. (1995). "Standard Practice for Determining Thermal Resistance of Building Envelope Components from the In-Situ Data". ASTM C1155,

ASTM. (2011a). "Standard Test Method for Core Shear Properties of Sandwich Constructions by Beam Flexure". ASTM C393/C393M, American Society for Testing and Materials, West Conshohocken.

ASTM. (2011b). "Standard Test Method for Shear Properties of Sandwich Core Materials". ASTM C273/C273M, American Society for Testing and Materials, West Conshohocken.

ASTM. (2014). "Standard Test Methods for Determining Structural Capacities of Insulated Panels". ASTM E1803, American Society for Testing and Materials, West Conshohocken.

ASTM. (2015). "Standard Test Method for Steady-State Thermal Transmission Properties by Means of the Heat Flow Meter Apparatus". ASTM C518, American Society for Testing and Materials, West Conshohocken.

Ballagh, K. (2010). "Adapting Simple Prediction Methods to Sound Transmission of Lightweight Foam Cored Panels". Building Acoustics, Vol. 17, Issue 4, pp. 269–276.

Balsa, J. (2013). "Avaliação destrutiva e não destrutiva de elementos retangulares de madeira de pinho bravo". MSc Thesis in Civil Engineering. Universidade de Coimbra - Departamento de Engenharia Civil, Coimbra.

Bella, A., Granzotto, N. and Barbaresi, L. (2016). "Analysis of acoustic behavior of bare CLT floors for the evaluation of impact sound insulation improvement". 22nd International Congress on Acoustics, Acoustical Society of America, Buenos Aires.

Betti, M., Brunetti, M., Lauriola, M., Nocetti, M., Ravalli, F. and Pizzo, B. (2016). "Comparison of newly proposed test methods to evaluate the bonding quality of Cross-Laminated Timber (CLT) panels by means of experimental data and finite element (FE) analysis". Construction and Building Materials, Vol. 125, pp. 952–963.

Brandner, R. (2013). "Production and Technology of Cross Laminated Timber (CLT): A state-of-the-art Report". COST Action FP1004, TU Graz, Graz.

Brandner, R, Flatscher, G, Ringhofer, A, Schickhofer, G and Thiel, A. (2016). "Cross laminated timber (CLT): overview and development". Eur. J. Wood Prod 74, pp. 331–351.

Buck, D., Wang, X., Hagman, O. and Gustafsson, A. (2016). "Further Development of Cross-Laminated Timber (CLT): Mechanical Tests on 45° Alternating Layers". World Conference on Timber Engineering 2016, WCTE 2016, Austria.

Bucur, V. (2016). "Handbook of Materials for String Musical Instruments". 1st ed. Springer, Melbourne, Australia.

Cadorel, X. and Crawford, R. (2018). "Life cycle analysis of cross laminated timber in buildings: a review". Engaging Architectural Science: Meeting the Challenges of Higher Density: 52nd International Conference of the Architectural Science Association 107–114.

Cárdenas, J, Muñoz, E, Riquelme, C and Hidalgo, F. (2015). "Simplified life cycle assessment applied to structural insulated panels homes". Revista Ingeniería de Construcción RIC, Vol. 30, Issue 1, pp. 33-38.

Carvalho, Albino. (1997). "Madeiras Portuguesas - Estrutura anatómica, Propriedades e Utilizações. Vol. 1 & 2.". Direcção Geral das Florestas, Lisboa.

CE. (2000). http://data.europa.eu/eli/dec/2000/532/oj. 2000/532/CE.

CEN. (1991). "Timber structures - Joints made with mechanical fasteners - General principles for the determination of strength and deformation characteristics". EN 26891, European Committee for Standardization, Brussels.

CEN. (1994). "Durability of wood and wood-based products - Natural durability of solid wood - Part 2: Guide to natural durability and treatability of selected wood species of importance in Europe". EN 350-2, European Committee for Standardization, Brussels.

CEN. (2000a). "Building materials and products. Hygrothermal properties. Tabulated design values". EN 12524, European Committee for Standardization, Brussels.

CEN. (2000b). "Building acoustics. Estimation of acoustic performance in buildings from the performance of elements. Airborne sound insulation between rooms". EN 12354-1, European Committee for Standardization, Brussels.

CEN. (2000c). "Building acoustics. Estimation of acoustic performance in buildings from the performance of elements. Impact sound insulation between rooms". EN 12354-2, European Committee for Standardization, Brussels.

CEN. (2004a). "Timber structures - Test methods - Determination of mechanical properties of wood based panels". EN 789, European Committee for Standardization, Brussels.

CEN. (2004b). "Eurocode 5: Design of timber structures - Part 1-1: General. Common rules and rules for buildings". EN 1995-1-1, European Committee for Standardization, Brussels.

CEN. (2004c). "Eurocode 5. Design of timber structures - Part 1-2: General. Structural fire design". EN 1995-1-2, European Committee for Standardization, Brussels.

CEN. (2007). "Fire classification of construction products and building elements. Classification using test data from reaction to fire tests". EN 13501-1, European Committe for Standardization, Brussels.

CEN. (2008). "Adhesives. One component polyurethane for load bearing timber structures. Classification and performance requirements". EN 15425, European Committee for Standardization, Brussels.

CEN. (2009). "Structural timber. Strength classes". EN 338, European Committee for Standardization, Brussels.

CEN. (2012a). "Timber structures - Structural timber and glued laminated timber - Determination of some physical and mechanical properties". EN 408, European Committee for Standardization, Brussels.

CEN. (2012b). "Wood and wood-based products - Calculation of sequestration of atmospheric carbon dioxide". EN 16449, European Committee for Standardization, Brussels.

CEN. (2012c). "Sustainability of construction works. Environmental product declarations. Core rules for the product category of construction products". EN 15804, European Committee for Standardization, Brussels.

CEN. (2013). "Self-supporting double skin metal faced insulating panels. Factory made products. Specifications". EN 14509, European Committee for Standardization, Brussels.

CEN. (2015). "Timber structures - Cross laminated timber - Requirements". EN 16351, European Committee for Standardization, Brussels.

Chen, Y. (2011). "Structural performance of box based cross laminated timber system used in floor applications". PhD Thesis. University of British Columbia, Vancouver.

Chen, W and Hao, H. (2015). "Performance of structural insulated panels with rigid skins subjected to windborne debris impacts – Experimental investigations". Construction and Building Materials, Vol. 77, pp. 241–252.

Chen, C., Pierobon, F. and Ganguly, I. (2019). "Life Cycle Assessment (LCA) of Cross-Laminated Timber (CLT) Produced in Western Washington: The Role of Logistics and Wood Species Mix". Sustainability, Vol. 11, pp. 1278.

Christovasilis, I., Brunetti, M., Follesa, M., Nocetti, M. and Vassallo, D. (2016). "Evaluation of the mechanical properties of cross laminated timber with elementary beam theories". Construction and Building Materials, Vol. 122, pp. 202–213.

CIB-W56, ECCS-TWG 7. 9. (2001). "European recommendations for sandwich panels part I: design". International Council for Building (CIB), Delft.

Clough, R. and Penzien, J. (1993). "Dynamics of structures". McGraw-Hill College, New York.

Colaço, A., Costa, P., Amado-Mendes, P., Magalhães, F. and Godinho, L. (2018). "Experimental validation of a FEM-MFS hybrid numerical approach for vibroacoustic prediction". Applied Acoustics, Vol. 141, pp. 79-92.

Crespell, P. and Gagnon, S. (2010). "Cross Laminated Timber: a Primer". FPInnovations, Quebec.

D'Alessandro, Vincenzo, Petrone, Giuseppe, Franco, Francesco and De Rosa, Sergio. (2013). "A review of the vibroacoustics of sandwich panels: Models and experiments". Journal of Sandwich Structures and Materials, Vol. 15, Issue 5, pp. 541–582.

Daniel, I, Gdoutos, E, Wang, K and Abot, J. (2002). "Failure Modes of Composite Sandwich Beams". International Journal of Damage Mechanics, Vol. 11, Issue 4, pp. 309-334.

Darby, H., Elmualim, A. and Kelly, F. (2013). "A case study to investigate the life cycle carbon emissions and carbon storage capacity of a cross laminated timber, multi-storey residential building". Sustainable Building Conference, SB13, 23-25 April 2013, Munich.

Davids, W., Willey, N., Lopez-Anido, R., Shaler, S., Gardner, D., Edgar, R. and Tajvidi, M. (2017). "Structural performance of hybrid SPFs-LSL cross-laminated timber panels". Construction and Building Materials, Vol. 149, pp. 156-163.

Davies, J. (2008). "Lightweight Sandwich Construction". John Wiley & Sons

Dias, A. and Arroja, L. (2012). "Environmental impacts of eucalypt and maritime pine wood production in Portugal". Journal of Cleaner Production, Vol. 37, pp. 368-376.

Dias, A., Machado, J. and Santos, P. (2014). "Uso de produtos de madeira de alto desempenho em aplicações estruturais". 5as Jornadas Portuguesas de Engenharia de Estruturas, Lisboa.

Dias, S., Tadeu, A., António, J., Almeida, J., Pedro, F., Martins, S. and Serra, C. (2018). "Experimental study of expanded cork agglomerate blocks – Compressive creep behavior and dynamic performance". Construction and Building Materials, Vol. 181, pp. 551-564.

Díaz, J, Nieto, P, Rabanal, F and Biempica, C. (2008). "Finite element analysis of thin-walled composite two-span wood-based loadbearing stressed skin roof panels and experimental validation". Thin-Walled Structures, Vol. 46, pp. 276–289.

Dong, W., Li, Q., Zhang, H., Wang, Z., Zhou, J. and Gong, M. (2019). "Embedment Strength of Cross-Laminated Timber for Smooth Dowel-type Fasteners". MATEC Web Conf., Vol. 275.

DR. (2008a). "Diário da República, 1.ª série — N.º 220 — 12 de Novembro de 2008". Decreto-Lei nº220 2008.

DR. (2008b). "Diário da República, 1.ª série — N.º 250 — 29 de Dezembro de 2008". Portaria n.º 1532/2008.

DR. (2013). "Despacho (extrato) n.º 15793-K/2013". Diário da República 2.ª série - N.º 234 - 3 de dezembro de 2013.

DR. (2015). "Portaria n.º 379-A 2015". Diário da República, 1.ª série — N.º 207 — 22 de outubro de 2015.

Durlinger, B, Crossin, E and Wong, J. (2013). "Life Cycle Assessment of a cross laminated timber building". Forest & Wood Products Australia, Victoria.

Du, Q, Zhang, H, Liu, N and Yin, X. (2013). "Comprehensive Life-cycle Assessment of SIP Building". Applied Mechanics and Materials, Vol. 353-356, pp. 2808-2812.

Ecoinvent. (2010). https://www.ecoinvent.org/. https://www.ecoinvent.org/.

Egoin. (2015). http://www.egoin.com/. Egoin, Bizkaia.

EOTA. (2000). "Test methods for Light Composite Wood-based Beams and Columns".

EOTA TR002, European Organisation for Technical Approvals, Brussels.

EOTA. (2003a). "Guideline for European Technical Approval of Self-Supporting Composite Lightweight Panels. Part 1: General.". ETAG 016-1, European Organisation for Technical Approvals, Brussels.

EOTA. (2003b). "Guideline for European Technical Approval of Self-Supporting Composite Lightweight Panels. Part 2: Specific aspects relating to Self-supporting Composite Lightweight Panels for use in roofs". ETAG 016-2, European Organisation for Technical Approvals, Brussels.

EOTA. (2005). "Calculation models for prefabricated wood-based loadbearing stressed skin panels for use in roofs". TR 019, European Organization for Technical Approvals, Brussels.

Espinoza, O, Trujillo, V, Mallo, M and Buehlman, U. (2016). "Cross-Laminated Timber: Status and Research Needs in Europe". BioResources, Vol. 11, Issue 1, pp. 281-295.

Estrada-Martínez, S, Mollón, V and Bonhomme, J. (2015). "Proposals to improve the durability assessment after ageing tests for wood-based sandwich panels". Journal of Sandwich Structures and Materials, Vol. 0, Issue 00, pp. 1-15.

ETA. (2010). "ARTUSO - CLT". ETA 10/0339, European Organisation for Technical Approvals, Vienna.

ETA. (2011). "KLH - Massivholzplatten". ETA 06/0138, European Organisation for Technical Approvals, Vienna.

Fernandez-Cabo, J, Majano-Majano, A, Ageo, L and Ávila-Nieto, M. (2011). "Development of a novel façade sandwich panel with low-density wood fibres core and wood-based panels as faces". Eur. J. Wood Prod., Vol. 69, pp. 459–470.

FERPFA. (2006). "Thermal insulation materials made of rigid polyurethane foam (PUR/PIR)". Polyurethane Foam Associations, Brussles.

Ferrão, P. (2009). "Ecologia industrial: princípios e ferramentas". IST Press - Instituto Superior Técnico, Lisboa.

FPInnovations. (2013). "CLT Handbook U.S. Edition". FPInnovations, Quebec.

FPL. (1959). "Structural Sandwich Design Criteria". Forest Products Laboratory, Wisconsin.

FPL. (2010). "Wood Handbook - Wood as an Engineering Material". Forest Products Laboratory, Madison.

Frangi, A, Fontana, M, Hugi, E and Jöbstl, R. (2009). "Experimental analysis of cross-laminated timber panels in fire". Fire Safety Journal, Vol. 44, pp. 1078–1087.

Frangi, A, Fontana, M, Knobloch, M and Bochicchio, G (2008). "Fire Behaviour of Cross-Laminated Solid Timber Panels". In Fire Safety Science - Proceedings of the Ninth international Symposium, Technical Research Centre of Finland.

Franzoni, L, Lebée, A, Forêt, G and Lyon, F (2015). "Advanced modelling for design helping of heterogeneous CLT panels in bending". International Network on Timber Engineering Research - INTER - Meeting 48, Sibenik.

Frechette, L. (1999). "Build Smarter with Alternative Materials". Craftsman Book Company, Carlsbad.

Freitas, S. (2012). "Steel plate reinforcement of orthotropic bridge decks". PhD Thesis. Delft University of Technology, Delft.

Garay, R. and Pino G., N. (2019). "Acoustic Behavior in Three Types of Housing: Brick Social Housing, Structural Insulated Panel (SIP) Emergency Housing and Mediagua Emergency Housing". Revista de la Construcción, Vol. 18, Issue 1, pp. 96-110.

Garrido, M. (2016). "Composite sandwich panel floors for building rehabilitation". PhD Thesis in Civil Engineering. Instituto Superior Técnico - Universidade de Lisboa, Lisboa.

Garrido, M, Correia, J and Keller, T. (2015). "Effects of elevated temperature on the shear response of PET and PUR foams used in composite sandwich panels". Construction and Building Materials, Vol. 76, pp. 150-157.

Gebhardt, G. and Blaß, H. (2010). "Wood Fibre Insulation Boards as Load-Carrying Sheathing Material of Wall Panels". World Conference on Timber Engineering 2010, Trentino, Italy.

Gereke, T, Gustafsson, P, Persson, K and Niemz, P. (2011). "The Hygroscopic Warping of Cross-Laminated". Springer

Glasø, G. and Nore, K. (2012). "Shear strength of cross laminated timber (CLT) with integrated acoustic properties". World Conference on Timber Engineering, Auckland.

Godinho, L., Masgalos, R., Pereira, A. and Branco, F. (2010). "On the use of a small-sized acoustic chamber for the analysis of impact sound reduction by floor coverings". Noise Control Eng. J., Vol. 58, Issue 6, pp. 658-668.

Goedkoop, M., Oele, M., Leijting, J., Ponsioen, T. and Meijer, E. (2016). "Introduction to LCA with SimaPro" Help book.

Goedkoop, M., Oele, M., Schryver, A., Vieira, M. and Hegger, S. (2010). "SimaPro Database Manual Methods Library" Help book.

Gonçalves, C. (2010). "Contributos para uma maior e melhor utilização da madeira de Pinho bravo em Portugal". MSc Thesis. Faculdade de Engenharia da Universidade do Porto, Porto.

Guggenberger, W and Moosbrugger, T (2006). "Mechanics of Cross-Laminated Timber Plates under Uniaxial Bending". World Conference on Timber Engineering 2006, Portland.

Gu, M., Pang, W. and Stoner, M. (2016). "Bending and Rolling Shear Capacities of Southern Pine Cross Laminated Timber (CLT)". World Conference on Timber Engineering, Vienna.

Homb, A., Carter, C. and Rabold, A. (2017). "Impact sound insulation of cross-laminated timber/massive wood floor constructions: Collection of laboratory measurements and result evaluation". Building Acoustics, Vol. 24, Issue 1, pp. 35–52.

Hopkin, D, Lennon, T, El-Rimawi, J and Silberschmidt, V. (2011). "Full-scale natural fire tests on gypsum lined structural insulated panel (SIP) and engineered floor joist assemblies". Fire Safety Journal, Vol. 46, pp. 528-542.

Huang, J and Gibson, L. (1991). "Creep of polymer foams". Journal of Materials Science, Vol. 26, Issue 3, pp. 637-647.

Huber, A. and Gibson, L. (1988). "Anisotropy of foams". Journal of Materials Science, Vol. 23, Issue 8, pp. 3031–3040.

IARC. (2006). "Monographs on the Evaluation of Carcinogenic Risks to Humans - Formaldehyde, 2-Butoxyethanol and 1-tert-Butoxypropan-2-ol". WHO Press.

ICNF. (2013a). "IFN6 – Áreas dos usos do solo e das espécies florestais de Portugal continental. Resultados preliminares". Instituto da Conservação da Natureza e das Florestas, Lisboa.

ICNF. (2013b). "Espécies arbóreas florestais utilizáveis em Portugal continental". Instituto da Conservação da Natureza e das Florestas, Lisboa.

IPCC. (2007). "Changes in Atmospheric Constituents and in Radiative Forcing". Intergovernmental Panel on Climate Change.

IPQ. (1995). "Madeira serrada de pinheiro bravo para estruturas". NP 4305,

IPQ. (2009). "Eurocódigo - Bases para projecto de estruturas". NP EN 1990,

ISO. (1997). "Acoustics - Measurement of sound insulation in buildings and of building elements - Part 1: Requirements for laboratory test facilities with suppressed flanking transmission". ISO 140-1, International Organization for Standardization, Geneva.

ISO. (1998). "Acoustics - Measurement of sound insulation in buildings and of building elements - Part 7: Field measurements of impact sound insulation of floors". ISO 140 - 7, International Organization for Standardization, Geneva.

ISO. (2003a). "Acoustics - Measurement of sound absorption in a reverberation room". ISO 354, International Organization for Standardization, Geneva.

ISO. (2003b). "Adhesives - Guide to the selection of standard laboratory ageing conditions for testing bonded joints". ISO 9142,

ISO. (2006a). "Environmental management - Life cycle assessment - Principles and framework". ISO 14040, International Organization for Standardization, Geneva.

ISO. (2006b). "Environmental management - Life cycle assessment - Requirments and guidelines". ISO 14044, International Organization for Standardization, Geneva.

ISO. (2010a). "Acoustics - Laboratory measurement of sound insulation of building elements - Part 2: Measurement of airborne sound insulation". ISO 10140-2, International Organization for Standardization, Geneve.

ISO. (2010b). "Acoustics - Laboratory measurement of sound insulation of building elements - Part 3: Measurement of impact sound insulation". ISO 10140-3, International Organization for Standardization, Geneva.

ISO. (2010c). "Acoustics - Laboratory measurement of sound insulation of building elements - Part 4: Measurement procedures and requirements". ISO 10140-4, International Organization for Standardization, Geneva.

ISO. (2013a). "Acoustics - Rating of sound insulation in buildings and of building elements - Part 2: Impact sound insulation". ISO 717-2, International Organization for Standardization, Geneva.

ISO. (2013b). "Plastics - Differential scanning calorimetry (DSC) - Part 2: Determination of glass transition temperature and glass transition step height". ISO 11357-2, International Organization for Standardization, Geneva.

ISO. (2014). "Acoustics - Field measurement of sound insulation in buildings and of building elements - Part 1: Airborne sound insulation". ISO 16283 - 1, International Organization for Standardization, Geneva.

Jelle, B. (2011). "Traditional, state-of-the-art and future thermal building insulation materials and solutions – Properties, requirements and possibilities". Energy and Buildings, Vol. 43, pp. 2549–2563.

Jöbstl, R and Schickhofer, G (2007). "Comparative examination of creep of GTL- and CLT- slabs in bending". CIB W18 2007, Bled.

Johansen, K. (1949). "Theory of timber connections". International Association of Bridge and Structural Engineering (IABSE), Vol. 9, pp. 249-262.

Johansson, C, Pizzi, T and Leemput, M. (2002). "Wood Adhesion and Glued Products - State of the Art – Report - COST Action E13". COST.

Jorissen, A., Rie, J., Houben, T. and Hofmeyer, H. (2016). "Sandwich panels with stiffeners". World Conference on Timber Engineering, Vienna.

Karacabeyli, E. and Douglas, B. (2013). "CLT Handbook U.S. Edition". FPInnovations, Quebec.

Kawasaki, T, Zhang, M, Wang, Q, Komatsu, K and Kawai, S. (2006). "Elastic moduli and stiffness optimization in four-point bending of wood-based sandwich panel for use as structural insulated walls and floors". J Wood Sci, Vol. 52, pp. 302–310.

Kennedy, S., Salenikovich, A., Munoz, W. and Mohammad, M. (2014). "Design equations for dowel embedment strength and withdrawal resistance for threaded fasteners in CLT". World Conference in Timber Engineering, Quebec.

Kermani, A. (2006). "Performance of structural insulated panels". Structures & Buildings, Vol. 159, pp. 13-19.

Kermani, A and Hairstans, R. (2006). "Racking Performance of Structural Insulated Panels". Journal of Structural Engineering, Vol. 132, Issue 11, pp. 1806-1812.

KLH. (2015). http://www.klh.at/. KLH, Katsch an der Mur.

Knapic, S, Tavares, F and Pereira, H. (2006). "Heartwood and sapwood variation in Acacia melanoxylon R. Br. trees in Portugal". Forestry, Vol. 79, Issue 4, pp. 371-380.

Knorz, M., Torno, S. and Kuilen, J-W. (2017). "Bonding quality of industrially produced cross-laminated timber (CLT) as determined in delamination tests". Construction and Building Materials, Vol. 133, pp. 219–225.

Krakers, L. (2009). "Parametric fuselage design - Integration of mechanics and acoustic & thermal insulation". PhD thesis in Aerospace Engineering. Delft University of Technology, Faculty of Aerospace Engineering, Netherlands.

Kreuzinger, H. (1999). "Platten, Scheiben und Schalen, ein Berechnungsmodell für gängige Statikprogramme". Bauen mit Holz, Vol. 1, pp. 34-99.

Künniger, T. (2008). "A semi-automatic method to determine thewood failure percentage on shear test specimens". Holz Roh Werkst, Vol. 66, pp. 229–232.

Leno. (2018). "https://www.zueblin-timber.com/".

Ley, Robert. (1999). "Facesheet Wrinkling in Sandwich Structures". NASA, California.

Liao, Y., Tu, D., Zhou, J., Zhou, H., Yun, H., Gu, J. and Hu, C. (2017). "Feasibility of manufacturing cross-laminated timber using fast-grown small diameter eucalyptus lumbers". Construction and Building Materials, Vol. 132, pp. 508-515.

Liu, Y., Guo, H., Sun, C. and Chang, W. (2016). "Assessing Cross Laminated Timber (CLT) as an Alternative Material for Mid-Rise Residential Buildings in Cold Regions in China—A Life-Cycle Assessment Approach". Sustainability, Vol. 8, Issue 10, pp. 1047.

Luedtke, J., Amen, C., Ofen, A. and Lehringer, C. (2015). "1C-PUR-bonded hardwoods for engineered wood products: influence of selected processing parameters". Eur. J. Wood Prod., Vol. 73, pp. 167–178.

Lu, Z., Zhou, H., Liao, Y. and Hu, C. (2018). "Effects of surface treatment and adhesives on bond performance and mechanical properties of cross-laminated timber (CLT) made from small diameter Eucalyptus timber". Construction and Building Materials, Vol. 161, pp. 9-15.

Machado, J., Louzada, J., Santos, A., Nunes, L., Anjos, O., Rodrigues, J., Simões, R. and Pereira, H. (2014). "Variation of wood density and mechanical properties of blackwood (Acacia melanoxylon R. Br.)". Materials and Design, Vol. 56, pp. 975–980.

Mapelli, A. (2012). "Analisi LCA del pannello XLAM – legno toscano". Politecnico di Milano, Milan.

Marini, M, Baccoli, R, Bella, A, Mastino, C, Trulli, N and Solinas, E (2015). "Comparison between calculated and measured performances of impact sound insulation for Cross Laminated Timber building elements". EuroNoise 2015, Maastricht.

Martins, C., Santos, P., Almeida, P., Godinho, L. and Dias, A. (2015). "Acoustic performance of timber and timber-concrete floors". Construction and Building Materials, Vol. 101, pp. 684–691.

Martins, C. (2018). "Avaliação estrutural de elementos de madeira lamelada colada". Universidade de Coimbra, PhD Thesis in Civil Engineering, Coimbra.

Mateo, R, Cabrero, J, Hermoso, E and Chillón, J. (2011). "Ageing tests study on wood-based sandwich panels". Materiales de Construcción, Vol. 61, Issue 304, pp. 583-596.

Mathworks. (2018). "MATLAB - https://www.mathworks.com/products/matlab.html".

Mechel, F. (2001). "Formulas of Acoustic". Springer-Verlag, Berlin.

Meier, Eric. (2020). https://www.wood-database.com/australian-blackwood/.

Messmer, A. (2015). "Life cycle assessment (LCA) of adhesives used in wood constructions". MSc Thesis. Institute of Ecological System Design ETH Zürich, Zürich.

Mindlin, R. (1951). "Influence of rotatory inertia and shear in flexural motions of isotropic elastic plates". J Appl Mech (ASME), Vol. 18, pp. 1031-1038.

Mohamed, M., Anandan, S., Huo, Z., Birman, V., Volz, J. and Chandrashekhara, K. (2015). "Manufacturing and characterization of polyurethane based sandwich composite structures". Composite Structures, Vol. 123, pp. 169-179.

Möhler, K. (1962). "Über das Tragverhalten von Biegeträgern und Druckstaben mit zusammengesetzten Querschnitten und nachgiebigen Verbindungsmitteln". Habilitation thesis - TH Karlsruhe.

Montgomery, W. (2014). "Hollow massive timber panels: a high-performance, long-span alternative to cross laminated timber". MSc Thesis. Clemson University, Clemson.

Mostafa, A., Shankar, K. and Morozov, E. (2013). "Insight into the shear behaviour of composite sandwich panels with foam core". Materials and Design, Vol. 50, pp. 92-101.

Mouritz, A. and Gardiner, C. (2002). "Compression properties of fire-damaged polymer sandwich composites". Composites Part A: Applied Science and Manufacturing, Vol. 33, Issue 5, pp. 609-620.

Mousa, Mohammed and Uddin, Nasim. (2011). "Global buckling of composite structural insulated wall panels". Materials and Design, Vol. 32, pp. 766-772.

Mousa, Mohammed and Uddin, Nasim. (2012). "Structural behavior and modeling of full-scale composite structural insulated wall panels". Engineering Structures, Vol. 41, pp. 320-334.

Nakajima, S., Miyatake, A., Shibusawa, T., Araki, Y., Shindo, K., Haramiishi, T. and Kudo, Y. (2016). "Evaluation of buckling strength of cross laminated timber". World Conference on Timber Engineering, Vienna.

Nunes, T. (2015). "Estudo da inflamabilidade de diversos tipos de madeiras e de cortiça usados na estrutura e na envolvente de edifícios". MsC Thesis, Universidade de Coimbra - Departamento de Engenharia Mecânica, Coimbra.

Nunes, F., Correia, J. and Silvestre, N. (2016). "Structural behaviour of hybrid FRP pultruded columns. Part 1: Experimental study". Composite Structures, Vol. 139, pp. 291-303.

Nur-Holz. (2015). http://www.nur-holz.com/text/687/en/product.html. Nur-Holz, Oberharmersbach.

OIB. (2014). "CLT – Cross Laminated Timber". ETA 14/0349, Austrian Institute of Construction Engineering, Vienna.

Pagnoncelli, L, Gadotti, A, Frattari, A, Bazzini, E and Moran, L (2014). "Acoustic performance of cross-laminated timber system (CLT): in situ measurements of airborne and impact sound insulation for different configurations". 40th IAHS World Congress on Housing - Sustainable Housing Construction, Funchal.

Pang, S., Kim, K., Park, S. and Lee, S. (2017). "Bending Behavior of Nailed-Jointed Cross-Laminated Timber Loaded Perpendicular to Plane". J. Korean Wood Sci. Technol., Vol. 45, Issue 6, pp. 728-736.

Panjehpour, M., Ali, A. and Voo, Y. (2013). "Structural Insulated Panels: Past, Present, and Future". Journal of Engineering, Project, and Production Management, Vol. 3, Issue 1, pp. 2-8.

Panobloc. (2018). "http://www.techniwood.fr".

Pérez, M. and Fuente, M. (2013). "Acoustic design through predictive methods in Cross Laminated Timber (CLT) panel structures for buildings". Inter-Noise 2013, Innsbruck.

Perret, O., Douthe, C., Lebée, A. and Sab, K. (2016). "Buckling of cross laminated timber walls". World Conference on Timber Engineering, Vienna.

Pico. (2019). "Pico Technology". https://www.picotech.com/.

Rasmussen, B. (2010). "Sound insulation between dwellings – Requirements in building regulations in Europe". Applied Acoustics, Vol. 71, Issue 2010, pp. 373–385.

Ren, J. (1986). "A new theory of laminated plate". Compos Sci Technol, Vol. 26, Issue 3, pp. 225-239.

RGEU. (1951). "Regulamento Geral das Edificações Urbanas".

Rungthonkit, P and Yang, J (2009). "Behaviour of structural insulated panels (SIPs) under both short-term and long-term loadings". Proceedings of the 11th International Conference on Non-conventional Materials and Technologies (NOCMAT 2009), Bath.

Santos, P. (2012). "Análise de Elementos Colados Cruzados de Pinho Bravo". MSc Thesis in Civil Engineering. DEC-UC, Coimbra.

Santos, C. (2016). "A crescente utilização de materiais combustíveis na construção de fachadas". 5ª Conferência de segurança - Proteger 2016, Estoril.

Santos, J. (2017). "A riqueza das madeiras portuguesas - Propriedades e fichas técnicas". AIMMP, Porto.

Santos, P., Martins, C., Skinner, J., Harris, R., Dias, A. and Godinho, L. (2015). "Modal Frequencies of a Reinforced Timber-Concrete Composite Floor: Testing and Modeling". Journal of Structural Engineering, Vol. 141, Issue 11.

Santos, C. and Matias, L. (2006). "Coeficientes de transmissão térmica de elementos da envolvente dos edifícios". (Book). Laboratório Nacional de Engenharia Civil, Lisboa.

Scalet, T. (2015). "Cross Laminated Timber as Sustainable Construction Technology for the Future, BSc Thesis". Helsinki Metropolia University of Applied Sciences, Helsinki.

Schiavoni, S., D'Alessandro, F., Bianchi, F. and Asdrubali, F. (2016). "Insulation materials for the building sector: A review and comparative analysis". Renewable and Sustainable Energy Reviews, Vol. 62, pp. 988-1011.

Schoenwald, S, Zeitler, B and Sabourin, I (2014). "Analysis on Structure-borne Sound Transmission at Junctions of Solid Wood Double Walls with Continuous Floors". Forum Acusticum 2014, Krakow.

Sebera, V, Muszynski, L, Tippner, J, Noyel, M, Pisaneschi, T and Sundberg, B. (2015). "FE analysis of CLT panel subjected to torsion and verified by DIC". Materials and Structure, Vol. 48, pp. 451–459.

Sika. (2012). "SikaForce 7710 L100 - Adesivo para painéis de sandwich de uso geral". Sika, V.N.Gaia.

Sikora, K, McPolin, D and Harte, A. (2016). "Shear Strength and Durability Testing of Adhesive Bonds in Cross-laminated Timber". The Journal of Adhesion, Vol. 92, Issue 7-9, pp. 758-777.

Silva, V. (2006). "Mechanics and Strength of Materials". Springer, Berlin.

Simonin. (2018). "https://www.simonin.com".

Simulia. (2014). "ABAQUS 6.14".

SIPA. (2015). http://www.sips.org/about/frequently-asked-questions-faqs-regarding-structural-insulated-panels-sips#a. Structural Insulated Panel Association.

SIPS. (2016). "Structural Insulated Panel Connection Details". Structural Insulated Panel Association.

Smith, R. (2011). "Interlocking cross-laminated timber: alternative use of waste wood in design and construction". BTES Conference 2011- Convergence and Confluence, Toronto, Canada.

Southwell, R. (1932). "On the analysis of experimental observations in problems of elastic stability". Proc R Soc A Math Phys Eng Sci, Vol. 135, pp. 601-616.

Srivaro, S., Matan, N. and Lam, F. (2015). "Stiffness and strength of oil palmwood core sandwich panel under center point bending". Materials and Design, Vol. 84, pp. 154-162.

Steiger, R, Gülzow, A, Czaderski, C, Howald, M and Niemz, P. (2012). "Comparison of bending stiffness of cross-laminated solid timber derived by modal analysis of full panels and by bending tests of strip-shaped specimens". Eur. J. Wood Prod., Vol. 70, pp. 141-153.

Structurlam. (2013). "Environmental Product Declaration - CrossLam". Structurlam.

Stürzenbecher, R, Hofstetter, K and Eberhardsteiner, J. (2010). "Structural design of Cross Laminated Timber (CLT) by advanced plate theories". Composites Science and Technology, Vol. 70, pp. 1368-1379.

Symons, K, Moncaster, A and Symons, D (2013). "An Application of the CEN/TC350 standards to an Energy and Carbon LCA of timber used in construction, and the effect of end-of-life scenarios". Australian Life Cycle Assessment Society (ALCAS) conference, Sydney.

Tadeu, A., Mateus, D., António, J., Godinho, L. and Mendes, P. (2010). "Acústica Aplicada" (Book). Departamento de Engenharia Civil - Faculdade de Ciências e Tecnologia- Universidade de Coimbra, Coimbra.

Tang, Z., Zha, X. and Ma, J. (2015). "Buckling of axially loaded sandwich composite panels with reinforced calcium silicate faces and polyurethane cores". Journal of Reinforced Plastics and Composites, Vol. 34, Issue 17, pp. 1378–1391.

Tcharkhtchi, A., Farzaneh, S., Abdallah-Elhirtsi, S., Esmaeillou, B., Nony, F. and Baron, A. (2014). "Thermal Aging Effect on Mechanical Properties of Polyurethane". International Journal of Polymer Analysis and Characterization, Vol. 19, Issue 7, pp. 571-584.

Thiel, A (2014). "ULS and SLS design of CLT and its implementation in the CLTdesigner". COST Action FP1004, University of Trento, Trento.

Thirumal, M., Khastgir, D., Singha, N., Manjunath, B. and Naik, Y. (2008). "Effect of Foam Density on the Properties of Water Blown Rigid Polyurethane Foam". Journal of Applied Polymer Science, Vol. 108, Issue 3, pp. 1810-1817.

Thoma. (2015). http://www.thoma.at/. Thoma, Goldegg.

Timoshenko, S. (1921). "On the correction factor for shear of the differential equation for transverse vibrations of bars of uniform cross-section". Philosophical Magazine, Vol. 41, pp. 744-746.

Tuwair, H, Hopkins, M, Volz, J, ElGawady, M, Mohamed, M, Chandrashekhara, K and Birman, V. (2015). "Evaluation of sandwich panels with various polyurethane foam-cores and ribs". Composites Part B: Engineering, Vol. 79, pp. 262-276.

Uibel, T and Blass, H (2006). "Load carrying capacity of joints with dowel type fasteners in solid wood panels". Proceedings. CIB-W18 Meeting, Florence.

Uibel, T and Blass, H (2007). "Edge joints with dowel type fasteners in cross laminated timber". Proceedings of the International Council for Research and Innovation in Building and Construction. Working Commission W18–Timber Structures. 40th meeting, Bled.

Uibel, T. and Blass, H. (2013). "Joints with Dowel Type Fasteners in CLT Structures". COST Action FP1004 - Focus Solid Timber Solutions - European Conference on Cross-Laminated Timber (CLT), Graz University of Technology, Graz.

Unterwieser, H. and Schickhofer, G. (2011). "Influence of moisture content of wood on sound velocity and dynamic MOE of natural frequency- and ultrasonic runtime measurement". Eur. J. Wood Prod., Vol. 69, pp. 171-181.

Veedu, V. and Carlsson, L. (2005). "Finite-element buckling analysis of sandwich columns containing a face/core debond". Composite Structures, Vol. 69, pp. 143-148.

Vinson, Jack. (2005). "Sandwich Structures 7: Advancing with Sandwich Structures and Materials". Springer, Netherlands.

Vries, P. and Gard, W. (1998). "The development of a strength grading system for small diameter roundwood". HERON, Vol. 43, Issue 4.

Wang, J., Mohammad, M., Lenardo, B. and Sultan, M. (2016). "CLT panels subjected to combined out-of-plane bending and compressive axial loads". World Conference on Timber Engineering, Vienna.

Wang, T., Sokolinsky, V., Rajaram, S. and Nutt, S. (2005). "Assessment of sandwich models for the prediction of sound transmission loss in unidirectional sandwich panels". Applied Acoustics, Vol. 66, pp. 245-262.

Wang, J., Wei, P., Gao, Z. and Dai, C. (2018). "The evaluation of panel bond quality and durability of hem-fir cross-laminated timber (CLT)". European Journal of Wood and Wood Products, Vol. 76, pp. 833–841.

Wawrzynowicz, A, Krzaczek, M and Tejchman, J. (2014). "Experiments and FE Analyses on Airborne Sound Properties of Composite Structural Insulated Panels". Archives of Acoustics, Vol. 39, Issue 3, pp. 351-364.

Weight, D. (2011). "Embodied through-life carbon dioxide equivalent assessment for timber products". Proceedings of the Institution of Civil Engineers - Energy, Vol. 164, Issue EN4, pp. 167–182.

Wittbecker, W., Daems, D. and Werther, U. (2011). "Performance of Polyurethane (PUR) building products in fire". European Isocyanate Producers Association, Brussels.

Wyss, S, Fazio, P, Rao, J and Kayello, A. (2015). "Investigation of Thermal Performance of Structural Insulated Panels for Northern Canada". Journal of Architectural Engineering, Vol. 21, Issue 4.

Xavier, J., Garrido, N., Oliveira, M., Morais, J., Camanho, P. and Pierron, F. (2004). "A comparison between the Iosipescu and off-axis shear test methods for the characterization of Pinus Pinaster Ait.". Composites Part A: Applied Science and Manufacturing, Vol. 35.

Xavier, J., Oliveira, M., Morais, J. and Pinto, T. (2009). "Measurement of the shear properties of clear wood by the Arcan test". Holzforschung, Vol. 63, pp. 217–225.

Yang, J, Li, Z and Du, Q. (2012). "An Experimental Study on Material and Structural Properties of Structural Insulated Panels (SIPs)". Applied Mechanics and Materials, Vol. 147, pp. 127-131.

Zeitler, B, Schoenwald, S and Sabourin, I (2014). "Direct impact sound insulation of cross laminate timber floors with and without toppings". Inter Noise 2014, Melbourne.

APPENDIX A – Mechanical characterization of the beams and panels. Additional results. Numerical models vs. experiments

A.1 - Comparison between experimental and numerical load-displacement curves for the SIP beams
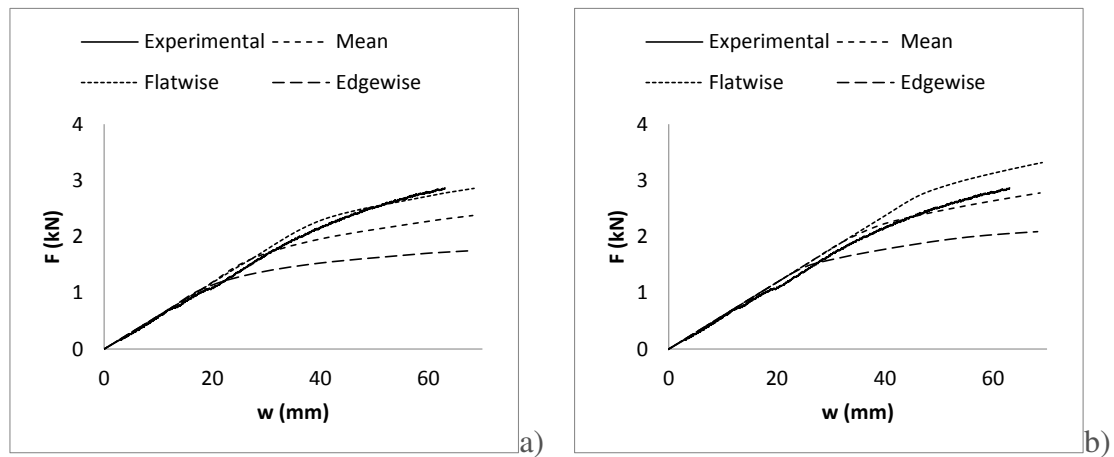
Figure A.1 - Comparison of the experimental and numerical load-displacement curves for SIP-10/40-B2: a) Plastic model; b) Crushable foam model.
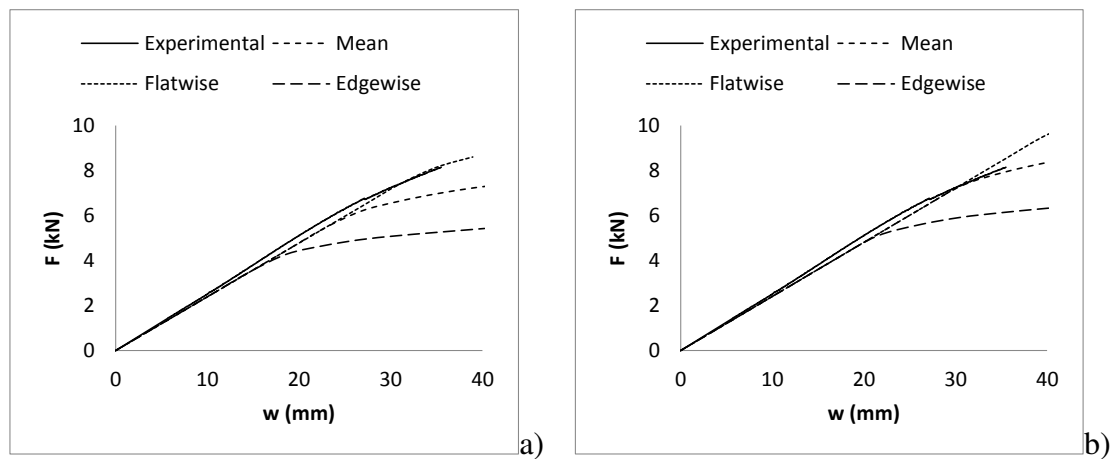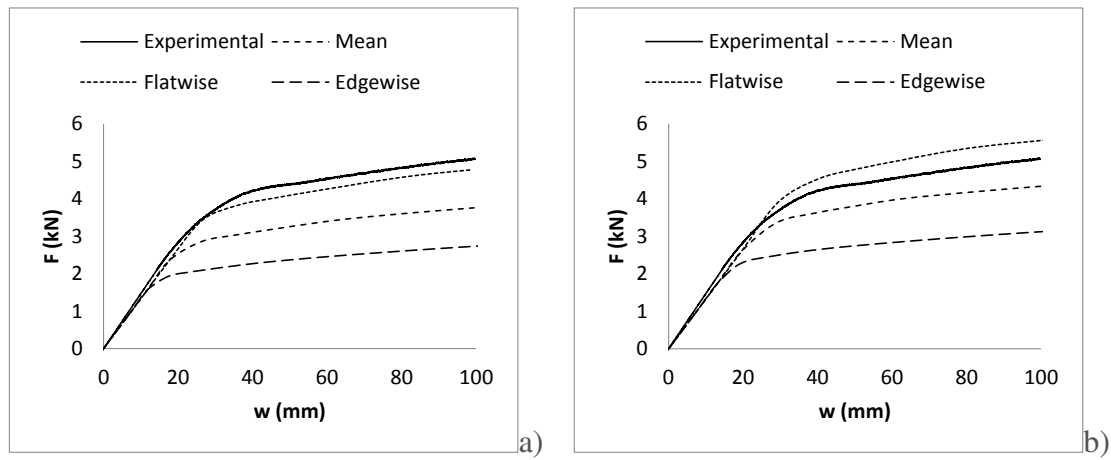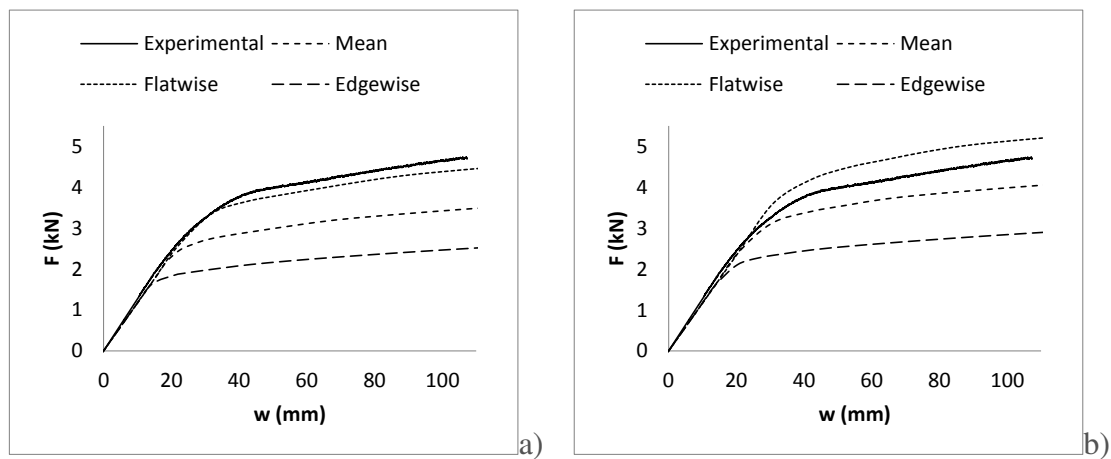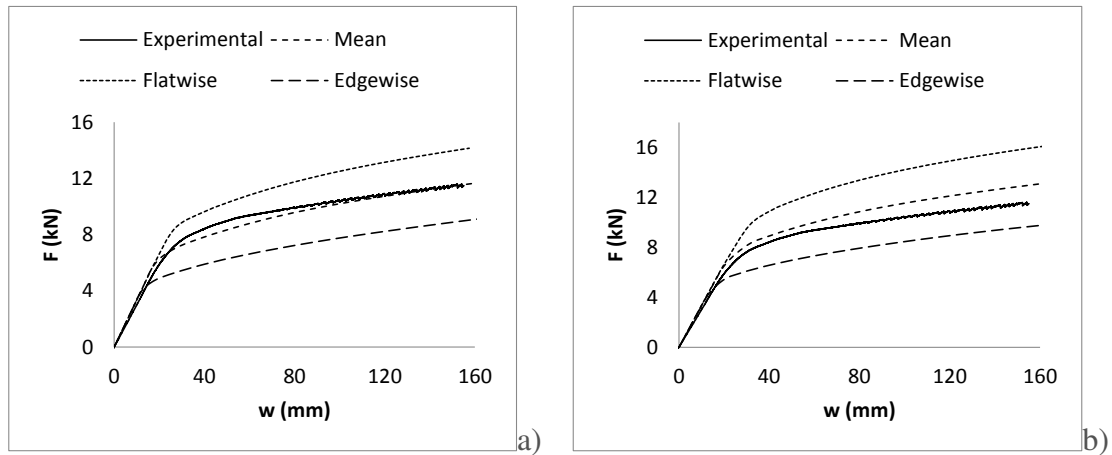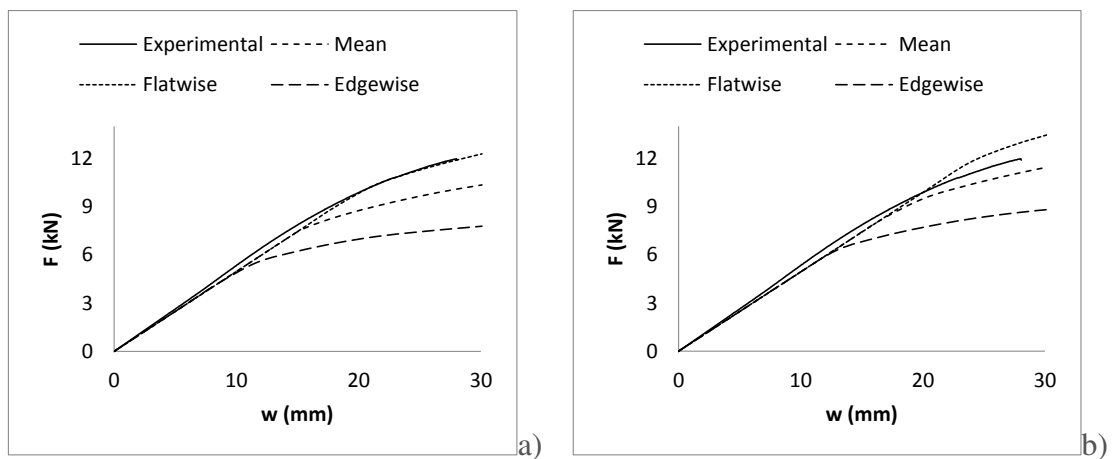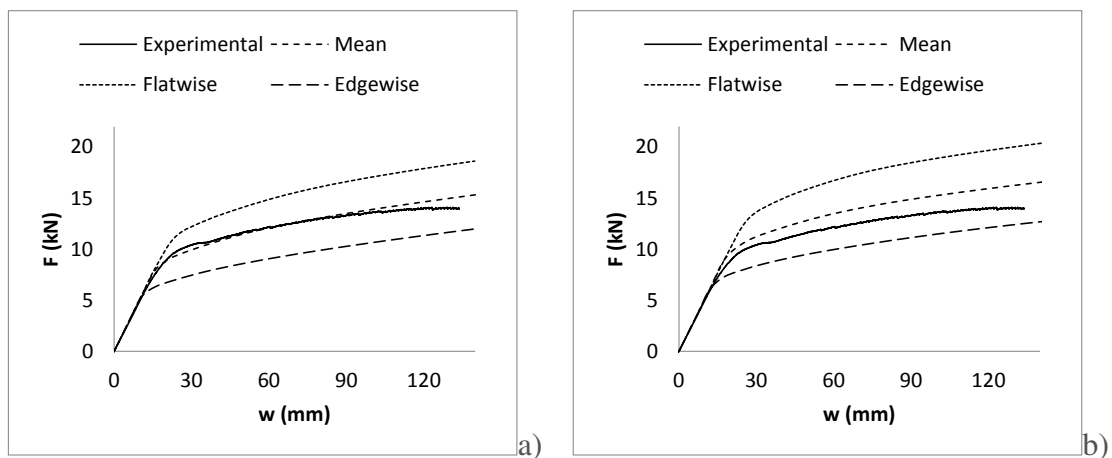
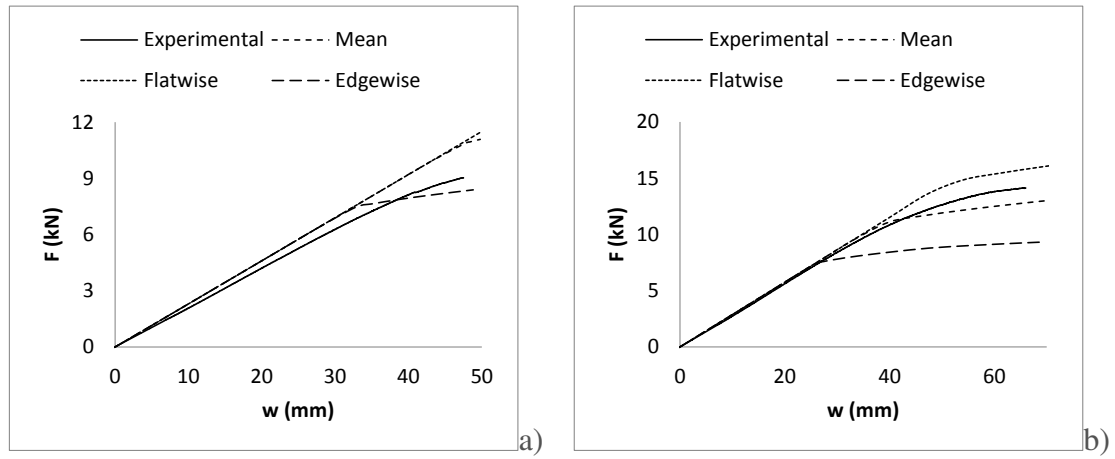Figure A.2 - Comparison of the experimental and numerical load-displacement curves for SIP-20/120-B1: a) Plastic model; b) Crushable foam model.

A.2 - Comparison between experimental and numerical load-displacement curves for the CIT beams

Figure A.3 - Comparison of the experimental and numerical load-displacement curves for CIT-10/40-B2: a) Plastic model; b) Crushable foam model.

Figure A.4 - Comparison of the experimental and numerical load-displacement curves for CIT-10/40-B3: a) Plastic model; b) Crushable foam model.

Figure A.5 - Comparison of the experimental and numerical load-displacement curves for CIT-20/120-B2: a) Plastic model; b) Crushable foam model.

Figure A.6 - Comparison of the experimental and numerical load-displacement curves for CIT-20/120-B3: a) Plastic model; b) Crushable foam model.

Figure A.7 - Comparison of the experimental and numerical load-displacement curves for CIT-20/120-B4: a) Plastic model; b) Crushable foam model.

A.3 - Comparison between experimental and numerical load-displacement curves for the CIT panels

Figure A.8 - Comparison of the experimental and numerical load-displacement curves for the CIT-10/30 panels: a) P1 and b) P3.
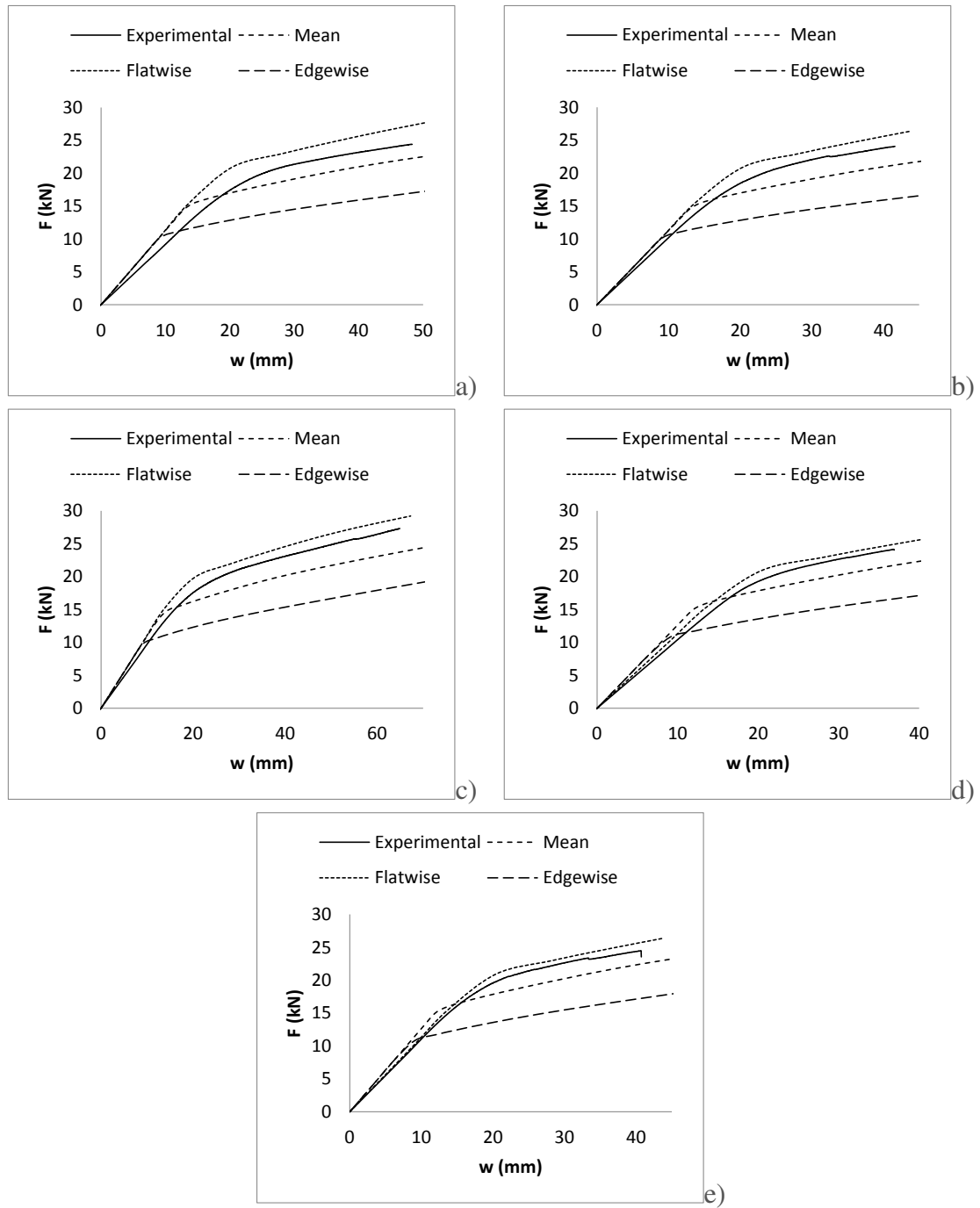
Figure A.9 - Comparison of the experimental and numerical load-displacement curves for the CIT-35/30 panels: a) P1; b) P3; c) P4; d) P5; e) P6.

APPENDIX B – Optimization of the panels. Additional results

B.1 – Optimization results as a function of span for exterior floor solutions - U≤0.35 W/(m².ºC)
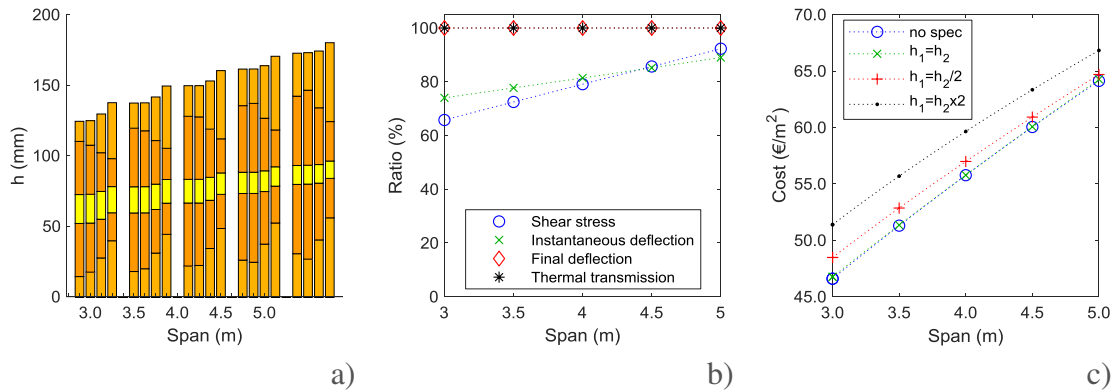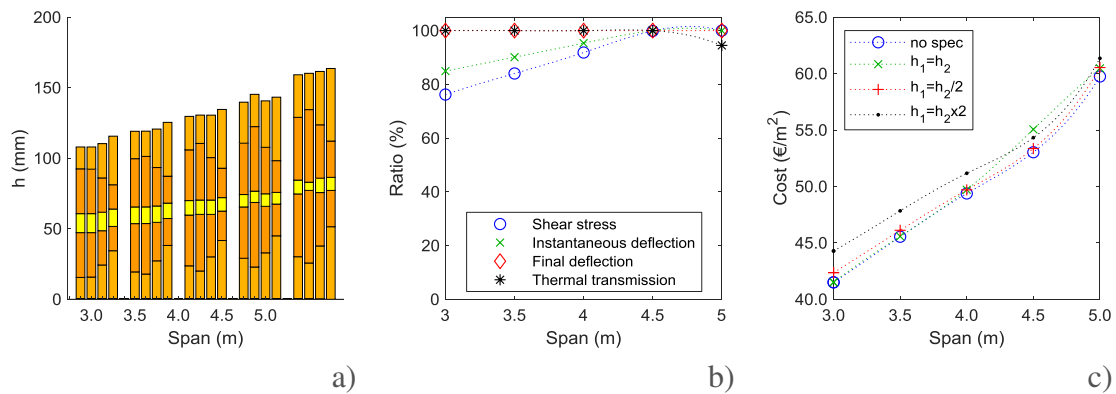

Figure B.1 – Results of the optimization in function of span for the CIT board's exterior floor solution: a) cross-sections; b) ratios of utilization; c) costs.
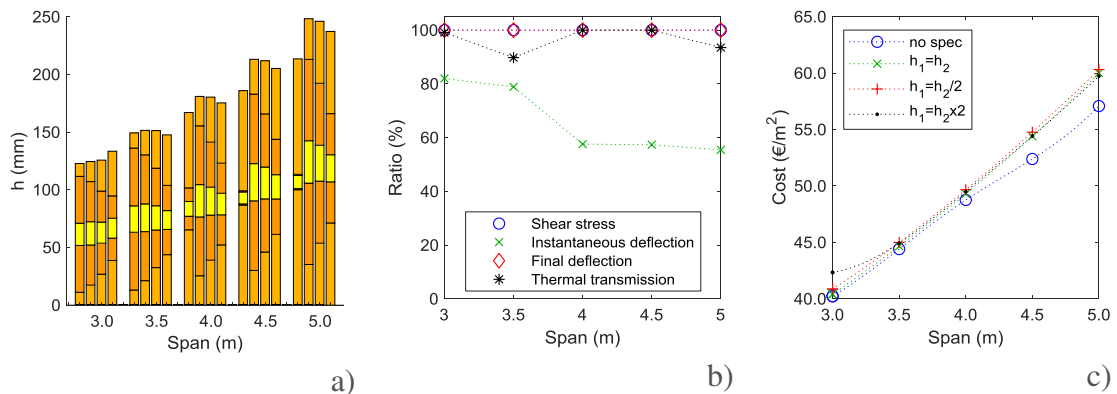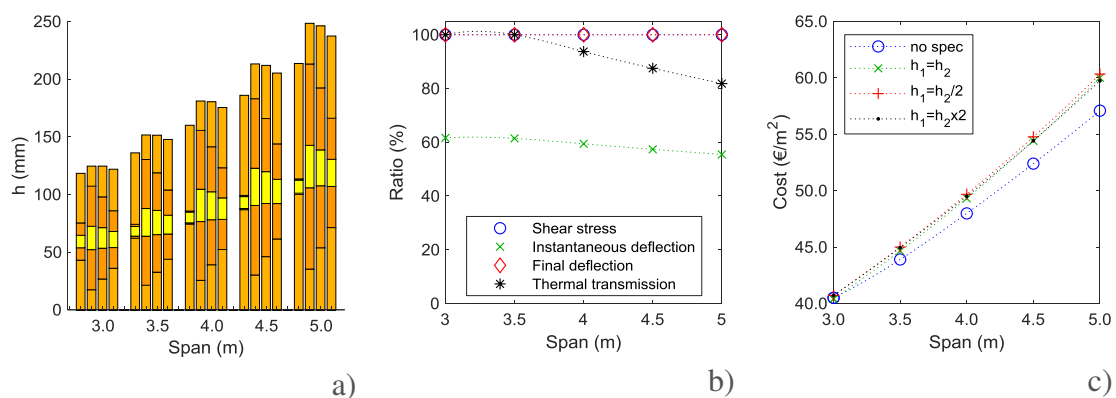

Figure B.2 – Results of the optimization in function of span for the CIT injected exterior floor solution: a) cross-sections; b) ratios of utilization; c) costs.
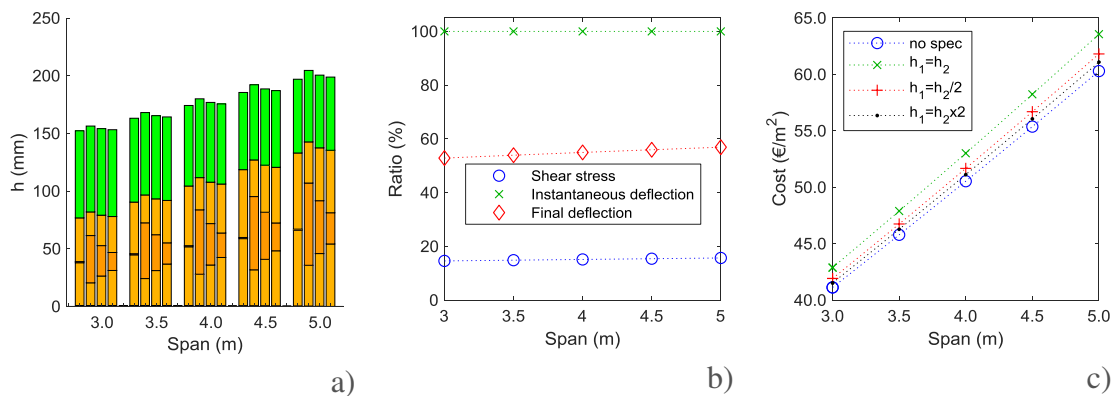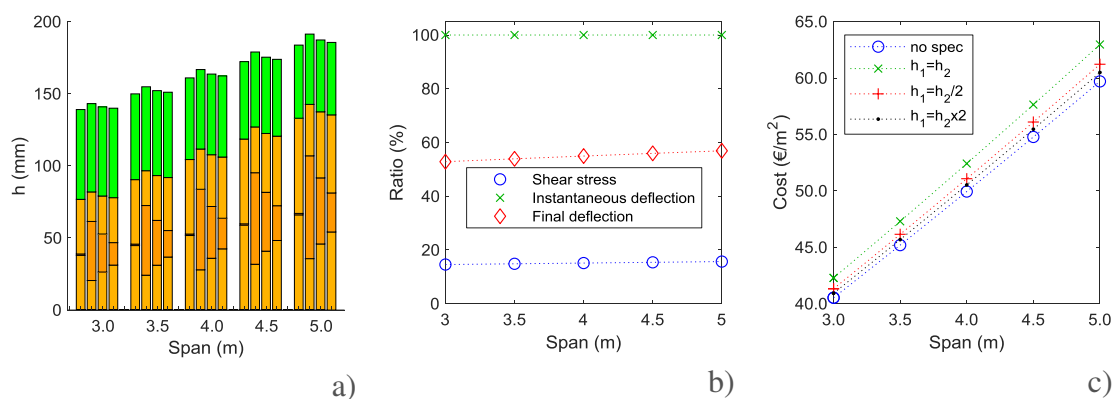

Figure B.3 – Results of the optimization in function of span for the CLT exterior floor solution: a) cross-sections; b) ratios of utilization; c) costs.

B.2 - Optimization results as a function of span for exterior floor solutions - U≤0.40 W/(m².ºC)

Figure B.4 – Results of the optimization in function of span for the CIT board's exterior floor solution: a) cross-sections; b) ratios of utilization; c) costs.

Figure B.5 – Results of the optimization in function of span for the CIT injected exterior floor solution: a) cross-sections; b) ratios of utilization; c) costs.

Figure B.6 – Results of the optimization in function of span for the CLT exterior floor solution: a) cross-sections; b) ratios of utilization; c) costs.

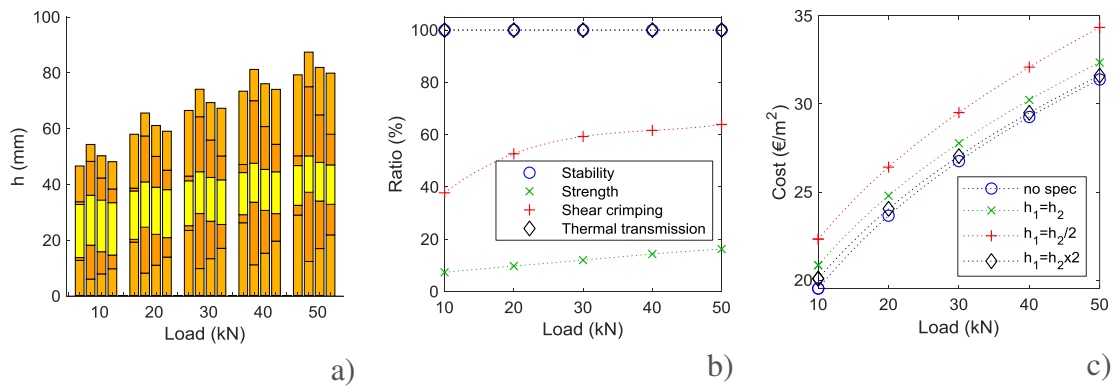## B.3 - Optimization results for exterior wall solutions - U≤0.40 W/(m².ºC)

Figure B.7 – Results of the optimization in function of load for the CIT board's exterior wall solution: a) cross-sections; b) ratios of utilization; c) costs.
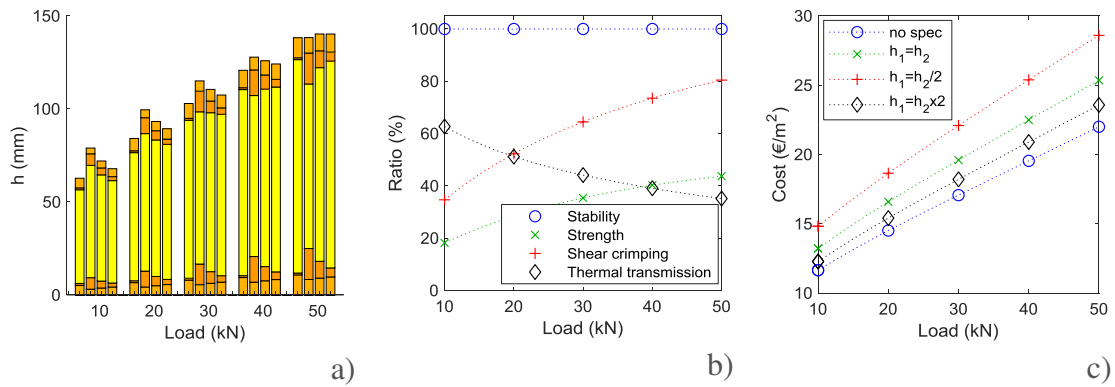

Figure B.8 – Results of the optimization in function of load for the CIT injected exterior wall solution: a) cross-sections; b) ratios of utilization; c) costs.
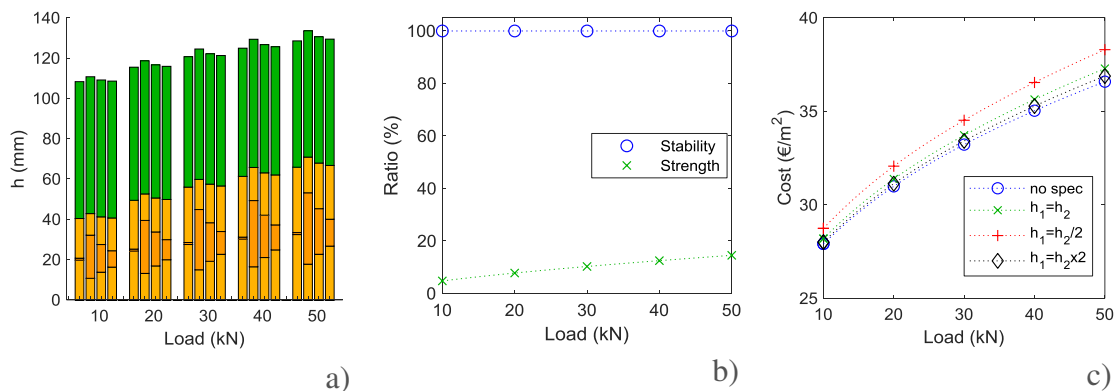

Figure B.9 – Results of the optimization in function of load for the CLT exterior wall solution: a) cross-sections; b) ratios of utilization; c) costs.

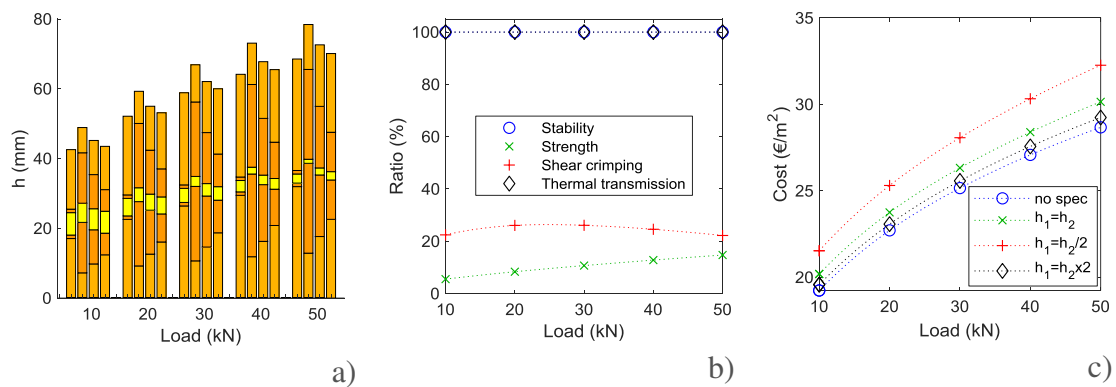## B.4 - Optimization results for exterior wall solutions - U≤0.50 W/(m².ºC)

Figure B.10 – Results of the optimization in function of load for the CIT board's exterior wall solution: a) cross-sections; b) ratios of utilization; c) costs.
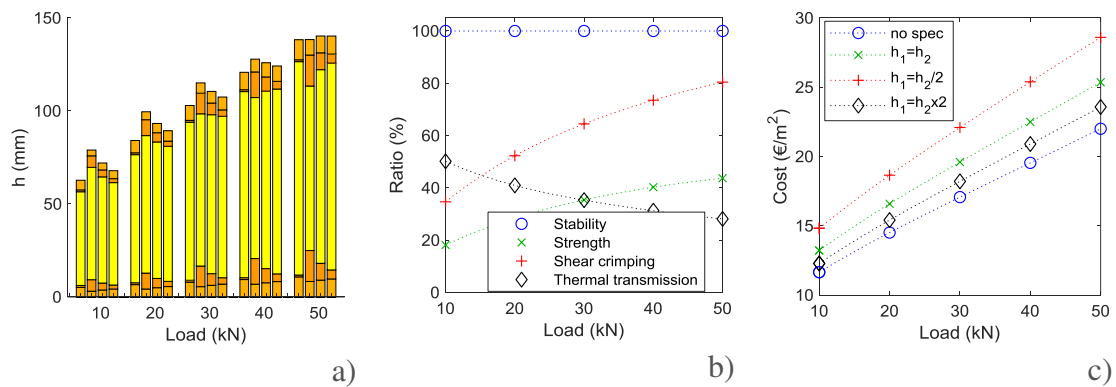

Figure B.11 – Results of the optimization in function of load for the CIT injected exterior wall solution: a) cross-sections; b) ratios of utilization; c) costs.
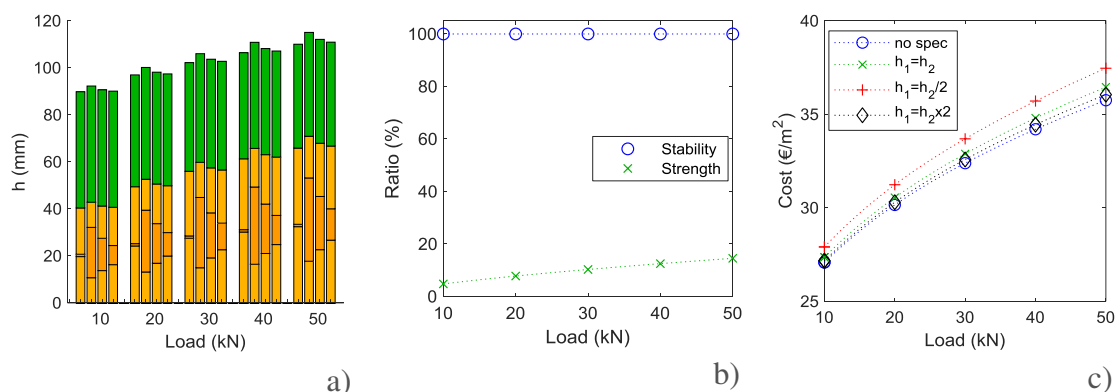

Figure B.12 – Results of the optimization in function of load for the CLT exterior wall solution: a) cross-sections; b) ratios of utilization; c) costs.

APPENDIX C – Life-Cycle Assessment. Additional results

C.1 – Results of the analysis of the contribution of each process on the environmental impact of the CIT panel wall

Table C.1 – Contribution of each process on each category indicator considered for the CIT wall.

| Process/Stage	Abiotic kg Sb eq.	Acidification kg SO$_2$ eq.	Eutrophication kg PO$_4$ eq.	Ozone layer kg CFC-11 eq.	Photochemical kg C$_2$H$_4$ eq.	Global warming kg CO$_2$ eq.
Logging and reforesting [with CO$_2$ seq.]	9.05E-03	9.92E-03	5.39E-03	1.69E-07	3.14E-04	1.3 [-95.2]
Transport of logs to sawmill	4.78E-03	3.58E-03	9.49E-04	1.06E-07	1.07E-04	0.7
Debarking and sawing	9.04E-03	1.06E-02	1.83E-03	7.17E-08	3.97E-04	1.2
Drying	7.37E-03	1.13E-02	2.61E-03	6.35E-08	4.28E-04	1.0
Grading	3.89E-05	4.74E-05	1.38E-05	5.01E-10	1.69E-06	0.0
Finger-jointing	1.19E-02	1.40E-02	2.26E-03	8.97E-08	5.23E-04	1.5
Planning	1.01E-02	1.19E-02	2.08E-03	7.91E-08	4.45E-04	1.4
Polyurethane 1C wood adhesive production	2.51E-04	1.78E-04	1.04E-05	6.05E-10	1.14E-05	0.0
Transport of wood adhesive to sawmill	1.07E-02	7.62E-03	5.30E-04	3.67E-08	4.74E-04	1.0
Transport of sandwich adhesive to sawmill	6.44E-04	4.82E-04	1.28E-04	1.43E-08	1.44E-05	0.1
Polyurethane foam production	4.31E-02	1.76E-02	3.59E-03	1.81E-08	2.05E-03	4.2
Transport of polyurethane foam to sawmill	2.80E-04	2.10E-04	5.56E-05	6.21E-09	6.27E-06	0.0
Wood adhesive application, press and curing	6.60E-02	7.76E-02	1.34E-02	5.24E-07	2.90E-03	8.7
Sandwich adhesive application, press and curing	1.49E-02	1.76E-02	3.03E-03	1.19E-07	6.57E-04	2.0
Cutting and trimming	5.77E-05	8.39E-05	3.06E-04	1.09E-09	3.07E-06	-0.1
Transport to construction site (A4)	2.67E-03	1.99E-03	5.29E-04	5.91E-08	5.96E-05	0.4
Transport to waste treatment (C2)	5.33E-04	3.99E-04	1.06E-04	1.18E-08	1.19E-05	0.1
Incineration [with energy recovery] (C3/C4)	3.19E-03	7.58E-03	9.20E-03	5.01E-08	2.58E-04	48.2 [37.3]
Landfill with partial rot [with energy recovery] (C3/C4)	4.27E-03	2.41E-03	8.23E-02	9.73E-08	5.39E-04	51.9 [29.0]
Landfill with total rot [with energy recovery] (C3/C4)	4.27E-03	2.41E-03	8.23E-02	9.73E-08	5.39E-04	251.1 [137.0]
A1 [with CO$_2$ seq.]	5.24E-02	2.77E-02	9.00E-03	1.88E-07	2.37E-03	5.6 [-90.9]
A2	1.64E-02	1.19E-02	1.66E-03	1.63E-07	6.02E-04	1.8
A3	1.19E-01	1.43E-01	2.55E-02	9.49E-07	5.36E-03	15.7
A1-A3	1.88E-01	1.83E-01	3.62E-02	1.30E-06	8.33E-03	23.1 [-73.4]
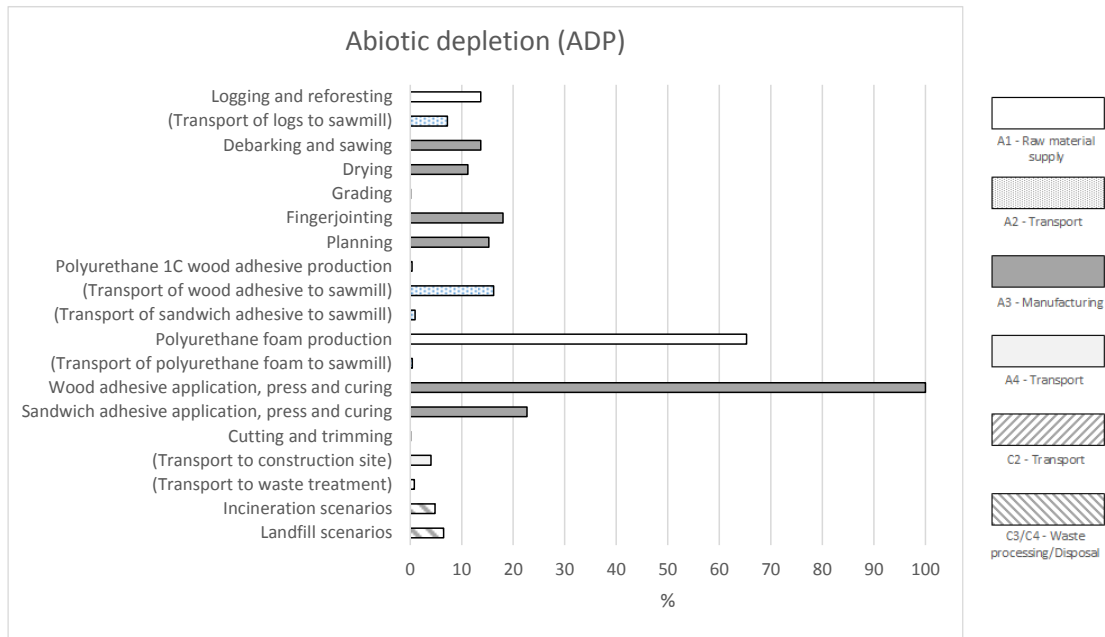
Figure C.1 – Relative contribution of each process on the environmental impact
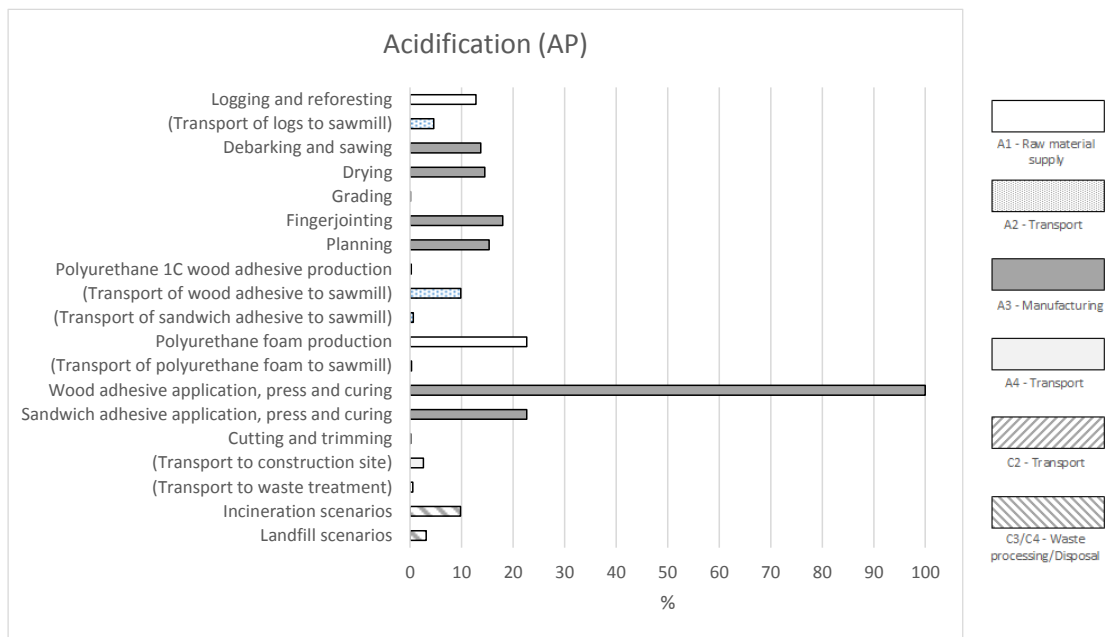(Abiotic depletion) of the CIT wall.

Figure C.2 – Relative contribution of each process on the environmental impact
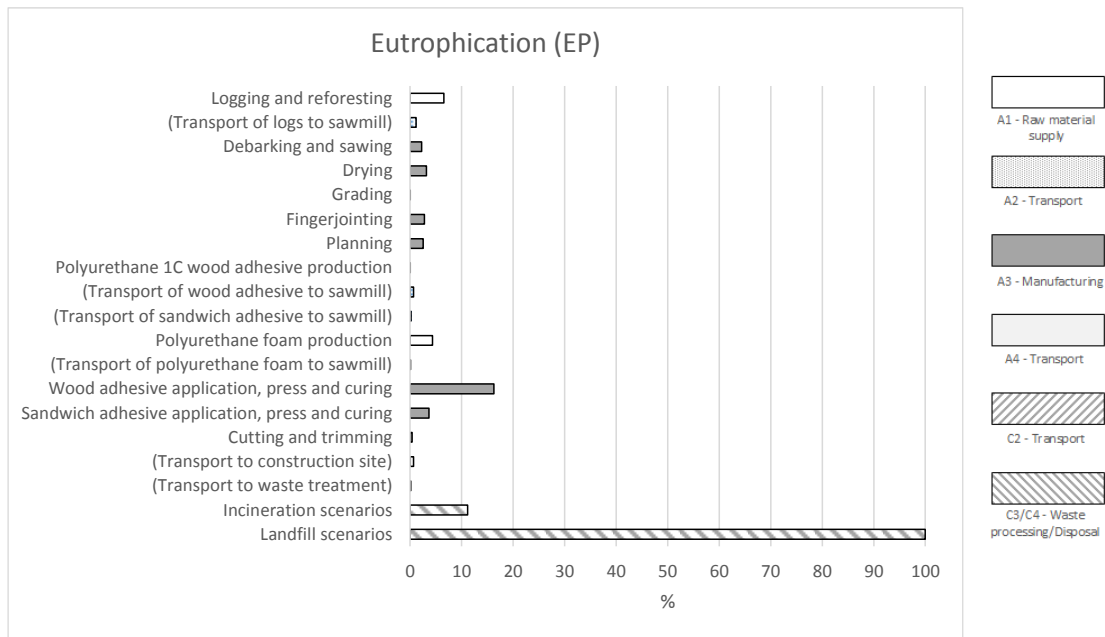(Acidification) of the CIT wall.

Figure C.3 – Relative contribution of each process on the environmental impact (Eutrophication) of the CIT wall.
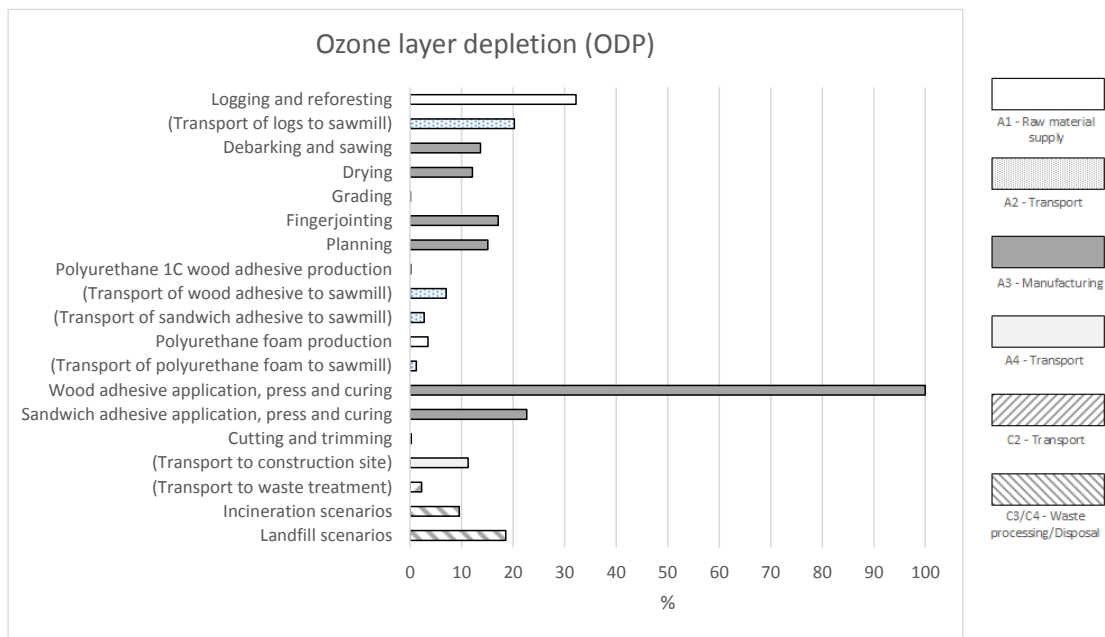

Figure C.4 – Relative contribution of each process on the environmental impact (Ozone layer depletion) of the CIT wall.
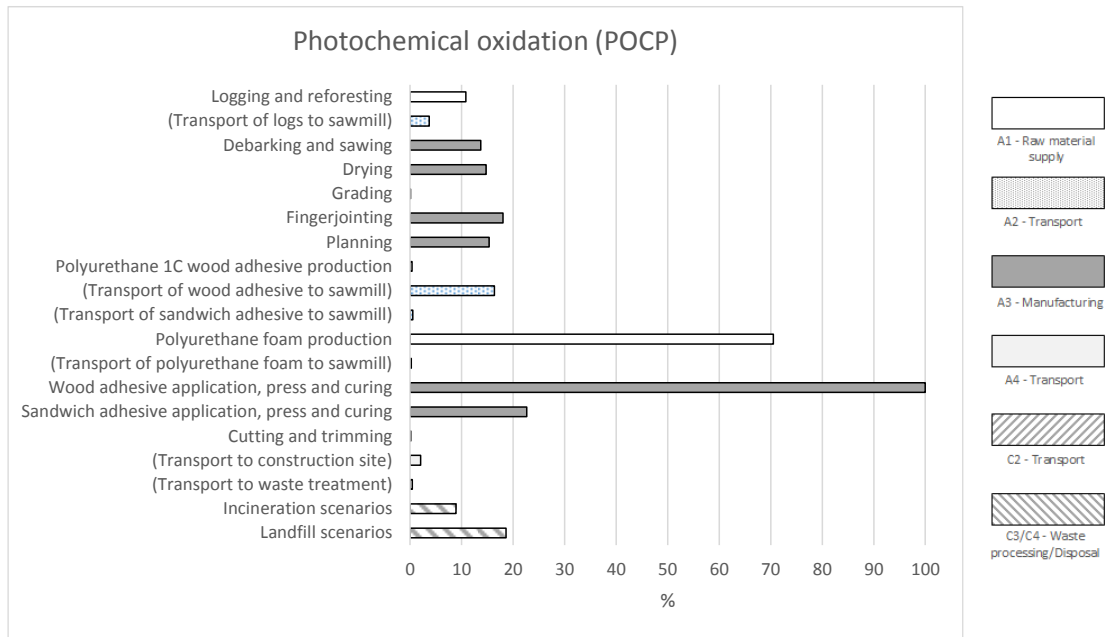
Figure C.5 – Relative contribution of each process on the environmental impact (Photochemical oxidation) of the CIT wall.
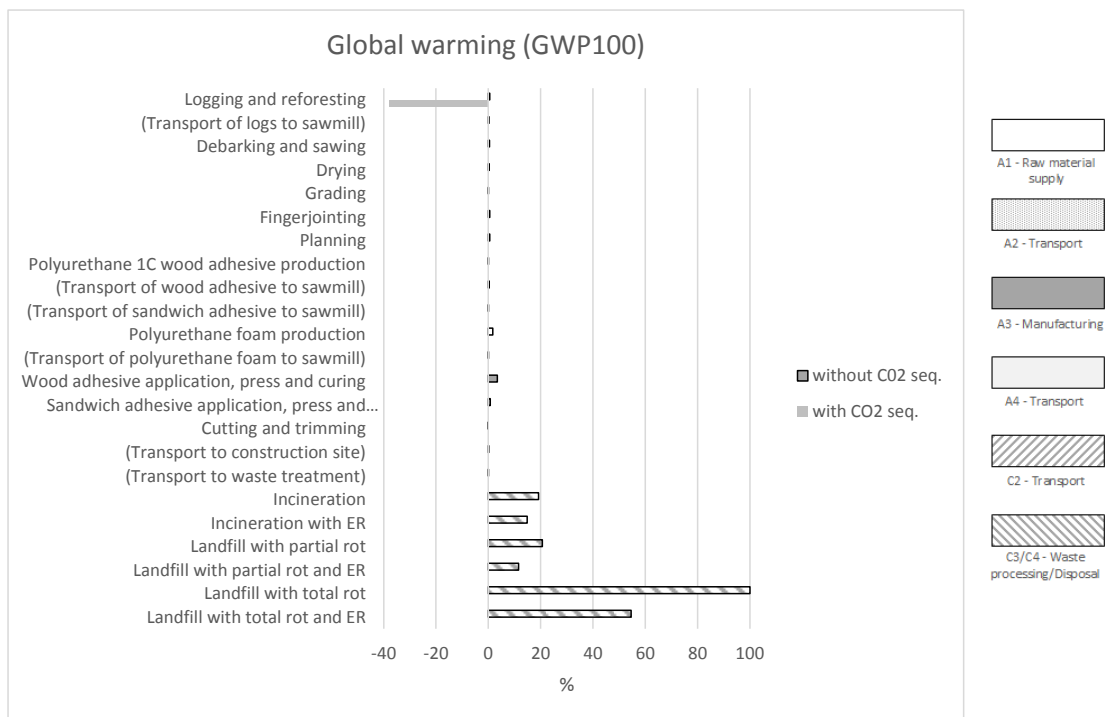

Figure C.6 – Relative contribution of each process on the environmental impact (Global warming) of the CIT wall.

C.2 – Results for different thicknesses of wood layers compared to the optimized one for the CIT wall

Figure C.7 – Impacts of each wall solution regarding the wood layer thickness for the cradle-to-gate stage (A1-A3).

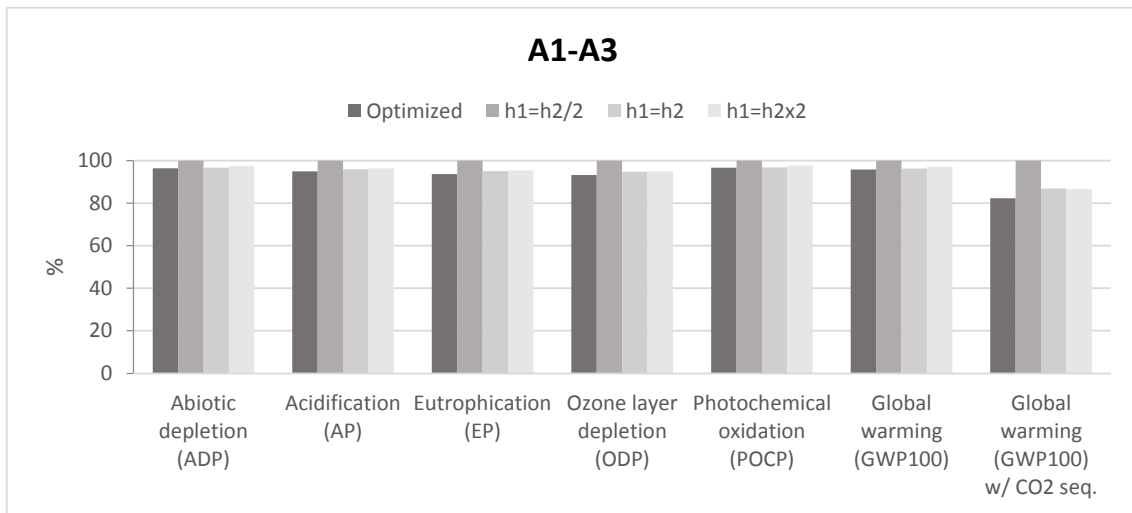| Wood layers' ratio	Abiotic depletion (ADP)	Acidification (AP)	Eutrophication (EP)	Ozone layer depletion (ODP)	Photochemical oxidation (POCP)	Global warming (GWP100)	Global warming (GWP100) w/ CO_2 seq.
	kg Sb eq.	kg SO_2 eq.	kg PO_4 eq.	kg CFC-11 eq.	kg C_2H_4 eq.	kg CO_2 eq.	kg CO_2 eq.
Optimized	1.88E-01	1.83E-01	3.62E-02	1.30E-06	8.33E-03	23.1	-73.4
$h_1=h_2/2$	1.95E-01	1.92E-01	3.86E-02	1.40E-06	8.62E-03	24.1	-89.2
$h_1=h_2$	1.89E-01	1.85E-01	3.67E-02	1.32E-06	8.34E-03	23.2	-77.5
$h_1=h_2x2$	1.90E-01	1.85E-01	3.68E-02	1.32E-06	8.43E-03	23.4	-77.3

Figure C.8 - Relative impacts of each wall solution regarding the wood layer thickness for the cradle-to-gate stage (A1-A3).

Table C.2 – Impacts at the end-of-life of each wall solution regarding the wood layer thickness as a function of the end-of-life scenario considered.

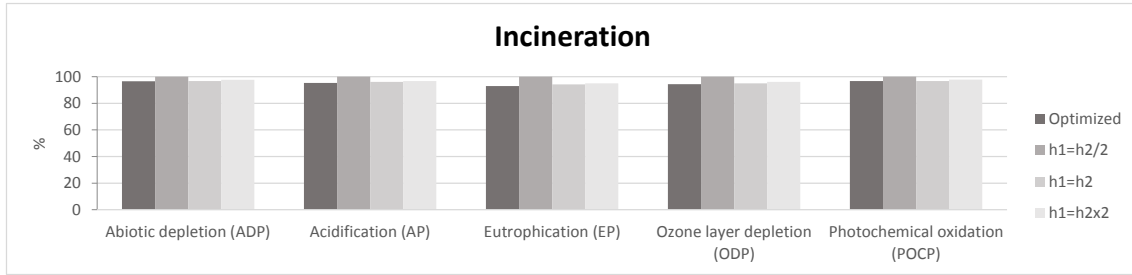| Wood layers' ratio	End-of-life scenario	Abiotic depletion (ADP) kg Sb eq.	Acidification (AP) kg SO$_2$ eq.	Eutrophication (EP) kg PO$_4$ eq.	Ozone layer depletion (ODP) kg CFC-11 eq.	Photochemical oxidation (POCP) kg C$_2$H$_4$ eq.	Global warming (GWP100) kg CO$_2$ eq.	Global warming (GWP100) w/ CO$_2$ seq. kg CO$_2$ eq.
Optimized	Incineration [with ER]	0.183	0.180	0.042	1.25E-06	0.008	70.0 [59.2]	25.1 [14.3]
	Landfill with partial rot [with ER]	0.184	0.175	0.115	1.29E-06	0.009	73.8 [50.9]	28.9 [6.0]
	Landfill with total rot [with ER]	0.184	0.175	0.115	1.29E-06	0.009	273.0 [158.9]	228.1 [114.0]
h$_1$=h$_2$/2	Incineration [with ER]	0.189	0.189	0.045	1.32E-06	0.009	78.6 [66.0]	25.9 [13.3]
	Landfill with partial rot [with ER]	0.191	0.184	0.128	1.39E-06	0.009	83.6 [56.8]	30.9 [4.1]
	Landfill with total rot [with ER]	0.191	0.184	0.128	1.39E-06	0.009	317.5 [183.5]	264.8 [130.8]
h$_1$=h$_2$	Incineration [with ER]	0.183	0.181	0.042	1.25E-06	0.008	71.9 [60.6]	25.1 [13.8]
	Landfill with partial rot [with ER]	0.184	0.177	0.118	1.32E-06	0.009	76.1 [52.3]	29.2 [5.4]
	Landfill with total rot [with ER]	0.184	0.177	0.118	1.32E-06	0.009	284.0 [284.0]	237.2 [118.1]
h$_1$=h$_2$x2	Incineration [with ER]	0.185	0.183	0.043	1.27E-06	0.008	72.3 [61.0]	25.4 [14.1]
	Landfill with partial rot [with ER]	0.186	0.177	0.119	1.32E-06	0.009	76.3 [52.4]	29.4 [5.6]
	Landfill with total rot [with ER]	0.186	0.177	0.119	1.32E-06	0.009	284.2 [165.1]	237.3 [118.2]

Figure C.9 – Relative impacts (at the end-of-life) of using different thicknesses of wood layers compared to the optimized one for the CIT wall, for the incineration end-of-life scenario.
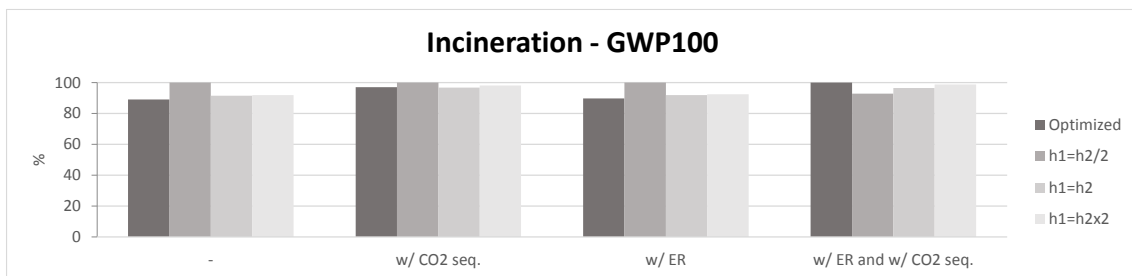

Figure C.10 – Relative impacts on GWP100 (at the end-of-life) regarding the use different thicknesses of wood layers compared to the optimized one for the CIT wall, for the incineration end-of-life scenario.
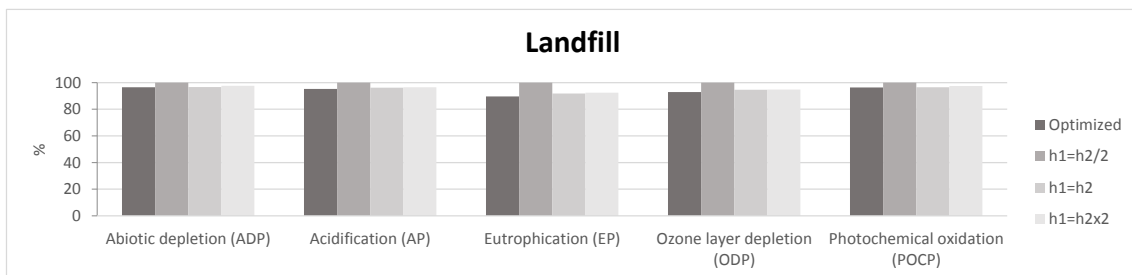

Figure C.11 – Relative impacts (at the end-of-life) of using different thicknesses of wood layers compared to the optimized one for the CIT wall, for the landfill end-of-life scenario.
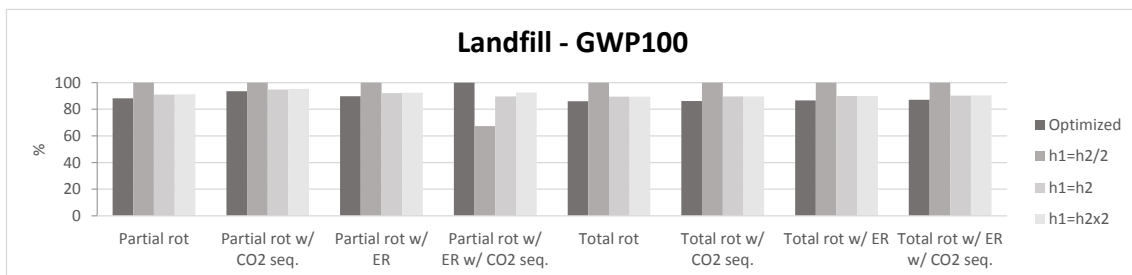

Figure C.12 – Relative impacts on GWP100 (at the end-of-life) regarding the use different thicknesses of wood layers compared to the optimized one for the CIT wall, for the landfill end-of-life scenario.

C.3 – Comparison between LCA results for the CIT wall panels with CIT with ICB core and CLT solutions with different insulation materials

Table C.3 – Impacts of each wall solution for the cradle-to-gate stage (A1-A3).

| Solution	Abiotic depletion (ADP)	Acidification (AP)	Eutrophication (EP)	Ozone layer depletion (ODP)	Photochemical oxidation (POCP)	Global warming (GWP100)	Global warming (GWP100) w/ CO_2 seq.
	kg Sb eq.	kg SO_2 eq.	kg PO_4 eq.	kg CFC-11 eq.	kg C_2H_4 eq.	kg CO_2 eq.	kg CO_2 eq.
CIT w/PUR	1.88E-01	1.83E-01	3.62E-02	1.30E-06	8.33E-03	23.1	-73.4
CIT w/ICB	1.94E-01	2.69E-01	5.94E-02	1.82E-06	1.24E-02	25.3	-159.3
CLT + RW	1.34E-01	1.45E-01	3.25E-02	1.17E-06	5.80E-03	17.1	-102.4
CLT + XPS	1.84E-01	1.43E-01	3.22E-02	1.14E-06	7.32E-03	20.7	-98.9
CLT + ICB	9.89E-02	2.32E-01	5.68E-02	9.97E-07	1.42E-02	13.2	-106.4
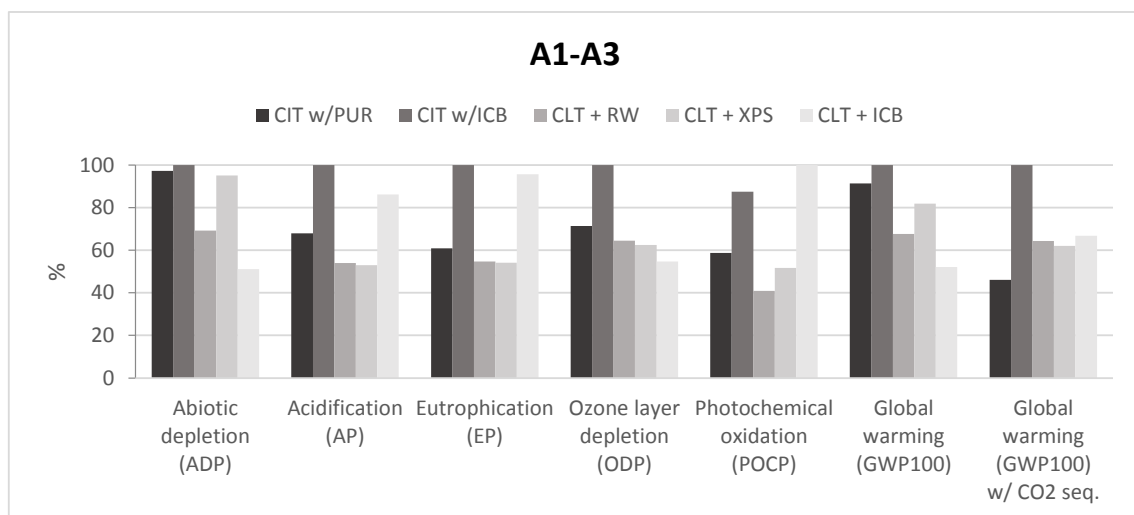
Figure C.13 – Relative impacts of each wall solution for the cradle-to-gate stage (A1-A3).

Table C.4 – Impacts at the end-of-life of each wall solution as a function of the end-of-life scenario considered.

| Panel Type	Wood layers' ratio	End-of-life scenario	Abiotic depletion (ADP)	Acidification (AP)	Eutrophication (EP)	Ozone layer depletion (ODP)	Photochemical oxidation (POCP)	Global warming (GWP100)	Global warming (GWP100) w/ CO_2 seq.
			kg Sb eq.	kg SO_2 eq.	kg PO_4 eq.	kg CFC-11 eq.	kg C_2H_4 eq.	kg CO_2 eq.	kg CO_2 eq.
CIT w/ PUR core	Optimized	Incineration [with ER]	0.183	0.180	0.042	1.25E-06	0.008	70.0 [59.2]	25.1 [14.3]
		Landfill with partial rot [with ER]	0.184	0.175	0.115	1.29E-06	0.009	73.8 [50.9]	28.9 [6.0]
		Landfill with total rot [with ER]	0.184	0.175	0.115	1.29E-06	0.009	273.0 [158.9]	228.1 [114.0]
CIT w/ ICB core	Optimized	Incineration [with ER]	0.183	0.263	0.069	1.71E-06	0.012	117.1 [94.6]	24.4 [1.9]
		Landfill with partial rot [with ER]	0.186	0.255	0.195	1.82E-06	0.013	129.6 [82.5]	36.9 [-10.2]
		Landfill with total rot [with ER]	0.186	0.255	0.195	1.82E-06	0.013	540.8 [305.3]	448.0 [212.5]
CLT + RW insulation	$h_1=h_2$	Incineration [with ER]	0.138	0.149	0.041	1.14E-06	0.006	25.3 [12.5]	19.2 [6.4]
		Landfill with partial rot [with ER]	0.139	0.143	0.123	1.21E-06	0.007	82.2 [53.9]	76.1 [47.8]
		Landfill with total rot [with ER]	0.139	0.143	0.123	1.21E-06	0.007	329.1 [187.7]	323.0 [181.6]
CLT + XPS insulation	$h_1=h_2$	Incineration [with ER]	0.187	0.145	0.039	1.09E-06	0.008	25.4 [10.7]	21.9 [7.2]
		Landfill with partial rot [with ER]	0.189	0.140	0.118	1.15E-06	0.008	85.0 [56.8]	81.6 [53.3]
		Landfill with total rot [with ER]	0.189	0.140	0.118	1.15E-06	0.008	331.9 [190.5]	328.5 [187.0]
CLT + ICB insulation	$h_1=h_2$	Incineration [with ER]	0.105	0.238	0.069	1.01E-06	0.015	35.3 [15.6]	18.5 [-1.2]
		Landfill with partial rot [with ER]	0.107	0.232	0.163	1.08E-06	0.016	81.8 [53.2]	65.0 [36.4]
		Landfill with total rot [with ER]	0.107	0.232	0.163	1.08E-06	0.016	330.9 [188.2]	314.1 [171.4]
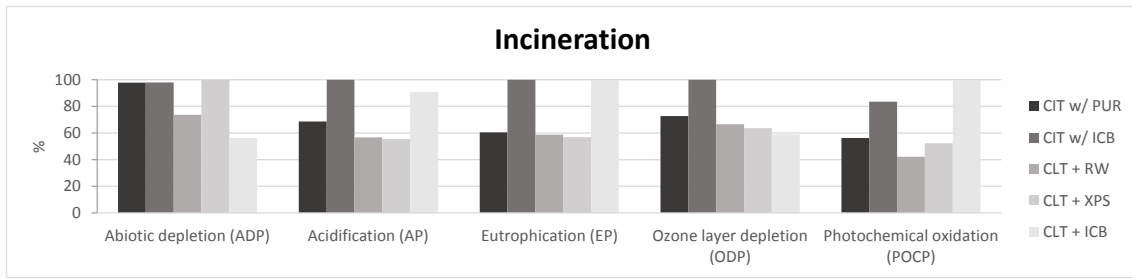
Figure C.14 – Comparison of the relative impacts (at the end-of-life) between the different CIT and CLT wall solutions for the incineration scenario.
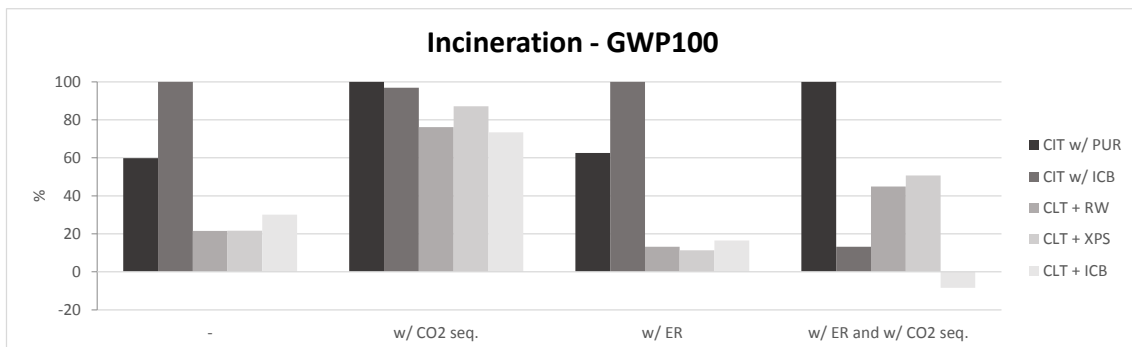

Figure C.15 – Comparison of the relative impacts (at the end-of-life) between the different CIT and CLT wall solutions for the incineration scenario regarding GWP100.
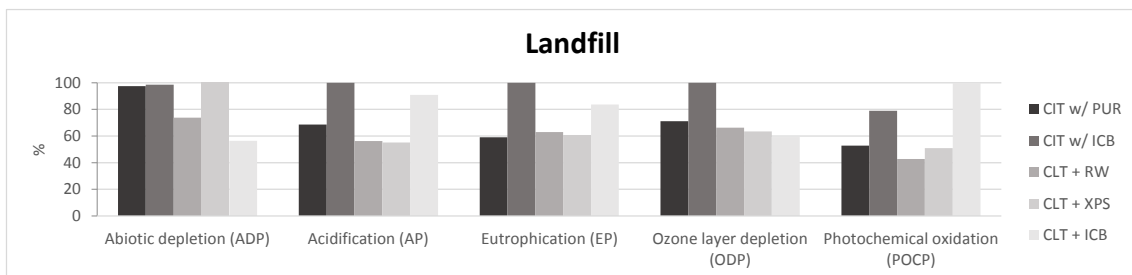

Figure C.16 – Comparison of the relative impacts (at the end-of-life) between the different CIT and CLT wall solutions for the landfill scenario.
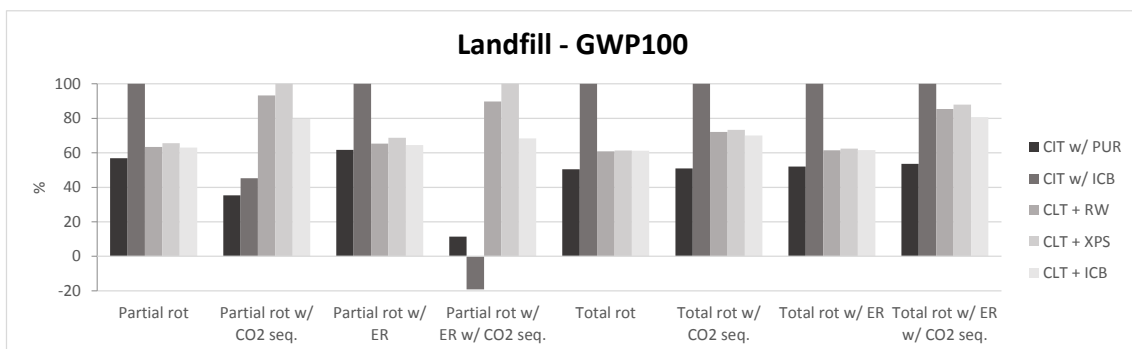

Figure C.17 – Comparison of the relative impacts (at the end-of-life) between the different CIT and CLT wall solutions for the landfill scenario regarding GWP100.